

Flue Gas Desulfurization

Flue Gas Desulfurization

John L. Hudson, EDITOR

University of Virginia

Gary T. Rochelle, EDITOR

University of Texas at Austin

Based on a symposium
sponsored by the
Division of Industrial
and Engineering Chemistry
at the 181st Meeting of the
American Chemical Society,
Atlanta, Georgia,
March 29–30, 1981.

A C S S Y M P O S I U M S E R I E S **188**

AMERICAN CHEMICAL SOCIETY
WASHINGTON, D. C. 1982



Library of Congress Cataloging in Publication Data

Flue gas desulfurization.
(ACS symposium series, ISSN 0097-6156; 188)

"Contains papers presented in the Symposium on
Advances in Flue Gas Desulfurization"—Pref.
Includes bibliographies and index.

1. Flue gases—Desulphurization—Congresses.
I. Hudson, John L. (John Lester), 1937- . II.
Rochelle, Gary T. III. American Chemical Society.
Division of Industrial and Engineering Chemistry. IV.
Symposium on Advances in Flue Gas Desulfurization
(1981: Atlanta, Ga.) V. Series.

TD885.5.S85F57 628.5'32 82-6818
ISBN 0-8412-0722-4 AACR2 ACSMC8 188 1-432
1982

Copyright © 1982

American Chemical Society

All Rights Reserved. The appearance of the code at the bottom of the first page of each article in this volume indicates the copyright owner's consent that reprographic copies of the article may be made for personal or internal use or for the personal or internal use of specific clients. This consent is given on the condition, however, that the copier pay the stated per copy fee through the Copyright Clearance Center, Inc. for copying beyond that permitted by Sections 107 or 108 of the U.S. Copyright Law. This consent does not extend to copying or transmission by any means—graphic or electronic—for any other purpose, such as for general distribution, for advertising or promotional purposes, for creating new collective work, for resale, or for information storage and retrieval systems.

The citation of trade names and/or names of manufacturers in this publication is not to be construed as an endorsement or as approval by ACS of the commercial products or services referenced herein; nor should the mere reference herein to any drawing, specification, chemical process, or other data be regarded as a license or as a conveyance of any right or permission, to the holder, reader, or any other person or corporation, to manufacture, reproduce, use, or sell any patented invention or copyrighted work that may in any way be related thereto.

PRINTED IN THE UNITED STATES OF AMERICA

American Chemical
Society Library
1155 16th St., N.W.

In Flue Gas Desulfurization, Hudson, John L., Rochelle, Gary T., et al.;
ACS Symposium Series; American Chemical Society: Washington, DC, 1982.

Washington, D. C. 20036

ACS Symposium Series

M. Joan Comstock, *Series Editor*

Advisory Board

David L. Allara

Robert Baker

Donald D. Dollberg

Robert E. Feeney

Brian M. Harney

W. Jeffrey Howe

James D. Idol, Jr.

Herbert D. Kaesz

Marvin Margoshes

Robert Ory

Leon Petrakis

Theodore Provder

Charles N. Satterfield

Dennis Schuetzle

Davis L. Temple, Jr.

Gunter Zweig

FOREWORD

The ACS SYMPOSIUM SERIES was founded in 1974 to provide a medium for publishing symposia quickly in book form. The format of the Series parallels that of the continuing ADVANCES IN CHEMISTRY SERIES except that in order to save time the papers are not typeset but are reproduced as they are submitted by the authors in camera-ready form. Papers are reviewed under the supervision of the Editors with the assistance of the Series Advisory Board and are selected to maintain the integrity of the symposia; however, verbatim reproductions of previously published papers are not accepted. Both reviews and reports of research are acceptable since symposia may embrace both types of presentation.

PREFACE

This volume contains papers presented in the Symposium on Advances in Flue Gas Desulfurization at the ACS National Meeting in Atlanta on March 29–30, 1981. The symposium was organized to provide a forum for fundamental work in flue gas desulfurization, rather than a forum for commercial process suppliers and users. Therefore, it differed substantially from symposia on flue gas desulfurization sponsored every 18 months by the U.S. Environmental Protection Agency.

Although there has long been talk of coal conversion processes, fluidized bed combustion, and other advanced technologies, flue gas desulfurization (FGD) is still the only commercially significant technology for abatement of sulfur dioxide from fossil-fired power plants. FGD has been used since the early 1970's, but is still not a mature technology. The chapters in this book present recent advances in the science and technology of FGD processes.

In spite of the effort to develop environmentally attractive processes that make marketable products, the lime/limestone slurry scrubbing process still dominates the commercial market for flue gas desulfurization. The limestone slurry scrubbing process requires only three pieces of major equipment: an absorber, a hold tank, and a liquid/solid separator. However, within this simple framework occur many interacting rate processes including gas/liquid mass transfer with chemical reaction, limestone dissolution, calcium sulfite dissolution and crystallization, gypsum crystallization, and sulfite oxidation. Each of these rate processes is itself a complex phenomenon involving solution and phase equilibria, reaction kinetics, and mass transfer. Therefore, although it is easy to design and construct a limestone slurry scrubbing process, it can be much more difficult to design and operate an optimal system. Numerous chapters in this book contribute to the quantitative understanding of the slurry scrubbing processes.

There is still active development of alternatives to throwaway slurry scrubbing. Advanced throwaway processes such as dual alkali and dry scrubbing offer improved economics, efficiency, and/or reliability. Regenerable processes such as MgO scrubbing and absorption/stripping produce marketable products and thereby minimize waste production. However, each of these new processes includes many of the same physical and chemical processes as in a throwaway slurry scrubbing. In addition,

there are new problems in solution equilibria, gas/solid reactions, temperature-induced side-reactions, and other phenomena that must be dealt with in each new process.

In 1979, the Department of Energy initiated support of a number of fundamental projects in the chemistry of flue gas desulfurization. Five chapters in this book report the initial results of this effort. The topics of fundamental work include thermodynamic properties, activity coefficients in aqueous solutions, sulfur and NO_x chemistry, and sulfite oxidation kinetics. The results provide the foundation for quantitative understanding of the FGD processes.

Eight chapters deal specifically with rate processes and innovations in throwaway slurry scrubbing. Data and models are given for limestone dissolution as a function of type and grind and as a function of solution composition. Two chapters present measured rates of sulfite oxidation catalyzed by Mn and Fe and models of the oxidation of CaSO_3 slurries. The effectiveness and degradation of organic acids are modeled and evaluated. Test results are presented for the use of adipic acid with the Shawnee 10 MW scrubbers. Energy requirements are evaluated as a function of scrubber type and additive concentration.

Four chapters address alternatives to throwaway slurry scrubbing. The development of the limestone dual alkali process is reviewed. Two chapters present results related to dry scrubbing with nahcolite or lime. A conceptual design and economics are given for MgO scrubbing using a spray dryer.

JOHN L. HUDSON
University of Virginia
Department of Chemical Engineering
Charlottesville, VA 22901

GARY T. ROCHELLE
University of Texas at Austin
Department of Chemical Engineering
Austin, TX 78712

January 7, 1982

Thermodynamic Values for Desulfurization Processes

LEO BREWER

University of California, Department of Chemistry, and Lawrence Berkeley Laboratory, Materials and Molecular Research Division, Berkeley, CA 94720

The thermodynamic properties of gases, liquids, solids and aqueous solutes of interest for desulfurization processes are tabulated for temperatures from 298 K to temperatures as high as 1000 K when possible. Major emphasis has been placed on aqueous lime or limestone scrubbing, but the data can also be used for high temperature gas processes and for NO_x processes.

The efficient design of processes for removal of sulfur dioxide resulting from coal and oil combustion requires thermodynamic and kinetic data for the various materials that might be used in the processes. Examination of the available thermodynamic data for sulfur compounds indicates serious uncertainties and the present review is a step toward providing the best set of internally consistent values obtainable from the literature and from current experiments.

Although the main emphasis is on information needed for aqueous limestone or lime slurry treatment, the data could also be used for other processes covering a wider temperature range. Thus data are tabulated, when possible, for the range from room temperature to at least 1000K. The present compilation covers most of the materials that might play a role in SO_2 extraction processes and for which data were found.

0097-6156/82/0188-0001\$10.75/0
© 1982 American Chemical Society

A convenient starting point is the list of recommended values (1) of the report of the CODATA Task Group on key values for thermodynamics, 1977. Some of these values were not considered up-to-date and, as discussed below, appropriate modifications and additions were made to provide what is considered the best set presently available. The present report covers values of ΔH_{298}° , S_{298}° , $H_{298}^{\circ}-H_0^{\circ}$, and C_p° at 298.15K. Values of $-(G^{\circ}-H_{298}^{\circ})/RT$ are tabulated to allow extension to higher temperatures. The values tabulated have been divided by R so that the data are in proper form for immediate calculation of the equilibrium constants (2) by $\ln K = -\Delta G^{\circ}/RT = -\Delta(G^{\circ}-H_{298}^{\circ})/RT - (\Delta H_{298}^{\circ}/R)/T$. As this procedure removes the uncertainty due to R in calculation of heat capacity and entropy values for gases, it was possible to improve the accuracy for some of the atomic species (3-7). The first version of this compilation was prepared for the FGD symposium held at Morgantown, West Virginia on Nov. 6-7, 1980, and subsequently extended for presentation at the FGD symposium of the American Chemical Society meeting in Atlanta, Georgia, held on March 30-31, 1981.

In such a thermodynamic compilation, it is very important to maintain internal consistency. When older data are replaced by more recent data as has been done here, one must ensure that all other values that depended upon the old data have been changed correspondingly. This is difficult to do and the present compilation is only one step in an iterative process that must be carried out continuously to incorporate newer data. The National Bureau of Standards is uniquely equipped to carry out such a process and it is hoped that the Bureau be able to continue the updating of the data that have been presented here.

TABLE I
Thermodynamic Properties of Common Gases at 298.15K

	$\Delta H_{298}^{\circ}/R, K$	S_{298}°/R	$(H_{298}^{\circ}-H_0^{\circ})/R, K$	C_p°/R
O(g)	29 970 ± 10	19.357 ± 0.002	809.2 ± 0.4	2.635
O ₂ (g)	0	24.660 ± 0.004	1 044.1 ± 0.5	3.533
O ₃ (g)	17 100 ± 200	28.733 ± 0.009	1 247 ± 2	4.736
H(g)	26 219 ± 1	13.784 ± 0.001	745.4	2.500
H ₂ (g)	0	15.704 ± 0.004	1 018.5 ± 0.4	3.468
OH(g)	4 700 ± 100	22.086 ± 0.005	1 060 ± 2	3.594
H ₂ O(g)	250 ± 1000	27.54 ± 0.01	1 203 ± 2	4.198
H ₂ O(g)	-29 084 ± 5	22.698 ± 0.005	1 192 ± 1	4.042
H ₂ O ₂ (g)	-16 340 ± 30	28.193 ± 0.02	1 342 ± 4	5.099
F(g)	9 548 ± 40	19.080 ± 0.002	783.9 ± 0.5	2.736
F ₂ (g)	0	24.378 ± 0.005	1 061.4 ± 0.5	3.765
HF(g)	-32 870 ± 80	20.887 ± 0.004	1 034.2 ± 0.5	3.504
Cl(g)	14 589 ± 1	19.854 ± 0.002	754.4 ± 0.4	2.627
Cl ₂ (g)	0	26.817 ± 0.005	1 104 ± 1	4.083
HCl(g)	-11 103 ± 16	22.465 ± 0.004	1 039.2 ± 0.5	3.504
Br(g)	13 457 ± 15	21.036 ± 0.002	745.4	2.500
Br ₂ (g)	3 718 ± 13	29.509 ± 0.006	1 170 ± 1	4.337
HBr(g)	-4 376 ± 20	23.884 ± 0.004	1 040.1 ± 0.5	3.505
I(g)	12 840 ± 2	21.730 ± 0.002	745.4	2.500
I ₂ (g)	7 508 ± 10	31.339 ± 0.008	1 217 ± 3	4.437
HI(g)	3 187 ± 15	24.834 ± 0.005	1 042.2 ± 0.7	3.507

Continued on next page.

TABLE I (continued)

	$\Delta H_{298}^{\circ}/R, K$	S_{298}°/R	$(H_{298}^{\circ}-H_0^{\circ})/R, K$	C_p°/R
S(g)	33 360 ± 50	20.172 ± 0.004	800.7 ± 0.5	2.847
S ₂ (g)	15 520 ± 80	27.429 ± 0.006	1 098 ± 1	3.909
S ₃ (g)	17 200 ± 400	32.85 ± 0.1	1 400 ± 5	5.78
S ₄ (g)	16 300 ± 400	35.29 ± 0.1	1 720 ± 5	7.93
S ₅ (g)	14 900 ± 400	40.6 ± 0.4	2 210 ± 20	10.73
S ₆ (g)	12 100 ± 400	42.55 ± 0.1	2 700 ± 10	13.54
S ₇ (g)	12 900 ± 400	48.1 ± 0.4	3 160 ± 20	16.1
S ₈ (g)	12 020 ± 180	51.20 ± 0.4	3 740 ± 20	18.71
HS(g)	16 800 ± 600	23.52 ± 0.01	1 100 ± 20	3.90
H ₂ S(g)	-2 470 ± 80	24.735 ± 0.006	1 198 ± 1	4.11
SO(g)	580 ± 50	26.680 ± 0.002	1 055 ± 5	3.625
SO ₂ (g)	-35 700 ± 20	29.841 ± 0.007	1 269 ± 2	4.792
SO ₃ (g)	-47 620 ± 80	30.84 ± 0.01	1 406 ± 2	6.088
SO ₄ (g)	(-37 000) ± 2500			
S ₂ O(g)	-5 400 ± 400	32.10 ± 0.02	1 338 ± 2	5.306
H ₂ SO ₃ (g)	(-64 000) ± 3000	(34.7) ± 1		
H ₂ SO ₄ (g)	-88 300 ± 300	35.9 ± 0.3	1 980 ± 20	10.1
H ₂ SO(g)	-(8 000) ± 2000			
H ₂ SO ₂ (g)	-(32 000) ± 2000			
(HO) ₂ S(g)	-(33 700) ± 2500	(35.2) ± 0.5		
HOS(g)	(2 500) ± 2000	(28.7) ± 0.5		
HOSO ₂ (g)	-(49 000) ± 1500	(33.7) ± 0.5		
HOSO ₃ (g)	-(63 000) ± 1000	(36.2) ± 0.5		
HOSO ₄ (g)	-(57 000) ± 2000			
(HO) ₂ SO ₄ (g)	-(124 000) ± 2500			
(HO) ₂ SO ₅ (g)	-(142 000) ± 1500			
(HO) ₂ SO ₆ (g)	-(137 000) ± 1000	(52) ± 1		

	$\Delta H_{298}^{\circ}, K$	S_{298}°/R	$(H_{298}^{\circ}-H_0^{\circ})/R, K$	C_p°/R
N(g)	56 850 ± 50	18.425 ± 0.001	745.4	2.500
N ₂ (g)	0	23.033 ± 0.003	1 042.7 ± 0.1	3.503
NH(g)	42 400 ± 1000	21.783 ± 0.002	1 034.5 ± 0.5	3.511
NH ₂ (g)	23 000 ± 1000	23.439 ± 0.006	1 195 ± 1	4.072
NH ₃ (g)	-5 525 ± 40	23.173 ± 0.01	1 208 ± 1	4.285
NO(g)	10 980 ± 50	25.334 ± 0.002	1 104.0 ± 1	3.592
NO ₂ (g)	4 110 ± 60	28.872 ± 0.004	1 227.7 ± 2	4.472
N ₂ O(g)	9 810 ± 60	26.448 ± 0.002	1 152.3 ± 1	4.646
N ₂ O ₃ (g)	10 420 ± 120	37.84 ± 0.04	2 060 ± 50	8.75
N ₂ O ₄ (g)	1 340 ± 120	36.606 ± 0.01	2 014 ± 4	9.52
N ₂ O ₅ (g)	1 600 ± 180	42.775 ± 0.8	2 500 ± 100	11.46
ONOSO ₂ (g)	-23 100 ± 2000			
HNO(g)	12 270 ± 360	26.557 ± 0.002	1 196 ± 1	4.075
H ₂ NNO ₂	-3 100 ± 1000	32.285 ± 0.1	1 463 ± 10	6.78
HONO(g)	-9 436 ± 70	30.544 ± 0.07	1 395 ± 5	5.57
HONO ₂ (g)	-16 106 ± 70	32.09 ± 0.02	1 430 ± 10	6.51
HONH ₂ (g)	-6 000 ± 1000	28.39 ± 0.3	1 350 ± 90	5.59
HO(SO ₂)NH ₂ (g)	-62 400 ± 1000			
HO(SO ₂)ONO(g)	-64 900 ± 1000			
HO(SO ₂)ONO ₂ (g)	-70 000 ± 1500			
C(g)	86 197 ± 60	19.002 ± 0.003	786 ± 1	2.507
CO(g)	-13 294 ± 20	23.761 ± 0.004	1 043 ± 1	3.505
CO ₂ (g)	-47 329 ± 15	25.700 ± 0.005	1 126 ± 1	4.466
CS(g)	33 460 ± 300	25.311 ± 0.005	1 047 ± 1	3.584
COS(g)	-17 090 ± 200	27.840 ± 0.004	1 194 ± 1	4.991
CS ₂ (g)	14 070 ± 100	28.61 ± 0.01	1 285 ± 3	5.492

Continued on next page.

TABLE I (continued)

	$\Delta H_{298}^{\circ}/R, K$	S_{298}°/R	$(H_{298}^{\circ}-H_0^{\circ})/R, K$	C_p°/R
$CH_4(g)$	-9 000 \pm 40	22.389 \pm 0.005	1 202 \pm 2	4.247
$CH_3OH(g)$	-24 185 \pm 50	28.83 \pm 0.02	1 375 \pm 2	5.30
$CH_2O(g)$	-13 060 \pm 100	26.30 \pm 0.05	1 205 \pm 10	4.26
$HCOOH(g)$	-45 530 \pm 75	29.93 \pm 0.02	1 314 \pm 5	5.494
$(HCOOH)_2(g)$	-98 740 \pm 300	40.01 \pm 0.5	2 360 \pm 100	11.56
$Mg(g)$	17 600 \pm 150	17.865 \pm 0.001	745.4	2.500
$Ca(g)$	21 500 \pm 150	18.615 \pm 0.001	745.4	2.500
$Li(g)$	19 170 \pm 50	16.678 \pm 0.002	745.4	2.500
$Na(g)$	12 880 \pm 50	18.475 \pm 0.001	745.4	2.500
$K(g)$	10 730 \pm 25	19.271 \pm 0.001	745.4	2.500

References to Table I on next page.

References to Table I

- O(g): (1) except Cp(8); O₂(g): (1,8); O₃(g): (8); H(g): ΔH(1), rest (3); H₂(g): (1) except Cp(8); OH(g): (8,9); HO₂(g): (8,9); H₂O(g): (1) except Cp(8,9); H₂O₂(g): (8); F(g): (1,8); F₂(g): (1) except Cp(8); HF(g): (1,8); Cl(g), Cl₂(g), and HCl(g): (1) except Cp(8); Br(g): ΔH(10,11), rest (3); Br₂(g) and HBr(g): (1) except Cp(8); I(g): ΔH(11), rest (3); I₂(g): (1) except Cp(8); HI(g): (1,12) except Cp(8); S(g): ΔH(13,14), rest (1,8); S₂(g): ΔH(10), S₂g (1,8,9), H₂g-H₀ (9), Cp(8); S₃(g) to S₈(g): (8). The calculated S₂g value (8) for S₇(g) using values for fifteen vibrational frequencies agrees closely with the calculation (15) using new determinations of the vibrational frequencies. However Steudel and Schuster (15) point out that Second law treatment of mass spectro-metric data (16,17) yield a higher entropy and they suggest addition of a contribution from pseudorotation. Since the number of degrees of freedom beyond translation and rotation is restricted to fifteen, addition of pseudorotation terms would be offset by removal of vibrational contributions. Although there would be a net increase in entropy, the uncertainty of the temperature coefficients of the mass spectro-metric measurements is comparable to the difference between Second and Third law values and no considerations of pseudorotation contributions was considered warranted at this time. HS(g), H₂S(g), and SO(g): (8, 9); SO₂(g): (1)
- except Cp(8). The S₂g/R value for SO₂(g) as determined by high-temperature cell measurements (18) is 1.0 lower than the CODATA value (1) and is claimed (18) to be more reliable. However the molecular constants of SO₂ are accurately known (19) and the value calculated using statistical mechanics is much more reliable than the value from cell measurements. SO₃(g): (8); SO₄(g): estimate by (20); S₂O(g): (8); H₂SO₃(g): estimate by (20); H₂SO₄(g): (8,9); H₂SO(g), H₂SO₂(g), HSO(OH)(g), (HO)₂S(g), HOS(g), HOSO₂(g), HOSO₃(g), HOSO₄(g), (HO)₂S₂O₄(g), (HO)₂S₂O₅(g), and (HO)₂S₂O₆(g): estimates from (20); N(g): ΔH(1), rest (3); N₂(g): (1,9); NH(g): (8,21); NH₂(g): (8); NH₃(g): (1) except Cp(8); NO(g), NO₂(g), N₂O(g), N₂O₃(g), N₂O₄(g) and N₂O₅(g): (8); ONOSO₂(g): estimate by (20); HNO(g), H₂NNO₂(g), HONO(g), HONO₂(g), and HONH₂(g): (8); HO(SO₂)NH₂(g), HO(SO₂)ONO(g), and HO(SO₂)ONO₂(g): estimates by (20); C(g): (1,9); CO(g) and CO₂(g): (1) except Cp(9); CS(g): (9) except revision of ΔH on basis of (22); COS(g): (9,23); CS₂(g): (9,23); CH₄(g): (9,23) except ΔH from (24); CH₃OH(g): (25); CH₂O(g): (9) except ΔH from (24); HCOOH(g) and (HCOOH)₂: (26); Mg(g) and Ca(g): (3) with ΔH(10,27); Li(g), Na(g), and K(g): (3) with ΔH(10).

TABLE II
Thermodynamic Properties of Solids and Liquids at 298.15 K

	$\Delta H_{298}^{\circ}/R, K$	S_{298}°/R	$(H_{298}^{\circ}-H_0^{\circ})/R, K$	C_p°/R
H ₂ O(l)	-34 378 ± 5	8.413 ± 0.01	1 599 ± 2	9.056
Br ₂ (l)	0	18.307 ± 0.005	2 950 ± 15	9.102
I ₂ (s)	0	13.968 ± 0.01	1 587 ± 5	6.548
S(orthorhombic)	0	3.855 ± 0.006	530 ± 7	2.730
H ₂ SO ₄ (l)	-97 930 ± 20	18.87 ± 0.01	3 396 ± 10	16.67
HNO ₃ (l)	-20 940 ± 60	18.72 ± 0.03	3 285 ± 5	13.215
NH ₄ NO ₃ (s)	-43 980 ± 35	18.18 ± 0.06	2 846 ± 10	16.728
NH ₄ Cl(s)	-37 900 ± 30	11.41 ± 0.06	1 887 ± 15	10.11
(NH ₄) ₂ SO ₄ (s)	-142 220 ± 60	26.49 ± 0.07	4 252 ± 50	22.55
NH ₂ SO ₂ OH(s)	-82 500 ± 100			
C(graphite)	0	0.690 ± 0.01	126 ± 2	1.025
Si(s)	0	2.262 ± 0.01	387 ± 1	2.405
SiO ₂ (α quartz)	-109 530 ± 120	4.987 ± 0.02	832 ± 2	5.36
SiO ₂ (α crist.)	-109 390 ± 150	5.22 ± 0.02	850 ± 4	5.40
Mg(s)	0	3.93 ± 0.01	601 ± 4	2.994
MgO(s)	-72 340 ± 40	3.24 ± 0.02	620 ± 3	4.46
Mg(OH) ₂ (s)	-111 200 ± 100	7.60 ± 0.025	1 372 ± 3	9.26
MgF ₂ (s)	-135 220 ± 150	6.89 ± 0.05	1 193 ± 5	7.407
MgCl ₂ (s)	-77 500 ± 100	10.77 ± 0.1	1 656 ± 10	8.57
MgCl ₂ ·6H ₂ O(s)	-300 550 ± 100	44.03 ± 0.5	6 710 ± 25	37.97
Mg(OH)Cl(s)	-96 170 ± 200	10.0 ± 1		8.9

	$\Delta H_{298}^0/R, K$	S_{298}^0/R	$(H_{298}^0 - H_0^0)/R, K$	C_p^0/R
MgS(s)	-41 600 ± 1500	6.054 ± 0.05	1 002 ± 5	5.480
MgSO ₃ (s)	-122 080 ± 400	10.4 ± 0.5		
MgSO ₃ ·3H ₂ O(s)	-233 140 ± 400	26 ± 1.5		
MgSO ₃ ·6H ₂ O(s)	-339 700 ± 400	42 ± 2.5		
MgSO ₄ (α)	-154 900 ± 100	11.0 ± 0.1	1 852 ± 10	11.59
MgSO ₄ ·H ₂ O(s)	-193 640 ± 100	15.2 ± 0.5	2 660 ± 50	16.1
MgSO ₄ ·6H ₂ O(s)	-371 580 ± 100	41.9 ± 0.1	6 665 ± 15	41.9
MgSO ₄ ·7H ₂ O(s)	-407 950 ± 80	47.3 ± 0.8	7 470 ± 50	44.8
MgCO ₃ (s)	-131 800 ± 200	7.83 ± 0.03	1 400 ± 4	9.15
MgCO ₃ ·3H ₂ O(s)	-237 790 ± 60	23.53 ± 0.08	3 880 ± 20	28.6
MgCO ₃ ·5H ₂ O(s)	-308 700 ± 400	33.7 ± 1		
Mg ₃ /4Ca ₁ /4CO ₃ (s)	-136 200 ± 50	9.006 ± 0.04	1 515 ± 6	9.32
Ca(s)	0	5.00 ± 0.05	689 ± 5	3.12
CaO(s)	-76 380 ± 100	4.59 ± 0.04	810 ± 5	5.07
CaO ₂ (s)	-79 600 ± 300	(7.7) ± 0.4		
CaO ₂ ·8H ₂ O(s)	-362 800 ± 500			
Ca(OH) ₂ (s)	-118 400 ± 30	10.015 ± 0.07	1 703 ± 8	10.52
CaF ₂ (s)	-146 800 ± 250	8.23 ± 0.05	1 400 ± 8	8.062
CaCl ₂ (s)	-95 700 ± 120	12.58 ± 0.05	1 858 ± 7	8.73
CaCl ₂ ·H ₂ O(s)	-133 450 ± 200	18.9 ± 0.8		
CaCl ₂ ·2H ₂ O(s)	-168 000 ± 150	24.2 ± 1		
CaCl ₂ ·4H ₂ O(s)	-240 300 ± 200	34.7 ± 1.5		
CaCl ₂ ·6H ₂ O(s)	-312 300 ± 150	47.1 ± 0.9		
CaClOH(s)	-109 550 ± 400			

Continued on next page.

TABLE II (continued)

	$\Delta H_{298}^{\circ}/R, K$	S_{298}°/R	$(H_{298}^{\circ}-H_0^{\circ})/R, K$	C_p°/R
CaS(s)	-57 900 ± 350	6.81 ± 0.15	1 082 ± 15	5.71
CaSO ₃ (s)	-139 400 ± 500	12.18 ± 0.15	1 940 ± 20	10.93
CaSO ₃ ·1/2H ₂ O(s)	-157 400 ± 300	(14.7) ± 0.2	(2 300) ± 100	(14.0)
CaSO ₄ (anhydride)	-172 500 ± 40	12.82 ± 0.07	2 070 ± 20	11.987
CaSO ₄ (sol. α)	-171 430 ± 50	13.03 ± 0.1	2 096 ± 20	12.05
CaSO ₄ (sol. β)	-170 900 ± 50	13.03 ± 0.1	2 091 ± 20	11.91
CaSO ₄ ·1/2H ₂ O(α)	-189 650 ± 50	15.70 ± 0.1	2 480 ± 15	14.36
CaSO ₄ ·1/2H ₂ O(β)	-189 400 ± 50	16.15 ± 0.1	2 544 ± 15	14.93
CaSO ₄ ·2H ₂ O(s)	-243 280 ± 40	23.33 ± 0.07	3 750 ± 20	22.3
CaS ₂ O ₃ ·4H ₂ O(s)	-348 430 ± 500			
Ca(NO ₂) ₂ (s)	-89 520 ± 100	(19.8) ± 0.5		
Ca(NO ₃) ₂ (s)	-112 840 ± 50	23.25 ± 0.09	3 420 ± 35	17.97
Ca(NO ₃) ₂ ·2H ₂ O(s)	-185 330 ± 130	32.7 ± 1.5		
Ca(NO ₃) ₂ ·3H ₂ O(s)	-220 200 ± 170	37.7 ± 2		
Ca(NO ₃) ₂ ·4H ₂ O(s)	-256 530 ± 140	42.8 ± 2.5		
CaCO ₃ (calcite)	-144 920 ± 50	10.03 ± 0.04	1 740 ± 10	10.04
CaCO ₃ ·H ₂ O(s)	-179 830 ± 100	15.807 ± 0.03		
CaCO ₃ ·6H ₂ O(s)	-356 200 ± 200	40.214 ± 0.07		
Li(s)	0	3.50 ± 0.02	557 ± 5	2.978
LiOH(s)	-58 625 ± 25	5.15 ± 0.06	892 ± 4	5.965
LiOH·H ₂ O(s)	-95 030 ± 25	8.61 ± 0.06	1 461	9.56
LiF(s)	-74 360 ± 40	4.32 ± 0.07	778 ± 3	5.03
LiCl(s)	-49 155 ± 25	7.11 ± 0.06	1 119 ± 3	5.776
Li ₂ SO ₄ (s)	-172 790 ± 45	13.71 ± 0.07	2 240 ± 5	14.145

	$\Delta H_{298}^{\circ}/R, K$	S_{298}°/R	$(H_{298}^{\circ}-H_0^{\circ})/R, K$	C_p°/R
Na(s)	0	6.17 ± 0.02	777 ± 2	3.397
NaOH(s)	-51 232 ± 20	7.79 ± 0.06	1 260 ± 4	7.16
NaOH·H ₂ O(s)	-88 370 ± 25	11.93 ± 0.06	1 875 ± 5	10.844
NaF(s)	-69 345 ± 40	6.16 ± 0.07	1 021 ± 5	5.635
NaCl(s)	-49 470 ± 20	8.66 ± 0.06	1 276 ± 4	6.075
Na ₂ S(s)	-44 000 ± 1500	11.6 ± 2		9.96
Na ₂ SO ₄ (s)	-166 930 ± 40	17.99 ± 0.06	2 790 ± 4	15.308
Na ₂ SO ₄ ·10H ₂ O(s)	-520 560 ± 40	71.15 ± 0.06		69.09
NaNO ₃ (s)	-56 240 ± 30	13.97 ± 0.06	2 071 ± 5	11.19
Na ₂ CO ₃ (s)	-135 820 ± 30	16.23 ± 0.1	2 503 ± 5	13.29
Na ₂ CO ₃ ·H ₂ O(s)	-171 960 ± 30	20.22 ± 0.1	3 168 ± 5	17.51
Na ₂ CO ₃ ·7H ₂ O(s)	-384 700 ± 50	51.3 ± 0.2		
NaHCO ₃ (s)	-114 130 ± 25	12.33 ± 0.15	1 917 ± 4	10.54
NaCHO ₂ (s)	-80 160 ± 50	12.48 ± 0.1	1 896 ± 5	9.94
K(s)	0	7.78 ± 0.02	852 ± 2	3.558
KF(s)	-68 520 ± 40	8.00 ± 0.07	1 203 ± 5	5.90
KF·2H ₂ O(s)	-140 245 ± 40	18.6 ± 0.2		
KCl(s)	-52 473 ± 20	9.97 ± 0.06	1 364 ± 3	6.17
K ₂ SO ₄ (s)	-172 900 ± 50	21.12 ± 0.07	3 059 ± 5	15.98
K ₂ S ₂ O ₆ (s)	-215 900 ± 600	37.244 ± 0.04	5 266 ± 5	27.76
KNO ₃ (s)	-59 395 ± 30	16.00 ± 0.06	2 258 ± 4	11.58

References to Table II on next page.

References to Table II

- $\text{H}_2\text{O}(\ell)$: (1) except Cp(9); Br₂(ℓ) and I₂(s):
 (1) except Cp(8); S(orthorhombic):(1) except
 Cp(8,9); H₂SO₄(ℓ): ΔH and S(28), rest (9,27,29);
 HNO₃(ℓ): (23,27); NH₄NO₃(s):(8,30); NH₄Cl(s)
 and (NH₄)₂SO₄(s): ΔH , S(30), rest (27);
 NH₂SO₂OH(s):(31); C(graphite):(1,9,23); Si(s):
 (1) except Cp(23,27); SiO₂ (α quartz):(1)
 except Cp(9,27); SiO₂(cristobalite): ΔH (32),
 rest (33); Mg(s):(1) except Cp(10); MgO(s):(1)
 except Cp(9,27); Mg(OH)₂(s):(27,29); MgF₂(s):
 (1,9); MgCl₂(s): ΔH (34), rest (27,9);
 MgCl \cdot 6H₂O(s) and Mg(OH)Cl(s): (27); MgS(s):
 (9,35); MgSO₃(s), MgSO₃ \cdot 3H₂O(s) and
 MgSO₃ \cdot 6H₂O(s):(27); α MgSO₄(s) and
 MgSO₄ \cdot 7H₂O(s):(27,36); MgSO₄ \cdot 6H₂O(s) and
 MgSO₄ \cdot 7H₂O(s):(27). MgCO₃(s), MgCO₃ \cdot 3H₂O(s),
 and MgCO₃ \cdot 5H₂O(s):(27,37); Mg₃/4Ca₁/4CO₃ (s):(37);
 Ca(s) and CaO(s):(1,9); CaO₂(s) and
 CaO₂ \cdot 8H₂O(s):(27); Ca(OH)₂(s): ΔH and
 S (28), rest (9); CaF₂(s), CaCl₂(s) and its
 hydrates, CaClOH(s), and CaS(s):(27); CaSO₃:(38)
 except H₂98-H₀(27); CaSO₃ \cdot 1/2H₂O(s):(39);
 CaSO₄ and its hydrates:(40); CaS₂O₃ \cdot 4H₂O(s)
 and Ca(NO₂)₂(s):(27); Ca(NO₃)₂(s): ΔH and
 S(28), rest (27); Ca(NO₃)₂ hydrates: (27) with
 addition of 68K to $\Delta\text{H}/\text{R}$ values to be consistent
 with Table III; CaCO₃(calcite): ΔH (28), rest
 (41); CaCO₃ hydrates:(27) with addition of 233K
 to $\Delta\text{H}/\text{R}$ values to be consistent with calcite
 value; Li(s):(1) except Cp(10); LiOH(s),
 LiOH \cdot H₂O(s), LiF(s) and LiCl(s): ΔH and
 S (30), rest (9); Li₂SO₄(s): ΔH , S(28)
 rest (9); Na(s):(1) except Cp(42); NaOH(s)
 NaOH \cdot H₂O(s), NaF(s), and NaCl(s):(30) except
 H₂98-H₀ and Cp from (9); Na₂S:(9); Na₂SO₄(s)
 and Na₂SO₄ \cdot 10H₂O(s): ΔH , S(30) with rest
 (9,43); NaNO₃(s): ΔH , S (30), rest (35,42);
 Na₂CO₃(s): ΔH , S(28,44), rest (9,43);
 Na₂CO₃(s) \cdot H₂O(s):(44); Na₂CO₃ \cdot 7H₂O(s):
 (42) corrected to agree with (28) and (44) for
 the other carbonates; NaHCO₃(s):(44) except
 Cp(35); NaCHO₂(s):(42); K(s):(1) except Cp(35,
 42); KF(s):(9,30,42); KF \cdot H₂O(s):(28);
 KCl(s) and K₂SO₄(s): ΔH and S(30), rest
 (9,43); K₂S₄O₆(s):(39); KNO₃(s):(30,35,42).

TABLE III
Thermodynamic Properties of Aqueous Species at 298.15K (m/kg for all species)

	$\Delta H_{298}^{\circ}/R, K$	S_{298}°/R	C_p°/R
H(aq)	25 800 ± 300	4.5 ± 1	
H ₂ (aq)	-486 ± 100	6.9 ± 0.3	21 ± 3
O ₂ (aq)	-1 460 ± 25	13.1 ± 0.1	27 ± 3
O ₃ (aq)	15 100 ± 300	17.8 ± 1	(28) ± 6
H ₂ O(l)	-34 378 ± 5	8.413 ± 0.01	9.056
H ⁺	0	0	0
OH ⁻	-27 666 ± 5	-1.305 ± 0.02	-16.9 ± 0.4
H ₂ O ₂ (aq)	-22 990 ± 10	17.51 ± 0.03	
HO ₂ ⁻	-19 280 ± 200	2.87 ± 0.5	
O ₂ ⁼²	(-4 500) ± 1500	(-5) ± 5	
HO ₂ (aq)	-4 400 ± 900	17 ± 2	
O ₂	-4 400 ± 1000	5 ± 4	
OH ⁻ (aq)	-600 ± 300	7.8 ± 1	
O ⁻	4 500 ± 1000	-2 ± 2	(-14) ± 3
F ⁻	-40 334 ± 80	-1.67 ± 0.10	-14.1 ± 0.5
Cl ₂ (aq)	-2 500 ± 500	16 ± 1	-10 ± 5
Cl ⁻	-20 095 ± 10	6.81 ± 0.02	-15.1 ± 0.5
Br ₂ (aq)	-260 ± 100	15.7 ± 0.2	
Br ⁻	-14 600 ± 20	9.95 ± 0.02	-15.9 ± 0.5
I ₂ (aq)	2 700 ± 50	16.4 ± 0.2	35 ± 4
I ⁻	-6 830 ± 10	12.80 ± 0.02	-14.5 ± 0.5
I ₃ ⁻	-6 300 ± 50	28.5 ± 0.2	0 ± 5
H ₂ S(aq)	-4 600 ± 120	15.3 ± 0.4	24 ± 1
HS ⁻	-1 800 ± 120	8.5 ± 0.5	-10 ± 3
S ⁼	4 000 ± 2000	-11 ± 5	
H ₂ S ₂ (aq)	(-6 300) ± 1500	(20) ± 3	

Continued on next page.

TABLE III (continued)

	$\Delta H_{298}^{\circ}/R, K$	S_{298}°/R	C_p°/R
HS_2^-	(-2 950) \pm 1500	(12) \pm 3	
S_2	3 600 \pm 1500	(-2) \pm 5	
$H_2S_3(aq)$	(-4 800) \pm 1500	(24) \pm 3	
HS_3^-	(-1 950) \pm 1500	(16) \pm 3	
S_3	3 100 \pm 1500	(4) \pm 5	
$H_2S_4(aq)$	-4 200 \pm 400	(28) \pm 3	
HS_4^-	-1 650 \pm 400	(20) \pm 3	
S_4	2 600 \pm 400	12.4 \pm 5	
$H_2S_5(aq)$	-3 450 \pm 500	(32) \pm 2	
HS_5^-	-1 100 \pm 500	(24) \pm 2	
S_5	2 750 \pm 500	17 \pm 5	
S_6	2 850 \pm 500	(22) \pm 5	
$SO_2(aq)$	-38 670 \pm 100	20.1 \pm 0.4	13.6 \pm 2
$H_2SO_3(aq)$	-73 050 \pm 100	28.5 \pm 0.4	22.7 \pm 2
HSO_3^-	-76 000 \pm 150	14.4 \pm 0.5	(0) \pm 4
S_2O_5	-118 200 \pm 600	15 \pm 2	
SO_3^-	-76 640 \pm 450	-4.2 \pm 1.5	-40 \pm 5
HSO_4^-	-106 560 \pm 200	16.2 \pm 0.15	-10 \pm 6
SO_4^-	-109 380 \pm 60	2.2 \pm 0.1	-33.4 \pm 0.8
$H_2S_2O_3(aq)$	-73 150 \pm 450	(30) \pm 3	
$HS_2O_3^-$	-76 300 \pm 400	(18) \pm 3	
S_2O_3	-79 300 \pm 360	4 \pm 1	-30 \pm 1
$S_2O_3^-$	-90 630 \pm 2000	11 \pm 2	
$S_2O_4^-$	-144 100 \pm 2000	13.4 \pm 3	
$S_2O_6^-$	-168 500 \pm 2000	(24) \pm 3	
$S_2O_7^-$	-161 700 \pm 1000	29.4 \pm 2	-13 \pm 1
$S_2O_8^-$	-144 300 \pm 2000	(30) \pm 3	
$S_3O_6^-$	-148 700 \pm 800	31.3 \pm 0.2	-6.1 \pm 1.5
$S_4O_6^-$	-148 700 \pm 2000	(33) \pm 3	

	$\Delta H_{298}^{\circ}/R, K$	S_{298}°/R	C_p°/R
$N_2(aq)$	-1 255 ± 100	11.5 ± 0.3	29.6 ± 3
$NH_3(aq)$	-9 780 ± 25	13.0 ± 0.1	9.0 ± 0.4
$NH_4OH(aq)$	-44 160 ± 25	21.80 ± 0.1	18.1 ± 0.4
NH_4	-16 030 ± 30	13.37 ± 0.05	8.3 ± 0.5
$NH_2OH(aq)$	-11 800 ± 400	19.5 ± 1	
NH_3OH^+	-16 070 ± 400	18.6 ± 0.8	
$N_2H_4^+$	4 130 ± 20	(16.6) ± 1	
N_2H_5	-910 ± 100	18 ± 1	8.45 ± 2
$HNO_2(aq)$	-14 300 ± 100	16.3 ± 1	
NO_2^-	-12 590 ± 100	14.8 ± 0.5	-11 ± 3
NO_2^-	-24 880 ± 50	17.63 ± 0.05	-8.7 ± 0.5
NO_3^-	-7 700 ± 400	26 ± 1	
$H_2N_2O_2(aq)$	-6 250 ± 800	17 ± 1	
HN_2O_2	-2 070 ± 800	3 ± 2	
N_2O_2	7 200 ± 300	14.1 ± 1	22 ± 5
$N_2O(aq)$	9 550 ± 300	14.3 ± 1	26 ± 5
$NO(aq)$			
$CH_4(aq)$	-10 660 ± 150	10.25 ± 0.4	29 ± 3
$HCN(aq)$	12 880 ± 100	15.3 ± 0.3	
CN^-	18 110 ± 100	11.6 ± 0.3	
$HCNO(aq)$	-18 800 ± 200	16.1 ± 1	
CNO^-	-17 550 ± 70	12.28 ± 0.5	
$HCNS(aq)$	11 150 ± 300	(22) ± 1	
CNS^-	9 190 ± 300	17.36 ± 0.2	-4.8 ± 2
$CO_2(aq)$	-49 704 ± 25	14.36 ± 0.07	25.5 ± 2
$H_2CO_3(aq)$	-84 080 ± 25	22.77 ± 0.07	34.5 ± 2
HCO_3^-	-82 980 ± 20	11.84 ± 0.07	-6.5 ± 0.5
CO_3^{2-}	-81 210 ± 30	-6.01 ± 0.1	-32.9 ± 0.5
$CO(aq)$	-14 630 ± 60	12.3 ± 0.2	27 ± 3

Continued on next page.

TABLE III (continued)

	$\Delta H_{298}^{\circ}/R, K$	S_{298}°/R	C_p°/R
$H_2CO(aq)$	-17 300 \pm 700	13.3 \pm 2	
$H_2C(OH)_2(aq)$	-55 200 \pm 700	17.7 \pm 2	
H_2COOH^-	-47 600 \pm 1500	11. \pm 3	
$HCOOH(aq)$	-51 200 \pm 50	19.7 \pm 0.5	10 \pm 4
$HCOO^-$	-51 220 \pm 50	11.0 \pm 0.5	-10.6 \pm 1
$CH_3COOH (aq)$	-58 410 \pm 50	21.5 \pm 0.3	20.4 \pm 0.3
CH_3COO^-	-58 454 \pm 50	10.4 \pm 0.3	3.2 \pm 0.3
$(COOH)_2(aq)$	-98 040 \pm 100	22.5 \pm 0.3	
$C_2O_4H^-$	-98 440 \pm 100	18.0 \pm 0.3	
$C_2O_4^{2-}$	-99 250 \pm 100	5.49 \pm 0.3	
$(CH_2)_2(COOH)_2(aq)$	-109 665 \pm 10	(30) \pm 2	27.1 \pm 0.5
$(CH_2)_2(COO)_2H^-$	-109 260 \pm 20	(21.65) \pm 2	
$(CH_2)_2(COO)_2^{2-}$	-109 200 \pm 20	(8.8) \pm 2	
$(CH_2)_4(COOH)_2(aq)$	-104 000 \pm 1000	(38) \pm 2	40.4 \pm 1
$(CH_2)_4(COO)_2H^-$	-104 200 \pm 1000	(27.15) \pm 2	
$(CH_2)_4(COO)_2^{2-}$	-104 520 \pm 1000	(13.6) \pm 2	
Mn^{++}	-26 600 \pm 150	-8.15	-1.3 \pm 0.4
Mn^{+++}	(-14 000) \pm 900		-0.5 \pm 4
Fe^{++}	-10 700 \pm 100	-16.6 \pm 0.3	
Fe^{+++}	-5 840 \pm 100	-38 \pm 0.5	
Mg^{++}	-56 100 \pm 130	-16.6 \pm 0.2	-1.9 \pm 1
Ca^{++}	-65 270 \pm 400	-6.74 \pm 0.1	-3.6 \pm 1
Li^+	-33 498 \pm 10	1.48 \pm 0.1	7.3 \pm 0.5
Na^+	-28 912 \pm 10	7.03 \pm 0.02	5.1 \pm 0.5
K^+	-30 322 \pm 10	12.17 \pm 0.02	1.6 \pm 0.5

References to Table III

- H(aq): (45); H₂(aq), O₂(aq), and O₃(aq): (46); H₂O(ℓ): (1) except Cp(9); OH⁻: ΔH(1), S(28), Cp(47, 48); H₂O₂(aq) and HO₂⁻(23); O₂: The Branch and Calvin equation (49) was used to calculate the ionization constant of HO₂⁻ and the entropy of ionization was estimated. HO₂(aq), O₂, OH(aq) and O: Baxendale, Ward, and Wardman (50) have reviewed earlier measurements of the ionization constants of HO₂ and OH and have carried out measurements over a range of temperature to obtain the enthalpies and entropies of ionization. They suggested that the enthalpies and entropies of solution would be closely the same for H₂O₂(g) and HO₂(g) and also for H₂O(g) and OH(g). Their suggested procedure was used with the data from Tables I and III and more recent data reviewed by Schwartz (45) to calculate the values tabulated in Table III for HO₂(aq) and OH(aq). Their ionization data were then used to obtain the values for O₂⁻ and O⁻. Their ΔG⁰ and ΔH⁰ values for the ionization of OH were shifted slightly to increase S⁰/R of O from -3 to -2 to better match the value for F⁻. The solvation enthalpies of O⁻ and F⁻ are almost the same and Cp for O⁻ was approximated by the value for F⁻. F⁻: ΔH(1), S(28), Cp(51); Cl₂(aq): (46); Cl⁻: ΔH(1), S(28), Cp(48, 52); Br₂(aq): Wu et al. (53) treated the solubility of Br₂(ℓ) in water as a function of temperature with a correction for deviation from Henry's law to obtain thermodynamic values for Br₂(aq). Their values combined with the later evaluation of Vasil'ev et al. (54) corresponds to $\ln \gamma_{Br} = -(0.689+735/T)m$ or $\gamma_{Br} = 0.5$ for $m_{Br} = 0.22M$ at 298K which seems to be too rapid a deviation from Henry's law. The deviation was reduced to $\ln \gamma_{Br} = -0.4m$ yielding $\Delta H_{298}^0/R = -260 \pm 100K$ and $\Delta S_{298}^0/R = -2.6 \pm 0.2$ for Br₂(ℓ) = Br₂(aq). Br: (28) except Cp(55); I₂(aq): (53, 56); I⁻: (12) and (28) except Cp(51); I₃⁻: Ramette and Sandford (56) have shown that I₅⁻ and I₆⁻ formation causes errors in the evaluation of thermodynamic values for I₃⁻ using either I₂ solubility in I⁻ solutions or calorimetric data with substantial I₂ and I₃⁻ activities. Johnson (12) has confirmed this effect by demonstrating that the molal enthalpy of solution of I₂ in HI(aq) varies with the amount of I₂ added. The solubility, calorimetric, and spectral measurements have been weighed with regard to influence of I₅⁻ and I₆⁻ to obtain the values of Table III. H₂S(aq): There have been a number of recent reviews of the solubility of H₂S in water as a function of temperature (46, 57, 58). The CODATA review (59) has also used calorimetric data to obtain recommended thermodynamic values, but their values yield solubilities as much as 13% low between 40 and 260°C. If $\Delta H_{298}^0/R$ for solution of H₂S is made 200K more positive, a good fit is obtained but this appears to be too large a shift from the calorimetric determinations

Continued on next page.

References to Table III (continued)

and the CODATA $\Delta H_{298}^{\circ}/R$ value was made only 95K more positive to obtain the values of Table III. HS^- : In addition to the data considered by CODATA (59), the determination of the first ionization constant of H_2S up to 150°C by Tsonopoulos et al. (60) and the calorimetric measurements by Jordan (61) were used. As noted below in the $S^=$ discussion, the tentative second ionization constant accepted by CODATA is believed to be too large by several orders of magnitude and the correction they applied to calorimetric data for hydrolysis of HS^- to $S^=$ would be too large. The tentative CODATA values yield for $OH^- + H_2S(g) = HS^- + H_2O$, $\Delta H_{298}^{\circ}/R = -6250K$. Jordan (61) has measured the enthalpy of solution of $H_2S(g)$ in 0.1M NaOH and in 0.2M ammonia buffer solutions and has obtained values corresponding to the OH^- reaction between -5890 and -5850K. The dilution correction should be small for this reaction. These values would appear to confirm that the CODATA values for the enthalpy of solution of H_2S and for the first ionization of H_2S should be more positive. As noted above, the CODATA value for the enthalpy of solution was made 95K more positive. The ionization enthalpy was made more positive by 110K resulting in a compromise between the Jordan and CODATA values of $-6040 \pm 120K$. $S^=$: The CODATA review (59) notes that reported values of the second ionization constant of H_2S range almost eight orders of magnitude. They selected

a tentative value of $\log K_2 = -13$. However, Gigenbach (62) has clearly shown that the ready oxidation of HS^- solutions to polysulfide species has invalidated previous measurements; he demonstrated that $\log K_2$ is at least 1.2 more negative than log K for the ionization of water at all temperatures and is of the order of -17 at 25°C. Tsonopoulos et al. (60) report identical pH titration curves for 0.1M HCl with 0.28M Na_2S or with NaOH. Thus the hydrolysis of $S^=$ must be very complete. They suggest $K_2 = 2 \times 10^{-16}$, but with the $S^=$ concentration so small, they can only set a limit. An additional confirmation of the value selected for K_2 of H_2S is given by the recent work of Meyer and Peter (63). They examined the Raman spectrum of HS^- in oxygen-free 1M NaOH and in a solution saturated with solid NaOH. Equal amounts of Na_2S had been added to each solution. The HS^- intensity was the same within experimental error in both solutions indicating complete hydrolysis even in a saturated NaOH solution and confirming a pK of at least 17. A value of $\log K_2 = -17 \pm 2$ is used for Table III. The enthalpy and entropy values suggested by Gigenbach were made somewhat more positive. It should be noted that changes in K_1K_2 or changes in ΔG° and ΔH° of $S^=$ can be disastrous in calculating the solubilities of metal sulfides if the K_{sp} values are not made consistent with the value of K_1K_2 selected. Whenever K_1K_2 is

Continued on next page.

References to Table III (continued)

increased by a factor q , the old value of K_{sp} must be divided by q to maintain the same equilibrium constant or ΔG° for $MS(s) + 2H^+ = M^{2+} + H_2S(g)$.

The ΔH values given by the NBS (23) for S_2^- and S_3^- were accepted. They are presumably based on the work of Maronny (64). The NBS entropies for S_4^- and S_5^- were also accepted. The remainder of the entropy and enthalpy of formation values were estimated to be consistent with the equilibrium measurements of Schwarzenbach and Fischer (65) for HS_4^- , HS_5^- , and their ions and with their estimates for HS_2^- , HS_3^- , and their ions and the measurements of Boulegue and Michard (66) on S_4^{2-} , S_5^- , and S_6^- . The ΔH values for S_2^- and S_3^- were given large uncertainty as Schwarzenbach and Fischer report that S_2^- and S_3^- are not detectable in solution and they discredit the cell measurements of Maronny.

$SO_2(aq)$, $H_2SO_3(aq)$: (58); HSO_3^- : Measurements of the ionization constant of sulfurous acid have grouped around 0.017 and 0.013. On the basis of the work of Huss and Eckert (67), 0.014 ± 0.001 was accepted and the thermodynamic values given by Cobble et al. (39) have been revised. Various estimates of C_p° of HSO_3^- vary from negative to positive; $C_p/R = 0 \pm 4$ seems to be the best estimate available at the moment. $S_{2O_5}^{2-}$: (68); SO_3^{2-} : (39), the calorimetric determination of the enthalpy of formation

of SO_3^{2-} was given preference to the temperature coefficient of the ionization constant between 5 and 50°C (70); HSO_4^- , SO_4^{2-} : (1,28,69) except C_p (51,71,72,73).

$H_2S_2O_3(aq)$, $HS_2O_3^-$: Ionization constants (74) were combined with $S_{2O_3}^{2-}$ value of Cobble et al. (39); C_p of $S_2O_3^{2-}$ (71). $S_{2O_4}^{2-}$, $S_2O_6^{2-}$, $S_{2O_8}^{2-}$, $S_3O_6^{2-}$: (42); C_p of $S_2O_8^{2-}$ (71). $S_{4O_6}^{2-}$: (39) except for correction of arithmetical error in ΔH calculation. $S_{5O_6}^{2-}$: (23,42).

$N_2(aq)$: (46); $NH_3(aq)$, $NH_4OH(aq)$, and NH_4^+ : New measurements and reviews of earlier values have been presented recently (75-78). The values in Table III are based on the CODATA selections (1,28) for ΔH_{298}° and S_{298}° of NH_4^+ (52,75); $NH_4OH(aq)$ and NH_3OH^+ : (23,79,80); $N_2H_4(aq)$ and $N_2H_5^+$: (23,79). $HNO_2(aq)$ and NO_2^- : (23,42); NO_3^- : $\Delta H(1,28)$, $S(28)$, $C_p(52)$; $H_2N_2O_2(aq)$, $HN_2O_2^-$, $N_2O_2^{2-}$: (42,79); $N_2O(aq)$ and $NO(aq)$: (46); $CH_4(aq)$: (46); $H_2CO(aq)$, CN^- , $H_2CNO(aq)$, and CNO^- : (27); $HCNS(aq)$ and CNS^- : (23,42). $CO_2(aq)$, $H_2CO_3(aq)$: (44,46); HCO_3^- : (28,44,81) except $C_p(51)$; CO_3^{2-} : (28,44,82) except $C_p(51)$; $CO(aq)$: (46); $H_2CO(aq)$: (23,83); $H_2C(OH)_2(aq)$: (23,28,83); H_3COOH^- : (83); $HCOOH(aq)$: (23,27,84,85); $HCOO^-$: (23,27); $CH_3COOH(aq)$: ΔH and ΔS based on ionization data tabulated by Christensen et al. (84), $C_p(75)$; CH_3COO^- : (42) except $C_p(51,75)$; $(COOH)_2(aq)$: Based on ionization data (84); $C_2O_4^{2-}$ and $C_2O_4^-$: (42). $(CH_2)_2(COOH)_2(aq)$: Continued on next page.

References to Table III (continued)

(86, 87); $(\text{CH}_2)_2(\text{COO})_2\text{H}^-$ and $(\text{CH}_2)(\text{COO})_2^-$: (84);
 $(\text{CH}_2)_4(\text{COOH})_2(\text{aq})$: (86, 87, 88); $(\text{CH}_2)_4(\text{COO})_2\text{H}$
 and $(\text{CH}_2)_4(\text{COO})_2$: (84).
 Mn^{++} : (81, 90, 91, 92); Mn^{+++} : (79); Fe^{++} and
 Fe^{+++} : (93, 94); Mg^{++} : $\Delta\text{H}(95)$, S(29),
 Ca^{++} : (28); $\text{Cp}(81, 91, 96)$; Li^+ : (28),
 $\text{Cp}(51)$; Na^+ : (28), $\text{Cp}(48, 52)$; K^+ : (28), $\text{Cp}(52)$.

TABLE IV
Equations for $-(G^{\circ}-H_{298}^{\circ})/RT$ for 298.15K to T_{\max}

Species	T_{\max} , K	$-(G^{\circ}-H_{298}^{\circ})/RT =$	Ref.
O(g)	1000	$20.151-7.110 \times 10^{-3}T+1.9800 \times 10^{-5}T^2-1.816 \times 10^{-8}T^3+5.987 \times 10^{-12}T^4$	(8,9)
O ₂ (g)	1000	$25.757-9.743 \times 10^{-3}T+2.6812 \times 10^{-5}T^2-2.4157 \times 10^{-8}T^3+7.8845 \times 10^{-12}T^4$	(8,9)
O ₃ (g)	1000	$30.370-1.4222 \times 10^{-2}T+3.8373 \times 10^{-5}T^2-3.385 \times 10^{-8}T^3+1.0885 \times 10^{-11}T^4$	(8)
H(g)	6000	$11.284+2.51298.15/T - \ln(298.15/T)$	(3)
H ₂ (g)	1000	$16.784-9.639 \times 10^{-3}T+2.6701 \times 10^{-5}T^2-2.436 \times 10^{-8}T^3+8.007 \times 10^{-12}T^4$	(8,9)
OH(g)	1000	$23.170-9.734 \times 10^{-3}T+2.7076 \times 10^{-5}T^2-2.4774 \times 10^{-8}T^3+8.162 \times 10^{-12}T^4$	(8)
HO ₂ (g)	1000	$28.909-1.2005 \times 10^{-2}T+3.2678 \times 10^{-5}T^2-2.9068 \times 10^{-8}T^3+9.4155 \times 10^{-12}T^4$	(8,9)
H ₂ O(g)	1000	$23.939-1.1055 \times 10^{-2}T+3.0494 \times 10^{-5}T^2-2.754 \times 10^{-8}T^3+9.016 \times 10^{-12}T^4$	(9)
H ₂ O ₂ (g)	1000	$29.901-1.490 \times 10^{-2}T+4.0313 \times 10^{-5}T^2-3.5592 \times 10^{-8}T^3+1.148 \times 10^{-11}T^4$	(8)
F(g)	1000	$19.906-7.426 \times 10^{-3}T+2.070 \times 10^{-5}T^2-1.901 \times 10^{-8}T^3+6.269 \times 10^{-12}T^4$	(8)
F ₂ (g)	1000	$25.601-1.0796 \times 10^{-2}T+2.9565 \times 10^{-5}T^2-2.658 \times 10^{-8}T^3+8.651 \times 10^{-12}T^4$	(8)
HF(g)	1000	$21.961-9.604 \times 10^{-3}T+2.6654 \times 10^{-5}T^2-2.4344 \times 10^{-8}T^3+8.008 \times 10^{-12}T^4$	(8)
Cl(g)	1000	$20.695-7.4565 \times 10^{-3}T+2.0567 \times 10^{-5}T^2-1.8693 \times 10^{-8}T^3+6.117 \times 10^{-12}T^4$	(8)
Cl ₂ (g)	1000	$28.130-1.1633 \times 10^{-2}T+3.2008 \times 10^{-5}T^2-2.8973 \times 10^{-8}T^3+9.465 \times 10^{-12}T^4$	(8)
HCl(g)	1000	$23.535-9.568 \times 10^{-3}T+2.6541 \times 10^{-5}T^2-2.421 \times 10^{-8}T^3+7.968 \times 10^{-12}T^4$	(8)
Br(g)	1000	$21.801-6.842 \times 10^{-3}T+1.899 \times 10^{-5}T^2-1.7341 \times 10^{-8}T^3+5.703 \times 10^{-12}T^4$	(8)
Br ₂ (g)	1000	$30.867-1.2101 \times 10^{-2}T+3.3458 \times 10^{-5}T^2-3.0435 \times 10^{-8}T^3+9.978 \times 10^{-12}T^4$	(8)
HBr(g)	1000	$24.950-9.534 \times 10^{-3}T+2.6434 \times 10^{-5}T^2-2.407 \times 10^{-8}T^3+7.914 \times 10^{-12}T^4$	(8)
I(g)	1000	$19.230+2.51298.15/T - \ln(298.15/T)$	(3)
I ₂ (g)	1000	$32.718-1.2287 \times 10^{-2}T+3.4019 \times 10^{-5}T^2-3.0998 \times 10^{-8}T^3+1.0176 \times 10^{-11}T^4$	(8)
HI(g)	1000	$26.090-1.0922 \times 10^{-2}T+2.9862 \times 10^{-5}T^2-2.7574 \times 10^{-8}T^3+9.204 \times 10^{-12}T^4$	(8)

Continued on next page.

TABLE IV (continued)

Species	T _{max} , K	$-(G^{\circ}-H_{298}^{\circ})/RT =$	Ref.
S(g)	1000	21.030-7.725 x10 ⁻³ T+2.1563x10 ⁻⁵ T ² -1.9851x10 ⁻⁸ T ³ +6.556 x10 ⁻¹² T ⁴	(8,9)
S ₂ (g)	1000	28.699-1.1222x10 ⁻² T+3.0796x10 ⁻⁵ T ² -2.7792x10 ⁻⁸ T ³ +9.067 x10 ⁻¹² T ⁴	(8,9)
S ₃ (g)	1000	33.068-4.357 x10 ⁻³ T+1.3802x10 ⁻⁵ T ² -2.6464 x10 ⁻⁹ T ³	(8)
S ₄ (g)	1000	35.63 -6.237 x10 ⁻³ T+1.944 x10 ⁻⁵ T ² -9.065 x10 ⁻⁹ T ³	(8)
S ₅ (g)	1000	40.99 -8.146 x10 ⁻³ T+2.576 x10 ⁻⁵ T ² -1.207 x10 ⁻⁸ T ³	(8)
S ₆ (g)	1000	47.079-3.984 x10 ⁻² T+1.0898x10 ⁻⁴ T ² -9.8128x10 ⁻⁸ T ³ +3.1944x10 ⁻¹¹ T ⁴	(8)
S ₇ (g)	1000	48.644-1.194 x10 ⁻² T+3.811 x10 ⁻⁵ T ² -1.791 x10 ⁻⁸ T ³	(8)
S ₈ (g)	1000	51.866-1.381 x10 ⁻² T+4.416 x10 ⁻⁵ T ² -2.0755x10 ⁻⁸ T ³	(8)
HS(g)	1000	24.670-1.0438x10 ⁻² T+2.9134x10 ⁻⁵ T ² -2.6763x10 ⁻⁸ T ³ +8.849 x10 ⁻¹² T ⁴	(8,9)
H ₂ S(g)	1000	26.031-1.1458x10 ⁻² T+3.1424x10 ⁻⁵ T ² -2.8197x10 ⁻⁸ T ³ +9.207 x10 ⁻¹² T ⁴	(8,9)
SO(g)	1000	27.844-1.0278x10 ⁻² T+2.8161x10 ⁻⁵ T ² -2.5297x10 ⁻⁸ T ³ +8.231 x10 ⁻¹² T ⁴	(8,9)
SO ₂ (g)	1000	31.444-1.4018x10 ⁻² T+3.8017x10 ⁻⁵ T ² -3.370 x10 ⁻⁸ T ³ +1.0875x10 ⁻¹¹ T ⁴	(8)
SO ₃ (g)	1000	32.988-1.8566x10 ⁻² T+4.9875x10 ⁻⁵ T ² -4.3737x10 ⁻⁸ T ³ +1.4012x10 ⁻¹¹ T ⁴	(8)
S ₂ O(g)	1000	33.876-1.5605x10 ⁻² T+4.2477x10 ⁻⁵ T ² -3.7926x10 ⁻⁸ T ³ +1.2285x10 ⁻¹¹ T ⁴	(8)
H ₂ SO ₄ (g)	1000	36.64 -9.61 x10 ⁻³ T+2.775 x10 ⁻⁵ T ² -1.25 x10 ⁻⁸ T ³	(8,9)
N(g)	2000	15.925+2.5[298.15/T - ln(298.15/T)]	(3)
N ₂ (g)	1000	24.0955-9.506x10 ⁻³ T+2.6323x10 ⁻⁵ T ² -2.3912x10 ⁻⁸ T ³ +7.849 x10 ⁻¹² T ⁴	(8,9)
NH(g)	1000	22.856-9.601 x10 ⁻³ T+2.644 x10 ⁻⁵ T ² -2.4321x10 ⁻⁸ T ³ +8.006 x10 ⁻¹² T ⁴	(8)
NH ₂ (g)	1000	24.703-1.1228x10 ⁻² T+3.0891x10 ⁻⁵ T ² -2.7835x10 ⁻⁸ T ³ +9.109 x10 ⁻¹² T ⁴	(8)
NH ₃ (g)	1000	24.570-1.2236x10 ⁻² T+3.3141x10 ⁻⁵ T ² -2.9206x10 ⁻⁸ T ³ +9.436 x10 ⁻¹² T ⁴	(8)
NO(g)	1000	26.422-9.721 x10 ⁻³ T+2.6892x10 ⁻⁵ T ² -2.4384x10 ⁻⁸ T ³ +7.997 x10 ⁻¹² T ⁴	(8)
NO ₂ (g)	1000	30.359-1.299 x10 ⁻² T+3.518 x10 ⁻⁵ T ² -3.109 x10 ⁻⁸ T ³ +1.0026x10 ⁻¹¹ T ⁴	(8)
N ₂ O(g)	1000	28.028-1.378 x10 ⁻² T+3.7298x10 ⁻⁵ T ² -3.3014x10 ⁻⁸ T ³ +1.0655x10 ⁻¹¹ T ⁴	(8)
N ₂ O ₃ (g)	1000	38.17 -6.50 x10 ⁻³ T+2.054 x10 ⁻⁵ T ² -9.474 x10 ⁻⁹ T ³	(8)
N ₂ O ₄ (g)	1000	39.99 -2.927 x10 ⁻² T+7.86 x10 ⁻⁵ T ² -6.898 x10 ⁻⁸ T ³ +2.212 x10 ⁻¹¹ T ⁴	(8)
N ₂ O ₅ (g)	1000	43.42 -9.960 x10 ⁻³ T+2.970 x10 ⁻⁵ T ² -1.357 x10 ⁻⁸ T ³	(8)

Species	T _{max} , K	$-(G^{\circ}-H_{298}^{\circ})/RT =$	Ref.
HNO(g)	1000	27.831-1.126 x10 ⁻² T+3.077 x10 ⁻⁵ T ² -2.740 x10 ⁻⁸ T ³ +8.903 x10 ⁻¹² T ⁴	(8)
H ₂ NNO ₂ (g)	1000	32.87 -7.224 x10 ⁻³ T+1.994 x10 ⁻⁵ T ² -8.743 x10 ⁻⁹ T ³	(8)
HONO(g)	1000	30.86 -4.853 x10 ⁻³ T+1.441 x10 ⁻⁵ T ² -6.523 x10 ⁻⁹ T ³	(8)
HONO ₂ (g)	1000	34.517-2.077 x10 ⁻² T+5.519 x10 ⁻⁵ T ² -4.778 x10 ⁻⁸ T ³ +1.5255x10 ⁻¹¹ T ⁴	(8)
HONH ₂ (g)	1000	28.77 -5.215 x10 ⁻³ T+1.504 x10 ⁻⁵ T ² -6.675 x10 ⁻⁹ T ³	(8)
C(g)	1000	19.772-6.884 x10 ⁻³ T+1.9091x10 ⁻⁵ T ² -1.7432x10 ⁻⁸ T ³ +5.728 x10 ⁻¹² T ⁴	(9)
CO(g)	1000	24.825-9.523 x10 ⁻³ T+6.323x10 ⁻⁵ T ² -2.3935x10 ⁻⁸ T ³ +7.858 x10 ⁻¹² T ⁴	(9)
CO ₂ (g)	1000	27.229-1.331 x10 ⁻² T+3.5974x10 ⁻⁵ T ² -3.177 x10 ⁻⁸ T ³ +1.024 x10 ⁻¹¹ T ⁴	(9)
CS(g)	1000	26.455-1.0117x10 ⁻² T+2.7736x10 ⁻⁵ T ² -2.4947x10 ⁻⁸ T ³ +8.130 x10 ⁻¹² T ⁴	(9)
COS(g)	1000	29.542-1.4862x10 ⁻² T+4.029 x10 ⁻⁵ T ² -3.5768x10 ⁻⁸ T ³ +1.1556x10 ⁻¹¹ T ⁴	(9)
CS ₂ (g)	1000	30.460-1.6203x10 ⁻² T+4.4067x10 ⁻⁵ T ² -3.9307x10 ⁻⁸ T ³ +1.2733x10 ⁻¹¹ T ⁴	(9)
CH ₄ (g)	1000	23.829-1.243 x10 ⁻² T+3.3115x10 ⁻⁵ T ² -2.841 x10 ⁻⁸ T ³ +9.068 x10 ⁻¹² T ⁴	(9)
CH ₃ OH(g)	1000	30.656-1.5764x10 ⁻² T+4.151 x10 ⁻⁵ T ² -3.5265x10 ⁻⁸ T ³ +1.1145x10 ⁻¹¹ T ⁴	(25)
CH ₂ O(g)	1000	26.55 -3.707 x10 ⁻³ T+1.083 x10 ⁻⁵ T ² -4.76 x10 ⁻⁹ T ³	(9)
HCOOH(g)	1000	32.052-1.8039x10 ⁻³ T+4.7926x10 ⁻⁵ T ² -4.1987x10 ⁻⁸ T ³ +1.370 x10 ⁻¹¹ T ⁴	(26)
(HCOOH) ₂ (g)	1000	40.97 -1.198 x10 ⁻² T+3.327 x10 ⁻⁵ T ² -1.45 x10 ⁻⁸ T ³	(26)
Mg(g)	2000	15.365+2.5[298.15/T - ln(298.15/T)]	(3)
Ca(g)	1500	16.115+2.5[298.15/T - ln(298.15/T)]	(3)
Li(g)	1600	14.1178+2.5[298.15/T - ln(298.15/T)]	(3)
Na(g)	1700	15.975+2.5[298.15/T - ln(298.15/T)]	(3)
K(g)	1400	16.771+2.5[298.15/T - ln(298.15/T)]	(3)
H ₂ O(l)	500	18.025-8.867 x10 ⁻² T+2.8856x10 ⁻⁴ T ² -3.9505x10 ⁻⁷ T ³ +2.08 x10 ⁻¹⁰ T ⁴	(9)
Br ₂ (l)	500	22.845-3.628 x10 ⁻² T+8.841 x10 ⁻⁵ T ² -5.95 x10 ⁻⁸ T ³	(8)
I ₂ (s)	387	15.897-1.333 x10 ⁻² T+2.30 x10 ⁻⁵ T ²	(8)
I ₂ (l)	760	-45.946+1204.8/T+9.569 lnT	(8)

Continued on next page.

TABLE IV (continued)

Species	T_{\max} , K	$-(G^0-H_{298}^0)/RT =$	Ref.
S(orthorhombic)	400	4.50 -4.58 $\times 10^{-3}T+8.11$	(8,9)
S(monoclinic)	400	4.27 -3.69 $\times 10^{-3}T+7.39$	(8,9)
S(λ)	1000	2.614-2.667 $\times 10^{-3}T+2.592$	(8)
H ₂ SO ₄ (λ)	700	23.435-3.773 $\times 10^{-2}T+8.96$	(9)
HNO ₃ (λ)	350	5.505+13.215[298,15/T - ln(298.15/T)]	(27)
NH ₄ NO ₃ (s)	450	21.94 -2.623 $\times 10^{-2}T+4.086$	(8)
NH ₄ NO ₃ (λ)	900	-108.40 +4468/T+19.364 lnT	(8)
NH ₄ Cl(s)	500	17.59 -4.927 $\times 10^{-2}T+1.204$	(35)
(NH ₄) ₂ SO ₄ (s)	600	17.61 -3.44 $\times 10^{-2}T+8.164$	(35)
C(graphite)	1000	1.125-3.593 $\times 10^{-3}T+9.165$	(9)
Si(s)	1000	3.095-7.270 $\times 10^{-3}T+1.976$	(9)
SiO ₂ (α, β quartz)	1000	6.94 -1.682 $\times 10^{-2}T+4.48$	(9)
SiO ₂ (α, β crist.)	1000	7.60 -1.975 $\times 10^{-2}T+5.146$	(33)
Mg(s)	922	4.88 -8.405 $\times 10^{-3}T+2.308$	(9)
MgO(s)	1000	4.85 -1.398 $\times 10^{-2}T+3.77$	(9)
Mg(OH) ₂ (s)	600	10.91 -2.664 $\times 10^{-2}T+6.355$	(35)
MgF ₂ (s)	1000	7.25 -6.14 $\times 10^{-3}T+1.872$	(9)
MgCl ₂ (s)	990	11.06 -6.19 $\times 10^{-3}T+1.993$	(9)
MgCl ₂ ·6H ₂ O(s)	385	44.03 -1.3 $\times 10^{-4}(T-298.15)^2$	(35,43)
MgOHC1(s)	850	5.49 -5.09 $\times 10^{-3}T+1.37$	(35)
MgS(s)	1000	6.22 -3.83 $\times 10^{-3}T+1.248$	(9)
MgSO ₄ (α)	1000	11.67 -1.025 $\times 10^{-2}T+3.031$	(9)
MgSO ₄ ·H ₂ O(s)	320	15.2 +8 $\times 10^{-5}(T-298.15)^2$	(27)
MgSO ₄ ·6H ₂ O(s)	320	41.9 +1 $\times 10^{-4}(T-298.15)^2$	(35)
MgSO ₄ ·7H ₂ O(s)	320	47.3 +2 $\times 10^{-4}(T-298.15)^2$	(35)

Species	T _{max} , K	$-(G^{\circ}-H_{298}^{\circ})/RT =$	Ref.
MgCO ₃ (s)	1000	9.05 -1.228 x10 ⁻² T+3.172 x10 ⁻⁵ T ² -1.496 x10 ⁻⁸ T ³	(9)
MgCO ₃ ·3H ₂ O(s)	320	23.53 +1x10 ⁻⁴ (T-298.15) ²	(27)
Ca(s)	721	5.49 -4.67 x10 ⁻³ T+1.20 x10 ⁻⁵ T ² -6.38 x10 ⁻⁹ T ³	(9)
CaO(s)	1000	4.82 -4.07 x10 ⁻³ T+1.26 x10 ⁻⁵ T ² -5.86 x10 ⁻⁹ T ³	(9)
Ca(OH) ₂ (s)	1000	13.73 -3.24 x10 ⁻² T+8.79 x10 ⁻⁵ T ² -7.846 x10 ⁻⁸ T ³ +2.544 x10 ⁻¹¹ T ⁴	(9)
CaF ₂ (s)	1000	10.97 -2.416 x10 ⁻² T+6.62 x10 ⁻⁵ T ² -5.967 x10 ⁻⁸ T ³ +1.95 x10 ⁻¹¹ T ⁴	(9)
CaCl ₂ (s)	1000	15.39 -2.49 x10 ⁻² T+6.862 x10 ⁻⁵ T ² -6.224 x10 ⁻⁸ T ³ +2.04 x10 ⁻¹¹ T ⁴	(9)
CaS(s)	1000	6.97 -3.93 x10 ⁻³ T+1.285 x10 ⁻⁵ T ² -6.05 x10 ⁻⁹ T ³	(9)
CaSO ₃ (s)	1000	12.75 -9.16 x10 ⁻³ T+2.75 x10 ⁻⁵ T ² -1.236 x10 ⁻⁸ T ³	(38)
CaSO ₃ ·1/2H ₂ O(s)	450	22.5 -6.24 x10 ⁻² T+1.53 x10 ⁻⁴ T ² -1.07 x10 ⁻⁷ T ³	(39,97)
CaSO ₄ (anhydride)	1000	13.31 -9.10 x10 ⁻³ T+2.824 ₅ x10 ⁻⁵ T ² -1.246 x10 ⁻⁸ T ³	(40)
CaSO ₄ (sol α)	320	13.03 +5.8x10 ⁻⁵ (T-298.15) ²	(40)
CaSO ₄ (sol β)	320	13.03 +5.7x10 ⁻⁵ (T-298.15) ²	(40)
CaSO ₄ ·1/2H ₂ O(α)	450	24.74 -7.22 x10 ⁻² T+1.778 x10 ⁻⁴ T ² -1.253 x10 ⁻⁷ T ³	(40)
CaSO ₄ ·1/2H ₂ O(β)	450	25.63 -7.533 x10 ⁻² T+1.842 x10 ⁻⁴ T ² -1.28 x10 ⁻⁷ T ³	(40)
CaSO ₄ ·2H ₂ O(s)	400	29.31 -4.183 x10 ⁻² T+7.30 x10 ⁻⁵ T ²	(40)
Ca(NO ₃) ₂ (s)	800	26.61 -3.036 x10 ⁻² T+7.497 x10 ⁻⁵ T ² -3.77 x10 ⁻⁸ T ³	(35)
CaCO ₃ (calcite)	1000	10.62 -9.025 x10 ⁻³ T+2.679 x10 ⁻⁵ T ² -1.221 x10 ⁻⁸ T ³	(35)
Li(s)	454	3.94 -3.45 x10 ⁻³ T+6.65 x10 ⁻⁶ T ²	(10)
LiOH(s)	800	6.35 -1.06 x10 ⁻² T+2.60 x10 ⁻⁵ T ² -1.33 x10 ⁻⁸ T ³	(9)
LiOH·H ₂ O(s)	350	8.61 +5.1x10 ⁻⁵ (T-298.15) ² - 1.6x10 ⁻⁷ (T-298.15) ³	(35)
LiF(s)	1000	4.55 -4.06 x10 ⁻³ T+1.25 x10 ⁻⁵ T ² -5.73 x10 ⁻⁹ T ³	(9,98)
LiCl(s)	900	7.67 -6.29 x10 ⁻³ T+1.73 x10 ⁻⁵ T ² -8.46 x10 ⁻⁹ T ³	(9)
Li ₂ SO ₄ (s)	900	15.53 -1.863 x10 ⁻² T+4.831 x10 ⁻⁵ T ² -2.264 x10 ⁻⁸ T ³	(9)
Na(s)	371	6.17 +1x10 ⁻⁴ (T-298.15)+1.30x10 ⁻⁵ (T-298.15) ²	(10)
NaOH(s)	600	9.50 -1.452 x10 ⁻² T+3.344 x10 ⁻⁵ T ² -1.619 x10 ⁻⁸ T ³	(9)

Continued on next page.

TABLE IV (continued)

Species	T _{max} , K	-(G°-H ₂₉₈ °)/RT =	Ref.
NaF(s)	1000	6.34 -4.00 x10 ⁻³ T+1.293 x10 ⁻⁵ T ² -6.03 x10 ⁻⁹ T ³	(9)
NaCl(s)	1000	8.83 -4.09 x10 ⁻³ T+1.346 x10 ⁻⁵ T ² -6.27 x10 ⁻⁹ T ³	(9,98)
Na ₂ S(s)	1000	11.81 -6.48 x10 ⁻³ T+2.167 x10 ⁻⁵ T ² -1.023x10 ⁻⁸ T ³	(9)
Na ₂ SO ₄ (s)	1000	23.81 -4.711x10 ⁻² T+1.1182x10 ⁻⁴ T ² -6.718x10 ⁻⁸ T ³	(9)
Na ₂ SO ₄ ·10H ₂ O	320	71.15 +3x10 ⁻⁴ (T-298.15) ²	(35)
NaN ₃ (s)	550	15.10 -1.026x10 ⁻² T+2.165 x10 ⁻⁵ T ²	(35)
Na ₂ CO ₃ (s)	900	18.15 -1.809x10 ⁻² T+4.595 x10 ⁻⁵ T ² -2.151x10 ⁻⁸ T ³	(9)
NaHCO ₃ (s)	400	15.17 -1.985x10 ⁻² T+3.46 x10 ⁻⁵ T ²	(35)
NaCHO ₂ (s)	330	12.48 +5x10 ⁻⁵ (T-298.15) ²	(42)
K(s)	336	7.78 +2x10 ⁻⁵ (T-298.15) ²	(10)
KF(s)	1000	8.175-4.07 x10 ⁻³ T+1.327 x10 ⁻⁵ T ² -6.185x10 ⁻⁹ T ³	(9,98)
KCl(s)	1000	10.14 -4.17 x10 ⁻³ T+1.37 x10 ⁻⁵ T ² -6.377x10 ⁻⁹ T ³	(9)
K ₂ SO ₄ (s)	900	22.88 -1.898x10 ⁻² T+5.042 x10 ⁻⁵ T ² -2.392x10 ⁻⁸ T ³	(9)
K ₂ S ₄ O ₆ (s)	330	37.24 -4x10 ⁻⁴ (T-298.15)+1.7x10 ⁻⁴ (T-298.15) ² -5x10 ⁻⁷ (T-298.15) ³	(39)
KNO ₃ (s)	400	19.60 -2.47 x10 ⁻² T+4.22 x10 ⁻⁵ T ²	(35)
AQUEOUS SOLUTES (99)			
H ₂ (aq)	500	6.91 +6.80 x10 ⁻⁴ t ² +3.14 x10 ⁻⁵ t ² -1.5 x10 ⁻⁹ t ³	(46,100,101)
O ₂ (aq)	500	13.01 +1.42 x10 ⁻³ t ² +6.34 x10 ⁻⁵ t ² -7.83 x10 ⁻⁸ t ³	(46,100,101,102)
O ₃ (aq)	400	17.77 -2.0 x10 ⁻³ t ² +1.034 x10 ⁻⁴ t ² -1.42 x10 ⁻⁷ t ³	(46,99)
H ₂ O(aq)	500	8.442-2.50 x10 ⁻³ t+5.795 x10 ⁻⁵ t ² -1.678x10 ⁻⁷ t ³ +2.08 x10 ⁻¹⁰ t ⁴	(9)
H ⁺	0.		
OH ⁻	500	-1.375+6.00 x10 ⁻³ t ² +7.464x10 ⁻⁷ t ³ -1.485x10 ⁻⁹ t ⁴	(103,104)
H ₂ O ₂ (aq)	400	17.68 -6.9 x10 ⁻³ t+2.8 x10 ⁻⁶ t ² +1.6 x10 ⁻⁷ t ³	(57,105)
HO ₂ ⁻	500	2.74 +1.02 x10 ⁻² t-1.96 x10 ⁻⁴ t ² +2.54 x10 ⁻⁷ t ³	(105,106)

(226.85°C)

Species	T _{max} , K	-(G ^o -H ₂₉₈ ^o)/RT =	Ref.
F ⁻	400	-1.25 -2.83 x10 ⁻² +5.86 x10 ⁻⁴ t ² -5.35 x10 ⁻⁶ t ³ +1.06 x10 ⁻⁸ t ⁴	(105-7)
Cl ₂ (aq)	350	16.0 +1.8 x10 ⁻³ t ⁻⁴ x10 ⁻⁵ t ²	(46)
Cl ⁻	500	6.62 +1.11 x10 ⁻² t ⁻¹ .827x10 ⁻⁴ t ² +6.72 x10 ⁻⁷ t ³ -9.62 x10 ⁻¹⁰ t ⁴	(105,108)
Br ⁻	400	9.62 +2.32 x10 ⁻² t ⁻⁴ .99 x10 ⁻⁴ t ² +2.713x10 ⁻⁶ t ³ -5.28 x10 ⁻⁹ t ⁴	(105,109)
I ⁻	500	13.56 -3.22 x10 ⁻² t ⁻¹ .46 x10 ⁻⁴ t ² +9.1 x10 ⁻⁷ t ³ -1.81 x10 ⁻⁹ t ⁴	(105,106)
H ₂ S(aq)	600	15.26 +8.8 x10 ⁻⁴ t ² +5.46 x10 ⁻⁵ t ² -7.8 x10 ⁻⁸ t ³	(46, 57, 110)
HS ⁻	550	8.38 +6.4 x10 ⁻³ t ⁻⁴ .9 x10 ⁻⁵ t ² +1.79 x10 ⁻⁷ t ³	(60, 111)
S ₃ =	500	3.78 +1.09 x10 ⁻² t ⁻⁸ .9 x10 ⁻⁵ t ² +2.1 x10 ⁻⁷ t ³	(105,106)
S ₄ =	500	12.32 +3.9 x10 ⁻³ t ⁻² .9 x10 ⁻⁵ t ² +6.6 x10 ⁻⁸ t ³	(105,106)
S ₅	500	16.82 +9 x10 ⁻³ t ⁻⁷ .2 x10 ⁻⁵ t ² +1.69 x10 ⁻⁷ t ³	(105,106)
SO ₂ (aq)	450	20.09 +5 x10 ⁻⁴ t ⁻⁶ x10 ⁻⁶ t ² +3.4 x10 ⁻⁷ t ³	(46, 57, 58, 105)
H ₂ SO ₃ (aq)	450	28.56 +4.5 x10 ⁻³ t ⁻⁷ .7 x10 ⁻⁵ t ² +1.1 x10 ⁻⁷ t ³	(46, 57, 58, 105)
HSO ₃	450	14.4 -2.8 x10 ⁻⁴ t ² +5.6 x10 ⁻⁶ t ²	(37, 105, 106)
SO ₃ =	450	-4.4 +1.18 x10 ⁻² t ⁻¹ .98 x10 ⁻⁴ t ² +3.2 x10 ⁻⁷ t ³	(37, 105, 106)
HSO ₄	450	16.05 +1.3 x10 ⁻² t ⁻³ .4 x10 ⁻⁴ t ² +2.29 x10 ⁻⁶ t ³ -8.0 x10 ⁻⁹ t ⁴	(72)
SO ₄	450	2.06 +1.17 x10 ⁻² t ⁻² .78 x10 ⁻⁴ t ² +1.34 x10 ⁻⁶ t ³ -4.1 x10 ⁻⁹ t ⁴	(73)
S ₂ O ₃ =	450	3.88 +7.57 x10 ⁻³ t ⁻¹ .1 x10 ⁻⁴ t ² +1.7 x10 ⁻⁷ t ³	(37, 105, 106)
S ₂ O ₄ =	450	10.89 +5.4 x10 ⁻³ t ⁻⁵ .2 x10 ⁻⁵ t ² +1 x10 ⁻⁷ t ³	(105, 106)
S ₂ O ₆ =	450	13.38 +9 x10 ⁻⁴ t ⁻¹ x10 ⁻⁶ t ² +2.4 x10 ⁻⁸ t ³	(105, 106)
S ₂ O ₈ =	450	30.43 -4.5 x10 ⁻³ t ² +1.385x10 ⁻⁴ t ² -1.53 x10 ⁻⁷ t ³	(105, 106)
S ₃ O ₆ =	450	29.91 +3.5 x10 ⁻³ t ² +3.4 x10 ⁻⁶ t ² +2.4 x10 ⁻⁸ t ³	(105, 106)
S ₄ O ₆ =	450	31.15 +6.4 x10 ⁻³ t ⁻² .2 x10 ⁻⁵ t ² +1.12 x10 ⁻⁷ t ³	(37, 105, 106)
S ₅ O ₆ =	450	32.91 +3 x10 ⁻³ t ² +2.4 x10 ⁻⁵ t ² +1.3 x10 ⁻⁸ t ³	(105, 106)

(176.85°C)

Continued on next page.

TABLE IV (continued)

Species	T _{max} , K	$-(G^0-H^0_{298})/RT =$	Ref.
N ₂ (aq)	450	11.39 +1.86 x10 ⁻³ t+4.95 x10 ⁻⁵ t ² -3.87 x10 ⁻⁸ t ³	(46,100,101)
NH ₃ (aq)	450	13.0 +2.5 x10 ⁻⁴ t+2.5 x10 ⁻⁵ t ² +1.3 x10 ⁻⁸ t ³	(58)
NH ₄ OH(aq)	450	21.4 -1.5 x10 ⁻³ t+6.94 x10 ⁻⁵ t ² -6.3 x10 ⁻⁸ t ³	(58)
NH ₄ ⁺	450	13.30 +2.8 x10 ⁻⁴ t+2.84 x10 ⁻⁵ t ² -3.0 x10 ⁻⁸ t ³	(60,75-85)
N ₂ H ₄ (aq)	500	16.54 +5.03 x10 ⁻³ t-1.17 x10 ⁻⁴ t ² +4.56 x10 ⁻⁷ t ³	(57,105)
N ₂ H ₅ ⁺	500	18.03 -2.47 x10 ⁻³ t+5.1 x10 ⁻⁵ t ² -5 x10 ⁻⁸ t ³	(99)
HNO ₂ (aq)	450	16.2 +5 x10 ⁻³ t-8 x10 ⁻⁵ t ² +2 x10 ⁻⁷ t ³	(57,105)
NO ₂ ⁻	500	14.76 +3.6 x10 ⁻³ t-7.8 x10 ⁻⁵ t ² +1.5 x10 ⁻⁷ t ³	(105,106)
NO ₃ ⁻	500	17.58 +3.75 x10 ⁻³ t-7.04 x10 ⁻⁵ t ² +1.26 x10 ⁻⁷ t ³	(105,106)
N ₂ O ₂	500	2.92 +5.8 x10 ⁻³ t-1.02 x10 ⁻⁴ t ² +1.5 x10 ⁻⁷ t ³	(105,106)
N ₂ O(aq)	400	14.14 -4.0 x10 ⁻³ t+1.10 x10 ⁻⁴ t ² -2.1 x10 ⁻⁷ t ³	(46)
NO(aq)	400	14.3 -5.2 x10 ⁻³ t+1.36 x10 ⁻⁴ t ² -2.6 x10 ⁻⁷ t ³	(46)
CH ₄ (aq)	500	10.215-1.26 x10 ⁻³ t+1.019x10 ⁻⁴ t ² -2.74 x10 ⁻⁷ t ³ +3.47 x10 ⁻¹⁰ t ⁴	(46,101)
HCN(aq)	450	15.24 +3.9 x10 ⁻³ t-6.55 x10 ⁻⁵ t ² +1.85 x10 ⁻⁷ t ³	(57,105)
CN ⁻	450	11.57 +3.9 x10 ⁻³ t-7.9 x10 ⁻⁵ t ² +1.2 x10 ⁻⁷ t ³	(60,105,106)
HCNO(aq)	450	16.14 -1.1 x10 ⁻³ t-2.1 x10 ⁻⁵ t ² +2.1 x10 ⁻⁷ t ³	(57,105)
CNO ⁻	450	12.2 +5 x10 ⁻³ t-9.8 x10 ⁻⁵ t ² +1.3 x10 ⁻⁷ t ³	(105,106)
CNS ⁻	450	12.8 +5 x10 ⁻³ t-9.8 x10 ⁻⁵ t ² +1.3 x10 ⁻⁷ t ³	(105,106)
CO ₂ (aq)	500	14.45 -7.0 x10 ⁻³ t+1.63 x10 ⁻⁴ t ² -5.49 x10 ⁻⁷ t ³ +7.95 x10 ⁻¹⁰ t ⁴	(46,57,58,112)
H ₂ CO ₃ (aq)	500	22.89 -9.6 x10 ⁻³ t+2.22 x10 ⁻⁴ t ² -7.21 x10 ⁻⁷ t ³ +1.01 x10 ⁻⁹ t ⁴	(46,57,58,112)
HCO ₃ ⁻	500	11.90 -2.96 x10 ⁻³ t+3.09 x10 ⁻⁵ t ² -2.52 x10 ⁻⁷ t ³ +5.4 x10 ⁻¹⁰ t ⁴	(57,58,81)
CO ₃ ⁼	500	-6.07 +5.85 x10 ⁻³ t-1.702x10 ⁻⁴ t ² +2.61 x10 ⁻⁷ t ³	(57,58,81,82)
CO(aq)	400	12.26 -5.2 x10 ⁻³ t+1.37x10 ⁻⁴ t ² -2.6 x10 ⁻⁷ t ³	(46)

(126.85°C)

Species	T _{max} , K	-(G ^o -H ₂₉₈ ^o)/RT =	Ref.
HCOOH(aq)	500	19.65 +1.7 x10 ⁻³ t+3 x10 ⁻⁶ t ² +2.5 x10 ⁻⁷ t ³	(57,85,105,113)
HCOO ⁻	500	10.90 +5.2 x10 ⁻³ t-5.6 x10 ⁻⁵ t ² +1.3 x10 ⁻⁷ t ³	(85,105,106)
CH ₃ COOH(aq)	500	21.43 +2.7 x10 ⁻³ t-1.17 x10 ⁻⁵ t ² +3.58 x10 ⁻⁷ t ³	(57,75,85,105,113)
CH ₃ COO ⁻	500	10.42 +1.64 x10 ⁻³ t-3.71 x10 ⁻⁵ t ² +9.1 x10 ⁻⁸ t ³	(75,85,105,106)
(COOH) ₂ (aq)	500	22.53 -3.5 x10 ⁻³ t+9.1 x10 ⁻⁵ t ² -5 x10 ⁻⁸ t ³	(57,105)
C ₂ O ₄ H ₂ ²⁻	500	18.04 -3.4 x10 ⁻³ t+6.75 x10 ⁻⁵ t ²	(105,106)
C ₂ O ₄ ²⁻	500	5.45 +3.3 x10 ⁻³ t-7.26 x10 ⁻⁵ t ² +1.1 x10 ⁻⁷ t ³	(105,106)
Mn ⁺⁺	500	-8.15 +4 x10 ⁻⁴ t-7 x10 ⁻⁶ t ²	(99)
Mn ⁺⁺⁺	500	-32.2 +6 x10 ⁻⁴ t-1.1 x10 ⁻⁵ t ²	(105,106)
Fe ⁺⁺	500	-16.6 +1 x10 ⁻⁴ t-3 x10 ⁻⁶ t ²	(99)
Fe ⁺⁺⁺	500	-38.0 -2 x10 ⁻⁵ t+8 x10 ⁻⁷ t ² -1 x10 ⁻⁸ t ³	(99)
Mg ⁺⁺	500	-16.6 +5 x10 ⁻⁴ t-1.1 x10 ⁻⁵ t ²	(115)
Ca ⁺⁺	500	-6.75 +1.0 x10 ⁻³ t-2.2 x10 ⁻⁵ t ² +2 x10 ⁻⁸ t ³	(105,106)
Li ⁺	500	1.51 -2.2 x10 ⁻³ t+4.6 x10 ⁻⁵ t ² -6 x10 ⁻⁸ t ³	(105,106,107)
Na ⁺	500	7.21 -9.53 x10 ⁻³ t+1.371x10 ⁻⁴ t ² -5.136x10 ⁻⁷ t ³ +5.68 x10 ⁻¹⁰ t ⁴	(109,113-6)
K ⁺	500	12.33 -8.28 x10 ⁻³ t+1.085x10 ⁻⁴ t ² -4.29 x10 ⁻⁷ t ³ +5.0 x10 ⁻¹⁰ t ⁴	(107,109,114)

(226.85°C)

Discussion of Table IV on next page.

Discussion of Table IV

The above tables represent an amalgamation of earlier tables by the National Bureau of Standards (23,29, 42,93) and CODATA (1,3,11,13,28, 30,59) with more recent data. However, as noted in the introduction, they suffer from the defect that it has not been possible to ensure that internal consistency has been maintained as the references to the National Bureau of Standards tables are not available. This is a very difficult task and it is hoped that the work of the NBS will be expanded to allow updating of their tables with maintenance of consistency. Until that time, the present tables will help with the need for utilization of recent measurements.

The extension to higher temperatures of the data for the aqueous species in Table IV constitutes a substantial step beyond the previous NBS compilations. The high temperature heat capacities are poorly known and many had to be estimated. Fortunately, because of the relative insensitivity of $-(G^{\circ}-H^{\circ}_{298})/RT$ to C_p , reasonably accurate values of the equilibrium constants can be given even with rather inaccurate heat capacities. However, it is important to note that the reverse process of differentiation of the equation given for $-(G^{\circ}-H^{\circ}_{298})/RT$ will not recover the heat capacities values used at their original accuracy. The choice was made to use a simple power series and t , the Centigrade temperature,

was used as the variable to reduce the number of terms and the number of places required for each parameter.

After Table III, references are given to the sources of S° and C_p° at 298 K which were used in generating the $-(G^{\circ}-H^{\circ}_{298})/RT$ equations. In Table IV, only those additional references which give information for higher temperatures are listed.

Appendix: Calculator Program for Use of Tables I-IV

For the reaction $aA + bB = cC + dD$, the constants of Table IV for each of the reactants and products can be combined to yield an equation for $-\Delta(G^{\circ}-H_{298}^{\circ})/RT$ as a function of temperature. The $\Delta H_{298}^{\circ}/R$ values of Tables I-III can be combined to yield $\Delta H_{298}^{\circ}/R$ for the overall reaction. $\Delta H_{298}^{\circ}/R = d(\Delta H_{298}^{\circ}/R)_D + c(\Delta H_{298}^{\circ}/R)_C - b(\Delta H_{298}^{\circ}/R)_B - a(\Delta H_{298}^{\circ}/R)_A$. The equilibrium constant can then be calculated by the equation $\ln K_T = -\Delta(G^{\circ}-H_{298}^{\circ})/RT - (\Delta H_{298}^{\circ}/R)/T$. If $\ln K$ is known, the above equation can be used to calculate $\Delta H_{298}^{\circ}/R$. The following program will carry out these operations using the constants of Tables I-IV. HP41C programming is used.

Directions

- | | | <u>Display</u> |
|---|-------------|---|
| (1) d ↑ c ↑ -b ↑ -a | XEQ 'AG' | 0 |
| The sign is negative for each reactant coefficient and positive for each product coefficient. If the total of reactants and products is three, enter d=0. For aA=cC, enter 0 ↑ 0 ↑ c ↑ -a. | | |
| (2) (a ₀) _D ↑ (a ₀) _C ↑ (a ₀) _B ↑ (a ₀) _A | User A | d(a ₀) _D |
| [(2') e ST09, (a ₀) _E | User E | e(a ₀) _E] |
| (2') is used only if the total of reactants and products is five. Step(2), and if necessary (2'), is repeated with a ₁ values from Table IV, and then again with the a ₂ values up to a ₄ values if there are a ₄ entries in Table IV for any of the reactants or products. If the sum of reactants and products is three, no entries are made for D. Similarly, if there are only two species, no entry is needed of (a _n) _B values. If there are only a ₀ terms which correspond to the C _p /R values at 298K given in Tables I-III, no entries are made after the a ₀ entries. However, if any reactant or product has a higher term, then entries, even when they are zero, are required through the highest a _n set with at least one non-zero value. | | |
| (3a) T ₁ | XEQ 1 | $-\Delta(G^{\circ}-H_{298}^{\circ})/RT_1$ |
| (3b) (If I stored in R12) | R/S | $-\Delta(G^{\circ}-H_{298}^{\circ})/RT$
for T = T ₁ + I |
| (4) After 10.1 ST010, $\Delta H_{298}^{\circ}/R$ for each product and reactant is inserted as in (2), and if necessary (2'). | | |
| (5a) To calculate average $\Delta H_{298}^{\circ}/R$ from a set of $\ln K_T$ values, XEQ5 to set up registers | | |
| T ↑ $\ln K_T$ | User H | $\Delta H_{298}^{\circ}/R$ |
| Repeat T ↑ $\ln K$ H for all T. | | |
| (5b) | R/S, SST | Av. $\Delta H_{298}^{\circ}/R$, Std. Dev. |
| (6a) After step 4 or 5 has stored $\Delta H_{298}^{\circ}/R$ in R11, | | |
| T ₁ | User E, SST | $\ln K_{T_1}, K_{T_1}$ |
| (6b) | R/S, SST | $\ln K_T, K_T$
for T = T ₁ +I |

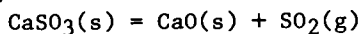
Note 1: When $-(G^0-H^0_{298})/RT$ is given as a function of $T-298.15$, e.g. $a_0' + a_1'(T-298.15) + a_2(T-298.15)^2$, it is necessary to expand to obtain power series in T . In the example cited, $a_0 = a_0' - 298.15a_1' + a_2(298.15)^2$ and $a_1 = a_1' - 2(298.15)a_2$.

Note 2: When the $-(G^0-H^0_{298})/RT$ equation in Table IV contains $\ln T$ and T^{-1} terms, these terms should be entered by step (2) after insertion of the a_0 terms and before insertion of the a_1 terms. For an equation with $\ln T$, T^{-1} as well as T and T^2 terms, LBL 01 would be modified after RCL 02 of step 51 to $R\uparrow / + R\uparrow LN RCL 01 X + RCL 00 + RTN$.

R 00	1	2	3	4	5	6	7	8	9	10
	Δa_0	Δa_1	Δa_3	Δa_4	-a	-b	c	d	e	Δa
										Index
	11	12	13				14		15	18
	$\frac{\Delta H^0_{298}}{R}$	I	$\Sigma \frac{\Delta H^0_{298}}{R}$				$\Sigma \left(\frac{\Delta H^0_{298}}{R}\right)^2$		lnK	n

SIZE 019, program has 94 steps using 124 bytes or 18 registers or a total of 37 registers needed. Program will set Σ registers starting at 13.

Test:



(1) 0 \uparrow 1 \uparrow 1 \uparrow 1 \uparrow -1

XEQ 'AG'

User

(2) 31.44 \uparrow 4.82 \uparrow 12.75
 -1.4018×10^{-2} \uparrow -4.07×10^{-3} \uparrow -9.16×10^{-3}
 3.8017×10^{-5} \uparrow 1.26×10^{-5} \uparrow 2.75×10^{-5}
 -3.37×10^{-8} \uparrow -5.86×10^{-9} \uparrow -1.23×10^{-9}
 1.0875×10^{-11} \uparrow 0 \uparrow 0

A

A

A

A

A

(3) EEX2 STO12, 800 XEQ1 21.694; (3b) R/S 21.510; R/S 21.378

(4) 10.1 STO10, -35 700 \uparrow -76 380 \uparrow -139 400; A 0; RCL11 27 320

(6a) 800 E -12.456 SST 3.90 $\times 10^{-6}$

(5a) XEQ5, 800 \uparrow -12.46 H 27 324; 900 \uparrow -8.85 H 27 324;

1000 \uparrow -5.94 H 27 318

(5b) R/S 27 322, SST 3

LBLAG	ST05	RDN	ST06	RDN	ST07	RDN	ST08	-1.1
STO10	0	STO1	STO2	STO3	STO4	STO12	RTN	
LBLA	ISG10	STIND10	CLX	RCL5	STXIND10			
		RDN	RCL6	X	ST+IND10	RDN	RCL7	X
ST+IND10		RDN	RCL8	X	ST+IND10	RTN		
LBL e	RCL9	X	ST+IND10	RTN				
LBL1	\uparrow	\uparrow	\uparrow	RCL4	X	RCL3	+	X
RCL2	+	X	RCL1	+	X	RCL00	+	RTN
RCL12	R \uparrow	+	GTO1					
LBL5	Σ REG13	CL Σ	RTN					
LBLH	STO15	RDN	XEQ1	RCL15	-	R \uparrow	X	Σ +
LASTX	RTN	MEAN	STO11	RTN	SDEV			
LBL E	XEQ1	RCL11	R \uparrow	/	-	RTN	E+X	RCL12
R \uparrow	+	GTOE						

Acknowledgment

This work was supported by the Assistant Secretary for Fossil Energy, Office of Coal Research, Advanced Environmental Control Division of the U.S. Department of Energy under Contract Number W-7405-ENG-48, through the Morgantown Energy Technology Center, Morgantown, West Virginia.

Literature Cited

1. CODATA recommended key values for thermodynamics, 1977, J. Chem. Thermodynamics 1978, 10, 903-6.
2. Pitzer, K. S.; Brewer, L. J. Phys. Chem. Ref. Data 1979, 8, 917-9; High-Temp. Sci. 1979, 11, 49-53.
3. For the atomic gases H, the alkali and alkaline earth elements, N, Br, and I which have no significant contribution to the heat capacity other than translational between 0 and 298 K, $(H_{298}^0 - H_0^0)/R = (5/2)(298.1500) = 745.4$ K with no uncertainty. For the same atoms, the entropy can be calculated very accurately from Eq. 27-3 of ref.(4). Appendix 3 of ref.(4) derives Eqs. A3-15 and 16 which are given again as Eq. 27-2 from which 27-3 is derived. $S_{298}^0/R = 13.0791 + (3/2)\ln M + \ln g_e$. M is the atomic weight and g_e is the electronic degeneracy which is 1 for the alkaline earth elements, 2 for H and the alkali elements, and 4 for N, Br, and I. The constant $13.0791 = 5/2 + (3/2)\ln(2\pi/N_0 h^2) + (5/2)\ln k - \ln 1013250$. The values used were $N_0 = 6.02209 \times 10^{23}$, $h = 6.62618 \times 10^{27}$ erg sec, and $k = 1.38065 \times 10^{-16}$ erg K^{-1} (5,6). The error in S_{298}^0/R due to uncertainties in the constants and atomic weights (7) or the use of an average molecular weight for an isotopic mixture is 0.001 or smaller for all of these elements. The values calculated here agree with the CODATA values (1) within rounding errors, but their uncertainties are too high.
4. Lewis, G. N.; Randall, M.; Pitzer, K. S.; Brewer, L. "Thermodynamics"; 2nd Ed., McGraw-Hill Book Co., New York, 1961.
5. Cohen, E. R.; Taylor, B. N. J. Phys. Chem. Ref. Data 1973, 2, 663-734.
6. Taylor, B. N.; Cohen, E. R. in "Atomic Masses and Fundamental Constants," Proc. 5th Int. Conf., 1975, Eds. Sanders, J. H., Wapstra, A. H., Plenum Press, New York, 1976.
7. Commission on Atomic Weights, Inorganic Chemistry Division of IUPAC, Atomic weights of the elements 1975, Pure Appl. Chem. 1976, 47, 75-95.
8. Glushko, V. P.; Gurvich, V. V.; Bergman, G. A.; Veitz, I. V.; Medvedev, V. A.; Khachkuruzov, G. A.; Yungman, V. S. "Thermodynamic Properties of Individual Substances," High-Temperature Institute, State Institute of Applied Chemistry, National Academy of Sciences of the U.S.S.R., Moscow, 1978. Vol. 1: Compounds of O, H, F, Cl, Br, I, He, Ne, Ar, Kr, Rn, S, N, and P.

9. Chase, M. W., Jr.; Curnutt, J. L.; McDonald, R. A.; Syverud, A. N. JANAF Thermochemical Tables, 1978 Supplement, J. Phys. Chem. Ref. Data 1978, 7, 793-940 and additional supplements.
10. Hultgren, R.; Desai, P. D.; Hawkins, D. T.; Gleiser, M.; Kelley, K. K.; and Wagman, D. D. Selected Values of the Thermodynamic Properties of the Elements, American Society for Metals, Metals Park, Ohio, 1973.
11. The CODATA enthalpy of formation values (1) for Br and I were slightly revised to correspond to the values reported by Barrow, R. F.; Broyd, D. F.; Pederson, L. V.; Yee, K. K. Chem. Phys. Letters 1973, 18, 357.
12. Johnson, G. K. J. Chem. Thermodynamics 1977, 9, 835-41.
13. The CODATA ΔH value for S(g) was changed in acknowledgment of the objection raised by K. P. Huber and G. Herzberg (14) and to be consistent with the value selected (10) for S₂(g).
14. Huber, K. P. and Herzberg, G. "Molecular Spectra and Molecular Structure. IV: Constants of Diatomic Molecules." Van Nostrand Reinhold, New York, 1979.
15. Steudel, R. and Schuster, F. J. Mol. Struct. 1978, 44, 143-57.
16. Rau, H.; Kutty, T. R. N.; Guedes De Carvalho, J. R. F. J. Chem. Thermodynamics 1973, 5, 833-44.
17. Detry, D.; Drowart, J.; Goldfinger, P.; Keller, H.; Rickert, H. Z. Phys. Chem. N.F. 1967, 55, 314-9.
18. Rosenquist, T.; Haugom, J. J.C.S. Faraday I 1977, 73, 913-9.
19. Lovas, F. J. J. Phys. Chem. Ref. Data 1978, 7, 1445.
20. Benson, S. W. Chem. Rev. 1978, 78, 23-35.
21. Piper, L. G. J. Chem. Phys. 1979, 70, 3417-9.
22. Drowart, J.; Smets, J.; Reynaert, J. C.; Coppens, P. Adv. Mass Spect. 1978, 7A, 647-50.
23. Wagman, D. D.; Evans, W. H.; Parker, V. B.; Halow, I.; Bailey, S. M.; Schumm, R. H. Nat. Bur. Stand. U.S. Technical Note, 270-3 (1968),
24. Domalski, E. S. J. Phys. Chem. Ref. Data 1972, 1, 221-77.
25. Chen, S. S.; Wilhoit, R. C.; Zwolinski, B. J. J. Phys. Chem. Ref. Data 1977, 6, 105-112.
26. Chao, J.; Zwolinski, B. J. J. Phys. Chem. Ref. Data 1978, 7, 363-77.
27. Clushkov, V. P.; Medvedev, V. A.; Yungman, V. S.; Bergman, G. A.; Kolesov, V. P.; Gurvich, L. V.; Vorob'yev, A. F.; Vasil'yev, V. P.; Kostryukov, V. N.; Reznitskii, L. A.; Ioffe, N. T., et al. Thermodynamic Constants of Materials, All Union Institute of Scientific and Technical Information (VINITI), Institute for High Temperature, Vol. II S, Se, Te, Po (1966), Vol. III N, P, As, Sb, Bi (1968), Vol. IV C, Si, Ge, Sn, Pb (1970), Vol. IX Be, Mg, Cu, Sr, Ba, Ra, (1979).

28. Wagman, D. D. U.S. National Bureau of Standards, private communication, June 1980, of proposed modifications of CODATA values (1). To be consistent with these changes, appropriate corrections have been applied to values taken from earlier tabulations when the accuracy of the data warranted the small corrections.
29. Parker, V. B.; Wagman, D. D.; Evans, W. H. Nat. Bur. Stand. U.S. Technical Note, 270-6 (1971).
30. Wagman (28) has listed values from references cited in CODATA Bulletin No. 10, 1973 as being the best data available up to June 1980.
31. Nash, G. A.; Skinner, H. A.; Zordan, T. A.; Hepler, L. G. J. Chem. Eng. Data 1968, 13, 271-2.
32. Navrotsky, A., Arizona State University, private communication, Aug. 1980, of determination of enthalpy difference of quartz and cristobalite.
33. The JANAF values (9) for cristobalite were revised using the measurements of A. J. Leadbetter and T. W. Smith, Phil. Mag. 1976, 33, 113-9.
34. Shin, C.; Criss, C. M. J. Chem. Thermodynamics 1979, 11, 663-6.
35. Kelley, K. K., Bureau of Mines Bulletin 584, U.S. Govt. Printing Office, Washington, D. C., 1960.
36. Ko, H. C.; Daut, G. E., Bur. Mines Report of Investigations RI 8409, 8 pg., 1980.
37. Hemingway, B. S.; Robie, R. A. J. Res. U.S. Geol. Surv. 1973, 1(5), 535-41, 543-7.
38. Cubicciotti, D.; Sanjuyo, A.; Hildenbrand, D. L. J. Electrochem. Soc. 1977, 124, 933-6.
39. The calculations of Cobble, J. W.; Stephens, H. P.; McKinnon, I. R.; Westrum, E. F., Jr. Inorg. Chem. 1972, 11, 1669-74, have been corrected to be consistent with the values of Table III.
40. Kelley, K. K.; Southard, J. C.; Anderson, C. T. U.S. Bur. Mines Tech. Paper 625, 1941. All of their $\Delta H/R$ values were made 2040 K more negative to be consistent with values for $SO_4^{=}$ and Ca^{++} of Table III and the values for $CaSO_4$ (anhydrite) and $CaSO_4 \cdot 2H_2O(s)$ recommended by Wagman (28).
41. Staveley, L. A. K.; Linford, R. G. J. Chem. Thermodynamics 1969, 1, 1-11.
42. Wagman, D. D.; Evans, W. H.; Parker, V. B.; Schumm, R. H.; Nuttall, R. L. Nat. Bur. of Standards Technical Note 270-8 (1981).
43. Kelley, K. K.; King, E. G. U.S. Bur. Mines Bull. 592, 1961.
44. Berg, R. L.; Vanderzee, C. E. J. Chem. Thermodynamics 1978, 10, 1113-36.
45. Schwartz, H.A. J. Chem. Educ. 1981, 58, 101-5.
46. Wilhelm, E.; Battino, R.; Wilcox, R. J. Chem. Rev. 1977, 77, 219-62.
47. Enea, O.; Singh, P. P.; Woolley, E. M.; McCurdy, K. G.; Hepler, L. G. J. Chem. Thermodynamics 1977, 9, 731-4.

48. Allred, G. C.; Woolley, E. M. J. Chem. Thermodynamics 1981, 13, 147-54.
49. Branch, G. E. K.; Calvin, M., "The Theory of Organic Chemistry," Prentice-Hall, 1941.
50. Baxendale, J. H.; Ward, M. D.; Wardman, P. Trans. Faraday Soc. 1971, 67, 2532-7.
51. Desnoyers, J. E.; de Visser, C.; Perron, G.; Picker, P. J. Solution Chem. 1976, 5, 605-16.
52. Roux, A.; Musbally, G. M.; Perron, G.; Desnoyers, J. E.; Singh, P. P.; Wooley, E. M.; Hepler, L. G. Can. J. Chem. 1978, 56, 24-8.
53. Wu, C.; Berky, M. M.; Hepler, L. G. J. Phys. Chem. 1963, 67, 1202-5.
54. Vasil'ev, V. P.; Kozlovskii, E. V.; Kunin, B. T. Izv. Vyssh. Ucheb. Zaved., Khim. Khim. Teknol. 1973, 16(3), 365-8.
55. Singh, P. P.; Woolley, E. M.; McCurdy, K. G.; Hepler, L. G. Can. J. Chem. 1976, 54, 3315-8.
56. Ramette, R. W.; Sandford, R. W., Jr. J. Am. Chem. Soc. 1965, 87, 5001-5.
57. Helgeson, H. C. J. Phys. Chem. 1967, 71, 3121-36.
58. Edwards, T. J.; Maurer, G.; Newman, J.; Prausnitz, J. M.; AIChE Journal 1978, 24, 966-76.
59. CODATA Special Report, Part VIII, April, 1980.
60. Tsonopoulos, C.; Coulson, D. M.; Inman, L. B. J. Chem. Eng. Data 1976, 21, 190-3.
61. Jordan, J., U.S. Dept. of Energy, Div. of Fossil Energy, Report FE-2710-1, pg. 24 (Jan. 1978) and FE-2710-3, p. 11, 17 (July 1978).
62. Giggenbach, W. Inorg. Chem. 1971, 10, 1333-8.
63. Meyer, B.; Peter, L., private communication, March 1981.
64. Maronny, G. J. chim. phys. et phys.-chim. biol. 1959, 56(2), 202-21.
65. Schwarzenbach, G., and Fischer, A. Helv. Chim. Acta 1960, 43, 1365-90.
66. Boulegue, J.; Michard, G. J. Fr. Hydrol. 1978, 9(1), 27-33.
67. Huss, A., Jr.; Eckert, C. A. J. Phys. Chem. 1977, 81, 2268-70.
68. Connick, R. E.; Tam, T. M.; Deuster, E. V. LBL-12272, 1981.
69. Pitzer, K. S.; Roy, R. N.; Silvester, L. F. J. Am. Chem. Soc. 1977, 99, 4930-6.
70. Hayon, E.; Treinin, A.; Wilf, J. J. Am. Chem. Soc. 1972, 94, 47-57.
71. Olofsson, G.; Spitzer, J. J.; Hepler, L. G. Can. J. Chem. 1978, 56, 1871-3.
72. Gardner, W. L.; Jekel, E. C.; Cobble, J. W. J. Phys. Chem. 1969, 73, 2017-20.
73. Rogers, P. S. Z.; Pitzer, K. S., LBL-12415 (March 1981).
74. Page, F. M. J. Chem. Soc., 1953, 1719-24.
75. Allred, G. C.; Woolley, E. M. J. Chem. Thermodynamics 1981, 13, 155-64.

76. Olofsson, G. J. Chem. Thermodynamics 1975, 7, 507-14.
77. Vanderzee, C. E.; King, D. L. J. Chem. Thermodynamics 1972, 4, 675-83.
78. Vanderzee, C. E.; King, D. L.; Wadsö, I. J. Chem. Thermodynamics 1972, 4, 685-9.
79. Latimer, W. M., "Oxidation Potentials," 2nd Ed., Prentice-Hall, N.Y., 1952.
80. Fraser, R. T. M. J. Chem. Soc., 1965, 1747-9.
81. Pitzer, K. S.; Peiper, J. C. J. Phys. Chem. 1980, 84, 2396-8
82. Peiper, J. C.; Pitzer, K. S. "Thermodynamics of Aqueous Carbonate Solutions Including Mixtures of Sodium Carbonate, Bicarbonate and Chloride," LBL-12725, 1981.
83. Meyer, B., "Urea-Formaldehyde Resins," Addison-Wesley, Reading, Massachusetts, 1979; pp. 26, 27, 31.
84. Christensen, J. J.; Hansen, L. D.; Izatt, R. M., Handbook of Proton Ionization Heats and Related Thermodynamic Quantities, John Wiley, N.Y., 1976.
85. Ackermann, Th.; Schreiner, F. Z. Electrochemie 1958, 62, 1143-51.
86. Pedley, J. B.; Rylance, J., Sussex-N.P.L. Computer Analysed Thermodynamic Data: Organic and Organometallic Compounds, Sussex Univ., 1977.
87. Nichols, N.; Sköld, R.; Spink, C.; Wadsö, I. J. Chem. Thermodynamics 1976, 8, 993-9.
88. Davies, M.; Griffiths, D. M. L. Trans. Far. Soc. 1953, 49, 1405-10.
89. Spitzer, J. J.; Singh, P. P.; Olofsson, I. V.; Hepler, L. G. J. Soln. Chem. 1978, 7, 623-9.
90. Gedansky, L. M.; Hepler, L. G. Can. J. Chem. 1969, 47, 699-701.
91. Spitzer, J. J.; Olofsson, I. V.; Singh, P. P.; Hepler, L. G. J. Chem. Thermodynamics 1979, 11, 233-8.
92. Spitzer, J. J.; Olofsson, I. V.; Singh, P. P.; Hepler, L. G. Thermochim. Acta 1979, 28, 155-60.
93. Wagman, D. D.; Evans, W. H.; Parker, V. B.; Halow, I.; Bailey, S. M.; and Schumm, R. H., Nat. Bur. Stand. U.S. Technical Note 270-4, 1969.
94. Bernarducci, E. E.; Morss, L. R.; Mikeztal, A. R. J. Soln. Chem. 1979, 8, 717-27.
95. Coffy, G.; Olofsson, G. J. Chem. Thermodynamics 1979, 11, 141-44.
96. Spitzer, J. J.; Singh, P. P.; McCurdy, K. G.; Hepler, L. G. J. Soln. Chem. 1978, 7, 81-6.
97. Lin, Bea-Jane, Ph.D. thesis, Lawrence Berkeley Laboratory Report Number 13466, October, 1981.
98. MacLeod, A. C. Trans. Far. Soc. 1973, 169, 2026-35.

99. All of the thermodynamics data for aqueous solutes tabulated in Tables III and IV are given for the solute standard state based on moles per kilogram of water. Up to 100°C, the conventional one-atmosphere (1.01325×10^5 Pa) standard state is used. At higher temperatures, the values are given for the equilibrium pressure of a pure water-steam system. The analytical equations given for $-(G^\circ - H_{298}^\circ)/RT$ incorporate the pressure change. The heat capacities for the aqueous ions are often very negative and change rapidly with temperature. As S° and C_p° for H^+ are taken as zero at all temperatures, the negative ion values will show the rapid changes. The $-(G^\circ - H_{298}^\circ)/RT$ function has the advantage that the heat capacity contributions are canceled out to a large extent and an analytical function for $-(G^\circ - H_{298}^\circ)/RT$ can be quite simple even if the heat capacity is behaving in a complex manner.

In many instances the heat capacities are unknown or poorly known and it was necessary to estimate the behavior of the heat capacity. A variety of models from the literature were used as indicated by the references. Where no reference is given to a model, the values were estimated by comparison with related species and reference (99) is cited.

100. Clever, H. L.; Han, C. H. "Am. Chem. Soc. Symp. Ser." 1980, 133, 513-36.
101. Schulze, G.; Prausnitz, J. M. Lawrence Berkeley Laboratory Report Number 12483 (1981).
102. Benson, B. B.; Krause, D., Jr. J. Chem. Phys. 1976, 64, 689-709.
103. Olofsson, G.; Olofsson, I. J. Chem. Thermodynamics 1981, 13, 437-440.
104. Marshall, W. L.; Franck, E. U. J. Phys. Chem. Ref. Data 1981, 10, 295-304.
105. Barner, H. E.; Scheuerman, R. V. "Handbook of Thermochemical Data for Compounds and Aqueous Species," John Wiley, N.Y., 1978.
106. Criss, C. M.; Cobble, J. W. J. Am. Chem. Soc. 1964, 86, 5385-90, 5390-93.
107. Rüterjans, H.; Schreiner, F.; Sage, U.; Ackermann, Th. J. Phys. Chem. 1969, 73, 986-994.
108. Ahluwalia, J. C.; Cobble, J. W. J. Am. Chem. Soc., 1964, 86, 5381-4.
109. Tanner, J. E.; Lamb, F. W. Journal of Solution Chemistry 1978, 7(4), 303-316.
110. Lee, J. H.; Mather, A. E. Ber. Bunsenges. Physik. Chem. 1977, 81, 1020-3.
111. Rao, S. R.; Hepler, L. G. Hydrometallurgy 1976/77, 2, 293-9.

112. Mason, D. M.; Kao, R. "Am. Chem. Soc. Symp. Ser." 1980, 133, 107-138.
113. Konicek, J.; Wadsö, I. Acta Chem. Scand. 1971, 25, 1541-51.
114. Likke, S.; Bromley, L. A. J. Chem. Eng. Data 1973, 18, 189-195.
115. Eigen, M.; Wicke, E. Z. f. Elektrochem. 1951, 55, 354-63.
116. Silvester, L. F.; Pitzer, K. S. J. Phys. Chem. 1977, 8, 1882-8.

RECEIVED December 23, 1981.

Reliable Data for Flue Gas Desulfurization Processes

BERT R. STAPLES

National Bureau of Standards, Electrolyte Data Center, Washington, DC 20234

A wide variety of physical chemical data and vapor liquid equilibria are required to predict and to extrapolate performance reliability of flue gas desulfurization processes. A chemical and physical model capable of predicting actual scrubber performance is a continuing goal, but any model is only as reliable as the input data. Carefully evaluated thermodynamic and kinetic data are needed to insure consistency, accuracy, and to provide a basis for comparing processes or models. The methodology for the critical evaluation of thermodynamic properties of electrolytes is discussed in general, with emphasis on processes important in flue gas washing systems. How we intend to use the present evaluation systems to provide updated data for flue gas washing processes is also discussed. A number of these specific processes were chosen to illustrate the evaluation procedure. Guidelines are provided for calculating an equilibrium constant, activity coefficient, Gibbs energy and enthalpy of reaction, enthalpy of dilution, and standard enthalpy, Gibbs energy, entropy, and heat capacity. Sources of data and how to use them are discussed.

The Chemical Thermodynamics Data Center and the Electrolyte Data Center are providing the Morgantown Energy Technology Center, Department of Energy, with an evaluated set of data for flue gas desulfurization processes. This data is advantageous to use.

The user is relieved of the burden of examining extensive literature sources to locate, then to judge, and finally to select a value for a thermodynamic property. These have already been done by experts in thermodynamic property evaluation. This provides an immediately usable source of data which is not only accepted as reliable but is also self-consistent with properties of other substances.

This chapter not subject to U.S. copyright.
Published 1982 American Chemical Society.

A critically evaluated and self consistent data base is needed for the thermodynamic properties (ΔH , ΔG , ΔS , C_p , γ_{\pm} , ϕ , K_{eq}) of chemical species important in flue gas desulfurization systems. Such a data base should form the foundation for the design of flue gas washing units and the modeling and predictive schemes used to describe the chemical processes and speciation occurring in these units.

Optimization of a flue desulfurization system depends on its operation and maintenance procedures, the design, the modeling and calculations used to produce the design, and the data base upon which all of these items rest. A 'standard' set of data can make it possible to test a variety of models or calculation schemes and can provide a common basis for comparing them.

The evaluation procedures presently employed at NBS will be briefly reviewed and the use of these procedures to provide updated values applicable to flue gas washing processes will be discussed in this chapter.

Generally, a critical evaluation of chemical thermodynamic data involves a network approach. A small sample of such a network approach is illustrated in Figure 1, for a few barium compounds. Each line represents a reaction (process), each node, represents a compound. The network approach has been discussed in reference (1). Various techniques are used by the analyst in evaluation of the thermodynamic consistency and reliability of individual reaction measurements. One of these is to analyze a given thermochemical network of measurements into various combinations of reactions that result in identical initial and final states. For each such 'loop' the algebraic sum of changes in a thermodynamic variable (ΔH , ΔG) should equal zero except for the combination of experimental uncertainties. Analysis of these residuals from the various loops may reveal certain measurements to be inconsistent with the remainder of the reactions. Similarly, solutions of the entire network using both least sums and least squares techniques are valuable (2). The least sums technique minimizes the sums of the residuals whereas the least squares technique minimizes the sum of the deviations squared. Large residuals found in the solution are indicative of thermodynamic inconsistency with respect to the total set of measurements.

Tests using loop analysis combined with least sums-least squares analysis can also be used to see whether a large-scale revision of data on compounds of a given element is needed or justified. The complexities of such networks can be great, as is the case for the lithium network. This network approach will assist us in evaluating data for flue gas washing processes.

A subset of chemical species have been selected to form the basis of an evaluation for flue gas washing processes. The selection is based on discussions with persons of DOE-Morgantown and from the 1979 FGD workshop proceedings (3). The chemical species include SO_2 and CO_2 , of course, and all combinations of the aqueous cations and anions listed in Table I. Other sulfur containing species will be added in future work.

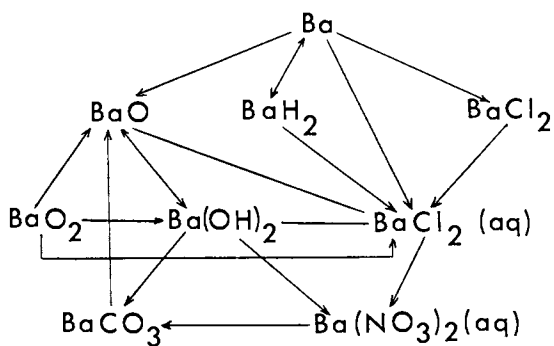


Figure 1. The barium network.

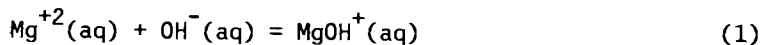
Table I. Chemical Species Important in Flue Gas Desulfurization

SO ₂	CO ₂
Mg ⁺²	OH ⁻
Ca ⁺²	SO ₃ ⁻
Fe ⁺³	HSO ₃ ⁻
Fe ⁺²	SO ₄ ⁼
Mn ⁺²	HSO ₄ ⁻
Na ⁺	CO ₃ ⁼
K ⁺	HCO ₃ ⁻

The properties selected for evaluation include most of the thermodynamic properties which we normally evaluate in the course of our work in the data centers. They include enthalpies of formation, solution, and dilution; Gibbs energies of formation and solution; entropies of formation and solution; heat capacities and equilibrium constants (solubility, ionization, etc); as well as activity and osmotic coefficients, relative apparent molal enthalpies and apparent molal heat capacities.

Properties for processes can be calculated from thermodynamic quantities for individual species. A sample (Table II) from the NBS Interim Report (4), 'A Report on Some Thermodynamic Data For Desulfurization Processes', shows typical values for selected quantities of some chemical species extracted from the NBS Technical Note 270-series (5). A sample (Table III) from the NBS Interim Report illustrates a set of processes for a few reactions related to the flue gas washing process. This reaction table can be constructed from the data on individual species. An example follows:

A calculation of an equilibrium constant for the formation of the ion pair MgOH⁺ from the reaction (1) is illustrated in equations (2) and (3) below.



$$\Delta G^{\circ} = \sum n_i (\Delta G^{\circ}f)_i \text{ products} - \sum n_i (\Delta G^{\circ}f)_i \text{ reactants} \quad (2)$$

$$\ln K = \frac{-\Delta G^{\circ}}{RT} = \frac{a(\text{MgOH}^{+})}{a(\text{Mg}^{+2})a(\text{OH}^{-})} \quad (3)$$

Equilibrium constants (ionization, complexation, and solubility) can be calculated from the data contained in the NBS Technical

Table II. Sample Property Table.

Enthalpy, Gibbs Energy of Formation, Entropy, and Heat Capacity

Substance Formula and Description	$\Delta_f H^\circ$	$\Delta_f G^\circ$	$H^\circ - H^\circ_0$	S°	C_p°
	298.15 K (25 °C)				
	kcal/mol			cal/deg·mol	
$\text{HSO}_3^-(\text{ao})$	-149.67	-126.15	---	33.4	---
$\text{HSO}_4^-(\text{ao})$	-212.08	-180.69	---	31.5	-20.
$\text{H}_2\text{SO}_3(\text{ao}) =$ $(\text{SO}_2 + \text{H}_2\text{O})$	-145.51	-128.56	---	55.5	---
$\text{H}_2\text{SO}_4(1)$	-194.548	-164.938	6.748	37.501	33.20
$\text{H}_2\text{SO}_4(\text{a})$	-217.32	-177.97	---	4.8	-70.
$\text{H}_2\text{SO}_4 \cdot \text{H}_2\text{O}(1)$	-269.508	-227.182	---	50.56	51.35
$\text{H}_2\text{SO}_4 \cdot 2\text{H}_2\text{O}(1)$	-341.085	-286.770	---	66.06	62.34
$\text{H}_2\text{SO}_4 \cdot 3\text{H}_2\text{O}(1)$	-411.186	-345.178	---	82.55	76.23
$\text{H}_2\text{SO}_4 \cdot 4\text{H}_2\text{O}(1)$	-480.688	-403.001	---	99.09	91.35
$\text{H}_2\text{SO}_4 \cdot 6.5\text{H}_2\text{O}(1)$	-653.264	-546.403	---	140.51	136.30
$\text{CO}_2(\text{g})$	-94.051	-94.254	2.2378	51.06	8.87
$\text{CO}_2(\text{ao})$	-98.90	-92.26	---	28.1	---
$\text{CO}_3^{2-}(\text{a})$	-161.84	-126.17	---	-13.6	---
$\text{HCO}_3^-(\text{ao})$	-165.39	-140.26	---	21.8	---
$\text{H}_2\text{CO}_3(\text{ao})$	-167.22	-148.94	---	44.8	---

Table III. Sample Table of Processes.
 Enthalpy and Gibbs Energy of Reaction Entropy and Heat Capacity Changes of Reaction and Equilibrium Constant

Reaction [298.15 K (25 °C)]	ΔH° kcal/mol	ΔG° kcal/mol	ΔS° cal/deg·mol	ΔC_p°	log K
$\text{CaO}(c) + \text{H}_2\text{O}(l) \rightarrow \text{Ca}(\text{OH})_2(c)$	-15.575	-13.703	-6.28	-6.315	10.044
$\text{Ca}(\text{OH})_2(c) \rightarrow \text{Ca}(\text{OH})_2(a)$	-4.00	7.27	-37.73	---	-5.329
$\text{Ca}(\text{OH})_2^{\frac{1}{2}}(ao) \rightarrow \text{Ca}^{+2}(a) + \text{OH}^-(a)$	---	1.81	---	---	-1.324
$\text{CaSO}_3(c) \rightarrow \text{CaSO}_3(a)$	---	---	-43.93	---	---
$\text{CaSO}_3 \cdot 0.5\text{H}_2\text{O}(c) \rightarrow \text{CaSO}_3(a) + 0.5\text{H}_2\text{O}(l)$	-2.30	9.70	-40.34	---	-7.108
$\text{CaSO}_4(c, \alpha, \text{soluble}) \rightarrow \text{CaSO}_4(a)$	-6.42	3.66	-33.8	---	-2.683
$\text{CaSO}_4(c, \beta, \text{soluble}) \rightarrow \text{CaSO}_4(a)$	-7.48	2.60	-33.8	---	-1.906
$\text{CaSO}_4(c, \text{insoluble, anhydrite}) \rightarrow \text{CaSO}_4(a)$	-4.30	5.66	-33.4	---	-4.149
$\text{CaSO}_4 \cdot 0.5\text{H}_2\text{O}(c, \alpha) \rightarrow \text{CaSO}_4(a) + 0.5\text{H}_2\text{O}(l)$	-4.368	4.796	-30.74	---	-3.5158
$\text{CaSO}_4 \cdot 0.5\text{H}_2\text{O}(c, \beta) \rightarrow \text{CaSO}_4(a) + 0.5\text{H}_2\text{O}(l)$	-4.868	4.566	-31.64	---	-3.3473
$\text{CaSO}_4 \cdot 2\text{H}_2\text{O}(c) \rightarrow \text{CaSO}_4(a) + 2\text{H}_2\text{O}(l)$	-0.270	5.956	-20.88	---	-4.3658
$\text{CaCO}_3(c, \text{calcite}) \rightarrow \text{CaCO}_3(a)$	-3.12	11.33	-48.5	---	-8.305
$\text{CaCO}_3(c, \text{aragonite}) \rightarrow \text{CaCO}_3(a)$	-3.07	11.08	-47.5	---	-8.122

Note 270-series (5), which is based on all available experimental data. Thus, a very large body of standard reference data can be applied immediately to the practical flue gas problem. This relieves the user of the burden of selecting values of ΔG_i .

The procedures for extracting such values from the 270-series, series, which were briefly outlined in equations (1-3), have been discussed more extensively by the present author (6).

Aqueous Solution Properties

Aqueous solution processes and the properties of aqueous species are of prime interest in wet lime-limestone and other liquid phase scrubber units. Accordingly, thermodynamics properties of interest include, but are not limited to ΔH_f° , γ_{\pm} , ϕ , ϕ_L , and K_{eq} .

The NBS Tech. Note 270-series provides some of these evaluated properties. Values of ΔH_f° and ΔG_f° are tabulated directly for aqueous species at 298 K. It has been illustrated (eqs 1-3, and ref. 6) that an equilibrium constant can be calculated from the tabulated values of ΔG_f° . Some of these values will change and will be based upon newer experimental results. This will be discussed later in the chapter.

The relative apparent molal enthalpy, ϕ_L , can be obtained from the tabulated ΔH_f° values, for example

$$\phi_L (\text{aq}, n \text{ H}_2\text{O}) = \Delta H_f^\circ (\text{aq}, n \text{ H}_2\text{O}) - \Delta H_f^\circ (\text{aq}, \infty) \quad (4)$$

Table IV shows the results of the ϕ_L calculation for $\text{CaSO}_4(\text{aq})$, as well as for the activity and osmotic coefficient results.

Activity and osmotic coefficients can be calculated using various semitheoretical equations. There have been two major efforts towards the evaluation of activity and osmotic coefficients during the past 10 years. Pitzer and coworkers have formulated a set of equations of the virial coefficient type consistent with both the modern statistical mechanical description of electrolyte solutions and the basic principles of thermodynamics of solutions. The Electrolyte Data Center at NBS (Goldberg, Nuttall, and Staples) has completed many detailed critical evaluations of electrolytes using an extensive data base of all available experimental data and have used extended forms of Hamer-Wu (8), Lietzke-Stoughton (9) equations, and more recently, extensions of the Pitzer equations. Basically all of these sets of equations have been employed in the representation of activity data for tables for FGD applications. The activity and dilution data are given in Tables IV-IX, for six salts. Pitzer equations, published thus far, sometimes do not cover the more concentrated ranges of interest (saturated or supersaturated solutions). Reevaluated Pitzer coefficients are being tabulated at NBS, which will cover wide ranges of concentration as do the Hamer-Wu and Lietzke-Stoughton equations.

**American Chemical
Society Library
1155 16th St., N.W.**

Table IV. CaSO_4 Relative Apparent Molal Enthalpy and Activity Coefficients
at 298.15 K

$n \text{ H}_2\text{O}$	$\Delta_f H$ kcal mol^{-1}	ϕ_L cal mol^{-1}	γ_{\pm}	ϕ	m mol kg^{-1}
5000.00	-346.414	646.	.3714	.7111	.01110
7500.00	-346.518	542.	.4276	.7410	.00740
10000.00	-346.566	494.	.4695	.7631	.00555
20000.00	-346.685	375.	.5729	.8166	.00278
50000.00	-346.827	233.	.7000	.8784	.00111
100000.00	-346.915	145.	.7791	.9140	.00056
500000.00	-347.009	51.	.8986	.9633	.00011
1000000.00	-347.026	34.	.9284	.9746	.00006
∞	-347.060	0			0

$$\Delta_f H^\circ = -347.060 \text{ kcal mol}^{-1} \quad \text{Number of molalities} = 8$$

Enthalpy data taken from NBS TN 270-Series [5]

Activity coefficient data from [7]

Constants for the activity coefficient equation (eqns. 5-11) :

$$b = 1.20\text{E}+00 \quad \alpha_1 = 1.40\text{E}+00 \quad \alpha_2 = 1.20\text{E}+01$$

$$\beta^0 = 2.00\text{E}-01 \quad \beta^1 = 2.65\text{E}+00 \quad \beta^2 = -5.57\text{E}+01$$

$$C^\phi = 0.00\text{E}+00$$

Table V. MgSO_4 Relative Apparent Molal Enthalpy and Activity Coefficients
at 298.15 K

$n \text{ H}_2\text{O}$	$\Delta_f H$ kca mol ⁻¹	ϕ_L cal mol ⁻¹	γ^\pm	ϕ	m mol kg ⁻¹
20.00	-327.100	1800.	.0513	.8481	2.77540
25.00	-327.200	1700.	.0469	.7072	2.22032
50.00	-327.410	1490.	.0522	.5340	1.11016
75.00	-327.520	1380.	.0624	.5194	.74011
100.00	-327.590	1310.	.0718	.5228	.55508
200.00	-327.740	1160.	.1016	.5459	.27754
300.00	-327.820	1080.	.1238	.5633	.18503
400.00	-327.880	1020.	.1421	.5772	.13877
500.00	-327.930	970.	.1578	.5888	.11102
600.00	-327.970	930.	.1716	.5989	.09251
800.00	-328.040	860.	.1954	.6156	.06939
1000.00	-328.080	820.	.2154	.6291	.05551
2000.00	-328.202	698.	.2866	.6722	.02775
5000.00	-328.358	542.	.4003	.7334	.01110
10000.00	-328.467	433.	.4976	.7835	.00555
20000.00	-328.581	319.	.5969	.8328	.00278
50000.00	-328.707	193.	.7163	.8883	.00111
100000.00	-328.774	126.	.7898	.9202	.00056
∞	-328.900	0			0

$$\Delta_f H^\circ = -328.900 \text{ kcal mol}^{-1} \quad \text{Number of molalities} = 18$$

Enthalpy data taken from NBS TN 270-Series [5]

Activity coefficient data from [7]

Constants for the activity coefficient equation (eqns. 5-11) :

$$b = 1.20\text{E}+00 \quad \alpha_1 = 1.40\text{E}+00 \quad \alpha_2 = 1.20\text{E}+01$$

$$\beta^\circ = 2.21\text{E}-01 \quad \beta^1 = 3.343\text{E}+00 \quad \beta^2 = -3.723\text{E}+01$$

$$c^\phi = 2.50\text{E}-02$$

Table VI. H_2SO_3 Relative Apparent Molal Enthalpy and Activity Coefficients
at 298.15 K

$n \text{ H}_2\text{O}$	$\Delta_f H$ kcal mol^{-1}	ϕ_L cal mol^{-1}	γ_{\pm}	ϕ	m mol kg^{-1}
100.00	-146.369	5531.			.55508
150.00	-146.541	5359.			.37005
200.00	-146.670	5230.			.27754
250.00	-146.773	5127.			.22203
300.00	-146.862	5038.			.18503
400.00	-147.006	4894.			.13877
500.00	-147.126	4774.			.11102
750.00	-147.351	4549.			.07401
1000.00	-147.516	4384.			.05551
1500.00	-147.776	4124.			.03701
2000.00	-147.957	3943.			.02775
2500.00	-148.091	3809.			.02220
3000.00	-148.206	3694.			.01850
3500.00	-148.304	3596.			.01586
4000.00	-148.383	3517.			.01388
5000.00	-148.524	3376.			.01110
7500.00	-148.758	3142.			.00740
10000.00	-148.899	3001.			.00555
∞	-151.900	0			0

$\Delta_f H^\circ = -151.900 \text{ kcal mol}^{-1}$ Number of molalities = 18
for $[2\text{H}^+ + \text{SO}_3^-]$

Enthalpy data taken from NBS TN 270-Series [5]
 H_2SO_3 is thermodynamically equivalent to $\text{SO}_2 + \text{H}_2\text{O}$. They are
not distinct species. Both the SO_2 and H_2SO_3 tables are for
the formation of the real solution, including all effects of
ionization.

Table VII. SO₂Relative Apparent Molal Enthalpy and Activity Coefficients
at 298.15 K

n H ₂ O	$\Delta_f H$ kcal mol ⁻¹	ϕ_L cal mol ⁻¹	γ_{\pm}	ϕ	m mol kg ⁻¹
100.00	-78.054	5531.			.55508
150.00	-78.226	5359.			.37005
200.00	-78.355	5230.			.27754
250.00	-78.458	5127.			.22203
300.00	-78.547	5038.			.18503
400.00	-78.691	4894.			.13877
500.00	-78.811	4774.			.11102
750.00	-79.036	4549.			.07401
1000.00	-79.201	4384.			.05551
1500.00	-79.461	4124.			.03701
2000.00	-79.642	3943.			.02775
2500.00	-79.776	3809.			.02220
3000.00	-79.891	3694.			.01850
3500.00	-79.989	3596.			.01586
4000.00	-80.068	3517.			.01388
5000.00	-80.209	3376.			.01110
7500.00	-80.443	3142.			.00740
10000.00	-80.584	3001.			.00555
∞	-83.585	0			0

$\Delta_f H^\circ = -83.585 \text{ kcal mol}^{-1}$ Number of molalities = 18
[completely ionized - See note on Table VI. H₂SO₃]

Enthalpy data taken from NBS TN 270-Series [5]

Table VIII. Na_2SO_3
Relative Apparent Molal Enthalpy and Activity Coefficients
at 298.15 K

$n \text{ H}_2\text{O}$	$\Delta_f H$ kcal mol^{-1}	ϕ_L cal mol^{-1}	γ_{\pm}	ϕ	m mol kg^{-1}
30.00	-266.290	0.	.1989	.7124	1.85027
50.00	-266.290	0.	.2292	.7026	1.11016
100.00	-266.290	0.	.2866	.7281	.55508
2000.00	-266.290	0.	.6074	.8581	.02775
10000.00	-266.290	0.	.7705	.9195	.00555
50000.00	-266.290	0.	.8812	.9593	.00111
200.00	-266.510	-220.	.3529	.7580	.27754
800.00	-266.410	-120.	.5029	.8177	.06939
∞	-266.290	0			0

$\Delta_f H^\circ = -266.290 \text{ kcal mol}^{-1}$ Number of molalities = 8

Enthalpy data taken from NBS TN 270-Series [5]

Activity coefficient data from [11]

Constants for the activity coefficient equation (eqns. 12,13) :

$$B = 1.32416014\text{E}+00$$

$$C = -2.69200069\text{E}-01$$

$$D = 6.67319796\text{E}-02$$

Table IX. Na_2SO_4
Relative Apparent Molal Enthalpy and Activity Coefficients
at 298.15 K

$n \text{ H}_2\text{O}$	$\Delta_f H$ kcal mol^{-1}	ϕ_L cal mol^{-1}	γ^\pm	ϕ	m mol kg^{-1}
18.00	-333.852	-1752.	.1389	.6735	3.08378
20.00	-333.800	-1700.	.1411	.6539	2.77540
25.00	-333.593	-1493.	.1494	.6303	2.22032
28.37	-333.491	-1391.	.1558	.6252	1.95658
30.00	-333.432	-1332.	.1590	.6244	1.85027
40.00	-333.165	-1065.	.1780	.6302	1.38770
50.00	-332.988	-888.	.1953	.6417	1.11016
60.00	-332.840	-740.	.2107	.6532	.92513
80.00	-332.605	-505.	.2367	.6726	.69385
100.00	-332.420	-320.	.2581	.6876	.55508
120.00	-332.275	-175.	.2762	.6996	.46257
140.00	-332.184	-84.	.2919	.7093	.39649
160.00	-332.122	-22.	.3058	.7175	.34693
180.00	-332.076	24.	.3183	.7246	.30838
200.00	-332.040	60.	.3296	.7308	.27754
250.00	-331.980	120.	.3540	.7435	.22203
300.00	-331.943	157.	.3743	.7537	.18503
350.00	-331.918	182.	.3919	.7622	.15859
400.00	-331.901	199.	.4072	.7694	.13877
500.00	-331.879	221.	.4333	.7813	.11102
600.00	-331.867	233.	.4549	.7910	.09251
800.00	-331.857	243.	.4894	.8060	.06939
1000.00	-331.855	245.	.5163	.8176	.05551
2000.00	-331.872	228.	.5991	.8520	.02775
3000.00	-331.892	208.	.6457	.8707	.01850
4000.00	-331.907	193.	.6774	.8832	.01388
5000.00	-331.920	180.	.7010	.8924	.01110
10000.00	-331.958	142.	.7677	.9178	.00555
20000.00	-331.992	108.	.8235	.9385	.00278
50000.00	-332.027	73.	.8805	.9589	.00111
∞	-332.100	0			0

$$\Delta_f H^\circ = -332.100 \text{ kcal mol}^{-1}$$

Number of molalities = 30

Enthalpy data taken from NBS TN 270-Series [5]

Activity coefficient data from [11]

Constants for the activity coefficient equation (eqns. 12,13) :

$$B = 1.21597315\text{E}+00 \quad E = -4.86954126\text{E}-03$$

$$C = -3.55728552\text{E}-01$$

$$D = 8.29465562\text{E}-02$$

For the NBS report (4), the activity and osmotic coefficients of 2 : 2 charge type electrolyte ($MgSO_4$, $CaSO_4$, and $MnSO_4$) have been calculated from the Pitzer equations (7).

For the activity coefficient of these 2:2 salts, the equation is

$$\ln \gamma = 4_f^Y + mB_{mx}^Y + m^2 C_{mx}^Y \quad (5)$$

where

$$f^Y = -A_\phi [I^{1/2}/(1 + bI^{1/2}) + (2/b) \ln(1 + bI^{1/2})] \quad (6)$$

and

$$B_{mx}^Y = 2\beta_{mx}^{(0)} + (2\beta_{mx}^{(1)}/\alpha_1^2 I) [1 - (1 + \alpha_1 I^{1/2} - \frac{1}{2}\alpha_1^2 I)e^{-\alpha_1 I^{1/2}}] \quad (7)$$

$$+ (2\beta_{mx}^{(2)}/\alpha_2^2 I) [1 - (1 + \alpha_2 I^{1/2} - \frac{1}{2}\alpha_2^2 I)e^{-\alpha_2 I^{1/2}}]$$

and

$$C_{mx}^Y = \frac{3}{2} C_{mx}^\phi \quad (8)$$

The osmotic coefficient equation is

$$\phi - 1 = 4_f^\phi + mB_{mx}^\phi + m^2 C_{mx}^\phi \quad (9)$$

where

$$f^\phi = -A_\phi [I^{1/2}/(1 + bI^{1/2})] \quad (10)$$

and

$$B_{mx}^\phi = \beta_{mx}^{(0)} + \beta_{mx}^{(1)} e^{-\alpha_1 I^{1/2}} + \beta_{mx}^{(2)} e^{-\alpha_2 I^{1/2}} \quad (11)$$

Definition of terms are detailed in reference (7) and parameters for these equations are given in the appropriate tables in reference (4).

For a more detailed discussion of the Pitzer equations the reader is referred to reference (7), as well as to G. Rosenblatt's paper in these proceedings.

For the uni-univalent compounds, and the unsymmetrical charge types, uni-bi and bi-univalent compounds the activity and osmotic coefficients have been calculated from the Hamer-Wu, Lietzke-Stoughton equations used in previous evaluations (8,9).

The equation for the osmotic coefficient is

$$\phi = 1 + \{ z_+ z_- A_m [-(1+B I^{1/2}) + 2 \ln(1+B I^{1/2})] + 1/(1 + B I^{1/2}) + 1/2 C_m + 2/3 D_m^2 + 3/4 E_m^3 + \dots \} \quad (12)$$

and the activity coefficient

$$\ln \gamma = \frac{-|z_+ z_-| A I^{1/2} + C_m + D_m^2 + E_m^3 + \dots}{1 + B I^{1/2}} \quad (13)$$

The parameters for these equations are tabulated in the appropriate tables in reference (4). Activity coefficients for these charge types may also be calculated from the Pitzer equations for the uni-univalent and uni-bi and bi-univalent salts. In these cases, the Pitzer equations are sometimes applicable to a more limited concentration range. If the concentration being investigated is beyond the range of validity specified by Pitzer, the Hamer-Wu, Lietzke-Stoughton equations are recommended.

Future Evaluations

Future directions for evaluation efforts at the NBS data centers include the following.

1. Adjustments must be made in the tables of thermodynamic properties to account for new, or better data, while maintaining the overall unity and consistency of these tables. For example, from the NBS Tech. Note 270-series, 'Selected Values of Thermodynamic Properties,' a ΔG° of solution of $\text{CaSO}_4 \cdot 2\text{H}_2\text{O}(c)$ of $5.96 \text{ kcal}\cdot\text{mol}^{-1}$ is obtained. This leads to a solubility constant, K_s° , of 4.3×10^{-5} (from equation 3). More recent data indicate a value of $\Delta G^\circ = 6.25 \text{ kcal}\cdot\text{mol}^{-1}$, which results in a $K_s^\circ = 2.63 \times 10^{-5}$, a difference of 65% in the K_s° value previously predicted.

2. Property values will be extended beyond 298 K and equations will be provided to calculate properties as a function of temperature, initially over the range of about 0 - 100°C. This range will bracket the 50-60° temperatures typically found in wet scrubbers.

3. The NBS data base on aqueous solutions will be used to obtain parameters for the Pitzer equations for activity data over extended ranges of concentration. Interaction parameters for mixed electrolytes will be evaluated.

4. Plans also include means to estimate and develop predictive schemes to obtain data where no measurements have been made and to develop methods to handle the properties of mixtures based on the Pitzer equations, particularly for the activity coefficients.

Acknowledgments

The data evaluation work and the formulation of flue gas data tables described in this paper have been carried out by Vivian Parker, David Neumann, and Thomas Jobe who deserve recognition for their significant efforts. Special thanks go to Kim Brandenburg for all of her assistance with this manuscript. This work was supported by the Department of Energy (METC) under contract #DE AT21-79MC11593.

Literature Cited

1. Wagman, D. D., Garvin, D., Parker, V. B., Schumm, R. H., Pedley, J. B., 'New Development in the Evaluation of Thermochemical Data', National Measurement Laboratory, 1979 Technical Highlights, National Bureau of Standards, NBS-SP572, U. S. Government Printing Office, Washington, DC, April 1980.
2. Garvin, D., Parker, V. B., Wagman, D. D., Evans, W. H., "A combined Least Sums and Least Squares Approach to the Evaluation of Thermodynamic Data Networks", NBSIR 76-1147, U. S. Department of Commerce, National Bureau of Standards, Washington, DC 20234, July 1976.
3. Workshop on Sulfur Chemistry in Flue Gas Desulfurization, U.S. Department of Energy, Morgantown Energy Technology Center, Morgantown, WV 26505, June 7-8, 1979.
4. Parker, V. B., B. R. Staples, T. L. Jobe, Jr., and D. Neumann, 'A Report on Some Thermodynamic Data for Desulfurization Processes', NBSIR 81-2345, U.S. Department of Commerce, National Bureau of Standards, Washington, DC 20234, September 1981.
5. Wagman, D. D., Evans, W. H., Parker, V. B., Halow, I., Bailey, S. M., and Schumm, R. H., NBS Tech Note 270-3 (1968) Idem, Tech Note 270-4 (1969) Wagman, D. D., Evans, W. H., Parker, V. B., Halow, I., Bailey, S. M., Schumm, R. H., and Churney, K. L., NBS Tech Note 270-5 (1971) Parker, V. B., Wagman, D. D., and Evans, W. H., NBS Tech Note 270-6 (1971) Schumm, R. H., Wagman, D. D., Bailey, S. M., Evans, W. H., and Parker, V. B., Tech Note 270-7 (1973) and Wagman, D. D., Evans, W. H., Parker, V. B., Schumm, R. H., and Nuttall, R. L., NBS Tech Note 270-8 (1981).
6. Staples, B. R., Environ. Sci. and Tech. 12, 339 (1978).
7. Pitzer, K. S., Mayorga, G., J. Solution Chem. 3, 539 (1974).
8. Hamer, W. J., and Wu, Y.-C., J. Phys. Chem. Reference Data, 1, 1047 (1972).
9. Lietzke, H., Stoughton, R. W., J. Phys. Chem. 64, 816 (1960).
10. Staples, B. R., Nuttall, R. L., J. Phys. Chem. Reference Data 6, 395 (1977).
11. Goldberg, R. N., J. Phys. Chem. Reference Data 10, 671 (1981).

RECEIVED February 25, 1982.

Use of Pitzer's Equations to Estimate Strong-Electrolyte Activity Coefficients in Aqueous Flue Gas Desulfurization Processes

GERD M. ROSENBLATT

University of California, Los Alamos National Laboratory, Los Alamos, NM 87545

The computer code which is in current widespread use for analyzing the chemistry taking place in aqueous flue-gas-desulfurization (FGD) processes is based upon modified Debye-Hückel single-ion activity coefficients and specific associations between oppositely charged ions. Recently, Pitzer and coworkers have presented equations for electrolyte activity coefficients in aqueous solutions which differ significantly in form and parameters, and also in predictions for model mixtures pertinent to FGD. The Pitzer equations have been shown to reproduce the behavior of complex, concentrated aqueous mixtures under a wide variety of conditions. In Pitzer's approach, both single- and mean-ion activity coefficients are calculated by summing over all interactions in the solution without involving specific associations, all interactions being described by the activity coefficients. Because they are a convergent series, the equations can be used at various levels of complexity and accuracy. When experimental data are unavailable, they can be truncated so that they contain only a few parameters. Those few parameters can be estimated empirically. Under these conditions, activity coefficients are estimated to an accuracy which will typically be better than 25%. It is concluded that Pitzer's equations offer a promising approach for thermodynamic modeling of FGD chemistry.

0097-6156/82/0188-0057\$06.00/0

© 1982 American Chemical Society

Introduction

It is more than a decade since P. S. Lowell and associates⁽¹⁾ developed the basic chemical thermodynamic approach underlying the widely used Bechtel-modified Radian equilibrium computer code for aqueous flue-gas-desulfurization systems. In that code, activities are calculated by combining association equilibria for strongly attractively-interacting ion-pairs with extended-Debye-Hückel single-ion activity coefficients. The Debye-Hückel coefficients depend upon a parameter for the ion and upon the ionic strength of the solution but not upon the nature of the other ions present. It has long been recognized that there are problems in using Debye-Hückel-based activity coefficients in solutions where the molal ionic strength is greater than ~ 0.2 . This leads one to ask:

- 1) In the intervening ten years, has there been developed a more accurate way (or ways) to describe activity coefficients in complex, concentrated aqueous solutions of strong electrolytes?
- 2) Can this be adapted to solutions, such as are encountered in FGD chemistry, for which the required thermodynamic parameters have not been measured?
- 3) Do activities and solubilities calculated from this alternate approach differ from those calculated with association-equilibrium extended-Debye-Hückel models under conditions of interest in FGD wet scrubbing?
- 4) Is there still more to be done to describe the thermodynamic properties of aqueous solutions of interest in flue-gas desulfurization?

In the author's opinion the answer to these four questions is "Yes." Pitzer and coworkers⁽²⁻¹²⁾ have put into practical form recent developments in the statistical mechanics of electrolyte solutions so as to obtain equations for activity and osmotic coefficients which sum over pairwise interactions for all ions present in the solution. The activity coefficients for ions in mixtures thus calculated reflect the differences in the degrees of interaction between various ions. Such calculations have been demonstrated to reproduce experiment closely even at high concentrations. Pitzer's equations require parameters for all ion pairs present in the mixture. When experimental data are not available, the required parameters may be estimated by empirical methods based upon a correlation between the parameters and the water "structure-making" or "breaking" tendencies of the ions⁽¹³⁾. When parameters must be estimated, Pitzer's equations can be truncated to reduce the number of parameters. Using the theory in this simplified form, approximate calculations can be made for complex mixtures using only pure-electrolyte quantities, either estimated or experimental. Pitzer's equations have been used previously as the basis for thermodynamic estimates, in a somewhat different way and for a different application, by Edwards et al.⁽¹⁴⁾

This paper first presents Pitzer's equations for single-ion activities in the truncated form appropriate to approximate calculations. Then, it describes sources of the experimental and

estimated parameters required for calculations on FGD mixtures. Next, it reviews the accuracy of such approximate calculations and their sensitivity to changes in input parameters. Then it compares Pitzer-equation calculations for simple model solutions relevant to FGD with Radian-code calculations, illustrating some potentially significant differences in the results.

Summary of Pitzer's Equations

The treatment starts from a generalized virial expansion for G^{XS} , the total Gibbs energy of the solution minus the Gibbs energy of an ideal solution of the same composition. Although the virial coefficients are not individually measurable, measurable combinations of the virial coefficients have been identified (2,5). Differentiation of G^{XS} with respect to the amount of water allows computation of the activity of the water and differentiation with respect to the amount of an ion yields the activity coefficient of that ion.

The expression (5,15,16) for the activity of water in a solution containing various cations c and anions a is

$$\ln a_{H_2O} = -0.018015 \left\{ \begin{aligned} & \sum_i m_i - 2A_\phi I^{3/2} / (1 + \rho I^{1/2}) \\ & + 2 \sum_{ca} \sum_c m_c m_a [B_{ca}^\phi + ZC_{ca}] \\ & - \sum_{cc'} m_c m_{c'} \theta_{cc'} + \sum_{aa'} m_a m_{a'} \theta_{aa'} \end{aligned} \right\} \quad (1)$$

In this equation m represents molality, z represents ion charge, $I = \frac{1}{2} \sum_i m_i z_i^2$ is the ionic strength, and $Z = \sum_i m_i z_i$. The quantities A_ϕ , B^ϕ , C and θ are related to the virial coefficients and are described further below, as is ρ .

Although one can usually only measure mean-ion activity coefficients for neutral combinations of ions, it is sometimes convenient to use expressions for single-ion activity coefficients which can then be combined to obtain mean-ion coefficients. For ion-pair $M_{\nu_M}^{z_M} X_{\nu_X}^{z_X}$

$$\ln \gamma_{MX} = (\nu_M/\nu) \ln \gamma_M + (\nu_X/\nu) \ln \gamma_X \quad (2)$$

where $\nu = \nu_M + \nu_X$. For the single ions M^{z_M} and X^{z_X} (12,16).

$$\begin{aligned} \ln \gamma_M = z_M^2 f^Y + \sum_a [2 B_{Ma} + ZC_{Ma}] \\ + 2 \sum_c \theta_{Mc} + \sum_{ca} \sum_c m_c [z_M^2 B_{ca}' + z_M^C C_{ca}] \end{aligned} \quad (3a)$$

$$\ln \gamma_X = z_X^2 f^\gamma + \sum_c [2B_{cX} + zC_{cX}] + 2 \sum_a \theta_{Xa} + \sum_{ca} \sum_c m_a [z_X^2 B'_{ca} + |z_X| C_{ca}] \quad (3b)$$

For the Debye-Hückel term f^γ (with γ a superscript, not a power), Pitzer⁽²⁾ chose the extended form

$$f^\gamma = -A_\phi [I^{1/2}/(1 + \rho I^{1/2}) + (2/\rho) \ln(1 + \rho I^{1/2})] \quad (4)$$

where $\rho = 1.2$ is related to an average ion hard-core diameter. Perhaps the most critical evaluation of the Debye-Hückel osmotic-coefficient constant A_ϕ is that of Clarke and Glew⁽¹⁷⁾ who obtain

$$A_\phi = -16.39023 + 261.3371 T^{-1} + 3.3689633 \ln T - 1.437167(T/100) + 0.111995(T/100)^2 \quad (5)$$

which at $T = 298.15$ K (25°C) yields $A_\phi = 0.392$. This value of A_ϕ was used by Pitzer and Mayorga^(13,14) in evaluating ion-pair parameters and it is necessary to use that same value when working with those parameters.

The virial coefficients B^ϕ , B , B' , and C describe the thermodynamic properties of a pure electrolyte. The second virial coefficients B^ϕ , B and B' arise from binary interactions and have an ionic strength dependence similar to that suggested by statistical mechanics:

$$B_{MX}^\phi = \beta_{MX}^{(0)} + \beta_{MX}^{(1)} e^{-\alpha_1 I^{1/2}} + \beta_{MX}^{(2)} e^{-\alpha_2 I^{1/2}} \quad (6)$$

$$B_{MX} = \beta_{MX}^{(0)} + \frac{2\beta_{MX}^{(0)}}{\alpha_1^2 I} \left[1 - (1 + \alpha_1 I^{1/2}) e^{-\alpha_1 I^{1/2}} \right] + \frac{2\beta_{MX}^{(1)}}{\alpha_2^2 I} \left[1 - (1 + \alpha_2 I^{1/2}) e^{-\alpha_2 I^{1/2}} \right] \quad (7)$$

$$B'_{MX} = \frac{2\beta_{MX}^{(1)}}{\alpha_1^2 I^2} \left[-1 + (1 + \alpha_1 I^{1/2}) + \frac{1}{2} \alpha_1^2 I e^{-\alpha_1 I^{1/2}} \right] + \frac{2\beta_{MX}^{(2)}}{\alpha_2^2 I^2} \left[-1 + (1 + \alpha_2 I^{1/2}) + \frac{1}{2} \alpha_2^2 I e^{-\alpha_2 I^{1/2}} \right] \quad (8)$$

The third virial coefficient C is related to ternary interactions. Its dependence upon ionic strength is negligible.

$$C_{MX}^{\phi} = \frac{C_{MX}^{\phi}}{2|z_M z_X|^{1/2}} \quad (9)$$

Equations (7)-(9) contain the parameters, $\beta^{(0)}$, $\beta^{(1)}$, $\beta^{(2)}$ and C^{ϕ} . These have been tabulated for a large number of pure electrolytes by Pitzer and Mayorga (13,4) who fit experimental data for 1-1, 1-2, 2-1, 1-3, 3-1, 1-4 and 1-5 electrolytes by taking $\alpha_1 = 2$ and neglecting the terms in α_2 and $\beta^{(2)}$ in Eqs. (6)-(8) (i.e., setting $\beta^{(2)} = 0$). For all 2-2 electrolytes, $\alpha_1 = 1.4$ and $\alpha_2 = 12.0$. The temperature dependencies of these pure-electrolyte parameters are found (10) to be small. Typical values for $d\beta^{(0)}/dT$ are about 10^{-3} . A consequence is that temperature changes of 25° or so lead to no significant change in $\beta^{(0)}$ or $\beta^{(1)}$. In addition, calculated activity coefficients are relatively insensitive to moderate changes in $\beta^{(0)}$ and $\beta^{(1)}$ (13). The third virial coefficient C^{ϕ} is small.

For mixtures (5) there is an additional parameter Θ in eqs. (1) and (3) which gives the deviation in the second virial coefficient MN for ions M and N of the same sign from the average for $M-M$ and $N-N$ interactions. As one might anticipate, Θ_{MN} is small, <0.1 . Apparently Θ significantly affects λ_{ν} only in systems involving mixing of singly-charged ions which differ greatly in their interaction with water (e.g., Cs^+ with H^+ or Cl^- with OH^-). Pitzer and Kim (5) introduced further mixing parameters Θ_{MN}^+ and ψ_{MNX} , the latter arising from the differences in mixture third-virial coefficients, but these terms are smaller than Θ and are neglected in approximate calculations. Neglect of such terms introduces little error in mixtures of 1-1 electrolytes (18) but can limit the accuracy of approximations for unsymmetrical mixtures at high concentrations (16). Also, for complex mixtures containing ions of various charges, such as are encountered in FGD chemistry and in geochemistry, accurate work (16) requires that one include additional, unparameterized, electrostatic mixing terms (6) which arise upon mixing ions of the same sign but different charge.

Approximate Calculations and Estimated Parameters.

Using eqs. (1)-(9), along with empirical pure-electrolyte parameters $\beta^{(0)}$, $\beta^{(1)}$, $\beta^{(2)}$ and C^{ϕ} and binary mixture parameters Θ , one can reproduce experimental activity-coefficient data typically to a few percent and in all cases to $\pm 20\%$. Of course, as noted above, the most accurate work on complex, concentrated mixtures requires that one include further mixing parameters and also, for calculations at temperatures other than 25°C , include the temperature dependencies of the parameters. However, for FGD applications, a more important point is that Pitzer's formulation appears to be a convergent series. The third virial coefficients

C^ϕ and mixture parameters Θ are small and their neglect, under most conditions, introduces errors of less than 10% in $\ln\gamma$ (2,3,4,5,19,20). This allows one to apply the formulation to mixtures which include chemical species for which experimental activity data are not at hand. Firstly, accepting that estimated activity coefficients will necessarily be approximate, a limited number of parameters, $\beta^{(0)}$ and $\beta^{(1)}$ (and for 2-2 electrolytes, $\beta^{(2)}$), must be estimated for those species. Secondly, because the equations are convergent, estimated pure-electrolyte parameters may be combined with more accurate, empirical, pure-electrolyte and interaction parameters where they exist. The complex solutions encountered in FGD chemistry encompass both types of chemical species--the well-known and the somewhat esoteric.

This leads one to the question of methods to estimate Pitzer-equation parameters for binary ion pairs. The parameters to be estimated, $\beta^{(0)}$ and $\beta^{(1)}$, depend upon short-range interactions and are not independent of each other, following generally parallel trends (3). The $\beta^{(2)}$ term describes additional attractive interactions unique to 2-2 and higher electrolytes at low concentrations and has only a small constant effect at concentrations above 0.1 M). Thus, if one estimates $\beta^{(0)}$, one can obtain (13) $\beta^{(1)}$ from $\beta^{(0)}:\beta^{(1)}$ ratios for similar ion-pairs, or from plots of $\beta^{(0)}$ vs. $\beta^{(1)}$ presented by Pitzer and Mayorga (3), or from an empirical equation (14) based upon those plots.

One way (13) to estimate $\beta^{(0)}$ and $\beta^{(1)}$ is based upon the observed correlation (3) of these parameters with the effect of the ions on the structure of liquid water. The more dissimilar the ions are in this respect, the greater the values of $\beta^{(0)}$ and $\beta^{(1)}$. The most "structure-making" cations are small and multiply charged (e.g., Mg^{2+}); the most "structure-breaking" anions are large and only singly charged (e.g., ClO_4^-). These trends have been used to estimate and tabulate parameters for 22 ion-pairs of interest in FGD chemistry (13). The estimated parameters, along with available experimental parameters summarized in that same paper (13), cover FGD solutions containing the following ions: Na^+ , K^+ , Mg^{2+} , Ca^{2+} , Cl^- , ClO_3^- , ClO_4^- , HCO_3^- , HSO_4^- , HSO_3^- , CO_3^{2-} , SO_4^{2-} , SO_3^{2-} , and $S_2O_5^{2-}$.

A somewhat similar estimation procedure has been used by Edwards et al. (14) who present an estimation "recipe" which may be somewhat easier to reproduce. In that procedure, tabulated values (3) of $\beta^{(0)}$ are broken up into individual ion components by taking $\beta_{Na^+}^{(0)} = 0$. $\beta_{MX}^{(0)}$ values for unmeasured ion combinations are then obtained by addition of $\beta_M^{(0)}$ and $\beta_X^{(0)}$. Additional single-ion $\beta^{(0)}$ values are obtained by correlation with the partial molal entropy of the ion in an infinitely dilute aqueous solution, as suggested by Bromley (21). A few $\beta_{MX}^{(0)}$ values estimated in this way are compared in Table I with experimental and estimated values from ref. (13). With the exception of the experimental value for Na_2CO_3 , the values compared are all very close to zero.

Table I. Estimated ion-pair parameters $\beta_{MX}^{(0)}$

	Edwards et al. (14)	Rosenblatt (13)
Na-HCO ₃	-0.049	0.0277 ^a
Na ₂ -CO ₃	-0.034	0.1898 ^b
Na-HSO ₃	-0.035	0.0249
Na ₂ -SO ₃	-0.017	0.021

a. Experimental value from ref. (11).

b. Experimental value from ref. (3).

Sensitivity of Activity Coefficients to Charges in Pitzer-Equation Parameters

Table II summarizes some Pitzer-equation computations (13) which assess the sensitivity of calculated activity coefficients to changes in estimated parameters and to changes in temperature, assuming only A_ϕ is temperature dependent. The solution is fairly typical of CaO/CaO₃ coal scrubbers but has a somewhat high ionic strength ($I = 1.17$). Ions present, in decreasing concentrations, are Mg²⁺, Cl⁻, SO₄²⁻, Ca²⁺, SO₃²⁻, and CO₃²⁻. The base ion-pair parameters are from ref. (13). The alternative Mg-SO₃ parameters are uniformly increased by 20% over the base estimates, a change which probably is an upper limit to the potential errors in the Mg-SO₃ parameters and is about the same as that produced by a 25° change in temperature. The alternative Ca-SO₃ parameters have a less negative value for $\beta^{(2)}$. The alternative estimates of $\beta^{(2)}$ for Ca-SO₃ and Mg-SO₃ assume, contrary to experiment, that the metal-sulfites are less associated than the metal-sulfates. The Table compares mean-ion activity coefficients for Ca-SO₄, Mg-SO₃, and Ca-SO₃ calculated using base and alternative estimates. It can be seen that γ_+ of Mg-SO₃ and of CaSO₃ change by about 13%. The effect of the $\bar{\nu}$ parameter changes on γ_{\pm} of Ca-SO₄ is insignificant. Raising the temperature from 25° to 50° also changes γ_{\pm} by 13%.

Two conclusions may be drawn from calculations of this type.

(1) Calculated activity coefficients are relatively insensitive to the Pitzer-equation parameters. This is particularly true for the parameters of ion-pairs which do not contain an ion whose activity coefficient is being calculated. Activity coefficients calculated with estimated parameters from eqs. (1)-(9) are probably accurate to better than $\pm 25\%$. This is not that different from the accuracy obtained with eqs. (1)-(9) when all parameters are based upon experiment (reported deviations up to 18% (22)). Achieving higher accuracy requires both better parameters and the inclusion of higher-order theoretical terms (C^ϕ , Θ , ψ , higher

electrostatic terms) as well as the temperature dependencies of those terms.

(2) The changes in computed activity coefficients brought about by uncertainties in estimated parameters, by the temperature dependence of those parameters, and by the temperature dependence of A_ϕ are roughly comparable. Thus, as long as one is restricted to the accuracy obtainable with estimated parameters and to the moderate temperature ranges typical of flue-gas-desulfurization practice, the temperature dependence of γ_+ is represented reasonably satisfactorily by the known temperature dependence of A_ϕ .

Table II. Calculated mean-ion activity coefficients in a sample FGD solution.

Temperature: Parameters:	25° Base	25° Alternate	50°C Base
γ_+ (CaSO ₄)	0.0918	0.0919	0.0799
γ_+ (MgSO ₃)	0.0975	0.1100	0.0848
γ_+ (CaSO ₃)	0.0865	0.0972	0.0752

Comparison with Association-Equilibrium Extended-Debye-Hückel Model

The Bechtel-Modified Radian Equilibrium Program⁽²³⁾ is a widely used computer code for modelling flue gas desulfurization processes. In that code, as was best practice at the time it was written⁽¹⁾, specific interactions between oppositely charged ions are treated as formation of ion pairs, described by a chemical equilibrium constant, and the activity coefficients of the remaining "free" ions are described by classical, extended Debye-Hückel theory. Extended Debye-Hückel activity coefficients depend upon concentration but not upon solution composition. Thus, all ion interactions must be described by the association equilibrium constants between specific pairs of oppositely charged ions. Comparisons of product activities for neutral ion-pairs calculated from this code with those calculated by Pitzer's equations show both some overall differences, reflecting differences in parameters, and, more fundamental, different behavior with changes in ionic strength and composition.

The reason for this goes back to the underlying theoretical foundations of the two approaches⁽¹³⁾. It is not surprising that an equilibrium constant approach is a rather limited way to sum over all possible binary and ternary interactions, particularly when one recalls that there are interactions between ions of like sign as well as those of opposite sign.

The differences in the two approaches, and their significance for FGD chemistry, can be illustrated by comparing activity products and activity coefficients in some simple model systems.

Figure 1 shows the computer activity product $a_2 = a_{Ca^{2+}} \cdot a_{SO_4^{2-}}$ when $MgSO_4$ is added to a nearly saturated 0.01 M $CaSO_4$ solution at 50°C. The a_2 values calculated from the Bechtel-Modified Radian Equilibrium Program continuously increase as $MgSO_4$ is added. (This may be inherent in the nature of the association-equilibrium model). The Radian program predicts that a_2 will equal the solubility-product constant of $CaSO_4$ when the $MgSO_4$ molality reaches 0.7 ($I \approx 3$) and that $CaSO_4$ will precipitate out of solution at $MgSO_4$ additions greater than this. In comparison, the Pitzer-equation calculations show a_2 to increase when $MgSO_4$ is first added, but then to decrease slowly at $MgSO_4$ molalities above 0.1, remaining below the solubility-product limit of $CaSO_4$ (22,24) over the whole range of $MgSO_4$ additions up to $I = 5$.

Figure 2 shows experimental solubility data. It can be seen that these faithfully mirror the behavior expected from the Pitzer-equation calculations in Figure 1. As $MgSO_4$ is added, the solubility of $CaSO_4$ first decreases, then slowly increases. In contrast, the Radian calculations predict a continuous decrease in $CaSO_4$ solubility as $MgSO_4$ is added, which is at first rapid and then tends to level off.

The way in which the two approaches yield different behavior in Figure 1 and different predictions of solubility is shown in Figure 3. This figure shows the variation of γ_+ for 0.01 M $CaSO_4$ at 50°C as the ionic strength is increased by adding $MgSO_4$. The Pitzer-equation curve indicates that addition of $MgSO_4$ causes γ_+ ($CaSO_4$) to decrease markedly, following essentially the same curve as the hypothetical addition of $CaSO_4$ beyond the saturation limit (dotted curve). The decrease in γ_+ with addition of $MgSO_4$ is sufficiently rapid that the product $a_2 = \gamma_+^2 \cdot m_{Ca^{2+}} \cdot m_{SO_4^{2-}}$ remains almost constant, and below the solubility product limit.

Mean-ion activity coefficients, $\gamma_+ = (\gamma_{Ca^{2+}} \cdot \gamma_{SO_4^{2-}})^{1/2}$, may be computed from the values of $\gamma_{Ca^{2+}}$ and $\gamma_{SO_4^{2-}}$ used in the Radian program. But because the ionic strength and activity of $CaSO_4$ in the Radian approach are modified by ion-pairing such mean-ion activity coefficients are not directly comparable to the Pitzer-equation values. However, one may use the Radian program to carry out calculations for the series of solutions in Figure 1, and then compute from the results "effective" activity coefficients which may be compared directly with the Pitzer-equation results. The Radian curves so obtained are also shown in Figure 3. The "effective" Radian γ_+ curve for the $CaSO_4 + MgSO_4$ solutions lies slightly below the Pitzer curve at low ionic strengths, crosses that curve at $I \approx 0.5$, then reaches a value about 0.01 above the Pitzer curve at high ionic strengths. This change in the shape of the curve is enough to lead to a different prediction of solubility.

Figure 4 shows similar calculations for the addition of NaCl to 0.01 M $CaSO_4$. Addition of NaCl lowers the activity coefficient of $CaSO_4$ considerably less than does addition of $MgSO_4$ and has only a small effect at ionic strengths above 1.5 M. The contrast

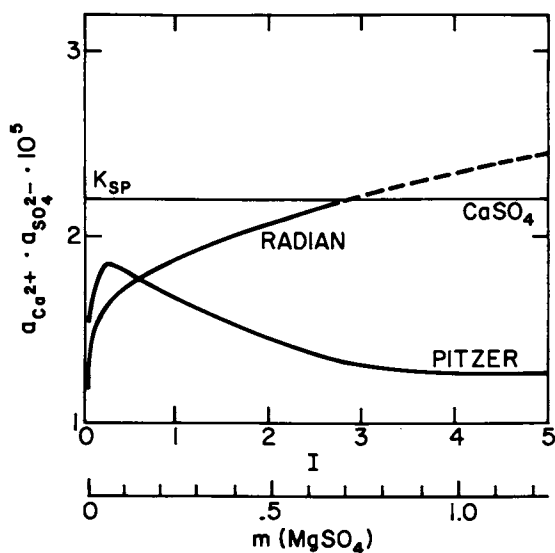


Figure 1. Activity of CaSO_4 when MgSO_4 is added to a 0.01 M CaSO_4 solution at 50°C as calculated from the Bechtel-modified Radian Equilibrium Program and from the Pitzer equations in this chapter. The horizontal line shows the solubility-product constant of CaSO_4 .

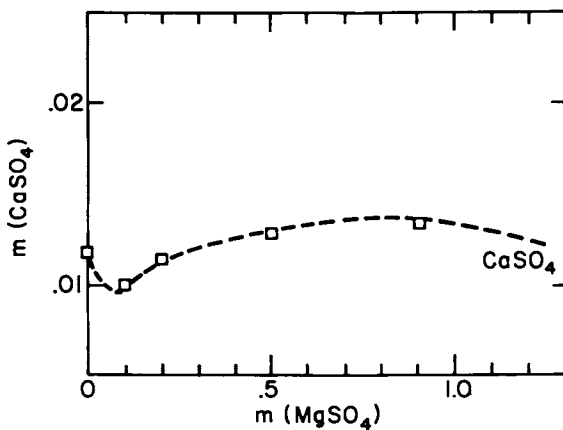


Figure 2. Experimental solubility data for CaSO_4 when MgSO_4 is added (24).

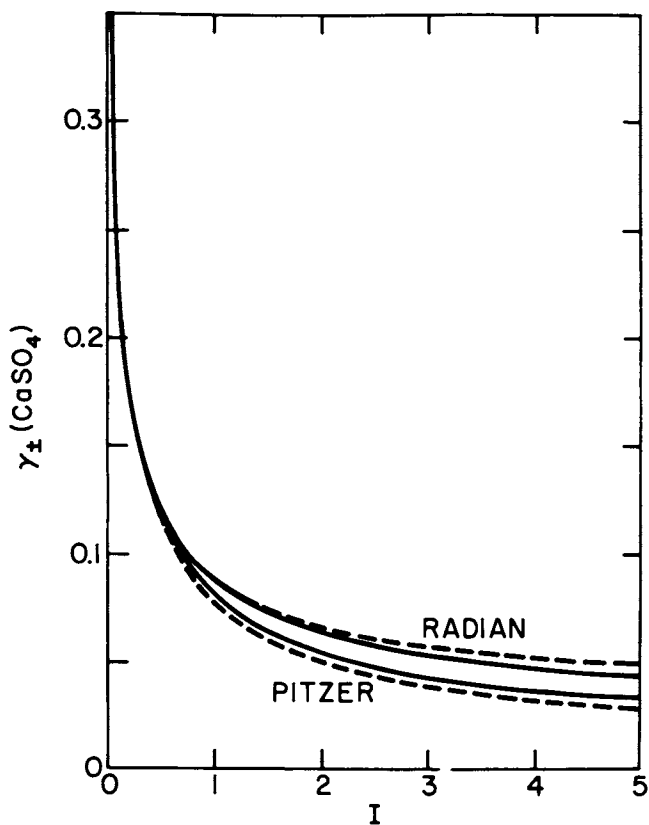


Figure 3. Pitzer and "effective" Radian mean-ion activity coefficients of CaSO_4 when MgSO_4 is added to a 0.01 M CaSO_4 solution at 50°C . The dotted lines represent the behavior of pure CaSO_4 (extrapolated beyond saturation).

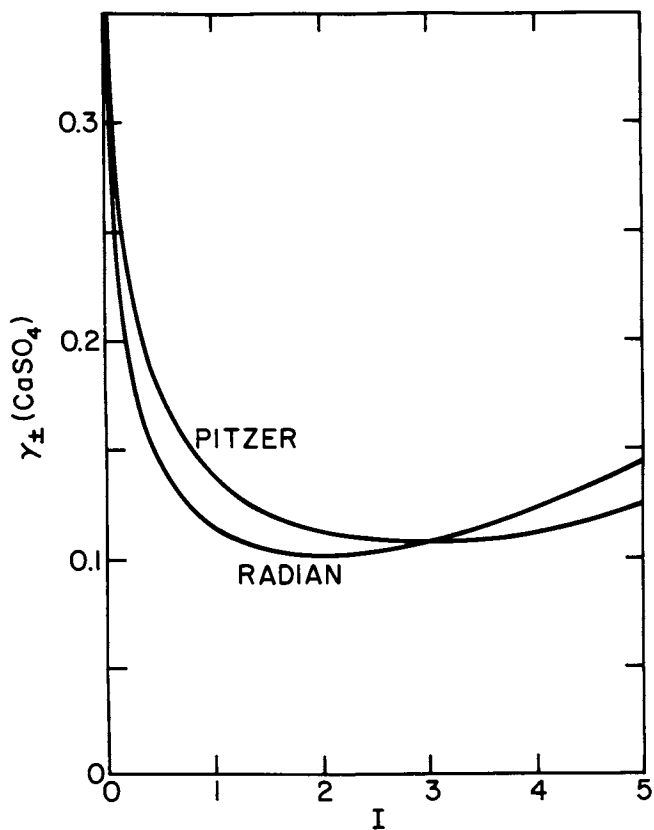


Figure 4. Pitzer and "effective" Radian mean-ion activity coefficients of CaSO_4 when NaCl is added to a 0.01 M CaSO_3 solution at 50°C .

with the "effective" Radian γ_{\pm} curve is more pronounced in this case, however.

The Pitzer-equation computations for Figures 3 and 4 are based upon experimentally derived 25°C ion-pair and interaction coefficients taken from the literature. From the extensive prior work validating the theory and parameters, these curves should deviate from experiment by less than 20%. However, as Figures 1-4 show, solubility calculations are very sensitive to variations in activity coefficients and the approximations made in eqs. (1)-(9) limit the accuracy of the solubility curves which can be calculated. When higher-order terms are included, Pitzer's equations accurately predict solubility in the CaSO_4 - MgSO_4 system up to $I = 12 \text{ M}$ (16).

Figure 5 shows similar Pitzer-equation curves for CaSO_3 based upon estimated parameters (13). The activity coefficients estimated for CaSO_3 are up to 20% below those for CaSO_4 at equal concentrations but the pattern of Figures 3 and 5 is very similar. The decrease in γ_{\pm} (CaSO_3) upon adding MgSO_3 is sufficiently large that the activity of CaSO_3 also is calculated to remain below the solubility product limit of CaSO_3 as MgSO_3 is added. Comparing with "effective" Radian γ_{\pm} values, the very strong specific associations invoked for SO_3^{2-} cause the Radian curves to decrease precipitously at very low ionic strengths. The Radian "effective" curve for CaSO_4 - MgSO_4 is about 50% below the Pitzer curves over the whole range of concentrations shown in Figure 5. Figure 6 may be compared with Figure 4. The Radian "effective" curve for CaSO_3 - NaCl is about 50% below the Pitzer curve at $I < 0.1$, crosses the Pitzer curve at $I \approx 2$, then rises above it by about 0.04 at high ionic strengths.

Conclusions

Pitzer's equations and available ion-pair parameters allow calculation of mean-ion activity coefficients γ_{\pm} in complex, concentrated electrolyte solutions with an accuracy estimated to be better than $\pm 25\%$ in the range 25° - 55°C. The accuracy of calculated activity coefficients is limited to about the same degree by uncertainties in the estimated parameters and by simplifications introduced in the theory both to reduce the number of parameters to be estimated and to reflect the uncertainties of the estimates. Because activity coefficients are determined to quite an extent by the form of Pitzer's equations and are not extremely sensitive to the exact values of parameters, ion-pair parameters only have to be estimated within a reasonable range.

Upon comparing Pitzer-theory calculations for typical scrubber and model solutions with the association-equilibrium, extended Debye-Hückel code in current use for FGD systems, one sees differences which reflect the differences in concentration range and applicability to mixtures of the two approaches.

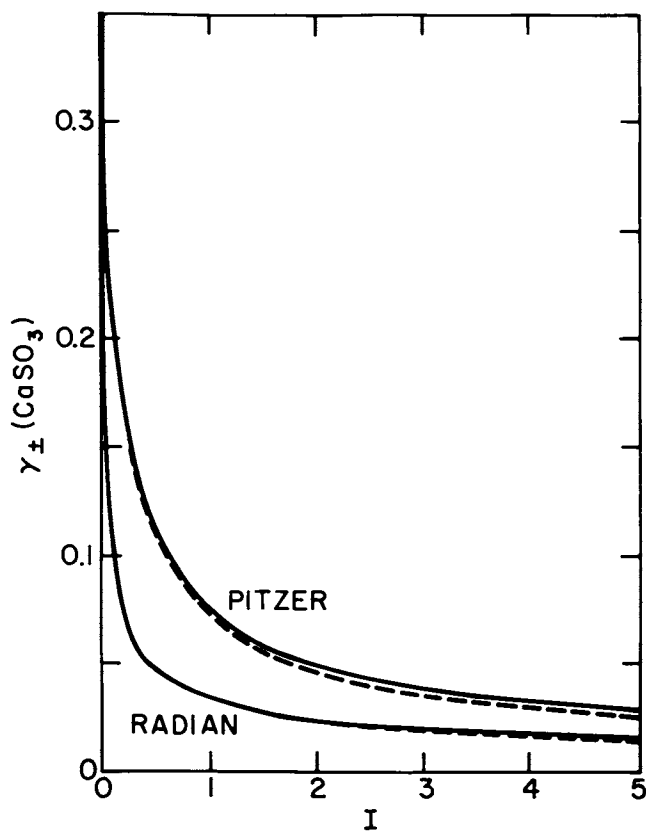


Figure 5. Pitzer and "effective" Radian mean-ion activity coefficients of CaSO_3 when MgSO_4 is added to a 0.01 M CaSO_3 solution at 50°C. The dotted lines represent pure CaSO_3 .

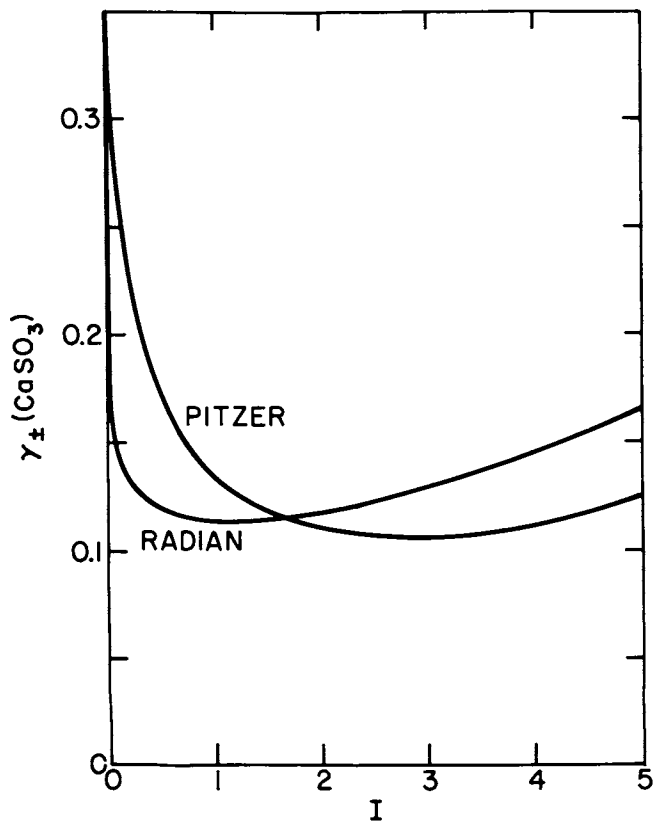


Figure 6. Pitzer and "effective" Radian mean-ion activity coefficients of CaSO_3 when NaCl is added to a 0.01 M CaSO_3 solution at 50°C.

Pitzer's formulation offers a satisfactory and desirable way to model strong electrolyte activity coefficients in concentrated and complex mixtures. When sufficient experimental data are available, one can make calculations which are considerably more accurate than those presented in this paper. Attaining high accuracy requires not only experimentally-based parameters but also that one employ third virial coefficients and additional mixing terms and include explicit temperature dependencies for the various parameters.

Further efforts based upon the Pitzer equation approach should allow one to model reasonably accurately the complex thermodynamics occurring in flue-gas-desulfurization aqueous scrubbers. Tasks to be pursued to this end include: (1) Replacing important estimated parameters by ones based upon experiment, particularly for sulfites. (2) Including higher-order terms (three-body, electrostatic, temperature dependence) where data are available. (3) Extending the treatment to include weak electrolytes.

Acknowledgments

The author thanks Professors Leo Brewer, Kenneth Pitzer, Robert Connick and Beat Meyer for helpful discussions. Professor Gary Rochelle, University of Texas, contributed information on the Radian program. Dr. Tom Pierce of EG&G contributed the Radian calculations. This work was supported by the Morgantown Energy Technology Center, U.S. Department of Energy under contract No. W-7405-Eng-48 to the University of California.

Literature Cited

1. Lowell, P. S.; Ottmers, D. M., Jr.; Schwitzgebel K.; Strange, T. I.; DeBarry D. W. Vol. I, Radian Corp. Final Report for PHS CPA-22-69-138 to National Air Pollution Administration (HEW), 1970, PB 193-029.
2. Pitzer, K. S. J. Phys. Chem. 1973, 77, 268.
3. Pitzer, K. S.; G. Mayorga. J. Phys. Chem. 1973, 77, 2300.
4. Pitzer, K. S.; G. Mayorga. J. Soln. Chem. 1974, 3, 539.
5. Pitzer, K. S.; Kim, J. J. J. Amer. Chem. 1974, 96, 5701.
6. Pitzer, K. S. J. Soln. Chem. 1975, 4, 249.
7. Pitzer, K. S.; Silvester, L. F. J. Soln. Chem. 1976, 5, 269.
8. Pitzer, K. S.; Roy, R. N.; Silvester, L. F. J. Amer. Chem. Soc. 1977, 99, 4930.
9. Pitzer, K. S. Accounts Chem. Res. 1977, 10, 371.
10. Silvester, L. F.; Pitzer, K. S. J. Soln. Chem. 1978, 7, 327.
11. Pitzer, K. S.; Peiper, J. C. J. Phys. Chem. 1980, 84, 2396.
12. Pitzer, K. S. "Thermodynamics of Aqueous Systems with Industrial Applications;" American Chemical Society: Washington, DC, 1980; p. 451.
13. Rosenblatt, G. M. AIChE J. 1981, 27, 619.

14. Edwards, T. J.; Mauer, G.; Newman, J.; Prausnitz J. M. AICHE J. 1978, 24, 966.
15. Lewis, G. N.; Randall, M.; Pitzer, K. S.; Brewer, L. "Thermodynamics," second edition, McGraw-Hill, 1961; p 570.
16. Harvie, C. E.; Weare, J. H. Geochimica Acta 1980, 44, 981.
17. Clarke, E. C. W.; Glew, D. N. JCS Faraday I 1980, 76, 1911.
18. Holmes, H. F.; Baes, C. F., Jr.; Mesmer, R. E. J. Chem. Thermodyn. 1979, 11, 1035.
19. Macaskill, J. B.; Bates, R. G. J. Soln. Chem. 1978, 7, 433.
20. Macaskill, J. B.; White, D. R.; Robinson, R. A.; Bates, R. G. J. Soln. Chem. 1978, 7, 339.
21. Bromley, L. A. J. Chem. Thermo. 1972, 4, 669.
22. Culberson, C. H.; Latham, G.; Bates, R. G. J. Phys. Chem. 1978, 82, 2693.
23. Epstein, M. U.S. Environmental Protection Agency, Environmental Protection Technology Series, EPA-650/2-75/074; Appendix G, 1975, PB-244901.
24. Bodaleva, N. V.; Lepeshkov, I.H. Zhur. Neorg. Khim 1956, 1, 995, [Engl. Trans. 1956, 1 (5), 123].

RECEIVED November 20, 1981.

Limestone Dissolution

Effects of pH, CO₂, and Buffers Modeled by Mass Transfer

PUI K. CHAN and GARY T. ROCHELLE

University of Texas at Austin, Department of Chemical Engineering, Austin, TX 78712

The rate of CaCO₃ dissolution in slurry scrubbers for flue gas desulfurization affects SO₂ absorption, CaSO₃/CaSO₄ scaling, and ultimate CaCO₃ utilization. The dissolution rate of reagent CaCO₃ has been measured in 0.1 M CaCl₂ at constant pH and CO₂ partial pressure by batch titration with HCl. A mass transfer model has been developed assuming that the calcite particles behave as spheres in an infinite stagnant solution. The model incorporates the effects of several equilibrium acid/base reactions and also includes the finite rate reaction involving CO₂ and HCO₃⁻. The cumulative rate of mass transfer is calculated by integrating over a particle size distribution obtained by a Coulter counter.

The results of this investigation show that CaCO₃ dissolution is controlled by mass transfer and not surface reaction kinetics. Buffer additives such as adipic acid enhance mass transfer by increasing acidity transport to the limestone surface. Dissolution is enhanced at low sulfite concentration but inhibited at high sulfite concentration, indicating some kind of surface adsorption or crystallization phenomenon. The rate of dissolution is a strong function of pH and temperature as predicted by mass transfer. At high CO₂ partial pressure, the rate of dissolution is enhanced due to the CO₂ hydrolysis reaction.

Limestone (CaCO₃) dissolution is an important phenomenon in stack gas desulfurization processes using limestone slurry to absorb SO₂ and produce CaSO₃/CaSO₄ waste solids (1). The rate of dissolution directly determines the need for excess limestone and interacts strongly with SO₂ removal and scale-free operation in the absorber. There is a need to know the dependence of dissolution rates on both solution composition and the type and grind of limestone. This paper presents a mass transfer model and

0097-6156/82/0188-0075\$6.75/0
© 1982 American Chemical Society

experimental results on the dissolution of reagent CaCO_3 (calcite) as a function of solution composition (2). A later paper will discuss the application of this mass transfer model to naturally occurring limestones (3,4).

In the slurry scrubbing process, limestone dissolves at pH 4 to 6 and 55°C in both absorber and the hold tank/crystallizer. Because of HCl accumulation from the flue gas, typical scrubbing solution contains 0.01 to 0.2 M CaCl_2 . CO_2 partial pressure can vary from near zero with forced oxidation to one atmosphere with CO_2 evolution from the hold tank and is typically 0.1 atm in the absorber. Sulfite/bisulfite buffer can be present in concentrations up to 0.1 M. CaSO_3 and/or CaSO_4 crystallization must occur simultaneously with limestone dissolution. Buffer additives such as adipic acid should enhance both SO_2 removal and CaCO_3 dissolution at concentrations of 3 to 10 mM (5).

Previous Work

The most significant previous work on calcite dissolution has been done by geochemists in pure water or a seawater environment as reviewed by Plummer *et al* (6). Berner and Morse (7) measured dissolution rates of reagent CaCO_3 using the pH-stat method. Plummer *et al* (8) studied dissolution of coarse Iceland spar using the free drift and pH-stat methods. These investigators both found a linear dependence of dissolution rate on H^+ concentration and PCO_2 and a constant forward rate in the near absence of H^+ and CO_2 . Near equilibrium pH Plummer observed a reverse reaction rate proportional to the product of Ca^{++} and HCO_3^- .

Some previous investigators have modeled calcite dissolution as limited by diffusion of H^+ at pH less than 4 to 5 (7,9). Other investigators have reported a dependence on agitation (10, 11).

The reported activation energy of calcite dissolution varies from 1.5 to 14 kcal/gmol (8,9,10,12,13). The trend of data gives low activation energy at pH 2 - 4 and high activation energy at pH 8 - 10.

Several investigators have studied inhibition of calcite dissolution near equilibrium pH by surface adsorption of insoluble salts. Berner and Morse (7) showed inhibition by phosphate at 10^{-6} M. Terjesen *et al* (14) modeled the inhibiting effects of metal ions as an apparent reduction in the equilibrium pH. Koss and Moller (15) studied the apparent equilibrium pH in the presence of Ni, Fe, Mg, and other metal ions. Sjoberg (13) measured inhibition by phosphate and by Mg^{++} .

Theory

The rate of CaCO_3 dissolution can be calculated by mass transfer theory assuming that the solution is in equilibrium with

calcite at the limestone surface. A steady-state solution of mass transfer theory is easily obtained by assuming spherical CaCO_3 particles in an infinite stagnant solution, corresponding to a mass transfer coefficient equal to the ratio of diffusivity and particle radius (D/r). The calculated rates from the stagnant model have been arbitrarily increased by a factor of 1.88 to fit the experimental rates. A factor of 1.25 would be consistent with the expected effect of agitation on mass transfer (3). The balance of the correction may be due to non-spherical shape or other factors.

The general model assumes instantaneous equilibria in the boundary layer of all solution species except CO_2 . It uses a different diffusivity for each species. It accounts for the finite-rate, reversible reaction of CO_2 and H_2O to give H^+ and HCO_3^- by iterative, numerical integration of a second-order, nonlinear differential equation and a set of nonlinear algebraic equations.

For many cases the CO_2 reaction can be neglected, and solution of the mass transfer theory requires iterative solution of a much simpler set of nonlinear algebraic equations.

Modeling of experimental data requires integration of the dissolution rate over a particle size distribution. This is simplified by assuming that the dissolution rate per particle is directly proportional to the particle diameter. Because of the CO_2 reaction, the dissolution rate of a particle in gmol/sec is not exactly proportional to the particle diameter. Therefore, the effect of the CO_2 reaction is assumed to be the same for all particles as for a $10 \mu\text{m}$ (effective diameter) particle. The general mass transfer model is used to calculate rates for $10 \mu\text{m}$ particles as a function of solution composition.

General Model. The general mass transfer model calculates dissolution rate as a function of bulk solution composition, particle diameter, and temperature. It assumes instantaneous equilibrium of the solution species H^+ , H_2O , OH^- , CaCO_3^0 , Ca^{++} , CO_3^{--} , HCO_3^- , SO_3^{--} , HSO_3^- , and a general buffer represented by the species H_2A , HA^- , and A^- . CaHCO_3^0 was not included, but should not affect the dissolution rate at most of the conditions modeled. This assumption gives the following equilibria which apply throughout the mass transfer boundary layer (constants at 25°C):

$$K_{\text{CaCO}_3^0} = \frac{a_{\text{Ca}^{++}} a_{\text{CO}_3^{--}}}{a_{\text{CaCO}_3^0}} = 6.3 \times 10^{-4} \quad (16) \quad (1)$$

$$K_{\text{HCO}_3^-} = \frac{a_{\text{H}^+} a_{\text{CO}_3^{--}}}{a_{\text{HCO}_3^-}} = 4.69 \times 10^{-11} \quad (17) \quad (2)$$

$$K_{\text{HSO}_3^-} = \frac{a_{\text{H}^+} a_{\text{SO}_3^{2-}}}{a_{\text{HSO}_3^-}} = 6.24 \times 10^{-8} \quad (18)$$

$$K_{\text{H}_2\text{O}} = a_{\text{H}^+} a_{\text{OH}^-} = 1.008 \times 10^{-14} \quad (4)$$

At 55°C, $K_{\text{H}_2\text{O}}$ was taken to be 7.26×10^{-14} and the other constants were evaluated according to Lowell *et al* (19). Activities were calculated as the product of concentration and activity coefficient. Activity coefficients were estimated using an extended Debye-Huckel limiting law as implemented by Lowell *et al* (19).

To account for the CaSO_3 ion pair, an effective $K'_{\text{HSO}_3^-}$ was defined as:

$$K'_{\text{HSO}_3^-} = K_{\text{HSO}_3^-} \left(1 + \frac{a_{\text{Ca}^{++}}}{K_{\text{CaSO}_3^0}} \right) \quad (5)$$

$$K_{\text{CaSO}_3^0} = \frac{a_{\text{Ca}^{++}} a_{\text{SO}_3^{2-}}}{a_{\text{CaSO}_3^0}} = 4.0 \times 10^{-4} \quad (19)$$

Similarly, to account for CaOH^+ ion pair, an effective $K'_{\text{H}_2\text{O}}$ was defined as:

$$K'_{\text{H}_2\text{O}} = K_{\text{H}_2\text{O}} \left(1 + \frac{a_{\text{Ca}^{++}}}{K_{\text{CaOH}^+}} \right) \quad (6)$$

$$K_{\text{CaOH}^+} = \frac{a_{\text{Ca}^{++}} a_{\text{OH}^-}}{a_{\text{CaOH}^+}} = 3.5 \times 10^{-2} \quad (19)$$

The general buffer equilibria were defined by the relations:

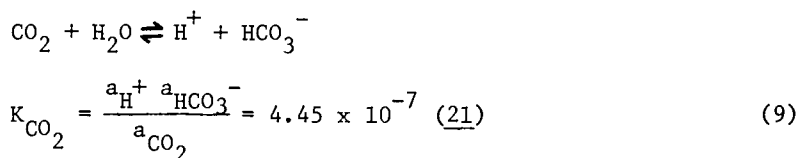
$$K_{\text{H}_2\text{A}} = \frac{a_{\text{H}^+} [\text{HA}^-]}{[\text{H}_2\text{A}]} \quad (7)$$

$$K_{\text{HA}^-} = \frac{a_{\text{H}^+} [\text{A}^-]}{[\text{HA}^-]} \quad (8)$$

In 0.1 M CaCl₂, the $K_{\text{H}_2\text{A}}$ and K_{HA^-} values were measured by Cavanaugh (20) and are 1.05×10^{-4} and 1.39×10^{-5} for adipic acid and 7.94×10^{-4} and 3.98×10^{-5} for sulfosuccinic acid. For acetic and acrylic acids, K_{HA^-} was estimated to be 3.55×10^{-5} and 9.54×10^{-5} , respectively.

The general model assumes that dissolved CO₂ is in equilibrium with other species in the bulk solution, but that its

concentration in the boundary layer is given by the finite-rate, reversible reaction:



The net rate of this reaction is given by:

$$\frac{d[\text{CO}_2]}{dt} = k_{\text{CO}_2} [\text{CO}_2] \left(\frac{a_{\text{H}^+} a_{\text{HCO}_3^-}}{K_{\text{CO}_2} a_{\text{CO}_2}} - 1 \right) \quad (10)$$

At infinite dilution, k_{CO_2} is 0.026s^{-1} at 25°C and 0.125s^{-1} at 55°C (22). The rate constant was assumed to be independent of ionic strength.

The differential material balance for total CO_2 species at steady state in spherical coordinates gives:

$$\frac{1}{r^2} \left[D_{\text{CO}_2} \frac{\partial}{\partial r} \left(r^2 \frac{\partial [\text{CO}_2]}{\partial r} \right) + D_{\text{HCO}_3^-} \frac{\partial}{\partial r} \left(r^2 \frac{\partial [\text{HCO}_3^-]}{\partial r} \right) + D_{\text{CaCO}_3^0} \frac{\partial}{\partial r} \left(r^2 \frac{\partial [\text{CaCO}_3^0]}{\partial r} \right) + D_{\text{CO}_3^{=}} \frac{\partial}{\partial r} \left(r^2 \frac{\partial [\text{CO}_3^{=}] }{\partial r} \right) \right] = 0 \quad (11)$$

Substituting $x = (1-d/2r)$ where d is the particle diameter and r the distance from the center of the sphere, equation (11) reduces to:

$$D_{\text{CO}_2} \frac{\partial^2 [\text{CO}_2]}{\partial x^2} + D_{\text{HCO}_3^-} \frac{\partial^2 [\text{HCO}_3^-]}{\partial x^2} + D_{\text{CaCO}_3^0} \frac{\partial^2 [\text{CaCO}_3^0]}{\partial x^2} + D_{\text{CO}_3^{=}} \frac{\partial^2 [\text{CO}_3^{=}] }{\partial x^2} = 0 \quad (12)$$

Integrating equation (12) with respect to x gives:

$$D_{\text{CO}_2} [\text{CO}_2] + D_{\text{HCO}_3^-} [\text{HCO}_3^-] + D_{\text{CaCO}_3^0} [\text{CaCO}_3^0] + D_{\text{CO}_3^{=}} [\text{CO}_3^{=}] = \alpha_1 + \beta_1 x \quad (13)$$

where α_1 ($\text{M cm}^2 \text{sec}^{-1}$) and β_1 ($\text{M cm}^2 \text{sec}^{-1}$) are constants of integration.

Similarly, other steady-state balances give for Ca^{++} species:

$$D_{\text{Ca}^{++}} [\text{Ca}^{++}] + D_{\text{CaCO}_3^0} [\text{CaCO}_3^0] = \alpha_2 + \beta_2 x \quad (14)$$

for charge balance:

$$\begin{aligned} D_{\text{H}^+} [\text{H}^+] + 2D_{\text{Ca}^{++}} [\text{Ca}^{++}] - D_{\text{HCO}_3^-} [\text{HCO}_3^-] - 2D_{\text{CO}_3^{=}} [\text{CO}_3^{=}] \\ - D_{\text{HA}^-} [\text{HA}^-] - 2D_{\text{A}^{=}} [\text{A}^{=}] - D_{\text{HSO}_3^-} [\text{HSO}_3^-] - 2D_{\text{SO}_3^{=}} [\text{SO}_3^{=}] \\ - D_{\text{OH}^-} [\text{OH}^-] = \alpha_3 + \beta_3 x \end{aligned} \quad (15)$$

for H_2A species:

$$D_{\text{H}_2\text{A}} [\text{H}_2\text{A}] + D_{\text{HA}^-} [\text{HA}^-] + D_{\text{A}^{=}} [\text{A}^{=}] = \alpha_4 + \beta_4 x \quad (16)$$

and for sulfite species:

$$D_{\text{HSO}_3^-} [\text{HSO}_3^-] + D_{\text{SO}_3^{=}} [\text{SO}_3^{=}] = \alpha_5 + \beta_5 x \quad (17)$$

By reaction stoichiometry, the flux of calcium from the limestone surface must be equal to the flux of total CO_2 :

$$\begin{aligned} \frac{\partial}{\partial x} (D_{\text{Ca}^{++}} [\text{Ca}^{++}] + D_{\text{CaCO}_3^0} [\text{CaCO}_3^0]) = \frac{\partial}{\partial x} (D_{\text{CO}_2} [\text{CO}_2] + \\ D_{\text{HCO}_3^-} [\text{HCO}_3^-] + D_{\text{CaCO}_3^0} [\text{CaCO}_3^0] + D_{\text{CO}_3^{=}} [\text{CO}_3^{=}]) \end{aligned} \quad (18)$$

Therefore $\beta_1 = \beta_2 = \beta$. Since the net fluxes of H_2A species, sulfite species, and charged species are zero, β_3 , β_4 , and β_5 are zero. If β is known, the constants α_1 , α_2 , α_3 , α_4 , and α_5 can be obtained from the compositions of the bulk solution (at $x=1.0$).

The finite-rate CO_2 reaction (equation 10) gives the following differential material balance for the CO_2 species alone:

$$(1-x)^4 D_{\text{CO}_2} \frac{d}{dx} \frac{\partial^2 [\text{CO}_2]}{\partial x^2} = k_{\text{CO}_2} [\text{CO}_2] \left(1 - \frac{a_{\text{H}^+} a_{\text{HCO}_3^-}}{K_{\text{CO}_2} a_{\text{CO}_2}} \right) \quad (19)$$

This equation is integrated numerically with a trial-and-error solution for the boundary conditions. A trial value of β is selected and the constants α_1 , α_2 , α_3 , α_4 , and α_5 are calculated from the bulk composition. At each step in the numeric integration, the algebraic equations representing equilibria (1,2,3,4,7, 8) and other differential material balances (13,14,15,16,17) are solved by trial and error to give a_{H^+} and $a_{\text{HCO}_3^-}$.

To initiate the numerical integration, the solution was assumed to be in equilibrium with calcite at the solid surface ($x = 0$) giving:

$$[\text{CaCO}_3^0] = 6.8 \times 10^{-6} \text{ M} \quad (19)$$

The CO_2 concentration at the surface was calculated from equations 1, 2, 3, 4, 7, and 8. Since no reaction of CO_2 with CO_3^{2-} can occur in the volume increment at the solid surface, $d[\text{CO}_2]/dx$ taken to be zero at $x = 0.0$. Equation 19 was then integrated by the Simpson-Kutta method (23) from $x = 0$ to $x = 0.85$. A cubic fit of $[\text{CO}_2]$ from $x = 0.7$ to $x = 0.85$ was used to extrapolate to $x = 1.0$. This extrapolation is expected to add little error since $[\text{CO}_2]$ varies little over this range. If the calculated value of $[\text{CO}_2]$ at $x = 1.0$ was equal to the specified solution composition, then the selected value of β was correct. Otherwise, a new value of β was selected and the integration was repeated.

The dissolution rate per unit radius is given by $4 \cdot 10^{-3} \beta \pi$. If CO_2 hydrolysis is neglected, β is independent of particle size. The rate per unit surface area ($\text{gmol}/\text{cm}^2\text{-sec}$) is given by $2 \cdot 10^{-3} \beta/d$. The rate in sec^{-1} is given by $12 \cdot 10^{-3} \beta/(\rho_m d^2)$.

Simplified Model. The dissolution rate of a single particle of volume V is given by:

$$\frac{dV}{dt} = \frac{-2 \cdot 10^{-3} \beta \pi d^2}{d \rho_m} \quad (20)$$

where ρ_m is the molar density of calcite ($0.0271 \text{ gmol}/\text{cm}^3$). Since d and V are related and β and ρ_m are constants, this equation can be integrated to give the fraction CaCO_3 remaining as a function of time:

$$f = \frac{V}{V_i} = \left(1 - \frac{8 \cdot 10^{-3} \beta t}{\rho_m d_i^2}\right)^{3/2} \quad (21)$$

The rate constant k (cm^2/sec) is defined:

$$k = 1.88 \cdot 8 \cdot 10^{-3} \beta / \rho_m \quad (22)$$

The factor 1.88 is an adjustable constant which accounts for deviation of experimental results from the unadjusted model. Values of β and k are obtained from the general mass transfer model as a function of solution composition and temperature at a particle diameter of $10 \mu\text{m}$. Use of k gives:

$$f = \left(1 - \frac{kt}{d_i^2}\right)^{1.5} \quad (23)$$

With a polydisperse size distribution, the total fraction remaining, F , can be determined by summing over the differential size distribution ϕ_j where ϕ_j is the fraction of total particle volume with initial diameters from d_j to d_{j+1} :

$$F = \sum_{j=1}^n \phi_j \cdot f_j = \sum_{j=1}^n \phi_j \left(1 - \frac{kt}{d_j d_{j+1}}\right)^{1.5} \quad (24)$$

$$f_j = 0 \text{ when } kt > d_j d_{j+1}$$

If a batch experiment gives the fraction remaining, F , as a function of time at constant composition, the rate constant, k , can be calculated from the experimental data and the mass transfer model. Two experimental data points (F_1, t_1) and (F_2, t_2) can be combined with two calculated data points at F_1 and F_2 with [$F_1, (kt)_1$] and [$F_2, (kt)_2$] to get the rate constant k_{exp} :

$$k_{\text{exp}} = \frac{(kt)_2 - (kt)_1}{t_2 - t_1} \quad (25)$$

Diffusivities. Values of diffusivities used in the general model are given in Table I. Diffusivities for ions are taken to be those in absence of a potential gradient, since there is usually a large excess of CaCl_2 to disperse any potential gradient. At 25°C and infinite dilution, ionic diffusivities are given by:

$$D = \frac{RT\lambda_o}{n_j (Fa)^2} \quad (26)$$

where Fa is the Farady number, n_j is the charge on the j th ion, and λ_o is the equivalent ionic conductivity.

Diffusivities at 55°C were estimated by the Stokes-Einstein relationship:

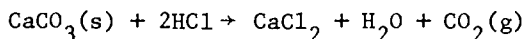
$$\frac{D_1 \eta_1}{T_1} = \frac{D_2 \eta_2}{T_2} \quad (27)$$

For the basic and monohydrogen species of sulfosuccinic acid, the diffusivities were reduced by 45% to 25% respectively to account for Ca^{++} interaction (24).

Experimental Apparatus and Procedure

Rates were measured in a pH-stat with batch dissolution of CaCO_3 at constant pH and solution composition (29). The pH was

automatically controlled ± 0.02 units by titration with 0.2 M HCl with the stoichiometry:



Either CO_2 or N_2 were sparged at 1750 cm^3/min into the solution to maintain a constant PCO_2 and HCO_3^- concentration. The relative change in calcium concentration was minimized by dissolving 5 mM CaCO_3 into solution with 0.1 M dissolved CaCl_2 . The cumulative dissolution was determined directly from a recording of HCl volume added versus time.

The dissolution reactor is shown in figure 1. It was agitated by a three-bladed, marine propellor at 720 rpm.

For runs at 55°C, the reactor temperature was controlled at $\pm 2^\circ\text{C}$ by a water bath. The CO_2 or N_2 gas was presaturated at reactor temperature. The pH (combination, Ag/AgCl) electrode was calibrated at reactor temperature in pH 4 phthalate and pH 7 phosphate buffers.

The reactor held one liter of 0.1 M CaCl_2 solution. Buffers were added in nominal concentrations as needed. The pH was adjusted to the desired value by adding HCl or NaOH. The experiment was initiated by addition of 0.5 g of Fisher Reagent CaCO_3 (precipitated calcite). In runs with sulfite the reactor solution was analyzed by iodimetric titration before and after the experiment.

The particle size distribution of the reagent CaCO_3 is given in Table II. It was determined by a Model TAI Coulter Counter using 0.18 M CaCl_2 electrolyte with a 100 μm aperture.

Typical results of two experiments are given in figure 2. The total fraction remaining, F, calculated from the volume of HCl added is given as a function of dimensionless time, t/t_{50} , where t_{50} is the time required to dissolve 50% of the CaCO_3 . Calculated curves are also given using the simplified mass transfer model with a single particle size (monodisperse) and with the actual polydisperse size distribution (Table 2). The polydisperse model fits the shape of the curve very well at all times. The monodisperse model is only satisfactory for t/t_{50} less than 1.

The experimental rate constant, k, was determined by using equation 25 with the calculated and measured values of F at kt_{50} and kt_{56} . For the run at pH 5, $t_{50} = 11.3$ min. From figure 2:

$$t_{56} - t_{50} = \left(\frac{t_{56}}{t_{50}} - 1.0 \right) 11.3 \text{ min} = 96.8 \text{ sec}$$

From the polydisperse model:

$$kt_{56} - kt_{50} = 6.14 \cdot 10^{-8} \text{ cm}^2$$

Therefore, $k = 6.34 \times 10^{-10} \text{ cm}^2/\text{sec}$.

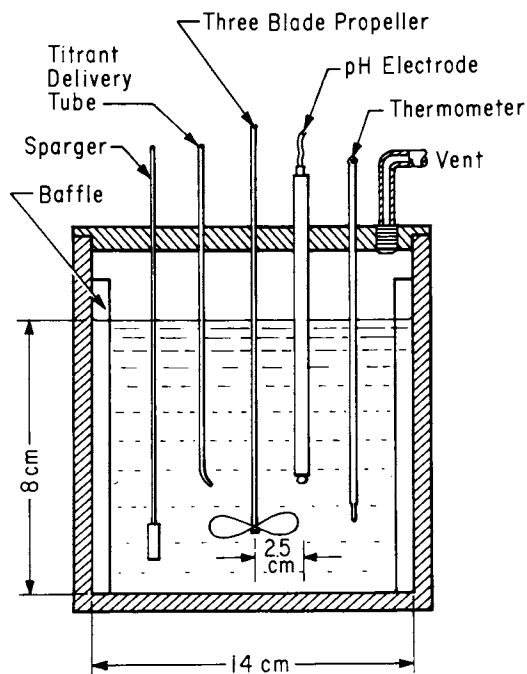


Figure 1. Dissolution reactor.

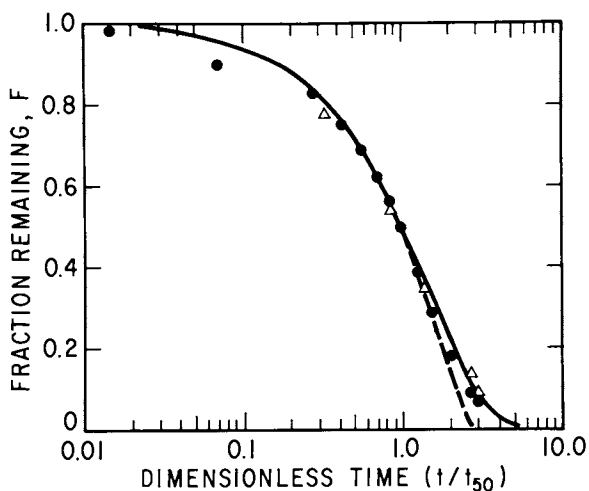


Figure 2. Dissolution curves for reagent grade CaCO_3 at 25°C with N_2 sparging. Key: Δ , pH 4; \bullet , pH 5; —, polydisperse model; and ---, monodisperse model.

Table I: Diffusivities at 25°C

<u>Species</u>	<u>D x 10⁻⁵ (cm²/sec)</u>	<u>Ref.</u>
CO ₂	2.00	25
HCO ₃ ⁻	1.20	26
CO ₃ ⁼	0.70	26
Ca ⁺⁺	0.79	26
H ⁺	9.30	26
CaCO ₃ ⁰	0.75	est.
SO ₃ ⁼	0.70	26
HSO ₃ ⁻	1.33	26
OH ⁻	5.27	26
Adipate ⁼	0.705	27
Hadipate ⁻	0.71	est.
Adipic acid	0.736	28
Acetate	1.09	26
Acetic acid	1.19	30
Sulfosuccinate ⁻³	0.73	28
H ₂ sulfosuccinate ⁼	0.53	24
H ₂ sulfosuccinate ⁻	0.41	24

Table II: Particle Size Distribution of
Reagent Grade CaCO₃ (Fisher)

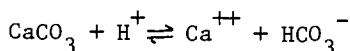
<u>Effective diameter (μm)</u>	<u>Volume % greater than given size</u>
4.0	100.0
5.04	99.8
6.35	98.4
8.00	91.7
10.08	69.7
12.7	30.7
16.0	5.2
20.2	0.6
25.4	0.2
32.0	0.0

Results and Discussion

The measured rate constants, k , for calcite dissolution in 0.1 M CaCl_2 are presented in figures 3 through 8 over the ranges of pH 4.0 to 7.0, 0.0 to 1.0 atm CO_2 , 25 to 55°C, 0 to 10 mM buffer additives, and 0 to 28 mM total sulfite.

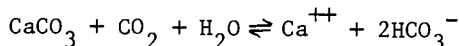
The curves given in figures 3 through 8 were calculated by the general mass transfer model with a 10 μm particle diameter and an empirical factor of 1.88. The mass transfer model accurately predicts the effects of all variables except for inhibition by selected organic acids. There is no evidence of any effect of surface kinetics, even at moderate and high values of pH. If surface kinetics were important the measured rate would be less than that predicted by the unadjusted model. However, the measured rate is 1.88 times greater than the unadjusted model. Therefore, it is highly probable that the distinguishing characteristic of natural, ground limestones will be their particle size distribution. Limestone reactivity should be independent of BET surface area, grain size, and other such variables.

Effect of pH. Figures 3 and 4 show that dissolution rate is a strong function of pH. With CO_2 sparging at 25°C the dissolution increases a factor of 6.7 from pH 4.0 to pH 5.0. At these conditions the dissolution is controlled primarily by H^+ diffusion from the bulk solution with a stoichiometry given approximately by:

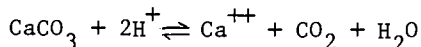


The adjusted model gives 0.36 cm/sec as the mass transfer coefficient of H^+ with a 10 μm particle. This compares to 0.05 cm/sec measured by Plummer *et al* (6) with much larger particles.

Effect of CO_2 . Figures 3 and 4 show that high CO_2 partial pressure generally enhances the dissolution rate by about 15% except close to equilibrium. Berner and Morse (7) observed a similar effect with precipitated CaCO_3 . At pH 4.5 to 5.0, CO_2 probably enhances by diffusion from the bulk solution with the following net finite-rate reaction and stoichiometry:



At pH less than 4 to 4.5, the finite-rate CO_2 reaction produces CO_2 in the boundary layer and requires somewhat higher H^+ stoichiometry as follows:



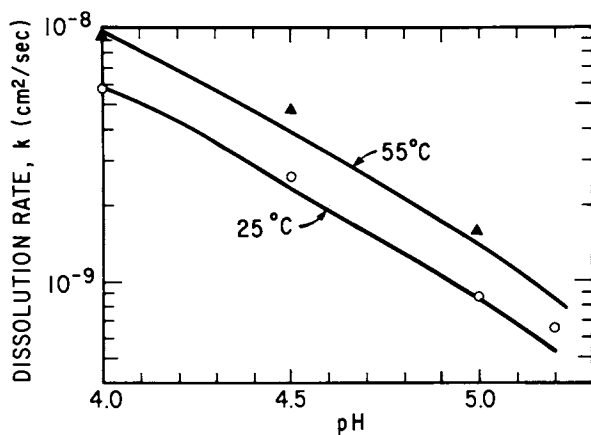


Figure 3. Dissolution rate of reagent grade CaCO_3 with CO_2 sparging in 0.1 M CaCl_2 .

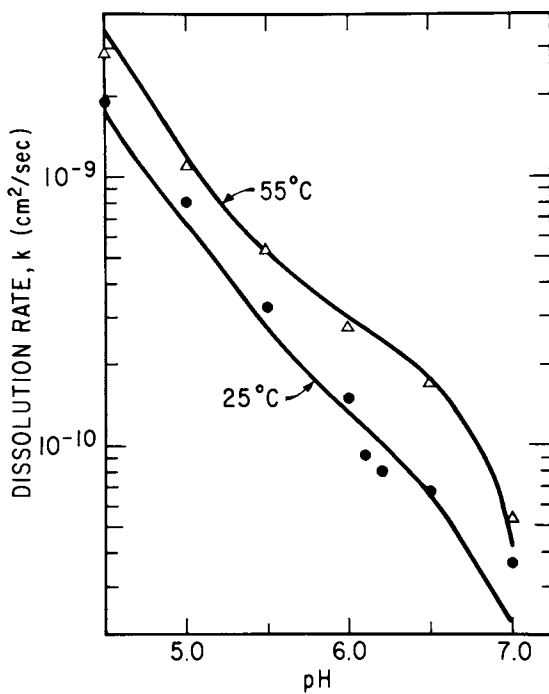


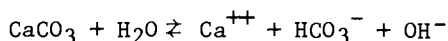
Figure 4. Dissolution rate of reagent grade CaCO_3 with N_2 sparging in 0.1 M CaCl_2 .

At pH 5.0, Plummer et al (6) found that 1 atm CO₂ increased the dissolution rate of coarse Iceland spar a factor of five. The participation of CO₂ is limited by a homogeneous reaction in the mass transfer boundary layer. The volume of the boundary layer is greater than the surface area in coarser particles. Therefore, a much larger effect is expected with coarse particles.

With CO₂ sparging the calculated equilibrium pH in 0.1 M CaCl₂ is 5.6 at 25°C and 5.4 at 55°C. Therefore, CO₂ sparging inhibits dissolution above about pH 5.2.

Effect of Temperature. At pH 5.0 or less, figures 3 and 4 show that the dissolution rate increases by a factor of 1.6 to 1.8 from 25 to 55°C. This gives an activation energy of about 4 kcal/gmol, corresponding to the effect of temperature on diffusivities.

Above pH 6.0, CaCO₃ dissolution is controlled mostly by diffusion of OH⁻ and HCO₃⁻ from the limestone surface. The driving force for this diffusion is determined to a large extent by the equilibrium:



This equilibrium changes significantly with temperature. Therefore, at pH 6 to 6.5 with N₂ sparging, the rate increases a factor of 3 from 25°C to 55°C, giving an activation energy of about 7 kcal/gmol. Other investigators have attributed this higher temperature dependence to surface kinetics, but our results showed that it arises from an effect of temperature on diffusivities and solution equilibria.

Effect of Organic Acids

Figures 5, 6, and 7 demonstrate the effect of organic acids on the dissolution rate at 25°C. Additives that provide buffer capacity between the bulk solution pH (4.0 to 5.5) and the pH at the limestone surface (5.5 to 8.0) enhance dissolution rate by providing an additional means of diffusing acidity to the limestone surface. Figure 5 shows that at pH 5.0, 3 mM total acetic acid enhances the dissolution rate a factor of 7. This enhancement is somewhat greater at higher pH, where H⁺ diffusion is much more limited.

At pH 5, the effect of CO₂ is insignificant in the presence of acetic acid. With CO₂ sparging at pH 5.5, very near the equilibrium pH of 5.6, the calculated rates with acetic acid (figure 5) are 2-3 times greater than the measured rates. This discrepancy may result from experimental pH error, or from error in accurately estimating the equilibrium pH.

Figure 6 shows that adipic acid is 20 to 50% more effective than acetic acid. Figure 7 shows that acrylic and sulfosuccinic acids are about equivalent. However, hydroxypropionic,

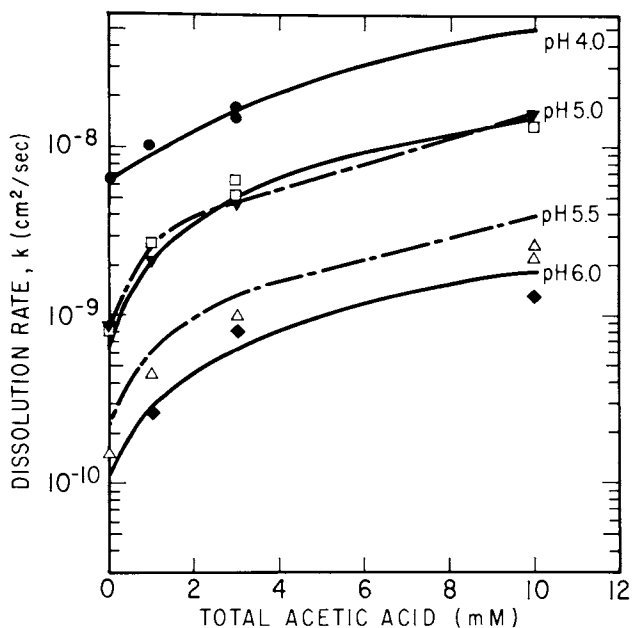


Figure 5. Effect of acetic acid on CaCO_3 dissolution at 25°C in 0.1 M CaCl_2 . N_2 sparge (—): ●, pH 4.0; □, pH 5.0; and △, pH 6.0. CO_2 sparge (---): ▼, pH 5.0; and ◆, pH 5.5.

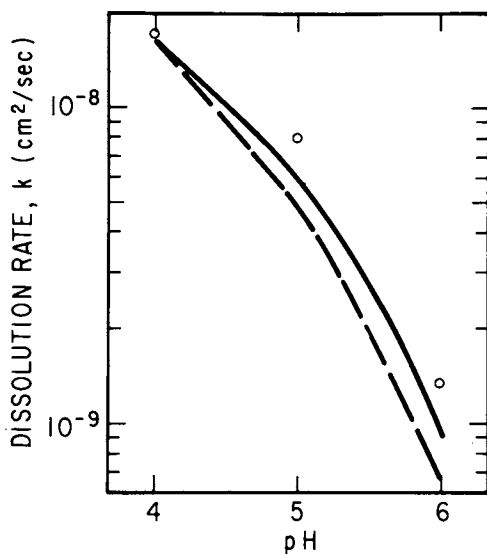


Figure 6. Dissolution rate of CaCO_3 in 0.1 M CaCl_2 with N_2 sparging at 25°C , and 3 mM adipic acid. Key: —, adipic; and ---, acetic.

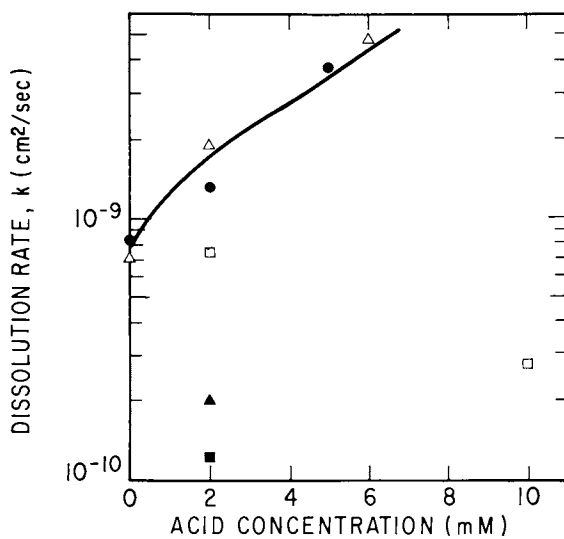


Figure 7. Effect of organic acids on dissolution rate in 0.1 M CaCl_2 with N_2 sparging at 25°C and $\text{pH } 5$. Key: Δ , acrylic; \bullet , sulfosuccinic; \square , sulfopropionic; \blacktriangle , hydroxypropionic; and \blacksquare , polyacrylic.

sulfopropionic, and polyacrylic acids inhibit limestone dissolution, probably by surface adsorption of polyacrylic acid. Sulfopropionic acid was synthesized by reaction of acrylic acid with SO_3^- in the presence of air (31). Hydroxypropionic acid was synthesized by hydration of 2 M acrylic acid at 100°C in 1 M H_2SO_4 for 20 hours (31). Both of these procedures could give some polyacrylic acid impurities by free radical polymerization.

Effects of Sulfite. The effects of total dissolved sulfite are given in figures 8 and 9. At low concentrations sulfite enhances dissolution by acting as a buffer. However, at concentrations greater than 1 mM, sulfite appears to inhibit CaCO_3 dissolution. This effect is more apparent at higher pH values. The range of sulfite concentration at which inhibition becomes apparent corresponds closely to the solubility of CaSO_3 solids in high pH solution, characteristic of the pH at the limestone surface. At lower pH values CaCO_3 dissolution rates do not actually decrease significantly until the bulk solution approaches the solubility limit of CaSO_3 . All of the measured rates were well-behaved, therefore irreversible CaSO_3 blinding of the surface is not occurring.

Figure 9 shows that at pH 5 3 mM sulfite enhances dissolution with less than 2 mM acetate, but inhibits above 2 mM acetate.

The enhancing and inhibiting effect of sulfite can be modeled as a shift in equilibrium at the calcite surface. Thus, the equilibrium $[\text{CaCO}_3^0]$ is reduced by increased $[\text{CaSO}_3^0]$, much like a solid solution at the CaCO_3 surface. Using the general mass transfer model, the solution composition at the CaCO_3 surface was calculated from the experimental rate data.

Figure 10 shows that the calculated surface concentrations of CaCO_3^0 and CaSO_3^0 are correlated by the equation:

$$\log [\text{CaCO}_3^0] = -10.76 - 1.29 \log [\text{CaSO}_3^0] \quad (28)$$

Thus, CaSO_3^0 concentration quantitatively reduces the equilibrium solubility of CaCO_3^0 , probably by forming a solid solution or adsorption layer at the calcite surface. For $[\text{CaSO}_3^0]$ less than 0.05 mM, $[\text{CaCO}_3^0]$ at the surface is equal to its normal equilibrium value, 6.80×10^{-7} M. The calculated rate is obtained by successive trial and error with β until the above solid solution equilibrium is satisfied.

As shown in figure 8, the modified mass transfer model predicts the measured rate well at pH 4.5, 5.0, and 6.0, but deviates significantly at pH 5.5 and 5.75. These deviations may result from the sensitivity of the calculated rates to the estimated equilibrium constants and diffusivities used in the model. The maximum dissolution rates at each pH correspond roughly to the CaSO_3 solubility, shifting to higher sulfite concentrations at lower pH. A higher dissolution rate was observed at 55°C , but the rates are still modeled well by mass

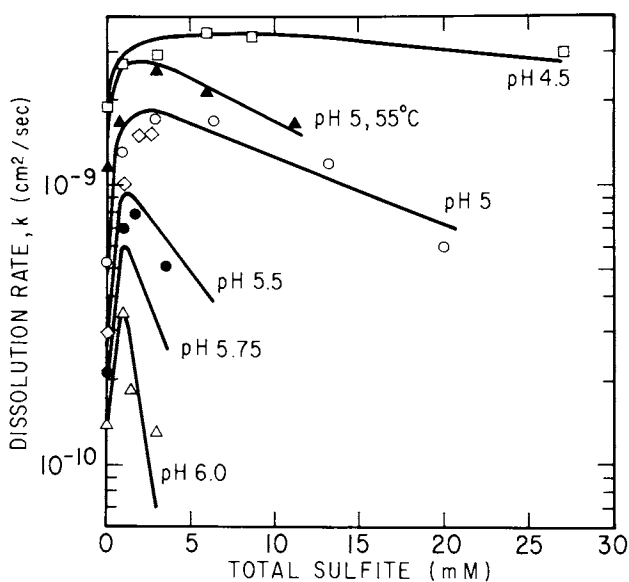


Figure 8. Effect of sulfite with N_2 sparging at 25 and 55°C. Curves calculated from mass transfer model. Including $CaCO_3^o/CaSO_3^o$ solid solution (Figure 10). pH: \square , 4.5; \circ and \blacktriangle , 5.0; \diamond , 5.5; \bullet , 5.75; and \triangle , 6.0; and \blacktriangle , 55°C.

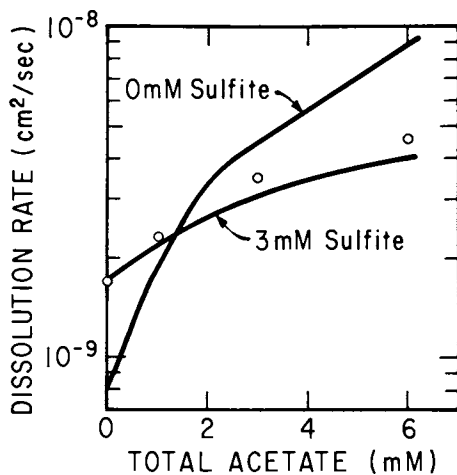


Figure 9. Effect of acetate on dissolution rate with 3 mM of total sulfite (pH 5 and 25°C).

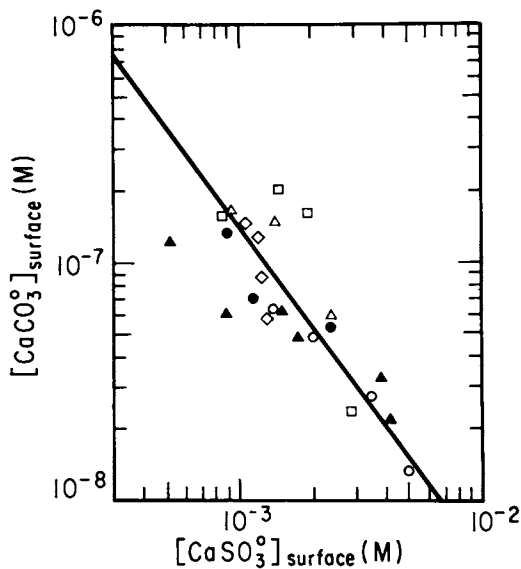


Figure 10. Calculated solution composition at CaCO_3 surface with N_2 sparging at 25°C. pH: ▲, 4.5; ○, 5.0; □, 5.5; △, 5.75; ●, 6.0; and ◇, 5.0 w/acetate.

transfer with the same $\text{CaSO}_3^0/\text{CaCO}_3^0$ equilibrium. It is significant that the solid solution equilibrium predicts well even with the higher rates in acetate buffer (figure 9). Therefore, sulfite affects surface equilibrium, not surface kinetics.

Inhibition by sulfite is analogous to inhibition by phosphate (7, 13) and metal ions (13, 14, 15). Inhibition by metal ions has also been modeled by a reduction in CaCO_3 solubility. Calcium phosphate and metal carbonates are relatively insoluble salts that could form adsorption layers or solid solutions at a calcite surface.

Sulfite inhibition is very significant for commercial applications in scrubber systems using CaCO_3 to produce CaSO_3 solids. CaSO_3 nucleation/crystallization may interact strongly with CaCO_3 utilization. Inhibitors of CaSO_3 crystallization such as Mg^{++} or dissolved iron may result in high CaSO_3 supersaturation which would in turn inhibit CaCO_3 dissolution. At very high CaSO_3 supersaturation irreversible blinding of the CaCO_3 surface could occur.

Conclusions and Recommendations

1. Limestone dissolution in throwaway scrubbing can be modeled by mass transfer. The mass transfer model accurately predicts effects of pH, PCO_2 , temperature, and buffers. For particles less than 10-20 μm , the mass transfer coefficient can be obtained by assuming a sphere in an infinite stagnant medium. This model underpredicts the absolute dissolution rate by a factor of 1.88, probably because it neglects agitation and actual particle shape.

2. Organic buffer additives such as acetic, adipic, acrylic, and sulfosuccinic acid enhance the rate of calcite dissolution by providing for mass transfer of acidity to the limestone surface.

3. At pH 4.5 to 5.5, PCO_2 of 1 atm increases the rate of dissolution by 15% because of the indirect reaction of CO_2 with CaCO_3 . However, at low pH (4.0), the effect of PCO_2 is insignificant. High PCO_2 is also a dominant factor in determining the equilibrium pH at which dissolution stops.

4. The rate of dissolution is enhanced at low sulfite concentration and inhibited at high sulfite concentration. These phenomena are modeled by mass transfer with a solid solution equilibrium of CaSO_3^0 and CaCO_3^0 .

5. The rate of calcite dissolution is a function of the solution composition and particle size distribution. The rate should be independent of surface roughness, internal surface area, and other variables.

6. The effects of temperature are predicted by the mass transfer model with appropriate physical constants. High temperature dependence at high pH results from the effect of temperature on OH^- equilibrium.

7. More experimental data are needed to establish better the validity of the mass transfer model near equilibrium pH.

Nomenclature

a	- activity, M
D	- diffusivity, cm^2/sec
d	- particle diameter, cm
Fa	- Faraday Number, 23,062 cal/volt-equiv
f	- fraction remaining of a given size fraction
F	- total fraction remaining
ΔH	- apparent heat of reaction, kcal/mol
k	- dissolution rate constant, cm^2/sec
M	- molar, gmol/liter
n_j	- charge on the jth ion
P_{CO_2}	- partial pressure of CO_2 , bar
pH	- negative logarithm of hydrogen ion activity
R	- universal gas constant, 0.08205 liter-atm/gmol-K
r	- distance from center of sphere, cm
T	- temperature, $^\circ\text{K}$
t	- time, sec
t_{50}	- time for 56% of CaCO_3 remaining, sec
t_{56}	- time for 56% of CaCO_3 remaining, sec
V	- volume of particle, cm^3
x	- dimensionless distance $(1 - d/2r)$
β	- rate of dissolution per unit radius, $\text{M cm}^2 \text{sec}^{-1}$
α_i, β_i	- constants of integration, $\text{M cm}^2 \text{sec}^{-1}$
γ	- activity coefficient
λ_0	- equivalent ionic conductivity at infinite dilution $\text{cm}^2/\text{gmol}/\text{ohm}$
η	- viscosity, poise
ϕ_j	- the fraction of total particle mass with diameter from d_j to d_{j+1}
[]	- concentration, M

Superscripts

o - ion pair, degrees

Subscripts

b - bulk
 exp - experimental
 s - surface
 i - initial

Acknowledgments

This work was performed under EPA Cooperative Agreement 806251. The EPA project officer was Robert H. Borgwardt.

Literature Cited

1. Rochelle, G.T., and King, C.J., Chem. Eng. Prog. 1978, 74, 65.
2. Chan, P.K.R., M.S. Thesis, University of Texas, Austin, Texas, 1981.
3. Toprac, A.J., and Rochelle, G.T., "Limestone Dissolution in Stack Gas Desulfurization Processes - Effect of Type and Grind", presented at AIChE Annual Meeting, New Orleans, November 8-12, 1981, in press, Env. Prog.
4. Toprac, A.J., M.S. Thesis, University of Texas, Austin, Texas, 1981.
5. Rochelle, G.T., "Process Synthesis and Innovation in Flue Gas Desulfurization", EPRI FP-463-SR, 1977.
6. Plummer, L.N., Parkhurst, D.L., and Wigley, T.M.L., ACS Symp. Ser., 1979, 93, 537.
7. Berner, R.A., and Morse, J.W., Amer. J. Sci. 1974, 274, 108.
8. Plummer, L.N., Wigley, T.M.L. and Parkhurst, D.L., Amer. J. Sci. 1978, 278, 179.
9. Barton, P., and Vatanatham, T., Env. Sci. and Tech. 1976, 10, 262.
10. Sjoberg, E.L., Geochim. Cosmochim. Acta. 1976, 40, 441.
11. Erga, O., and Terjesen, S.G., Acta. Chem. Scand. 1956, 10, 872.
12. Ottmers, D., Phillips, J., Burklin, C., Corbett, W., Phillips N., and Shelton, C., "A Theoretical and Experimental Study of the Lime/Limestone Wet Scrubbing Process", EPA Report No. EPA-650/2-75-006, 1974.
13. Sjoberg, E.L., Stock. Contr. Geol., 1981, 32(1), 1.
14. Terjesen, S.G., Erga, O., Thersen, G., and Ve, A., Chem. Eng. Sci. 1961, 14, 277.
15. Koss, V., and Moller, P., Z. Anorg. Allg. Chem. 1974, 410, 165.
16. Garrels, R.M., and Thompson, M.E., Am. J. Sci. 1962, 260, 57.
17. Harned, H.S., and Scholes, S.R. Jr., J. Am. Chem. Soc. 1941, 63, 1706.
18. Tartar, H.V., and Garretson, H.H., J. Am. Chem. Soc. 1941, 63, 808.
19. Lowell, P.S., Ottmers, D.M., Schwitzgebel, K., Strange, T.I., and Deberry, D.W., "A Theoretical Description of the Limestone Injection - Wet Scrubbing Process", PB 193-029, U.S. Environmental Protection Agency, 1970.
20. Cavanaugh, C.M., M.S. Thesis, University of Texas at Austin, Austin, Texas, 1978.
21. Harned, H.S., and Bonner, F.T., J. Am. Chem. Soc. 1945, 67 1026.
22. Pinsent, R.W., Pearson, L., and Roughton, F.J.W., Trans. Far. Soc. 1956, 52, 1512.
23. Nielsen, K.L., "Methods in Numerical Analysis", 2nd Edition, New York, MacMillan, 1964.

24. Weems, W.T., M.S. Thesis, University of Texas, Austin, Texas, 1981.
25. Sherwood, T.K., Pigford, R.L., and Wilke, C.R., "Mass Transfer" McGraw-Hill, 1975.
26. Landolt-Bornstein Physikalisch-Chemische Tabellen, Bd. II-7 225, Springer-Verlag, Berlin, Germany, 1960.
27. Jeffrey, G.H., and Vogel, A.I., J. Chem Soc. 1935, 21.
28. Albery, W.J., Greenwood, A.R., and Ribble, R.F., Trans. Far. Soc. 1967, 63, 360.
29. Morse, J.W., Amer. J. Sci. 1974, 274, 97.
30. Lewis, J.B., J. Appl. Chem. 1955, 5, 225.
31. Smith, R.C., M.S. Thesis, The University of Texas, Austin, Texas, 1981.

RECEIVED December 10, 1981.

Studies of the Major Factors Affecting Magnesium Limestone Dissolution

FRANK B. MESEROLE and ROBERT L. GLOVER
Radian Corporation, Austin, TX 78759

DOROTHY A. STEWART
Electric Power Research Institute, Palo Alto, CA 94394

This paper summarizes the results from a laboratory study funded by the Electric Power Research Institute (EPRI) to examine the factors which affect limestone reactivity and the availability of magnesium in limestone. The use of limestone in calcium-based SO₂ wet scrubbers is well demonstrated technology. However, guidelines to assess the acceptability of a given limestone for a specific scrubbing system are incomplete. Size, calcium concentration, and inert content are generally the only criteria included in the limestone specifications. Experience as well as theoretical considerations indicate that these properties are insufficient to uniquely gauge the reactivity of the limestone. The chemical composition, the crystal lattice imperfections, and the composition of the specific scrubber solution may also affect the dissolution rate and hence the acceptability of the limestone. The availability of the magnesium in limestone to dissolve is also important since the presence of magnesium is beneficial to scrubber efficiency. However, not all the magnesium in limestones will dissolve under scrubber conditions. Therefore, this study was funded to examine key variables including temperature, particle size, pH, stir rate, and the magnesium level in the dissolving solution.

The use of limestone in calcium-based SO₂ wet scrubbers is economically preferable at large facilities such as electrical utilities' coal-fired generating plants because of the increasing cost differential between limestone and lime. This differential is caused by the continually rising fuel costs incurred in the calcination of limestone to lime. However, the economic advantage of limestone is diminished if its utilization in a particular process is low. Low utilization results in higher reagent costs as well as increased disposal burden. This paper presents a laboratory apparatus and test procedure to measure the reactivity of different limestones at a variety of simulated scrubber operating conditions. The results from this test can then be used to choose the most appropriate limestone.

0097-6156/82/0188-0099\$6.00/0
© 1982 American Chemical Society

The limestone reactivity test procedure calls for the samples to be ground and screened to produce material in narrow particle size ranges for testing. Solution composition and pH are maintained constant throughout the measurement period (up to 20 hours) at preselected values. The selection of pH and solution compositions is based upon several design criteria including:

- desired operating pH,
- forced versus natural oxidation,
- quality of makeup water,
- degree of solids dewatering, and
- scrubber design.

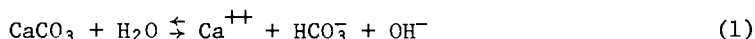
Using an SO₂ wet scrubber computer model, the above information can be used to predict the solution composition in a system at steady-state conditions. Further descriptions of the test equipment and procedure as well as recent experimental data on a variety of limestones are presented in the following sections.

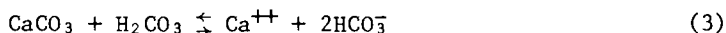
Discussion

The dissolution of limestone is known to be controlled by both diffusion of ions in solution and surface reaction rates. The pH value influences which of these steps dominates in the limestone dissolution. For example, at pH values less than 5 the diffusion process dominates the dissolution with little dependence on surface reaction. On the other hand, at pH values greater than 7 the reaction at the limestone surface begins to dominate the dissolution process. In the pH range between 5 and 7 both dissolution steps can influence the overall rate.

The bulk of the limestone dissolution in most SO₂ scrubbers occurs in the 5-6 pH range. Thus, both solution mass transfer properties and the nature of the limestone must be considered at typical operating conditions. Therefore, the pH, solution composition, solution buffer capacity, and the nature of the limestone are important considerations when designing for maximum limestone utilization. This paper deals primarily with the measurement of the influence of limestone properties on the overall dissolution rate.

The chemical reactions involving calcium carbonate at the surface of the solids in the scrubber pH operating range are:





Reaction (2) is thought to have a more rapid rate than reactions (1) and (3). This is substantiated by experimental data that show the log of the dissolution rate to be inversely proportional to the pH in the range of 2 to 5 (1). However, at pH values above 5, the hydrogen ion concentration decreases significantly and thus this step becomes less significant. This is also the case for the reaction shown in equation (3). Therefore, equation (1) represents the predominate dissolution mechanism at high pH.

Since water is the reactant in equation (1), the diffusion should be important only in removing the products from the reaction zone. The measurements presented in the Experimental Results Section were designed to determine the relative effects of the surface reaction rate and the diffusion of products on the overall dissolution rate. The variables in these tests were temperature, pH, stirring rate, and type of limestone.

The equation used for correlating the data is:

$$\text{D.R.} = k \cdot \text{SA} \cdot (\text{RS}-1)^n \quad (4)$$

where,

D.R. = dissolution rate,

k = reaction rate constant, constant with temperature and limestone type,

SA = limestone surface area,

RS = degree of subsaturation of calcium carbonate in the boundary layer, and

n = exponent usually equal to 1.

The difficulty with applying equation (4) is the uncertainty as to whether the RS value measured in the bulk liquor (which can be measured) is the same as the RS in the boundary layer surrounding the limestone particles (which cannot be measured). Test conditions employing high stirring rates and relative large particles (~100 μm) have been chosen to minimize the differences in these two RS values.

Experimental Approach

The experimental apparatus shown in Figure 1 was used to evaluate limestone reactivity. Conditions in the reactor approximate conditions in the reaction tank of a limestone scrubbing system. As the limestone dissolves, the pH in the reactor will begin to rise. Therefore, to insure a constant pH in the experimental reactor, a low pH test solution (see Table I) is metered to the reactor. As the low pH feed is added, an equal amount of reactor liquor is also withdrawn to maintain the reactor volume also remains constant (2.5L). In an actual scrubbing system, SO₂ absorbed from the flue gas will provide enough acidity such that the pH remains approximately constant.

TABLE I. SCRUBBER FEED COMPOSITION (mmol/L)

	<u>Normal Conditions</u>	<u>High Magnesium Scrubber Feed</u>
Na ₂ SO ₄	24	24
HCl	25	25
MgCl ₂	0	87
pH	2.0	2.0

Prior to testing, 3.0–3.5L of scrubber feed solution are saturated overnight with approximately 10 g of the limestone of interest. Saturation is accomplished at the temperature at which the run is to be performed. Ten grams of the limestone are ground and sized to the desired mesh. Pictures were taken using an optical microscope to document the size distribution.

The next day the filtered solution is then used as the initial charge to the reactor. In this way, the initial reactor composition will be approximately the same in the beginning as during the run. The pH controller is then set to the desired value. The pH controller is used to meter scrubber feed liquor (pH 2) into the reactor to maintain a constant reactor pH. After the stirring rate has been set and the desired temperature reached, 10.00 g of sized limestone are added to the reactor.

As the run proceeds, the accumulated volume leaving the reactor is recorded. Samples of the reactor liquor are also taken periodically and analyzed for calcium and magnesium by atomic absorption. By maintaining a constant reactor pH, the composition remains fairly constant throughout the run. Based upon the flow rate data and the solution composition, the fraction of the stone dissolved and dissolution rate can then be calculated.

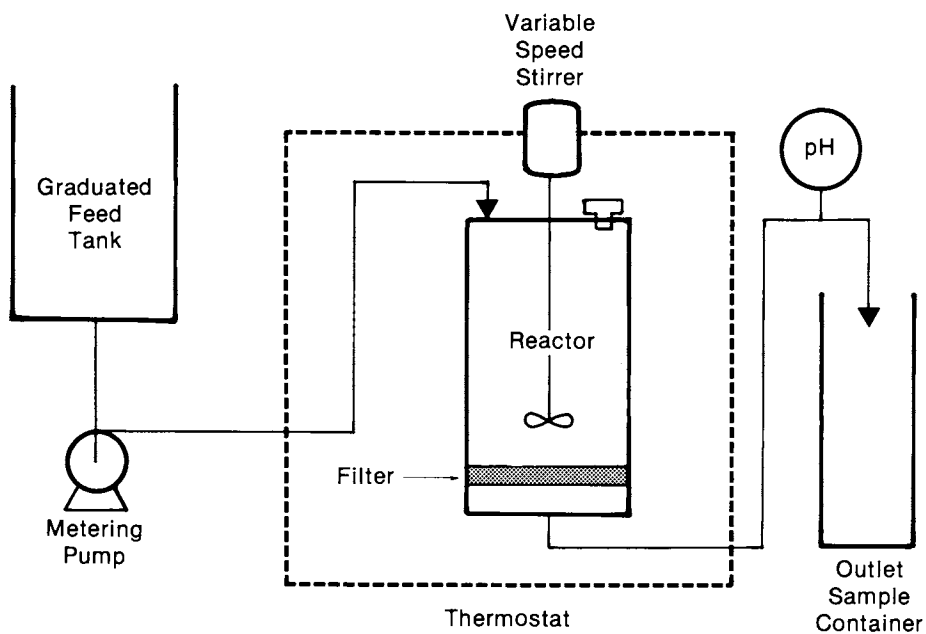


Figure 1. Limestone reactivity apparatus.

Experimental Results

Fifteen runs using three limestones are reported for various reactor conditions. A base case experiment was performed for each of three limestones: 1) Fredonia, 2) Brassfield, and 3) Pfizer (see Tables II and III). Operating conditions were then varied to show the effect of stir rate, temperature, and pH as well as reactor feed composition.

Each stone was ground and sized to 120-200 mesh in an attempt to minimize differences in surface area between the samples. Based upon optical counts of the three sized stones, each sample used in the experiments had approximately the same average particle diameter (Fredonia - 134 μm , Pfizer - 147 μm , Brassfield - 133 μm). However, no attempt was made to correct for any surface area differences due to different limestone porosities.

The experimental results are summarized in Table IV. The run condition describes the operating variable which was changed from the base line conditions. For Fredonia, the effects of temperature (30°C, 50°C, 60°C), stir rate (500 rpm, 1000 rpm, 1500 rpm) and pH (5.0, 5.8) were examined. For Brassfield, a high temperature (60°C), low pH (5.0), and high magnesium (87 mmol/L) cases were run in addition to the base case. Base, low pH (5.0), and high magnesium (87 mmol/L) cases were conducted for Pfizer.

TABLE II. BASE CASE OPERATING CONDITIONS

Stir Rate	500 rpm
Temperature	50°C
pH	5.8
Particle Size	120-200 mesh
Reactor Feed Composition	
Na_2SO_4	24 mmol/L
HCl	25 mmol/L
MgCl_2	0 mmol/L

TABLE III. COMPOSITIONS OF LIMESTONE SAMPLES TESTED

<u>Limestone</u>	<u>Composition (wt%)</u>		
	<u>CaCO₃</u>	<u>MgCO₃</u>	<u>Inerts</u>
Fredonia	96.8	1.5	1.7
Brassfield	88.3	9.0	2.7
Pfizer	94.6	4.8	0.6

The calcium and magnesium dissolved from the limestones are calculated by multiplying their respective liquid concentrations (mg/L) by the volume of liquor leaving the reactor during some increment of time. By summing over the various time increments, the total amounts of calcium and magnesium which have dissolved can be calculated.

To aid in analyzing the data and to allow extrapolation to greater dissolution fractions (typically only 40-50 percent of the stone dissolves in a 6 hour run), the data are fit to a power function of the form:

$$1 - W/W_0 = at^b \quad (5)$$

where,

W = weight (g) of calcium or magnesium remaining in limestone at time t ;

W_0 = initial weight (g) of calcium or magnesium in limestone;

a, b = constants; and

t = time (min.).

By differentiating equation (5), the rate of dissolution at any time (t) can be calculated from:

$$\frac{dW}{dt} = -W_0 abt^{b-1} \quad (6)$$

Using equation (6), the dissolution rates of CaCO₃ and MgCO₃ were calculated when 50 percent of the calcium and magnesium had dissolved (see Table IV). The values reported in Table IV represent the rate of dissolution (dW/dt) divided by the amount of CaCO₃ or MgCO₃ left in the limestone (50 percent of W_0). The Fredonia base case dissolution rates from three replicate tests were calculated to be 1.77×10^{-3} , 1.75×10^{-3} , and 2.05×10^{-3} g/min/g CaCO₃(s) at 50 percent CaCO₃ dissolved.

TABLE IV. SUMMARY OF RESULTS

Limestone	Run Condition	CaCO ₃ Dissolution		MgCO ₃ Dissolution	
		Dissolution Rate at $t=t^{1/2}$ $\left(\frac{\text{g/min}}{\text{g CaCO}_3(\text{S})}\right)$	Correlation Coefficient	Dissolution Rate at $t=t^{1/2}$ $\left(\frac{\text{g/min}}{\text{g MgCO}_3(\text{S})}\right)$	Correlation Coefficient
Fredonia	Base ³	1.8 x 10 ⁻³	0.999	0.78 x 10 ⁻³	0.999
	Base	1.8 x 10 ⁻³	1.000	0.78 x 10 ⁻³	1.000
	Base	2.0 x 10 ⁻³	0.999	0.85 x 10 ⁻³	0.999
	60°C	3.8 x 10 ⁻³	0.996	1.7 x 10 ⁻³	0.996
	pH 5.0	8.9 x 10 ⁻³	0.964	4.9 x 10 ⁻³	0.972
	1000 rpm	2.2 x 10 ⁻³	1.000	0.87 x 10 ⁻³	1.000
	1500 rpm	2.5 x 10 ⁻³	0.989	0.76 x 10 ⁻³	0.992
	30°C	0.63 x 10 ⁻³	0.999	0.21 x 10 ⁻³	1.000
	Base	1.4 x 10 ⁻³	1.000	0.16 x 10 ⁻³	1.000
	60°C	1.8 x 10 ⁻³	1.000	0.26 x 10 ⁻³	1.000
Brassfield	pH 5.0	4.0 x 10 ⁻³	0.998	1.4 x 10 ⁻³	0.998
	High Mg	1.3 x 10 ⁻³	0.997	--	--
	Base	1.6 x 10 ⁻³	1.000	0.48 x 10 ⁻³	1.000
Pfizer	pH 5.0	3.6 x 10 ⁻³	0.998	1.4 x 10 ⁻³	0.999
	High Mg	1.5 x 10 ⁻³	0.996	--	--

¹ $t^{1/2}$ = time required to dissolve 50% of the CaCO₃

² $t^{1/2}$ = time required to dissolve 50% of the MgCO₃

³ Stir Rate = 500 rpm, T = 50°C, pH = 5.8, Low Mg

Comparing the CaCO_3 dissolution rates for the three stones, Fredonia appears to dissolve only slightly faster than either Pfizer or Brassfield with Brassfield the slowest of the three. The differences in the MgCO_3 dissolution rates are more significant; again, Fredonia appears to be the fastest dissolving.

Low pH increased the dissolution rates of both CaCO_3 and MgCO_3 for all the stones as expected. Figure 2 graphically illustrates the effect of pH on the CaCO_3 dissolution rate. Fredonia shows the greatest increase in dissolution at the lower pH. However, both Brassfield and Pfizer also show substantial increases in dissolution rate.

Higher temperature seemed to increase the dissolution rates of CaCO_3 and MgCO_3 for both Fredonia and Brassfield. Figure 3 shows the effect of temperature on the CaCO_3 and MgCO_3 dissolution rates for the Fredonia stone. The linear nature of the graphs suggests an Arrhenius form for the temperature dependence. This indicates that a temperature dependent reaction(s) (such as the surface dissolution) may play a major role in limiting the dissolution of the Fredonia limestone at pH 5.8.

Several runs were also made for the Fredonia stone at various stirring rates. As shown in Table IV and Figure 4, the stirring rate did not have a drastic effect on either the calcium or magnesium dissolution rates. There was a slight increase seen in the CaCO_3 dissolution rate at 1000 rpm and 1500 rpm. However, the change in the CaCO_3 dissolution (approximately 30 percent from 500 rpm to 1500 rpm) is not that significant when compared to other factors such as temperature. Finally, the magnesium level in the dissolving solution did not seem to affect the CaCO_3 dissolution rate of either Brassfield or Pfizer.

Conclusions

The results reported in this paper represent only three of the seven limestones which will be tested during this study. However, based upon the results to date the following conclusions can be made.

1. CaCO_3 and MgCO_3 dissolution data at various temperatures suggest an Arrhenius form of the temperature dependence. The calculated activation energy of 11 Kcal/mole indicate that the dissolution at pH 5.8 is reaction rate, not diffusion, limited.
2. There does appear to be some difference between limestones in the CaCO_3 dissolution rate. However, the most significant difference between stones is the rate of dissolution of MgCO_3 .

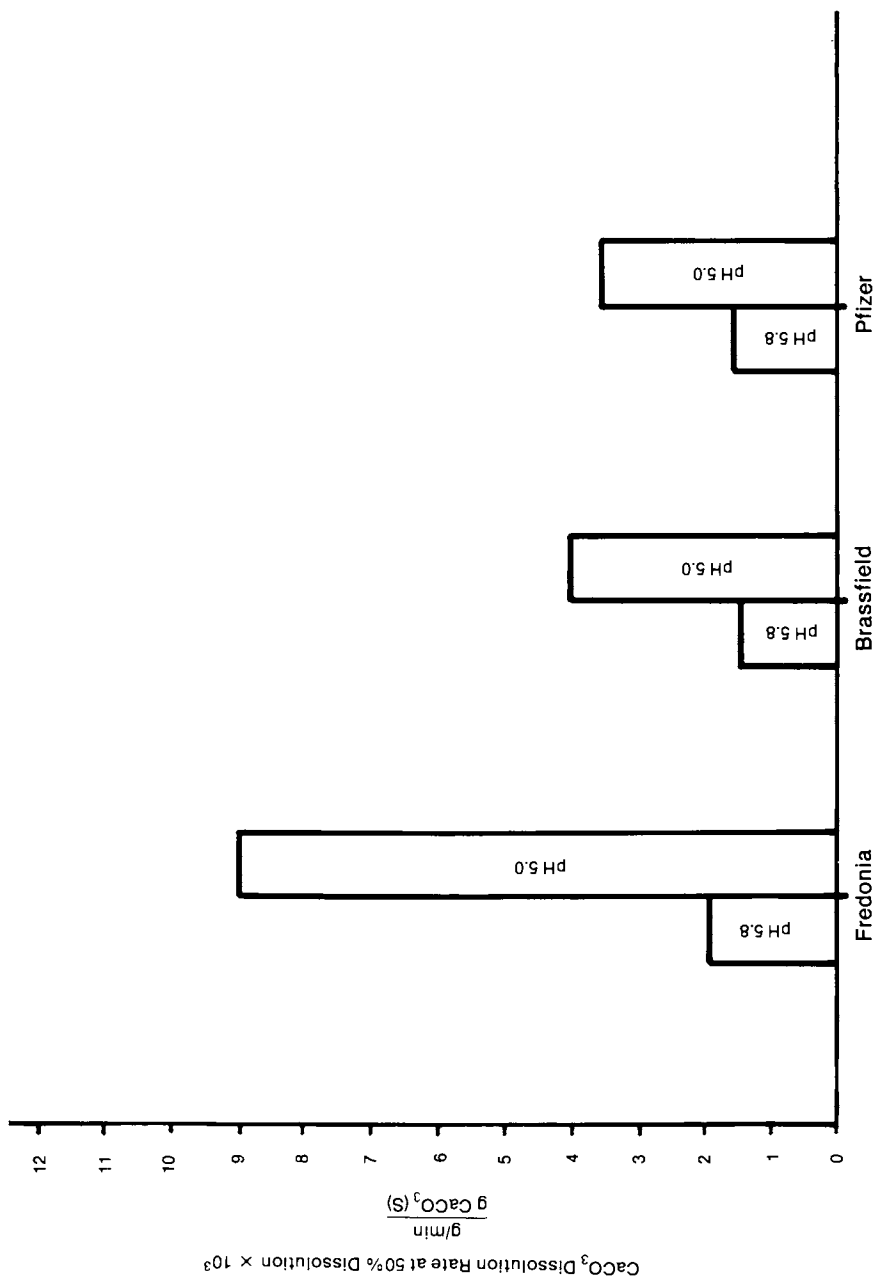


Figure 2. Effect of pH on CaCO₃ dissolution rate.

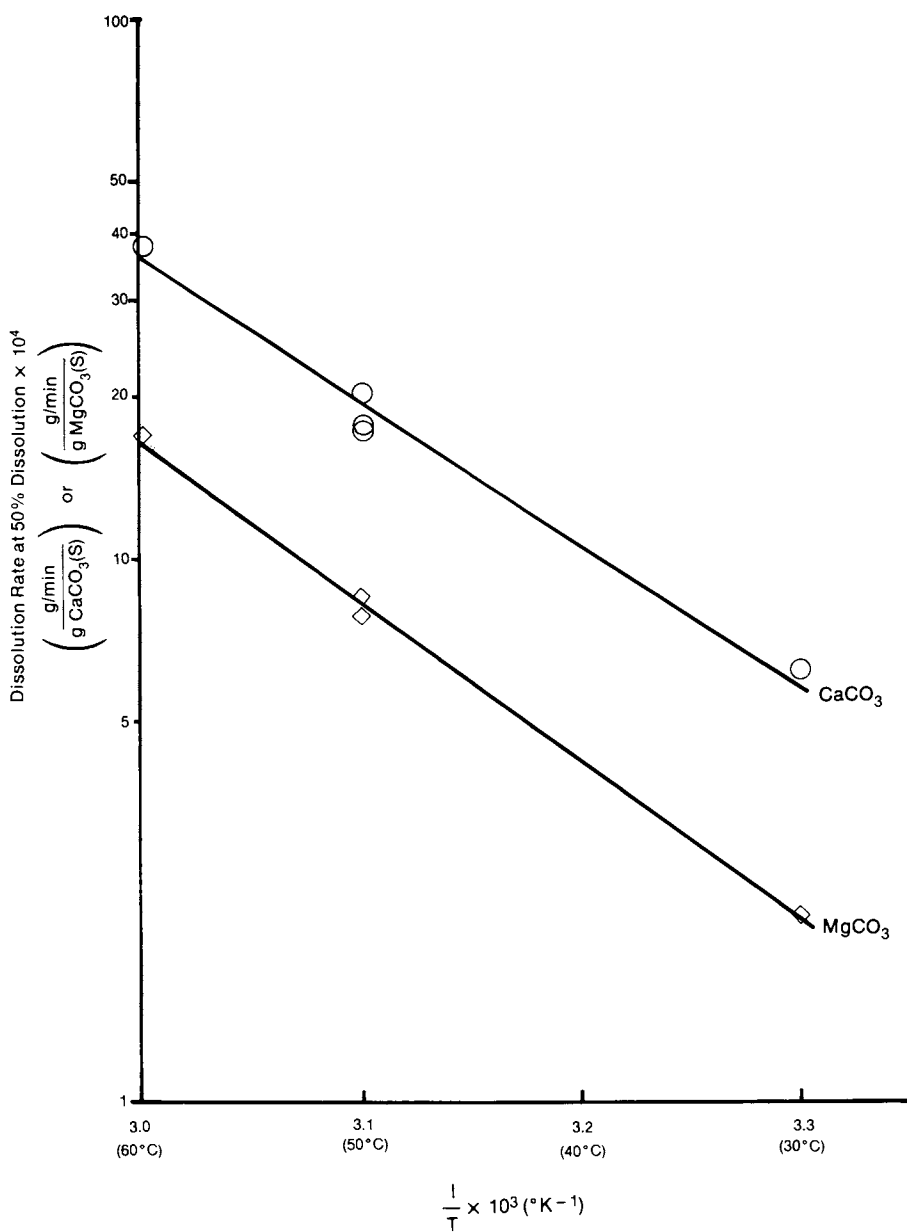


Figure 3. Dissolution rate at pH 5.8 vs. reciprocal temperature—Fredonia limestone.

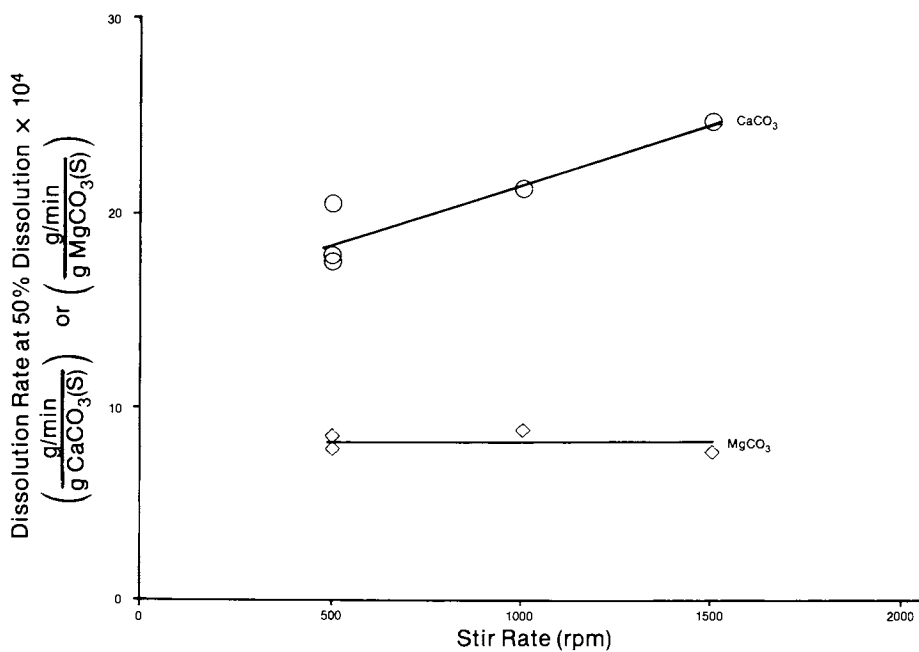


Figure 4. Fredonia limestone dissolution rate vs. stirring rate, (50°C; pH 5.8).

3. A low pH dissolving environment does increase both the CaCO_3 and MgCO_3 dissolution rates as expected.
4. High magnesium dissolving solutions did not significantly impede the CaCO_3 dissolution rate for either the Brassfield or Pfizer stones.
5. Stirring rate appeared to have little effect on the CaCO_3 and MgCO_3 dissolution rates for the Fredonia limestone at pH 5.8.

Literature Cited

- (1) Plummer, L. N.; Parkhurst, D. L. "Critical Review of the Kinetics of Calcite Dissolution and Precipitation, Chemical Modeling in Aqueous Systems," Everett A. Jenne, Editor; ACS Symposium Series 93, 1979.

RECEIVED November 20, 1981.

Thermal Decomposition of Sulfite, Bisulfite, and Disulfite Solutions

B. MEYER, M. RIGDON, T. BURNER, M. OSPINA, and K. WARD

University of Washington, Department of Chemistry, Seattle, WA 98195, and
University of California, Lawrence Berkeley Laboratory, Materials and
Molecular Research Division, Berkeley, CA 94720

K. KOSHLAP

University of California, Lawrence Berkeley Laboratory, Materials and
Molecular Research Division, Berkeley, CA 94720

This work shows that oxygen-free sulfite in lime/limestone slurries, exposed to sulfur dioxide, slowly decomposes under process conditions. In fact, auto-redox reactions of sulfur oxyacids can occur in all coal desulfurization systems, including coal-gasification systems and impurities present in commercial flue gas systems are capable of catalyzing the reaction under process conditions. Our experiments indicate that any large-scale coal utilization will depend on appropriate control of the auto-redox reactions of sulfur species.

It is well known that sulfite and bisulfite can be oxidized to sulfate by oxygen in air. It is less widely recognized that sulfite can be converted to sulfate by auto-redox decomposition reactions, even if no oxygen is present. This latter reaction was first described by Priestley in 1790 (1). Priestley conducted his experiments with sulfurous acid solution ("volatile acid of sulfur") sealed in a soft-glass tube. The latter was stored in a sand bath at 180°C for several months until brownish solid and liquid phases formed. Priestley recognized that the reaction products included elemental sulfur as well as sulfate. This auto-redox reaction was all but forgotten for almost a hundred and fifty years and has been widely ignored by chemists and chemical engineers during the last fifty years, probably because it was assumed to be slow and insignificant.

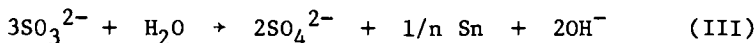
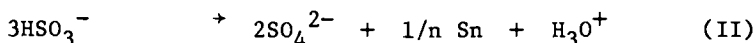
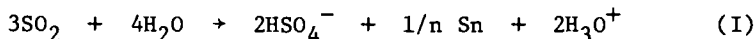
This assumption is incorrect. Already the earliest patent literature on desulfurization of coal gasification, "city gas", and coal combustion gas desulfurization (2) contains persistent and recurring reports of decomposition of sulfur scrubbing liquids, yielding unexpected and difficult-to-handle products, among them nascent, polymeric elemental sulfur which forms rubbery and sticky films causing breakdown of equipment. Our

0097-6156/82/0188-0113\$6.00/0
© 1982 American Chemical Society

research group has studied a variety of systems, including lime/limestone slurries, as well as magnesium, sodium and potassium systems, including impurities containing transition metal ions and nitrogen compounds. The latter are almost absent in oil-desulfurization systems, but quite abundant in heterocycles in coal and therefore in coal gases.

We have found that ammonia solution saturated with sulfur dioxide gas sealed in glass tubes precipitate sulfate crystals, as well as elemental sulfur within less than 72 hrs at 70°C. We also observed the same products at room temperature after less than two months.

Thus, the decomposition of sulfite occurs at lower temperature and far quicker than generally assumed, under conditions well within the temperature range of many desulfurization processes. The reaction involves the auto-redox decomposition of sulfur (IV). Depending on the pH of the system, the overall reaction can be summarized as shown in Equations I-III.



Equation I applies at $\text{pH} < 2$, the pK_1 for H_2SO_3 . The reaction must be conducted in a sealed tube to exclude oxygen and to confine sulfur dioxide gas, the solubility of which is 22.24 wt% at 20°C, yielding a 4.1 M saturated solution. Equation II applies at $2 < \text{pH} < 7$. In this range bisulfite prevails. At high concentration it is accompanied by up to approximately 4% $\text{S}_2\text{O}_5^{2-}$, disulfite. Equation III is valid above $\text{pH} 7$, i.e. pK_2 of H_2SO_3 .

Experimental

Fortunately, we are no longer dependent on visual identification of reaction products, as Priestley was (1), nor are we dependent on complex analytical wet-chemistry as were Bichowsky (3) and others who investigated these systems during the last fifty years. We use now a Raman spectrometric method, details of which have been recently reported (4). This method makes possible continuous in situ determination of the components, free of interference by analytical reagents which intrinsically shift equilibria. The method is based on the fact that each of the aqueous sulfur species has distinct and characteristic vibrational modes. The frequency of these vibrational modes is used to identify the species; the intensity is a measure of the concentration.

We employ the blue line at 488.0 nm and the green line at 514.5 nm of an argon laser to illuminate about 2 ml of the

degassed, aqueous solution sealed in an 8 mm diameter pyrex tube. The Raman scattered light is collected in a J-Y double spectrometer. The light intensity is displayed as a function of wavelength on a TV screen and the data is stored on a magnetic disc. A microcomputer is used for integration spectra, and for conducting a semi-quantitative analysis of the solution. This is achieved by comparison of the spectrum of the unknown sample with that of a standard solution of known composition and concentration (4). The chemical analysis can be conducted while the experiment is in progress, and instant feed-back makes it possible to adjust and control the chemical parameters as desired. This reduced the need for repetitive experimentation. The chemical analysis is based on standard spectra of standard solution and synthetic mixtures of known composition.

The reaction systems of interest in this study include both research samples containing reagent grade solution, which are carefully purged of oxygen, as well as samples drawn from pilot scale sulfur dioxide scrubbers using commercial grade lime and limestone slurries exposed to air.

Results

Preliminary experiments confirmed that bisulfite solutions autodissociate into elemental sulfur and sulfate, and that the reverse reaction also proceeds readily (5). However, it was immediately apparent that the reaction proceeded at a far higher rate at 120°C than one would predict from extrapolation of experiments at 180°C on the basis of activation energy estimation. In fact, it was found that 0.1 M barium chloride solution could precipitate barium sulfate from a pure barium sulfite solution after only nine hours at room temperature. The barium sulfate, which has a solubility product of 10^{-10} , is readily recognized by the strong vibration frequency of 981 cm^{-1} . Following this discovery, a search was undertaken to identify intermediates indicative of possible low temperature reaction mechanisms. Among the potential intermediates are all oxyacids of sulfur with oxidation states from +2 to +6, as well as sulfur and sulfides. A summary of the fourteen best known species is provided in Table I, which also lists the oxidation states of sulfur. The pertinent Raman data has been published (4,19,20).

Ammonia Solutions. It has long been suggested that ammonia solutions age quicker than sodium or potassium solutions of sulfite. We have recorded Raman spectra of three year old 1 M ammonium bisulfite solutions in sealed ampules. These contain not only a solid elemental sulfur phase and solid ammonium sulfate phase, but the liquid phase contains also several percent of dithionate, recognizable by the vibration frequencies of 710 cm^{-1} and 1206 cm^{-1} , with an intensity ratio of $I_{710}/I_{1206} = 3.2$. A search for other oxyacids yielded traces of thiosulfate

TABLE I
Oxyacids Ions of Sulfur

Species	Oxidation State	name
SO_4^{-2}	+6	sulfate
HSO_4^-	+6	bisulfate
$\text{S}_2\text{O}_6^{-2}$	+5	dithionate
SO_3^{-2}	+4	sulfite
HSO_3^-	+4	bisulfite
$\text{S}_2\text{O}_5^{-2}$	+4	disulfite
$\text{S}_3\text{O}_6^{-2}$	3.3	trithionate
$\text{S}_2\text{O}_4^{-2}$	+3	dithionate
$\text{S}_4\text{O}_6^{-2}$	2.5	tetrathionate
$\text{S}_2\text{O}_3^{-2}$	+2	thiosulfate
$\text{S}_5\text{O}_6^{-2}$	2	pentathionate
$\text{S}_x\text{O}_6^{-2}$	10/x	polythionate
SSSO_3^{-2}	1.3	disulfane monosulfonate
$\text{S-S}_x\text{O}_3^{-2}$	4/(x+1)	polysulfane sulfonate

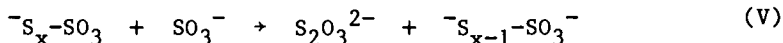
when fresh samples were temperature cycled between 25°C and 100°C. The reaction mechanism for the formation of these species is not yet clear. Dithionate contains sulfur in the oxidation state V. It is possible that this intermediate oxidation state results from a multimolecular reaction. It should be possible to verify this through concentration studies. The reaction is clearly pH dependent. At high pH the reaction proceeds substantially more slowly.

Figure 1 shows the decomposition of a saturated ammonia-sulfur dioxide solution at 70°C. At the beginning, the yellow liquor displays the strong characteristic spectrum of bisulfite and disulfite, Figure 1a. After 18 hrs, a weak sulfate peak appears at 981 cm^{-1} , Figure 1b. During subsequent periods, the concentrations of bisulfite and disulfite decrease, while that of sulfate increases, Figures 1c and 1d. After 4x18 hrs, sulfate dominates the spectrum of the liquid, which shows also colloidal sulfur recognizable by the peak at 450 cm^{-1} and below. A white solid also forms, Figures 2a and 2b, which contains sulfate as well as specks of elemental sulfur.

Solutions of Sodium and Potassium Sulfite and Bisulfite. Oxygen free, pure sulfite and bisulfite solution containing sodium or potassium ions are stable for more than a year at room temperature. However, at 100°C or above, the sulfate spectrum can be observed already after a few days. Elemental sulfur does not immediately appear. Sometimes, at intermediate and high pH, thiosulfate can be observed in a few experiments. The appearance of these species indicates that they are intermediates in the auto-redox reaction Equations I-III, or that they are formed in a secondary reaction of sulfur (IV) with the product elemental sulfur. The latter reactions are already known. They occur during the degradation of elemental sulfur with sulfite, yielding thiosulfate, as a stepwise process, consisting of ring open, Equation IV:



followed by chain degradation according to Equation V:



These reactions are reversible. The intermediate species contain sulfur in three different oxidation states: The sulfonate group contains sulfur in the oxidation state (VI), the sulfide tail sulfur (-II) and the chain links are in the oxidation state sulfur (0). These sulfane-sulfonate species were first proposed by Schmidt (6); the charge distribution in these species was evaluated by Peter (7). These ions have not yet been identified in pure form.

As long as excess sulfite is present under appropriate pH

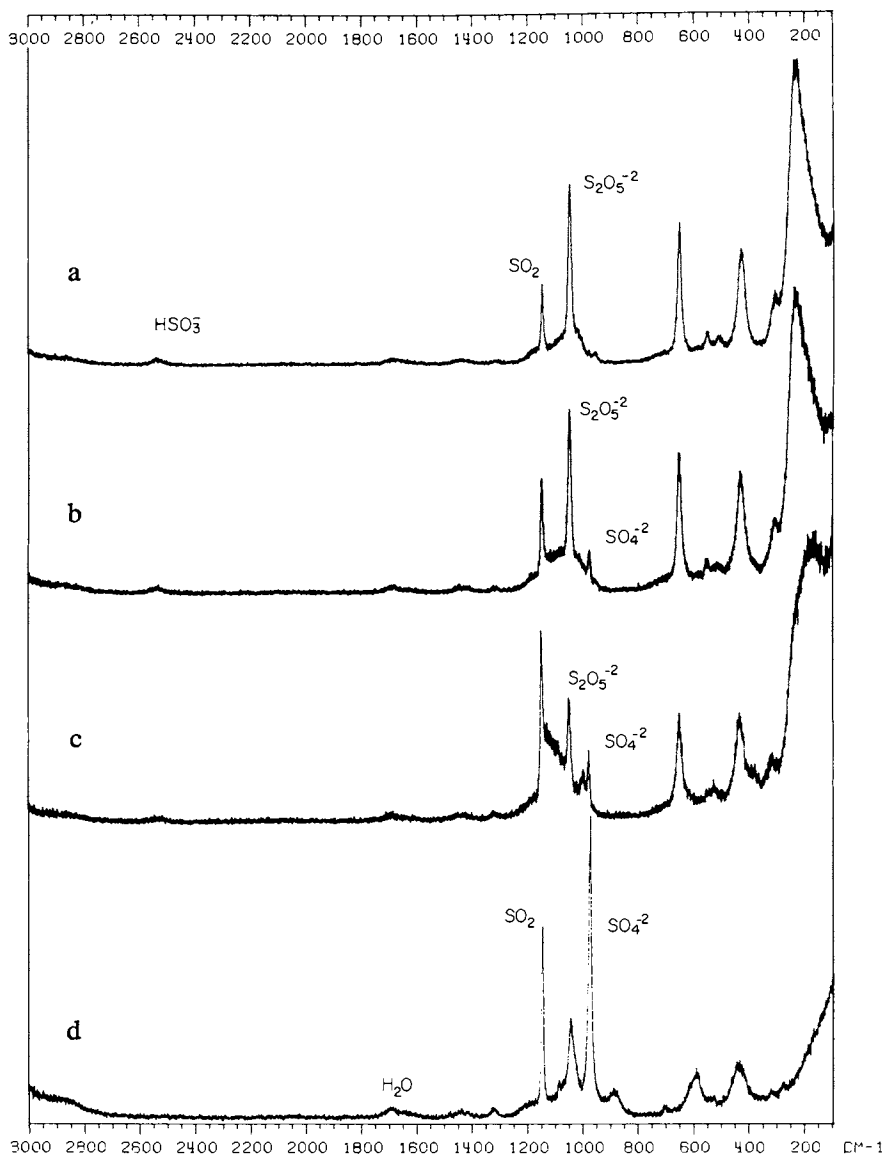


Figure 1. Raman spectra of ammonium bisulfite solution.

Key: a, Yellow liquid (time = 0) saturated with SO_2 . The peaks are identified in Ref. 4. b, Yellow liquid after 36 hrs at 70°C . The sulfate peak appears at 981 cm^{-1} . c, Yellow liquid after 48 hrs at 70°C . The spectrum below 450 cm^{-1} indicates the presence of colloidal sulfur. d, After 72 hrs at 70°C , the liquid is clear and colorless. The solution is saturated with sulfate, of which the bulk has precipitated (Figure 2). The peak at 1650 cm^{-1} belongs to water.

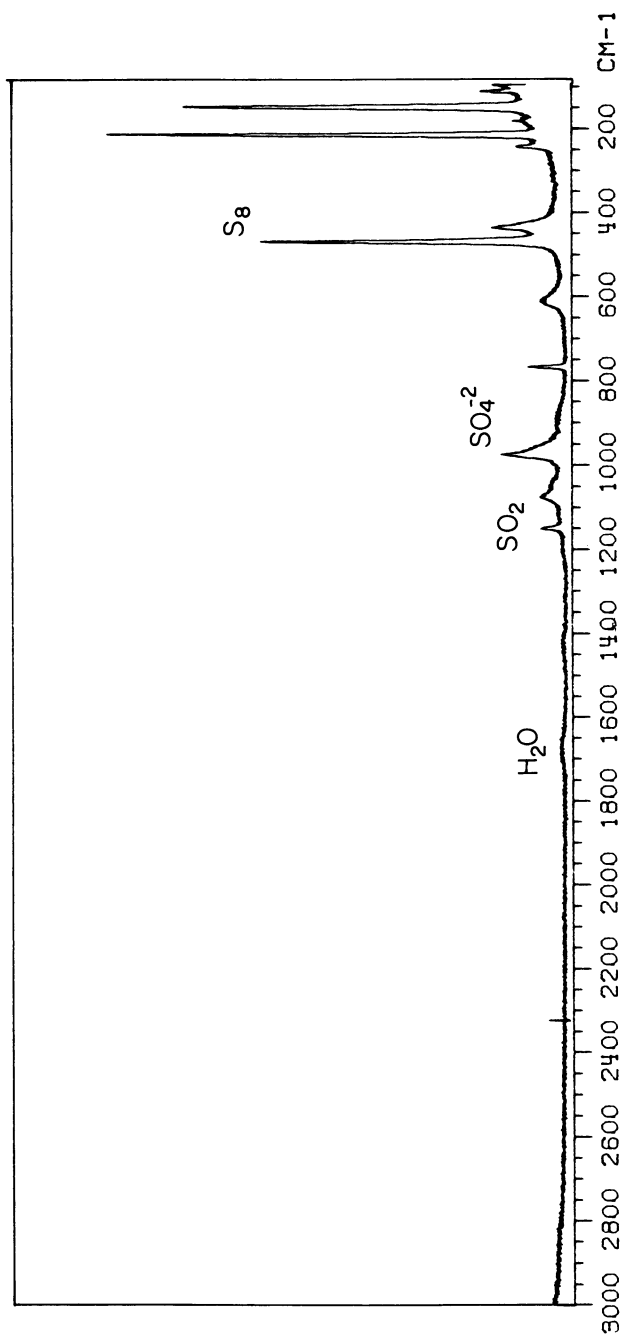


Figure 2. Raman spectrum of white solid collected after 72 hrs at 70°C from auto-redox products of an NH_3 solution saturated with SO_2 . The solid contains ammonium sulfate, elemental sulfur, and dissolved SO_2 .

conditions, all elemental sulfur converts to thiosulfate by this mechanism. The speed of the reaction and the yield of the products depend on the sulfite concentration. The reverse reaction has been invoked by Davis and Bartlett (8) to explain the decomposition of thiosulfate at low pH which yields S_6 , S_8 , S_{10} and various other elemental sulfur allotropes.

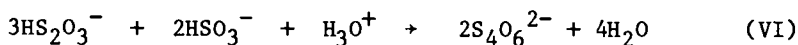
These reactions show that the study of any redox-reaction involving sulfite and elemental sulfur must be based on a sound understanding of reactions of pure thiosulfate solutions.

Thiosulfate Solutions. Aqueous thiosulfate is stable at room temperature for several weeks, but it decomposes within days at 100°C . The reaction products depend on the pH. Our Raman study essentially confirms the formation of products found by earlier authors (8,9). Figure 3 summarizes our results. At high pH thiosulfate prevails; at $\text{pH} < 7$ two different product groups appear: either elemental sulfur and sulfate appear, or polythionates; rarely both product groups form simultaneously. At $2 < \text{pH} < 4$ trithionate is metastable; between $1 < \text{pH} < 5$ tetrathionate seems to be the preferred products. Eventually, polythionate decomposes to thiosulfate, sulfur and sulfate.

The study of these complex, metastable systems has been previously hampered by difficulties in analyzing oxyacid mixtures and, especially, polythionate mixtures.

Figure 4 shows that the problem can be solved by high-resolution Raman spectroscopy. However, the interpretation of our data is far from complete.

The formation of polythionates can be rationalized by the reaction shown in Equation VI.



Our work indicates that polythionates are far more stable intermediates than previously assumed. In fact, we find polythionates among the prevailing species in HCl-thiosulfate mixtures at and below room temperature for several days.

The Influence of Catalysts. The effect of ammonia has already been described above. At low pH the catalytic effect of ammonia is clearly due to chemical interactions between ammonia and sulfur dioxide, because in very concentrated solution, and in non-aqueous systems, N-S bonded compounds can be found and identified (10). At high pH, ammonia clearly catalyzes the decomposition of oxyacids, and, in liquid ammonia, even elemental sulfur is activated, even though N-S bonded products have not yet been clearly identified (11).

We have also studied the effect of metal ions, and found that the heavy metals, such as Se, Mn, Cr, and V do not only catalyze the oxidation by oxygen from air, but also strongly catalyze the oxygen-free auto-redox reaction described above.

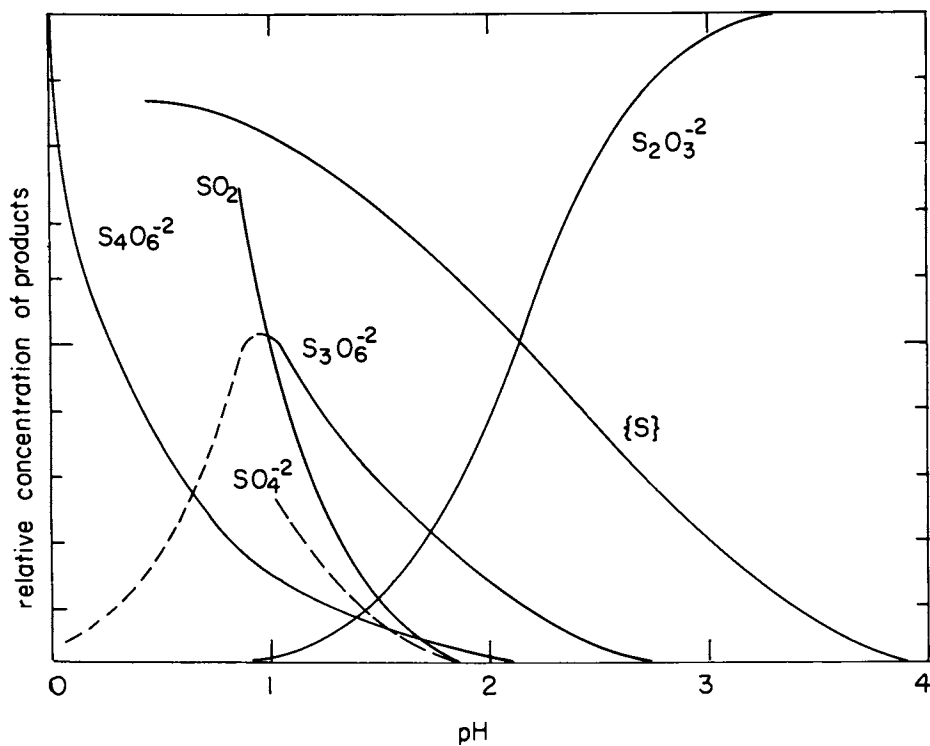


Figure 3. Relative concentration of products of the decomposition of thiosulfate (1 M at 20°C) as a function of pH. The products also depend on concentration and the speed of acidification.

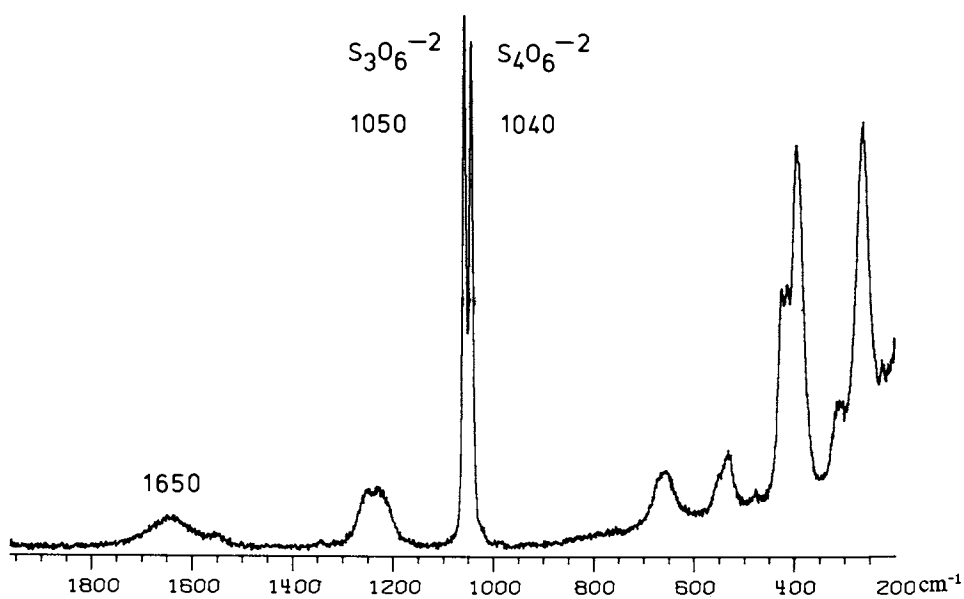


Figure 4. Raman spectra of a mixture of trithionate and tetrathionate. The peak at 1650 cm^{-1} belongs to water.

Thus, Se and Cr cause the decomposition of sulfite and bisulfite already at 90°C within two or three days. However, we have found that the reaction speed is not always readily reproducible, with reaction speeds varying by factors of up to 10^3 for given conditions. Furthermore, the reaction speed changes in some systems during the course of the reaction, and finally, with some metals different end products can be formed. Thus, one MnO_2 modification yields preferentially sulfate, while another yields dithionate. A careful study of these systems will require substantial experimentation.

Solid Calcium Sulfite. Recent thermodynamic studies of calcium sulfite by mass spectroscopy indicated that calcium sulfite dissociates into calcium oxide and sulfur dioxide (12). Under atmospheric pressure, this dissociation reaction is slow in the range below 250°C. We find under these conditions substantial decomposition of sulfite, yielding sulfate, elemental sulfur as well as thiosulfate. These observations are consistent with experiments by Brewer (13), and confirm old observations made by wet-analysis of these complex solids (14). Our work confirms seventy year old literature reports which suggested evidence for thiosulfate, trithionate and dithionate in old pulping sulfite liquor which yellows when kept in air-free, sealed ampules (15-18).

While our Raman spectroscopic method is useful for the identification of the solid reaction products and the analysis of surface products, it is not suitable for direct, total quantitative in situ analysis of solids.

Summary

Oxidation of sulfite to sulfate can proceed by mechanisms other than those involving oxygen from air. The reaction kinetics and the mechanics are not yet understood, but our experiments show that oxygen-free sulfite in lime/limestone slurries, exposed to sulfur dioxide, slowly decomposes under process conditions. In fact, our experiments indicate that auto-redox reactions of sulfur oxyacids can occur in all coal desulfurization systems, including coal-gasification systems and that impurities present in commercial flue gas systems are capable of catalyzing the reaction under process conditions.

Our experiments indicate that any large-scale coal utilization will depend on appropriate control of the auto-redox reactions of sulfur species.

Acknowledgments

This work was supported by the Assistant Secretary for Fossil Energy, Office of Coal Research, Advanced Environmental Control Division of the U.S. Department of Energy under Contract

Number W-7405-ENG-48 through the Morgantown Energy Technology Center, Morgantown, WV. The authors wish to thank Professor L. Brewer and Professor R. E. Connick for valuable discussion and for the use of their laboratory facilities. Drs. O'Brien, Friggens, and Case of METC and Mr. R. Borgwardt of the U.S. Environmental Protection Agency supported this work with helpful suggestions.

Literature Cited

1. Priestley, J. "Experiments and Observations on Different Kinds of Air and Other Branches of Natural Philosophy"; J. Johnson: London, Vol. VI, 1790; p. 333.
2. Meyer, B. "Sulfur, Energy and Environment"; Elsevier Publishers, Amsterdam, 2nd printing, 1978; pages 195-201.
3. Bichowsky, F. R. Equilibrium in the reaction between sulfur dioxide and water. J. Am. Chem. Soc. 1922, 44, 116.
4. Meyer, B.; Ospina, M.; Peter, L. Absolute Raman Intensities of Aqueous Oxyacid Ions of Sulfur. Anal. Chem. Acta 1980, 117, 301.
5. Meyer, B.; Peter, L.; Ospina, M. Sulfur Cycles on Venus and in Terrestrial Pollution Abatement Systems. Geochimica et Cosmochimica Acta 1979, 43, 1579.
6. Schmidt, M. Angew. Chem. (Int. Ed.) 1975, 14, 638.
7. Meyer, B.; Peter, L.; Spitzer, K. Charge Distribution in Elemental Sulfur Molecules and Ions. Rheingold, A. L., Ed.; "Homoatomic Rings, Chains and Macromolecules of Main Group Elements"; Elsevier, Amsterdam, 1977; page 477.
8. Bartlett, P. D.; David, R. E.; Cox, E. F. J. Am. Chem. Soc. 1961, 83, 103.
9. Mizoguchi, T.; Takei, Y.; Okabe, T. Chemical Behavior of Low Valence Sulfur Compounds. Bull. Chem. Soc. Jap. 1976, 49, 70.
10. Meyer, B.; Mulliken, B.; Weeks, H. The Reaction of Sulfur Dioxide with Excess Ammonia. Phosphorus and Sulfur 1980, 8, 281.
11. Meyer, B.; Mulliken, B.; Weeks, H. The Reaction of Ammonia with Excess Sulfur Dioxide. Phosphorus and Sulfur 1980, 8, 291.
12. Cubicciotti, D.; Sanjugo, A.; Hildenbrand, D. L. The Thermal Decomposition of CaSO_3 and its Enthalpy of Formation. J. Electrochem. Soc. 1929, 117, 17 and 1977, 124, 933.
13. Brewer, L. Thermodynamic Data for Flue-Gas Desulfurization Processes. LBL-11758; this conference.
14. Foerster, F.; Lange, F.; Drossbach, O.; Seidl, W.; Self Decomposition of Aqueous Bisulfite. Z. Anorg. Allg. Chem. 1928, 128, 245.
15. Klason, P. Papier Z. 1910, 35, 357.

16. Klason, P. Decomposition of Calcium Sulfite Pulping Liquors. Ark. Kem. Min. 1912/13, 4(1), 1-27.
17. Ryabinina, A. S. Thermal Decomposition of Bisulfite. Trudy Ural. Lesot. Inst. 1973, 31, 83-90.
18. Stavik, J. Svensk Papper Tidn. 1961, 11, 427.
19. Peter, L. Ph.D. Thesis, University of Washington, 1979.
20. Ospina, M. Ph.D. Thesis, University of Washington, 1981.

RECEIVED December 10, 1981.

Kinetics of Reactions in a Wet Flue Gas Simultaneous Desulfurization and Denitrification System

S. G. CHANG, D. LITTLEJOHN, and N. H. LIN

University of California, Lawrence Berkeley Laboratory, Berkeley CA 94720

A number of processes currently undergoing development for simultaneous removal of SO_2 and NO_x have been based on either the oxidation of relatively insoluble NO to more soluble NO_2 or the employment of a water-soluble ferrous-chelating compound as a catalyst to aid in the absorption of the insoluble NO . These ferrous compounds have the ability to form complexes with the NO and thus promote the absorption of the NO . Once in solution NO_x can be reduced by the absorbed SO_2 to form molecular N_2 , N_2O , or reduced nitrogen compounds such as $\text{NOH}(\text{SO}_3)\text{NH}_2\text{SO}_3^-$, and NH_4^+ ; while SO_2 is oxidized to sulfate. The kinetics and mechanisms of reactions involved in this system are discussed.

Power plant flue gas contains several hundred ppm NO_x and hundreds or thousands ppm SO_2 . Most NO_x is in the form of NO . Several processes, still in the development stage, are based on using NO_x as an oxidizing agent for SO_2 in aqueous solution to simultaneously control the emission of both SO_2 and NO_x in the flue gases. These processes can be divided into two different types: one is classified as an oxidation-absorption-reduction technique, and the other as an absorption-reduction technique. Table I (1, 2) summarizes additives, products, testing conditions, and SO_2 and NO_x removal efficiencies of some of these processes.

Both types of process are being developed mainly in Japan and have not approached the stage of commercial use. Part of the reason for this is that these processes are recent developments and have not been tested extensively and the chemistry involved in these systems is not yet well understood. This paper discusses the kinetics and mechanisms of reactions involved in both types of process.

0097-6156/82/0188-0127\$7.50/0
© 1982 American Chemical Society

Table I.
Additives and products of some wet simultaneous desulfurization and denitrification processes.^a

Type	Process	Reagents/Additives	Products	Testing conditions and removal efficiency
Oxidation-	Chiyoda	O ₃ , CaCO ₃	CaSO ₄ · 2H ₂ O, N ₂ O↑, N ₂ ↑	2000 ppm SO ₂ , 90-98%; 250 ppm NO _x , 80%; flow rate = 1000 m ³ /hr
	Ishikawajima	O ₃ , CaO/CaO ₃	CaSO ₄ · 2H ₂ O Ca(NH ₂ SO ₃) ₂ , N ₂ ↑, N ₂ O↑	1150 ppm SO ₂ , 90%; 180 ppm NO _x , 80%; flow rate = 5000 m ³ /hr
Absorption- Reduction	Mitsubishi	O ₃ , CaCO ₃	CaSO ₄ · 2H ₂ O, Ca[NH(SO ₃) ₂], Ca[NOH(SO ₃) ₂], N ₂ ↑, N ₂ O↑	1100 ppm SO ₂ , 95%; 220 ppm NO _x , 80-90%; flow rate = 2000 m ³ /hr
	Asahi	Na ₂ SO ₃ , Fe ⁺² (EDTA), CaCO ₃	CaSO ₄ · 2H ₂ O, Na ₂ SO ₄ , NH(SO ₃ Na) ₂ , N ₂ ↑	1500 ppm SO ₂ , 99%; 200 ppm NO _x , 80-85%; flow rate = 50 m ³ /hr
Absorption- Reduction	Chisso	(NH ₄) ₂ SO ₃ , Fe ⁺² (PCC)	NH(SO ₃ NH ₄) ₂ , NH ₂ SO ₃ NH ₄ , (NH ₄) ₂ SO ₄	1600 ppm SO ₂ , 95%; 200 ppm NO _x , 80%; flow rate = 300 m ³ /hr

^aFrom references 1 and 2.

Oxidation-Absorption-Reduction Processes

This type of process is based on injecting a gas-phase oxidant, such as O_3 or ClO_2 , into the flue gas to selectively oxidize the relatively insoluble NO to the more soluble NO_2 . Nitrous and nitric acids are produced in the aqueous phase after NO_2 and/or N_2O_3 are absorbed into solution; and sulfur oxyacids, such as sulfite/bisulfite or pyrosulfite, are formed if SO_2 dissolves in the solution. Interaction among oxides of nitrogen, nitrogen oxyacids, sulfur oxyacids, oxygen, and trace metal ions such as Fe(III) or Mn(II) can take place in a flue gas wet scrubber. Identifying all reactions involved in this complex system is impossible. However, important reactions must be identified and characterized in order to improve the performance of a scrubber.

Several Japanese processes (1, 2), such as the Ishikawajima, Chiyoda, or Mitsubishi processes in which the NO in the flue gas is oxidized to NO_2 by O_3 and subsequently passed to a NO_2/SO_2 absorber, have shown that a major fraction of the absorbed NO_x is in the form of nitrogen-sulfur complexes, which are the compounds produced in the reaction between nitrite and sulfite ions.

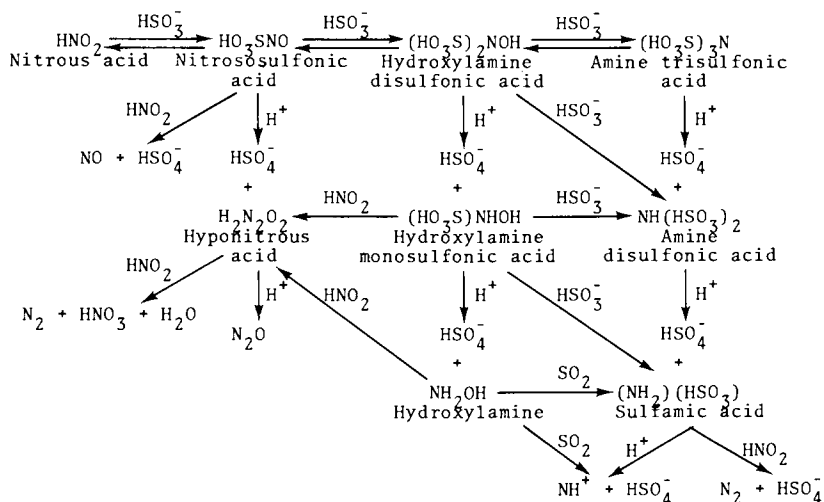
We have reviewed the literature (3-20) and found that many concurrent and consecutive chemical reactions can occur as a result of the interaction between nitrite and sulfite ions. We will summarize the kinetic results of these reactions and present the results of model calculations that give the concentration profile of species produced in this system as a function of reaction time. The effects of temperature, pH, and concentrations of reactant will be demonstrated.

Review of Previous Kinetic Studies

Nitrous acid and sulfite react to form nitrososulfonic acid, which then continues along one or more of three reaction paths:

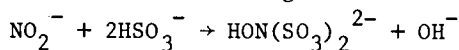
1. Further sulfonation to produce hydroxylamine disulfonate and amine trisulfonate. These sulfonates can hydrolyze to form sulfuric acid and reduced nitrogen species. The latter can undergo further reaction with bisulfite and nitrite.
2. Hydrolysis to form sulfuric acid and hyponitrous acid. The latter decomposes to produce nitrous oxide.
3. A reaction with nitrous acid to yield sulfuric acid and nitric oxide.

The extent to which these three different paths will contribute to the system depends on the pH, temperature, and concentration of nitrite and sulfite species. It is believed that process 1 is favored by a neutral or mildly acidic solution; processes 2 and 3 are expected to become increasingly important as the pH of the solution decreases. A summary of reactions that can take place as a result of interactions between sulfite and nitrite ions is shown in the following reaction scheme:



The kinetic information of reactions involved in this system is outlined below.

Formation of Hydroxylamine Disulfonate by Reaction of Nitrous Acid with Bisulfite Ion. Hydroxylamine disulfonate (HADS) is formed according to the following net reaction:



The kinetics of this reaction was first studied (at pH between 5 and 7) by Seel and Degener (10) over two decades ago. They found two concurrent processes for the HADS production as summarized by the following rate law:

$$\frac{d[\text{HADS}]}{dt} = k_{1a}[\text{H}^+]^2[\text{NO}_2^-] + k_{1b}[\text{H}^+][\text{NO}_2^-][\text{HSO}_3^-] \quad (1)$$

Yamamoto and Kaneda (11) identified the same two processes. However, they found that the first term was really a combination of both general acid and acetic acid specific catalyzed reactions. Seel and Knorre (12) later investigated this reaction (at pH between 6.13 and 6.92) and interpreted their results as a single process having the following rate law:

$$\frac{d[\text{HADS}]}{dt} = \frac{k_{2a}[\text{NO}_2^-][\text{HSO}_3^-]^2}{1 + k_{2b}[\text{SO}_3^{2-}]} \quad (2)$$

Because of the discrepancies between these results, we have undertaken a systematic investigation (7) of this reaction over the pH range between 4.5 and 7. The reaction has been found to consist of two concurrent processes. The rate law was shown as

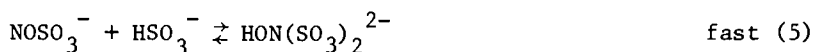
$$\frac{d[\text{HADS}]}{dt} = k_{3a}[\text{H}^+][\text{NO}_2^-][\text{HSO}_3^-] + k_{3b}[\text{NO}_2^-][\text{HSO}_3^-]^2 \quad (3)$$

The dependence of k_{3a} and k_{3b} on temperature and ion strength was also studied:

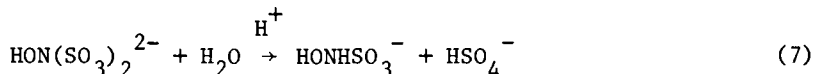
$$k_{3a} = 3.7 \times 10^{12} e^{-6100/T} \text{ liter}^2/\text{mole}^2\text{-sec} \quad (a)$$

$$k_{3b} = 9.0 \times 10^{-4} e^{2.1\sqrt{\mu}} \text{ liter}^2/\text{mole}^2\text{-sec} \quad (b)$$

The following reaction mechanisms are suggested:



Hydrolysis of Hydroxylamine Disulfonate (HADS). HADS hydrolyzes to give hydroxylamine monosulfonate (HAMS) and sulfates:



The rate and mechanism of this hydrolysis was performed by Naiditch and Yost (13). These authors found that hydrolysis is catalyzed by acid as well as water, but the effect of water is much less than that of acid. The rate equation can be expressed as

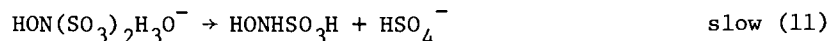
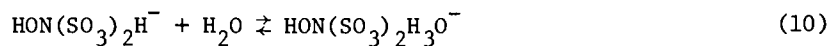
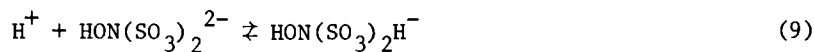
$$-\frac{d[\text{HADS}]}{dt} = \{k_{8a}[\text{H}^+] + k_{8b}[\text{H}_2\text{O}]\} [\text{HON}(\text{SO}_3)_2^{2-}] \quad (8)$$

k_{8a} and k_{8b} are respectively the rate constants for acid- and water-catalyzed reactions. At zero ionic strength:

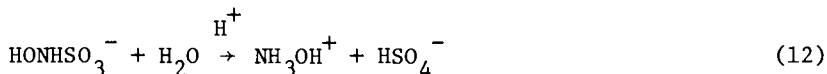
$$k_{8a} = 2.1 \times 10^{11} e^{-17600/RT} \text{ liter/mole-sec} \quad (c)$$

$$k_{8b} = 1.67 \times 10^{11} e^{-23000/RT} \text{ sec}^{-1} \quad (d)$$

The proposed mechanism assumes that the ion $\text{HON}(\text{SO}_3)_2\text{H}^-$ forms a reaction complex with water. The overall rate is determined by the rate at which the complex is converted into the hydrolytic products:



Hydrolysis of Hydroxylamine Monosulfonate (HAMS). HAMS hydrolyzes in acidic solution, but at a much slower rate than that of HADS (13). The hydrolysis of HAMS produced hydroxylamine (HA) and sulfates:



The rate equation may be assumed to be

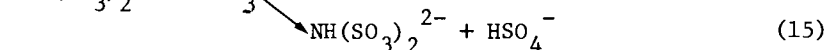
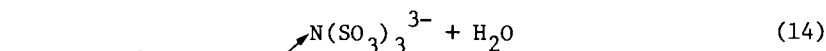
$$-\frac{d[\text{HAMS}]}{dt} = k[\text{HONHSO}_3^-][\text{H}^+] \quad (13)$$

The rate constant was not determined; however, an upper limit can be obtained from the result of Naiditch and Yost (13):

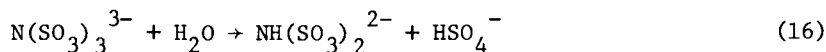
$$k \leq 2.65 \times 10^{11} e^{-19500/RT} \text{ liter/mole-sec} \quad (e)$$

at an ionic strength $\mu = 0.01 \text{ M}$

Sulfonation of Hydroxylamine Disulfonate. Seel et al. (14) studied the reaction between HADS and bisulfite and found that this reaction produced about 70% aminetrisulfonate (ATS) and 30% aminedisulfonate (ADS) in the temperature range from 25 to 60°C and ionic strength from 1.0 to 1.2 M, with reaction times ranging up to 4.5 hr at a pH of 7. The reaction proceeds according to Eqs. (14) and (15):



Aminedisulfonate can also be formed through the hydrolysis of hydroxylamine trisulfonate:



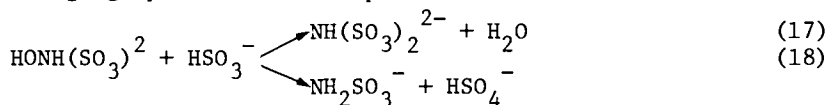
The rate of disappearance of HADS can be expressed as

$$-\frac{d[\text{HADS}]}{dt} = A e^{-\Delta E_a/RT} [\text{HON}(\text{SO}_3)_2^{2-}][\text{HSO}_3^-] \quad (f)$$

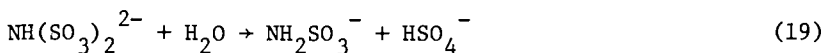
where $A = 7.2 \times 10^9$ liter/mole-sec, and $\Delta E_a = 18.0$ kcal/mole. This rate equation indicates that the rate determining step is reaction 14 and/or 15, while Eq. (16) is a fast reaction; and the activation energy determined is a weighted value of reactions 14, 15, and 16, leading to the formation of a mixture of products.

Yamamoto and Kaneda (11) measured the rate of formation of ATS and obtained an identical rate equation with $A = 3.4 \times 10^{10}$ liter/mole-sec, and $\Delta E_a = 19.2$ kcal/mole at $\mu = 1.0 \text{ M}$.

Sulfonation of Hydroxylamine Monosulfonate (HAMS). According to Seel et al. (14), the reactions between HAMS and bisulfite are branched ones (Eqs. 17 and 18), producing about 70% aminedisulfonate (ADS) and 30% sulfamate (SAM) in the temperature range 25-60°C and ionic strength range 1.0-1.2 M, with reaction times ranging up to 12 hr at a pH of 7:



Aminedisulfonate can undergo hydrolysis to form sulfamate:



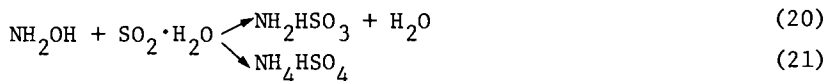
The rate determining step is reaction 17 and/or 18. The rate equation is:

$$-\frac{d[\text{HAMS}]}{dt} = A e^{-\Delta E_a/RT} [\text{HONH}(\text{SO}_3)^-] [\text{HSO}_3^-] \quad (g)$$

where $A = 2.0 \times 10^{13}$ liter/mole-sec, and $\Delta E_a = 24.5$ kcal/mole. Hydroxylamine O-sulfonic acids are assumed to be intermediate products.

Sulfonation of Hydroxylamine (HA). Sisler and Audrieth (15) studied the formation of sulfamic acid by the reaction of hydroxylamine with sulfur dioxide in an aqueous solution and proposed that the reaction mechanism involved coordination between NH_2OH and SO_2 molecules with subsequent rearrangement to sulfamic acid. The kinetics of this reaction was investigated by Brackman and Higginson (16) at room temperature. They found that in addition to sulfamic acid, trace amounts of ammonium bisulfate were also formed and that the percentage of ammonium bisulfate produced appeared to be independent of pH. Fraser (17) and Gomiscek et al. (9) studied the kinetics of this reaction as a function of temperature. The kinetic studies by both Brackman and Higginson (16) and Fraser (17) were performed by monitoring the rate of disappearance of total sulfite during the course of the reaction, while Gomiscek et al. (9) studied this reaction by monitoring the rate of disappearance of total hydroxylamine.

This reaction can be expressed as



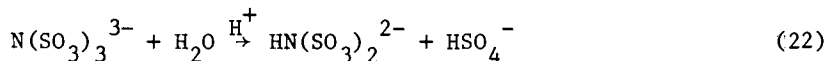
The rate law can be written as

$$-\frac{d[\text{HA}]}{dt} = (k_{20} + k_{21}) [\text{NH}_2\text{OH}] [\text{SO}_2 \cdot \text{H}_2\text{O}] \quad (h)$$

The enthalpy and entropy of activation for the formation of sulfamic acid and ammonium bisulfate are:

	Sulfamic acid		Ammonium bisulfate	
	ΔH_{20}^\ddagger (kcal/mole)	ΔS_{21}^\ddagger (e.u.)	ΔH_{21}^\ddagger (kcal/mole)	ΔS_{21}^\ddagger (e.u.)
^a Fraser	10.9	-16	1	-56
Gomiscek et al. ^b	13.4	- 6.1	3	-45.8
^a Ref. 17	^b Ref. 9			

Hydrolysis of Aminetrisulfonate (ATS). The hydrolysis of potassium aminetrisulfonate has been studied by Sisler and Audrieth (15) at 25, 40, 67, and 100°C. They found that this reaction (Eq. 22) is acid catalyzed and that the ATS was rapidly converted into aminedisulfonate and sulfates even in a neutral solution and at 25°C:

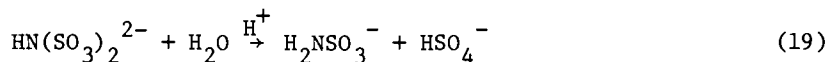


The rate equation may be written as

$$-\frac{d[\text{ATS}]}{dt} = k_{22}[\text{N}(\text{SO}_3)_3^{3-}][\text{H}_3\text{O}^+] \quad (i)$$

The rate constant has not been determined, however.

Hydrolysis of Amine Disulfonates (ADS). ADS hydrolyzes irreversibly and quantitatively to form sulfamate (SAM) and sulfates according to Eq. 23 (18, 19, 20):



The rate of the acid-catalyzed reaction has been studied (20) over the temperature range 25-45°C. The results at constant ionic strength conform to the rate equation:

$$-\frac{d[\text{ADS}]}{dt} = k_{23}[\text{HN}(\text{SO}_3)_2^{2-}][\text{H}^+] \quad (j)$$

The variation of the rate constant k_{23} at zero ionic strength with temperature is described by the equation

$$k_{23} = 2.54 \times 10^{14} e^{-23500/RT} \text{ liter/mole-sec}$$

The relatively large value of the frequency factor was explained on the basis of a large positive entropy ($\Delta S^\ddagger = 21.3$ e.u.) of

formation of the activated complex due to its electrostatic interaction with the solvent.

The dependence of the specific rate constant on ionic strength at 25°C, based on the Brønsted-Debye-Hückel theory (21), was studied.

$$\log_{10} k_{23} = \log_{10} k_{23}^{\circ} + \frac{2Az_1z_2\mu^{1/2}}{1 + \mu^{1/2}} + \beta\mu \quad (k)$$

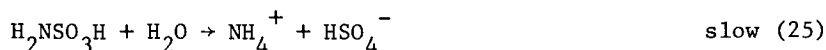
where $A = 0.5065$, $z_1z_2 = -2$, and $\beta\mu = +0.092$. The uncatalyzed hydrolysis was found to have an undetectable rate compared to the rate of the acid-catalyzed reaction.

The ionization constant for reaction 23



in a sodium chloride solution at an ionic strength of 1.0 at 25°C is 3.2×10^{-9} mole/liter.

Hydrolysis of Sulfamate (SAM). The kinetics of hydrolysis of sulfamate ion was investigated by Maron and Berens (22) (in dilute acid at 80–98°C) and by Candlin and Wilkins (23) (in 10^{-3} M to 6 M perchloric acid at 95°C). A reaction mechanism involving a pre-equilibrium between sulfamate ion and sulfamic acid (Eq. 24), followed by slow hydrolysis of the acid (Eq. 25), was proposed:



The rate equation can be expressed as

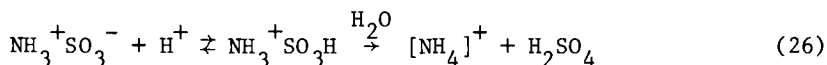
$$-\frac{d[\text{SAM}]}{dt} = \frac{k[\text{H}^+]}{K + [\text{H}^+]} [\text{NH}_2\text{SO}_3^- + \text{NH}_2\text{SO}_3\text{H}] \quad (1)$$

where $k = 2.3 \times 10^{-4} \text{ sec}^{-1}$ at 95°C, ionic strength $\mu = 1\text{M}$, and K is the ionization constant of sulfamic acid, which has been determined by E.M.F. (24) and conductance (25) measurements. A relationship, $-\log K = (3792.8/T) - 24.122 + 0.041544 T$, has been deduced from the measurements between 10 and 50°C ($K = 0.1$ mole/liter at 25°C, and 0.266 at 95°C).

The energies and entropies of activation determined by Maron and Berens (22) (30.5 kcal/mole and 9.7 e.u.) include the energy and entropy of formation of sulfamic acid (i.e., both reactions 24 and 25). The latter values can be estimated from the data of King and King (24) as +0.9 kcal/mole and +9 e.u., and this will mean values for the energy and entropy of activation of hydrolysis of sulfamic acid (Eq. 25) of 29.6 kcal/mole and 0.7 e.u.

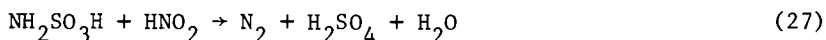
respectively, which are in good agreement with those determined by Candlin and Wilkins (23) (29.7 kcal/mole and 3.2 e.u.).

In addition to the A 1 acid-catalyzed decomposition of sulfamate ion, proposed by Maron and Berens (22) and Candlin and Wilkins (23), Hughes and Lusty (26) present evidence that an additional A 2 path involving sulfamic acid (Eq. 26) also occurs:

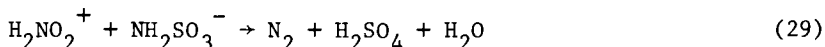
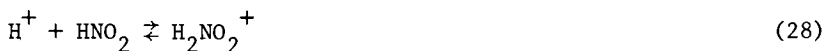


This mechanism would predominate or occur exclusively above 2 M perchloric acid.

Reaction of Sulfamic Acid with Nitrous Acid. A kinetic study of the reaction of sulfamic acid with nitrous acid (Eq. 27) by Hughes (27) revealed that the mechanism



at acidities less than 0.248 M, proceeded according to reactions 28 and 29:



The protonated nitrous acid species reacts with sulfamate ion in a slow step. The rate equation can be written as

$$-\frac{d[\text{HNO}_2]}{dt} = k_{29}[\text{H}^+][\text{HNO}_2][\text{NH}_2\text{SO}_3^-] \quad (m)$$

At an ionic strength $\mu = 0.25$ M, k_{29} is 170, 667, 1130, and 2040 liter² mole⁻² sec⁻¹ at 0, 18, 25, and 34.5°C respectively. This temperature dependence study reveals that $\Delta S^\ddagger = -6.6$ e.u., and $\Delta H^\ddagger = 11.3$ kcal/mole.

In the acid range 0.25–3 M, a second pathway emerges in which H_2NO_2^+ attacks sulfamic acid. As the concentration of sulfamate ion becomes very small at these higher acidities, the reaction with sulfamic acid will become more important although sulfamate ion is more reactive than sulfamic acid. The two mechanisms are operating side by side, with an increase of acidity favoring the reaction through sulfamic acid.

Several more reactions are known to take place in this system in addition to those discussed above. However, their kinetics and mechanisms have not been well characterized. Some of these reactions are:

1. Formation of hyponitrous acid ($\text{H}_2\text{N}_2\text{O}_2$) from the acid-catalyzed hydrolysis of nitrosulfonic acid.
2. Reaction of nitrosulfonic acid with nitrous acid to form sulfates and liberate NO.

3. Production of hyponitrous acid and sulfates from the reaction of hydroxylamine monosulfonate with nitrous acid.

4. Reaction of hydroxylamine with nitrous acid to yield hyponitrous acid or N_2O .

5. Reaction of hyponitrous acid with nitrous acid to form nitric acid and N_2 .

Chemical Kinetics Modeling. The concentration profiles of HADS, HAMS, HA, ATS, ADS, SAM, NH_4^+ , N_2 , and sulfate as a function of time resulting from the reaction of sulfite and nitrite ions in aqueous solutions was calculated at various conditions (Figures 1-6). A CHEMK software package developed by Systems Applications, Inc., of San Rafael, California, was used for this computation. Three different initial SO_2 and NO_x concentrations were considered (in ppm): 1000, 450, and 50; 1000, 250, and 250; 2000, 250, and 250 respectively for SO_2 , NO, and NO_2 . Calculations were carried out at two different temperatures (55 and 25°C) and three different pH's (3, 5, and 7). The pH of the solution was assumed to be constant throughout the reaction. Table I lists elementary reactions considered and rate constants used. The following additional assumptions were made in this calculation:

1. Gas dissolution and liberation rates are much larger than chemical reaction rates.

2. Any reaction involving aqueous HNO_3 , NO, NO_2 , N_2O_3 , and N_2O_4 is neglected.

3. The equilibrium is maintained all the time for reactions 1 through 7. The rate constant of the 14 reversible reactions was adjusted to satisfy the equilibrium condition.

4. Oxidation of NO to NO_2 (both in gas phase and aqueous solution) is discounted.

Figures 1-4, 5, and 6 show the time-resolved concentration of species in a batch reactor at various pH's, temperatures, and initial partial pressures of SO_2 and NO_x for the first 2 and 24 hours respectively. The gas-to-liquid ratio (G/L) is 75. Figure 1 (at $P_{SO_2} = 1000$, $P_{NO} = 450$, and $P_{NO_2} = 50$ ppm, pH = 5, and $T = 328K$) demonstrated that the removal efficiency of NO is only about 10%, although NO_2 can be removed nearly completely. This is because NO alone cannot be converted into nitrous acid. The major product is HADS within the initial 1-1/2 hr; the concentrations of HAMS and sulfate increase while that of HADS decreases as the reaction time continues. If the reaction is allowed to continue, the final products will be NH_4^+ , N_2 , and sulfate. Because we disregard the reaction of HAMS and HA with HNO_2 and the hydrolysis of nitrosulfonic acid, no N_2O is formed.

The effect of the oxidation of NO to NO_2 by an oxidant such as O_3 is illustrated in Figure 2 ($P_{SO_2} = 1000$, $P_{NO} = P_{NO_2} = 250$ ppm, pH = 5, and $T = 328K$). The result indicates enormous

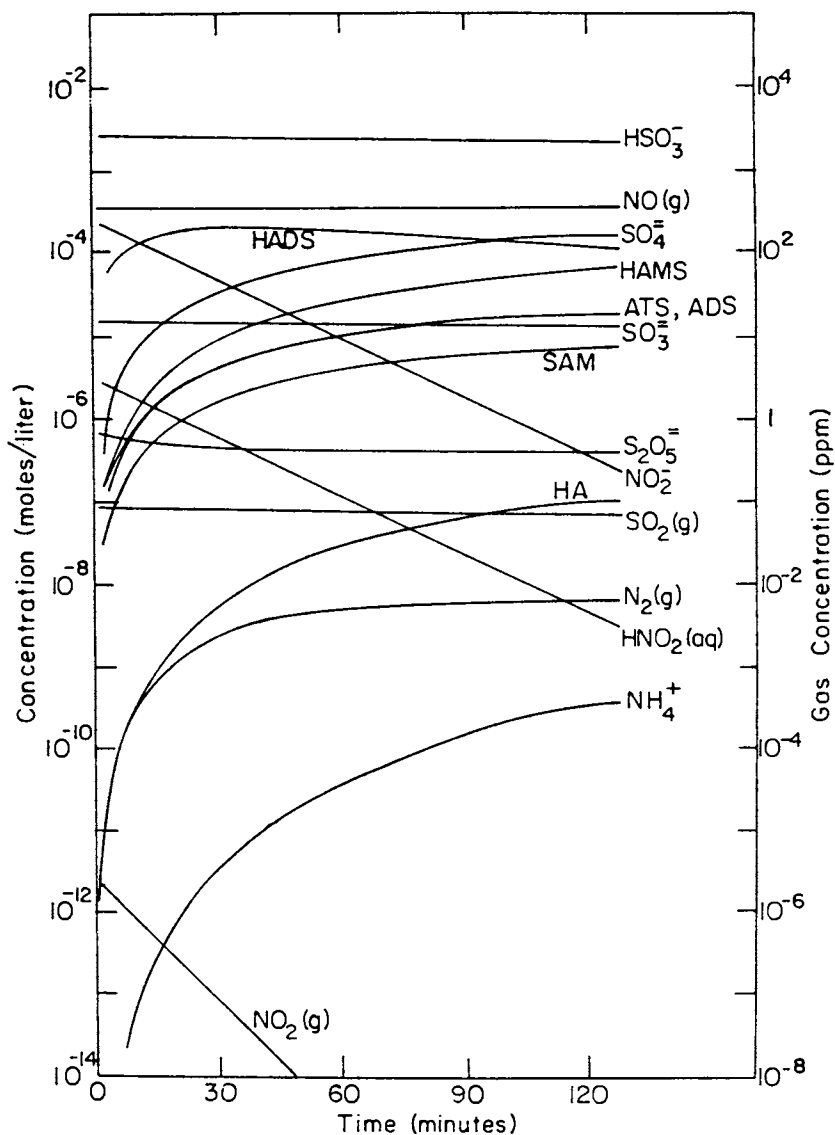


Figure 1. The concentration profile of species as a function of reaction time in a batch reactor (pH 5 and 328 K) at the following initial condition: $P_{\text{SO}_2} = 1000$, $P_{\text{NO}} = 450$, and $P_{\text{NO}_2} = 50$ ppm. The gas-to-liquid ratio, G/L, is 75.

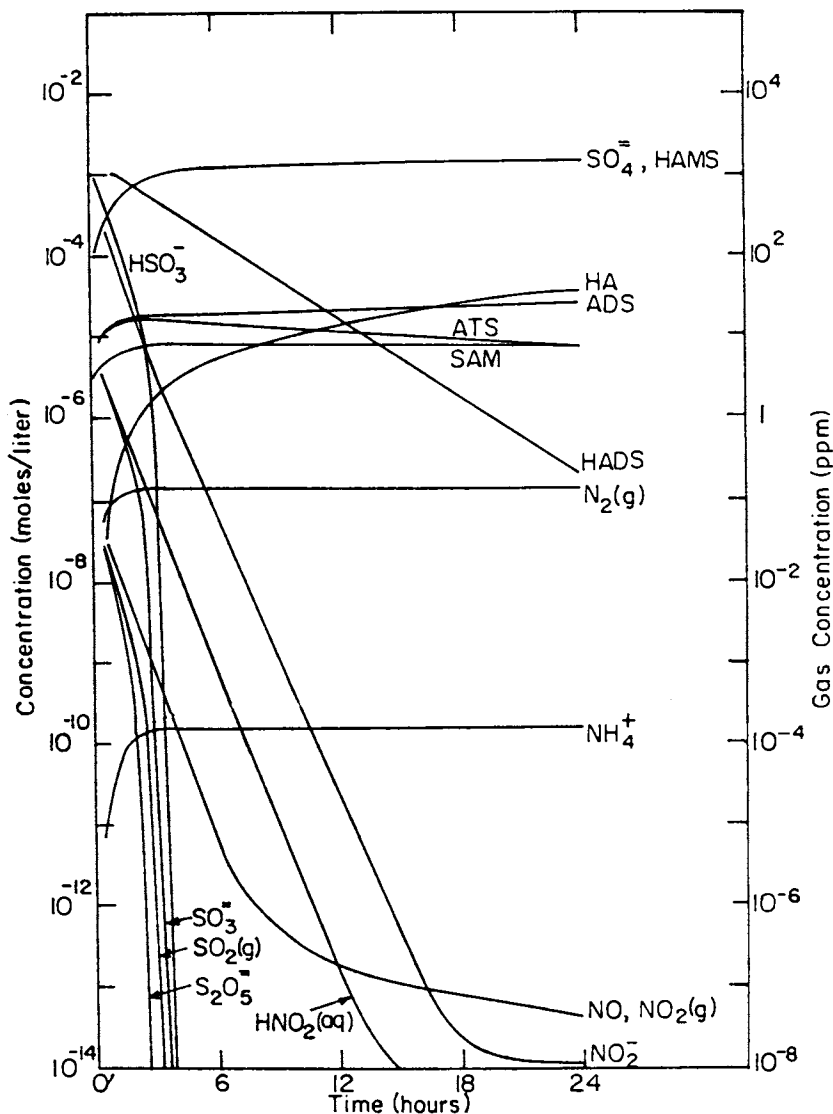


Figure 2. The concentration profile of species as a function of reaction time in a batch reactor (pH 5 and 328 K) at the following initial condition: $P_{\text{SO}_2} = 1000$, $P_{\text{NO}} = P_{\text{NO}_2} = 250$ ppm. G/L, 75.

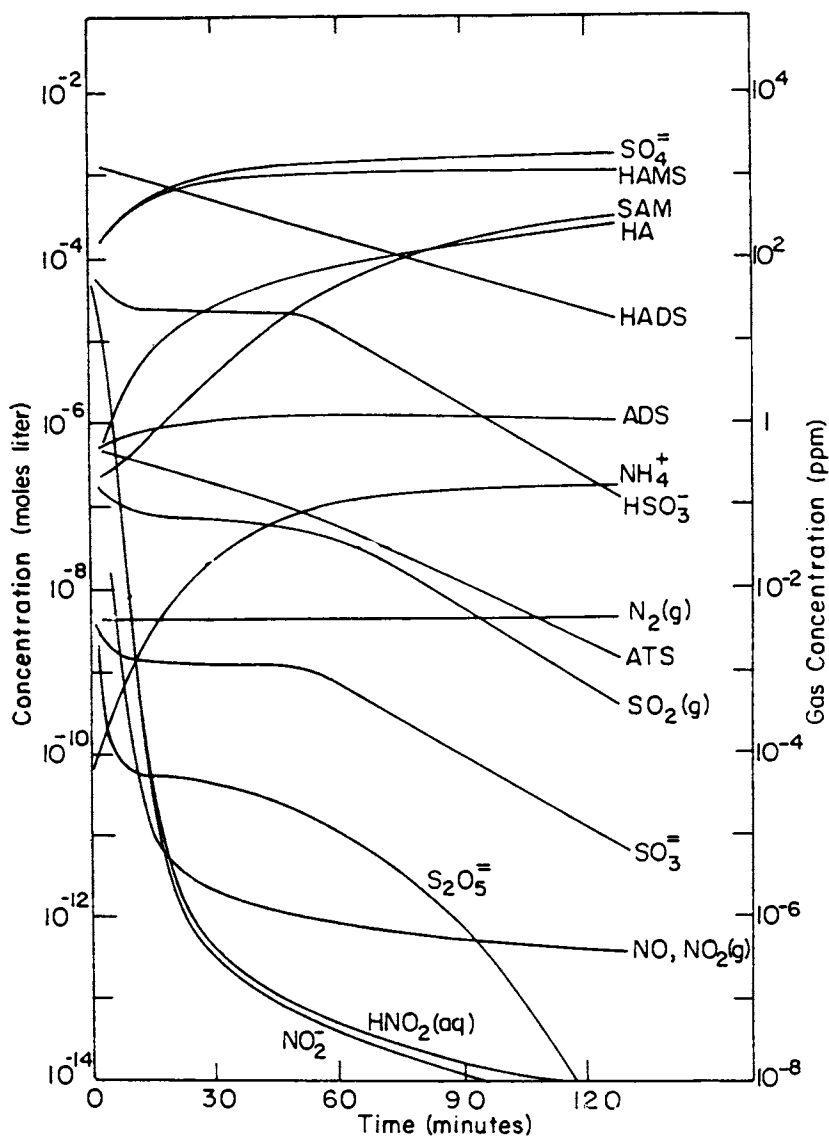


Figure 3. The concentration profile of species as a function of reaction time in a batch reactor (pH 3 and 328 K) at the following initial condition: $P_{\text{SO}_2} = 1000$, $P_{\text{NO}} = P_{\text{NO}_2} = 250$ ppm. G/L, 75.

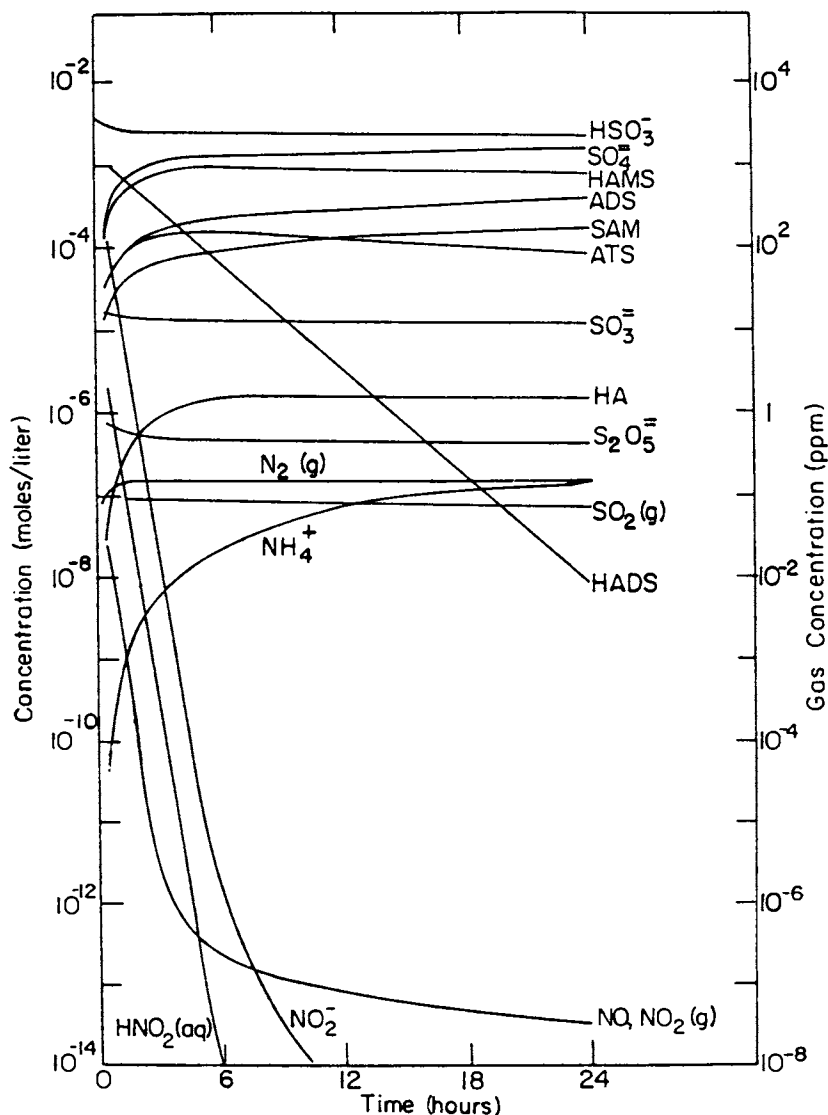


Figure 4. The concentration profile of species as a function of reaction time in a batch reactor (pH 5 and 328 K) at the following initial condition: $P_{\text{SO}_2} = 2000$, $P_{\text{NO}} = P_{\text{NO}_2} = 250$ ppm. G/L, 75.

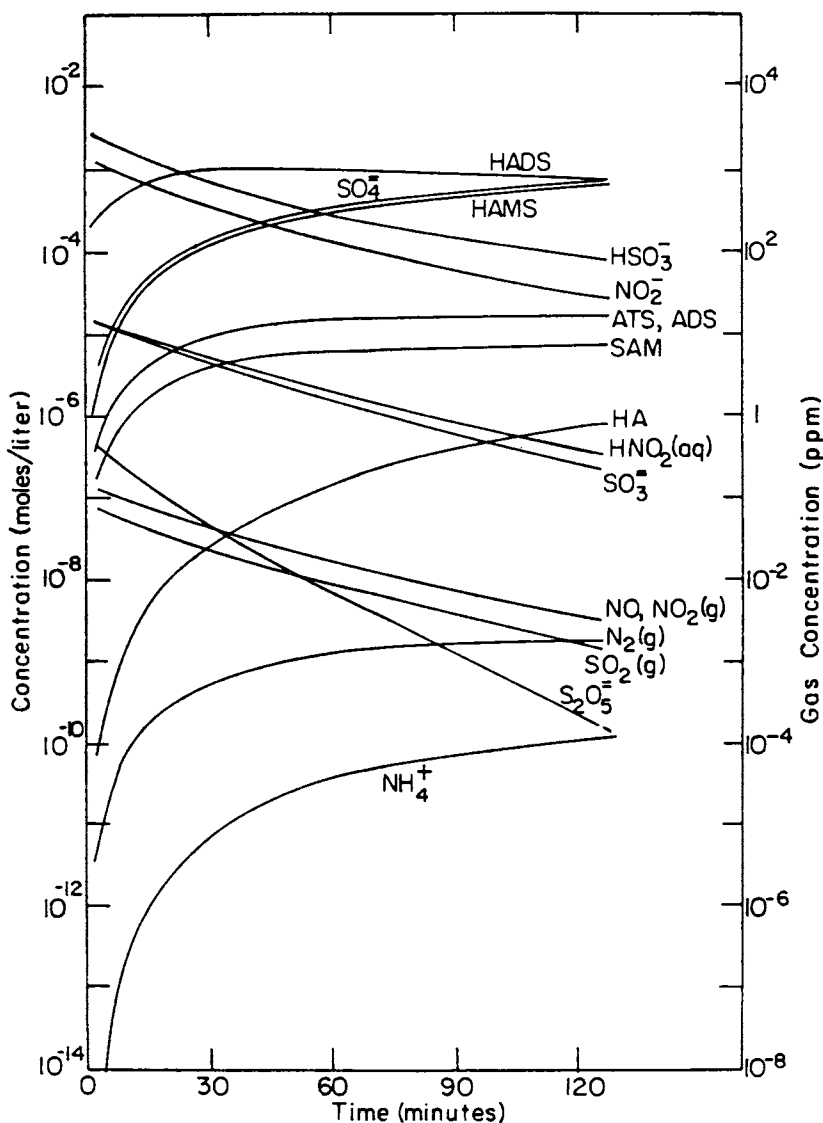


Figure 5. The concentration profile of species as a function of reaction time in a batch reactor (pH 5 and 328 K) at the following initial condition: $P_{SO_2} = 1000$, $P_{NO} = P_{NO_2} = 250$ ppm. G/L, 75.

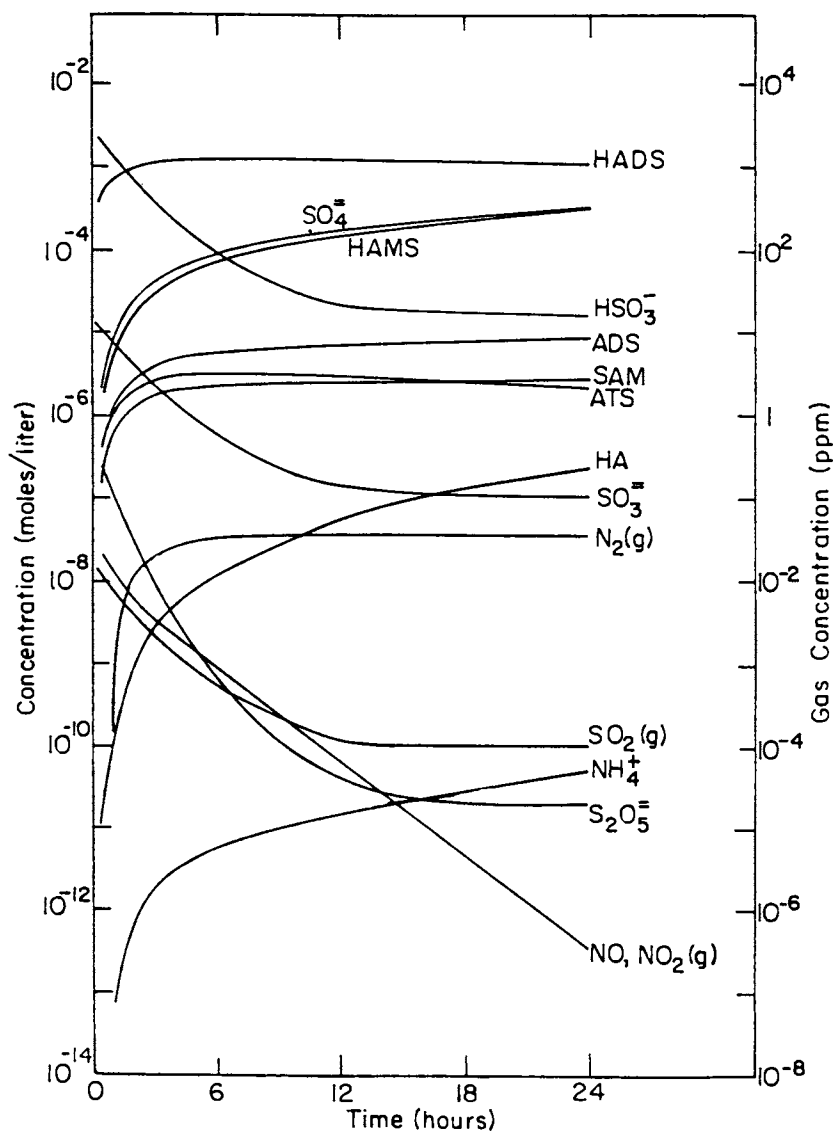


Figure 6. The concentration profile of species as a function of reaction time in a batch reactor (pH 5 and 298 K) at the following initial condition: $P_{\text{SO}_2} = 1000$, $P_{\text{NO}} = P_{\text{NO}_2} = 250$ ppm. $G/L, 75$.

improvement in NO_x removal efficiency. The concentration of HADS, HAMS, ATS, etc., species is larger (compared to Figure 1) because of the larger concentration of nitrite/nitrous acid in the solution. By the same token, HSO_3^- is consumed at a larger rate.

The effect of the pH of the solution on the reaction is shown in Figure 3 ($P_{\text{SO}_2} = 1000$, $P_{\text{NO}} = P_{\text{NO}_2} = 250$ ppm, $\text{pH} = 3$, and $T = 328\text{K}$). The reactions speed up at a lower pH (between $\text{pH} = 5$ and 3), and NO_x is reduced at a larger rate. The concentration of HAMS is larger than HADS after about 20 min. Similarly, larger concentrations of HA, SAM, N_2 , and NH_4^+ are observed at a given time. These are due to the fact that the hydrolysis reaction is acid catalyzed, and therefore low pH conditions would favor the formation of hydrolysis products.

If the SO_2 concentration is increased while that of NO_x is held constant, i.e., at a larger SO_2/NO_x ratio (Figure 4, with $P_{\text{SO}_2} = 2000$, $P_{\text{NO}} = P_{\text{NO}_2} = 250$ ppm, $\text{pH} = 5$, and $T = 328\text{K}$), the production rate of ATS, ADS, and SAM increases because a larger SO_2/NO_x ratio favors sulfonation reactions. The NH_4^+/N_2 ratio increases with an increase of the SO_2/NO_x ratio because the N_2 formation rate is only slightly affected by the change in the SO_2/NO_x ratio. (The effect due to the increase in SAM concentration is offset by that due to the decrease in HNO_2 concentration.) However, the NH_4^+ rate of formation increases as the concentration of SAM increases at a constant pH of the solution.

The effect of temperature is demonstrated in Figure 5 ($P_{\text{SO}_2} = 1000$, $P_{\text{NO}} = P_{\text{NO}_2} = 250$ ppm, $\text{pH} = 5$, and $T = 328\text{K}$) and Figure 6 ($P_{\text{SO}_2} = 1000$, $P_{\text{NO}} = P_{\text{NO}_2} = 250$ ppm, $\text{pH} = 5$, and $T = 298\text{K}$). The results indicate that the overall reaction rate speeds up at higher temperatures.

Absorption-Reduction Processes

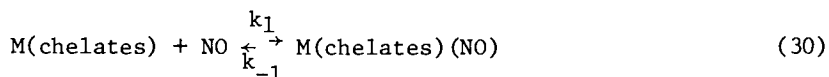
This type of process is based on the addition of metal chelates such as Fe(II)EDTA in aqueous solution to promote absorption of NO in solutions (1, 2). These metal chelates can bind NO to form nitrosyl metal chelates which can react with absorbed SO_2 in aqueous solution to produce reduced nitrogen species and sulfate while metal chelates are regenerated.

Identification of an efficient metal chelate for optimum absorption of NO requires knowledge of the thermodynamics and kinetics of the coordination of NO to various metal chelates. Knowledge is also needed of the kinetics and mechanisms of the reaction between nitrosyl metal chelates and absorbed SO_2 in solution to calculate the regeneration rate of metal chelates and to control the products of reaction by adjusting the scrubber operating conditions. Not much of this information is available in the literature, although several ferrous and cobalt chelates have been used as additives for testing in bench-scale wet flue gas simultaneous desulfurization and denitrification scrubbers.

Equilibrium Constants, Enthalpy, and Entropy of the Coordination of NO to Metal Chelates. Complexes of NO have been known for centuries. Many studies have been done on determining the structure of these complexes, yet few have been done on determining their thermodynamic properties and reaction kinetics. Hishinuma et al. (28) and our group (29) have recently determined the equilibrium constants, enthalpy, and entropy for the coordination of NO to Fe(II)EDTA and Fe(II)NTA. Both these groups performed their experiments by bubbling a mixture of NO and N₂ of known NO concentration through a metal chelate solution and then measuring the NO concentration in the outlet gas with a NO_x analyzer. NO absorption was carried out until the NO concentration in the outlet gas became equal to that in the inlet gas, i.e., until equilibrium was reached. The experiments were performed at several temperatures to evaluate enthalpy and entropy of the reaction. The results of this study are shown in Table III.

We recently determined the equilibrium constant for the coordination of NO to Fe(II)(H₂O)₅, Fe(II)(citrate), and Fe(II)(acac)₂ using a temperature-jump apparatus (30). The source of the temperature jump is a high-voltage d.c. power supply connected to a capacitor through a solenoid switch. After the capacitor is charged, the switch is disconnected. By closing a variable spark gap, the energy stored in the capacitor can be discharged through a cell containing the reaction under study. A temperature jump of 8°C occurs within several microseconds. The temperature jump induces a change in the concentration of reactants and products as the reaction shifts to a new equilibrium. The shift is monitored by a photomultiplier that responds to changes in absorption of a nitrosyl ferrous chelate. The results are displayed on an oscilloscope, which is triggered by the closing of the spark gap.

The coordination of NO to metal chelates can be written as



The reciprocal of the relaxation time equals the forward rate constant times the sum of the final equilibrium concentrations of M(chelates) and NO plus the backward rate constant. When the reciprocal of the relaxation time is plotted against the final concentrations of M(chelate) + NO, the slope of the curve gives the forward rate constant (k₁) and the point of interception gives the backward rate constant (k₋₁). The results are summarized in Table III.

By comparing the equilibrium constants of reactions listed in Table III, it is obvious that Fe(II)(EDTA) and Fe(II)(NTA) have much larger absorption capacities for NO than Fe(II)(H₂O)₅, Fe(II)(citrate), and Fe(II)(acac)₂ have.

Formation and Dissociation Rate Constants of Nitrosyl Metal Chelates. The absorption rates of NO in an aqueous solution of Fe(II)EDTA were measured by Teramoto et al. (31) and Sado et al. (32) using a stirred vessel with a free flat gas-liquid interface. The forward rate constants of the complexing reaction were derived on the basis of the theory of gas absorption. The results are given in Table II.

With a temperature-jump technique we have directly measured the formation and dissociation rate constants (30) of Fe(II)(H₂O)₅NO, Fe(II)(citrate)NO, Fe(II)(acac)₂NO, Fe(II)(EDTA)NO, and Fe(II)(NTA)NO (Table II). Values for the rate and equilibrium constants for the formation of Fe(II)(H₂O)₅NO determined in this study agree well with those determined by Kustin et al. (33). The forward and reverse rate constants for the formation of Fe(II)(citrate)NO are somewhat smaller than the values for the Fe(II)(H₂O)₅NO complex, while the equilibrium constant is larger. The kinetics for the formation and dissociation of the Fe(II)(acac)₂NO complex are much slower than any other complex studied.

For both Fe(II)(EDTA)NO and Fe(II)(NTA)NO, the relaxation times due to the temperature jump were too fast to be measured. However, an upper limit of 10 microseconds was established for the relaxation times for both complexes. Using this value with the equilibrium constants determined for Fe(II)(EDTA)NO and Fe(II)(NTA)NO by Hishinuma et al. and our group respectively, the lower limits of forward and reverse rate constants were calculated (Table III).

Kinetics of Reactions of NO and SO₂ in Aqueous Solutions Containing Metal Chelates. Under O₂-free conditions, NO and SO₂ can react with metal chelates such as Fe(II)EDTA in aqueous solution to form Fe(II)(EDTA)NO and Fe(II)(EDTA)(SO₃²⁻) respectively. However, when both NO and SO₂ are bubbled into an aqueous solution containing Fe(II)EDTA, species such as N₂O, sulfamate, disulfamate, dithionate, and sulfate are produced (34). The kinetics and mechanisms of reactions involved in this NO-SO₂-metal chelates-*l*.H₂O system have not been characterized yet. Teramoto et al. (31) have recently proposed the following reactions that could take place in this system:

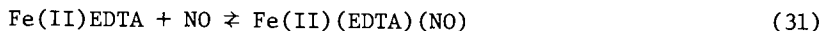


Table II.
Reactions considered and rate constants used for modeling.

Reaction	k, K or H (298OK) ^a	ΔE_a (kcal/mole)
1. $\text{SO}_2(\text{g}) + \text{H}_2\text{O} \rightarrow \text{SO}_2 \text{H}_2\text{O}$	1.24	
2. $\text{SO}_2 + \text{H}_2\text{O} \rightleftharpoons \text{H}^+ + \text{HSO}_3^-$	1.27×10^{-2}	
3. $\text{HSO}_3^- \rightleftharpoons \text{H}^+ + \text{SO}_3^{2-}$	6.24×10^{-8}	
4. $2\text{HSO}_3^- \rightleftharpoons \text{S}_2\text{O}_5^{2-} + \text{H}_2\text{O}$	7.0×10^{-2}	
5. $\text{NO}(\text{g}) + \text{NO}_2(\text{g}) + \text{H}_2\text{O}(\text{g}) \rightarrow 2\text{HNO}_2(\text{g})$	5.31×10^{-2}	
6. $\text{HNO}_2(\text{g}) \xrightarrow{\text{H}_2\text{O}} \text{HNO}_2$	49	
7. $\text{HNO}_2 \rightleftharpoons \text{H}^+ + \text{NO}_2^-$	5.1×10^{-4}	
8. $\text{H}^+ + \text{HNO}_2 \rightarrow \text{NO}^+ + \text{H}_2\text{O}$	4.08×10^2	11.5
9. $\text{NO}^+ + \text{HSO}_3^- \rightarrow \text{NOSO}_3^+ + \text{H}^+$ b		
10. $\text{HNO}_2 + \text{HSO}_3^- \rightarrow \text{NOSO}_3^- + \text{H}_2\text{O}$	2.43	12.1
11. $\text{NOSO}_3^- + \text{HSO}_3^- \rightarrow \text{HON}(\text{SO}_3)_2^{2-}$ b		
12. $\text{NO}_2^- + \text{S}_2\text{O}_5^{2-} \rightarrow \text{ON}(\text{SO}_3)_2^{3-}$ b		
13. $\text{ON}(\text{SO}_3)_2^{3-} + \text{H}^+ \rightarrow \text{HON}(\text{SO}_3)_2^{2-}$ b	1.29×10^{-2}	

Continued on next page.

American Chemical
Society Library
1155 16th St., N.W.

Table II. Continued.

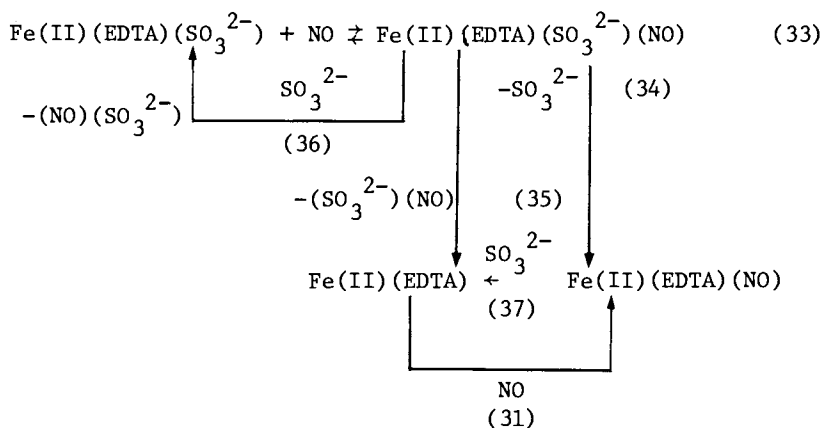
14.	$\text{HON}(\text{SO}_3)_2^{2-} + \text{H}^+ \xrightarrow{\text{H}_2\text{O}} \text{HONHSO}_3^- + \text{H}^+ + \text{HSO}_4^-$	1.92×10^{-2}	17.6
15.	$\text{HON}(\text{SO}_3)_2^{2-} \xrightarrow{\text{H}_2\text{O}} \text{HONHSO}_3^- + \text{HSO}_4^-$	1.52×10^{-6}	23.0
16.	$\text{HONHSO}_3^- + \text{H}^+ \xrightarrow{\text{H}_2\text{O}} \text{NH}_2\text{OH} + \text{H}^+ + \text{HSO}_4^-$	9.45×10^{-4}	19.5
17.	$\text{HON}(\text{SO}_3)_2^{2-} + \text{HSO}_3^- \rightarrow \text{N}(\text{SO}_3)_3^{3-} + \text{H}_2\text{O}$	2.02×10^{-4}	19.2
18.	$\text{N}(\text{SO}_3)_3^{3-} + \text{H}^+ \xrightarrow{\text{H}_2\text{O}} \text{HN}(\text{SO}_3)_2^{2-} + \text{HSO}_4^-$ $\text{H}_2\text{O} \rightarrow \text{H}_2\text{NSO}_3^- + \text{HSO}_4^-$ ^b	9.85×10^{-4}	23.5
19.	$\text{HN}(\text{SO}_3)_2^{2-} + \text{H}^+ \rightarrow \text{H}_2\text{NSO}_3^- + \text{HSO}_4^-$	2.84×10^{-4}	18.0
20.	$\text{HON}(\text{SO}_3)_2^{2-} + \text{HSO}_3^- \rightarrow \text{N}(\text{SO}_3)_3^{3-} + \text{H}_2\text{O}$	1.22×10^{-4}	18.0
21.	$\text{HON}(\text{SO}_3)_2^{2-} + \text{HSO}_3^- \rightarrow \text{HN}(\text{SO}_3)_2^{2-} + \text{HSO}_4^-$	1.50×10^{-5}	24.5
22.	$\text{HONHSO}_3^- + \text{HSO}_3^- \rightarrow \text{HN}(\text{SO}_3)_2^{2-} + \text{H}_2\text{O}$	6.44×10^{-6}	24.5
23.	$\text{HONHSO}_3^- + \text{HSO}_3^- \rightarrow \text{H}_2\text{NSO}_3^- + \text{HSO}_4^-$	2.58×10^1	13.4
24.	$\text{NH}_2\text{OH} + \text{SO}_2 \cdot \text{H}_2\text{O} \rightarrow \text{H}_2\text{NSO}_3^- + \text{H}_2\text{O} + \text{H}^+$	6.7×10^{-1}	3
25.	$\text{HN}_2\text{OH} + \text{SO}_2 \cdot \text{H}_2\text{O} \rightarrow \text{NH}_4^+ + \text{HSO}_4^-$	1.13×10^2	11.3
26.	$\text{H}_2\text{NSO}_3 + \text{HONO} \rightarrow \text{N}_2 + \text{HSO}_4^- + \text{H}_2\text{O}$		

^aUnits are mole liter⁻¹ for aqueous species and atm for gaseous species.

^bRate constants of 9, 11, 13 and 18 are assumed to be fast.

Table III
Kinetic and thermodynamic data for reversible NO coordination to ferrous chelates.

Ferrous chelates	k_1 $M^{-1} sec^{-1}$	k_{-1} sec^{-1}	K M^{-1} at 298°K	ΔH Kcal/mole	ΔS e.u.
Fe(II)(H ₂ O) ₅ (NO)	$(7.1 \pm 1.0) \times 10^5$	$(1.5 \pm 0.6) \times 10^3$	$(4.7 \pm 2.0) \times 10^2$		
Fe(II)(citrate)(NO)	$(4.4 \pm 0.8) \times 10^5$	$(6.6 \pm 2.4) \times 10^2$	$(6.7 \pm 2.0) \times 10^2$		
Fe(II)(acac) ₂ (NO)	$(4.0 \pm 3.0) \times 10^2$	24 ± 2	17 ± 14		
Fe(II)(NTA)(NO)	$\geq 7 \times 10^7$	≥ 35	2.14×10^6	-11.94	-11.0
Fe(II)(EDTA)(NO)	$\geq 6 \times 10^7$	≥ 60	1.15×10^7	-15.8	-20.7



They suggested that reactions (34), (35), and (36) are slow compared to reaction (37); and the activation energies of reactions (34) and (37) are larger than those of reactions (31) and (33). From the absorption rate study using a stirred vessel, they derived the forward rate constant of reaction (33) to be $1.4 \times 10^8 \text{ M}^{-1} \text{ sec}^{-1}$ at 25°C . The rate constants of other reactions, the rate law, and the products of all reactions involved have not yet been reported.

We are investigating the kinetics of aqueous reactions between Fe(II)(NTA)NO and sodium sulfite under well-controlled conditions. Our preliminary results indicate that the reaction rate is second order with respect to the concentration of Fe(II)(NTA)NO and first order with respect to the concentration of SO_3^{2-} . The major nitrogen product is N_2O . The rate constant is about $2.15 \times 10^3 \text{ M}^{-2} \text{ sec}^{-1}$ at 20°C . Work is in progress to determine the temperature and ionic strength dependence of the reaction and to identify all products for mass balance. We are also studying the kinetics of the reaction between Fe(II)(NTA)(SO_3^{2-}) and NO.

Conclusion. Considering the current lack of understanding of the chemistry involved and the present elementary stage of development for this type of process, J. Ando (35) suggested that this wet simultaneous SO_2/NO_x removal technique may be economically competitive with the sequential installation of NO_x control by selective catalytic reduction (SCR) followed by SO_2 control by flue gas desulfurization. Further research to identify a more effective metal chelate and to characterize important reactions involved could make this type of process an effective and economic scrubber for SO_2/NO_x control in a power plant.

Acknowledgment

We thank Professors Leo Brewer, Robert Connick, and Scott

Lynn for helpful discussions; and we appreciate the support and encouragement of Mr. Gary Friggen and Dr. Jack Halow. This work was supported by the Morgantown Energy Technology Center, contract no. 81MC14002, through the Assistant Secretary of Fossil Energy of the U.S. Department of Energy under contract no. W-7405-ENG-48.

Literature Cited

1. Yaverbaum, L.H. "Nitrogen Oxides Control and Removal, Recent Developments"; Noyes Data Corp.: Park Ridge, NJ, 1979.
2. Martin, A.E., ed. "Emission Control Technology for Industrial Boilers"; Noyes Data Corp.: Park Ridge, NJ, 1981.
3. Duecker, W.; West, J.; eds. "The Manufacture of Sulfuric Acid"; American Chemical Society Monograph Series No. 144, 1959.
4. Raschig, F. "Schwefel und Stickstoffstudien"; Verlag Chemie: Berlin, 1924.
5. Latimer, W.; Hildebrand, J.H. "Reference Book of Inorganic Chemistry"; Macmillan: New York, 1951; p. 208.
6. Chang, S.G. Paper presented at Technical Advisory Committee, DOE/Advanced Environmental Control Technology Program: Morgantown, WV, November 6-7, 1980; LBL Report 11800, 1980.
7. Oblath, S.B.; Markowitz, S.S.; Novakov, T.; Chang, S.G. J. Phys. Chem. 1981, 85, 1017.
8. Chang, S.G.; Toossi, R.; Novakov, T. Atmos. Environ. 1981, 15, 1287.
9. Gomiscek, S.; Clem, R.; Novakov, T.; Chang, S.G. J. Phys. Chem. 1981, 85, 2567.
10. Seel, V.F.; Degener, E. Z. anorg. allg. Chem. 1956, 284, 101.
11. Yamamoto, S.; Kaneda, T. Nippon Kagaku Zasshi 1959, 80, 1908.
12. Seel, V.F.; Knorre, H. Z. anorg. allg. Chem. 1961, 313, 70.
13. Naiditch, S.; Yost, D.M. J. Am. Chem. Soc. 1941, 63, 2123.
14. Seel, V.F.; Degener, E.; Knorre, H. Z. anorg. allg. Chem. 1959, 299, 122.
15. Sisler, H.H.; Audrieth, L.F. J. Am. Chem. Soc. 1939, 61, 3389.
16. Brackman, D.S.; Higginson, W.C.E. J. Chem. Soc. London 1953, 3896.
17. Fraser, R.T.M. J. Chem. Soc. London 1965, 1747.
18. Raschig, F. Ann. 1887, 241, 161.
19. Sisler, H.H.; Audrieth, L.F. J. Am. Chem. Soc. 1938, 60, 1947.
20. Doyle, G.J.; Davidson, N. J. Am. Chem. Soc. 1949, 71, 3491.
21. Benson, S.W. "The Foundations of Chemical Kinetics"; McGraw-Hill: New York, 1960.
22. Maron, S.H.; Berens, A.R. J. Am. Chem. Soc. 1950, 72, 3571.
23. Candlin, J.P.; Wilkins, R.G.; J. Chem. Soc. London 1960, 4236.
24. King, E.J.; King, G.W. J. Am. Chem. Soc. 1952, 74, 1212.

25. Spiro, M. Trans. Faraday Soc. 1959, 55, 1746.
26. Hughes, M.N.; Lusty, J.R. J. Chem. Soc., Dalton Trans. 1977, 509.
27. Hughes, M.N. J. Chem. Soc. (A) 1967, 902.
28. Hishinuma, Y.; Kaji, R.; Akimoto, H.; Nakajima, F.; Mori, T.; Kamo, T.; Arikawa, Y.; Nozawa, S. Chem. Soc. Japan Bull. 1979, 52, 2863.
29. Lin, N.H.; Littlejohn, D.; Chang, S.G. Submitted to J. Phys. Chem.
30. Littlejohn, D.; Chang, S.G. Submitted to J. Phys. Chem.
31. Teramoto, M.; Hiramane, S.; Shimada, Y.; Sugimoto, Y.; Teranishi, H. J. Chem. Eng. Japan 1978, 11, 450.
32. Sado, E.; Kumazawa, H.; Kudo, I.; Kondo, T. Ind. Eng. Chem. Process Dec. Dev. 1980, 19, 377.
33. Kustin, K.; Taub, I.A.; Weinstock, E. Inorg. Chem. 1966, 5, 1966.
34. Sawai, K.; Gorai, T. Kyusan to Kogyo 1976, 187.
35. Cichanowicz, ed. "Proceedings: Second NO_x Control Technology Center"; EPRI FP-1109-SR, 1979.

RECEIVED November 20, 1981.

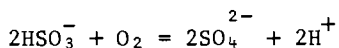
Kinetics of the Oxidation of Bisulfite Ion by Oxygen

THOMAS G. BRAGA and ROBERT E. CONNICK

University of California, Department of Chemistry, and Lawrence Berkeley Laboratory, Materials and Molecular Research Division, Berkeley, CA 94720

The chain reaction between sulfur (IV) and oxygen has been studied in the pH region of 3.0 and 4.7 where bisulfite ion, HSO_3^- , is the principal species. Preliminary measurements were made with a two-phase gas-aqueous system. To avoid mass-transfer problems, the remaining studies were done on a single aqueous phase with no gas phase present and using an oxygen meter to follow the concentration of dissolved oxygen as a function of time. Empirical rate laws were determined for a variety of conditions, including the presence of ethanol, manganous ion and ultra violet light. Without additives the chain appears to be terminated by a bimolecular reaction of chain carriers, since the rate law contains powers of multiples of 1/2. Ethanol inhibits the reaction by chain termination involving a single chain carrier. Manganous ion is a strong catalyst, apparently through the introduction of a new propagating path as well as participation in the initiation. Ultra violet light presumably initiates the chain. The "simplest" resolution of the rate laws into the three components: initiation, propagation and termination is suggested. The data do not establish the identity of the intermediates; other information will be necessary to fix mechanisms of the reaction.

The oxidation of bisulfite ion by oxygen:



is of importance in the lime/limestone processes for removing sulfur dioxide from stack gases of coal-burning power plants as well as in the conversion of atmospheric SO_2 to sulfuric acid, the principal component of acid rain. In the various Flue Gas Desul-

0097-6156/82/0188-0153\$6.00/0
© 1982 American Chemical Society

furization processes, there are advantages to be gained in accelerating this oxidation in some cases and in slowing it down in others. Thus a basic understanding of the kinetics of the reaction is a desirable goal.

Since Bäckström (1,2) reported studies of the thermal and photo-oxidation of sodium sulfite solutions, the oxidation of S(IV) species by oxygen has been known to proceed by a chain mechanism. The details of the mechanism, however, are still a matter of much controversy.

A review of the extensive literature (3,4) shows considerable disagreement concerning the rate law and rate constants. Most of the studies were done on sulfite solutions around pH 9. The rate law appears to vary depending on the experimental conditions, and no consistent law has been obtained. The rate has been reported to be proportional to the sulfite concentration and independent of the oxygen concentration (5-7) as well as proportional to both the sulfite and oxygen concentrations (8-10). Although some reports (11) distinguish between the rate laws at sulfite concentrations less than or greater than ~ 0.01 M, both expressions have been reported for both ranges. Dramatic effects of many metal ions (12-14) and organic molecules (15-16) have been cited, however in many cases the role of these additives has not been determined.

The effects of impurities have been well documented, with investigators reporting that consistent results could only be approached after extensive purification (7,9), although even then the rate may have been controlled by impurities. This sensitivity is not surprising since, as a chain reaction, the process involves highly reactive chain carriers.

We have chosen to attack the control of this reaction not by exhaustive purification, which has proven to be a difficult task owing to the large effects produced by some catalysts even in trace amounts, but by attempting to control or define the chain processes by the introduction of known catalysts and inhibitors.

The present studies were carried out at acidities where HSO_3^- is the principal S(IV) species. The dependences of the oxidation rate on the concentration of bisulfite, oxygen and H^+ were studied in the pH range of 3.0 to 4.7. The effects of ethanol, manganese ion and ultraviolet radiation on the rate and above dependences were investigated in order to gain information concerning the feasibility of controlling the oxidation reaction through their presence.

Experimental.

Two Phase Experiments. The rate of O_2 uptake by bisulfite solutions was measured by following the change in the volume of oxygen gas at one atmosphere pressure in a closed, thermostated system at 25°C . The solution was violently agitated using a Vibro Mischer (Ag. für Chemie-Apparatebau, Zürich, Switzerland) which vibrated a perforated plate vertically about 5 mm below the

surface of the liquid at 7200 rpm with ca. 2 mm amplitude. This action forces many small gas bubbles into the solution below the plate and produces almost a froth above the plate. The mixing was further enhanced by a magnetic stirring bar operating on the bottom of the vessel at its maximum speed.

Aliquots of HSO_3^- solution were introduced into the system by means of a pressure equalizing buret.

Single Phase Experiments. In order to eliminate the possibility of gas-liquid mass transfer control, the rate of the disappearance of dissolved oxygen in bisulfite solutions was determined in the liquid phase in the absence of a gas phase using the vessel shown in Figure 1. Concentrations were varied by introducing aliquots of the reagents through the port of the vessel both at the beginning and sometimes during a kinetic run. The initial oxygen concentration was usually 2.6×10^{-4} M but in a few cases was as high as 4.3×10^{-4} M. The direct measurement of the change in the concentration of oxygen with time was achieved by using a Yellow Springs Instrument model 57 oxygen meter and model 5739 probe. This probe consists of a Clark-type membrane covering a gold and AgCl electrode system. Output was recorded on a Leeds and Northrup Speedomax strip chart recorder.

The response time of the oxygen probe was determined by measuring the response of the probe to a sudden change in oxygen concentration. This was accomplished by physically transferring the probe from air saturated water to deoxygenated water. Analyzing these data in terms of a two layer diffusion model (17) indicated that a zero order rate of O_2 disappearance of less than $\sim 3 \times 10^{-6}$ M sec^{-1} could be determined without applying any corrections due to diffusional processes. Larger zero order rates were determined by graphically fitting the decay to a series of plots calculated using a mathematical treatment analogous to that of Benedek and Heideger (17) for the oxygen probe. Rates less than $\sim 2 \times 10^{-5}$ M sec^{-1} were measurable, i.e., appreciably slower than the diffusion control limit.

The pH of the solution was measured with an Orion Research model 601A digital meter and a Markson model 788 combination electrode.

Ultraviolet radiation was produced by a General Electric H100A4/T bulb, with the glass outer casing removed, located approximately 6 cm above the upper solution. The UV light was allowed to shine into the solution through the quartz tube indicated (Figure 1). The intensity of the light on the solution was varied by masking the cross sectional area of the tube close to the light source with a foil perforated with holes. All experiments were at 25°C.

Results

Two Phase Experiments. Figure 2 shows typical data for the

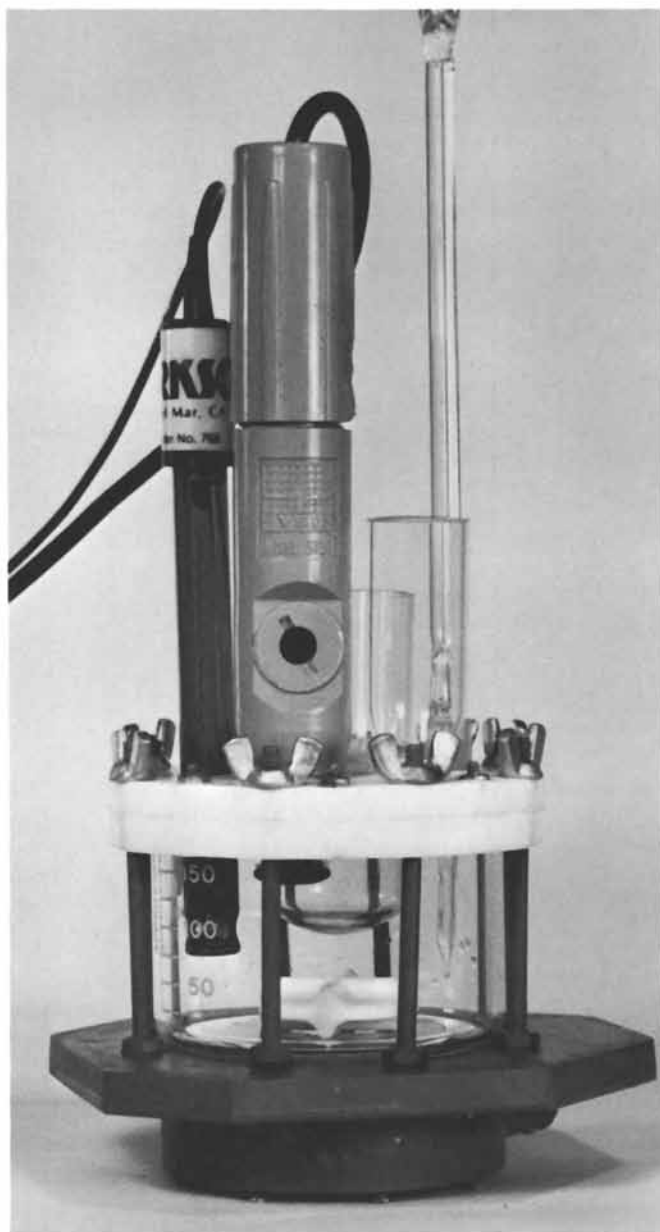


Figure 1. Reaction vessel used for single phase experiments.

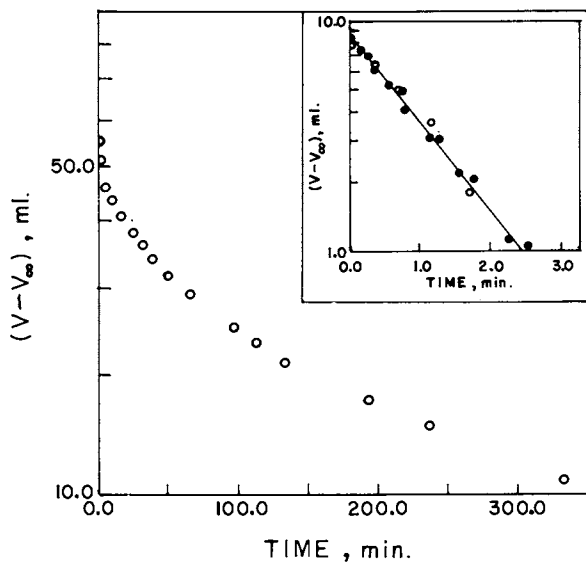


Figure 2. Typical gas volume data for the absorption of gaseous O_2 into a bisulfite solution. Sodium acetate-acetic acid buffer at 0.5 M; initial $[HSO_3^-] = 0.012$ M; $[O_2] = 1.23 \times 10^{-3}$ M. Insert: \circ , O_2 absorption into H_2O ; \bullet , initial O_2 absorption into HSO_3^- solution.

absorption of gaseous O_2 into a bisulfite solution. To maintain pH control, an acetic acid-sodium acetate buffer (pH = 3.7 to 4.7) was used. Since the solution was prepared from oxygen depleted water, the initial rapid drop in volume of oxygen occurs as the solution is quickly being saturated, followed by the slower decrease in volume as the oxidation proceeds. When the data for the first few minutes have subtracted from them values of the smoothly extrapolated remainder of the curve, it is found that the first order rate agrees closely with the rate at which $O_2(g)$ goes into water under the same mixing conditions (insert, Figure 2). The rate of reaction between HSO_3^- and O_2 is shown to be much slower than the mass transfer rate and therefore is kinetically controlled. This rate, on analysis, is found to be 3/2 order in bisulfite concentration during a single experiment (Figure 3).

Rates were not reproducible between runs, varying usually 10 to 20 percent but sometimes much more. Varying the source and purity of the water and the source of bisulfite failed to eliminate the problem. However, comparison of rates between experiments seemed consistent with 3/2 order for HSO_3^- and indicated the rate was inverse first order in H^+ concentration. The oxygen dependence was not tested.

Single Phase Experiments.

Buffered Solutions. Single phase experiments in 0.5 M acetic acid-0.5 M sodium acetate buffer solutions, with HSO_3^- (0.01 to 0.04 M) in large excess over oxygen, gave approximately a zero order dependence on oxygen. The data actually indicated a somewhat less than zero order initially which gradually became zero order as the reaction approached completion. The complete rate law for these buffered solutions at pH \sim 4.7 appears to be

$$\frac{-d[O_2]}{dt} = \text{Rate} = \frac{k[HSO_3^-]^{3/2}[O_2]^0}{[H^+]} \quad (2)$$

with $k \approx 3 \times 10^{-8} \text{ M}^{1/2} \text{ s}^{-1}$. The addition of 0.2 M $CuSO_4$ increased the rate by a factor of 3 for 0.016 M HSO_3^- in the equimolar buffer.

Buffered Solutions with $MnSO_4$ and Ethanol. A series of experiments at constant $[HSO_3^-]$, buffer and initial $[O_2]$ showed a first order dependence of the rate on concentration of manganous ion (Figure 4, curve A).

A series of experiments at constant $[HSO_3^-]$, buffer and initial $[O_2]$ gave an inverse dependence of the rate on ethanol concentration as shown in Figure 5 where the reciprocal of the rate, normalized to the value at zero ethanol is plotted. For sulfite solutions Bäckström (1) found an alcohol dependence of the form

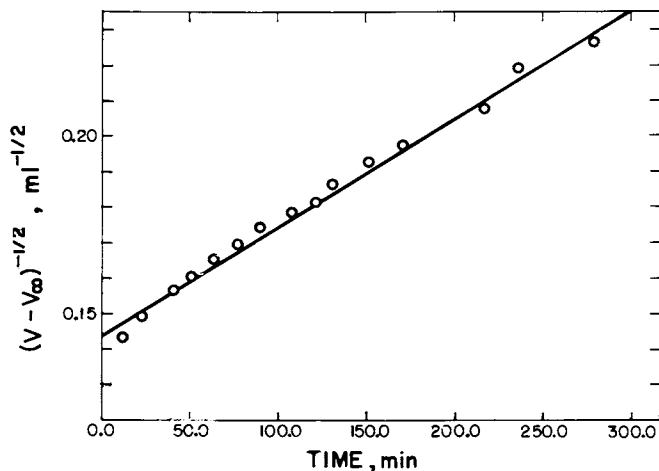


Figure 3. Plot indicating three-half-order dependence of rate on $[\text{HSO}_3^-]$ for the reaction: $\text{HSO}_3^- + \text{O}_2$ in 0.5 M acetic acid-sodium acetate buffer. Initial $[\text{HSO}_3^-] = 0.012 \text{ M}$; $[\text{O}_2] = 1.23 \times 10^{-3} \text{ M}$.

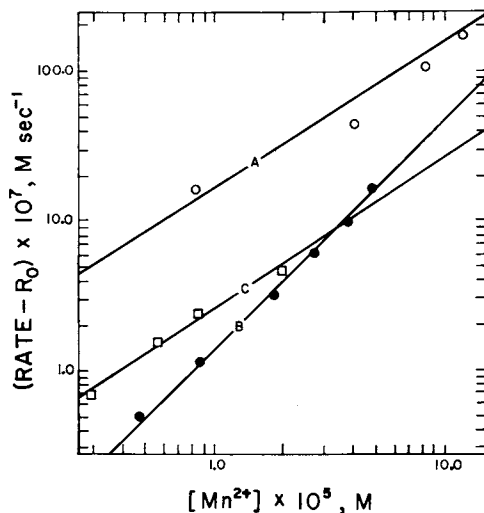


Figure 4. Effect of Mn^{2+} on the rate of oxidation of HSO_3^- . Curve A: 0.25 M acetic acid-0.25 M sodium acetate buffer, 0.02 M HSO_3^- , $1.8 \times 10^{-4} \text{ M O}_2$, rate without Mn^{2+} (R_0) = $9.6 \times 10^{-7} \text{ M/s}$. Line of slope 1.0 indicated. Curve B: $9.0 \times 10^{-3} \text{ M HSO}_3^-$, pH 4.2, $R_0 = 5.70 \times 10^{-8} \text{ M/s}$. Line of slope 1.5 indicated. Curve C: $1.04 \times 10^{-2} \text{ M HSO}_3^-$, pH 3.00, $R_0 = 2.40 \times 10^{-7} \text{ M/s}$. Line of slope 1.0 indicated.

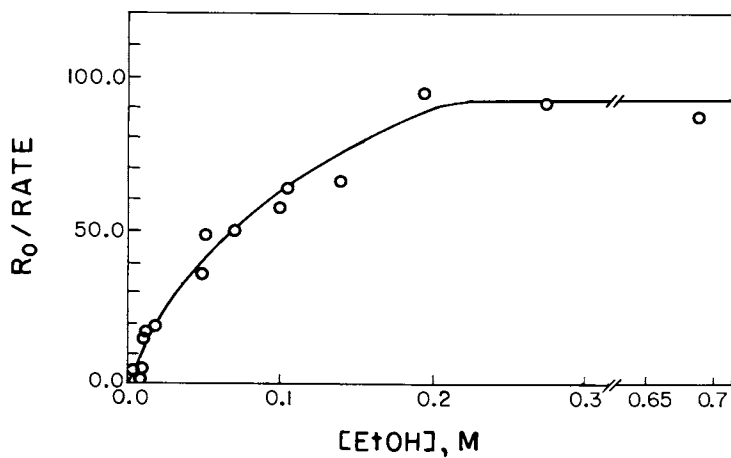


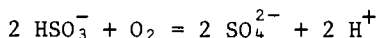
Figure 5. Effect of EtOH on the rate of oxidation of HSO_3^- in a 0.25 M acetic acid-0.25 M sodium acetate buffer. $[\text{HSO}_3^-] = 0.02 \text{ M}$; $[\text{O}_2] = 1.8 \times 10^{-4} \text{ M}$. Rate without EtOH (R_0) = $8.7 \times 10^{-7} \text{ M/s}$.

$$\text{Rate} \propto \frac{1}{1 + k [\text{EtOH}]} \quad (3)$$

The present results at low ethanol concentrations are probably consistent with this relationship. At higher ethanol, a new reaction path becomes observable (Figure 5). This path is roughly 100 fold slower than the original path and is independent of the ethanol concentration. Further experiments showed that the new path had a 3/2 order dependence on oxygen and increased in rate as the buffer concentration was increased.

Experiments were attempted with both ethanol and manganous ion present. The results conformed to no simple rate law and seemed only understandable if it was assumed that the manganous ion (at $<4 \times 10^{-4}$ M) was being complexed by an impurity in the ethanol. Purification of the ethanol by distillation increased the rate ca. 4 fold but did not eliminate the effect. Because of the apparent participation of the buffer in the rate law, work on buffered systems was discontinued.

Non-buffered Solutions. The net reaction



produces one H^+ per HSO_3^- consumed so it is necessary to add base to the reacting system if the pH is to be kept constant. This was done by addition of NaHCO_3 solution by means of a finely-tipped buret inserted into the solution in the cell (Figure 1). The addition was done manually using the pH meter as an indicator of acidity.

As in the buffered solutions, the rate was initially less than zero order in $[\text{O}_2]$. It was discovered, however, that the rate increased somewhat and became zero order if the reaction was repeated several times by introducing fresh oxygen. For this reason, the following procedure was adopted. After an aliquot of a HSO_3^- solution was injected into the reaction vessel, the $[\text{O}_2]$ was recorded until the oxygen was completely depleted. The solution was then re-oxygenated by bubbling O_2 through it. After the removal of all bubbles, the time dependence of the $[\text{O}_2]$ was again recorded. This procedure was continued until the rate became constant. Usually two complete reactions sufficed.

As the rate was generally zero order in $[\text{O}_2]$ with HSO_3^- in large excess, the constant slope of the $[\text{O}_2]$ vs. time plot made it easy to determine the rate. Because of this circumstance and in order to minimize changes in the solution that could lead to irreproducibility, many of the experiments on the order with respect to HSO_3^- , Mn^{2+} , ethanol and light intensity were done by following the O_2 disappearance long enough to establish the rate, adding a small volume of the species whose order was being determined, following long enough to get the new rate, adding more of

the species, etc. In this way changes in the reaction solution were kept to a minimum and hopefully irreproducibility was minimized.

Figure 6, curve A, and Figure 7, curve A, show the dependence of the rate on the concentrations of bisulfite and hydrogen ion for the oxidation where the pH was controlled by the addition of NaHCO_3 . These data indicate that under the described conditions, the rate is $3/2$ order with respect to $[\text{HSO}_3^-]$ and approximately inverse $3/2$ order with respect to $[\text{H}^+]$. Also, since the concentration of O_2 was observed to decrease linearly with time, the rate is independent of $[\text{O}_2]$, as in the buffered systems.

An earlier series of experiments using different distilled water, bisulfite and sodium bicarbonate solutions gave a second order dependence on bisulfite concentration and an inverse second order dependence on $[\text{H}^+]$. The rate of reaction was approximately 3 fold less. Since these inconsistencies could possibly be attributed to the introduction of impurities, another method of varying the $[\text{HSO}_3^-]$ was tried. After making a run with a given HSO_3^- concentration, a small volume of ca. 2 M H_2O_2 (prepared from 30% H_2O_2 Mallinckrodt Superoxol) was added to reduce the HSO_3^- concentration by oxidation of a part of it to SO_4^{2-} . The solution was then reoxygenated and run again, etc. These experiments gave a $3/2$ order with respect to bisulfite, thus adding support to the first cited rate law, although, as in other cases, it was still not possible to rule out contributions from impurities.

Non-buffered Solution with Ethanol. The effect of ethanol on the non-buffered solutions at constant $[\text{HSO}_3^-]$ is shown in Figure 8, curve A. These data indicate that the effect of ethanol under these conditions is qualitatively the same as in the buffered solutions and is described by equation 3 at low alcohol.

The dependence of the reaction on $[\text{HSO}_3^-]$ and pH in the presence of ethanol were investigated under the conditions shown in Figure 6, curve B, and Figure 7, curve B. The reaction is shown to be second order in $[\text{HSO}_3^-]$ and inverse second order in $[\text{H}^+]$. In all cases the rate was still independent of $[\text{O}_2]$.

Non-buffered Solution with MnSO_4 . The effect of the addition of Mn^{2+} on the non-buffered rate is shown in Figure 4, curve B, where rates corrected for the rate for zero manganous concentration are plotted. This treatment suggests that the manganous catalyzed rate is dependent on $[\text{Mn}^{2+}]^{3/2}$.

In the presence of manganous, the rate is shown to be independent of $[\text{HSO}_3^-]$ (Table I) and inversely proportional to $[\text{H}^+]$ (Figure 7, curve C), while still independent of $[\text{O}_2]$. Therefore, it appears that the rate law for the path catalyzed by Mn^{2+} under these conditions is of the form

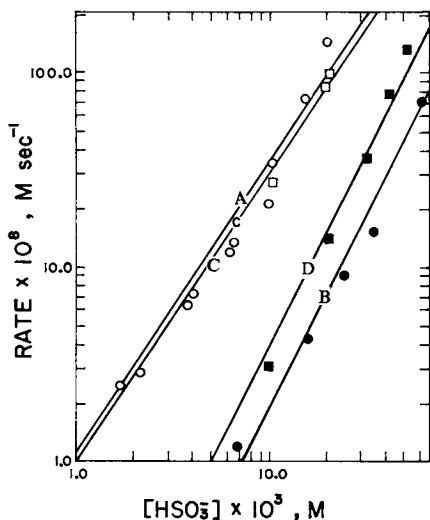


Figure 6. Dependence of the rate of oxidation on $[\text{HSO}_3^-]$. Curve A: \circ , pH 4.2, line of slope $3/2$ indicated. Curve B: pH 4.2, 1.28×10^{-3} M EtOH, line of slope 2.0 indicated. Curve C: \square , pH 3.90, line of slope 1.5 indicated. Dark reaction negligible. Curve D: pH 3.90, 5.84×10^{-3} M EtOH, line of slope 2.0 indicated. Dark reaction negligible.

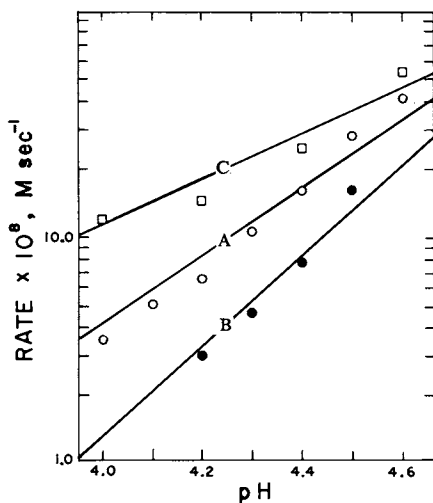


Figure 7. Dependence on pH of the rate of oxidation of HSO_3^- . Curve A: 8.7×10^{-3} M HSO_3^- , line for $[\text{H}^+]^{-1.5}$ dependence indicated. Curve B: 6.94×10^{-2} M HSO_3^- , 2.51×10^{-3} M EtOH, line for $[\text{H}^+]^{-2}$ dependence indicated. Curve C: 8.47×10^{-3} M HSO_3^- , 8.80×10^{-6} M Mn^{2+} , line for $[\text{H}^+]^{-1}$ dependence indicated. Ordinate is rate minus rate without Mn^{2+} (R_0) where $R_0 = 2.8 \times 10^{-14} [\text{H}^+]^{-3/2}$.

Table I

Dependence of Rate on $[\text{HSO}_3^-]$ with $[\text{Mn}^{2+}] = 9.14 \times 10^{-6} \text{ M}$.

$[\text{HSO}_3^-] \times 10^3$ M	Rate(observed) $\times 10^7 \text{ M sec}^{-1}$	Rate(without Mn^{2+}) $\times 10^8 \text{ M sec}^{-1}$	Rate(with Mn^{2+}) $\times 10^7 \text{ M sec}^{-1}$
3.47	1.50	0.85	1.41
4.65	1.48	1.30	1.35
8.47	1.95	4.50	1.50
8.96	1.95	5.70	1.38

$$\text{Rate} = \frac{k[\text{Mn}^{2+}]^{3/2} [\text{HSO}_3^-]^0 [\text{O}_2]^0}{[\text{H}^+]} \quad (4)$$

Non-buffered Solutions with Ultraviolet Light. Analysis of the photooxidation data was made with the assumption that although only part of the solution was illuminated (<50%), a correction for the dark reaction could be made by subtracting the dark rate from the observed rate.

The rate of the oxidation under these conditions was shown to be dependent on $[\text{HSO}_3^-]^{3/2}$ (Figure 6, curve C). Also, it is independent of both $[\text{O}_2]$ and pH over the pH range of 3.0 - 4.2.

Rough measurements with variable intensity of light suggest that the rate depends on the square root of the light intensity (Figure 9, curve A).

Non-buffered Solutions with Ultraviolet Light and Ethanol. As in the case of the thermal oxidation, the rate expression for the photooxidation with ethanol is initially of the form of equation 3. At higher ethanol concentrations, however, the rate is becoming independent of ethanol, as was the case of the buffered solution experiments, indicating the contribution of a new pathway (Figure 8, curve B). Under conditions where the rate was inversely proportional to the ethanol concentration, the rate was independent of pH (3.0 - 4.2) and $[\text{O}_2]$, was second order in $[\text{HSO}_3^-]$ (Figure 6, curve D), and was proportional to the intensity of light (Figure 9, curve B).

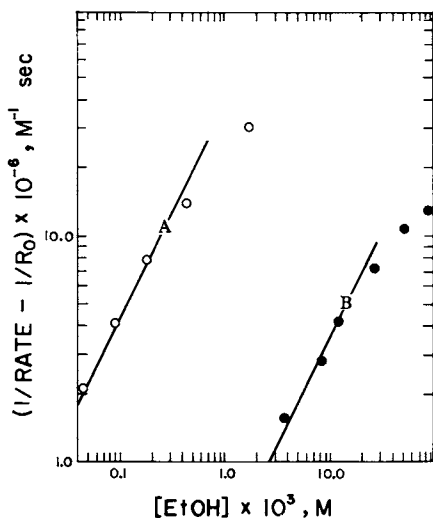


Figure 8. Effect of EtOH on the rate of oxidation of HSO_3^- . Curve A: 3.76×10^{-2} M HSO_3^- , pH 4.2, line of slope 1.0 indicated. Rate without EtOH (R_0) = 4.65×10^{-7} M/s. Curve B: 1.97×10^{-2} M HSO_3^- , pH 3.90, line of slope 1.0 indicated, $R_0 = 8.7 \times 10^{-7}$ M/s.

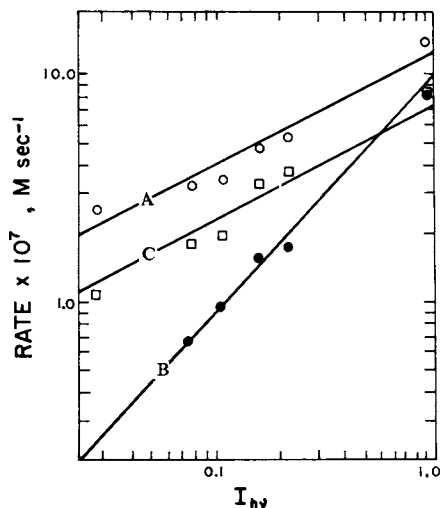


Figure 9. Dependence of the rate of photooxidation of HSO_3^- on the intensity of UV light. Curve A: 3.20×10^{-2} M HSO_3^- , pH 3.90, line of slope 0.5 indicated. Dark reaction negligible. Curve B: 5.84×10^{-3} M EtOH, 4.36×10^{-2} M HSO_3^- , pH 3.90, rate without EtOH (R_0) = 2.0×10^{-6} M/s, line of slope 1.0 indicated. Dark reaction negligible. Ordinate is $10^7 (1/R - 1/R_0)^{-1}$. Curve C: 6.7×10^{-6} M Mn^{2+} , 1.00×10^{-2} M HSO_3^- , pH 3.00, dark rate = 2.83×10^{-7} M/s, slope of 0.5 indicated. Ordinate is $10^7 (\text{rate} - \text{dark rate})$.

Non-buffered Solutions with Ultraviolet Light and MnSO₄.

The photooxidation rate was found to be proportional to the concentration of Mn²⁺ (Figure 4, curve C), independent of [O₂] and hydrogen ion concentration, and proportional to the intensity of light to the 0.5 power (Figure 9, curve C). The order with respect to HSO₃⁻ is somewhat greater than 0.5 but less than 1.0 (Figure 10).

Reproducibility. As all other investigators have found, the rate of the reaction is not reproducible within the experimental accuracy, even when careful precautions are taken to use the same chemicals and containers. No satisfactory explanation has been advanced other than the presence of variable amounts of unknown impurities. In our experience, experiments done under as identical conditions as possible usually gave rates within 10% of each, but sometimes varied as much as 20% and infrequently more. Experiments with different solutions of reagents gave greater variations, sometimes as much as several fold. Within a single run in the one-phase system the [O₂] vs. time plot was quite linear, within the experimental accuracy. The two-phase system showed some irreproducibility in a single run. The use of ethanol as a terminator and manganous ion as a presumed propagator did not eliminate the irreproducibility. Therefore it is suspected that it arises at least in part in the initiation. The experiments with UV light were not sufficiently well controlled to determine whether the reproducibility was improved.

Discussion. The rate of a chain reaction of long chain length may be represented symbolically by a chain initiating step I, a chain propagating step P, and a chain terminating step T:

$$\text{Rate} = P \left(\frac{I}{T} \right)^{\frac{1}{n}} \quad (5)$$

where n is a small integer, usually 1 or 2. The rates of initiation and termination are equal, i.e., $I = T$. The factor I/T is introduced to cancel from the rate law the concentration(s) of chain carrier(s) which appear in P and T. If the termination involves one chain carrier, n will be unity; if it involves two chain carriers, n will be two. Analysis of rate expressions in terms of equation 5 can help in the determination of the role of catalysts or inhibitors in the chain process.

In the treatment of the data, the effects of Mn²⁺ and ultraviolet light were assumed to be separable from the processes without these additives. Therefore, the rates of the catalyzed reaction paths were determined by correcting the observed rate for contributions from the rate without the additives. It must be understood, however, that this assumption is exact only when the catalyzed reaction is independent of the non-catalyzed reaction

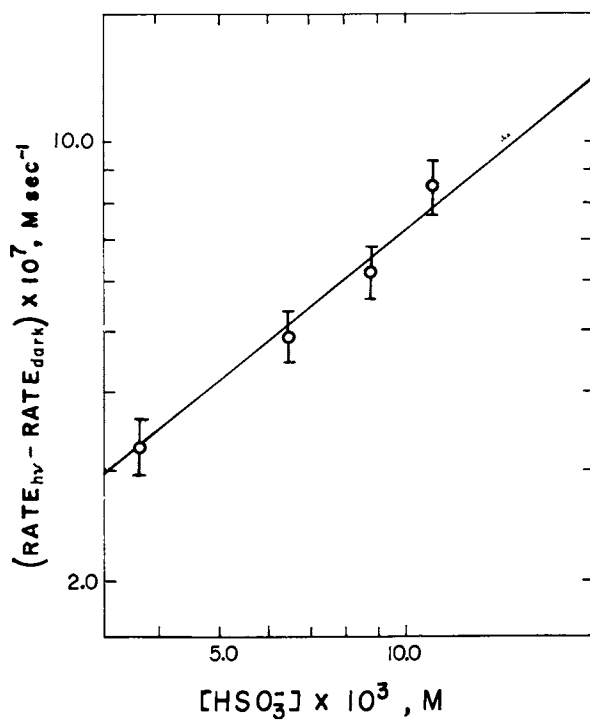


Figure 10. Dependence on $[\text{HSO}_3^-]$ of the rate of photooxidation in the presence of Mn^{2+} . $[\text{Mn}^{2+}] = 6.7 \times 10^{-6} \text{ M}$; pH 3.00. Slope = 0.8.

or when the catalyst only affects one process (i.e., initiation or propagation) additively while the other processes are unchanged. However, the assumption yields a first order correction if the catalyst is involved in more than one process.

The order of the reaction with respect to a particular reagent was generally determined by changing the concentration through additions of the reagent. Exceptions were HSO_3^- in the two-phase experiments and O_2 in the single-phase experiments, where the order could be determined from the change in concentration during a single run. For the usual case, i.e., where reagent was added, there was always the possibility of the presence in the reagent of an impurity which entered into the rate, with the consequence that a false order for the reagent would be obtained. In an attempt to guard against this possibility different sources of each reagent were tried with no evidence of a significant effect within the general level of reproducibility of the rate, except for the case of ethanol in the presence of Mn^{2+} cited earlier. Yet the possibility that the orders might be flawed by impurities must be kept in mind. Accepting these assumptions in the treatment of the data, a qualitative explanation of the results can be obtained by analyzing the rate laws for the various conditions in terms of equation 5. A possible analysis which utilizes the minimum number of paths is shown in Table II.

The discerning reader will notice that the alcohol dependence given in equation (3) is not that predicted from the proper combination of the second and third rate laws of Table II. The difference is small, however, and probably not detectable within the reproducibility of the experiments. The inability of the analysis to explain completely the bisulfite dependence shown in rate law 7 may be due to over-simplification. A contribution of another term in the propagation process which is proportional to $[\text{HSO}_3^-][\text{X}]$ (i.e., the propagation term for the rate laws without the presence of Mn^{2+}), may not be negligible. The addition of this term would produce a gradual increase in the order of the rate with respect to $[\text{HSO}_3^-]$ from 0.5 to 1.5 with increasing $[\text{HSO}_3^-]$. This is not unlike the effect shown in Figure 10.

The most serious discrepancy in Table II occurs in rate law 2 where the $[\text{H}^+]$ dependence measured is $-3/2$ while that predicted is -1 , as found in rate law 1. Unless the results are in error, the system is more complex than pictured.

The suggested breakdown of the rate laws in Table II into initiation, propagation and termination is of course not unique, but rather the simplest interpretation for a chain mechanism. For example, wherever an $[\text{X}][\text{X}]$ termination was used, it could equally well be an $[\text{X}][\text{Y}]$ termination involving two intermediates. The propagation term would then be the square root of the product of two of the propagating steps - one involving $[\text{X}]$ and the other $[\text{Y}]$. Further, the concentration terms in the rate law that are to be attributed to each of the three terms is not unique, but the choice given seems the most reasonable of the possibilities. The

Table II

Possible Interpretation of the Rate Laws

Conditions	Rate Law	Analysis
1) Buffered solutions	$\text{Rate} \propto \frac{[\text{HSO}_3^-]^{3/2} [\text{O}_2]^0}{[\text{H}^+]}$	$\begin{aligned} I &\propto [\text{HSO}_3^-][\text{H}^+]^{-2} \\ P &\propto [\text{HSO}_3^-][\text{X}] \\ T &\propto [\text{X}][\text{X}] \end{aligned}$
2) Non-buffered solutions	$\text{Rate} \propto \frac{[\text{HSO}_3^-]^{3/2} [\text{O}_2]^0}{[\text{H}^+]^{3/2}}$	$\begin{aligned} I &\propto [\text{HSO}_3^-][\text{H}^+]^{-2} \\ P &\propto [\text{HSO}_3^-][\text{X}] \\ T &\propto [\text{X}][\text{X}] \end{aligned}$
3) Non-buffered solutions with ethanol	$\text{Rate} \propto \frac{[\text{HSO}_3^-]^2 [\text{O}_2]^0}{[\text{H}^+]^2 [\text{EtOH}]}$	$\begin{aligned} I &\propto [\text{HSO}_3^-][\text{H}^+]^{-2} \\ P &\propto [\text{HSO}_3^-][\text{X}] \\ T &\propto [\text{EtOH}][\text{X}] \end{aligned}$
4) Non-buffered solutions with MnSO_4	$\text{Rate} \propto \frac{[\text{Mn}^{2+}]^{3/2} [\text{HSO}_3^-]^0 [\text{O}_2]^0}{[\text{H}^+]}$	$\begin{aligned} I &\propto [\text{Mn}^{2+}][\text{H}^+]^{-2} \\ P &\propto [\text{Mn}^{2+}][\text{X}] \\ T &\propto [\text{X}][\text{X}] \end{aligned}$
5) Non-buffered solutions with UV light	$\text{Rate} \propto I_{\text{hv}}^{1/2} [\text{HSO}_3^-]^{3/2} [\text{O}_2]^0$	$\begin{aligned} I &\propto I_{\text{hv}} [\text{HSO}_3^-] \\ P &\propto [\text{HSO}_3^-][\text{X}] \\ T &\propto [\text{X}][\text{X}] \end{aligned}$
6) Non-buffered solutions with UV light and ethanol	$\text{Rate} \propto \frac{I_{\text{hv}} [\text{HSO}_3^-]^2 [\text{O}_2]^0}{[\text{EtOH}]}$	$\begin{aligned} I &\propto I_{\text{hv}} [\text{HSO}_3^-] \\ P &\propto [\text{HSO}_3^-][\text{X}] \\ T &\propto [\text{EtOH}][\text{X}] \end{aligned}$
7) Non-buffered solutions with UV light and MnSO_4	$\text{Rate} \propto I_{\text{hv}}^{1/2} [\text{Mn}^{2+}] [\text{HSO}_3^-]^{0.8} [\text{O}_2]^0$	$\begin{aligned} I &\propto I_{\text{hv}} [\text{HSO}_3^-] \\ P &\propto [\text{Mn}^{2+}][\text{X}] \\ T &\propto [\text{X}][\text{X}] \end{aligned}$

selection of a termination step involving two chain carriers is strongly suggested whenever the rate law contains an odd multiple of one half order, corresponding to $n = 2$, although other sources of such orders are possible in principle. If there are no half orders in the rate law it is likely, although not necessary, that the termination involves only a single chain carrier.

These results suggest the following:

Ultraviolet light appears to affect only the initiation. This is indicated by the change in the dependence on the intensity of light from 0.5 to 1.0 order upon the addition of ethanol, a known terminator (1) which switches the termination from $[X][X]$ to $[EtOH][X]$ and n from 1 to 2.

The $3/2$ order in $[Mn^{2+}]$ suggests that manganous is involved in both the initiation and propagation, although other explanations involving more complex mechanisms and higher order terms are possible.

In the resolution of the rate laws of Table II into their component parts, intermediates (chain carriers) have always been symbolized by X. The simplest interpretation would have X the same species for all of the rate laws. Assuming this to be the case, it is possible to combine the rate laws of Table II into a single master rate law that allows comparison of a calculated rate with the experimental rate for each data set. The irreproducibility of the experiments, however, makes such a procedure questionable. The results are generally consistent qualitatively with such an analysis, but there is not perfect quantitative agreement.

Of course there may be impurities involved in some of the steps in Table II, and in particular it seems likely that some impurity participates in the initiation step of the first three rate laws.

From the analysis of the rate laws in Table II one can write plausible mechanisms for the reaction, but always more than one. The chain initiation reaction is in no case defined by the rate law, and the chain carriers cannot be uniquely fixed from the rate law. Therefore no attempt will be made to give mechanisms until further information is available to limit the possibilities.

Acknowledgment

This work was supported by the Assistant Secretary for Fossil Energy, Office of Coal Research, Advanced Environment Control Division of the U. S. Department of Energy under contract number W7405 ENG-48 through the Morgantown Energy Technology Center, Morgantown, WV.

Literature Cited

1. Bäckström, H. L. J. J. Am. Chem. Soc. 1927, 49, 1460.
2. Alyea, H. N.; Bäckström, H. L. J. Ibid 1929, 51, 90.
3. The older literature, up to 1949, is analyzed in Gmelins Handbuch Der Anorganischen Chemie 1963, 9, 1293-1514.
4. Most of the recent literature is cited by J. L. Hudson in "Sulfur Dioxide Oxidation in Scrubber Systems," EPA-600/7-80-083, April, 1980.
5. Reinders, W.; Dingemans, P. Rec. Trav. Chim. 1934, 53, 231.
6. Titoff, A. Z. Physik. Chem. 1903, 45, 641.
7. Winkelmann, V. D. Z. Elektrochem. 1955, 59, 891.
8. Schultz, J. S.; Gaden, E. L. Ind. Eng. Chem. 1956, 48, 2209.
9. Fuller, E. C.; Crist, R. H. J. Am. Chem. Soc. 1941, 63, 1644.
10. Yagi, S.; Inoue, H. Chem. Eng. Sci. 1962, 17, 411.
11. Srivastava, R. D.; McMillan, A. F.; Harris, I. J. Can. J. Chem. Eng. 1968, 46, 181.
12. Hoather, R. C.; Goodeve, C. F. Trans. Faraday Soc. 1934, 30, 626, 1149.
13. Chen, T-I.; Barron, C. H. Ind. Eng. Chem. Fundam. 1972, 11(4), 466.
14. Alper, E. Trans. Inst. Chem. Eng. 1973, 51(2), 159.
15. Altwicker, E. R. Trans. Inst. Chem. Eng. 1977, 55, 281.
16. Mathews, J. H.; Weeks, M. E. J. Am. Chem. Soc. 1917, 39, 635.
17. Benedek, A. A.; Heideger, W. J. Water Res. 1970, 4, 627.

RECEIVED December 10, 1981.

Sulfite Oxidation in Organic Acid Solutions

D. B. NURMI, J. W. OVERMAN, J. ERWIN, and J. L. HUDSON

University of Virginia, Department of Chemical Engineering, Charlottesville, VA 22901

The rates of the catalytic oxidation of sodium and calcium sulfite in several organic acid buffers have been determined. In the paper particular attention is given to oxidation in succinic acid.

The experiments with sodium sulfite were done at pH 4.6, 40°C, and with 0.2 m/l succinic acid, with catalysts iron, manganese, and a mixture of iron and manganese. With manganese catalyst, the order of the reaction with respect to both S IV and manganese was about one whereas with iron the orders were 1.7 and 0.2 on S IV and iron respectively. Although iron catalyzes the reaction when acting alone, it has no marked influence when manganese is also present, i.e., mixed manganese-iron solutions behave essentially like solutions containing only manganese catalyst.

The experiments with calcium sulfite were done with succinic acid concentrations from 0 to 0.2 m/l and it is seen that the organic acid is a substantial inhibitor for the oxidation. The inhibition by succinic acid is compared to that of glycolic acid and adipic acid.

Forced oxidation in flue gas desulfurization (FGD) systems converts calcium sulfite ($\text{CaSO}_3 \cdot \frac{1}{2}\text{H}_2\text{O}$) to calcium sulfate, or gypsum ($\text{CaSO}_4 \cdot 2\text{H}_2\text{O}$). This oxidized gypsum product is far superior to the calcium sulfite product now produced in FGD scrubbers since the gypsum has less disposal volume and settles by an order of magnitude faster than the unoxidized material. The gypsum filters to better than 80% solids and handles like moist soil compared to the unoxidized material which filters to only about 50 to 60% solids and is thixotropic.

Borgwardt (1,2) has recently discussed forced oxidation in limestone FGD scrubbing systems. It is shown (2) that even in a single loop limestone scrubber that forced oxidation increases the SO_2 removal efficiency and utilization of limestone.

0097-6156/82/0188-0173\$6.00/0
© 1982 American Chemical Society

Furthermore, forced oxidation can cause a decrease of scale formation in the scrubber tower since there is more CaSO_4 seed crystal available in the scrubber.

Oxidation in a three phase system is a very complicated process. The rate of oxidation can depend on mass transfer of oxygen from the gas to the liquid, on the rate of solid dissolution, and on chemical kinetics. These three processes are closely interrelated and the relative importance of any one depends on the conditions in the scrubber or hold tank. The individual steps of these processes include the gas to liquid transport of oxygen, the solid to liquid mass transfer of sulfite, the precipitation of sulfates, and the chemical reaction. The rates of these steps depend on the concentrations of reacting and nonreacting species in the slurry, on pH, on slurry density, and on the design of the reactor.

In this paper we consider only one part of the overall oxidation process, viz., the liquid phase oxidation reaction to sulfate. We discuss the effects of manganese and iron catalysts on the oxidation of sulfite in aqueous solutions buffered with organic acids. These two catalysts were chosen since they are both known to influence the rate of the oxidation reaction and since they are both present in scrubbing systems. For example, typical flyash (3) and limestone analyses are given in Table I (4); these impurities find their way into the scrubbing system and are available to catalyze the oxidation. Results are presented in this work on the effects of manganese and iron acting independently and simultaneously. The study was carried out in organic acid buffers since weak organic acids can improve the rate of absorption of sulfur dioxide into limestone slurries (5,6) and it is likely that buffers will thus be present in commercial scrubbing loops. However, these organic acids also inhibit the rate of oxidation to sulfate. In this paper emphasis is given to succinic acid; other acids, particularly glycolic and adipic, are discussed in reference (7).

This work is not meant to be a basic kinetic study of the mechanism of the reaction. Rather it has as a goal the development of a simple kinetic rate expression which can be used in an overall model of oxidation including the complicating effects of solid dissolution and gas absorption. The goal is to accumulate kinetic data necessary to design a scrubber undergoing oxidation rather than to explore the mechanism of the complicated chemical reactions.

There are several organic compounds which are known to inhibit the aqueous phase oxidation of sulfite (7, 8, 9, 10). Several metals are known to have a catalytic effect on the rate of oxidation. Fuller and Christ (10) demonstrated that copper sulfate is an effective catalyst. Cobalt also catalyzes the oxidation of sodium sulfite (11).

Table I. COMMON CATALYTIC IMPURITIES IN FLY ASH AND LIMESTONE

Fly Ash Analysis (3)

<u>Component</u>	<u>Weight Percent</u>
Al ₂ O ₃	20 - 30
Fe ₂ O ₃	12 - 23
CaO	2 - 7
MgO	0.5 - 1.5

Limestone Analysis (4)

<u>Component</u>	<u>Weight Percent</u>
Al ₂ O ₃	6.01
Fe ₂ O ₃	0.19
MnO	0.06
CaO	55.5
Cl	0.004
Cu	0.00044
Cr	0.00011
As	0.0002
Hg	6 x 10 ⁻⁶

Experiments

The experiments were carried out in a semi-batch stirred reactor with continuous oxygen feed. The reactor is a one liter Pyrex flask with flattened bottom and baffles which is fitted with five standard 24/40 necks to accommodate the gas inlet, gas vent, sampling tube, and pH electrode. The reactor is immersed in a standard water bath for temperature control. Gas is fed at a flow rate of 3.0 ± 0.1 l/min through a rotameter. The solution is stirred at 1620 rpm.

All chemicals except the calcium sulfite and gases were reagent grade with catalytic impurities less than 0.0008%. The oxygen and nitrogen were 99.5% pure. The calcium sulfite analysis is given in Table II. The water was distilled in tin and passed over activated carbon and mixed-resin ion exchange beds such that the specific resistance exceeded a megohm.

Further details on the experiments are available in (7).

Results: Oxidation of Sodium Sulfite

All experiments with sodium sulfite reported in this paper were carried out with 0.2 gmol/l succinic acid and a pH of 4.6. The concentration is higher than that used in commercial practice; it was chosen in order to hold the pH constant during the experiments. The succinic acid concentration was varied in the experiments with calcium sulfite as is seen below. No other pH control was required.

In Figure 1 is shown the mole fractions of $\text{SO}_2 \cdot \text{H}_2\text{O}$, HSO_3^- , and SO_3^{2-} in a Na_2SO_3 solution at 40°C. It can be seen that pH = 4.6 corresponds to the maximum in HSO_3^- mole fraction. Temperature has only a moderate influence on the behavior shown in Figure 1. The initial pH was adjusted to 4.6 with NaOH. The manganese was added in the form manganous sulfate monohydrate ($\text{MnSO}_4 \cdot \text{H}_2\text{O}$) at concentrations from 0.83 to 4.0 ppm manganese. The iron was added in the form ferric sulfate ($\text{Fe}_2(\text{SO}_4)_3 \cdot x\text{H}_2\text{O}$) with the iron concentration being varied from 1.0 to 5.0 ppm.

Manganese Catalyzed Na_2SO_3 Oxidation. We first consider sodium sulfite oxidation catalyzed by manganese. Typical results for $[\text{S}^{+4}]$ vs time are shown in Figure 2 for manganese concentrations from 0.83 to 4.0 ppm. It is evident that the manganese has a substantial effect on the rate of reaction. For all manganese concentrations there was an induction period of about four minutes.

The experimental data (neglecting the induction period) were fitted to an expression of the form

Table II

ANALYSIS OF CALCIUM SULFITE SOLID

Species	Weight %
CaSO ₃	50.6
Manganese	0.0062
Iron	0.0248
Copper	0.0004
Magnesium	0.0505
Cobalt	0.0008
Zinc	0.0009

Atomic Absorption Analysis by North American
Exploration, Inc., Charlottesville, Virginia 22901

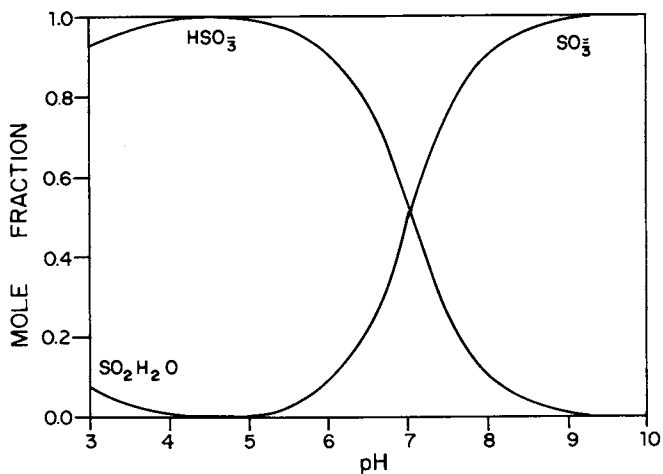


Figure 1. Effect of pH on S(IV) species. Conditions: 0.02 M Na_2SO_3 , 40°C.

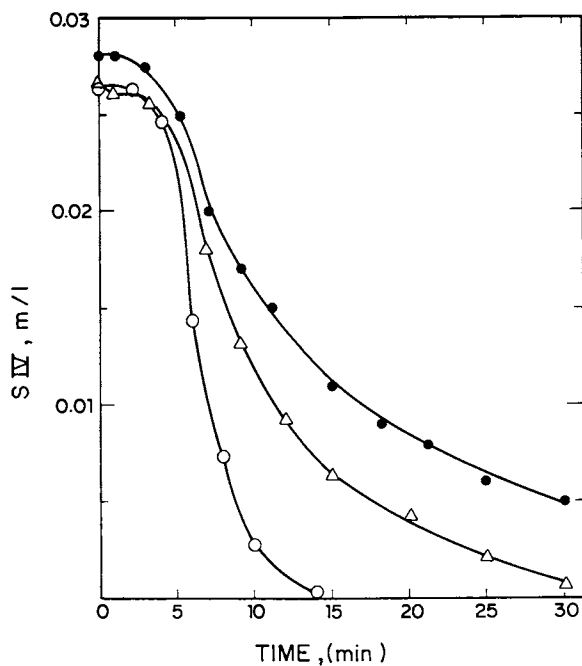


Figure 2. S(IV) concentration vs. time for Mn-catalyzed oxidation of Na_2SO_3 . Key: ●, 0.83 ppm Mn; △, 1.33 ppm Mn; and ○, 4.00 ppm Mn. pH 4.6; and T, 40°C.

$$\text{Rate} = k S^\alpha \quad (1)$$

where the rate has units gmol/l.s and S is the concentration of S(IV) having units gmol/l. The results are shown in Table III from which it can be seen that the reaction is approximately the same order in sulfur for all manganese concentrations investigated; since the order in sulfur is independent of the concentration of manganese, it seems reasonable to fit the rate to an expression of the form

$$\text{Rate} = k S^\alpha \text{Mn}^\beta \quad (2)$$

The maximum likelihood estimates of $\log_{10} k$, α , and β are 2.00, 0.95, and 1.03 and the standard deviations of the estimates of $\log_{10} k$, α , and β are 0.43, 0.04, and 0.09. In equation (2) and subsequent similar equations all species, including the catalyst concentrations, have units of moles per liter.

Iron Catalyzed Na_2SO_3 Oxidation. Similar experiments were carried out with iron catalyst and typical results are shown in Figure 3. A series of runs was carried out at pH = 4.6 and T = 40°C similar to that done with manganese catalyst, and results are given in Table IV. Again the order in sulfur appears to be independent of iron concentration; therefore, these data were fit to an equation of the form

$$\text{Rate} = k S^\alpha \text{Fe}^\gamma \quad (3)$$

The maximum likelihood estimates of $\log_{10} k$, α , and γ are -0.81, 1.69, and 0.18 and the standard deviation of the estimates of $\log_{10} k$, α , and γ are 0.39, 0.06, and 0.08.

Experiments were also carried out at 30°C and 50°C with an iron concentration of 5 ppm in order to obtain an activation energy for the reaction. The data were simply fit to

$$\text{Rate} = k_0 S^\alpha \exp(-E/RT) \quad (4)$$

where k_0 is the pre-exponential factor.

The maximum likelihood estimates of $\log_{10} k_0$, α , and E are 9.91, 1.41, and 17.09 and the standard deviations of the estimates of $\log_{10} k_0$, α , and E are 0.91, 0.06, and 1.22. E has units of kcal/mole. Of course, a different subset of data were used with equation (4) than that used with equation (3), and therefore a somewhat different order in sulfur was obtained (1.41 vs 1.69).

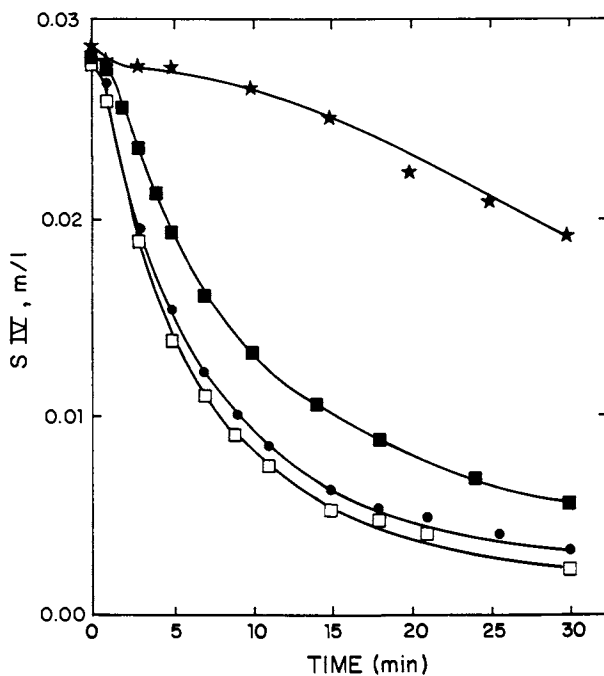


Figure 3. $S(IV)$ concentration vs. time for Fe-catalyzed oxidation of Na_2SO_3 . Key: ★, 0 ppm Fe; ■, 1 ppm Fe; ●, 3 ppm Fe; and □, 5 ppm Fe. pH 4.6; T, 40°C; and succinic acid, 0.2 m/L.

Table III
REGRESSION ANALYSES OF MANGANESE
CATALYZED Na_2SO_3 OXIDATION

<u>Mn Concentration Added (ppm)</u>	<u>Number of Data Points</u>	<u>Order With Respect to $[\text{S}^{4+}]$</u>	<u>Standard Deviations of Order</u>
0.83	21	0.91	0.14
1.33	14	0.90	0.06
2.67	11	1.03	0.08
4.00	10	0.96	0.09

Conditions:

pH = 4.6; Temperature = 40°C; Mn added as MnSO_4 .

Table IV
REGRESSION ANALYSES OF IRON CATALYZED Na_2SO_3 OXIDATION

<u>Fe Concentration Added (ppm)</u>	<u>Number of Data Points</u>	<u>Order With Respect to $[\text{S}^{4+}]$</u>	<u>Standard Deviations of Order</u>
1.00	21	1.78	0.10
3.00	19	1.78	0.10
5.00	123	1.68	0.08

Conditions:

$\text{pH}_I = 4.6$; Temperature = 40°C; Fe added as $\text{Fe}_2(\text{SO}_4)_3$.

Mixed Manganese and Iron Catalysts. Finally, experiments were carried out with mixed manganese and iron catalysts and the results again fitted by means of a regression analysis to an expression of the form

$$\text{Rate} = k S^{\alpha} \text{Mn}^{\beta} \text{Fe}^{\gamma} \quad (5)$$

The results are shown in the third row of Table V; the table also includes the results of the experiments catalyzed with manganese alone and with iron alone. It is interesting to note that the results with mixed manganese and iron resemble those with manganese alone, i.e., the orders in S(IV) and Mn are about 1.0 in both cases. Furthermore, the order in iron is approximately zero when both iron and manganese are present. Thus the presence of manganese causes the reaction to behave as if no iron were present for all iron concentrations used in these experiments. To further test this result we carried out a second regression analysis on the mixed catalyst data but omitting the iron from the analysis, i.e., the data used for line 3 of Table V were fit to equation 2. The results are shown in line 4 of Table V. These results show that the order with respect to iron is not significantly different than zero.

We thus see that although iron when present alone is a catalyst for the oxidation reaction, it has almost no effect on the rate of reaction when manganese is present. Since several catalysts are normally present in scrubbing system liquors, care must be taken in predicting oxidation rates based on information on individual catalysts.

Results: Oxidation of Calcium Sulfite

Effect of Succinic Acid. We carried out similar experiments using CaSO_3 in place of Na_2SO_3 . The rate of oxidation with calcium was always faster than that with sodium, partly because of the presence of impurities in the CaSO_3 which catalyze the reaction.

We first varied the concentration of the succinic acid buffer from 0 to 0.2 m/l. As is noted above, the succinic acid also acts as an inhibitor for the reaction.

Results of these experiments are shown in Table VI for pH = 4.0 and Table VII for pH = 5.0. At the lower succinic acid concentrations a pH controller was used to hold the pH at the desired level by addition of NaOH. At higher concentrations the controller was not necessary because of the buffering action of the organic acid.

The effect of the succinic acid can best be seen by comparing the rates of reaction calculated from the rate expressions at a fixed S IV concentration, chosen arbitrarily to be 0.01 gmol/l. The results of such a comparison are shown in Figure 4 where it can be seen that the effect of the organic acid is substantial.

Table V
SUMMARY OF REGRESSION ANALYSES OF Na₂SO₃ OXIDATION

Catalyst	# of Data pts	S ⁺⁴ Order	Std Dev	Mn Order	Std Dev	Fe Order	Std Dev	log ₁₀ k	Std Dev
Mn	56	0.95	(0.04)	1.03	(0.09)	----	----	2.00	(0.43)
Fe	163	1.69	(0.06)	----	----	0.18	(0.08)	-0.81	(0.39)
Mixed Mn + Fe	88	0.96	(0.03)	0.94	(0.06)	0.04	(0.07)	1.86	(0.28)
Mixed Neglecting Fe in Order Determination	88	0.96	(0.03)	0.96	(0.05)	----	----	1.78	(0.25)

Table VI
 EFFECT OF SUCCINIC ACID ON OXIDATION OF CaSO_3 ($\text{pH} = 4.0$, $T = 50^\circ\text{C}$)

Succinic Acid Concentration m/l	Order with $[\text{S}^{+4}]$ Respect to $[\text{S}^{+4}]$	Standards Deviations of Order	$\log_{10}k$ Rate	Standard Deviations of $\log_{10}k$ Rate	Rate at $[\text{S}^{+4}] = 0.01$ m/l (mole/l s)
0	1.21	0.07	-0.87	0.21	5.18×10^{-4}
0.0014	0.94	0.08	-1.72	0.24	2.49×10^{-4}
0.00136	1.19	0.08	-1.63	0.20	9.75×10^{-5}
0.0423	1.34	0.11	-1.68	0.28	4.36×10^{-5}
0.100	1.33	0.16	-2.12	0.38	1.66×10^{-5}
0.200	1.35	0.10	-2.40	0.27	7.9×10^{-6}

Table VII

EFFECT OF SUCCINIC ACID ON OXIDATION OF CaSO_3 (pH = 5.0, T = 50°C)

Succinic Acid Concentration m/l	Order with Respect to $[\text{S}^{+4}]$	Standard Deviations of Order	Rate Constant	Rate at $[\text{S}^{+4}] = 0.01 \text{ m/l}$ (mol/l-sec)
0.01	1.45	0.06	0.231	2.91×10^{-4}
0.05	1.82	0.15	0.350	8.02×10^{-5}
0.1	1.84	0.12	0.245	5.12×10^{-5}
0.2	1.64	0.12	0.0823	4.32×10^{-5}

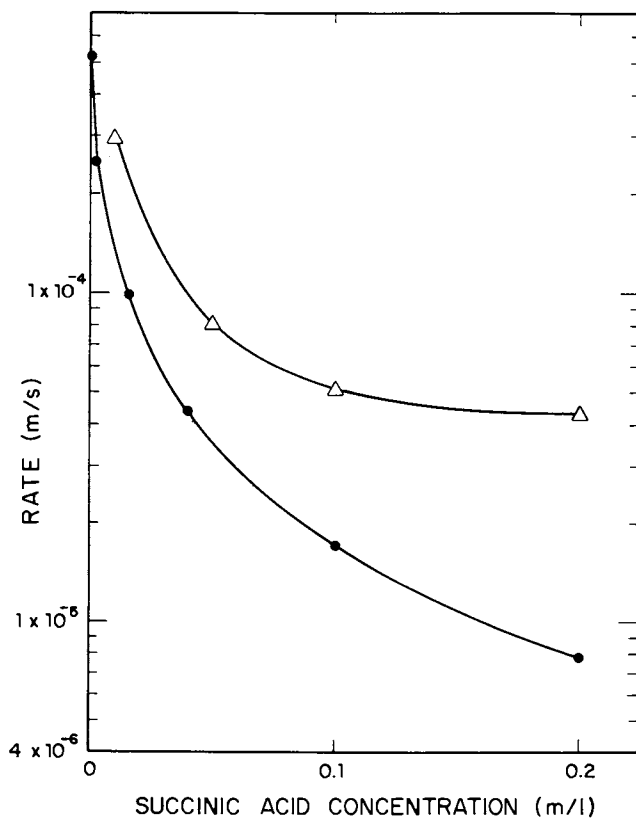


Figure 4. Dependence of oxidation rate of calcium sulfite on succinic acid concentration. Key: Δ , pH 5.0; and \bullet , pH 4.0. T , 50°C .

Manganese Catalyzed CaSO₃ Oxidation. We also investigated the effect of manganese catalyst on the oxidation of CaSO₃. These experiments were done in 0.2 gmol/l succinic acid, the same concentration as was used in the sodium sulfite study.

Representative results are shown in Table VIII for T = 50°C; pH = 5.0. The manganese concentration was varied from 0.1 to 1.0 ppm, values which are representative of those found in scrubber liquors (12). The concentration of manganese is the total value, i.e., the sum of that contributed by the calcium sulfite and that added to the solution. These results were also fit to an expression of the form of equation (2) with the maximum likelihood estimates being:

$$\alpha = 1.63, \text{ standard deviation} = 0.07$$

$$\beta = 1.03, \text{ standard deviation} = 0.13$$

$$\log_{10} k = 4.77, \text{ standard deviation} = 0.74$$

It should be noted that the dependency on manganese is about the same as that found with sodium sulfite but the order in S IV is larger with CaSO₃ than with Na₂SO₃.

Other Organic Acids. Experiments were also carried out using other organic acid buffers; details can be found in (7). The three most carefully studied acids were succinic, adipic, and glycolic. Adipic acid is the most likely candidate for use as a buffer in commercial scrubbers. The order of inhibition power is

glycolic >> adipic > succinic > no acid.

Glycolic acid is a very strong inhibitor and under most conditions will essentially stop the oxidation. Adipic acid has only a slightly greater effect than succinic acid.

Discussion

We have measured the rate of oxidation of sodium and calcium sulfite to sulfate in a solution containing an organic buffer and the catalysts manganese and iron. The work was carried out in order to develop kinetic rate expressions rather than to explore the fundamentals of the reaction scheme.

The catalysts cause a considerable increase in the rate of reaction and are thus able to counteract the inhibiting effect of the succinic acid. Although both manganese and iron catalyze the reaction, the iron has little effect on the rate of reaction in sodium sulfite when mixed with manganese under the conditions of these experiments.

Table VIII
MANGANESE CATALYZED CaSO_3 OXIDATIONS

Added Mn Conc. ppm	# of Data Points	Order with Respect to $[\text{S}^{+4}]$	Standard Deviations of Order
0.1	17	1.79	0.08
0.2	11	1.53	0.15
0.3	12	1.41	0.27
0.4	11	1.47	0.23
0.5	15	1.71	0.14
1.0	5	1.82	0.07

Conditions :

Temp = 50°C initial pH = 5.0;

0.2 m/l succinic acid.

In subsequent publications we will describe the entire oxidation process including the mass transfer steps, viz., the dissolution of solid and the adsorption of oxygen into the slurry.

Acknowledgment

This work was supported in part by Grant Number R805227 from the Environmental Protection Agency.

Literature Cited

1. Borgwardt, R. H., "IERL-RTP Scrubber Studies Related to Forced Oxidation", in proceedings: Symposium on Flue Gas Desulfurization, New Orleans, 1976, Volume I, EPA-600/2-76-136a (NTIS No. PB 255-317/AS), 117-143.
2. Borgwardt, R. H., "Effect of Forced Oxidation on Limestone SO_x Scrubber Performance", in proceedings: Symposium on Flue Gas Desulfurization, Hollywood, FL, 1977, Volume I, EPA-600/7-78-058a (NTIS No. PB 282-090/OG1), 205-228.
3. Harpel, W. I., D. T. Murray, A. J. Graffeo and J. C. Steelhammer, "The Chemistry of Scrubbers", *Combustion*, March 1976, 33.
4. Harvey, R. D. and John D. Steinmetz, "Petrographic Properties of Carbonate Rocks Related to their Sorption of Sulfur Dioxide," Sept. 1971, EGN50, Illinois State Geological Survey.
5. Rochelle, Gary T. and C. Judson King, "The Effect of Additives on Mass Transfer in CaCO₃ on CaO Slurry Scrubbing of SO₂ from Waste Gases," 1977, IEC Fund 16, 67.
6. Hatfield, J. O., Y. K. Kim and R. C. Mullins, "Study of the Effect of Organic Acids on the Wet-Limestone Scrubbing Process", 1972, EPA Report, Contract No. T-V-34425A (NTIS No. PB 210-793).
7. Hudson, J. L., "Sulfur Dioxide Oxidation in Scrubber Systems", 1980, Final Report to EPA, EPA-600/7-80-083.
8. Altwicker, E. R., "The role of inhibition in the kinetics of sulphite oxidation", 1977, Trans. Inst. Chem Eng 55, 281.
9. Altwicker, E. R., "Oxidation/Inhibition of Sulfur Dioxide in Aqueous Solution", 1977, Paper 27d AIChE Annual Meeting, New York.
10. Fuller, E. C. and R. H. Crist, "The Rate of Oxidation of Sulfite Ions by Oxygen", 1941, *JACS*, 63, 1644.
11. Linek, V. and J. Tvrdik, "A Generalization of Kinetic Data on Sulphite Oxidation Systems", *Biotechnology and Bioengineering*, 1971, Volume XIII, 353-369.
12. Bornstein, L. J., R. B. Fling, F. D. Hess, R. C. Rossi and J. Rossoff, "Reuse of Power Plant Desulfurization Waste Water, Feb. 1976, EPA-600/2-76-024.

RECEIVED December 9, 1981.

A Model of Oxidation in Calcium Sulfite Slurries

J. ERWIN

Southwest Research Institute, San Antonio, TX 78284

C. C. WANG and J. L. HUDSON

University of Virginia, Department of Chemical Engineering, Charlottesville, VA 22901

A model has been developed for oxidation of calcium sulfite in a three-phase, semibatch reactor. The overall rate of conversion to sulfate depends on the rates of solid dissolution and liquid phase chemical reaction. In this first treatment of the problem, gas-liquid mass transfer resistance did not affect the overall rate of oxidation.

An initial distribution of particle sizes was obtained with a particle size analyzer. The size distribution was calculated as a function of time. The rate of dissolution depends on both the concentrations in the bulk liquid and at the particle surface.

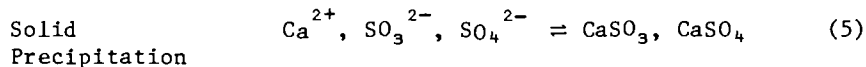
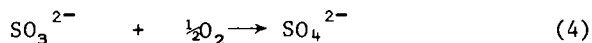
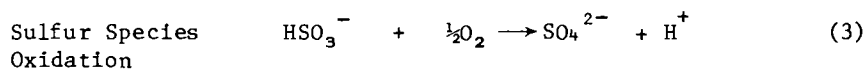
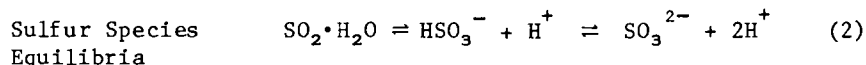
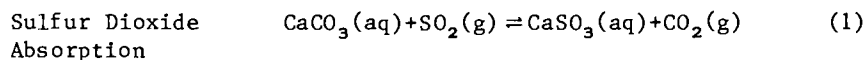
A solid-liquid mass transfer coefficient of 0.015 cm/s was found by comparing the predictions of [S(IV)] to experimental results obtained under conditions in which the liquid phase kinetics were fast. The model was then applied to slurry oxidation under more general conditions by using liquid phase reaction rate kinetics obtained in clear solutions. The results of the model agree with experimental findings for the total rate of oxidation.

The sulfite oxidation rate in hold tanks of antipollution scrubbers is central to flue gas desulfurization technology. The accurate description of the rate of disappearance of sulfite slurry particles (from the scrubber liquor) bears upon both process selection and economics. This article will describe a mathematical model for a semi-batch, stirred tank reactor in which S(IV) anions, sulfite and bisulfite, are reacted with dissolved oxygen gas at saturation. Experimental work to secure several physical parameters and to verify the

0097-6156/82/0188-0191\$8.50/0
© 1982 American Chemical Society

model is reported as well. The model was then used to study the bulk S(IV) concentration in various cases of slurry oxidation as well as to infer the conditions at the particle surface.

In recent years considerable effort has been devoted to investigating the ever-growing problem of atmospheric SO₂ emission. For instance, a power plant burning 5000 tons of eastern coal may discharge 500 tons per day of sulfur dioxide into the air(1). The primary removal process, absorption of sulfur dioxide by a slurry of lime or limestone and discarding this loaded absorbent, has the outstanding advantages of relative simplicity, lowest first cost, and freedom from marketing a byproduct(2). The important processes in SO₂ scrubbing may be represented by:



The slurry falls from the scrubber to a mixing/hold tank, where fresh lime or limestone is added and from which a side stream containing the various sulfur species is removed. The rest of the slurry is returned to the scrubber. Oxidation in the scrubber solution, leads to gypsum scale formation(3). Calcium sulfate is preferable to calcium sulfite from the point of view of solids disposal since,

- It settles by an order-of-magnitude faster than the unoxidized material(4).
- It filters to 80% solids and handles like moist soil compared to sulfites which filter to only 50-60% solids and are thixotropic(5).
- The sulfate has no chemical oxygen demand which contributes to water pollution.
- It is insoluble with respect to the sulfite, which in landfills may be subject to leaching.

By promoting the oxidation and precipitation outside the scrubbing loop(6), the disposal benefits of sulfate may be realized while decreasing the potential for scale formation(7,8).

Synopsis

The current model is a step closer toward a reliable working description of the sulfite oxidation rate in scrubber slurries. By incorporating a boundary layer description of the film around each particle, this model predicts the conditions at the particle surface which drive the mass transfer. The interfacial area for mass transfer was discovered to be more closely represented by a sphere than by a plate-like shape. From the model, using highly catalyzed experiments, a mass transfer coefficient of $0.015 \text{ cm sec}^{-1}$ was found - quite close to literature correlation predictions.

The model is able to track the level of sulfite in an experimental slurry well. The predicted pH behavior, while not as closely predicted as sulfite concentration, does respond to changes in initial pH the way the experimental slurries did. This overall good agreement of the model may be put to use most directly in forced oxidation systems. The saturation concentration for oxygen was constant in the neighborhood of 0.0005 Mol/l in the present experiments - much higher than in conventional hold tanks, but likely in a pressure or jet oxidizer. Note that in this kind of system where mass transfer has a dominant role (and where the sulfite concentration in solution usually is assumed to be zero because of the fast reaction), the current model predicts (and slurry measurements confirmed) a changing, appreciable sulfite level in the bulk solution. In this regime, neither mass transfer nor reaction kinetics is in full rate control.

Previous Work

A considerable amount of work has been done on the oxidation of sulfite and bisulfite anions in aqueous solutions (25). In this paper the discussion is limited to oxidation of calcium sulfite (9), which has received much less attention than oxidation of sodium salts. The attention here is on the oxidation of calcium sulfite, catalyzed by metal ions in the presence of organic acid buffers, occurring in solid-liquid-gas slurry reactors. The organic acid buffers not only moderate pH changes during the reaction, but also inhibit the rate of chemical reaction (10).

Clear Solution Kinetics. Without buffer, clear solutions of calcium sulfite have such low saturation concentrations in the pH range of interest that the resulting oxidation is quite slow, subject to low-level extraneous influences, and hard to work with. There are few reports in the literature which contain experiments at the needed conditions (11,12). Of the

few studies available, only one will be mentioned because of its connection with the determination of the mass transfer coefficient in the current work.

Erwin(13) investigated the calcium sulfite oxidation at high manganese concentrations in a flow calorimeter under the following conditions:

pH_i	: 4.6	
$[\text{S(IV)}]$: 0.00136 - 0.00456	mol/l
$[\text{O}_2]$: 0.00642 - 0.0172	mol/l
$[\text{Mn}]$: 10 - 2000	ppm (wt)
T_i	: 25 ± 0.02	$^{\circ}\text{C}$

For the extremely catalyzed solutions (2000 ppm Mn) like those employed in the current work to assess k_1 , the rate expression was:

$$R = 85 C_1^{1.5} \quad \text{at } 40^{\circ}\text{C}$$

Experiments in Slurries. In a slurry system, Borgwardt (14,8) studied enhanced oxidation in a pilot-scale scrubbing system (pH 4.5) with a forced oxidation tank. Even with advanced-design gas distributors, he found the overall rate of oxidation was limited by the mass transfer of oxygen to the solution. An air stoichiometry of 2.6 was used in this investigation. Neither gas distributor orifice size nor chloride concentration had an effect on the rate.

Takeda reported a series of experiments in which he determined the amount of SO_2 absorbed by limestone slurries (15). He observed significant differences in the rate of SO_2 absorption at different slurry concentrations. Here limestone dissolution probably plays an important role in the gas absorption process.

Gladkii(16) at the State Scientific Research Institute of Industrial and Sanitary Gas Cleaning at Moscow did work on the three-phase calcium sulfite slurry oxidation system, finding that the liquid phase oxidation (pH 3.6-6) is first order with respect to the sulfite species. He pointed out, on the basis of pH versus time data from his semi-batch reaction, that the slurry oxidation had different periods in which either reaction kinetics or solid-liquid mass transfer controlled the oxidation rate. He also presented an omnibus empirical correlation between pH, temperature, and the liquid phase saturation concentration of calcium sulfite solution for predicting the slurry oxidation rate. The catalytic effect of manganese

sulfate (100 ppm MnSO_4) greatly accelerated the reaction and reduced the activation⁴ energy from 21.5 to 13.8 Kcal/mol and the order in sulfite to $\frac{1}{2}$.

A continuous stirred tank reactor was used by Wen, McMichael, and Nelson(17) to study the oxidation of aqueous solutions of sodium and calcium sulfite. In their experiments, the oxidations were gas phase to liquid phase mass transfer limited (rate \propto impeller speed) for sodium sulfite solutions of 0.1 Mol/l at impeller speeds up to 700 RPM. Their results showed the oxidation was first order in oxygen, slightly less than zeroth order in hydronium ion concentration, and independent of the sulfite ion concentration.

Modeling of the Slurry Oxidation. In 1969 Ramachandran and Sharma(18) first proposed a film model for gas absorption accompanied by a fast chemical reaction in a slurry containing sparingly soluble, fine particles. A first case assumed that the solid dissolution in the liquid film next to the gas-liquid interface was unimportant. The second case assumed that it was important. Numerical solutions were given for the second case which indicated that the specific rate of absorption of gas in the presence of fine particles could be considerably higher than in the absence of solids.

In the Ramachandran-Sharma model, the rate constant of solid dissolution did not change. For the purpose of applying this model to the lime or limestone scrubbing processes, Uchida, et al.(19) modified the model by considering that the rate of limestone dissolution is accelerated by a higher concentration of hydronium ions(20). In a numerical example, Uchida showed that when the rate of the solid dissolution was enhanced by the absorbed gas, the oxidation rate would be higher than predicted by Ramachandran and Sharma's model. The data of Takeda agree with the Uchida, et al. model.

Sada, Kumazawa, and Butt extended the Ramachandran and Sharma and Uchida, et al. model, applying it to several special cases: (1) single gas absorption with a finite rate of reaction, (2) simultaneous absorption of two gases with parallel reactions in a slurry, (3) gas absorption into a finite slurry with an instantaneous reaction. Tests for all the cases were presented (21,22,23). In this model as well as the others, emphasis was placed on the gas dissolution step; whereas the current model emphasizes the chemical kinetics in solution as well as solid dissolution.

Experimental

The experimental system, Figure 1, comprised a semi-batch slurry reactor with mechanical stirring and gas sparging. The particulars for the reactor include(24):

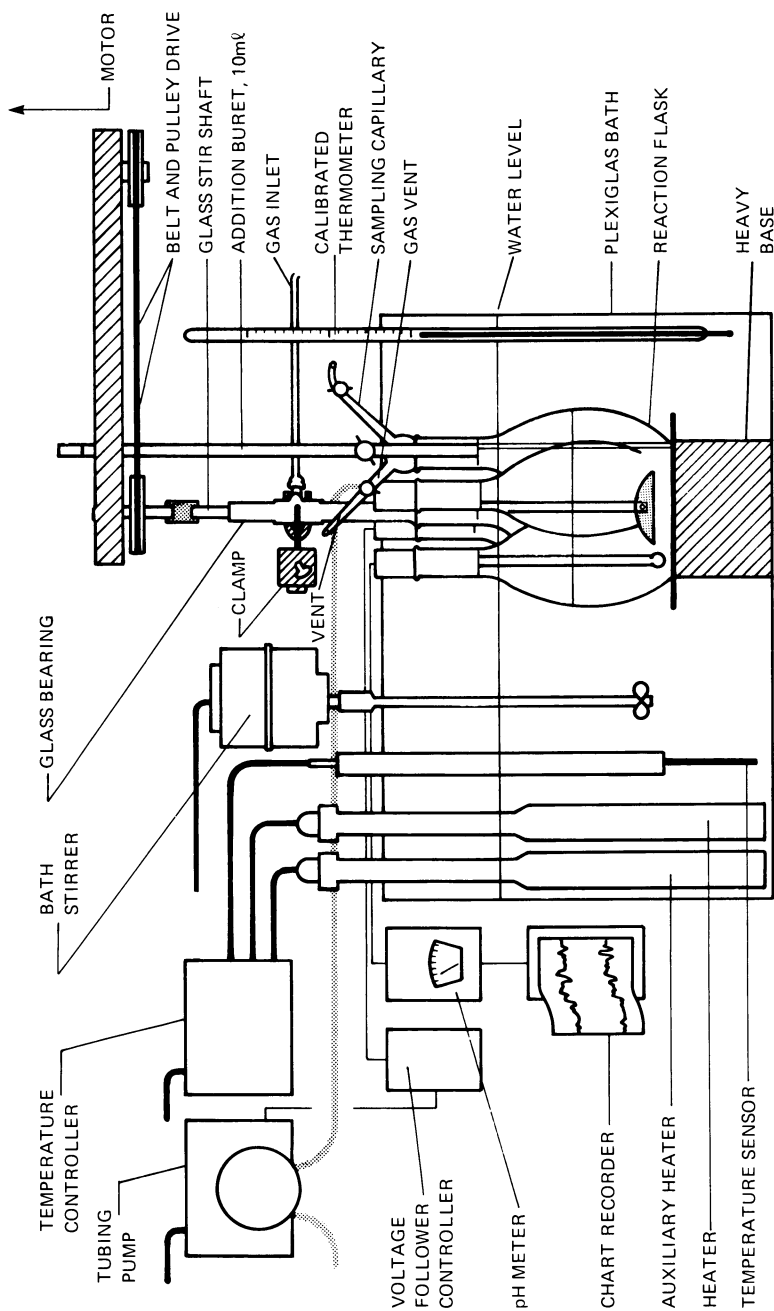


Figure 1. Experimental system.

Water thermostat at $40^{\circ} \pm 0.1^{\circ}\text{C}$
1000 cc pyrex, baffled Florence flask reactor
0.6 ℓ liquid reaction mixture
Mechanical stirring at 1800 RPM
6.4 cm stirrer blade of TFE
 O_2 or N_2 sparging at 3 ℓ pm
Continuous pH monitoring via glass electrode
pH control when required by automated base addition

The stir rate and gas flow rate assure adequate mass transfer of oxygen to the reaction mixture during oxidation (except those with 2000 ppm Mn) to prevent any rate limitation by diffusion of oxygen. The stir shaft was lubricated sparingly with silicone stopcock grease before each experiment. Before each run, the reactor was thoroughly rinsed with deionized water. (Chromic acid cleaning was used periodically.) A nitrogen purge was started into 600 ml of stirred, deionized water before addition of weighed CaSO_3 powder to produce the required slurry density in grams per litre. At least 30 minutes elapsed before oxygen was admitted and the timer started. Samples were withdrawn via capillary dip tube and pipetted into excess buffered iodine/iodide solution to react immediately with S(IV) present in the reacting solution. Remaining iodine was "back titrated" with primary standard (H_3AsO_3). Clear samples were withdrawn through a Millipore filter under vacuum before pipetting and titration. Blank trials showed the resolution for the titration to be $\pm 0.0003 \text{ Mol}/\ell$.

The chemicals used in the experiments were all of reagent grade except the calcium sulfite. This material was a hemihydrate of commercial quality ($\sim 47 \text{ wt\%}$ anhydrous CaSO_3) product containing about 0.006 wt% Mn and 0.024 wt% Fe. [A complete analysis appears in reference (12)].

Using this commercial sulfite is pertinent to industrial equipment. All of the water for cleaning and for solutions was of exceptional purity, being distilled and passed through a carbon bed before thorough deionizing.

Physical System

The experiments were designed to present an idealization of the complex oxidizing system in a scrubber (hold tank) slurry which is amenable to mathematical description and yet close enough to practice to be useful. The temperature of 40°C is chosen as appropriate to both commercial scrubbers and the experimental apparatus. A similar compromise was the choice of calcium sulfite as the reacting solid, considering that in a working scrubber, the process begins with the dissolving carbonate. However, since the carbonate anion was not directly

involved in the reaction, we take up the model at the point where sulfite has formed, is dissolving, and is ready to react.

The sulfite crystals themselves are small platelets which aggregate with the larger sulfate parallelepiped rods, Figure 2, to form the roughly spherical particles which are present in slurries, Figure 3. A schematic representation of the situation in a slurry is summarized in Figure 4, where the boundary layer configuration adopted in the model is included. The enlargement at the bottom collects the variables of interest and shows their relations with the solid surface, the liquid film, or the bulk liquid.

The overall initial particle size distribution used for the computations in this paper is on Figure 5. This thirteen-step distribution was the most recent of several taken by the Coulter Method (MeOH, LiCl) and is in agreement by shape and mean diameter to previous Coulter and other determinations (16,34). This determination, as well as the percent sulfite in the solid is critical to calculating the initial number of particles in an experimental run:

$$\left(\begin{array}{c} \text{initial} \\ \text{total} \\ \text{number of} \\ \text{particles} \end{array} \right) = \sum_{i=1}^{13} \frac{\left(\begin{array}{c} \text{volume fraction of} \\ \text{i-sized particles} \end{array} \right) \times \left(\begin{array}{c} \text{total volume of} \\ \text{solid particles} \end{array} \right)}{\left(\begin{array}{c} \text{volume per i-sized particle} \end{array} \right)} \quad (6)$$

An equally important parameter is the solubility of the sulfite. In principle, this quantity may be inferred from the simultaneous obedience to the conditions in solution at fixed pH (40°C):

$$\begin{aligned} \text{Sulfite Solubility(27): } [Ca^{2+}] [SO_3^{2-}] &= K_{sp1} \\ &= 1.631 \times 10^{-7} (\text{mol}/\ell)^2 \quad (7) \end{aligned}$$

$$\begin{aligned} \text{Sulfate Solubility(27): } [Ca^{2+}] [SO_4^{2-}] &= K_{sp2} \\ &= 2.45 \times 10^{-5} (\text{mol}/\ell)^2 \quad (8) \end{aligned}$$

These equations ignore ion-pair formation ($CaSO_3^\circ$ and $CaSO_4^\circ$) because all of the solubilities are quite low(27). This condition is certainly not true in operating scrubber systems; the current considerations are an approximation used to simplify the model.



Figure 2. Sulfite/sulfate slurry particles (showing sulfite plates and sulfate rods).

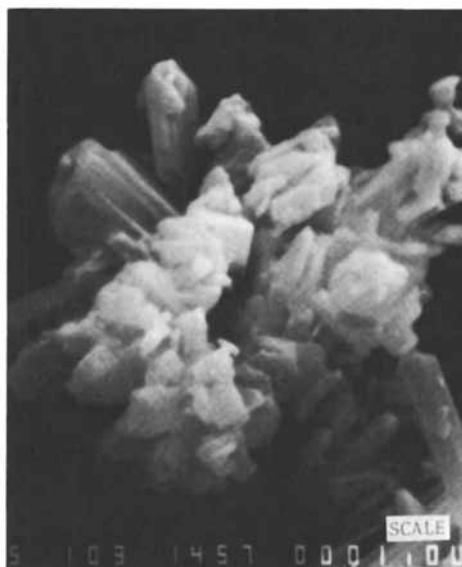


Figure 3. A single particle agglomerate (rough spherical aggregate).

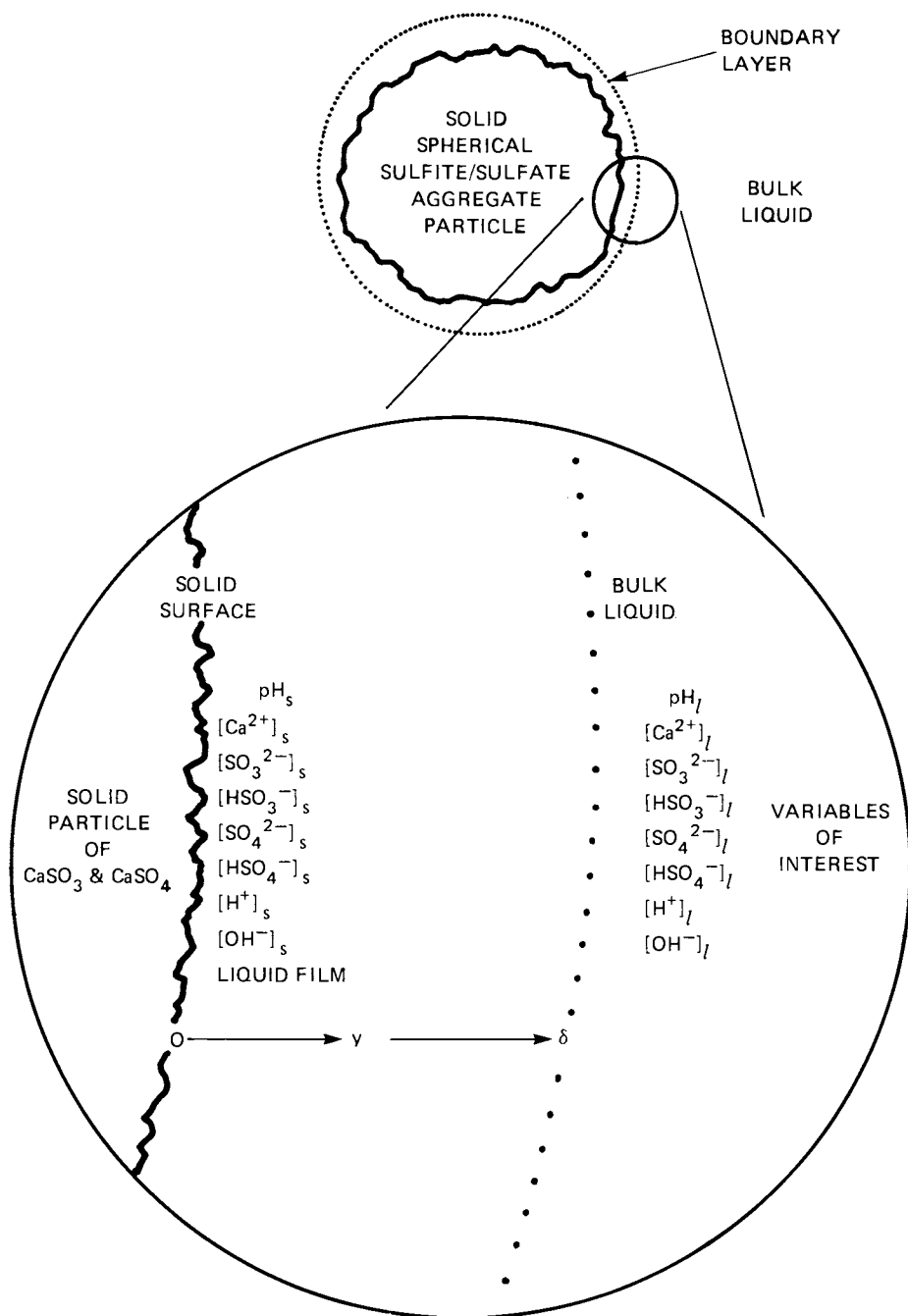


Figure 4. Representation of a slurry particle.

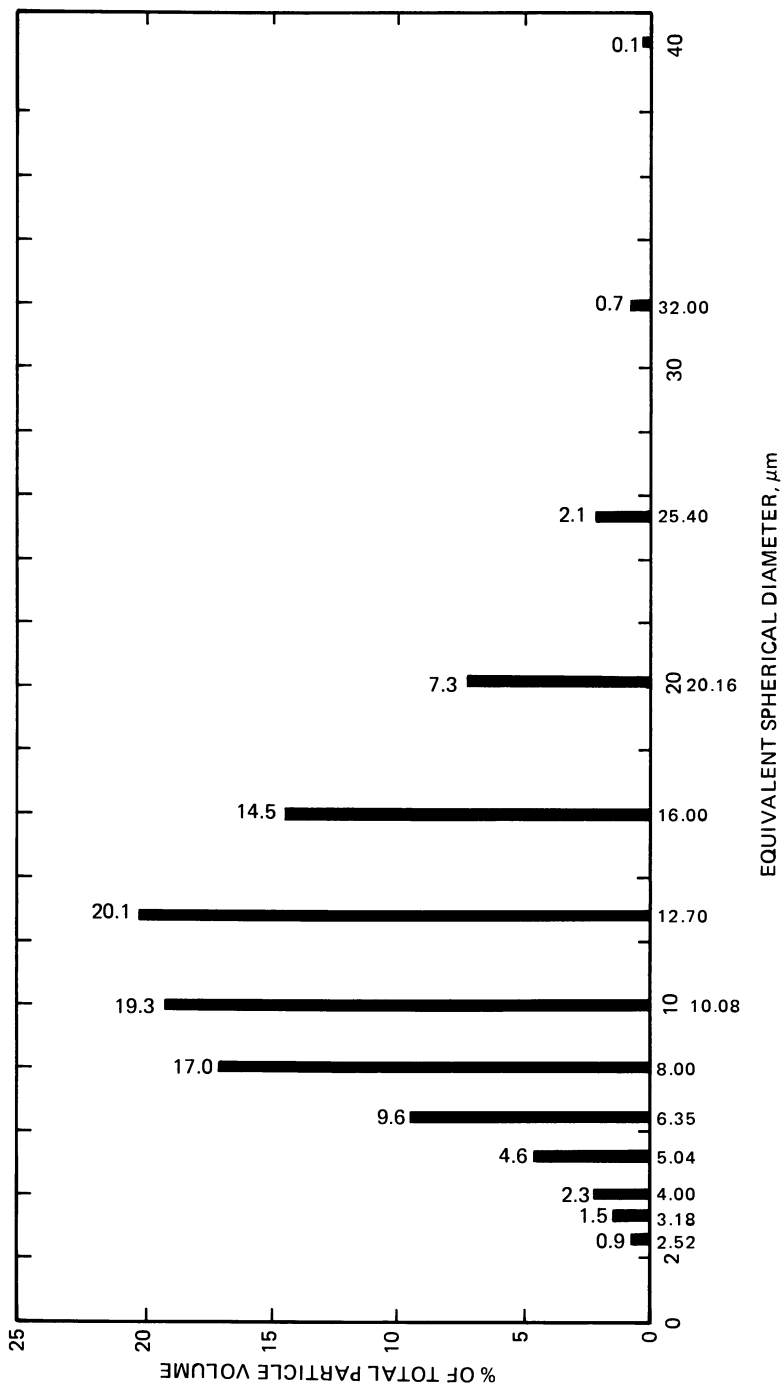
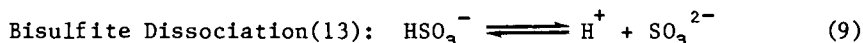
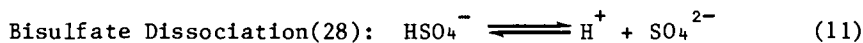


Figure 5. Particle size distribution. Geometric mean diameter, 11.62 μm; median, 11.94 μm; mode, 13.07 μm; and standard deviation, 1.59 μm.



$$\frac{[\text{H}^+][\text{SO}_3^{2-}]}{[\text{HSO}_3^-]} = K_s = 4.94 \times 10^{-8} \text{ (mol/ l)} \quad (10)$$



$$\frac{[\text{H}^+][\text{SO}_4^{2-}]}{[\text{HSO}_4^-]} = K_2 = 6.4565 \times 10^{-3} \text{ (mol/l)} \quad (12)$$



$$[\text{H}^+][\text{OH}^-] = K_w = 10^{-13.5348} \text{ (mol/l)}^2 \quad (14)$$

Electroneutrality for the whole solution:

$$2[\text{Ca}^{2+}] + [\text{H}^+] = [\text{OH}^-] + 2[\text{SO}_3^{2-}] + [\text{HSO}_3^-] + 2[\text{SO}_4^{2-}] + [\text{HSO}_4^-] \quad (15)$$

In all cases, molar concentrations are used in favor of activities since the activity coefficients are very close to 1.0 (Handbook of Chemistry and Physics, q.v. section D-205)(28) at the current low concentrations (less than 0.01 Mol/l). At a fixed pH value, there are then six equations and six unknowns (i.e., $[\text{Ca}^{2+}]$, $[\text{OH}^-]$, $[\text{SO}_3^{2-}]$, $[\text{HSO}_3^-]$, $[\text{SO}_4^{2-}]$, and $[\text{HSO}_4^-]$), and one may construct a solubility curve with respect to pH.

Experimental measurements along with the calculated solubilities appear on Figure 6. Because the saturation changes quickly with pH in the region of interest and the solubility concentration figures strongly in the driving force for mass transfer, these carefully determined experimental values were employed in calculations for the model. Note the low saturation concentrations in the pH range of interest (4.5-5).

Surface Conditions During Dissolution

The first case is calcium sulfite dissolution without chemical reaction. Using a film model will allow the calculation of the surface concentrations of all the species and the rate of dissolution. With a knowledge of the particle population and solution concentrations, most of the variables are known when the experiment starts. To specify all the starting values of the variables, the conditions at the particle surface are required. From the consideration of saturation concentration in the previous section during dissolution, the bulk liquid must obey:

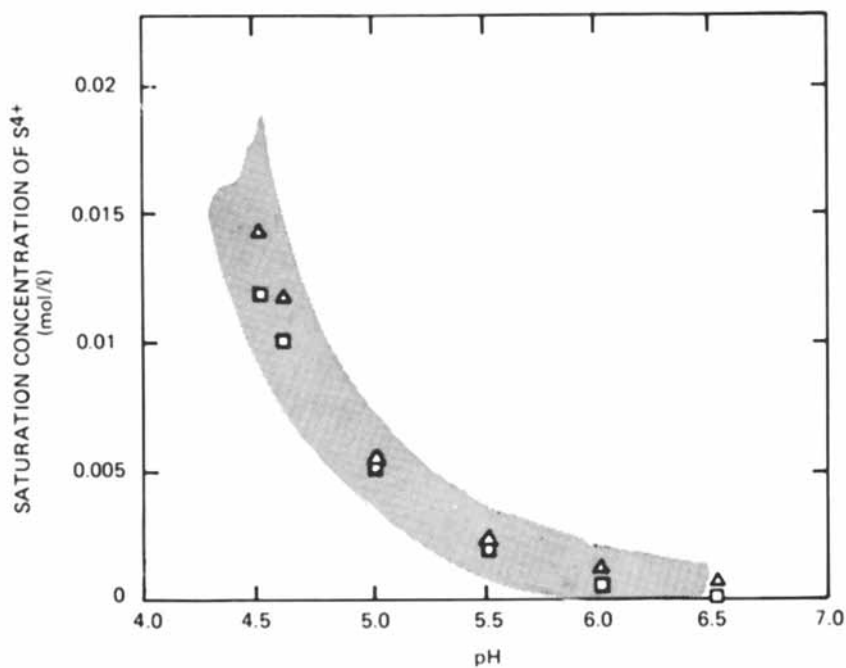


Figure 6. Effect of pH on solubility. Key: □, calculated value; and △, experimental data.

- Water dissociation
- S(IV) equilibrium
- S(VI) equilibrium
- Electroneutrality

Since the system will no longer be at equilibrium conditions when dissolution starts, a balance on the entering ions must exist:

- Ca^{2+} and sulfur balance

$$[\text{Ca}^{2+}]_1 = [\text{SO}_3^{2-}]_1 + [\text{HSO}_3^-]_1 + [\text{SO}_4^{2-}]_1 + [\text{HSO}_4^-]_1 \quad (16)$$

The conditions at the particle surface must obey:

- Water dissociation
- Calcium sulfite solubility product
- Calcium sulfate solubility product
- S(IV) equilibrium
- S(VI) equilibrium
- Electroneutrality
- A molar diffusion flux balance at the surface

$$\sum_i \mathcal{J}_i^+ \Big|_{\text{surface}} = \sum_j \mathcal{J}_j^- \Big|_{\text{surface}} \quad (17)$$

where \mathcal{J}_i = molar flux of i^{th} (cationic) species
[similarly for j (anionic) species].

This molar flux balance merits a brief discussion. Two factors dictate the necessity and form of the diffusion flux balance. Because each ion exhibits a characteristic valance and ionic conductance (at prevailing temperature and ionic strength), its progress along the diffusion gradient will be unlike the other diffusing species. Thus a simple ion balance like the one in the bulk (for Ca^{2+} and sulfur) can be ruled out. All of the diffusing species are electrically charged. The concentration gradient is reflected in a concomitant electrical gradient which in turn influences the charged species. The diffusion flux is most readily written, therefore, in terms of the measurable ionic properties like valance and ionic conductance that are expressed in terms of gram-ion equivalents [p. 380, (31)]. Hence, the diffusion flux balance at a particle surface is:

$$\begin{aligned} \frac{1}{2} J_{\text{Ca}^{2+}} \Big|_{y=0} &= \frac{1}{2} J_{\text{SO}_3^{2-}} \Big|_{y=0} + J_{\text{HSO}_3^-} \Big|_{y=0} \\ &+ \frac{1}{2} J_{\text{SO}_4^{2-}} \Big|_{y=0} + J_{\text{HSO}_4^-} \Big|_{y=0} \quad (18) \end{aligned}$$

where: J_+ , J_- = diffusion flux densities of cation
and anion, respectively, g equiv. / (cm²)(sec).

Vinograd and McBain(30) express these fluxes quantitatively in terms of ionic:

Conductance
Charge
Concentration
Electrical gradient

The electrical gradient is taken to be linear for each species across the film, yielding a flux balance in terms of ionic properties, bulk concentrations, surface concentrations, and film thickness(24).

Therefore, in the bulk liquid there are seven variables (i.e., $[H^+]_l$, $[OH^-]_l$, $[SO_3^{2-}]_l$, $[HSO_3^-]_l$, $[SO_4^{2-}]_l$, $[HSO_4^-]_l$, and $[Ca^{2+}]_l$), but only five equations [10,12,14,15,16]. The degrees of freedom in the bulk liquid equal two. At the particle surface there are seven variables: $[H^+]_s$, $[OH^-]_s$, $[SO_3^{2-}]_s$, $[HSO_3^-]_s$, $[SO_4^{2-}]_s$, $[HSO_4^-]_s$, and $[Ca^{2+}]_s$ and seven equations [7,8,10,12,14,15,17], but the diffusion flux equation involves the bulk liquid concentrations. Thus, at any instant during the dissolution, by specifying any two variables in the liquid phase, all the other bulk liquid concentrations can be calculated. Then the surface equations, along with all these bulk liquid concentrations, can be used to calculate the surface concentrations of all ionic species for three characteristic film thicknesses(31) during dissolution. These results appear in Table I. From the results, observe that the surface pH (or the corresponding surface S(IV) concentration) remains almost constant at 8.18 during the course of dissolution. Furthermore, the effect of the change of film thickness is almost negligible on all values but the surface pH.

The results in this preliminary analysis give important information about the driving force, $(C - C_l)$, which governs the calcium sulfite dissolution that is used in the model of the oxidation. The constant surface pH 8.18, which is naturally the pH of the saturated solution, can be used in the transient state analysis of the dissolution.

The Model - Dissolution with Chemical Reaction

With the conditions in the slurry determined, consider the oxidation process; four assumptions are made:

1. The only loss of S(IV) from the slurry occurs from the liquid phase oxidation of sulfite. There is no S(IV) precipitation or stripping.
2. There is no gas-liquid mass transfer limit during the reaction(26). The oxygen concentration is constant at saturation at all times during the oxidation.

TABLE I
Surface and Bulk Conditions During Particle
Dissolution with no Reaction

$\delta = 1.0 \times 10^{-5}$ cm			$\delta = 6.66 \times 10^{-5}$ cm			$\delta = 1.25 \times 10^{-4}$ cm		
$[\text{SO}_3^{2-}]_s = 3.3 \times 10^{-5} \text{ M/l}$			$[\text{SO}_3^{2-}]_s = 3.3 \times 10^{-5} \text{ M/l}$			$[\text{SO}_3^{2-}]_s = 3.3 \times 10^{-5} \text{ M/l}$		
Bulk Surface $[\text{SO}_3^{2-}]_s$			Bulk Surface $[\text{SO}_3^{2-}]_s$			Bulk Surface $[\text{SO}_3^{2-}]_s$		
pH	pH	$\times 10^6$	pH	pH	$\times 10^6$	pH	pH	$\times 10^6$
6.77	8.07	0	6.77	8.07	0	6.77	8.06	0
7.68	8.11	3.3	7.68	8.11	3.3	7.68	8.11	3.3
7.83	8.13	6.6	7.83	8.12	6.6	7.83	8.12	6.6
7.92	8.14	9.8	7.92	8.13	9.8	7.92	8.13	9.8
7.98	8.15	1.3	7.98	8.14	1.3	7.98	8.14	1.3
8.03	8.15	1.6	8.03	8.15	1.6	8.03	8.15	1.6
8.07	8.16	2.0	8.07	8.16	2.0	8.07	8.16	2.0
8.10	8.17	2.3	8.10	8.16	2.3	8.10	8.16	2.3
8.13	8.17	2.6	8.13	8.17	2.6	8.13	8.17	2.6
8.16	8.18	3.0	8.16	8.17	2.9	8.16	8.17	2.9
8.18	8.18	3.3	8.18	8.18	3.3	8.18	8.18	3.3
8.20	8.13	3.6	8.20	8.18	3.6	8.20	8.18	3.6

3. The presence of a film around the particle surface available for solid-liquid mass transfer is assumed. The dissolved ions diffuse from the particle surface to the bulk liquid until bulk equilibrium is reached. The concentration of each species at the particle surface is its saturation concentration which equals the bulk concentration when the solution is at equilibrium.
4. During the course of reaction, the S(VI) ions are continuously produced. Assume that $\text{CaSO}_4(\text{s})$ precipitates at new nuclei as soon as the solution is over-saturated in calcium sulfate. The change in size of the solid particles of interest is only caused by the dissolution of calcium sulfite, not by the $\text{CaSO}_4(\text{s})$ leaving the solution, *i.e.*, there is no "blinding". The precipitating $\text{CaSO}_4(\text{s})$ does not influence the sulfite mass transfer.

The liquid phase concentration of sulfite in the slurry is governed by two competing mechanisms. Sulfite in the liquid is lost due to the oxidation reaction, but is replenished by the dissolution of the solid calcium sulfite. The sulfite concentration is represented by a differential equation of the form:

$$\frac{d(V C_l)}{dt} = -V R_r + V R_m \quad (19)$$

where:

- V = reactor volume, 0.6 ℓ
- C_l = sulfite concentration in liquid phase, Mol/ ℓ
- R_l = reaction rate, Mol/ ℓ sec
- R_r = dissolution rate, Mol/ ℓ sec
- t^m = time, sec.

The kinetic rate expression has been shown elsewhere⁽¹²⁾ to be,

$$R_r = -k_{1.5} C_l^{1.5} \quad (20)$$

The mass transfer of S(IV) ions from solid to liquid will be given by,

$$R_m = k_l a (C_s - C_l) \quad (21)$$

where:

- k_l = mass transfer coefficient, cm/sec
- a = interfacial area, cm^2/cm^3
- C_s = [S(IV)] at particle surface, *i.e.*, saturation concentration, Mol/ ℓ

The interfacial area per unit volume, a , changes with time as the particles shrink and disappear:

$$a = \frac{4 \pi w N_{t=0} \sum_{i=1}^{13} r_i^2 h_i f_i}{v} \quad (22)$$

where:

- r_i = the radius of i type particles which is a function of time, cm
- $N_{t=0}$ = the initial total numbers of particles
- h_i = number fraction of "i-size" particles
- f_i = fraction of the original number of "i-size" particles remaining in the reactor; f_i equals 1 when present, but f_i equals 0 when all i -size particles dissolve away
- w = fraction of particle composed of CaSO_3 and hence available for mass transfer of sulfite (i.e. = 0.47 wt%).

The summation is over the 13 size classes of particles. Substitution of these rates and cancelling the reactor volume gives the equation,

$$\frac{dC_l}{dt} = -k_l^{1.5} + \frac{(0.47) 4 \pi N_{t=0} k_l (C_s - C_l)}{v} \sum_{i=1}^{13} r_i^2 h_i f_i \quad (23)$$

The rate of sulfite transfer from the solid particles to the liquid phase is given by the expression:

$$\frac{d \left(\begin{array}{c} \text{total moles of sulfite} \\ \text{in solid particles} \end{array} \right)}{dt} = -VR_m \quad (24)$$

or

$$\frac{dW}{dt} = \frac{-Vmk_l a}{0.47} (C_s - C_l) \quad (25)$$

where: m = molecular weight of calcium sulfite, gm/mol
 ρ = solid density, gm/cm³
 W = total mass of solid particles, gm

or

$$W = \frac{4}{3} \pi \rho N_{t=0} \left\{ \sum_{i=1}^{13} r_i^3 h_i f_i \right\} \quad (26)$$

in which case,

$$\begin{aligned} \frac{4}{3} \pi \rho N_{t=0} \frac{d}{dt} \left\{ \sum_{i=1}^{13} r_i^3 h_i f_i \right\} \\ = -4 \pi m k_l N_{t=0} (C_s - C_l) \left\{ \sum_{i=1}^{13} r_i^2 h_i f_i \right\} \end{aligned} \quad (27)$$

This equation can be split into 13 separate equations corresponding to 13 sizes of solid particles, each equation describing the rate of change of one size of particle.

The total concentration of sulfite in the slurry at any time, C_T , is the sum of liquid phase concentration and the remaining solid phase concentration:

$$C_T = C_l + \frac{(0.47) \frac{4}{3} \pi \rho N_{t=0}}{V m} \left\{ \sum_{i=1}^{13} r_i^3 h_i f_i \right\} \quad (28)$$

The 14 equations, sulfite rate of change in the liquid and the rates of sulfite transfer (in terms of r_i) from the 13 sized particles, may be solved simultaneously for C_l and the r_i 's. Then the total sulfite concentration is calculated at each increment of time. In addition, to compute the proper surface conditions for the mass transfer driving force, all of the governing equations for the bulk listed in the section above on the surface conditions during dissolution must be solved at each time step. Two differences should be noted: the solubility product for sulfate must now be satisfied and in the Ca^{2+} and sulfur balance, the effect of oxidation must be accounted for:

$$\begin{aligned} & \left[\begin{array}{c} \text{initial moles} \\ \text{of } \text{Ca}^{2+} \end{array} \right]_l + \left[\begin{array}{c} \text{moles of } \text{Ca}^{2+} \\ \text{produced from} \\ \text{dissolution of} \\ \text{CaSO}_3 \end{array} \right]_l - \left[\begin{array}{c} \text{moles of } \text{Ca}^{2+} \\ \text{at time } t \end{array} \right]_l \quad (29) \\ = & \left[\begin{array}{c} \text{initial moles} \\ \text{of S(VI)} \end{array} \right]_l + \left[\begin{array}{c} \text{moles of S(VI) produced} \\ \text{from oxidation of S(IV)} \end{array} \right]_l - \left[\begin{array}{c} \text{moles of S(VI)} \\ \text{at time } t \end{array} \right]_l \end{aligned}$$

or:

$$\begin{aligned}
 [\text{Ca}^{2+}]_l, t=0 + \int_0^t k_l a (C_s - C_l) dt - [\text{Ca}^{2+}] = [\text{S(VI)}]_l, t=0 \\
 + \int_0^t k C_l^{1.5} dt - [\text{S(VI)}] \quad (30)
 \end{aligned}$$

A fourth order Runge-Kutta-Gill algorithm was utilized to solve this system of 14 simultaneous differential equations. Starting from $t = 0$, with all the corresponding initial conditions (initial pH, initial liquid phase and surface S(IV) concentrations, initial total S(IV) concentration, and initial number of particles, and the other initial concentrations), those equations can be solved step by step in time to give $C_l(t)$ and $r_l(t)$. At each step, once the $C_l(t)$ (where $C_l = [\text{SO}_3^{2-}] + [\text{HSO}_3^-]$) is known, the liquid phase concentrations of all species can be calculated from the governing equations, and the surface concentrations are then determined. The calculated saturation concentration of sulfite at the surface, $C(t)$, is in turn substituted into the system of differential equations in the model for the next step of calculation to give $C(t+\Delta t)$ and $r_l(t+\Delta t)$ (Δt is the step size of time used in this numerical calculation). Then this new C_l will be used to repeat the above calculations. The change of the interfacial area, $a(t)$, is also taken into consideration in this manner. The solution of the model will continue with the above loop-like calculations until all solid calcium sulfite is dissolved and the reaction is over.

Solutions of the Model

Highly Catalyzed Experiments. In conjunction with experiments in which the manganese concentration was 2000 ppm, the model was first used to determine the mass transfer coefficient of calcium sulfite ($T=40^\circ\text{C}$, $\text{pH}=5.0$). A reaction order of 1.5 was obtained from previous liquid phase kinetic studies with a rate constant of $85 \ell^{0.5} \text{mol}^{-0.5} \text{sec}^{-1}$ (25). Computer curves were generated using a series of mass transfer coefficients and plotted along with the experimental kinetic results on Figure 7. A mass transfer coefficient of 0.015 cm/sec most closely fits the data. The bulk pH drops quickly during the initial several seconds and then stays around 2.9, but the surface pH remains almost constant at 5.15 which implies that the oxidation only has small influence on the surface conditions.

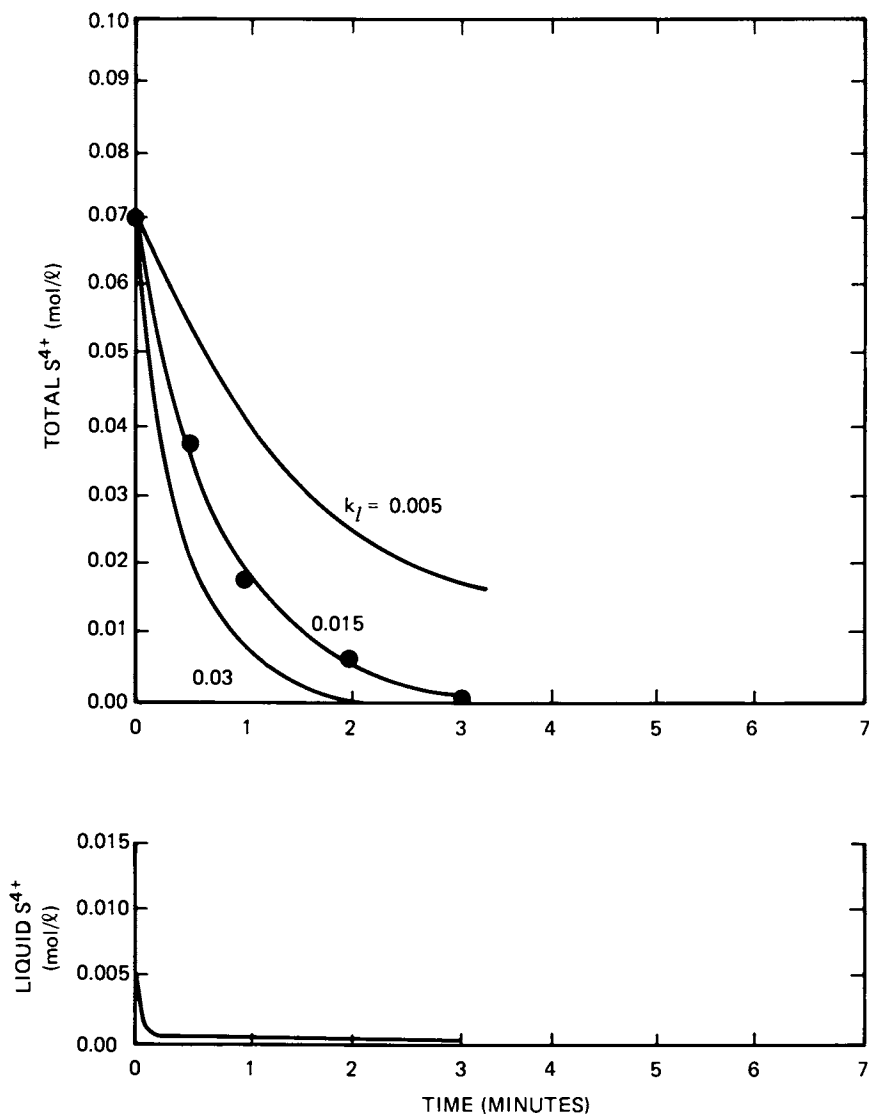


Figure 7. Determination of mass transfer coefficient. Key: ●, experimental data (9). One and one-half order rate constant $k = 85$. Conditions: pH_4 , 5.0; slurry density, 20 g/L; stirring speed, 1800 rpm; and 40°C. All three k_i 's gave the same liquid phase behavior.

The model was then tested to assess the effect of the value of the 1.5 order rate constant at values of 15, 20, and 30 $\ell^0.5 \text{ mol}^{-0.5} \text{ sec}^{-1}$ (12). This comparison showed that the determination of mass transfer coefficient to be unaffected by the value of the 1.5 order rate constant as long as it is large. This confirms that the use of 85 $\ell^0.5 \text{ mol}^{-0.5} \text{ sec}^{-1}$ as the 1.5 order rate constant for the simulation of the extremely catalyzed oxidation is not a sensitive parameter.

Variable Catalyst Concentration Solutions. Using the mass transfer coefficient of 0.015 cm/sec, the model was then used to simulate the slurry oxidation with three concentrations of added Mn catalyst. Results are presented in Figure 8. The 1.5 order homogeneous reaction rate constants for 0, 6.66, and 200 ppm added Mn reactions were found from the model to be 0.35, 2.25, and 5.5 $\ell^0.5 \text{ mol}^{-0.5} \text{ sec}^{-1}$ respectively. The corresponding values of 1.5 order rate constants from the comparable clear solution experiments are 0.162, 0.35, and 0.8 to 5 $\ell^0.5 \text{ mol}^{-0.5} \text{ sec}^{-1}$ (25). The computer-predicted values show good agreement with the experimental data, particularly considering unavoidable differences in the two systems, e.g., increases in catalyst concentration in the solution phase of the slurries caused by addition of catalytic solutes as the solid particles dissolve.

The bulk and surface pH curves predicted by the model for the above cases were considered as well. All of the surface pH's remain almost constant around 5.0. The bulk pH's change differently within the initial several minutes, but eventually drop and stay around pH 3.0.

Slurry Density Variations. The model was also used to simulate the slurry oxidations with different initial conditions. Initial pH's of 4.5 and 5.5 were both tested. Results (total concentration and solution phase concentration curves) for the initial pH 4.5 are presented in Figure 9. By using the predicted mass transfer coefficient and rate constants, the computer curves can match these experimental results very well.

pH Behavior. The pH behavior in the bulk and at the particle surface of the slurry oxidation with pH = 4.5, 5.0, and 5.5 is shown in Figure 10. There are two clear observations: the calculated and bulk pH (for an initial pH 5.0) do not agree well until the oxidation is nearly complete, and there is a marked sensitivity of the pH behavior of the model to initial pH.

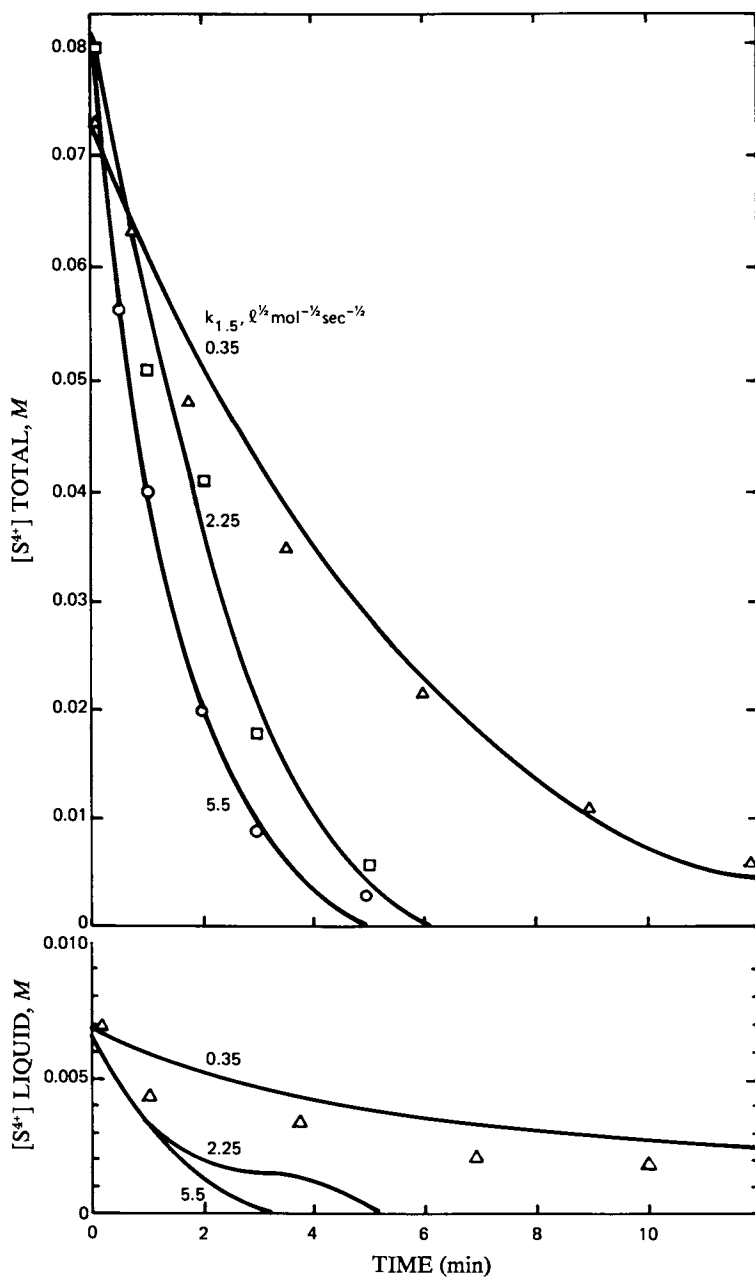


Figure 8. Effect of Mn concentration on the oxidation. Measured $[S^{4+}]$ (26). Mn (ppm): Δ , 0; \square , 6.66; and \circ , 200. Model: solid lines with $k_{1.5}$ as marked. pH_w , 5.0; slurry density, 20 g/L; and 40°C .

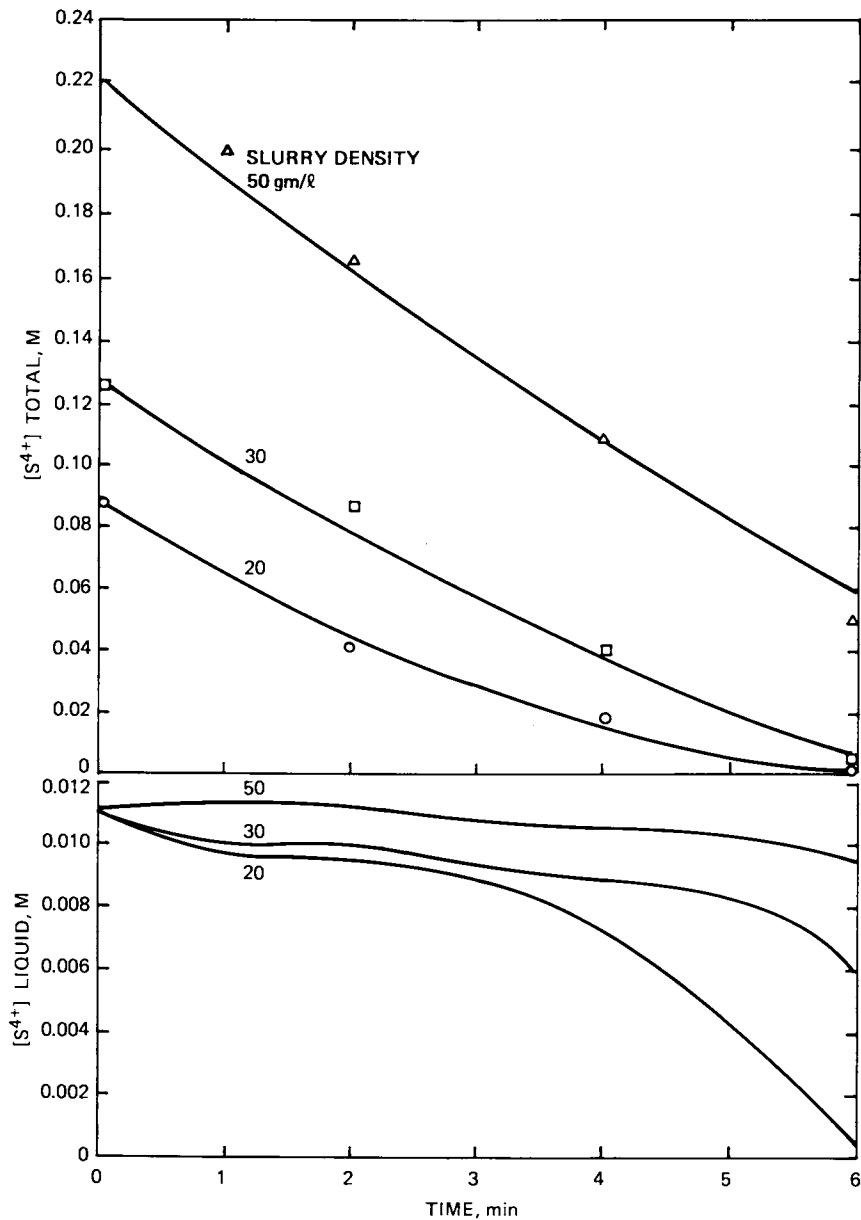


Figure 9. Oxidation in variable concentration slurries. Measured $[S^{4+}]$ (26): \circ , 20; \square , 30; and \triangle , 50 g/L. Model: solid lines for each slurry density shown. $k_{1.5} = 0.35 \text{ L}^{1/2} \text{ mol}^{-1/2} \text{ s}^{-1/2}$. pH_i , 4.5; and 40°C .

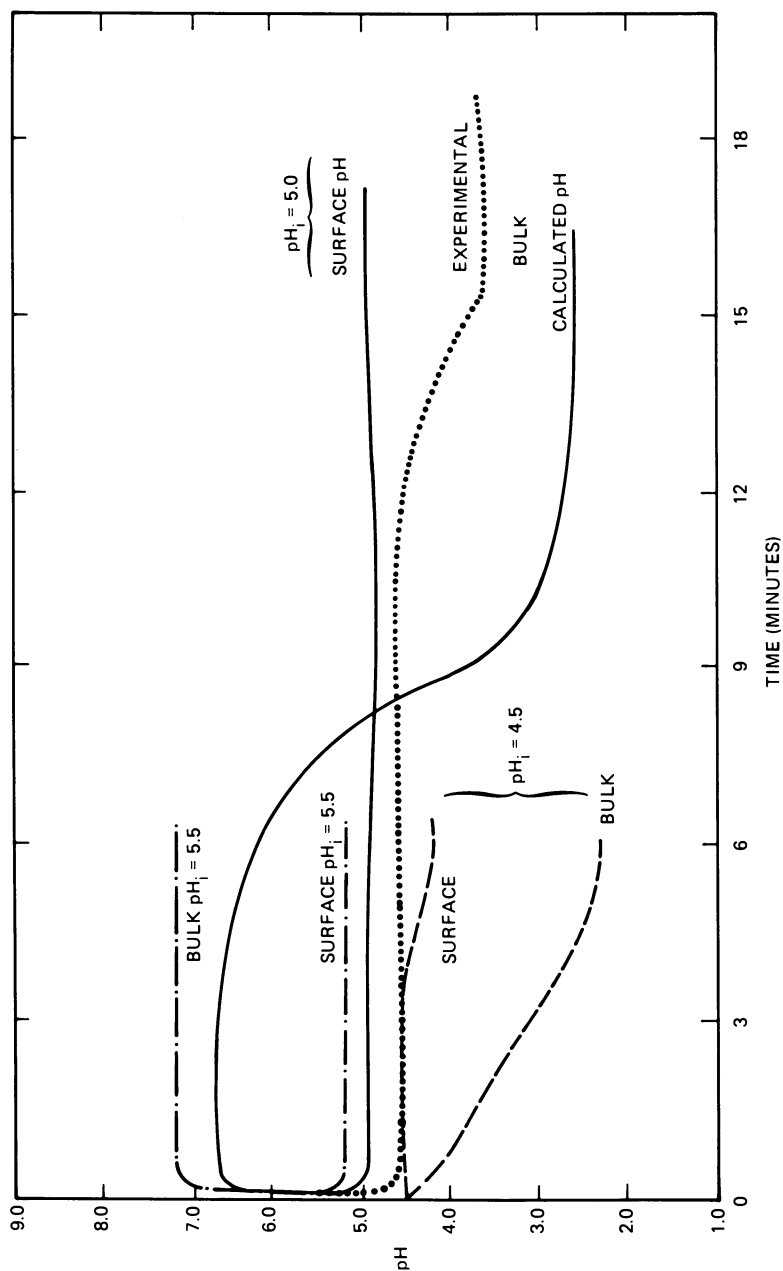


Figure 10. Oxidations beginning at three pH values. Temperature: 40°C. pH_i : 4.5, 5.0, and 5.5. Slurry density: 20 g/L. No Mn added. $k_1 = 0.015$ cm/s and $k_{i,5} = 0.35$ L^{0.5} mol^{-0.5} s⁻¹.

Discussion

The model developed in this paper is part of the growing body of knowledge describing the conditions in scrubber slurries. Even as an interim step, the current work has produced useful results. At the outset, the choice of a spherical geometry was an improvement over an earlier tendency toward flat plate geometries encouraged by the flat sulfite platelets themselves. Moreover, in preparing the initial conditions, the present calculations/measurements of solubility confirm the helpfulness of including the bisulfate species by the good agreement in Figure 6.

A film theory was employed in the model for the description of the solid-liquid mass transfer. It is important because it builds a relation between the surface of the particles and the solution phase. The particle surface condition is believed to be governed only by the $\text{CaSO}_3/\text{CaSO}_4$ solubilities, the electroneutrality of solutions, and the ion species equilibria, while the bulk liquid condition is the result of a complex relationship between the solid-liquid mass transfer, ion species equilibria, ion charge balance, and the kinetic rate of oxidation.

All the computer calculations show that there are drastic changes in the liquid phase behavior (viz., the bulk pH change) during the reaction, but the surface conditions are almost not affected by the oxidation (as shown by the constant surface pH during reaction). This result reflects the important fact that although the bulk pH (i.e., the measured pH) changes as the reaction proceeds, the saturation concentration of sulfite remains almost constant and does not correspond to the changing bulk pH.

In actual measurements, the initial pH had a profound influence on the pH vs time curve, for example, Figure 11 (26). With such sensitivity to initial pH, it is very hard to replicate experiments. Beside the obvious changes in initial concentrations, a variety of possible catalytic complexes may form at the different pH levels. The initial bulk pH has the most marked effect on the course of the subsequent pH change during oxidation. For the model to predict correctly the pH curve, both for changes in the initial pH and to produce agreement at the end of oxidation, suggests that the construction of the model is sound and that it could be revised to track the pH even more closely during oxidation.

By incorporating the film theory into the mathematical model for the batch slurry oxidation, a mass transfer coefficient of 0.015 cm/sec was obtained by matching the model to highly catalyzed (2000 ppm Mn added) slurry oxidation data. Saturation concentration of sulfite is most important in determining mass transfer coefficient(32). A correlation is given

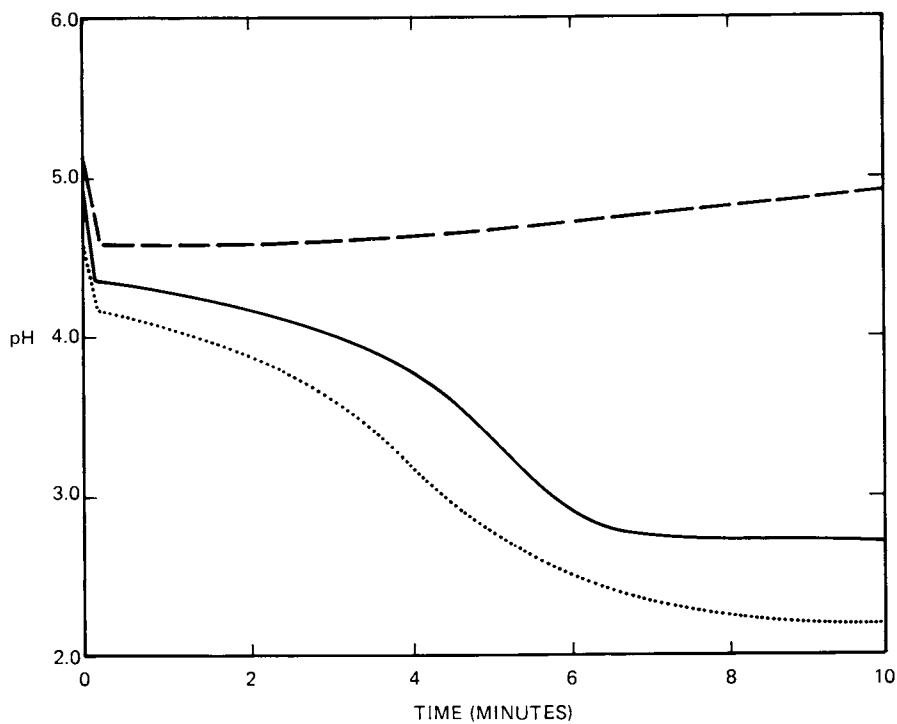


Figure 11. Experimental pH measurements for oxidations starting from variable initial pH. Slurry density, 20 g/L. pH: ---, 5.0; —, 4.7; ···, 4.5; 40°C.

by Sherwood, Pigford, and Wilke to predict the solid-liquid mass transfer coefficients for spherical particles suspended in an agitated vessel(31). Assuming a diffusivity of 10^{-5} cm²/sec, this correlation indicates a mass transfer coefficient larger than 0.01 cm/sec based on the average particle size encountered here. Therefore, the mass transfer coefficient predicted by the model closely matches this calculated literature correlation. A further endorsement of the model using this mass transfer coefficient comes from the agreement of the kinetic rate constants found by the model with the experimental range of the $k_{1.5}$ values.

An outstanding finding is the consonance of the model's prediction of the liquid phase S(IV) concentration and the measured values. In the reactions under investigation, the liquid phase concentrations are predicted to be higher than zero and lower than the saturation concentration, except for the highly catalyzed oxidation. This intermediate liquid phase concentration forecast by the model is in general agreement with the experimental data, and marks an instance of neither strict mass transfer nor kinetic control.

Acknowledgment

The United States Environmental Protection Agency supported this work through its grant R805227010. Robert Borgwardt was the project monitor.

Literature Cited

1. Magill, P. L., Holden, F. R., and Ackley, C., "Air Pollution Handbook," McGraw-Hill Book Company, Inc., New York (1956).
2. Esche, M., "Saarbery-Holter FGD Process-Regeneration in Lime Based FGD System," FGD Symposium, Hollywood, FL (1977).
3. Borgwardt, R. H., Combustion, 37 (1975).
4. Graffeo, A.J., Harpell, W.J. and Hsu, "Kinetics of CaSO₄ Crystallization Applied to FGD Problems," AIChE Meeting, Washington, D.C. (December 1974).
5. Head, N. N., Wang, S. C., and Keen, R. T., "Results of Lime and Limestone Testing with Forced Oxidation at the RPA Alkali Scrubbing Test Facility," Bechtel Corp. (1977).
6. Goodwin, R. W., "Oxidation of Flue Gas Desulfurization Waste and the Effect on Treatment Modes," J. Air Pollution Control Assn. 28, 35 (1978).

7. Borgwardt, R. H., "Limestone Scrubbing of SO_2 at EPA/RTP Pilot Plant," Progress Report 23-27 (April 1976).
8. Borgwardt, R. H., "Effect of Forced Oxidation on Limestone/ SO_x Scrubber Performance," EPA (1977).
9. Hatfield, J. D., Kim, Y. K., and Mullins, R. C., "Study of the Report to EPA, Contract No. T-V-34425 A (1972).
10. Gorman, D. N., "The Effect of Organic Acids on the Sulfur Dioxide Oxidation," B.S. Thesis, University of Virginia (1979).
11. Walter, P. E., " SO_2 Oxidation Kinetics," M.S. Thesis, University of Illinois, Urbana (1972).
12. Wang, C. C., "Experiments and Modeling of Calcium Sulfite Slurry Oxidation," M.S. Thesis, University of Virginia (1980).
13. Erwin, J., "Chemical Kinetics of the Manganese Catalyzed Autooxidation of Sulfite Anion That Occurs in the Solution Phase of Slurries," Ph.D. Thesis, University of Illinois, Urbana (1980).
14. Borgwardt, R. H., "IERL-RTP Scrubber Studies Related to Forced Oxidation," FGD Symposium, EPA, New Orleans, LA (1976).
15. Takeda, T., Moriguchi, H., Uchida, S., and Koide, K., a paper submitted to 12th fall meeting of the Society of Chemical Engineers, Nagoya, Japan (1976).
16. Gladkii, A.V., Working Group on Stationary Source Air Pollution Control in Technology; State Scientific Research Institute of Industrial and Sanitary Gas Cleaning, Moscow, USSR (1974).
17. Wen, C. Y., McMichael, W. J., and Nelson, R. D., "Scale Control in Limestone Wet-Scrubbing Systems," Report to EPA by A. D. Little, Inc., 37-57 (1975).
18. Ramachandran, P., and Sharma, M., "Absorption with Fast Reaction in a Slurry Containing Sparingly Soluble Fine Particles," Chem. Eng. Sci., 24, 1681-1686 (1969).
19. Uchida, S., Koide, K., and Shindo, M., "Gas Absorption with Fast Reaction into a Slurry Containing Fine Particles," Chem. Eng. Sci., 30, 644-645 (1975).

20. Uchida, S., Wen, C. Y., and McMichael, W. J., Progress Report to EPA, Contract No. EHS-D-71-20, No. 21 (1973); also Chi. Ch.E. J. No. 2, 5, 111-114 (1974).
21. Sada, E., Kumazawa, H., and Butt, M. A., "Single Gas Absorption with Reaction in a Slurry Containing Fine Particles," Chem. Eng. Sci., 32, 1165-1170 (1977).
22. Sada, E., Kumazawa, H., and Butt, M. A., "Simultaneous Absorption with Reaction in a Slurry Containing Fine Particles," Chem. Eng. Sci., 32, 1499-1503 (1977).
23. Sada, E., Kumazawa, H., and Butt, M. A., "Chemical Absorption into a Finite Slurry," Chem. Eng. Sci., 34, 715-718 (1979).
24. Wang, H. J., "Oxidation of Sulfites in a Batch Reactor," M.S. Thesis, University of Virginia (1979).
25. Hudson, J. L., Erwin, J., Dove, C., Gorman, D., Nurmi, D.B., Overman, J., Wang, C.C., Wang, H.J., Weishicht, W., "Sulfur Dioxide Oxidation in Scrubber Systems," Final Report EPA-60017-80-083 (1980).
26. Weisnicht, W., "Forced Oxidation in Calcium Sulfite Slurries," M.S. Thesis, University of Virginia (1978).
27. Seidell, A., "Solubilities of Inorganic and Metal Organic Compounds," D. Van Nostrand Company, Inc., New York, 327-328 (1940).
28. Weast, R. C., "Handbook of Chemistry and Physics," CRC Press, 53rd edition, D-122, Cleveland, OH (1972-73).
29. Brescia, F., Arents, J., Meislick, H., Turk, A., Fundamentals of Chemistry, Academic Press, New York (1967).
30. Vinograd, J. R., and McBain, J. W., "Diffusion of Electrolytes and of the Ions in Their Mixtures," J. Amer. Chem. Soc., 63, 2008 (1941).
31. Sherwood, T. K., Pigford, R. L., and Wilke, C. R., "Mass Transfer," McGraw-Hill Book Company, Inc., New York, 214-17 (1975).
32. Weisnicht, W. L., Overman, J., Wang, C. C., Wang, H. J., Erwin, J., and Hudson, J. L., "Calcium Sulfite Oxidation in a Slurry Reactor," Chem. Eng. Sci. 35, 463-468 (1980).

RECEIVED March 4, 1982.

Laboratory Investigation of Adipic Acid Degradation in Flue Gas Desulfurization Scrubbers

J. C. TERRY, J. B. JARVIS, D. L. UTLEY, and E. E. ELLSWORTH

Radian Corporation, Austin, TX 78766

The addition of adipic acid to FGD scrubber liquor results in improved limestone utilization and enhanced SO_2 sorption kinetics. During scrubber operation, however, adipic acid is lost from the system in the liquid and solid phase purge streams and by chemical degradation. In order to assess the effects of scrubber operating parameters on the loss of adipic acid, a series of laboratory tests have been performed. These include both bench-scale closed loop scrubber tests and batch mode jar tests. The parameters investigated include pH, adipic acid concentration, trace metal catalysts, degree of sulfite oxidation, sulfite concentration, SO_2 gas loading, and scrubber slurry temperature. Results indicate that the amount of adipic acid coprecipitated with the scrubber solids decreases significantly with increasing sulfate in the solids. Chemical degradation increased dramatically with forced sulfite oxidation. Chemical degradation was also found to increase with increasing adipic acid concentration and temperature. Reduced chemical degradation was observed with Mn^{+2} in the liquor. pH also affected chemical degradation but only when Mn^{+2} was present.

The addition of adipic acid to limestone-based FGD wet scrubbers results in improved limestone utilization and enhanced SO_2 sorption kinetics. The use of adipic acid was first proposed by Rochelle (1) and has been tested by the EPA in pilot systems at the Industrial Environmental Research Laboratory, Research Triangle Park, North Carolina and at the TVA Shawnee Test Facility at Paducah, Kentucky. Adipic acid in the concentration range of 1,000-2,000 mg/l has been found effective as a scrubber additive. During scrubber operation, however, adipic acid is lost from the system in the liquid and solid phase purge streams and by chemical degradation (2,3).

0097-6156/82/0188-0221\$6.50/0
© 1982 American Chemical Society

Tests conducted at the Shawnee Test Facility indicated that adipic acid added to their limestone FGD scrubber did not degrade at pH's below 5. Since these unexpected but favorable results were important to the future application of adipic acid as an FGD additive, independent verification was desired. Radian was contracted by the EPA to carry out a systematic study of the effects of scrubber operating conditions on adipic acid degradation.

The specific objectives of the study were to:

- setup a bench-scale SO₂ scrubber capable of closed loop operation;
- verify the quenching of adipic acid degradation at low pH observed at Shawnee; and
- conduct parametric studies to more fully characterize the effects of key operating variables on adipic acid degradation.

The topics presented in this paper include a description of the bench-scale system, the experimental approach, and the results of degradation testing. Also included are the results of batch precipitation experiments designed to study coprecipitation of adipic acid in scrubber waste solids.

Experimental Approach

The design of the bench-scale system was influenced by two important considerations:

- The desire to simulate the operation of full-scale FGD systems which would allow results from the bench-scale system to be used to anticipate adipic acid degradation in larger systems, and
- The need for accurate mass balance determinations since certain sets of operating conditions were anticipated to produce low degradation rates.

The experimental equipment design which resulted from the above considerations is illustrated schematically in Figure 1. In general terms, the operation of the system consisted of contacting synthetic or boiler flue gas in a packed scrubber with recirculating slurry from the hold tank. The pH of the hold tank slurry was maintained at a constant level by addition of reagent grade CaCO₃ or limestone.

At the start of each run, various materials were added to the hold tank. These materials included deionized water, adipic acid, calcium sulfite seed crystals, NaCl, MnSO₄·H₂O, Fe₂(SO₄)₃, fly ash, etc. depending on the purpose of the test. The resulting thin slurry was circulated through the scrubber where it was contacted with flue gas. This procedure was continued for several hours, allowing time for the mass of solids in the hold tank to increase and the concentration of ionic species (particularly SO₃⁼) to reach a constant level. At this point, a quantitative amount of slurry was withdrawn from the hold tank.

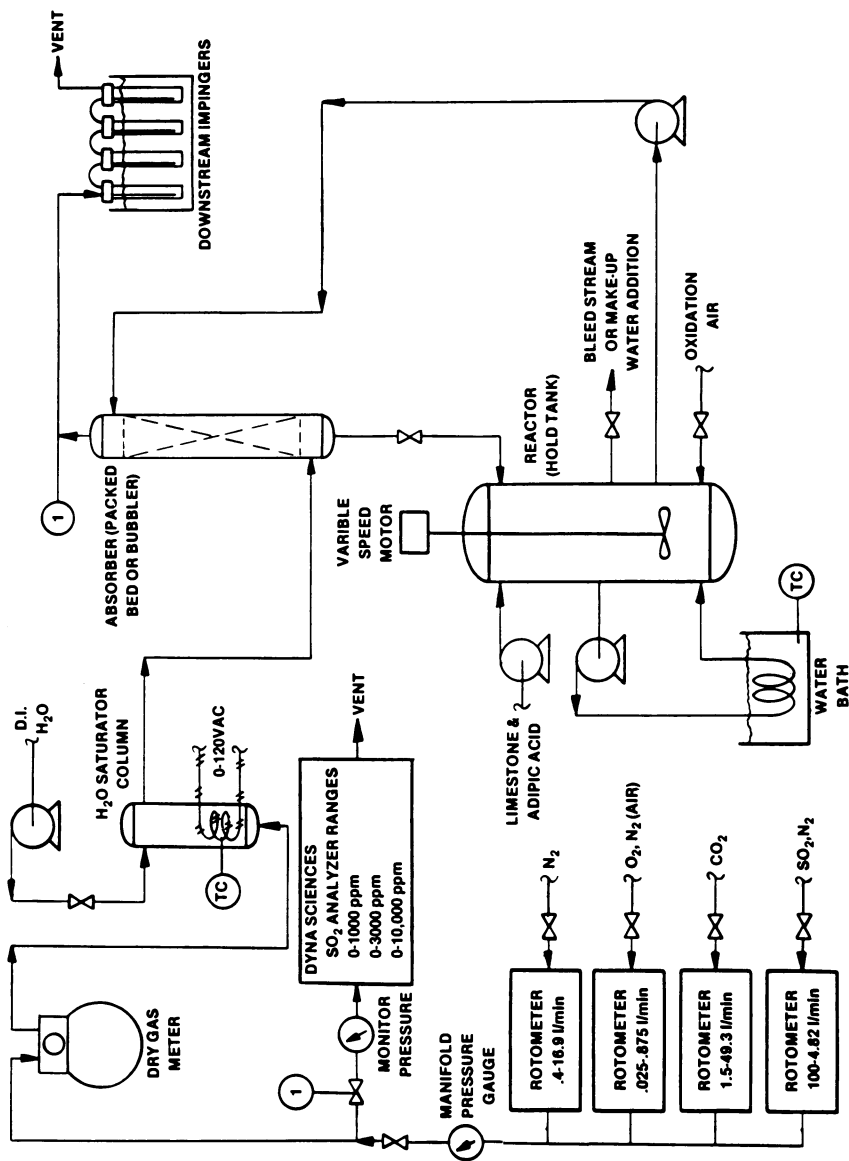


Figure 1. Diagram of closed loop SO₂ scrubber.

Analysis for adipic acid in both the solid and liquid phase, plus data for the hold tank volume, slurry density, and weight percent solids, provided sufficient information to calculate the inventory of adipic acid remaining in the hold tank. At the end of the run, a second sample was withdrawn from the hold tank and the adipic acid inventory was again calculated. The absolute amount of adipic acid which had degraded during the run was represented by the difference between the initial and final inventories.

Several features were incorporated into the design of the bench-scale unit which facilitated the study of the effects of operating conditions on adipic acid degradation. Some of the more important features are described below:

- Synthetic flue gas, rather than combustion gases, was used during the laboratory phase of testing. This allowed an independent determination of the effect on degradation of components of flue gas such as fly ash, percent O₂, and certain sulfur species.
- Calcium carbonate, rather than limestone was used as the source of alkalinity for baseline testing. Again, this permitted independent study of limestone components (notably trace metals) on adipic acid degradation.

In addition to the measurements required for determining the adipic acid degradation rate, a variety of other variables were monitored:

- pH (continuously),
- Inlet and outlet SO₂ concentration,
- Percent oxidation in the solids,
- Temperature (hold tank and gas inlet),
- Limestone consumption rate,
- Limestone utilization,
- Liquid to gas ratio (L/G),
- Sulfite concentration,
- Chloride concentration (used as a tracer), and
- Trace metals concentration (if added to system).

With this information, the adipic acid degradation rate and other aspects of operation with adipic acid can be related to specific process variables. And, results obtained with the bench-scale system can then be used to anticipate adipic acid degradation rates in full-scale systems.

Bench-Scale Scrubber Test Results

The results of bench-scale tests were obtained during three phases of experimentation. The first phase consisted of laboratory testing at Radian. The second phase consisted of testing at the Shawnee test facility in Paducah, KY, and at the City Utilities of Springfield Southwest Power Station in Springfield, MO. The third phase consisted of additional laboratory testing at Radian.

A total of 43 bench-scale runs were performed. The results

of these runs, including the observed degradation rates and a summary of run conditions, are listed in Table I. Twenty-one of these runs were baseline tests in which the variables under consideration were limited to the SO₂ absorption/oxidation rate, the adipic acid concentration, and pH. CaCO₃ was used as the alkaline species for all baseline tests. The ranges for the variables investigated in the baseline tests were:

<u>Variable</u>	Range
SO ₂ absorption rate	2.07 - 7.86 g SO ₂ /hr
Percent solids oxidation (a measure of the total absorbed SO ₂ that is oxidized to sulfate)	9.7 - 100%
Adipic acid concentration	876 - 10,080 ppm
pH	4.6 - 5.5

The resulting adipic acid degradation rates ranged from 15.4 to 600 mg/hr. A computer program was used to perform a statistical analysis on the baseline test data. This analysis showed that the adipic acid degradation rate was a function of the overall SO₂ oxidation rate and the adipic acid concentration. The degradation rate was found not to depend on pH, at least over the range tested. The sulfite ion concentration was also included in this analysis. However, the sulfite concentration was generally a function of pH and was also found not to influence the adipic acid degradation rate. A weighted least squares analysis was used to correlate the significant variables. The resulting correlation, which represents the best fit of the experimental data, is given below:

$$\text{adipic acid degradation rate, mg/g SO}_2 \text{ removed} = 0.00308 \left(\begin{array}{c} \text{adipic acid} \\ \text{concentration, ppm} \end{array} \right)^{0.5542} \left(\begin{array}{c} \text{percent oxidation} \end{array} \right)^{1.185}$$

(correlation coefficient, $r^2 = 0.96$)

This correlation indicates that the adipic acid degradation rate, normalized by the SO₂ removal rate, is roughly proportional to the percent oxidation of the solids times the square root of the adipic acid concentration. A graph of the above correlation is shown in Figure 2.

Nine forced oxidation runs were performed with manganese, manganese plus iron, Springfield limestone, or Springfield limestone plus fly ash. The common factor involved in all these runs was the presence of manganese ions in the scrubber liquor. The presence of manganese caused a significant reduction in the adipic

Table I. Summary of Bench-Scale System Adipic Acid Degradation Results

Run No.	Degradation of Adipic Acid as:		Degradation Rate Constant K_d , H^{-1}	Uncertainty ¹ Level, %	Run Characteristics
	Absolute Degradation, g/hr	mg Adipic Degraded/g SO ₂ Removed			
R-1	0.068	9.4	0.86	54	Natural oxidation, pH 5.5 (baseline)
R-2	0.030	4.7	0.14	116	Natural oxidation, pH 4.6 (baseline)
R-3	0.018	3.1	0.21	70	Natural oxidation, pH 4.6 (baseline)
R-4	0.30	63	1.38	7.5	Forced oxidation, pH 4.6 (baseline)
R-5	0.66	105	0.74	14	Forced oxidation, pH 4.6, High adipic acid conc. (baseline)
R-6	0.30	143	0.92	19	Forced oxidation, pH 4.6, high adipic acid conc., low SO ₂ inlet conc. (baseline)
R-7	0.66	96	0.69	16	Forced oxidation, pH 5.5, high adipic acid conc. (baseline)
R-8	0.50	75	0.59	20	Forced oxidation, pH 5.5, high adipic acid conc., high sulfite conc.
S-1	0.041	8.6	0.66	37	Natural oxidation, pH 4.6
S-2	0.061	11.9	1.43	26	Natural oxidation, pH 4.6
S-3	0.053	10.5	0.89	36	Natural oxidation, pH 4.6, exclude O ₂ from hold tank
P-1	0.026	6.5	1.27	67	Natural oxidation, pH 4.6
P-2	0.032	6.3	2.23	50	Natural oxidation, pH 5.5
P-3	0.018	4.2	0.40	97	Natural oxidation, pH 4.6, manganese
P-4	0.027	6.6	1.15	91	Natural oxidation, pH 4.6
R-9	0.025	4.5	1.01	39	Natural oxidation, pH 4.6 (baseline)
R-10	0.028	4.2	1.22	35	Natural oxidation, pH 5.1 (baseline)
R-11	0.016	2.0	0.49	121	Natural oxidation, pH 5.5 (baseline)
R-12	0.189	24.7	1.01	5.5	Partial forced oxidation, pH 5.1 (baseline)
R-13	0.298	45.4	1.39	3.3	Forced oxidation, pH 4.6 (baseline)
R-14	0.136	18.1	0.41	9.0	Forced oxidation, pH 5.1, manganese

¹Uncertainty level reflects experimental uncertainty in the absolute degradation rate only.

Run No.	Degradation of Adipic Acid as:			Degradation Rate Constant K _d , M ⁻¹	Uncertainty ¹ Level, ±%	Run Characteristics
	Absolute Degradation, g/hr	mg Adipic Degraded/g SO ₂ Removed	Degradation, g/hr			
R-15	0.131	22.8	1.27	8.3	Partial forced oxidation, pH 4.6 (baseline)	
R-16	0.038	5.9	1.62	23	Natural oxidation, pH 5.1, low manganese	
R-17	0.154	20.0	0.52	7.7	Forced oxidation, pH 4.6, low temperature	
R-18	0.145	20.2	0.63	5.5	Forced oxidation, pH 5.1, manganese	
R-19	0.346	49.3	1.90	2.1	Forced oxidation, pH 5.1 (baseline)	
R-20	0.041	5.3	1.12	30	Natural oxidation, pH 5.5 (baseline)	
R-21	0.079	10.7	0.98	16	Natural oxidation, pH 5.5, high sulfite	
R-22	0.076	10.4	1.16	17	Natural oxidation, pH 5.1 (baseline)	
R-23	0.015	2.7	1.53	24	Natural oxidation, pH 5.1, low adipic acid conc. (baseline)	
R-24	0.074	11.2	0.38	48	Natural oxidation, pH 5.1, high adipic acid conc. (baseline)	
R-25	0.436	81.7	2.33	1.9	Forced oxidation, pH 4.6, high temperature	
R-26	0.295	53.2	2.05	2.3	Forced oxidation, pH 4.6 (baseline)	
R-27	0.047	8.6	0.20	25	Forced oxidation, pH 4.6, manganese	
R-28	0.010	1.7	1.26	123	Forced oxidation, pH 5.1, thiosulfate	
R-29	0.236	30.0	0.65	5.7	Forced oxidation, pH 5.1, limestone (manganese)	
R-30	0.204	25.6	0.49	7.5	Forced oxidation, pH 5.1, limestone + fly ash (manganese)	
R-31	0.097	15.5	0.49	7.6	Forced oxidation, pH 5.1, manganese + iron	
R-32	0.123	19.0	1.42	30	Natural oxidation, pH 5.1, high adipic acid conc. (baseline)	
R-33	0.047	9.1	0.22	21	Forced oxidation, pH 4.1, manganese	
R-34	0.178	26.6	0.93	5.1	Forced oxidation, pH 5.5, manganese	
R-35	0.076	12.1	0.33	12	Forced oxidation, pH 4.6, manganese + iron	
R-36	0.640	81.4	0.93	4	Forced oxidation, pH 5.1, high adipic acid conc. (baseline)	

¹Uncertainty level reflects experimental uncertainty in the absolute degradation rate only.

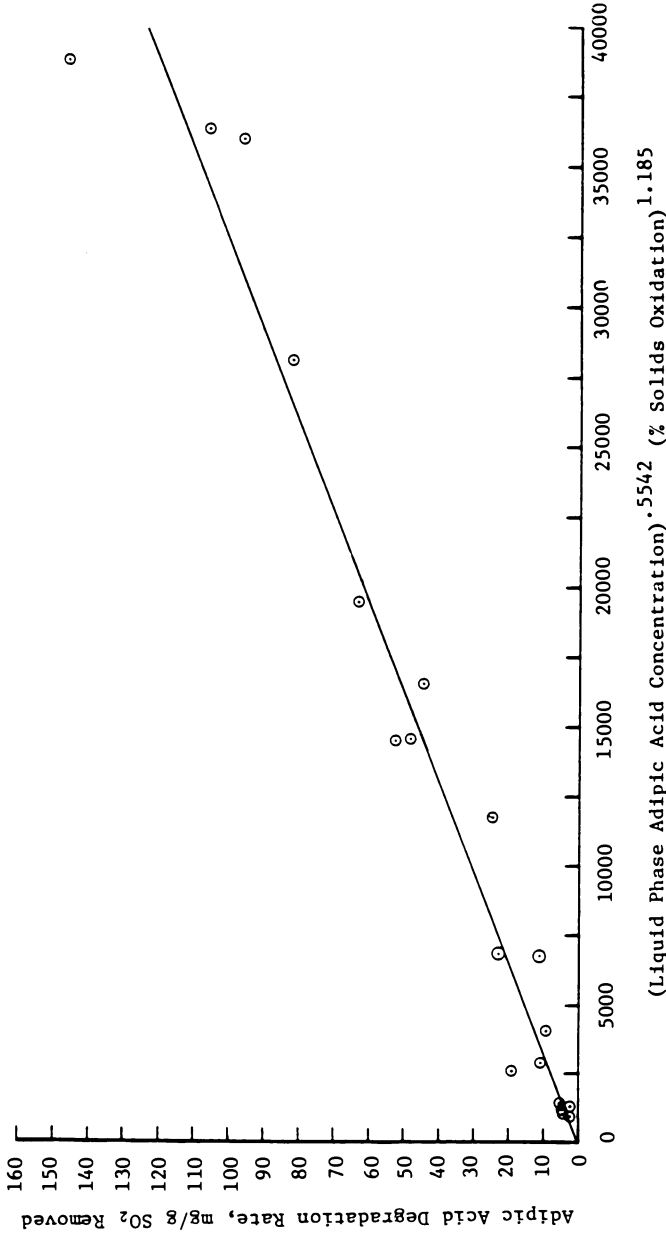


Figure 2. Correlated relationship between the adipic acid degradation rate, the liquid phase adipic acid concentration, and the percent solids oxidation for the baseline data set.

acid degradation rate. Reductions of 42.5 to 85.4 percent below the adipic acid degradation rates predicted from the baseline correlation were observed for forced oxidation runs. Data from these runs are listed in Table II.

The adipic acid degradation rate was found to be a function of pH when manganese ions were present. The results show that a decrease in pH is accompanied by a decrease in the adipic acid degradation rate. In the baseline runs, in which no manganese was present, no pH effect was observed.

The effect of manganese and pH on the adipic acid degradation rate is illustrated in Figure 3. Here, the adipic acid degradation rate has been presented in the form of a degradation rate constant, K_d . K_d is based on the following simple rate model:

$$\text{Adipic Acid Degradation Rate, mass/unit time} = K_d \left(\frac{\text{Adipic Acid Concentration}}{\text{Sulfite Oxidation Rate, mass/unit time}} \right)$$

When solved for K_d , the above model suggests that the adipic acid degradation rate, normalized by the adipic acid concentration and the sulfite oxidation rate, should be constant. This feature makes K_d useful in evaluating the effects of variables not included in the correlation; in this case, manganese and pH. The results in Figure 3 show that values of K_d ranging from 0.20 to 0.93 were obtained for runs in which manganese ions were present in the hold tank. This compares to predicted values of K_d ranging from 1.2 to 1.6 for baseline tests at similar conditions without the presence of manganese ions.

Several of the runs illustrated in Figure 3 were performed with Springfield limestone rather than CaCO_3 . The adipic acid degradation rates seen in the limestone tests were significantly below those seen in similar baseline tests with CaCO_3 . This limestone was analyzed for trace metals and a concentration of 430 ppm manganese was found. Some of this manganese dissolved in the scrubber liquor during the bench-scale tests. The resulting adipic acid degradation rates were about the same as those seen in runs with CaCO_3 in which manganese was added to the hold tank.

The combination of limestone and fly ash was also tested. The resulting adipic acid degradation rate did not differ significantly from that of limestone alone. In bench-scale tests at Shawnee and Springfield, in which boiler flue gas with fly ash was utilized, no significant effect of fly ash was observed.

Several forced oxidation tests with both manganese and iron were attempted. However, iron was found to be essentially insoluble and only small concentrations of iron could be held in solution. Again, the resulting adipic acid degradation rates were about as expected, based on the pH and the concentration of manganese in the hold tank.

A natural oxidation run with manganese was also performed. However, under natural oxidation conditions, only a small amount of the added manganese remained in solution and the resulting

Table II. Results of Bench-Scale Runs with Manganese, Iron, Limestone, and Fly Ash

Run #	Degradation Rate Constant K_d , M^{-1}	Degradation as $mg/g SO_2$ Removed	Predicted Degradation Rate, $mg/g SO_2$ Removed ¹	% Reduction from Predicted Degradation	pH	Run Conditions
<u>Runs with manganese only (CaCO₃)</u>						
R-33	0.22	9.14	56.6	83.9	4.1	[Mn ²⁺] = 18 ppm forced oxidation
R-27	0.20	8.61	58.7	85.4	4.6	[Mn ²⁺] = 15 ppm forced oxidation
R-14	0.41	18.0	58.6	69.3	5.1	[Mn ²⁺] = 21 ppm forced oxidation
R-18	0.63	20.3	49.5	59.1	5.1	[Mn ²⁺] = 6 ppm forced oxidation
R-34	0.93	26.6	46.3	42.5	5.5	[Mn ²⁺] = 9 ppm forced oxidation
<u>Runs with manganese and iron (CaCO₃)</u>						
R-35	0.33	12.1	52.9	77.1	4.6	[Mn ²⁺] = 16 ppm; [Fe ³⁺] ≤ 1.5 ppm forced oxidation
R-31	0.49	15.5	49.2	68.5	5.1	[Mn ²⁺] = 6 ppm; [Fe ³⁺] = 2 ppm forced oxidation
<u>Runs with Springfield limestone</u>						
R-29	0.65	30.0	60.6	50.5	5.1	[Mn ²⁺] = 5 ppm; [Fe ³⁺] ≤ 0.6 ppm forced oxidation
R-30	0.49	25.6	64.5	60.3	5.1	[Mn ²⁺] = 5 ppm; [Fe ³⁺] ≤ 0.6 ppm forced oxidation + fly ash

¹Predicted degradation rate from baseline correlation:

$$\text{adipic acid degradation rate, mg/g SO}_2 \text{ removed} = 0.00308 \left(\text{adipic acid concentration, ppm} \right)^{0.5542} \left(\text{percent oxidation} \right)^{1.185}$$

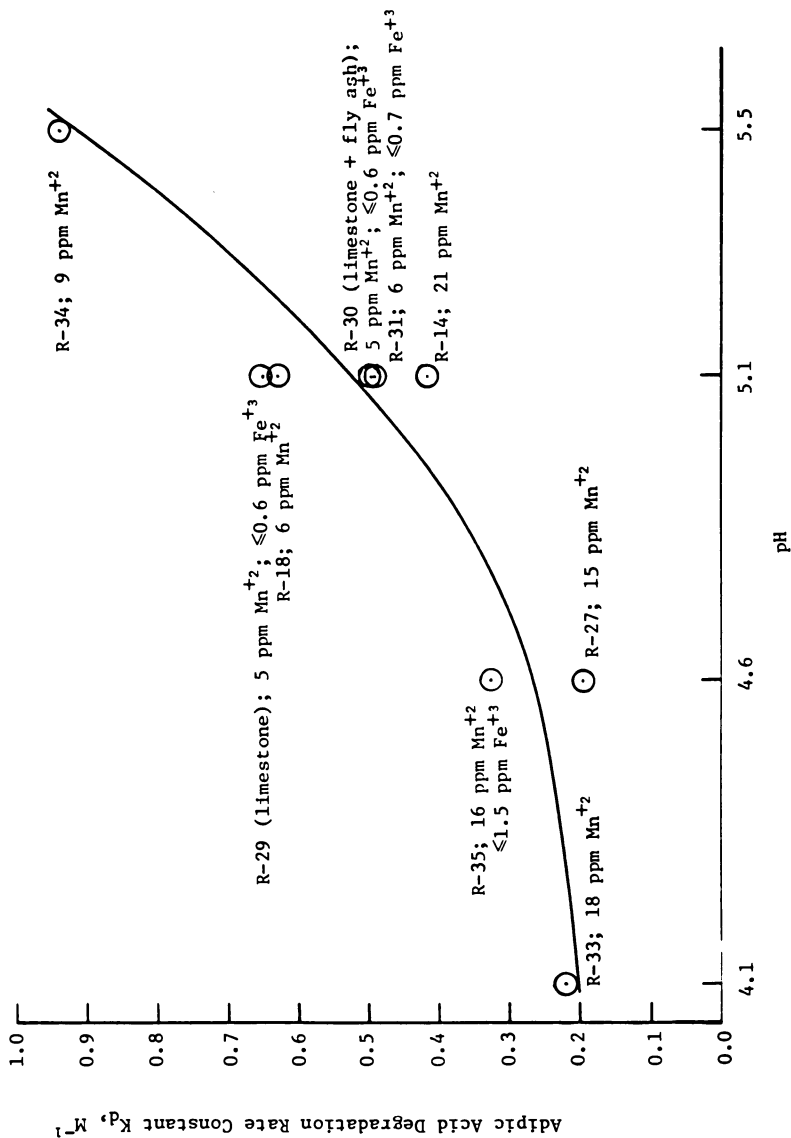


Figure 3. Effect of pH on the adipic acid degradation rate constant, K_d , for forced oxidation runs with Mn, Mn + Fe, limestone, and limestone + fly ash.

adipic acid degradation rate was actually above that predicted from the baseline correlation.

Three runs were performed in which the temperature of the hold tank was varied. Selected results from these runs are shown in Table III.

Table III. Effect of Hold Tank Temperature on the Adipic Acid Degradation Rate

Run #	Adipic Acid Degradation Rate Constant K_d, M^{-1}	Adipic Acid Degradation Rate, mg/g SO ₂ Removed	Temperature, °F (°C)	Average Adipic Acid Concentration, ppm
R-17	0.52	20.0 ±7.7%	93 (33.9)	2449
R-13	1.39	45.4 ±3.3%	125 (51.7)	2159
R-25	2.33	81.7 ±1.9%	146 (63.3)	2246

Note: All three runs were performed at pH 4.6 - forced oxidation (100%).

The results of these runs show that the adipic acid degradation rate increased with increasing temperature. The effect of temperature on the rate of chemical reaction can often be modeled by the following empirical equation (4):

$$K = A \exp\{-E_a/RT\}$$

where K = the chemical rate constant or an equivalent expression for the reaction rate,

A = a pre-exponential constant,

E_a = the Arrhenius activation energy,

R = the ideal gas constant, and

T = the absolute temperature.

This equation can be written in the logarithmic form:

$$\log_{10} K = \left(\frac{-E_a}{2.303R} \right) \frac{1}{T} + \log_{10} A$$

According to this equation: A plot of $\log_{10} K$ versus the reciprocal of the absolute temperature should be a line with a slope of $(-E_a/2.303 R)$. A plot of this type is shown in Figure 4 in which the logarithm of the adipic acid rate constant, K_d , is

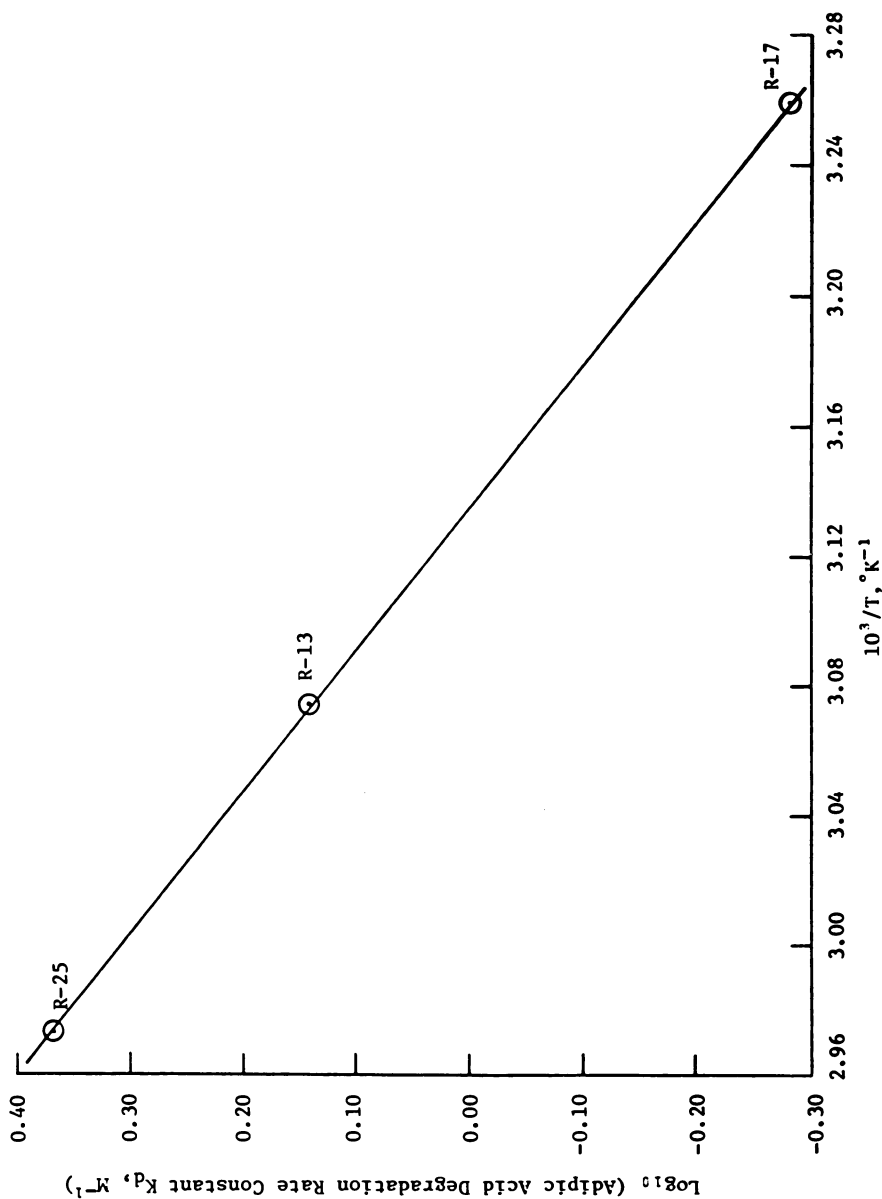


Figure 4. Plot of $\text{Log}_{10} (K_d)$ vs. reciprocal absolute temperature for the determination of the Arrhenius activation energy, E_a .

is plotted against the reciprocal of the absolute temperature. The use of K_d is appropriate here only because the percent oxidation and the average adipic acid concentration for the three runs are close. From the slope of the line shown in Figure 4, the Arrhenius activation energy was determined to be 10.6 Kcals/mole. This activation energy is typical for an organic reaction in which the rate is controlled by a chemical reaction rather than a physical process such as diffusion.

In the analysis of the baseline test results, the sulfite ion concentration was not found to have an effect on the adipic acid degradation rate. However, in these tests, the equilibrium sulfite ion concentration was a strong function of pH. To obtain an independent determination of the effect of the sulfite ion concentration, the sulfite concentration was increased via the addition of sodium ions (as Na_2SO_4). In this way, the effect of different sulfite ion concentrations could be evaluated at the same pH. A comparison of the degradation rates from these tests with the values predicted from the baseline correlation indicates that the sulfite ion concentration has little, if any, impact on the adipic acid degradation rate mechanism.

Coprecipitation of Adipic Acid in Scrubber Solids

A major factor in determining the degradation rate of adipic acid is differentiating between physical loss of adipic acid and actual chemical degradation. There are at least two mechanisms for physical loss of adipic acid including liquor loss with the wet filter cake and coprecipitation with calcium sulfite hemihydrate and gypsum solids. The bench-scale data, as well as earlier work (2, 3), indicated that adipic acid coprecipitation with scrubber solids was a potentially important factor in mass balance calculations. Further, the bench-scale data, shown in Figure 5, indicated that the amount of coprecipitated adipic acid was a strong function of the level of sulfite oxidation.

In order to further characterize this mechanism for adipic acid loss, two series of batch precipitation experiments were performed. The tests were designed to study:

- The mechanism for adipic acid coprecipitation (surface adsorption versus occlusion or solid solution formation),
- The effect of liquid phase adipic acid concentration on adipic acid concentration in the scrubber solids, and
- The effect of sulfite to sulfate ratio (oxidation fraction) on adipic acid coprecipitation.

In the first series of tests 1.0 M Na_2SO_3 and 1.0 M Na_2SO_4 were separately dripped into stirred solutions of 0.5 M CaCl_2 at 50°C. In tests with Na_2SO_3 , a nitrogen blanket was maintained over the solutions and boiled deionized water was used to prepare reagents. The pH was maintained at 4.6 and 5.5 by dropwise addition of hydrochloric acid. To test the surface absorption mechanism, about 3,000 ppm adipic acid was added to the slurries after

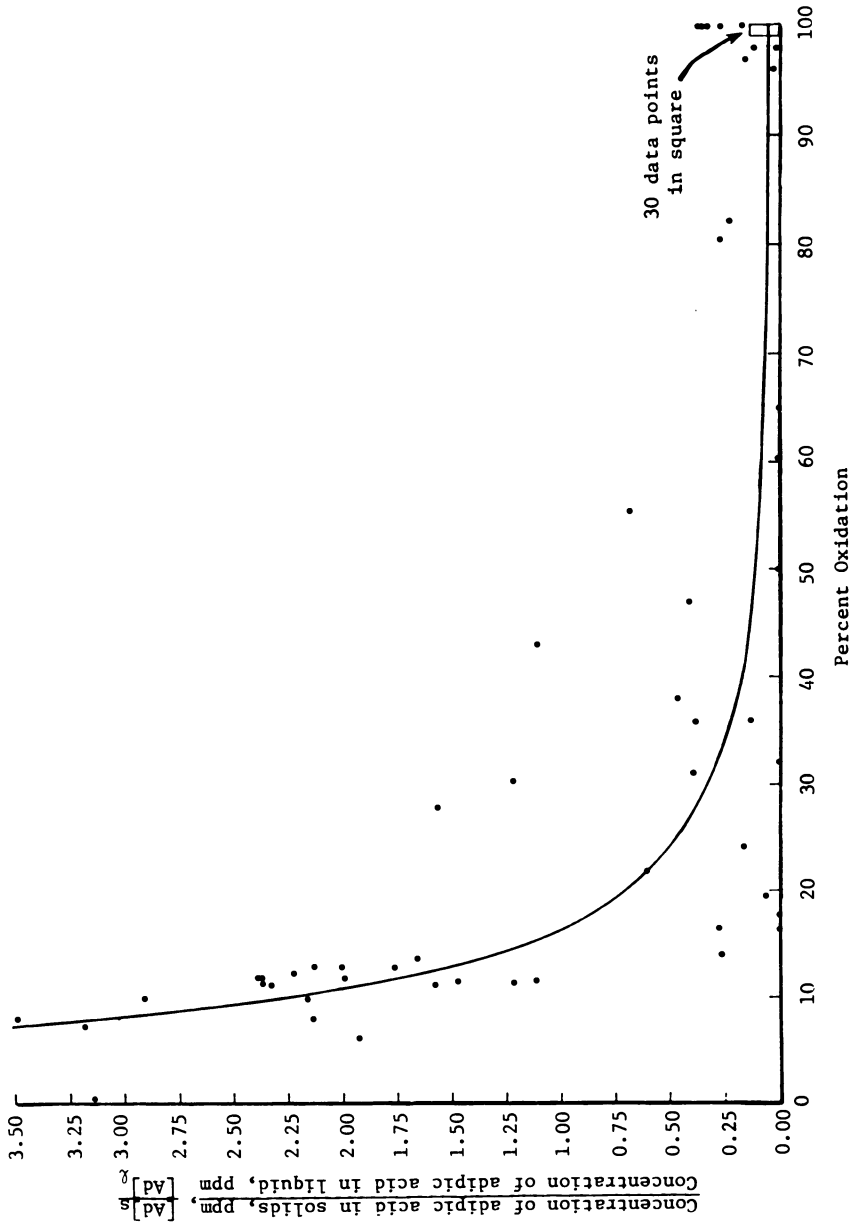


Figure 5. Relationship of adipic acid content of bench-scale solids to percent oxidation.

precipitation had occurred. To test occlusion/solid solution formation, about 3,000 ppm adipic acid was added before precipitation occurred. The amount of absorbed and occluded adipic acid was then determined by analysis of filtered and dried solids. The cake analysis was corrected for the amount of adipic acid calculated to have been associated with the water in the wet cake based on weight percent solids in the cake and the measured concentration of adipic acid in the slurry liquor. A summary of test results is given in Table IV.

Table IV. Summary of Test Results for Addition of Adipic Acid Before and After Solids Precipitation

Solids Phase	Solution pH			
	4.6		5.5	
	Before	After	Before	After
$\text{CaSO}_3 \cdot \frac{1}{2}\text{H}_2\text{O}$	15,500 $\mu\text{g/g}$	<500 $\mu\text{g/g}$	15,000 $\mu\text{g/g}$	<500 $\mu\text{g/g}$
$\text{CaSO}_4 \cdot 2\text{H}_2\text{O}$	640 $\mu\text{g/g}$	<500 $\mu\text{g/g}$	770 $\mu\text{g/g}$	<500 $\mu\text{g/g}$

Several conclusions can be made based on these results:

- The major mechanism for adipic acid coprecipitation is occlusion or solid solution formation and not surface absorption although absorption could still occur at the <500 ppm level.
- The extent of adipic acid coprecipitation is highly influenced by the oxidation fraction of the scrubber solids (sulfite versus sulfate),
- The scrubber slurry pH does not significantly effect adipic acid coprecipitation (at least over the pH range tests).

The second series of batch precipitation tests was performed at pH 4.6 with various levels of adipic acid added before solids were precipitated and at intermediate levels of sulfate fraction in the product solids. The results of these tests and selected similar tests from the first test sequence are summarized in Table V. The ratio of $[\text{Ad}]_s/[\text{Ad}]_l$ is plotted against the percent sulfate in the solids in Figure 6. Examination of the plot in Figure 6 as well as a simple inspection of the data shows that the concentration of adipic acid in the solids is directly proportional to the concentration of adipic acid in the slurry solution but inversely proportional to the fraction of sulfate in the solids formed. The exact relationship for solids adipic acid concentration versus solids sulfate fraction does not appear to be linear and this may be related to a change in mechanism from predominately sulfate coprecipitation at low oxidation levels to gypsum formation at high oxidation levels. Note the similarity of the data in Figure 6 with that from the bench-scale tests shown in Figure 5.

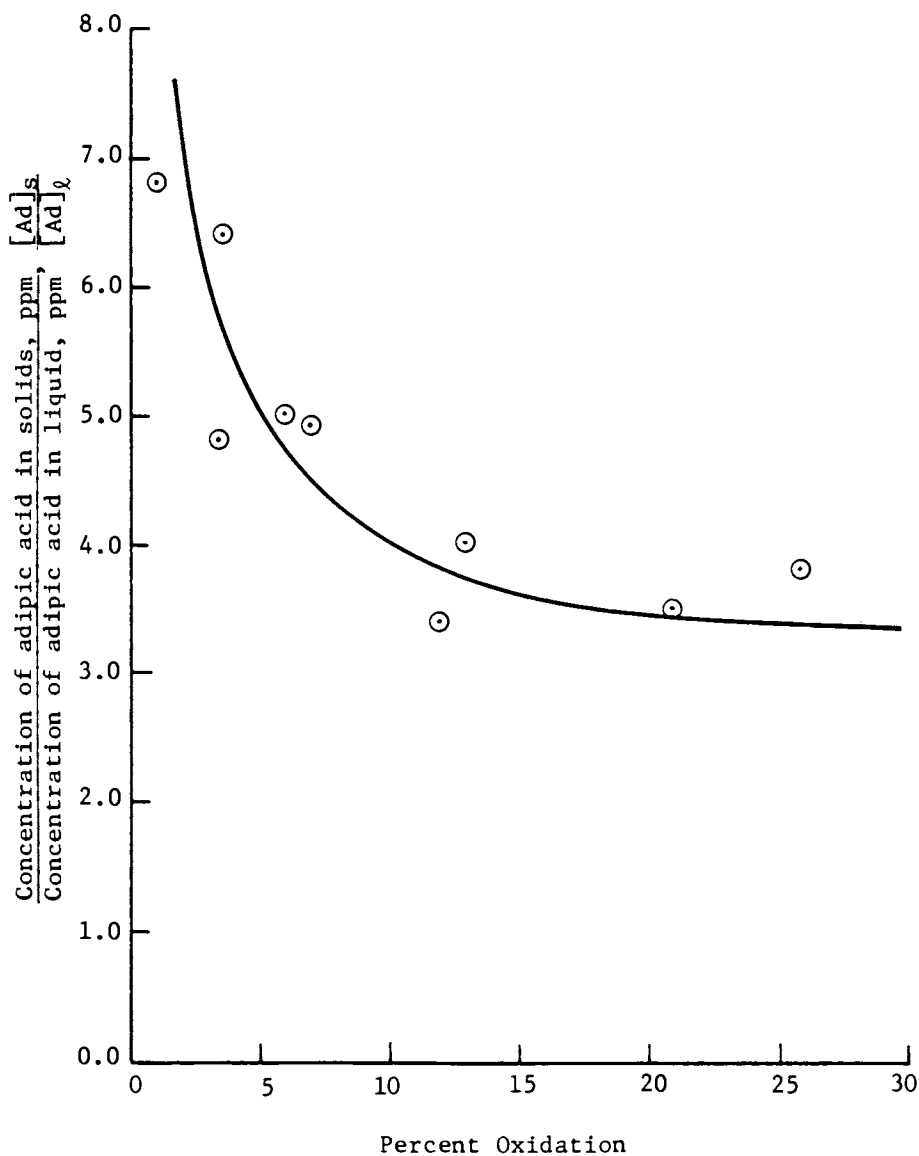


Figure 6. Normalized concentration of adipic acid in solids vs. percent sulfate in solids.

Table V. Summary of Test Results for Various Adipic Acid Concentration and Solids Oxidation Levels

% Oxidation In Solids	Adipic acid Concentration In Solution (ppm)	Acipid Acid Concentration In Solids (ppm)	$[Ad]_s/[Ad]_l$
<1.0	2,400	16,200	6.8
3.4	3,100	15,000	4.8
3.7	2,300	14,800	6.4
6.0	9,300	46,500	5.0
7.0	5,800	28,400	4.9
12.0	9,100	31,300	3.4
13.0	6,600	26,600	4.0
21.0	3,500	12,300	3.5
26.0	3,600	13,800	3.8
100.0	3,100	640	0.2
100.0	3,500	770	0.2

Solids from the batch precipitation tests were also examined by scanning electron microscopy. In tests where no adipic acid was added, the calcium sulfite solids formed a single platelet crystal. However, upon addition of 3,000 ppm adipic acid prior to solids precipitation, the calcium sulfite crystals formed as platelet clusters or rosettes. As the concentration of adipic acid was increased the crystals became smaller and less plate-like until at 10,000 ppm adipic acid in the slurry solution the crystals were submicron in size and resembled popcorn shaped spheres (5). These results suggest that adipic acid effects the nucleation rate of calcium sulfite and certainly can drastically change the particle size distribution and crystal morphology of precipitated solids.

The batch precipitation tests show dramatic effects of adipic acid slurry concentration and solid phase oxidation fraction on coprecipitation of adipic acid in scrubber solids. Real world scrubbers would probably never operate at adipic acid concentrations as high as those tested and would also not likely ever produce pure phase calcium sulfite hemihydrate. Therefore, the magnitude of the results observed is somewhat a product of the laboratory test conditions. The results do, however, establish the potential importance of adipic acid coprecipitation and, hence, the need for analysis of scrubber solids for adipic acid when determining adipic acid chemical degradation rates by a mass balance calculation approach.

Conclusions

Conclusions resulting from the bench-scale investigation of adipic acid degradation are listed below.

- 1) Sulfite oxidation is a necessary and sufficient condition for adipic acid degradation. The results of baseline testing, show that the degradation rate is directly proportional to the sulfite oxidation rate. The adipic acid degradation rate is also dependent on the adipic acid concentration.
- 2) Manganese ions in the hold tank resulted in a decrease in the adipic acid degradation rate. Since manganese is a sulfite oxidation catalyst, the decrease in the degradation rate is most likely associated with a change in the sulfite oxidation mechanism. The adipic acid degradation rate was found to depend on pH when manganese ions were present.
- 3) Lower adipic acid degradation rates were observed when Springfield limestone, rather than CaCO_3 , was used as the alkaline species. This result is due to the presence of soluble manganese in the limestone.
- 4) Adipic acid degradation was found to depend on temperature. An Arrhenius activation energy of 10.6 Kcals/mole was observed.
- 5) Large amounts of adipic acid were coprecipitated or occluded in the scrubber solids. The concentration of adipic acid in the solids was a function of both the liquid phase adipic acid concentration and the oxidation fraction in the solids.

The results from bench-scale adipic acid degradation testing can be used to estimate the adipic acid degradation rate and the total consumption rate of adipic acid for full-scale systems. An example of such an estimate is given in Figure 7. This figure shows the total consumption of adipic acid resulting from losses due to chemical degradation and losses in both the solid and liquid phases of the filter cake as a function of percent solids oxidation. The bases of this estimate are given below:

- The chemical adipic acid degradation rate constant, K_d , was assumed to be 0.5 M^{-1} . This is typical of the degradation expected at pH 5.1 for systems in which manganese is present at concentrations of about 20 ppm.
- The liquid phase adipic acid concentration was assumed to be 2000 ppm.
- The weight percent solids in the filter cake, from which the adipic acid loss in liquid associated with the filter cake is calculated, was assumed to be that determined during full-scale testing in Springfield. Ten percent of the total solids were assumed to be inert, either from the fly ash or the limestone.
- The loss of adipic acid coprecipitated or occluded in the waste solids was estimated from the bench-scale relationship illustrated in Figure 5.
- Closed loop operation was assumed. That is, no blow-down or miscellaneous slurry losses were considered.

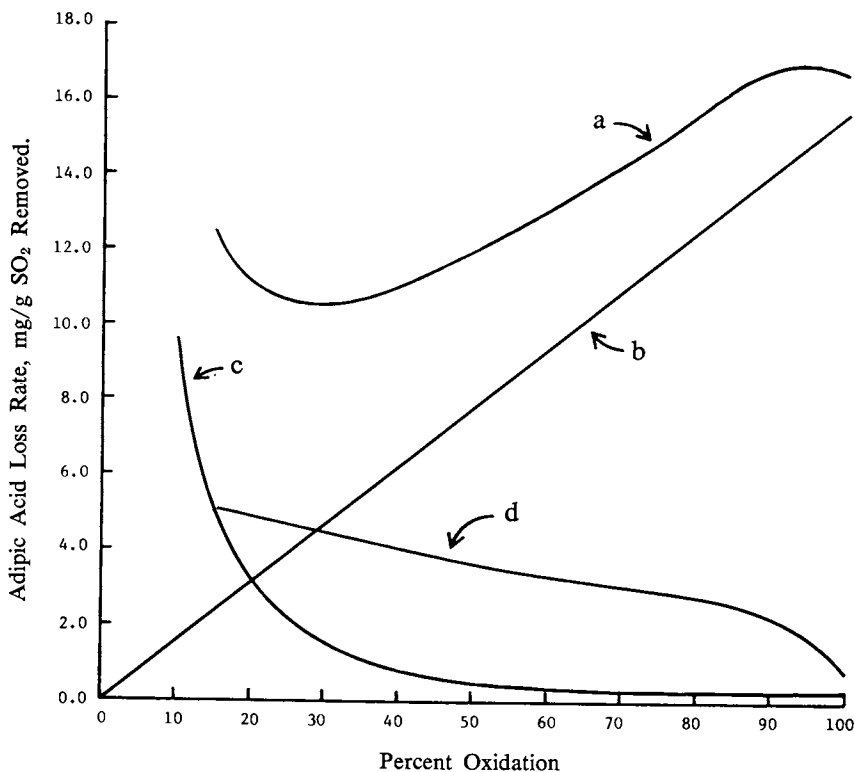


Figure 7. Estimated total adipic acid losses due to chemical degradation, coprecipitation or occlusion in the solids, and liquid entrained in the filter cake vs. percent oxidation. Key: a, total loss of adipic acid; b, loss of adipic acid due to chemical degradation; c, loss of adipic acid due to coprecipitation or occlusion in the solids; and d, loss of adipic acid in liquid entrained in the filter cake solids.

The results given in Figure 7 show that each of the three major loss mechanisms can be responsible for the largest fraction of the total adipic acid loss, depending on the percent oxidation. At oxidation levels up to 15 percent, the largest loss of adipic acid is due to coprecipitation in the solids. From 15 to 20 percent oxidation, the loss of adipic acid in the liquid associated with the filter cake represents the largest loss. About 30 percent oxidation, the chemical degradation of adipic acid predominates. Also, the total loss function is seen to pass through a minimum at roughly 30 percent oxidation.

The above example is intended to illustrate the adipic acid loss profile for a typical full-scale FGD system. Naturally, this profile can change considerably depending on operating conditions and site-specific factors. In the above example, degradation losses were based on a value of $K_d = 0.5 \text{ M}^{-1}$. This is the predicted adipic acid degradation rate of pH 5.1 with 20 ppm manganese. If the pH was reduced to 4.6 for example, a lower chemical degradation rate would be expected and the total loss curve would become flatter and less dependent on percent oxidation. The opposite would be the case for operation at pH 5.5. Losses due to chemical degradation are also affected by the concentration of manganese, the hold tank temperature, and the adipic acid concentration.

Losses of adipic acid in liquid associated with the filter cake can also be expected to be site-specific due to differences in solids dewatering equipment. The percent solids achieved in the filter cake may also be affected by the concentration of adipic acid.

Losses of adipic acid through blowdown or spills were not considered in this example. In some FGD installations this loss mechanism may represent a large fraction of total adipic acid losses.

Literature Cited

1. Rochelle, G., "The Effect of Additives on Mass Transfer in CaCO_3 and CaO Slurry Scrubbing of SO_2 from Waste Gases," *Ind. Eng. Chem. Fundam.*, 16: 67-75, 1977.
2. Meserole, F.B.; Lewis, D.L.; Nichols, A.W.; and Rochelle, G. "Adipic Acid Degradation Mechanism in Aqueous FGD System," Final Report, EPA-600/7-79-224, Environmental Protection Agency, Research Triangle Park, NC, September, 1979.
3. Meserole, F.B.; Lewis, D.L.; and Kurzawa, F.T. "Further Study of Adipic Acid Degradation in FGD Scrubbers," Final Report, EPA-600/7-80-152, Environmental Protection Agency, Research Triangle Park, NC, August, 1980.
4. Daniels, F. and Alberty, R.A. "Physical Chemistry," Fourth Edition, John Wiley and Sons, Inc., 1975, pp. 316-18.

5. Jarvis, J.B.; Terry, J.C.; Schubert, S.A.; and Utley, D.L. "Effect of Trace Metals and Sulfite Oxidation on Adipic Acid Degradation," Draft Final Report, Environmental Protection Agency, Contract No. 68-02-3171 with Radian Corporation, Austin, TX, July, 1981.

RECEIVED January 12, 1982.

Buffer Additives for Lime/Limestone Slurry Scrubbing

GARY T. ROCHELLE, WILLIAM T. WEEMS, RAYMOND J. SMITH,
and MARY W. HSIANG

University of Texas at Austin, Department of Chemical Engineering, Austin, TX 78712

Buffer additives are attractive for enhancing SO₂ removal and/or CaCO₃ utilization in lime/limestone slurry scrubbing processes for flue gas desulfurization. This work was sponsored by EPA to provide experimental data on commercial synthesis, gas/liquid mass transfer enhancement, and oxidative degradation of useful buffer additives.

Sulfopropionic and sulfosuccinic acids were synthesized by addition of bisulfite to unsaturated acids. At pH 5, 55°C, and 0.5 N ionic strength, the second-order rate constants and activation energies for sulfonation of acrylic, fumaric, and maleic acids were, respectively; 0.21 M⁻¹ min⁻¹, 14 kcal/gmol; 0.031 M⁻¹ min⁻¹, 6.1 kcal/gmol; and 0.52 M⁻¹ min⁻¹, 17 kcal/gmol. β-Hydroxypropionic acid was synthesized by hydration of acrylic acid at 100 to 140°C with catalysis by H₂SO₄ or H⁺-loaded cation exchange resin. At 100°C the second-order hydration rate constant was 0.11 M⁻¹ hr⁻¹ with an activation energy of 17 kcal/gmol.

Enhancement of SO₂ absorption by buffers was measured at 55°C in 0.3 M NaCl and 0.1 M CaCl₂ for acetic, adipic, hydroxypropionic, sulfopropionic, and sulfosuccinic acids and for basic aluminum sulfate. These results were correlated by mass transfer with equilibrium reactions. Sulfopropionic acid and basic aluminum sulfate were less effective than expected. Relative economics were developed for these and seven additional buffers.

Organic acid oxidation in conjugation with oxidation of CaSO₃ slurry was studied for seven acids. Degradation of adipic acid and other aliphatic and sulfo carboxylic acids was least at pH 4.3 with 1.0 mM dissolved Mn and greatest at pH 5.5 without Mn. Hydroxypropionic and hydroxyacetic acids inhibited sulfite oxidation and were less subject to degradation. Fumaric acid degraded faster than the other alternatives.

0097-6156/82/0188-0243\$6.75/0
© 1982 American Chemical Society

The most attractive acids for further testing are adipic, sulfosuccinic, hydroxypropionic, and hydroxyacetic.

Lime/limestone slurry scrubbing is the dominant commercial technology for flue gas desulfurization (1). SO_2 is absorbed at 50-55°C and pH 5.5-6.0 in an aqueous slurry of excess CaCO_3 and product solids. The $\text{CaSO}_3/\text{CaSO}_4$ product is disposed of as solid waste. With greater than 500-1000 ppm SO_2 in the flue gas, SO_2 absorption is controlled by liquid-film mass transfer resistance because of the limited solubility of SO_2 gas and alkaline solids. Additives that buffer between pH 3 and pH 5.5 enhance SO_2 absorption by providing dissolved alkaline species for reaction with SO_2 (8).

The most extensive early work on buffer additives was done by TVA who screened a large number of organic acids including adipic, phthalic, and hydroxyacetic (2) and tested benzoic acid in laboratory and pilot plant CaCO_3 scrubbing systems (3,4). Independently at the same time, Chemico Corp. tested and was issued a patent on the use of formic, acetic, and propionic acids in CaCO_3 slurry scrubbing (5). Wasag *et al.* (6) tested several organic acids in a bench-scale scrubber and concluded that citric acid was a superior alternative.

Rochelle evaluated additional organic acids including sulfopropionic and sulfosuccinic. He developed a model for mass transfer with irreversible reactions which predicted that as little as 3 to 12 mM organic buffer would be effective in improving SO_2 absorption (8). He showed that buffer additives should be especially attractive when used with forced oxidation in a limestone slurry scrubbing system (1). At the advice of Rochelle, adipic acid was tested by EPA in the 300cfm pilot plant at Research Triangle Park (9) and in the 10 MW scrubbers at the TVA Shawnee power plant (10, 11, 12). The EPA development program has culminated in a 194 MW demonstration at Springfield, Missouri (13).

The testing at Shawnee has shown that adipic acid is effective at concentration levels of 3 to 20 mM. SO_2 removal at typical operating conditions was increased from 80-85% without adipic acid to 95-99% with 10 to 20 mM adipic acid. Simultaneously limestone utilization was increased from 70-80% to 90-95%.

An attractive buffer additive should be inexpensive, should provide mass transfer enhancement at low concentrations, and should be nonvolatile and chemically stable at scrubber conditions. This paper is a report of work sponsored by EPA to provide experimental data for the evaluation of buffer additive alternatives.

The important classes of inexpensive, nonvolatile buffers include polycarboxylic acids such as adipic, hydroxycarboxylic acids such as hydroxypropionic, and sulfocarboxylic acids such

as sulfopropionic. Some of these alternatives are not commercially available and must be synthesized from inexpensive raw materials. Cavanaugh (14) demonstrated the synthesis of hydroxypropionic, sulfopropionic, and sulfosuccinic acids. In this paper, we present quantitative reaction kinetics for the synthesis of these three alternatives (15).

Mass transfer enhancement depends on the buffering properties and diffusivity of the additive. Cavanaugh (14) measured effective pK_a values of buffer alternatives at scrubber conditions. Chang and Rochelle (16) developed a model of enhancement based on mass transfer with equilibrium reactions and experimentally demonstrated its effectiveness with acetic and adipic acid at 25°C. In this paper, we present experimental and model results at 55°C with several buffer alternatives (17).

Organic acids are normally stable to oxidation, but laboratory and pilot plant results (18) have shown that adipic acid oxidizes in conjugation with sulfite oxidation in the scrubber. This paper reports oxidative degradation rate of adipic acid as a function of pH and Mn concentration (19). Results are also presented on sulfopropionic, sulfosuccinic, succinic, hydroxypropionic, and hydroxyacetic acids (20).

Buffer Synthesis

Sulfo and hydroxy carboxylic acids are attractive as buffer additives because the additional hydrophilic groups make both the buffer and its degradation products nonvolatile in aqueous solution. Keller (21) patented the use of sulfosuccinic acid in a flue gas desulfurization process using H_2S regeneration. Rochelle (7) evaluated available kinetic data on sulfite addition to maleic or acrylic acid to give sulfosuccinic or β -sulfopropionic acid. Cavanaugh (14) demonstrated the feasibility of hydrating acrylic acid with H_2SO_4 catalysis at 100°C to get β -hydroxypropionic acid.

This paper reports measurements of reaction kinetics for sulfonation of maleic, fumaric, and acrylic acids by sulfite addition and for hydration of acrylic acid with catalysis by H_2SO_4 or cation exchange resin. The kinetics were measured by sampling of isothermal batch reactors.

In sulfonation experiments the extent of reaction was determined by iodine titration for total sulfite. Solutions initially containing 0.05 to 0.20 M unsaturated acid were maintained at approximate pH values by lactate, acetate, or phosphate buffers. NaCl, $CaCl_2$, or $MgCl_2$ were added to give changes in ionic environment.

In hydration experiments, acrylic acid was determined by ion exclusion chromatography (ICE) on a Dionex ion chromatograph. Hydroxypropionic acid was evident on the chromatograms, but was not quantified because of the lack of an adequate standard. Hydration was catalyzed at 100 to 140°C by 0.1 to 1.5 M H_2SO_4 or

by H^+ -loaded sulfonated polystyrene resin (Dowex 50W-X4) with an exchange capacity of 1.3 meq/cm^3 (wet basis) and 67% moisture content.

Sulfocarboxylic Acids. Measured sulfonation rate constants are presented in Table I. The sulfonation reactions follow a second-order mechanism:

$$\text{rate (M/min)} = k_s [\text{acid}]_T [\text{SO}_3^-]_T$$

The rate constants do not vary significantly from pH 3.5 to 7.0, but no reaction occurs at pH 2 or 13. The sulfonation rates increase with ionic strength. With fumaric and maleic acids, there may also be an additional catalytic effect of Mg^{++} or Ca^{++} .

The second-order rate constants ($M^{-1} \text{ min}^{-1}$) for sulfonation at 1.2 N ionic strength in Na^+ solutions at pH are given by:

$$\text{acrylic: } k_s = 4.48 \times 10^8 \exp(-14,100/RT)$$

$$\text{fumaric: } k_s = 372 \exp(-6100/RT)$$

$$\text{maleic: } k_s = 2.38 \times 10^{11} \exp(-17,500/RT)$$

At 55°C with 0.5N ionic strength the constants are $0.21 \text{ M}^{-1} \text{ min}^{-1}$ for acrylic, $0.031 \text{ M}^{-1} \text{ min}^{-1}$ for fumaric, and $0.52 \text{ M}^{-1} \text{ min}^{-1}$ for maleic.

At 80°C , Hagglund and Ringbom (22) measured rate constants of 0.3 to $0.8 \text{ M}^{-1} \text{ min}^{-1}$ for acrylic acid, $0.086 \text{ M}^{-1} \text{ min}^{-1}$ for fumaric acid, and $0.16 \text{ M}^{-1} \text{ min}^{-1}$ for maleic acid. These compare to our extrapolated values at 80°C of 0.96 , 0.062 and $3.5 \text{ M}^{-1} \text{ min}^{-1}$, respectively. Our higher value with maleic acid may be a result of higher ionic strength or different pH. At 25°C and pH 3-5, Van Der Zanden (23) measured rate constants of $0.0019 \text{ M}^{-1} \text{ min}^{-1}$ and $0.0040 \text{ M}^{-1} \text{ min}^{-1}$ for fumaric and maleic acids, respectively, compared to our higher values of 0.012 and $0.035 \text{ M}^{-1} \text{ min}^{-1}$. Morton and Landfield (24) measured activation energies of 12.4 to 18.0 kcal/gmol for sulfonation of several unsaturated nitriles and esters, comparable to our values for maleic and acrylic acids. However, our sulfonation rates at 25°C for acrylic and maleic acids are 50 to 100 times faster than the measured rates for acrylonitrile and methyl acrylate.

Because dissolved sulfite is present in a typical $CaO/CaCO_3$ scrubber system, it is conceivable that unsaturated acids would sulfonate if added directly to the scrubber system. For the sulfonation reactions, a scrubber system can be characterized as a completely stirred tank reactor with a residence time equal to the ratio of solution inventory and the rate of loss of solution with the waste solids. Assuming 10 mM total dissolved sulfite, 55°C , 0.5 N ionic strength, and 130 hours residence time, the fraction of unsulfonated acid that would leave the system is 6%

Table I: Sulfonation Rates of Unsaturated Acids

<u>T(°C)</u>	<u>pH</u>	<u>Total Na (M)</u>	<u>Ionic Strength (N)</u>	<u>k_s (M⁻¹ min⁻¹)</u>
<u>Acrylic Acid</u>				
25	4.2	0.90	0.45	0.020
24	4.8	0.70	0.35	0.022
24	4.8	0.80	0.40	0.021
25	4.9	0.80	0.45	0.025
26	4.9	0.90	0.45	0.027
55	3.3	0.10 ^a	1.05	0.21
55	3.6	0.70	0.35	0.21
55	4.3	3.20	1.60	0.43
55	4.3	0.20 ^c	2.10	0.46
55	4.9	0.70	0.35	0.20
55	6.8	0.95	0.47	0.20
<u>Fumaric Acid</u>				
25	5.4	1.24	0.45	0.012
55	4.3	0.98	0.49	0.033
55	4.7	1.26	0.63	0.031
55	4.9	0.40 ^b	1.0	0.11
55	6.1	1.32	0.66	0.038
55	7.1	1.25	0.62	0.031
55	12.9	1.21	0.60	NR
<u>Maleic Acid</u>				
25	4.7	0.90	0.45	0.035
55	3.3	0.10 ^a	1.05	0.31
55	4.6	1.08	0.54	0.52
55	5.1	0.20 ^b	0.90	0.97

^a plus 0.5 M Ca⁺⁺, ^b plus 0.4 M Mg⁺⁺, ^c plus 1.0 M Mg⁺⁺.

Table II: Hydration of Acrylic Acid ^a

<u>T(°C)</u>	<u>Acrylic Acid (M)</u>	<u>H₂SO₄ (M)</u>	<u>k_h (M⁻¹ hr⁻¹)</u>
55	2.0	1.5	NR
100	2.0	1.0	0.11
100	2.0	resin	0.11
105	2.0	1.5	0.20
105	2.0	0.5	0.15
105	4.0	0.5	0.26 ^b
105	2.0	0.1	0.18
105	2.0	0	NR
120	1.9	1.0	0.38
140	2.0	1.5	>1.6

^a forward + reverse rate constants (M⁻¹ hr⁻¹)

^b includes polymerization

American Chemical
Society Library
1155 16th St., N.W.

for acrylic, 29% for fumaric, and 4% for maleic. Therefore, in situ sulfonation is feasible for acrylic acid and maleic acid, but is only partially effective for fumaric acid.

Acrylic acid and maleic anhydride (the commercial form of maleic acid) require some precautions for safe handling. If these precautions are unacceptable to the user, these unsaturated acids can be easily sulfonated offsite by reaction with sodium sulfite. Sodium sulfosuccinate was prepared successfully by adding 3.3 gmol Na_2SO_3 and 3.0 gmol maleic anhydride to one liter of water. The temperature increased from 25 to 80°C and the solids dissolved within one minute. The solution did not precipitate when cooled to 6°C. Therefore, the sulfonated acids could probably be prepared in a tank car and shipped as concentrated solution directly to the user.

Sulfopropionic and sulfosuccinic acids were prepared for subsequent laboratory use by mixing 1 gmol Na_2SO_3 and 1 gmol acrylic or maleic acid in 1 liter of water at 55°C for 10 to 15 hours. Utilization of the sulfite was 95 to 98% as determined by iodine titration.

Hydroxypropionic Acid (HP). Measured hydration rate for acrylic acid are presented in Table II. The hydration reaction is first-order in acrylic acid (AA) and first-order in H^+ . The reaction is reversible at high conversions, but the data in Table 2 were taken at low conversions and assume the reaction is irreversible so that only the forward rate constant is given. The net reaction rate is given by:

$$\text{rate (M/hr)} = k_f [\text{H}^+] [\text{AA}] - (k_f/K) [\text{H}^+] [\text{HP}]$$

where the equilibrium constant K is defined by:

$$K = [\text{HP}] / [\text{AA}]$$

In Table 2, the H^+ concentrations were estimated assuming 1 mole H^+ /mole H_2SO_4 or from the nominal exchange capacity of the resin. The second-order forward rate constant ($\text{M}^{-1} \text{hr}^{-1}$) for both resin and H_2SO_4 catalysis is correlated by:

$$k_h = 1.14 \times 10^9 \exp (-17,000/RT)$$

In at least one experiment (105°C, 4 M AA, 0.5 M H_2SO_4) there was visual evidence of acrylic acid polymerization, giving a faster apparent rate constant. Polymerization should be minimized by reduced acrylic acid concentrations and increased catalyst concentrations.

Pressman and Lucas (25) measured rates and equilibrium for up to 0.05 M acrylic acid in perchloric acid with the following results:

$T(^{\circ}\text{C})$	$k_f (\text{M}^{-1} \text{hr}^{-1})$	K
110.6	0.159	11.3
119.8	0.296	9.27
134.7	---	6.79

Their activation energy (20.4 kcal/gmol) was somewhat higher than ours (17 kcal/gmol). Their rate constant at 120°C (0.296 M⁻¹hr⁻¹) was somewhat lower than ours (0.38 M⁻¹hr⁻¹).

Using our measured rate data and equilibria from Pressman and Lucas, the estimated reactor residence times for 85% conversion with 1 M H₂SO₄ at 105°C are 14 hours for a batch or plug flow reactor, 85 hours for a single completely stirred tank reactor (CSTR), or 33 hours for two CSTR's in series. If the reaction was carried out at the scrubber site, no additional purification should be required, but there would be a makeup requirement for sulfuric acid.

Hydroxypropionic acid for subsequent laboratory tests was taken from the final solution of the experiment at 105°C with 2 M acrylic acid and 1.5 M H₂SO₄. After 13 hours the total conversion of acrylic acid to hydroxypropionic acid was 85%.

Gas/Liquid Mass Transfer Enhancement

Chang and Rochelle (16) measured SO₂ absorption at 25°C in a continuous stirred reactor with an unbroken gas/liquid interface. They varied P_{SO₂}, pH, and concentrations of acetic acid and adipic acid in 0.3 M NaCl. Because SO₂ absorption was quantified by liquid-phase material balance, there were no experiments with greater than 1 mM total dissolved sulfite.

The apparatus used by Chang and Rochelle was modified for this work (17). Heating tape was added to liquid and gas stream inlets to permit operation at 55°C. Gas phase analysis and flow measurement were refined, and SO₂ absorption rate was determined by gas-phase material balance, permitting operation with high concentrations of sulfate and total sulfite. Tighter pH control was achieved by continuously adding 1.0 M NaOH directly to the reactor.

The apparatus was characterized at 55°C and 540 rpm by SO₂ absorption into 0.3 M NaOH giving k_{oA} of 4.93×10^{-3} gmol/bar-sec and into 0.3 M HCl giving k_{oA} of 1.5×10^{-3} l²/sec. Experiments were performed in 0.3 M NaCl or 0.1 M CaCl₂ at pH 5.5 or 4.2 with 0 to 40 mM of adipic, acetic, sulfopropionic, sulfosuccinic, or hydroxypropionic acids or AlCl₃. The gas-phase SO₂ concentration was adjusted to give about 1000 ppm at the gas-liquid interface. The enhancement of the liquid-film mass transfer coefficient by

chemical reaction was calculated from SO_2 absorption rate, SO_2 gas concentration, SO_2 Henry's constant, $k_{\lambda}^{\circ}\text{A}$, and $k_g\text{A}$ as in Chang and Rochelle (16).

Chang and Rochelle (16) developed an enhancement factor model based on approximate surface renewal with multiple equilibrium reactions. Their model included equilibria among and diffusion of the solution species: H^+ , SO_2 , HSO_3^- , SO_3^{2-} , H_2A , HA^- , and A^{2-} . The pK_a values of the buffer species, H_2A , HA^- , and A^{2-} , could be adjusted to represent any appropriate buffer. Activity coefficients were calculated from a modified Debye-Huckel limiting law (26).

The model of Chang and Rochelle (16) was used in this work with appropriate equilibrium constants and diffusivities to represent operation at 55°C in 0.3 M NaCl or 0.1 M CaCl_2 (Tables III and IV). Because the model uses only diffusivity ratios, the diffusivities in NaCl solution were taken to be the same as those at infinite dilution and 25°C (16), assuming that the diffusivity ratios were independent of temperature and NaCl concentration. The equilibrium constants in NaCl solution were generally assumed to be independent of temperature and are based primarily on measurements by Cavanaugh (14) and the equilibrium program by Lowell et al., (26). The solubility of undissociated SO_2 in water was given by Rabe and Harris (27):

$$[\text{SO}_2] = P_{\text{SO}_2}/H$$

$$H = \exp(-9.3795 + 2851.1/T)$$

Effective equilibrium constants in 0.1 M CaCl_2 were measured by Cavanaugh (14) or estimated by the Radian equilibrium program (26). As given in Table IV, these constants include the effects of ionic strength and ion pairing on the activity of the anions. Ion pairs, such as CaSO_3° , are not treated as separate species, but are accounted for as an effect on the activity of simple ions, such as SO_3^{2-} .

Empirically, it was found that diffusivities in 0.1 M CaCl_2 were consistently less than in 0.3 M NaCl. To get good correlation of the experimental data the diffusivities of all monovalent anions were reduced 25% and the diffusivities of all divalent anions were reduced 45% from their values in 0.3 M NaCl. Weems (17) presents more extensive data on the effects of Na^+ , Mg^{++} , and Ca^{++} on the diffusivities of SO_3^{2-} and HSO_3^- .

Figure 1 compares calculated and measured values of the liquid-film enhancement factor with five buffers. The calculated values are within 10% of the measured values. In order to fit the measured data, the diffusivity of sulfopropionic acid was reduced by an additional 50% from the value estimated by Chang and Rochelle (16).

Table III. Physical Properties at 55°C, 0.3 M NaCl

Buffer	Diffusivities x 10 ⁵ (cm ² /sec)			pK _a ^g Values	
	H ₂ A	HA	A	pK ₁	pK ₂
Acetic		1.19 ^d	1.09 ^b	4.66	
Adipic	0.74 ^a	0.72	0.71 ^c	4.07 ^f	5.10 ^f
Benzoic		1.21 ^a	0.87 ^b	4.05 ^f	
Formic		1.46 ^a	1.43 ^b	3.60	
Hydroxyacetic		0.98 ^a	0.91	3.60	
Hydroxypropionic		0.99 ^a	0.91	4.33 ^f	
Lactic		0.99 ^a	0.91	3.60 ^f	
Phthalic	0.72 ^a	0.71	0.69 ^b	3.02 ^f	4.6 ^f
Succinic	0.86 ^a	0.84	0.81 ^b	4.10	5.25
Sulfopropionic		0.45	0.40	4.06	
Sulfosuccinic	0.73 ^a	0.70	0.66	3.33 ^f	4.84 ^f
Fumaric	0.86 ^a	0.84	0.81 ^b	2.97	4.08
Sulfate		1.20 ^b	0.90 ^b	1.55	
Sulfite	1.76 ^e	1.33 ^b	0.98 ^b	2.02	7.4

^a Measured by Albery *et al.* (28) or estimated by his method,

^b Estimated from ionic conductivities in Ref. 29,

^c Ref. 30, ^d Ref. 31, ^e Ref. 32, ^f Ref. 14, ^g K_a = a_{H+}[A⁻]/[HA].

Table IV: Physical Properties at 55°C, 0.1 M CaCl₂

Buffer	Diffusivities x 10 ⁵ (cm ² /sec)			pK _a ^a Values	
	H ₂ A	HA	A	pK ₁	pK ₂
Acetic		1.19	0.82	4.45	
Adipic	0.74	0.54	0.39	3.98 ^c	4.86 ^c
Benzoic		1.21	0.65	3.90 ^c	
Formic		1.46	1.07	3.45	
Clycolic		0.98	0.68	3.42	
Hydroxypropionic		0.99	0.68	4.26 ^c	
Lactic		0.99	0.68	3.36 ^c	
Phthalic	0.72	0.53	0.38	2.82 ^c	4.4 ^c
Succinic	0.86	0.53	0.45	3.86	5.01
Sulfopropionic		0.45	0.30	4.06 ^c	
Sulfosuccinic	0.55	0.39	0.36	3.14 ^c	4.43 ^c
Fumaric	0.86	0.53	0.45	2.73	3.84
Sulfate		1.20 ^a	0.68	1.60 ^b	
Sulfite	1.76	1.00	0.57	2.02 ^b	6.2 ^b

^a K_a = a_{H+}[A⁻]/[HA], ^b Ref. 26, ^c Ref. 14.

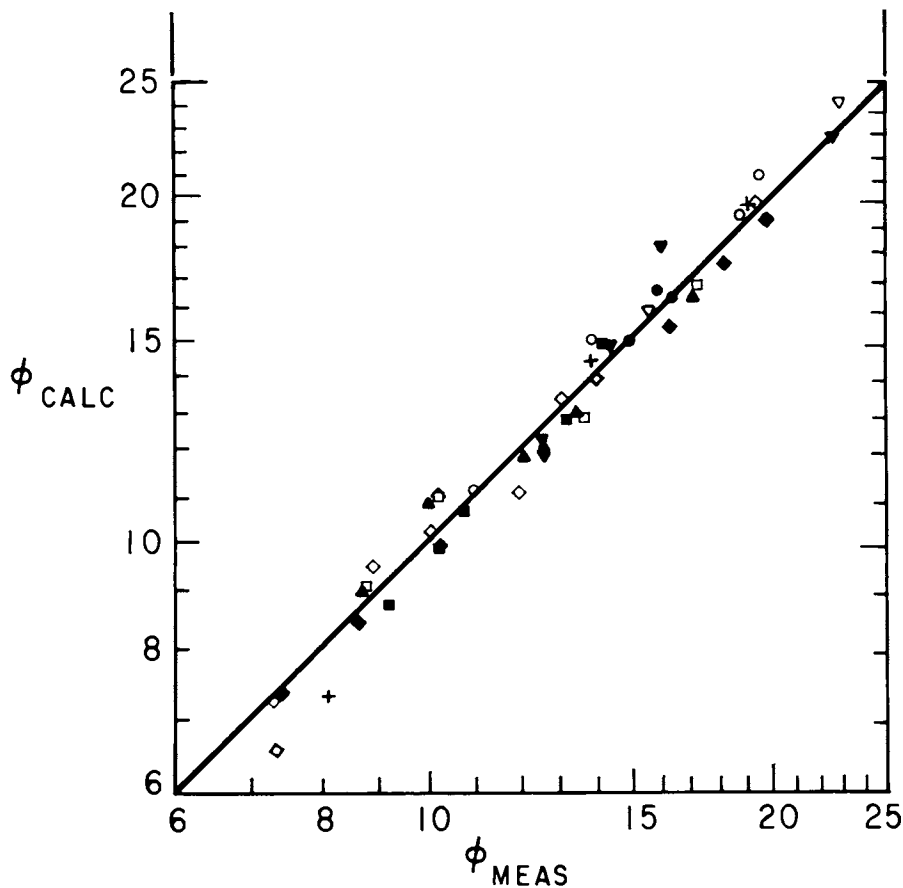


Figure 1. Comparison of measured and calculated liquid-film enhancement factors with 0 to 40 mM buffer and 1000 ppm SO_2 at pH 5.5 and 25°C. Key: \circ , sulfosuccinic in 0.3 M NaCl; \bullet , sulfosuccinic in 0.1 M CaCl_2 ; \blacktriangle , hydroxypropionic in 0.1 M CaCl_2 ; \square , sulfopropionic in 0.3 M NaCl; \blacksquare , sulfopropionic in 0.1 M CaCl_2 ; ∇ , acetic in 0.3 M NaCl; \blacktriangledown , acetic in 0.1 M CaCl_2 ; $+$, adipic in 0.1 M CaCl_2 ; \diamond , adipic in 0.3 M NaCl (pH 4.2); and \blacklozenge , adipic in 0.1 M CaCl_2 (pH 4.2).

Experiments with up to 20mM AlCl_3 in 0.1 M CaCl_2 at pH 3.8 gave no measureable enhancement of SO_2 absorption, even though basic aluminum chloride is an excellent buffer at pH 3.8. The lack of effectiveness of the aluminum buffer may result from the formation of large, slow-moving polynuclear aluminum complexes, or it may reflect a slow reaction rate between aluminum complexes and H^+ .

Figure 2 shows the calculated liquid-film enhancement factor for five buffers as a function of buffer concentration in 0.1 M CaCl_2 at pH 5.5 with 1000 ppm SO_2 at the gas/liquid interface. On a molarity basis, adipic acid is most attractive and sulfo-propionic acid is least attractive. With no buffer, the enhancement factor is 7.2 because of the hydrolysis of SO_2 and because of enhancement by SO_3^- . At 10 mM total adipic acid, the enhancement factor is 20, or about 3 times greater than in the absence of buffer.

Figure 3 illustrates the effect of adipic acid on the overall enhancement of SO_2 absorption. It gives the ratio of the overall mass transfer coefficient, K_g , to the gas-film coefficient, k_g , as a function of a dimensionless parameters including adipic acid concentration. The overall coefficient includes an effect of k^0 and the liquid-film enhancement factor which increases with adipic acid concentration. The ratio, K_g/k_g , represents the fraction resistance of the gas film and cannot exceed 1.0.

Greater values of K_g/k_g represent proportionately better scrubber performance. This specific figure is valid for scrubbers with ratio of mass transfer coefficients without enhancement given by $\text{H}^+ k^0/k_g$ equal to 0.2.

As shown in Figure 3, adipic acid will have a greater effect with higher SO_2 gas concentration, because at lower concentration SO_2 absorption is already controlled mostly by gas film resistance. With less total dissolved sulfite, liquid-film resistance is reduced by SO_2 hydrolysis to H^+ and HSO_3^- , even in the absence of buffer.

In all cases, the curves asymptote to gas phase control with an abscissa value of 10 to 40. 10 mM adipic acid and 10 mM sulfite at pH 5 with 2500 ppm SO_2 gives K_g/k_g of 0.91. This corresponds to an improvement of 1.8 because of adipic acid addition.

Table V gives the calculated concentrations of twelve buffers required to get an enhancement factor of 20 in 0.1 M CaCl_2 with 10 mM total sulfite at pH 5.0 with 1000 ppm SO_2 at the gas liquid interface. Relative costs have been calculated assuming that makeup rates would be proportional to concentration

Formic and acetic acids are most attractive, but would probably be volatile under scrubber conditions (8). Succinic and lactic acids would not be cost-effective if purchased at market price. Fumaric acid is more subject to oxidative degradation. Phthalic and Benzoic acids may give undesirable aromatic degradation products. Therefore, the most useful buffers appear to be hydroxypropionic, sulfosuccinic, fumaric, sulfo-propionic, adipic, and hydroxyacetic.

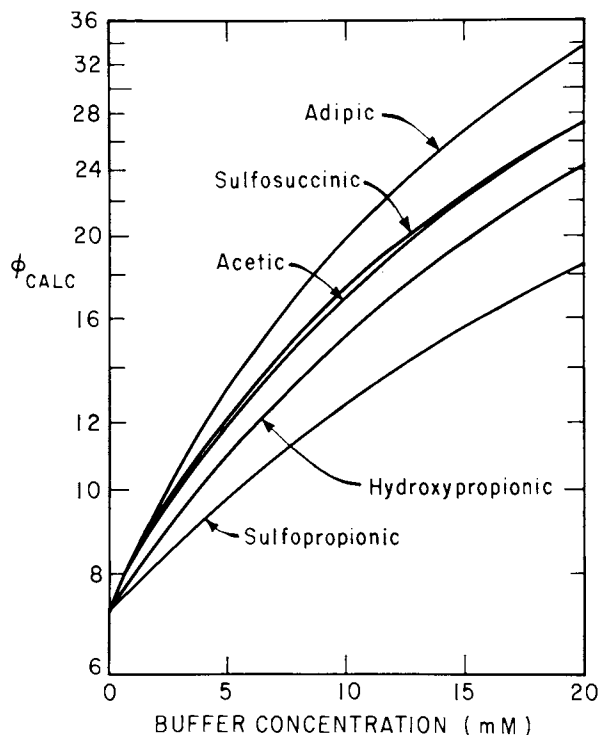


Figure 2. Calculated effect of buffer alternatives on the liquid-film enhancement factor, 0.1 M CaCl_2 , 55°C, pH 5.5, 3 mM total sulfite, 1000 ppm SO_{2t} .

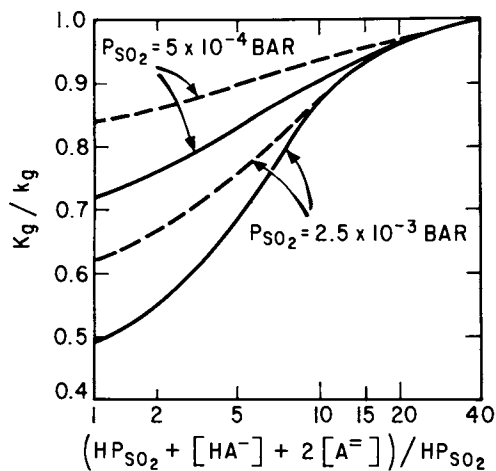


Figure 3. Overall mass transfer enhancement by adipic acid, 55°C, 0.1 M CaCl_2 , pH 5. Total sulfite: ---, 0 mM; and —, 10 mM.

Table V: Relative Costs of Organic Acids,
 $\phi=20$, 55°C , $\text{pH } 5.0$, 0.1 M CaCl_2 , $10 \text{ mM total sulfite}$, 1000ppm SO_2

<u>Organic Acid</u>	<u>Concentration</u> (mM)	<u>Price</u> (\$/lb mol)	<u>Relative</u> <u>Cost</u>
Formic	21.1	12.28	0.28
Acetic	15.6	21.62	0.37
Hydrosypropionic	19.7	34.59	0.75
Sulfosuccinic	16.3	43.15	0.77
Sulfopropionic	25.6	34.59	0.97
Adipic	11.8	77.45	1.00
Phthalic	18.1	55.58	1.10
Benzoic	17.0	57.46	1.13
Fumaric	19.1	66.16	1.38
Hydroxyacetic	32.0	39.66	1.39
Succinic	12.3	134.11	1.80
Lactic	34.4	78.82	2.97

Oxidative Degradation

Unexpected loss of adipic acid accompanied by valeric acid odor was first observed by Borgwardt (9) in pilot plant testing of adipic acid with forced oxidation. These observations were confirmed by larger scale tests at the Shawnee test facility (10). Additional Shawnee results have shown that unexpected losses are reduced at pH less than 5.0 and increased by forced oxidation (12). Radian analyzed field samples and found significant quantities of valeric acid and glutaric acid (18). They were able to duplicate this degradation of adipic acid by oxidizing CaSO_3 slurry in the presence of adipic acid (33, 34). Later more extensive work by Radian has shown that unexpected losses of adipic acid can also occur by its coprecipitation in CaSO_3 solids (35).

Conjugated oxidation of carboxylic acids probably occurs by reaction with free radicals generated by sulfite oxidation. There is extensive literature on the conjugated oxidation of carboxylic acids with the oxidation of hydrocarbons or alcohols (36, 37, 38). The products of such conjugated oxidation are CO_2 and mono or dicarboxylic acids of shorter chain length than the original acid. Hence, conjugated oxidation of adipic acid could give CO_2 , glutaric acid, valeric acid and perhaps succinic acid and butyric acid.

The rate of carboxylic acid oxidation should be proportional to the rate of sulfite oxidation and the acid concentration:

$$\frac{d[A]}{dt} = k_d[A] \frac{d[\text{SO}_3^-]}{dt} T$$

or

$$\frac{d[A]}{d[\text{SO}_3^-]T} = k_d[A]$$

With batch oxidation of CaSO_3 slurry the integrated rate equation is:

$$\ln([A]_i/[A]) = k_d([\text{SO}_3^-]_{T_i} - [\text{SO}_3^-]_T)$$

The rate constant, k_d , should be reduced at higher dissolved sulfite because of reduced free radical concentrations at a given oxidation rate. The degradation rate may also be affected by sulfite oxidation catalysts or inhibitors that would change the concentrations and types of intermediate free radical species.

In this work, oxidation of 5 to 20 mM carboxylic acid has been measured during batch oxidation of 1 to 2 M CaSO_3 slurry at 55°C with pure oxygen sparged into an agitated reactor. CaSO_3 solids were usually synthesized by titration of 1 M CaCl_2 with 1 M Na_2SO_3 followed by filtering, washing, and drying. Slurry was analyzed for total sulfite by iodine titration. Filtered solution was analyzed for the specific carboxylic acids by a Dionex ion chromatograph using ion chromatography (IC) or ion exclusion chromatography (ICE) (19).

Initial work was performed in a glass reactor with good temperature control but no pH control. During the experiment pH drifted upward and the rate of oxidation decreased. The glass reactor was poorly agitated and complete oxidation of 2 M CaSO_3 slurry required 15 to 20 hours, even with 110 ml/min of oxygen.

Later work was performed in a plexiglass reactor with pH control by continuous addition of H_2SO_4 . Because of poor thermal conductivity, the temperature in this reactor increased from 55 to 70 or 80°C during the course of an experiment. The oxygen flow rate was 110 cm^3/min . With agitation at 950 rpm, the maximum sulfite oxidation rate was 0.4 to 0.5 M/hr; at 1340 rpm, it was 0.6 to 0.7 M/hr.

In a typical experiment 5 to 10 samples were analyzed for carboxylic acid and total sulfite. The rate constant, k_d , was obtained from a plot of $\ln[A]$ versus total sulfite. Figures 4 and 5 show results of a typical experiment.

Table VI summarizes the results of experiments with adipic, sulfosuccinic, sulfopropionic, succinic, glycolic and hydroxypropionic acids. The results are reported as the sulfite oxidation rate (M/hr) and the degradation rate constant, $k_d (\text{M}^{-1})$. Analytical accuracy generally allowed determination of k_d within $\pm 0.1 \text{ M}^{-1}$. In experiments with little or no sulfite oxidation, (A11, HP3, HP5, HA1, HA3, HA4), there was no measurable degradation of the carboxylic acid. Experiments with 5, 10, and 20 mM adipic acid (A21, A14, A18, A15, A23) showed that the degradation reaction is first order in the carboxylic acid concentration, as expected and modelled by k_d .

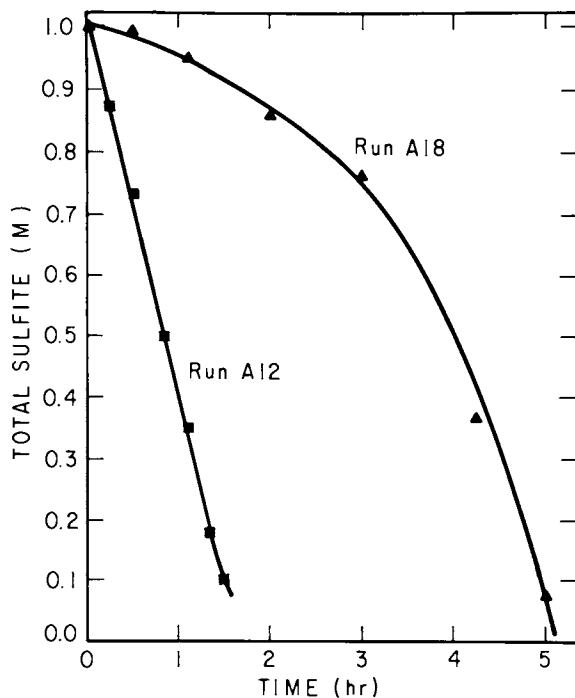


Figure 4. Sulfite oxidation in two typical experiments.

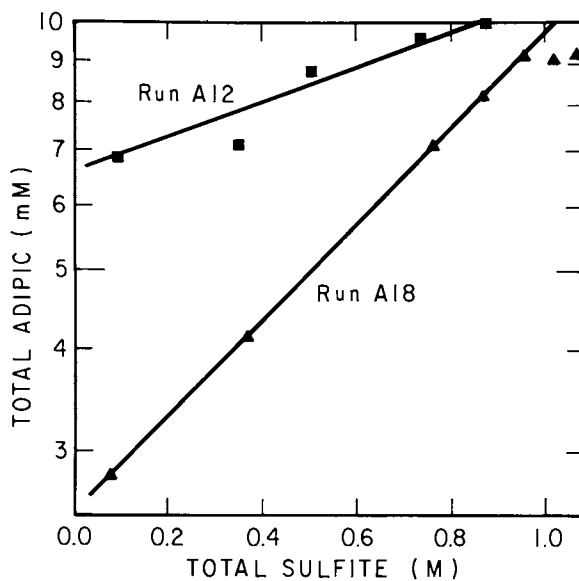


Figure 5. Adipic acid degradation in two typical experiments.

Table VI: Oxidative Degradation of Carboxylic Acids

Run	pH	Other Component ^a (mM)	Sulfite Oxidation Rate (M/hr)	Degradation Rate k_d (M ⁻¹)
Glass Reactor, 110 ml/min O ₂ , 500 ml slurry				
Sulfosuccinic (SS)				
SS1	5.0+	---	0.07	~1.0
Sulfopropionic (SP)				
SP1	5.0+	---	0.07	~1.0
Adipic (A)				
A1	5.0+	---	0.06	~1.5
A4	4.3+	---	0.04	~1.1
A5	5.0+	---	0.04	1.7
Plexiglass reactor, 110 ml/min O ₂ , 950 rpm, 1 L slurry				
A7	4.3	1 Fe ⁺⁺	0.46	1.2
A81 ^c	5.0	0.1+ Mn	0.37	0.3
A82	5.0	---	0.38	2.0
A83 ^c	5.0	0.1+ Mn	0.35	0.4
A9	5.0	300 Na ₂ SO ₄	0.44	0.3
A10	4.3	1 Fe ²⁺ , 1 Mn	0.38	0.3
A11	6.0	---	0.0	0.0
Plexiglass reactor, 1340 rpm				
A12	4.3	---	0.64	0.7
A13	4.3	1 Mn	0.67	0.1
A14	5.0	---	0.08	1.4
A15	5.0	1 Mn	0.68	0.2
A16	5.5	1 Mn	0.67	0.6
A17	4.7	1 Mn	0.70	0.2
A18	5.0	---	0.20	1.4
A19	5.5	---	0.13	1.3
A20	5.0	300 CaCl ₂	0.45	1.1
A21	5.0	5 A	0.26	1.6
A22	5.0	300 MgSO ₄	0.36	0.6
A23	5.0	1 Mn, 20A	0.78	0.3
A24	4.3	---	0.61	0.6
A25	5.0	0.1 Mn	0.62	1.3
A26	5.5	1 Mn	0.96	0.2
AA1	5.5	1 Mn	0.33	0.6
AA2	5.5	1 Mn, 10 HA	0.23	0.5
AA3	4.5	1 Mn, 10 HA	0.55	0.07
AA4	4.5	1 Na ₂ S ₂ O ₃	0.01	0
AA5	4.5	1 Mn, 1 Na ₂ S ₂ O ₃	0.42	0.11

Continued on next page.

Table VI -- continued

Succinic (S)				
S1	4.5	---	0.56	0.5
S2	4.5	1 Mn	0.69	~0
S3A	5.5	---	0.06	~5
S3B	5.5	1 Mn ⁺⁺ , 6.3 S	0.38	0.2
S4	4.5	0.33 Mn	0.41	~0
S5	4.4	0.1 Mn	0.54	0.5
β -Hydroxypropionic (HP)				
HP1	4.5	2HP	0.52	0.2
HP2	4.5	1 Mn	0.49	~0.1
HP3	4.5	25 HP	0.06	~0
HP4	5.5	25 HP, 1 Mn	0.57	~0
HP5	4.5	---	0.06	~0
Hydroxyacetic (HA)				
HA1	4.5	---	0.04	~0
HA2	5.5	1 Mn	0.74	~0
HA3	5.0	---	0.02	~0
HA4	5.0	0.1 Mn	0.06	~0
HA5	5.0	0.3 Mn	0.37	~0.1
AA2	5.5	1 Mn, 10 A	0.23	~0
AA3	4.5	1 Mn, 10 A	0.55	~0
Fumaric (F)				
F1	5.5	1 Mn	0.21	2.4

^aInitial carboxylic acid concentration is 10 mM unless noted

$$^b k_d = d \ln[\text{acid}] / d[\text{SO}_3^-]_T$$

^cThese runs used purchased CaSO₃ with Mn impurities

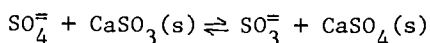
The sulfite oxidation was usually at a maximum rate at pH 4.3 or 4.5 or in the presence of 1 mM Mn. This rate was probably limited by oxygen mass transfer and increased with increasing agitation. Without Mn, the sulfite oxidation rate decreased with increasing pH and essentially stopped at pH 6.0. With agitation at 1390 rpm, the sulfite oxidation rate without catalysts or inhibitors was typically 0.5 to 0.7 M/hr at pH 4.3, 0.08 or 0.26 M/hr at pH 5.0, and 0.06 to 0.13 M/hr at pH 5.5. In the absence of Mn, the oxidation rate was typically faster at the end of an experiment than at its beginning.

Manganese had a catalytic effect on sulfite oxidation at concentrations as low as 0.1 mM (A25). At pH 5 or 5.5, 1 mM Mn permitted oxidation at the maximum rate of 0.6-0.7 M/hr.

Hydroxyacetic and hydroxypropionic acids inhibited sulfite oxidation at concentrations as low as 10 mM. At pH 5.0, 0.3 mM Mn was sufficient to overcome the inhibiting effects of 10 mM hydroxyacetic acid (HA4, HA5). In general, the hydroxy acids had little effect on the oxidation rate in the presence of 1 mM Mn.

Thiosulfate at 1 mM inhibited sulfite oxidation at pH 4.5 in the absence of Mn (AA4). However 1 mM Mn was enough to minimize the inhibiting effect of thiosulfate (AA5).

The addition of 0.3 M CaCl₂ or 0.3 M MgSO₄ increased the sulfite oxidation rate at pH 5. MgSO₄ increases the level of dissolved sulfite by the equilibrium:



CaCl₂ may introduce catalytic impurities or change oxygen bubble size in the reactor.

In the absence of dissolved Mn, the dicarboxylic or sulfo-carboxylic acids have degradation rate constants of 0.5-1.1 M⁻¹ at pH 4.3 or 4.5 and 1.4 to 2.0 M⁻¹ at pH 5 to 5.5. Mn has a definite inhibiting effect on the degradation of all the carboxylic acids. At pH 4.5 with succinic acid 0.33 mM Mn is sufficient to reduce *k_d* to 0.03 M⁻¹ from 0.45 M⁻¹ at 0.1 mM Mn (S4, S5). At pH 5.0, Mn of 0.1 to 0.3 mM introduced as an impurity in purchased CaSO₃ was sufficient to reduce the adipic acid degradation constant from 2.0 to 0.4 M⁻¹ (A81, A82, A83).

The effect of Mn is not as great at higher pH. 1 mM Mn gives adipic acid degradation constants of 0.1-0.2 M⁻¹ at pH 4.3 to 4.7, 0.3 M⁻¹ at pH 5, and 0.6 M⁻¹ at pH 5.5. Two experiments at pH 5.5 did give low values of *k_d*, but these may not be representative results (S3B, A26).

The addition of 0.3 M Na₂SO₄ or MgSO₄ at pH 5.0 reduced the degradation rate of adipic acid from 1.6 to 2.0 M⁻¹ to 0.3 to 0.6 M⁻¹. This effect was expected because of increased dissolved sulfite generated by the dissolved sulfate. The addition of 0.3 M CaCl₂ did not increase the degradation rate.

The hydroxy acids did not degrade as fast as the dicarboxylic and sulfocarboxylic acids. The maximum degradation constant observed with these acids was 0.2 M^{-1} with hydroxypropionic acid at pH 4.5 with no Mn. Run AA2 with 10 mM adipic, 10 mM hydroxyacetic, and 1 mM Mn at pH 5.5 gave k_d values of 0.5 M^{-1} for adipic and less than 0.1 for hydroxyacetic.

Fumaric acid degraded 2 to 4 times faster than adipic acid at pH 5.5 with 1 mM Mn (F1). The carbon-carbon double bond is apparently more susceptible to oxidation. Therefore, unsaturated acids should be sulfonated to avoid degradation. Since fumaric acid does not sulfonate rapidly in the scrubber, it is not an attractive buffer alternative.

Complete carbon material balances were not obtained on any of the degraded solutions. Valeric and glutaric acids were identified as degradation products of adipic acid, but account for less than 20% of the adipic acid loss. Sulfopropionic acid was identified as a degradation product of sulfosuccinic acid, but accounts for less than 10% of the total degradation.

Work on oxidative degradation is continuing. The objectives of future work will be to obtain better analyses of degradation products, to screen additional buffer alternatives, and to evaluate more potential catalysts and inhibitors.

Other Factors

The ultimate utility of a buffer additive will depend on a number of other factors. Because most systems will operate near CaCO_3 and CaSO_3 saturation, buffer properties should be primarily useful for gas/liquid mass transfer. However, additional buffer capacity at pH 5-6 would be useful in enhancing CaCO_3 dissolution (39) and in providing capacity for SO_2 absorption without CaCO_3 or CaSO_3 dissolution in the absorber. Therefore, the buffers with higher $\text{p}K_a$ values (adipic, phthalic, acetic, and sulfosuccinic) should give relatively greater overall effectiveness.

Specific results with hydroxypropionic and sulfopropionic acids indicate that these buffers inhibit CaCO_3 dissolution, probably because of polyacrylic acid impurities (39). These impurities are derived from the specific synthesis processes. In actual operation, the polyacrylic acid may be removed from the scrubber solution by precipitation of its calcium salt. If not, modifications of and/or separation of polyacrylic acid after synthesis may be necessary to make these buffers useful.

Coprecipitation of buffer with CaSO_3 may be an important additional source of buffer losses. Radian has shown that adipic acid is present in significant concentrations in CaSO_3 solids, especially with low concentrations of CaSO_4 in the solids (35). No results are available on other buffers.

Volatility of formic, acetic, and benzoic acids can be economically and environmentally significant at scrubber conditions. Even though these buffers are mostly dissociated and therefore nonvolatile at the pH of the bulk solution, they are mostly protonated and therefore volatile at the pH of the gas/liquid interface (2.5 to 3.5). In relatively open-loop scrubber systems with large solution losses, volatility losses are economically less significant and formic and acetic acids would be competitive with adipic acid. In staged or countercurrent absorbers with high pH solution in the last stage for gas contacting, it may be possible to minimize losses of volatile acids.

Waste or byproduct organic acids could be cost-effective alternatives. Adipic acid production by nitric acid oxidation of cyclohexanol/cyclohexanone generates byproduct consisting of glutaric and succinic acids which should perform like adipic acid. Air oxidation of cyclohexane to produce cyclohexanone as an intermediate for caprolactam generates a waste solution of adipic, hydroxyvaleric, glutaric, and other acids. This product should be comparable to a mixture of adipic and hydroxypropionic acids.

Conclusions

1. Adipic acid has attractive buffer properties and it is cost-effective, non toxic, and commercially available in large quantities. It coprecipitates with CaSO_3 and is subject to oxidative degradation, but these problems should be minimized by using forced oxidation at low pH with high concentrations of dissolved Mn.

2. The hydroxycarboxylic acids are uniquely inert to oxidative degradation and inhibit sulfite oxidation in the absence of Mn. Hydroxypropionic acid is economically attractive; however, its synthesis from acrylic acid gives polyacrylic acid impurities that would probably have to be separated. Glycolic acid is commercially available but economically somewhat less attractive.

3. Sulfosuccinic and sulfopropionic acids are economically attractive when synthesized in situ or offsite from maleic anhydride or acrylic acid. Both are subject to oxidation, but should give nonvolatile degradation products. Synthesis of sulfopropionic acid can give undesirable polyacrylic acid impurities.

4. Acetic and formic acids could be economically superior if volatilization were minimized or tolerated.

5. Benzoic acid is nearly competitive with adipic, but is volatile and aromatic.

6. Basic aluminum salts are ineffective for mass transfer enhancement.

Recommendations

1. Adipic acid should be used commercially in systems with forced oxidation at low pH with dissolved Mn.

2. Glycolic, sulfosuccinic, and waste acids should be tested in a pilot plant.

3. Additional laboratory work should be conducted on the following topics:

- a) coprecipitation of CaSO_3 and buffers other than adipic acid
- b) oxidative degradation catalysts and inhibitors
- c) oxidative degradation of buffers other than adipic acid
- d) elimination of polyacrylic acid from hydroxypropionic and sulfopropionic acids.

Nomenclature

A	= Gas/Liquid contact area, cm^2
H	= Henry's constant, bar M^{-1}
K	= Equilibrium constant for acrylic acid hydration, dimensionless
k_d	= Degradation rate constant, M^{-1}
k_f	= Forward rate constant of the hydration of acrylic acid, M hr^{-1}
k_g	= Gas film mass transfer coefficient, $\text{gmol}/\text{bar}\cdot\text{sec}\cdot\text{cm}^2$
K_g	= Overall gas film mass transfer coefficient, $\text{gmol}/\text{bar}\cdot\text{sec}\cdot\text{cm}^2$
k_h	= Apparent total rate constant of acrylic acid hydration, $\text{M}^{-1} \text{hr}^{-1}$
k_ℓ^o	= Liquid-film mass transfer coefficient for physical absorption, $\text{L}/\text{sec}\cdot\text{cm}^2$
k_s	= Sulfonation rate constant, $\text{M}^{-1}\text{min}^{-1}$
M	= Molation, gmol/L
mM	= Millimolarity, $10^{-3} \text{ gmol}/\text{L}$
P_{SO_2}	= Partial pressure of SO_2 , bar
R	= Gas constant, $1.987 \text{ cal}/\text{gmol} - ^\circ\text{K}$
T	= Temperature, $^\circ\text{K}$
[]	= Molarity, gmol/L

Acknowledgments

This work was performed under EPA Cooperative Agreement No. 806743. The EPA project officer was Robert H. Borgwardt. Additional experimental data has been taken from the work of Neyma E. Garcia, Curtis M. Cavanaugh, and Yungli Lee. Experimental assistance was provided by Jack Broodo, Kirk Limbach, Alvin Sturm, and Kim Marma.

Literature Cited

1. Rochelle, G.T., and King, C.J., Chem. Eng. Prog. 1978, 65-70.
2. Hatfield, J.D., Kim, Y.K. and Mullins, R.C., "Study of the Effect of Organic Acids on the Wet Limestone Scrubbing Process", 1972, APTD 1137, PB 210-793, U.S. EPA.
3. Hatfield, J.D., and Potts, J.M., Proceedings of Second International Lime/Limestone Wet Scrubbing Symposium, 1972, APTD01161, U.S. EPA, p.263.
4. Hollinden, G.A., Moore, N.D., and Schultz, J.J., "Removal of Sulfur Dioxide from Stack Gases by Scrubbing with Limestone Slurry: Effect of an Organic Additive at TVA Pilot Plant", 1974, presented at Fourth Annual Environmental Engineering and Science Conference.
5. Villiers-Fisher, J.F. and Warshaw, A., 1972, U.S. Patent 3,632,306.
6. Wasag, T., Galka, J., and Fraczak, M., 1975, Air Conservation 9(3), 16.
7. Rochelle, G.T., "Process Synthesis and Innovation in Flue Gas Desulfurization", 1977, EPRI Report No. FP-463-SR.
8. Rochelle, G.T., and King, C.J., Ind. Eng. Chem. Fund., 1977, 16, 67.
9. Borgwardt, R.H., Proceedings: Industry Briefing on EPA Lime/Limestone Wet Scrubbing Test Programs, 1979, EPA-600/7-79-092 p.1-9.
10. Head, H.N., Wang, S.C., Rabb, D.T., Borgwardt, R.H., Williams, J.E., and Maxwell, M.A., Proceedings: Symposium on Flue Gas Desulfurization, Las Vegas, Nevada, 1979, EPA-600/7-79-167a, 343.
11. Burbank, D.A., and Wang, S.C., "Test Results on Adipic Acid-Enhanced Lime/Limestone Scrubbing at the EPA Shawnee Test Facility", presented at the Industry Briefing on EPA Lime/Limestone Wet Scrubbing Test Program, Raleigh, N.C., Dec. 5, 1979.
12. Burbank, D.A. and Wang, S.C., Proceedings: Symposium on Flue Gas Desulfurization - Houston, 1980; Vol. I, pp.233-286, EPA-600/9-81-019a, 1981.
13. Hicks, N.D., Hargrove, O.W., and Colley, J.D., "FGD Experiences - Southwest Unit I", Proceedings: Symposium on Flue Gas Desulfurization, Houston, 1980; EPA-600/9-81-019a, pp.327-49.
14. Cavanaugh, C.M., M.S. Thesis, University of Texas, Austin, 1978.
15. Smith, R.J., M.S. Thesis, University of Texas, Austin, 1981.
16. Chang, C.S., and Rochelle, G.T., "Effect of Organic Acid Additives on SO₂ Absorption into CaO/CaCO₃ Slurries", in press AIChE.J., 1981.
17. Weems, W.T., M.S. Thesis, The University of Texas, Austin, 1981.
18. Meserole, F.N., Lewis, D.L., Nichols, A.W., and Rochelle, G.T., "Adipic Acid Degradation Mechanism in Aqueous FGD Systems", 1979, EPA-600/7-79-224.

19. Hsiang, M.W., M.S. Thesis, University of Texas, Austin, 1981.
20. Garcia, N.F., M.S. Thesis, University of Texas, Austin, 1980.
21. Keller, J.E., 1956, U.S. Patent 2,729,543.
22. Hagglund, E., and Ringbom, A., Z. Anorg. Allgem. Chem., 1926, 150, 231-53.
23. Van Der Zanden, J.M., Rec. Trav. Chim., 1926, 45, 424-27.
24. Morton, M., and Landfield, H., J. Am. Chem. Soc., 1952, 74, 3523-27.
25. Pressman, D., and Lucas, H.J., J. Am. Chem. Soc., 1942, 64, 1953-57.
26. Lowell, P.S., Ottmers, D.M., Schwitzgebel, K., Strange, T.I., and Deberry, D.W., 1970, PB 193-029, U.S. Environmental Protection Agency.
27. Rabe, A.E., and Harris, J.F., J. Chem. Engr. Data, 1963, 8, 333.
28. Albery, W.J. Greenwood, A.R., and Ribble, R.F., Trans. Far. Soc., 1967, 63, 360.
29. Landolt-Bornstein Physikalisch-Chemische Tabellen, Bd. II-7 225, Springer-Verlag, Berlin, Germany, 1960.
30. Jeffery, G.H., and Vogel, A.F., J. Chem. Soc., 1935, 21-30.
31. Lewis, J.B., J. Appl. Chem., 1955, 5, 228.
32. Peaceman, D.W., Sc. D. Thesis, Mass. Inst. Technol., Cambridge, Ma., 1951.
33. Meserole, F.B., Lewis, D.L., and Kurzawa, F.T., "Further Study of Adipic Acid Degradation in FGD Systems", 1980, Draft report, EPA Contract 68-02-2508, Task 72.
34. Meserole, F.B., "Fate of Adipic Acid Used in FGD Systems", presented at ACS Southwest Regional Meeting, Austin, Texas, December 5-7, 1979.
35. Terry, J.C., Jarvis, J.B., Utley, D.L., and Ellsworth, E.E., Chapter in this book.
36. Tinker, H.B., J. Catalysis, 1970, 19, 237-44.
37. Denisov, E.T., Mitskevich, N.I., and Agabekov, V.E., "Liquid-phase Oxidation of Oxygen-containing Compounds", 1977, Consultant Bureau, New York.
38. Berezin, I.V., Denisov, E.T., and Emanuel, N.M., "The Oxidation of Cyclohexane", Pergamon Press, New York, 1966.
39. Chan, P.K., and Rochelle, G.T., Chapter in this book.

RECEIVED December 10, 1981.

Adipic Acid-Enhanced Lime/Limestone Test Results at the EPA Alkali Scrubbing Test Facility

SHIH-CHUNG WANG and DEWEY A. BURBANK

Bechtel Group, Inc., San Francisco, CA 94119

This paper summarizes the results of tests conducted from July 1978 through March 1981 at the EPA, 10-MW equivalent, lime/limestone wet-scrubbing FGD test facility, during which adipic acid as an additive was tested and shown to be a powerful scrubber additive for improving SO₂ removal. The optimum concentration of adipic acid is only 700 to 1500 ppm at a scrubber inlet pH of 5.2 or higher. SO₂ removal efficiencies in excess of 90 percent and reliable operation were demonstrated in four long term, limestone/adipic acid runs. Factorial tests were also conducted to characterize SO₂ removal as a function of gas and slurry flow rates, pH, and adipic acid concentration. Intermediate duration optimization runs and favorable economics are also reported.

Introduction and Background

This report describes the results of the Shawnee Lime and Limestone Wet Scrubbing Test Program conducted by EPA's Industrial Environmental Research Laboratory, Research Triangle Park, North Carolina (IERL-RTP). In this program, flue gas desulfurization (FGD) tests were conducted at the EPA 10 MW prototype Shawnee Test Facility located at the Tennessee Valley Authority (TVA) coal-fired Shawnee Power Station near Paducah, Kentucky. Bechtel Group, Inc. of San Francisco was the major contractor and test director, and TVA was the constructor and facility operator. Results of the program before July 1978 have been reported elsewhere (1,2).

This report describes the results of adipic acid-enhanced lime and limestone testing at the Shawnee Test Facility from July 1978 through March 1981. It also summarizes earlier adipic acid additive test results from the IERL-RTP 0.1 MW pilot plant, which led to the testing at Shawnee. Also reported are preliminary results from the 100 MW full-scale demonstration being

0097-6156/82/0188-0267\$11.00/0
© 1982 American Chemical Society

conducted at the Southwest Power Plant of Springfield City Utilities, Springfield, Missouri and from the 27 MW equivalent industrial boiler test at Rickenbacker Air Force Base.

As the emission standards for sulfur dioxide become increasingly stringent and the fossil-fueled utilities become hard pressed to meet these standards, there is a strong incentive to improve the FGD system performance while minimizing the operating costs.

A primary objective of the EPA alkali wet scrubbing test program during the last several years has been to enhance SO₂ removal and improve the reliability and economics of lime and limestone wet scrubbing systems by use of adipic acid as a chemical additive.

Adipic acid is a six-carbon dicarboxylic organic acid, HOOC(CH₂)₄COOH, that buffers the pH in the scrubber slurry. In theory, any acid which is intermediate in strength between carbonic acid and sulfurous acid, and whose calcium salt is reasonably soluble, may be employed. However, adipic acid was selected because it is one of the most cost-effective organic acid buffers on a molar basis and is commercially abundant. Its main use is as a raw material in the manufacturing of nylon.

The buffering activity of adipic acid limits the drop in pH that normally occurs at the gas-liquid interface during SO₂ absorption, and the resultant higher concentration of SO₂ at the interface significantly accelerates the liquid-phase mass transfer. The capacity of the bulk liquor for reaction with SO₂ is also increased by the presence of calcium adipate in solution. Thus, the SO₂ absorption becomes less dependent on the dissolution rate of limestone or calcium sulfite in the absorber to provide the necessary alkalinity.

In the case of limestone scrubbing, it logically follows that a given SO₂ removal efficiency can be achieved at a lower limestone stoichiometry, thereby improving scrubber reliability.

Adipic acid degrades to lower molecular weight (C₁-C₅) monocarboxylic acids, paraffinic hydrocarbons, and carbon dioxide and water. The feed rate of adipic acid varies depending on the operating conditions, such as pH and oxidation, which influence the degree of degradation, but is usually less than five times the theoretical requirement. Most of the carboxylic acid degradation products, such as valeric acid, still offer a proper pH buffer range for effective SO₂ removal enhancement. At Shawnee, all reported concentrations of adipic acid (in ppm) are, in reality, the concentrations of total carboxylic acid expressed in terms of "adipic acid."

At the Shawnee Test Facility, major emphasis has been placed on the use of adipic acid in conjunction with forced oxidation of calcium sulfite to calcium sulfate, since this system results in better sludge dewatering properties and reduced waste solids disposal costs. Furthermore, the more tightly closed liquor loop,

achievable as a result of forced oxidation, reduces the adipic acid makeup requirements.

Advantages of Adipic Acid as a Scrubber Additive

A number of attractive features of adipic acid as a scrubber additive are presented below.

Handling. Adipic acid is non-toxic, non-hygroscopic, and usually comes in powder form. It is easy to handle and no hazards are encountered in the usual applications other than possible dust explosions, which are typical of any organic dust. At Shawnee, it is routinely dry-fed directly to the effluent hold tank, although it has been added to the fresh limestone slurry makeup tank in some instances.

Buffer Reaction Mechanism. The mechanism by which adipic acid buffers the pH is simple. It reacts with lime or limestone in the effluent hold tank to form calcium adipate. In the absorber, calcium adipate reacts with absorbed $\text{SO}_2(\text{H}_2\text{SO}_3)$ to form CaSO_3 and simultaneously regenerates adipic acid (the buffer reaction). The regenerated adipic acid is returned to the effluent hold tank for further reaction with lime or limestone. With a sufficiently high concentration of calcium adipate in solution, usually on the order of 10 m-moles/liter to react with the absorbed SO_2 , the overall reaction rate is no longer controlled by the dissolution rate of limestone or calcium sulfite.

Retrofit. Use of adipic acid in an existing lime or limestone system does not require modification of process flow configuration or absorber design; therefore, it is particularly suited for retrofit applications. The fact that it may be added at any point in the slurry circuit provides a greater flexibility in the location and installation of a simple solids storage and feed system, a minimal capital investment.

Quantity and Concentration. Depending on the operating parameters, the degree of degradation, and the tightness of the liquor loop, the quantity of adipic acid required is quite small in relation to the alkali feed. At Shawnee, where a filter is normally used as the final sludge dewatering device, the adipic acid consumption rate is usually less than 10 lb/ton of limestone fed to the system, and sometimes as low as 2 lb/ton of limestone. These values correspond to only 0.6 to 3.0 tons of adipic acid per day for a 500 MW plant.

Adipic acid has two pH buffer points. These are pH 4.5 and 5.5 in the absence of chloride in the liquor, and about 4 and 5 with 5,000 to 7,000 ppm chloride. To fully utilize the buffer capacity of adipic acid, therefore, the slurry pH should be kept above these values. At Shawnee, where the chloride concentration

is usually a few thousand ppm, a slurry pH above about 5.2 is sufficient to keep adipic acid fully active (or ionized). The optimum concentration range of adipic acid at a pH above 5.2 is only 700 to 1,500 ppm for 90 percent removal of approximately 2,500 ppm inlet SO₂. Higher concentrations would be required at a lower pH to maintain equivalent buffer capacity in the liquid. It should be noted that most of the degradation products of adipic acid, such as valeric and glutaric acid, are also effective buffers.

Limestone Utilization. At a scrubber inlet pH of about 5.2, the corresponding limestone utilization is normally 80 percent or higher for an adipic acid-enhanced system, as compared to 65 to 70 percent in unenhanced limestone systems at an equivalent SO₂ removal. Thus the quantity of waste solids generated is reduced in an adipic acid-enhanced system. Higher limestone utilization also contributes to more reliable scrubber operation by reducing the fouling tendency. This increased reliability is a very attractive feature of adipic acid-enhanced systems, since reliability problems have historically plagued limestone FGD.

Operating pH. With proper pH control and sufficiently high adipic acid concentration (sufficient buffer capacity), the scrubber performance is more stable, and steady outlet SO₂ concentrations can be maintained, even with wide fluctuations of inlet SO₂ concentrations.

With the lower operating pH (about 4.6 to 5.4) in an adipic acid-enhanced limestone system, compared to the higher pH (about 5.5 to 5.8) usually needed for an unenhanced limestone system, the system becomes more amenable to other process concepts and improvements. Potential advantages of low pH operation are:

- Reduced adipic acid consumption. Adipic acid degradation has been found to decrease with decreasing pH
- Easier forced oxidation in the scrubber slurry loop or bleed stream, and a smaller air (and compressor energy) requirement
- Potential for essentially complete limestone utilization with improved scrubber operating reliability
- Reduced sensitivity of the system to limestone type and grind. Fine grinding of limestone is probably not required
- Lower sulfite scaling potential
- Better prospects (sensitivity) for automatic pH control
- Greater flexibility for SO₂ emission control. Higher sensitivity of SO₂ removal at lower pH

allows raising pH to increase the adipic acid buffer capacity and SO₂ removal when needed

- Applicability to low-sulfur subbituminous and lignite coals containing alkaline ashes, which are extractable only at low pH
- Lower costs due to all of the above factors

Economics. Since limestone dissolution is not a rate-controlling step in SO₂ absorption for an adipic acid-enhanced limestone system, adipic acid should promote use of less expensive and less energy-intensive limestone rather than lime.

Adipic acid-enhanced limestone scrubbing has lower projected capital and operating costs than unenhanced limestone or MgO-enhanced limestone scrubbing. This is due primarily to the reduced limestone consumption at the lower operating pH, the reduced grinding cost, and the reduced quantity of waste sludge generated.

Forced Oxidation. The mechanism by which adipic acid promotes SO₂ removal is not affected by forced oxidation. Therefore, it can be used with both lime and limestone in systems with or without forced oxidation.

Since forced oxidation converts sulfite to sulfate, it has an adverse effect on SO₂ removal in an unenhanced lime system in which sulfite is the major SO₂ scrubbing species. This is also true in MgO-enhanced lime and limestone systems in which the promotion of SO₂ removal relies on an increased sulfite-bisulfite buffer. When adipic acid is used with lime, calcium adipate becomes a major buffer species; therefore, both good SO₂ removal and sulfite oxidation can be achieved using within-scrubber-loop forced oxidation.

Chloride Effect. The effectiveness of adipic acid is not adversely affected by chlorides, as is the effectiveness of MgO in an MgO-enhanced process. Tests at the IERL-RTP pilot plant showed that SO₂ removal efficiency obtained with 17,000 ppm chloride in the scrubbing liquor was not significantly different from that obtained without chloride under similar levels of adipic acid concentration. Thus, use of adipic acid is especially attractive for systems with a very tightly closed liquor loop.

Solids Dewatering. Adipic acid does not significantly affect the settling and filtration properties of oxidized or unoxidized slurry solids, whereas magnesium does.

Total Dissolved Solids. Addition of adipic acid does not significantly increase the total dissolved solids in liquid as does magnesium. High total dissolved solids in liquid entrainment can increase particulate emissions and fouling tendencies of equipment downstream of the scrubber.

Test Programs

The theoretical basis for the effect of adipic acid on the performance of lime and limestone scrubbers was first developed in detail by G. Rochelle in 1977 (3). In October 1977, EPA began an investigation of adipic acid with the 0.1 MW IERL-RTP pilot plant to determine its effectiveness as an additive to limestone scrubbers for improving SO₂ removal efficiency (4). Initial results demonstrated, as predicted by Rochelle, that adipic acid was indeed an attractive and powerful additive.

Based on the findings at the IERL-RTP pilot plant, a program was set up at the 10 MW Shawnee Test Facility to develop commercially usable design data for adipic acid as a chemical additive. Actual testing at Shawnee began in July 1978, and lasted through March 1981. Some of the significant test results during the first two-thirds of this period have been presented elsewhere (5,6,7). The test schedule for this period is shown in Figure 1. Tests were conducted over a period of 33 months, using both lime and limestone with and without forced oxidation. As can be seen, major emphasis was placed on limestone testing with forced oxidation.

As part of EPA's continuing program of FGD technology transfer, and to further demonstrate the effectiveness of adipic acid and to encourage its use, EPA contracted with Radian Corporation in the spring of 1980 to conduct a full-scale demonstration program of adipic acid-enhanced limestone scrubbing (8). The program, being conducted with two 100 MW Turbulent Contact Absorbers (TCA) located at the Springfield City Utilities' Southwest Station near Springfield, Missouri, will continue through September 1981. Some preliminary test results are included in this report, as are data from the industrial-sized (27 MW) scrubber test conducted by PEDCo Environmental, Inc. on the Bahco system at Rickenbacker Air Force Base.

During some factorial tests conducted at the Shawnee Test Facility in 1979, it was noticed that the rate of adipic acid addition required to maintain a desired concentration in the scrubber liquor was substantially reduced when the scrubber inlet pH was controlled at 5.0 or lower. In order to verify the Shawnee findings, the EPA initiated several programs to study the adipic acid degradation phenomenon. Contractors involved included University of Texas at Austin, Radian Corporation, Acurex Corporation, and the Research Triangle Institute. Programs were set up to investigate the effects of pH, oxidation, and catalysts such as manganese and iron on adipic acid degradation, to develop analytical procedures and to identify the degradation products. Although the adipic acid degradation mechanism is complex, the principal variables affecting degradation and its major products have been identified. The results of these studies are beyond the scope of this report and will be reported separately.

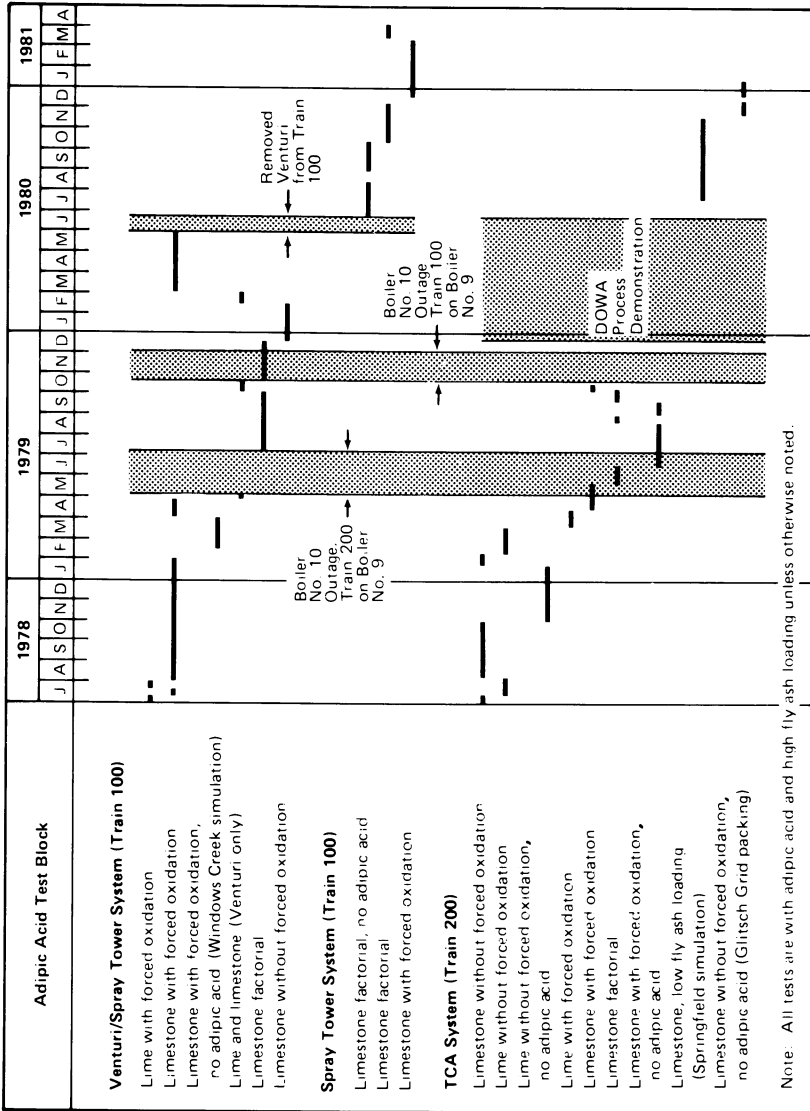


Figure 1. Shawnee adipic acid test schedule.

Shawnee Test Facility. Tests with adipic acid at Shawnee have been conducted on two parallel scrubber systems: a venturi/spray tower system (Train 100) and a TCA system (Train 200). Each system has its own slurry handling and dewatering facilities, and each is designed to remove both SO₂ and particulate from approximately 10 MW equivalent of flue gas (up to 35,000 acfm at 300°F). The flue gas which normally contains 1,400 to 3,500 ppm by volume of SO₂, is obtained either upstream (containing high fly ash loading of 2 to 7 grains/dry scf) or downstream (containing low fly ash loading of 0.2 to 0.6 grain/dry scf) from Boiler No. 10 particulate removal equipment.

In June 1980, the venturi scrubber was removed from Train 100, allowing operation with the spray tower only. Prior to the removal of the venturi scrubber, operation with a true spray tower-only configuration was not possible without some interference from the venturi, even with its adjustable plug wide open and minimum slurry flow for flue gas cooling.

Shawnee Test Blocks. Tests conducted at the Shawnee Test Facility can be classified into blocks according to type of alkali, fly ash loading in the flue gas, adipic acid addition, and forced oxidation scheme. Table 1 lists the combinations of these variables which have been tested at Shawnee, including factorial tests.

Forced oxidation is achieved by air sparging of the slurry in an oxidation tank, either on the bleed stream to the solids dewatering system or on the recirculated slurry within the scrubber slurry loop. For a one-scrubber-loop forced oxidation system, the slurry effluent from all scrubbers in the system (e.g., the venturi scrubber and spray tower at Shawnee constitute a two-scrubber system, and the spray tower alone or TCA, a one-scrubber system) are sent to a single effluent hold tank, which is the oxidation tank. For a two-loop forced oxidation system, there are two scrubbers in series (e.g., venturi and spray tower at Shawnee) with effluent from each scrubber going to a separate tank; the effluent hold tank for the upstream scrubber (with respect to gas flow) is the oxidation tank. For either one-loop or two-loop forced oxidation systems, the oxidation tank may be followed by a second tank, in series, to provide further limestone dissolution and gypsum desupersaturation time prior to recycle to the scrubber.

Test Results

It is beyond the scope of this report to present all of the Shawnee test results from the test blocks listed in Table 1. Therefore, only the typical and important test results are presented below. Results of long-term tests (longer than one month) are included. Results from factorial or partial factorial tests, which normally lasted a minimum of 12 hours including 5 to 7 hours

Table 1.
Test Blocks Conducted at Shawnee

Test Block	Alkali	Fly Ash Loading	Adipic Acid Addition	Oxidation Scheme	No. of Tanks in Oxid. Loop
Venturi/Spray Tower System:					
1	Lime	High	Yes	2-Loop	2
2	Lime	High	Yes	No	—
3(a)	Limestone	High	Yes	2-Loop	2
4	Limestone	High	Yes	2-Loop	1
5	Limestone	High	Yes	1-Loop	2
6	Limestone	High	Yes	1-Loop	1
7	Limestone	High	Yes	Bleed Stream	—
8	Limestone	High	Yes	No	—
9(b)	Limestone	High	No	2-Loop	2
Spray Tower System:					
10(a)	Limestone	High	Yes	1-Loop	2
11	Limestone	High	Yes	No	—
12	Limestone	High	No	1-Loop	2
13	Limestone	High	No	No	—
TCA System:					
14	Lime	High	Yes	1-Loop	1
15	Lime	High	Yes	No	—
16(a)	Lime	High	No	No	—
17	Limestone	High	Yes	1-Loop	2
18	Limestone	High	Yes	1-Loop	1
19(a)	Limestone	High	Yes	No	—
20	Limestone	High	No	1-Loop	1
21(c)	Limestone	High	No	No	—
22(d)	Limestone	Low	Yes	1-Loop	1
23(d)	Limestone	Low	Yes	No	—

(a) Includes long-term (greater than one month) tests.

(b) Widows Creek forced oxidation simulation tests.

(c) Glitsch Grid packing tests.

(d) Springfield adipic acid simulation tests.

of steady state operation, are also included as figures to illustrate the effects of pH and adipic acid concentration on SO₂ removal.

A summary of initial tests at the IERL-RTP pilot plant and the preliminary results from the full-scale TCA tests at Springfield are also given.

IERL-RTP Pilot Plant Test Results. The initial testing of adipic acid as a scrubber additive was carried out by EPA beginning in October 1977 in the 0.1 MW in-house pilot plant located at IERL-RTP (4). A single-loop limestone scrubber was used for this purpose, operated with forced oxidation in the scrubbing loop. In addition to effects on SO₂ removal and oxidation efficiencies, these tests sought to determine whether adipic acid caused any change in the properties of the oxidized sludge. So that these properties could be clearly seen, the system was operated without fly ash. Chloride was added as HCl and controlled at the high levels expected for tightly closed loop systems.

The results of the tests showed adipic acid to be very effective in improving SO₂ removal efficiency, even when operating at chloride levels as high as 17,000 ppm. A TCA scrubber, which removed 82 percent of the inlet SO₂ without the additive, yielded 89 percent SO₂ removal with 700 ppm adipic acid, 91 percent removal with 1,000 ppm, and 93 percent removal with 2,000 ppm adipic acid. The limestone utilization was concurrently increased from 77 percent without the additive to 91 percent with 1,600 ppm adipic acid. The observed effects thus confirmed the theoretical expectations in all respects. In addition, the tests showed no serious interference by adipic acid on the performance of the oxidizer, operating at pH 6.1.

The quality of the oxidized sludge was similar to that obtained when operating without adipic acid, although small differences were detected. For example, the filtered sludge averaged 80 percent solids (for 13 one-week tests) vs 84 percent solids for 11 tests without the additive, when operating at 97 to 99 percent oxidation in both cases. The settling rate of the slurry (fly ash free at 50°C) averaged 2.3 cm/min during the adipic acid tests and 3.4 cm/min without adipic acid; bulk settled densities averaged 1.0 and 1.2 gm solids/cm³ slurry, respectively. It was concluded from these results that the large improvements in sludge quality that can be achieved by forced oxidation are not compromised by the use of adipic acid as a scrubber additive.

Tests without forced oxidation also demonstrated the efficacy of adipic acid. Operating a TCA scrubber with 2,000 ppm adipic acid and 6 inches H₂O pressure drop, 92 percent SO₂ removal was obtained at a limestone utilization level of 88 percent. By comparison, only 75 percent SO₂ removal would be expected in the pilot plant at these test conditions without the additive. At this adipic acid level, the unoxidized sludge filtered to 49 percent solids; at lower adipic acid levels (1,500 ppm or less), the

filterability of the slurry was the same as that obtained without additives: 55 percent solids.

During the testing with adipic acid, the scrubbing liquor had a noticeable odor, even though the additive feed did not. The odor has been identified as that of valeric acid, $\text{CH}_3(\text{CH}_2)_3\text{COOH}$, an intermediate product formed by side reactions that degrade adipic acid at scrubber operating conditions. At Shawnee, this odor was rarely noticed and was not a problem.

Limestone Long-Term Tests with Two Scrubber Loops and Forced Oxidation. The venturi/spray tower system was modified for two-scrubber-loop operation with forced oxidation as shown in Figure 2. Two tanks were used in the oxidation loop (venturi loop); air was injected to the first of these tanks through a simple 3-inch diameter pipe below the agitator. Adipic acid was dry-fed to the spray tower effluent hold tank. This was accomplished by manually adding one-pound increments hourly to maintain specified concentration, usually totaling only a few pounds per hour. A small screw feeder would serve the purpose in a full-scale plant.

The main advantage of this two-loop system, as far as forced oxidation is concerned, is that it permits operation of the first loop (venturi loop) at lower pH for good oxidation efficiency, while maintaining higher pH in the second loop (spray tower loop) for good SO_2 removal. This configuration also maximizes the limestone utilization. With adipic acid-enhancement, however, some of these advantages can also be obtained in a single-loop scrubber because an adipic acid enhanced system can be operated at a lower pH (4.6 to 5.4). Thus, both good oxidation and good SO_2 removal can be achieved without an independent first loop.

Table 2 summarizes the results of two long-term tests (exceeding one month), Runs 907-1A and 907-1B, with adipic acid addition and with a variable gas flow rate. The results of Run 901-1A, a base case run without additive and with a constant spray tower gas velocity of 9.4 ft/sec, are also included for comparison.

Run 907-1A was a month-long adipic acid-enhanced limestone run with forced oxidation, designed to demonstrate operational reliability with respect to scaling and plugging and to demonstrate the removal enhancement capability of the adipic acid additive. This run was controlled at a nominal limestone stoichiometry of 1.7 (compared to 1.4 for the base case run, Run 901-1A) and 1,500 ppm adipic acid in the spray tower. Venturi inlet pH was controlled at a minimum of 4.5 by the occasional addition of limestone to the venturi loop.

Flue gas flow rate was varied from 18,000 acfm to a maximum of 35,000 acfm (spray tower gas velocity between 4.8 and 9.4 ft/sec) to follow the daily boiler load cycle, which normally fluctuated between 100 and 150 MW. The adjustable venturi plug was fixed in a position such that the pressure drop across the venturi

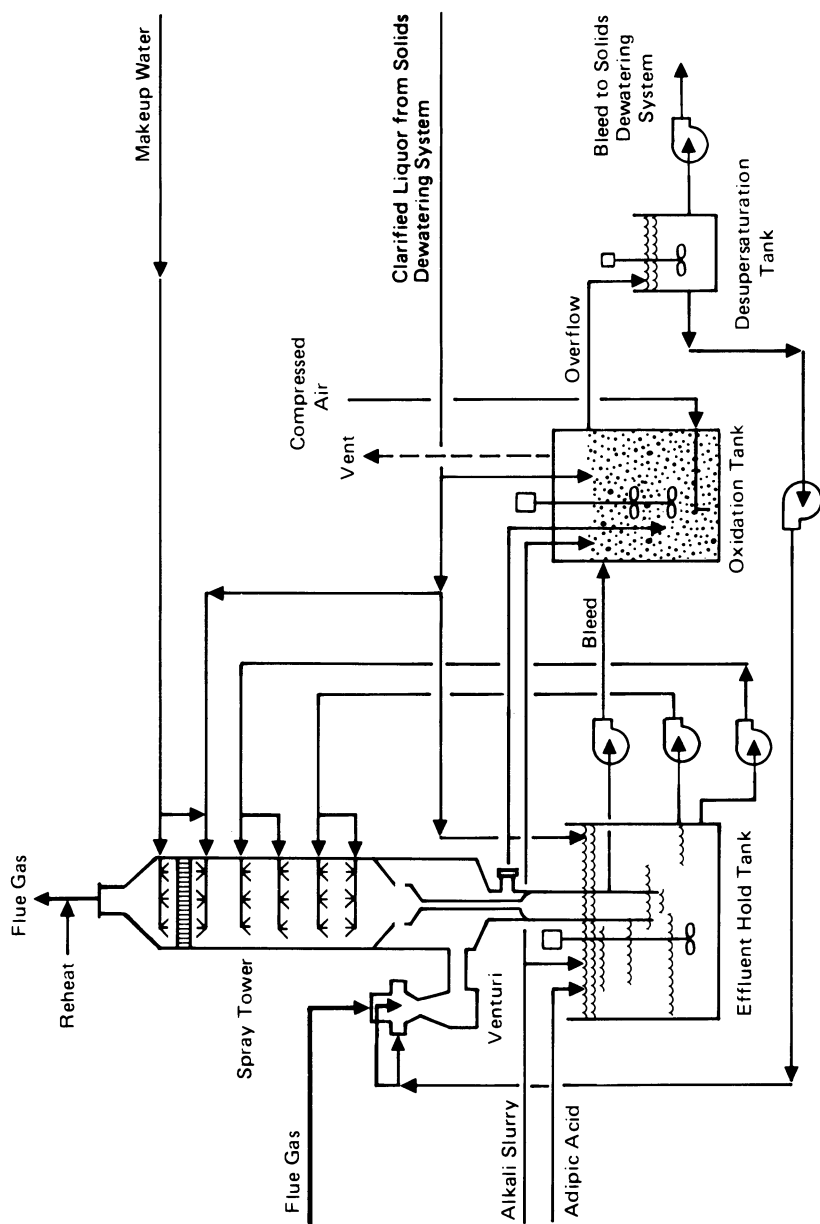


Figure 2. Flow diagram for adipic acid-enhanced scrubbing in the venturi/spray tower system with two scrubber loops and forced oxidation.

Table 2.
Adipic Acid-Enhanced Limestone Tests on the Two-Loop Venturi/Spray Tower System with Forced Oxidation

Run No.	901-1A	907-1A	907-1B
Onstream hours	187	719	1,666
Fly ash loading	High	High	High
Adipic acid conc. in venturi, ppm	0	2,360	2,180
Adipic acid conc. in spray tower, ppm (controlled)	0	1,560	1,510
Spray tower gas velocity, ft/sec	9.4	4.8-9.4	5.4-9.4
Venturi liquid-to-gas ratio, gal/Mcf	21	21-42	21-37
Spray tower liquid-to-gas ratio, gal/Mcf	57	57-111	57-100
Venturi slurry solids conc., wt % (controlled)	15	15	15
Spray tower slurry solids conc., wt %	5.9	6.1	5.9
Venturi inlet pH (controlled)	4.50	4.65	4.65
Spray tower inlet pH	5.45	5.45	5.35
Venturi pressure drop, in. H ₂ O	9.0	3.0-9.6	3.5-9.2
Oxidation tank level, ft	18	18	18
Oxidation tank residence time, min	11.3	11.3	11.3
Desupersaturation tank residence time, min	4.7	4.7	4.7
Spray tower effluent tank residence time, min	14.7	14.7	14.7
Spray tower limestone stoich. ratio (controlled)	1.36	1.77	1.70
Average percent SO ₂ removal	57	97.5	97
Average inlet SO ₂ concentration, ppm	2,800	2,350	2,500
Percent oxidation of sulfite to sulfate	98	98.5	98
Air stoichiometry, atoms oxygen/mole SO ₂ absorbed	2.30	2.0-3.85	1.9-3.3
Overall percent limestone utilization	97	88	92
Venturi inlet liquor gypsum saturation, %	95	110	105
Spray tower inlet liquor gypsum saturation, %	95	105	110
Filter cake solids content, wt %	85	87	85

was 9 inches H₂O at 35,000 acfm maximum gas rate. Actual pressure drop ranged from 3.0 to 9.6 inches H₂O.

The slurry recirculation rates to the venturi and spray tower were fixed at 600 gpm (L/G = 21 to 42 gal/Mcf) and 1,600 gpm (L/G = 57 to 111 gal/Mcf), respectively.

The oxidation tank level was 18 ft and the air flow rate was held constant at 260 scfm.

The run began on October 8, 1978 and terminated November 13, 1978. It ran for 719 onstream hours (30 days) with no unscheduled outages. The scrubber was down once for a scheduled 3-hour inspection and again when the boiler came down for 135 hours to install a new station power transformer.

Average SO₂ removal for Run 907-1A was 97.5 percent at 2,350 ppm average inlet SO₂ concentration. The SO₂ removal stayed within a narrow range of 96 to 99 percent throughout almost the entire run. This was a significant improvement over the 57 percent SO₂ removal for the base case run, Run 901-1A, at 9.4 ft/sec spray tower gas velocity under similar conditions. On October 19 and on October 27, SO₂ removal dropped briefly to less than 90 percent when the pump which supplied the slurry to the top two spray headers was brought offstream for repacking, and the spray tower slurry flow rate was cut in half to 800 gpm. At the reduced slurry recirculation rate, SO₂ removal was 82 to 87 percent.

Venturi and spray tower inlet pH averaged 4.65 and 5.45, respectively. Overall limestone utilization was 88 percent and the spray tower limestone utilization was 56 percent, demonstrating the advantage of good limestone utilization in a two-scrubber-loop operation.

Average adipic acid concentrations were 2,360 ppm in the venturi loop and 1,560 ppm in the spray tower loop.

Sulfite oxidation in the system bleed slurry averaged 98.5 percent, with the air stoichiometric ratio varied between 2.0 and 3.85 atoms oxygen/mole SO₂ absorbed. The filter cake solids content was 87 percent.

The mist eliminator was clean during the entire run. The system was free of plugging and scaling and there was no increase in solids or scale deposits on the scrubber internals during Run 907-1A.

Following Run 907-1A, a second adipic acid-enhanced limestone long-term run with forced oxidation was made during which flue gas monitoring procedures were evaluated by EPA. This run, Run 907-1B, was made under the same conditions as Run 907-1A except that the gas flow rate was varied according to a "typical" utility boiler load cycle rather than the actual Unit No. 10 boiler load. Run 907-1B began on November 13, 1978 and terminated January 29, 1979. It ran for 1,666 onstream hours (69 days) with only 27 hours of scrubber-related outages. The scrubber was also out of service 146 hours when Unit 10 came down for replacement of a broken turbine thrust bearing.

Excluding boiler outages and scheduled inspections, the combined Runs 907-1A and 907-1B operated for a period of over 3 months with an onstream factor of 98.9 percent. No deposits whatsoever were observed in the mist eliminator for the entire 3-month test period. On only one occasion did solids accumulation cause an outage; the cross-over line carrying slurry effluent from the venturi to the oxidation tank plugged with soft solids and had to be cleaned out. Because of problems associated with converting the Shawnee venturi/spray tower system to two-scrubber-loop operation, this cross-over line followed a tortuous path (see Figure 2). A properly designed system would not have this problem.

Results of Run 907-1B were as good in every respect as those of Run 907-1A. Average SO₂ removal remained within a narrow band of 95 to 99 percent. SO₂ removal dropped briefly (typically 30 minutes) below 90 percent five times when one of the two spray tower recirculation pumps was taken out of service for maintenance, effectively cutting the slurry recirculation rate in half.

Overall limestone utilization during this run was 92 percent. Sulfite oxidation averaged 98 percent and the waste sludge filter cake quality was excellent, having a solids content of 85 percent.

SO₂ emissions for Run 907-1A and 907-1B were calculated based on an assumed coal heating value of 10,500 Btu/lb, on 100 percent sulfur overhead (none in bottom ash), and on an assumed excess air of 30 percent. This excess air rate resulted in about 700 ppm inlet SO₂ per 1.0 weight percent sulfur in coal for the above conditions. The average SO₂ emission for the entire 3-month operating period was only 0.20 lb/10⁶ Btu. The highest 24-hour average SO₂ emission during Run 907-1A was 0.37 lb/10⁶ Btu, and during Run 907-1B was 0.41 lb/10⁶ Btu.

A material balance calculation for the adipic acid consumption was made for Run 907-1B. Actual adipic acid feed rate was 8.3 lb/ton of limestone fed to the system, of which 1.8 lb/ton were discharged with the filter cake (theoretical requirement) and 6.5 lb/ton were unaccounted for, giving an actual-to-theoretical consumption ratio of 4.6.

Limestone Long-Term Test with One Scrubber Loop and Without Forced Oxidation. Perhaps the most straightforward illustration of the effectiveness of adipic acid is demonstrated by a long-term limestone test conducted on the Shawnee TCA system, in which the additive was introduced without any system modifications.

Table 3 lists the results of the long-term test, Run 932-2A, with adipic acid enhancement. The results of a base case run, Run 926-2A, without the additive, are also included in the table for comparison.

Figure 3 depicts the simple single-loop, one-tank configuration of the TCA system used for these runs. The TCA contained three beds of 1-7/8 inch diameter, 11.5-gram nitrile foam spheres

Table 3.

Adipic Acid-Enhanced Limestone Test on the Single-Loop TCA System without Forced Oxidation

Run No.	926-2A	932-2A
Onstream hours	192	833
Fly ash loading	High	High
Adipic acid concentration, ppm (controlled)	0	1,620
Scrubber gas velocity, ft/sec	12.5	8.4-12.5
Liquid-to-gas ratio, gal/Mcf	50	50-75
Slurry solids concentration, wt % (controlled)	15	15
Limestone stoichiometric ratio (controlled)	1.2	1.2
Total static bed height, inches of 11.5 gram nitrile spheres	15	15
Effluent hold tank residence time, min	4.1	4.1
Average percent SO ₂ removal	71	96
Average inlet SO ₂ concentration, ppm	2,750	2,450
SO ₂ make-per-pass, m-moles/liter	10.1	4-18
Percent oxidation of sulfite to sulfate	13	21
Scrubber inlet pH	5.65	5.30
Percent limestone utilization	80	82
Scrubber inlet liquor gypsum saturation, %	90	110
Centrifuge cake solids content, wt %	37*	61

*Clarifier underflow solids content.

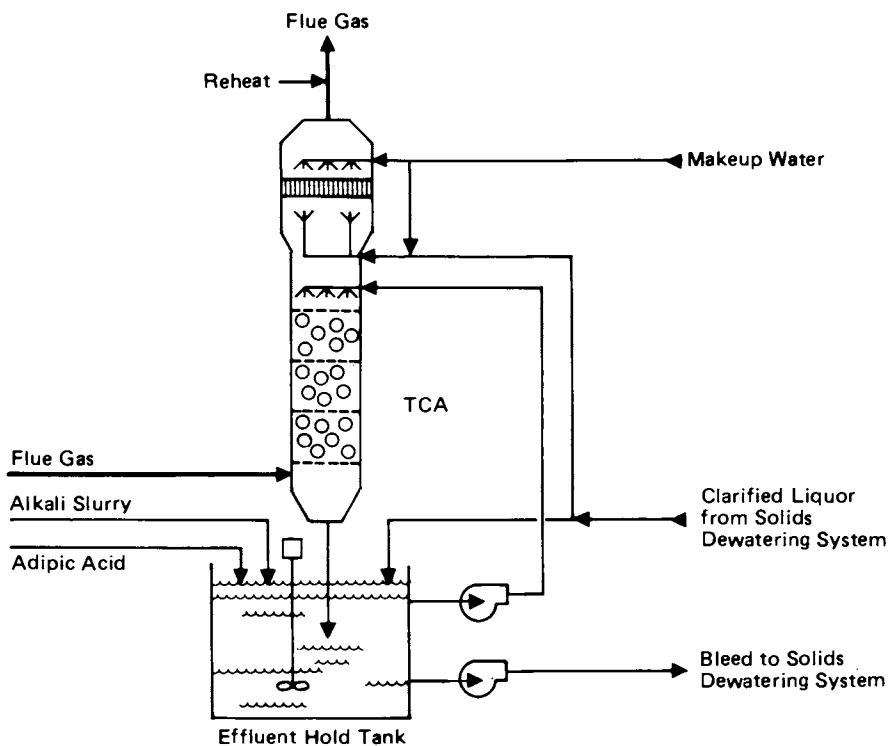


Figure 3. Flow diagram for adipic acid-enhanced scrubbing in the TCA system without forced oxidation.

retained between bar grids. Each bed contained 5 inches static height of spheres. Adipic acid was manually fed by the operator to the effluent hold tank.

Run 932-2A was made to demonstrate both operational reliability with respect to scaling and plugging of the TCA and the SO₂ removal enhancement capability of the adipic acid additive. The run began on September 26, 1978 and terminated on November 2, 1978, for a total of 833 onstream hours (35 days). During the run, the scrubber was out of service for 48 hours due to a boiler outage caused by a tube leak, 5 hours for a scheduled inspection, and 8 hours for unscheduled outages to clean and repair the scrubber induced-draft fan damper. Excluding boiler outages and scheduled inspections, Run 932-2A operated with an onstream factor of 99.0 percent. As was typical of all long-term runs, the scrubber was more reliable than the boiler.

The run was controlled at a nominal limestone stoichiometric ratio of 1.2 and 1,500 ppm adipic acid concentration in the slurry liquor. Slurry solids concentration was controlled at 15 percent. The flue gas flow rate was varied between 20,000 and 30,000 acfm (8.4 to 12.5 ft/sec superficial gas velocity) as the boiler load fluctuated between 100 and 150 MW. The slurry recirculation rate was fixed at 1,200 gpm (L/G = 50 to 75 gal/Mcf). The effluent hold tank residence time was only 4.1 minutes.

SO₂ removal during Run 932-2A averaged 96 percent at an average inlet SO₂ concentration of 2,450 ppm. Excluding the first few days of unsteady state operation, SO₂ removal stayed within a narrow range of 94 to 98 percent as the inlet SO₂ concentration varied widely between 1,400 and 3,500 ppm. By contrast, SO₂ removal during the base case run without adipic acid, Run 926-2A, averaged only 71 percent at 2,750 ppm average inlet SO₂ concentration, and at constant 12.5 ft/sec gas velocity and 50 gal/Mcf liquid-to-gas ratio.

SO₂ emissions were calculated for Run 932-2A on the same basis as for the venturi/spray tower runs, Runs 907-1A and 907-1B. Excluding the first few days of unsteady state operation, the SO₂ emissions for the 27-day period from October 6 through the end of the run on November 2, 1978, averaged only 0.26 lb/10⁶ Btu. The highest 24-hour average SO₂ emission during this period was only 0.44 lb/10⁶ Btu.

The mist eliminator was completely clean at the end of Run 932-2A and the entire scrubber system free of scaling and plugging. Limestone utilization during the run averaged 82 percent. Solids discharged from the centrifuge averaged about 61 percent, which is typical of unoxidized limestone sludge.

An adipic acid material balance calculation was made for a 21-day period during Run 932-2A. The actual adipic acid feed rate was 9.2 lb/ton limestone feed, of which 4.2 lb/ton were discharged with the centrifuge cake (theoretical requirement) and 5.0 lb/ton were unaccounted loss, giving an actual-to-theoretical consumption

ratio of 2.2. This ratio was less than the value of 4.6 for venturi/spray tower Run 907-1B when oxidation was forced, indicating that forced oxidation promotes adipic acid degradation. However, the actual feed rate of 9.2 lb/ton limestone for Run 932-2A was higher than the 8.3 lb/ton limestone for Run 907-1B, because of the higher moisture content in the discharge cake for Run 932-2A without forced oxidation. Thus, the net effect of forced oxidation was to reduce the adipic acid makeup requirements by approximately 10 percent.

In summary, the objectives of this long-term test were met. High removal was consistently achieved at a good limestone utilization, and no fouling, scaling, or plugging occurred.

Lime tests with One Scrubber Loop and Without Forced Oxidation. Tests with adipic acid in lime scrubbing also were impressive in enhancing SO₂ removal, both on the venturi/spray tower and TCA systems. Table 4 shows some typical results of adipic acid-enhanced lime tests from the Shawnee TCA without forced oxidation. The flow diagram for these tests is shown in Figure 3.

All three runs listed in Table 4 were operated under the same conditions, except for the adipic acid concentration. Run 978-2A was a base case test without adipic acid. For Runs 979-2A and 980-2A, adipic acid concentration was controlled at a nominal 600 ppm and 1,200 ppm, respectively (615 ppm and 1,305 ppm actual). The scrubber inlet pH was controlled at 7.0 for all runs.

Average SO₂ removal improved from 83 percent at 2,350 ppm average inlet SO₂ concentration for the base case run, to 93 percent SO₂ removal at the higher inlet SO₂ concentration of 2,900 ppm with 615 ppm adipic acid, and to 97.5 percent removal at 2,750 ppm inlet SO₂ with 1,305 ppm adipic acid. Thus, with 600 to 1,300 ppm adipic acid, SO₂ removal improved by 10 to 15 percent over the base case removal of 83 percent at 50 gal/Mcf liquid-to-gas ratio and 7.0 scrubber inlet pH.

Lime Test with One Scrubber Loop and Forced Oxidation. Within-scrubber-loop forced oxidation in a single-loop scrubbing system would not be expected to give good SO₂ removal for a lime scrubber because of the oxidation of the major scrubbing species, sulfite ion, into nonreactive sulfate ion. With adipic acid addition, however, satisfactory SO₂ removal should be possible because calcium adipate becomes the major scrubbing species. In addition, the lower pH at which a lime/adipic acid system operates should facilitate sulfite oxidation.

Table 5 lists the test results of such a lime run, Run 951-2E, using within-scrubber-loop forced oxidation with 1,330 ppm adipic acid. The system configuration used for this run was the same as that shown in Figure 3, except that the oxidizing air was injected into the effluent hold tank (oxidation tank). A single

Table 4.

Adipic Acid-Enhanced Lime Tests on the Single-Loop TCA System without Forced Oxidation

Run No.	978-2A	979-2A	980-2A
Onstream hours	116	177	247
Fly ash loading	High	High	High
Adipic acid concentration, ppm (controlled)	0	615	1,305
Scrubber gas velocity, ft/sec	12.5	12.5	12.5
Liquid-to-gas ratio, gal/Mcf	50	50	50
Slurry solids concentration, wt % (controlled)	8	8	8
Scrubber inlet pH (controlled)	7.0	7.2	6.95
Total static bed height, inches of 11.5 gram nitrile spheres	15	15	15
Effluent hold tank residence time, min	4.1	4.1	4.1
Average percent SO ₂ removal	83	93	97.5
Average inlet SO ₂ concentration, ppm	2,350	2,900	2,750
SO ₂ make-per-pass, m-moles/liter	10.3	14.3	14.3
Percent oxidation of sulfite to sulfate	21	14	10
Percent lime utilization	92	92	88
Scrubber inlet liquor gypsum saturation, %	125	90	75

Table 5.

Adipic Acid-Enhanced Lime Test on the Single-Loop TCA System with Forced Oxidation

Run No.	951-2E
Onstream hours	103
Fly ash loading	High
Adipic acid concentration, ppm (controlled)	1,330
Scrubber gas velocity, ft/sec	12.5
Liquid-to-gas ratio, gal/Mcf	50
Slurry solids concentration, wt % (controlled)	8
Scrubber inlet pH (controlled)	5.0
Total static bed height, inches of 11.5 gram nitrile spheres	15
Oxidation tank level, ft	17
Oxidation tank residence time, min	4.1
Average percent SO ₂ removal	82
Average inlet SO ₂ concentration, ppm	2,400
SO ₂ make-per-pass, m-moles/liter	10.4
Percent oxidation of sulfite to sulfate	98
Air stoichiometry, atoms oxygen/mole SO ₂ absorbed	1.95
Percent lime utilization	97
Scrubber inlet liquor gypsum saturation, %	105
Scrubber inlet liquor SO ₃ ²⁻ /HSO ₃ ⁻ concentration, ppm	100
Centrifuge cake solids content, wt %	72

3-inch diameter pipe was used for this purpose, with the air discharging downwards at the center of the oxidation tank 5 inches from the tank bottom.

Run 951-2E was made with a scrubber inlet pH of 5.0 (oxidation tank pH). Higher pH increases the calcium sulfite scaling tendency and also decreases oxidation efficiency. Lower pH reduces the calcium adipate buffer capacity and SO₂ removal efficiency.

At 5.0 scrubber inlet pH and 50 gal/Mcf liquid-to-gas ratio, sulfite oxidation averaged 98 percent and the SO₂ removal was satisfactory at 82 percent.

It should be noted that under the operating conditions chosen for Run 951-2E, the major SO₂ scrubbing species was calcium adipate because there was little sulfite available, both in liquor or solids, normally the major scrubbing species in an unenhanced lime system without forced oxidation. Higher SO₂ removal than the 82 percent in Run 951-2E should be achievable by simply raising the adipic acid concentration beyond the 1,330 ppm tested.

An SO₂ removal of only 65 percent would be predicted under the same operating conditions as Run 951-2E, but without forced oxidation and without adipic acid addition. With forced oxidation and without adipic acid enhancement, the expected SO₂ removal should be significantly lower than 65 percent.

Limestone Long-Term Test with One Scrubber Loop and Forced Oxidation. A one-scrubber-loop system has an inherent advantage over a two-scrubber-loop system in its simple design and lower capital and operating costs. If a simple one-loop limestone (or lime) system is operated with adipic acid, which offers the advantage of lower operating pH, then both good SO₂ removal and sulfite oxidation can be achieved with minimum cost.

This was illustrated in a long-term adipic acid-enhanced limestone run, Run 917-1A, conducted on the Shawnee spray tower system from December 26, 1980, to March 13, 1981. Figure 4 shows the flow diagram for this long-term run with forced oxidation using two series tanks in the slurry loop. Oxidation was forced in the first tank while fresh limestone was added to the second. Use of two tanks in series in a within-scrubber-loop forced oxidation system has several advantages over a single tank:

- Lower pH in the first tank (oxidation tank), which receives the scrubber effluent slurry, gives better oxidation efficiency
- Limestone blinding potential by calcium sulfite is reduced because liquor sulfite is oxidized in the first tank before fresh limestone is added to the second tank
- Limestone utilization is improved with two tanks in series

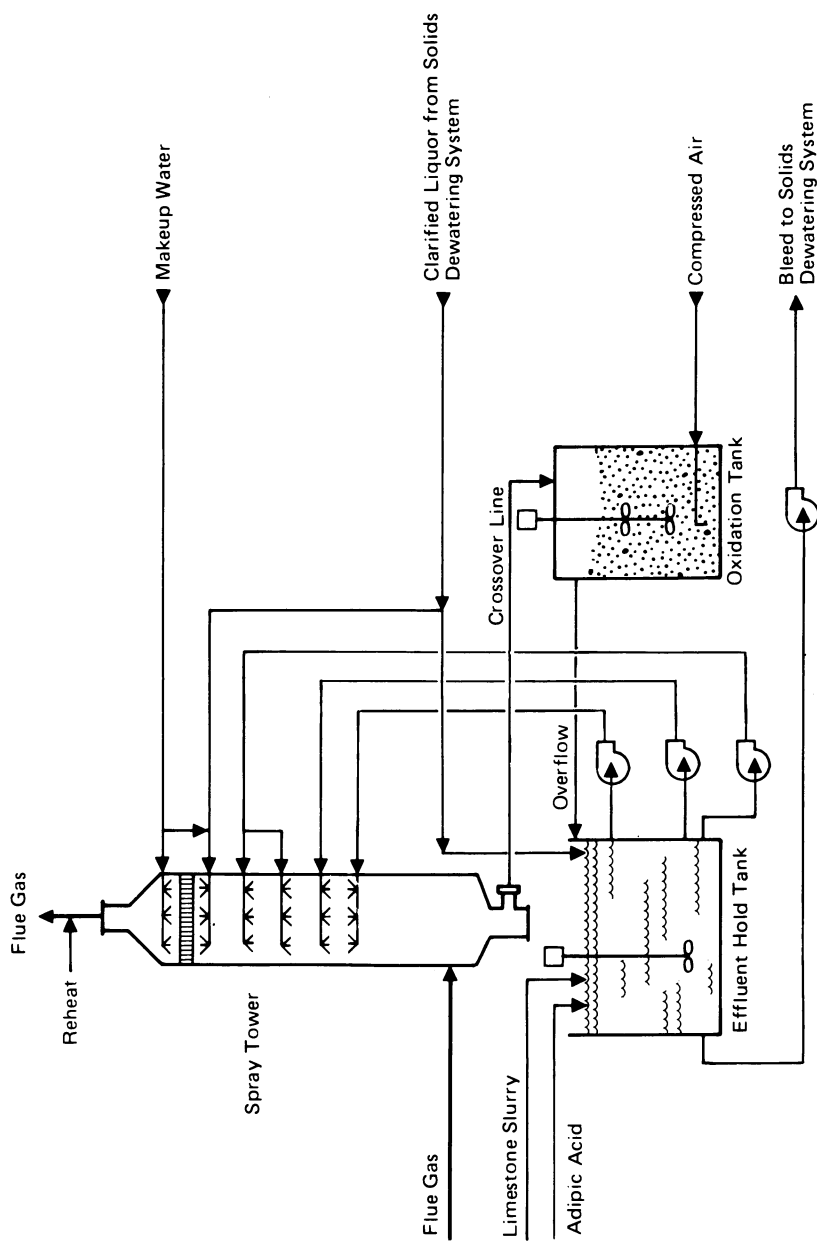


Figure 4. Flow diagram for adipic acid-enhanced limestone scrubbing in the spray tower system with forced oxidation and two tanks.

- The second tank offers extra time for gypsum desupersaturation and precipitation
- The second tank provides air-free suction for slurry recirculation pumps

In any within-scrubber-loop forced oxidation system, irrespective of whether it is additive promoted or not, the possibility exists for calcium sulfite blinding of limestone because the recirculated slurry lacks the solid CaSO_3 crystal seeds. Under this environment, and if the oxidation intensity is not sufficiently high, liquor sulfite could build up to a level at which CaSO_3 begins to precipitate on alkaline limestone particles, causing limestone blinding, reduced dissolution, and a pH drop. The problem is usually avoided by increasing the air stoichiometry to prevent the buildup of sulfite in the liquor. The potential of limestone blinding is further reduced by the use of two tanks in series, as described above, to permit sulfite oxidation before limestone addition.

Table 6 summarizes the important test results of Run 917-1A. As in the previous runs with forced oxidation, air was injected into the oxidation tank through a single 3-inch diameter pipe. The system was onstream for 1,688 hours. During the run, the scrubber was out of service for 78 hours due to equipment problems and 84 hours due to boiler outages. Excluding boiler outages, Run 917-1A operated with an onstream factor of 95.6 percent.

The run was controlled at a scrubber inlet pH of 5.0 to 5.1 and an adipic acid concentration of 1,300 to 1,700 ppm to obtain 90 percent or higher SO_2 removal. The flue gas flow rate was varied between 20,000 and 35,000 acfm (5.4 to 9.4 ft/sec superficial gas velocity) according to a "typical daily boiler load cycle." The slurry flow rate was fixed at 2,400 gpm ($\text{L/G} = 85$ to 150 gal/Mcf). Slurry solids concentration was controlled at 15 percent.

SO_2 removal during the run averaged 93.4 percent at 2,660 ppm average inlet SO_2 concentration. At the low L/G of 85 gal/Mcf, SO_2 removal varied from 87 to 92 percent with 1,300 ppm adipic acid, and from 90 to 93 percent with 1,700 ppm adipic acid. At the high L/G of 150 gal/Mcf, the removal was 97 to 99 percent. Daily average SO_2 removal was 92 to 95 percent.

Limestone utilization averaged 92.6 percent. Sulfite oxidation was excellent at 99.8 percent and the filter cake solids content was high, averaging 86 percent. Gypsum saturation in the scrubber inlet liquor was only 93 percent.

The mist eliminator was completely clean at the end of the run, and there was no evidence of plugging or scaling within the spray tower.

The actual adipic acid consumption rate during Run 917-1A was only 5.4 lb/ton of limestone feed, four times the theoretical requirement.

Table 6.
Adipic Acid-Enhanced Limestone Test on the Single-Loop Spray Tower
System with Forced Oxidation and Two Tanks

Run No.	917-1A
Onstream hours	1,688
Fly ash loading	High
Adipic acid concentration, ppm (controlled)	1,300-1,700
Scrubber gas velocity, ft/sec	5.4-9.4
Liquid-to-gas ratio, gal/Mcf	85-150
Slurry solids concentration, wt % (controlled)	15
Scrubber inlet pH (controlled)	5.0-5.1
Oxidation tank level, ft	18
Oxidation tank residence time, min	2.8
Effluent hold tank residence time, min	8.3
Average percent SO ₂ removal	93.4
Average inlet SO ₂ concentration, ppm	2,660
SO ₂ make-per-pass, m-moles/liter	4.0-8.9
Percent oxidation of sulfite to sulfate	99.8
Air stoichiometry, atoms oxygen/mole SO ₂ absorbed	1.4-2.4
Oxidation tank pH	4.9
Percent limestone utilization	92.6
Scrubber inlet liquor gypsum saturation, %	93
Filter cake solids content, wt %	86

Limestone Tests with Bleed Stream Oxidation. A major advantage of the bleed stream oxidation is its simple flow configuration. In operation without forced oxidation, the scrubber bleed stream would be sent directly to the solids dewatering system. To oxidize this bleed stream, it is necessary only to install an oxidation tank and the associated agitator and compressed air system anywhere between the effluent hold tank and the solids dewatering area. Thus, the bleed stream oxidation scheme is particularly well suited for retrofit when modifications of the existing scrubber system for within-scrubber-loop forced oxidation are not possible due to physical constraints.

Bleed stream oxidation of unenhanced lime or limestone slurry is usually not feasible because the pH rise caused by the residual alkali in the oxidation tank makes it difficult to redissolve the solid calcium sulfite. With adipic acid-enhanced limestone scrubbing, however, this constraint is removed because of the low operating pH and low residual alkali in the bleed slurry. Thus, the oxidation tank can be maintained at a low pH for good sulfite oxidation, while achieving high SO₂ removal efficiency with a sufficiently high concentration of adipic acid in the scrubber liquor.

Table 7 gives the results of a typical bleed stream oxidation test, Run 915-1C, which was conducted with adipic acid-enhanced limestone on the venturi/spray tower system. The effluent slurries from the venturi and the spray tower were discharged into a common effluent hold tank. The scrubber bleed stream was pumped from the effluent hold tank to an oxidation tank into which air was injected through a 3-inch diameter pipe. The final system bleed was withdrawn from the oxidation tank and sent to the solids dewatering system.

Good sulfite oxidation of 98 percent was achieved in the oxidation tank at 4.8 pH and 1.8 air stoichiometry. SO₂ removal was high at 96 percent with 4.8 scrubber inlet pH, 4,140 ppm adipic acid, and 2,030 ppm inlet SO₂ concentration.

Degradation of adipic acid was low, as expected with the low pH operation. The actual-to-theoretical adipic acid consumption ratio was only 1.26 for a rate of 8.7 lb/ton of limestone feed. The centrifuge cake solids content was 79 percent.

Factorial Test Results. Full or partial factorial tests have been conducted at Shawnee, primarily to investigate the effects of adipic acid concentration and pH on SO₂ removal. These tests usually lasted 12 hours or longer, including at least 5 to 7 hours of steady-state operation. Scrubber configurations used were: venturi alone, spray tower alone, combined venturi and spray tower, and TCA. Limestone was used in all scrubber configurations. Lime was used only with the venturi alone. Only the typical results from the TCA and spray tower tests are presented below to show the degree of effect of pH and adipic acid concentration on SO₂ removal.

Table 7.
Adipic Acid-Enhanced Limestone Test on the Venturi/Spray Tower System
with Bleed Stream Oxidation

Run No.	915-1C
Onstream hours	127
Fly ash loading	High
Adipic acid concentration, ppm (controlled)	4,140
Spray tower gas velocity, ft/sec	9.4
Venturi liquid-to-gas ratio, gal/Mcf	21
Spray tower liquid-to-gas ratio, gal/Mcf	57
Slurry solids concentration, wt % (controlled)	15
Scrubber inlet pH (controlled)	4.8
Venturi pressure drop, in. H ₂ O	9
Oxidation tank level, ft	17
Effluent hold tank residence time, min	9.1
Average percent SO ₂ removal	96
Average inlet SO ₂ concentration, ppm	2,030
Percent sulfite oxidation in effluent hold tank	54
Percent sulfite oxidation in oxidation tank	98
Air stoichiometry, atoms oxygen/mole SO ₂ absorbed	1.8
Oxidation tank pH	4.8
Percent limestone utilization	88
Scrubber inlet liquor gypsum saturation, %	105
Oxidation tank liquor gypsum saturation, %	100
Centrifuge cake solids content, wt %	79

Figures 5 through 7 show the results of partial factorial limestone runs conducted on the TCA system using two tanks in series. Operating conditions common to all runs were:

Fly ash loading: High (2 to 7 grains/dry scf)
Slurry solids concentration: 15 percent
Oxidation tank level (7 ft diameter): 18 ft
Effluent hold tank level (20 ft diameter): 6.2 ft
Air flow to oxidizer: 220 scfm (for runs with
forced oxidation)

Figure 5 shows the SO₂ removal as a function of adipic acid concentration and slurry flow rate for the TCA without spheres (grid tower). With a controlled limestone stoichiometry of 1.2 (5.6 to 6.1 scrubber inlet pH) and a slurry flow rate of 37 gpm/ft², adipic acid concentration greater than 2,000 ppm would be required to achieve 90 percent SO₂ removal.

Figure 6 is similar to Figure 5 except that the data used for Figure 6 were obtained using 15 inches (5 inches per bed) of static height of spheres in the TCA. With a controlled limestone stoichiometry of 1.2, 90 percent SO₂ removal could be obtained with 2,000 ppm adipic acid and only 19 gpm/ft² slurry flow rate, or with only 600 ppm adipic acid at 28 gpm/ft² slurry flow rate. With 37 gpm/ft², the required adipic acid concentration is only 300 ppm to achieve 90 percent removal. Both Figures 5 and 6 show that, at 1.2 limestone stoichiometry (5.6 to 6.1 scrubber inlet pH), SO₂ removal begins to "taper off" at about 600 ppm adipic acid concentration.

The effects of scrubber inlet pH and adipic acid concentration on SO₂ removal in the TCA are given in Figure 7. In comparing Figure 7 with Figures 5 and 6 (high pH data) at the same slurry flow rate of 28 gpm/ft², the low pH curves of Figure 7 have a noticeably steeper slope for adipic acid concentration above 600 ppm than is the case for the high pH data. At low pH, the adipic acid is partially ineffective because of a significant amount of unionized adipic acid. For example, Figure 6 shows that at a scrubber inlet pH of 5.6 to 6.1 and 28 gpm/ft², 75 percent SO₂ removal can be achieved without adipic acid. To achieve this same 75 percent removal, Figure 7 indicates that 600 ppm adipic acid is required at 5.3 scrubber inlet pH and 1,700 ppm at 4.6 inlet pH. Therefore, operation at a very low pH with adipic acid-enhanced limestone is not as attractive as at the higher pH from the process standpoint, since adipic acid is only partially utilized for SO₂ scrubbing, and the SO₂ removal is far more sensitive to fluctuations in both pH and adipic acid concentration.

Figures 8 and 9 show the results of partial factorial limestone runs made on the spray tower. Common operating conditions for these runs were:

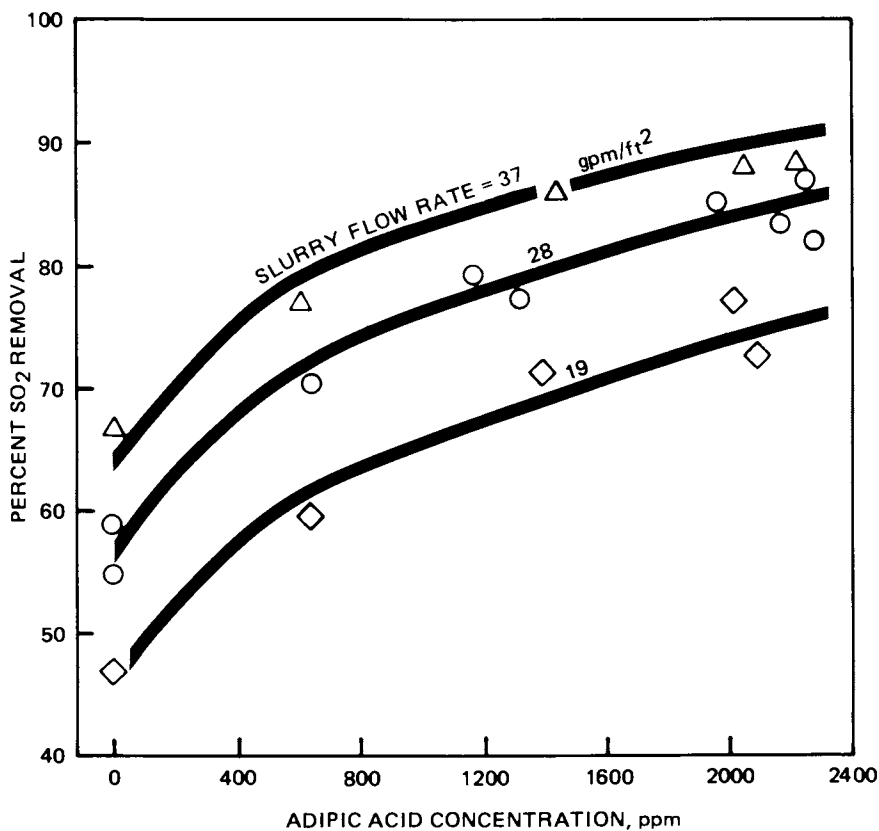


Figure 5. Effect of adipic acid concentration and slurry flow rate on SO_2 removal in the TCA with four grids and without spheres. Key: Δ , 37 gpm/ft²; \circ , 28 gpm/ft²; and \diamond , 19 gpm/ft². Inlet SO_2 , 1800–2800 ppm; gas velocity, 8.4–12.5 ft/s; scrubber inlet pH, 5.6–6.1 (limestone stoich., 1.2); height of spheres, 0 in. with forced oxidation.

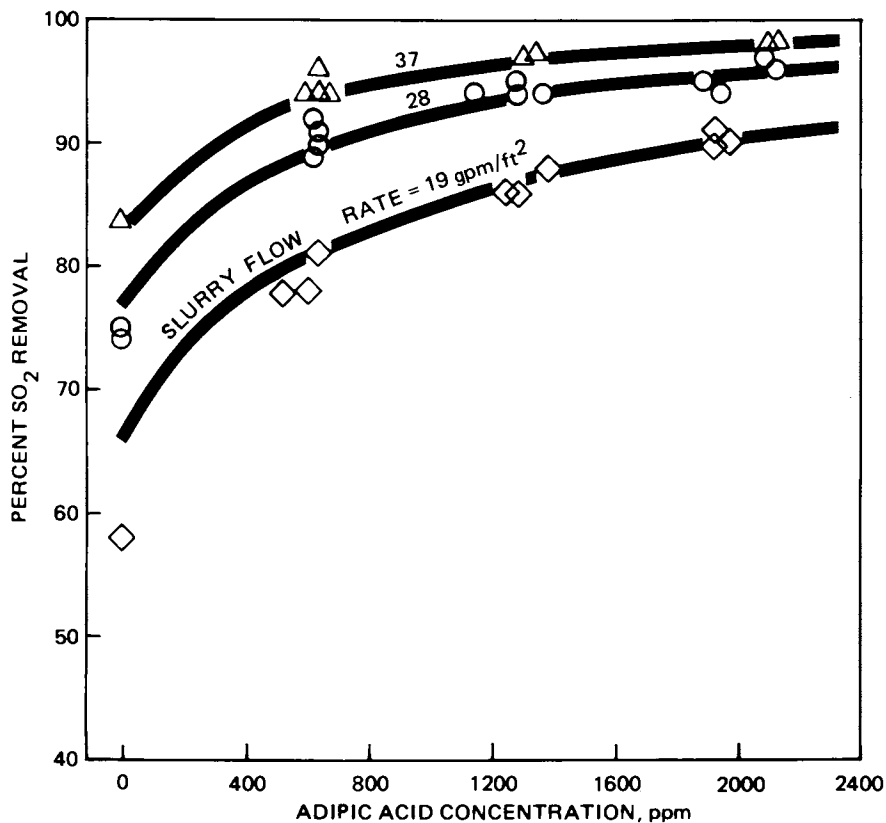


Figure 6. Effect of adipic acid concentration and slurry flow rate on SO_2 removal in the TCA with four grids and 15 in. of spheres. Key: ∇ , pH 5.6; \diamond , pH 5.3; \circ , 28 gpm/ft²; and \square , 19 gpm/ft². Inlet SO_2 , 1800–2800 ppm; gas velocity, 8.4–12.5 ft/s; scrubber inlet pH, 5.6–6.1 (limestone stoich., 1.2); height of spheres, 15 in. with and without forced oxidation.

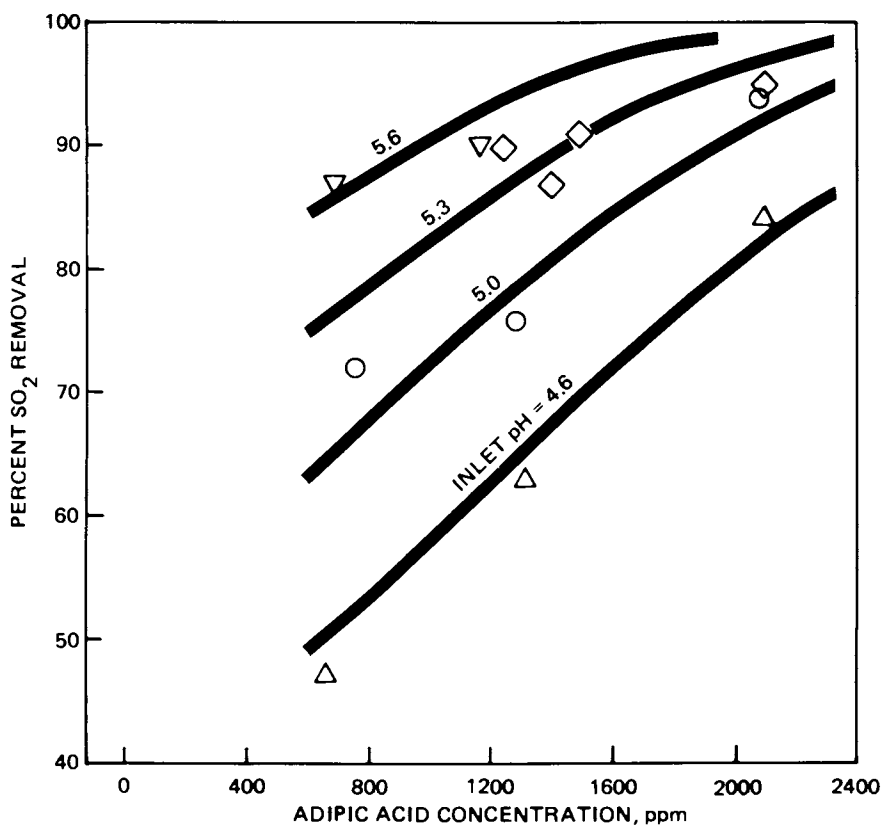


Figure 7. Effect of adipic acid concentration and scrubber inlet pH on SO₂ removal in the TCA with four grids and 15 in. of spheres. Key: ▽, pH 5.6; ◇, pH 5.3; ○, pH 5.0; and △, pH 4.6. Inlet SO₂, 1800–2800 ppm; gas velocity, 10.4 ft/s; slurry flow rate, 28 gpm/ft²; height of spheres, 15 in. with forced oxidation.

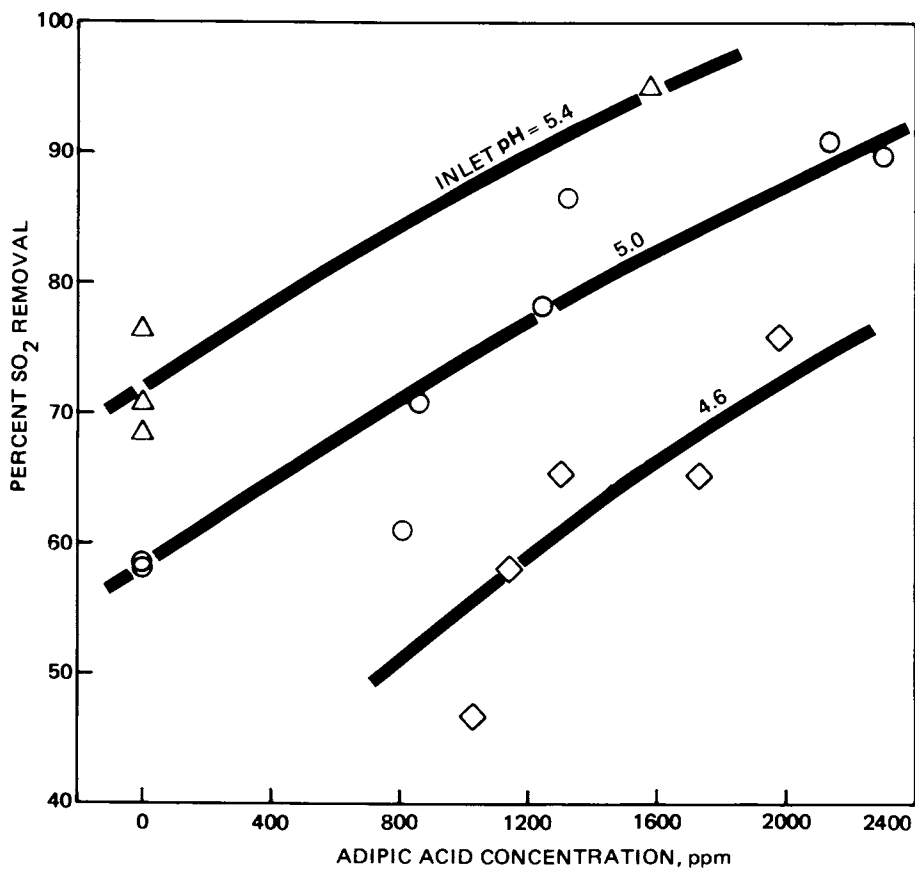


Figure 8. Effect of adipic acid concentration and scrubber inlet pH on SO₂ removal in the spray tower without forced oxidation. Key: Δ , pH 5.4; \circ , pH 5.0; and \diamond , pH 4.6. Inlet SO₂, 2380–3000 ppm; gas velocity, 9.4 ft/s; and L/G, 85 gal/Mcf.

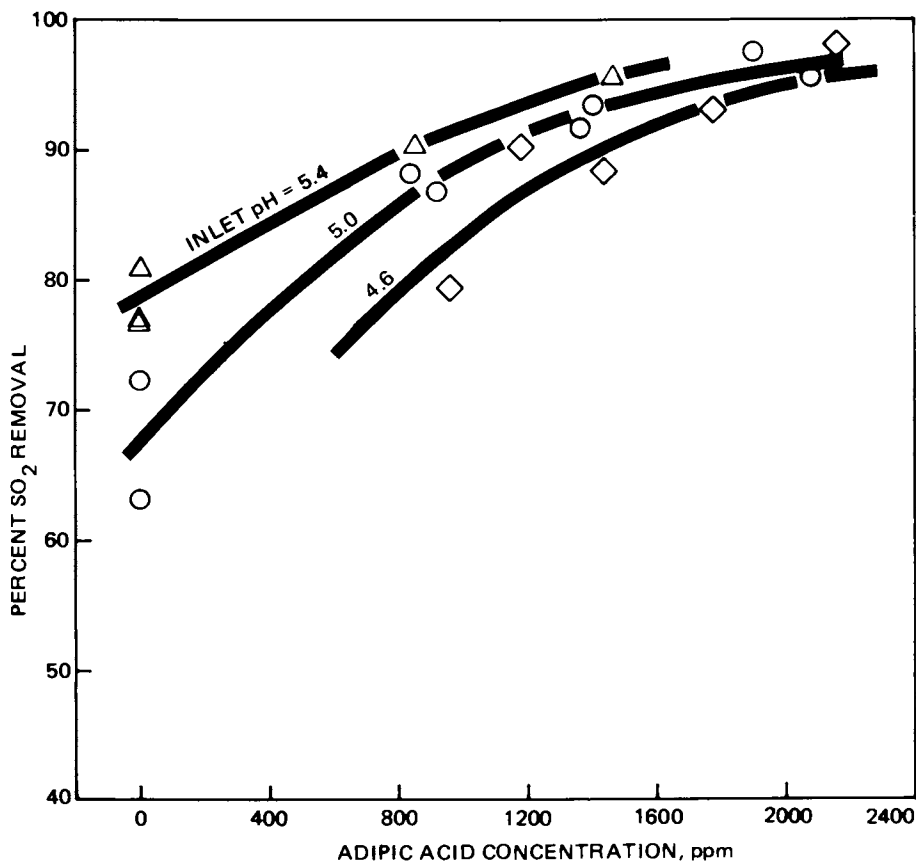


Figure 9. Effect of adipic acid concentration and scrubber inlet pH on SO₂ removal in the spray tower with forced oxidation. Key: Δ , pH 5.4; \circ , pH 5.0; and \diamond , pH 4.6. Inlet SO₂, 2360–3090 ppm; gas velocity, 9.4 ft/s; and L/G, 85 gal/Mcf.

Fly ash loading: High (2 to 7 grains/dry scf)
Slurry solids concentration: 15 percent
Gas velocity: 9.4 ft/sec
Liquid-to-gas ratio: 85 gal/Mcf (2,400 gpm)
Air flow to oxidizer: 250 scfm (for runs with forced oxidation)

For runs without forced oxidation, a single effluent tank 20 ft in diameter with 8.5-ft tank level was used. For runs with forced oxidation, two tanks in series were used with an oxidation tank preceding the effluent hold tank. The oxidation tank was 8 ft in diameter with an 18-ft tank level.

Figure 8 gives the SO₂ removal as a function of adipic acid concentration and spray tower inlet pH for runs made without forced oxidation and at a constant liquid-to-gas ratio of 85 gal/Mcf. SO₂ removal is sensitive to both pH and adipic acid concentration within the ranges shown in the figure. At a liquid-to-gas ratio of 85 gal/Mcf, 90 percent SO₂ removal could be achieved at 5.4 scrubber inlet pH and 1,200 ppm adipic acid, or 5.0 inlet pH and 2,200 ppm adipic acid. At 4.6 inlet pH, the required adipic acid concentration is estimated to be in excess of 3,000 ppm to yield 90 percent SO₂ removal.

Figure 9 shows the effects of scrubber inlet pH and adipic acid concentration on SO₂ removal for runs made with forced oxidation. As in Figure 8, the liquid-to-gas ratio was held constant at 85 gal/Mcf for the runs shown in Figure 9. By comparing the two figures, it is seen that forced oxidation dramatically improved the SO₂ removal, especially at the scrubber inlet pH below about 5.0. For example, at 1,200 ppm adipic acid concentration and without forced oxidation, SO₂ removals were 59.77, and 90 percent at scrubber inlet pH of 4.6, 5.0, and 5.4, respectively. The corresponding SO₂ removals with forced oxidation were 87, 91, and 94 percent.

The reason for improved SO₂ removal, particularly at low pH, is that forced oxidation eliminates bisulfite species, thereby reducing the SO₂ vapor pressure at the gas-liquid interface and improving the SO₂ mass transfer efficiency. This mechanism of improved SO₂ removal holds true when sulfite is not a major scrubbing species and the SO₂ removal does not depend on the sulfite-bisulfite buffer. In the case of Figure 8 and 9, calcium adipate is the major scrubbing reagent.

Therefore, it would be advantageous to operate a low pH, adipic acid-enhanced limestone or lime system with within-scrubber-loop forced oxidation which, in addition to improved SO₂ removal, requires low adipic acid makeup, minimizes gypsum scaling potential, and produces a sludge with good disposal properties. Based on Figure 9, 90 percent SO₂ removal can be achieved at 5.0 inlet pH and only 1,100 ppm adipic acid, or at 4.6 inlet pH with 1,400 ppm adipic acid.

Springfield Full-Scale Demonstration. In August and September 1980, the EPA, through its contractor, Radian Corporation, conducted the first demonstration of the commercial feasibility of adipic acid addition to a full-scale limestone scrubber (8). The host facility was the Southwest Power Plant of the City Utilities of Springfield, Missouri. In that facility, 3.5 percent sulfur eastern coal is burned in two boilers with a total generating capacity of 200 MW. The flue gas from the electrostatic precipitators is scrubbed by two parallel 100 MW TCA's.

During this initial two-month test period, seven different sets of test conditions were examined. Table 8 presents the major results of two baseline tests without adipic acid conducted on Modules S-1 and S-2, and seven tests with adipic acid conducted on Module S-1. All tests were without forced oxidation.

SO₂ removal improved from 68 to 72 percent for the baseline tests to 91, 95, and 96 percent with 840, 1,040, and 1,650 ppm adipic acid, respectively, at the same scrubber inlet pH of 5.5. At 5.0 inlet pH, SO₂ removal remained high at 84, 90, and 93 percent with 1,250, 13,00, and 1,800 ppm adipic acid, respectively. At the lower pH of 5.0, the limestone utilization also increased from 76 to 84 percent for the baseline tests (pH 5.5) to 84 to 97 percent.

The results are consistent with the Shawnee findings. Furthermore, the SO₂ removal obtained at Springfield lay within 1 to 3 percentage points of model prediction based on the Shawnee data under similar operating conditions.

It should be noted that the odor associated with the adipic acid testing also was not a problem at Springfield.

Following these initial tests, the scrubber system was shut down for scheduled maintenance. Subsequently, the demonstration continued with adipic acid testing, both with and without forced oxidation. These results will be reported separately by others.

Rickenbacker Industrial Boiler Demonstration. In February, March, and April 1981, the EPA, through its contractor, PEDCo Environmental, Inc., conducted adipic acid-enhanced limestone scrubber tests on an industrial-sized system. The testing was carried out at the Rickenbacker Air Force Base on a Research-Cottrell/Bahco system rated at 55,000 scfm, or about 27 MW equivalent. The tests, conducted with certified instrumentation, indicated an SO₂ removal efficiency increase from 55 percent without adipic acid, to 90 to 95 percent with adipic acid. This improvement was achieved at a scrubber inlet pH of 5.0 and adipic acid concentrations of between 2,000 and 2,500 ppm. More complete data will be reported separately by others.

Economics

The economics of limestone scrubbing, with or without additive, have been projected for forced oxidation systems designed to

Table 8.
Results of Springfield Full-Scale Adipic Acid Demonstration

Test	Gas Flow 10 ³ dscfm	Slurry Flow* gpm	Inlet SO ₂ ppm dry	Scrubber Inlet pH	Adipic Acid Conc. ppm	Av. SO ₂ Removal %	Limestone Util. %	Test Period hrs.
Baseline								
S-1	171	13,500	2,410	5.5	0	68	76	497
S-2	163	13,500	2,410	5.5	0	72	84	408
Adipic Acid (S-1)								
1	201	13,500	2,460	5.5	840	91	82	122
2	187	13,500	2,360	5.5	1,040	95	75	50
3	190	13,500	2,420	5.2	1,000	88	94	74
4	193	13,500	2,500	5.0	1,250	84	91	44
5	192	13,500	2,540	5.0	1,800	93	84	33
6	196	13,500	2,500	5.5	1,650	96	73	89
7	175	13,500	2,640	5.0	1,300	90	97	84

*Slurry contains approximately 10 wt % solids.

achieve an average of 90 percent SO₂ removal from high-sulfur flue gas. The capital investment and revenue requirements are calculated using a Design/Economics Computer Program which was jointly developed by TVA and Bechtel under EPA sponsorship (9,10).

For the purposes of this report, four cases were studied, including a limestone case with MgO additive. The operating conditions for these cases are presented in Table 9. The evaluations were based on a 500 MW scrubbing facility incorporating forced oxidation, and operating on flue gas from a boiler burning eastern coal containing 4 percent sulfur by weight. The cases evaluated were:

- Case 1 - A limestone base case without additive operated at relatively high limestone stoichiometry and liquid-to-gas-ratio to achieve 90 percent SO₂ removal. It should be noted that long-term reliability with this mode of operation has not been demonstrated at Shawnee.
- Case 2 - A limestone case with MgO addition. Oxidation of the scrubber bleed stream was chosen because in-loop oxidation is incompatible with magnesium-enhanced scrubbing. As in Case 1, long-term reliability has not been demonstrated at Shawnee for this mode of operation.
- Case 3 - A limestone case with adipic acid addition operated at high pH. Although only 800 ppm adipic acid is required to obtain 90 percent SO₂ removal, degradation of adipic acid at high pH requires about five times the theoretical adipic acid addition rate.
- Case 4 - A limestone case with adipic acid addition operated at low pH. For this case, 2,000 ppm adipic acid is required. However, the low pH operation requires only 1.4 times the theoretical adipic acid addition rate and 1.05 limestone stoichiometry.

The results of the economic evaluations are presented in Tables 10 and 11. The capital investment and the first-year revenue requirement in Table 10 include the dewatering equipment (thickener and filter) but exclude the waste sludge (filter cake) disposal area. Table 11 lists separately the first-year revenue requirement for the waste sludge disposal area.

As shown in Table 10, both the total capital investment and the first-year revenue requirement are the lowest for adipic acid-enhanced limestone scrubbing at low pH (Case 4). The total capital investment is reduced by 4.8 percent, and the first year revenue requirement reduced by 5.8 percent for the limestone/adipic acid/low pH case (Case 4), compared with the conventional

Table 9.

Conditions for Economic Analysis of Limestone Scrubbing with Forced Oxidation and with or without Additive

Capacity:	500 MW			
Coal:	4 wt % sulfur			
Scrubber:	TCA with 3 beds, 4 grids, and 5 inches of static height of spheres per bed			
SO ₂ removal efficiency:	90%			
Superficial gas velocity:	12.5 ft/sec			
Number of trains:	5, including one spare train			
Solids dewatering:	To 80% solids by thickener and rotary drum vacuum filter			
Onstream factor:	5,500 hr/yr			
Effluent hold tank residence time:	5 min			
Oxidation tank residence time:	5 min			
Oxidation tank level:	18 ft			
Air sparger pressure drop:	5 psi			
Oxidation tank agitator Hp:	0.002 brake Hp/gal			
Solid sulfite oxidation:	99%			
Air stoichiometry:	1.7 lb-atoms O/lb mole SO ₂ absorbed			
Number of tanks:	2 (effluent hold tank and oxidation tank)			
Alkali:	Limestone			
Case No.	1	2	3	4
Additive	—	MgO	Adipic Acid	Adipic Acid
Additive concentration, ppm	—	5,500 ^(a)	800	2,000
Additive rate, lb/hr	—	104	83.3 ^(b)	53.6 ^(c)
L/G, gal/Mcf	58	50	50	50
Limestone stoichiometry, moles Ca/mole SO ₂ absorbed	1.52	1.20	1.20	1.05
TCA inlet pH	5.8	5.4	5.6	4.8
Mode of oxidation	1 loop, 2 tanks	bleed stream	1 loop, 2 tanks	1 loop, 2 tanks

(a) Excess of molar equivalent of chloride.

(b) Five times theoretical consumption.

(c) 1.4 times theoretical consumption.

Table 10.
Results of Economic Analysis Excluding Waste Sludge Disposal Area

Case No.	Total Capital Investment			First Year Revenue Requirement		
	\$ MM (1982)	\$/kW	Cost Factor	\$ MM (1984)	Mills/kWh	Cost Factor
1	87.40	174.8	1.000	25.01	9.09	1.000
2	85.26	170.5	0.975	24.15	8.78	0.966
3	83.97	167.9	0.961	24.01	8.73	0.960
4	83.22	166.4	0.952	23.56	8.57	0.942

Revenue requirement includes 14.7% annual capital charge.

Raw material costs (1984):
 Limestone — \$8.5/ton
 MgO — \$460/ton
 Adipic Acid — \$1200/ton

Table 11.
Revenue Requirement in Waste Sludge Disposal Area

Case No.	Filter Cake, dry tons/hr	First Year Revenue Requirement, Mills/kWh (1984)			
		Total Excluding Sludge Disposal	Sludge Disposal	Total	Cost Factor
1	48.7	9.09	0.97	10.06	1.000
2	41.6	8.78	0.83	9.61	0.955
3	41.6	8.73	0.83	9.56	0.950
4	38.3	8.57	0.77	9.34	0.928

Revenue requirement includes 14.7% annual capital charges.

Sludge disposal cost assumes \$10/dry ton, including 14.7% annual capital charge.

limestone case (Case 1). The revenue requirement includes 14.7 percent annual capital charge.

Total capital investment and operating costs for adipic acid-enhanced limestone at high pH (Case 3) are higher than those for limestone/adipic acid at low pH (Case 4), but are still lower than those for the conventional limestone (Case 1) or the limestone/MgO case (Case 2). Total capital investment is lower by 3.9 percent, and the first-year revenue requirement is lower by 4.0 percent for Case 3, compared with Case 1.

Table 11 illustrates the additional savings that result from adipic acid addition. Because of the lower pH operation, and thus lower limestone consumption, the amount of waste solids produced is lower for limestone/adipic acid cases (Cases 3 and 4) than for a limestone case (Case 1). Assuming a landfill disposal cost of \$10/dry ton, including 14.7 percent annual capital charge, the first-year revenue requirements for the sludge disposal area are 0.97, 0.83, and 0.77 mills/kWh for Cases 1, 3, and 4, respectively. Thus, the total first-year revenue requirement, including the sludge disposal area, is 9.34 mills/kWh for Case 4, compared with 10.06 mills/kWh for Case 1. This is a reduction of 7.2 percent, compared with 5.8 percent when the sludge disposal cost is not included.

These cost figures are cited as representative of typical scenarios only, and some variation from them would be normally expected. Moreover, the differences in total capital investments and operating costs between these cases are small. The principal conclusion from these evaluations is that adipic acid addition to a limestone scrubbing system decreases cost consistently when compared on the same basis.

It should be noted that adipic acid use provides a level of flexibility in fuel and reagent choice and control level not available with other systems, and in site-specific cases, may prove to be much more economically advantageous than indicated above.

Acknowledgment

This paper utilizes data that were acquired as part of the Environmental Protection Agency's Shawnee Wet Scrubbing Test Program under Contract No. 68-02-3114. J. E. Williams, R. H. Borgwardt, and J. D. Mobley were the EPA Project Officers.

Literature Cited

1. Bechtel Corporation, "EPA Alkali Scrubbing Test Facility: Summary of Testing through October 1974," EPA-650/2-75-047, NTIS PB 244901, June 1975.

2. Bechtel National, Inc., "EPA Alkali Scrubbing Test Facility: Advanced Program, Final Report (October 1974-June 1978)," EPA-600/7-80-115, NTIS PB 80-204241, May 1980.
3. Rochelle, G. T.; King, C. J. Ind. Eng. Chem. Fundam. 1977, 16, 67-75.
4. Borgwardt, R. H. Proceedings: Industry Briefing on EPA Lime/Limestone Wet Scrubbing Test Programs (August 1978), EPA-600/7-79-092, NTIS PB 296517, March 1979, pp. 1-9.
5. Head, H. N.; Wang, S. C.; Rabb, D. T.; Borgwardt, R. H.; Williams, J. E.; Maxwell, M. A. Proceedings: Symposium on Flue Gas Desulfurization - Las Vegas, Nevada, March 1979; Volume I, EPA-600/7-79-167a, NTIS PB 80-133168, July 1979, pp. 342-385.
6. Burbank, D. A.; Wang, S. C. Proceedings: The Fifth Industry Briefing on IERL-RTP Lime/Limestone Wet Scrubbing Test Programs (December 1979), EPA-600/9-80-032, NTIS PB 80-199813, July 1980, pp. 27-113.
7. Burbank, D. A.; Wang, S.C.; McKinsey, R. R.; Williams, J. E. Proceedings: Symposium on Flue Gas Desulfurization - Houston, October 1980; Volume 1, EPA-600/9-81-019a, April 1981, pp. 233-286.
8. Radian Corporation, "Technical Note - Results of Baseline and Adipic Acid Testing at City Utilities Southwest Power Plant, August-September 1980," EPA Contract No. 68-02-3191, October 20, 1980.
9. Stephenson, C. D.; Torstrick, R. L. Proceedings: The Fifth Industry Briefing on IERL-RTP Lime/Limestone Wet Scrubbing Test Programs (December 1979), EPA-600/9-80-032, NTIS PB 80-199813, July 1980, pp. 167-222.
10. Anders, W. L.; Torstrick, R. L. "Computerized Shawnee Lime/Limestone Scrubbing Model Users Manual," EPA-600/8-81-008, TVA/OP/EDT-81/15, March 1981.

RECEIVED December 21, 1981.

Energy Requirements for SO₂ Absorption in Limestone Scrubbers

ROBERT H. BORGWARDT

U.S. Environmental Protection Agency, Industrial Environmental Research Laboratory, Utilities and Industrial Processes Division, Research Triangle Park, NC 27711

The energy needed to operate limestone scrubbers for flue gas desulfurization (FGD) has been estimated to be as much as 8 percent of the total energy produced by power plants. A major part of the energy demand is electrical power consumed by the fans and pumps of the SO₂ absorber. This paper examines the net work input and gross specific electric demand of three types of limestone scrubbers, using data reported in the literature on pressure drop and slurry recirculation rates for high-sulfur coal applications. It shows that the net work required for 90 percent SO₂ removal is 70 ft-lb/cu ft of flue gas scrubbed in a turbulent contacting absorber (TCA) and 82 ft-lb/cu ft in a spray tower (gas volumes at 125°F and saturated). At 60 percent pump efficiency and 70 percent fan efficiency, the gross electric energy demand for 90 percent SO₂ removal in the TCA and spray tower is 2.8 and 3.4 W/cfm, respectively. A spray tower will nevertheless require only 0.16 percent more of the total plant power production than a TCA scrubber. The data on a high-velocity cocurrent grid tower indicate that it will be more energy efficient than a counter-current spray tower, in addition to reducing the capital cost. Well designed FGD systems using no reheat should not require more than 1.3 percent of the total plant power production. Adipic acid, added at a concentration of 1400 ppm to the scrubbing liquor, can reduce the electric power demand of the absorber by 30 percent. The additive is most cost-effective, however, when used to increase the limestone utilization. New dual-alkali limestone scrubbers can reduce the total energy demand of a FGD system to less than that generated by the combustion of the sulfur in most high sulfur coals.

This chapter not subject to U.S. copyright.
Published 1982 American Chemical Society.

An analysis of the energy and economic impacts of pollution control for coal-fired power plants (1) estimated that as much as 8 percent of the net power production would be required to achieve 92 percent SO₂ removal with limestone flue gas desulfurization (FGD) systems. Others (2) have reported that 2 to 5 percent of the total power generating capacity of a boiler unit is generally required to operate SO₂ scrubbers--exclusive of the energy used to reheat the cooled flue gas--and that the power plant's net generating capacity is effectively "de-rated" by that amount. A study prepared by TVA (3) estimates that 3.5 percent of the total power-plant energy input will be required to meet the current emission standard of 1.2 lb SO₂/M Btu, or 90 percent removal, for new plants burning high sulfur coals. TVA's analysis showed that the total energy demand of the FGD system is divided about equally between the steam requirements for flue gas reheat and the electricity required as "process energy." The process energy can be broken down into four categories, each accounting for the approximate fraction of total electric demand indicated in parentheses:

- 1) Electric power required by the scrubber fans and recycle pumps to effect SO₂ absorption (60 percent).
- 2) Electric power consumed by the scrubber fans to overcome the pressure drop in the connecting ductwork and dampers, and to move the air leaked through the ductwork--primarily at the air preheater (24 percent).
- 3) Electric power used for raw materials handling and preparation; e.g., limestone grinding and waste disposal pumps (9 percent).
- 4) Electric power needed to operate ancillary scrubber equipment such as effluent hold-tank mixers, saturation spray pumps, and thickener rake (7 percent).

Since the energy required for reheat is as great as the sum of all other energy demands, most of the effort to reduce FGD energy consumption has focused on the reheat problem. Bypass reheat has been proven the most energy-efficient technique for use at power plants burning low sulfur coals. A limestone scrubber of this type is said to operate on less than 1.3 percent of plant power production (4). For most coals, the 1979 EPA New Source Performance Standards will effectively disallow bypass reheat in new power plants. Although reheat may provide a slight reduction in ground level pollution (5) in the immediate vicinity of a power plant, its principal function is not pollution control, but corrosion control. Some plants are avoiding reheat altogether by using new stack liner designs and more costly materials of construction, including Inconel 625, to protect equipment downstream of the scrubber; Muela's survey of 103 existing and proposed utility FGD systems in the U.S. showed 20 using this approach. A more innovative solution to the problem is now being

used in Japan and Europe: Ljungstrom type heat exchangers which reheat the scrubbed flue gas with the hot (320°F) scrubber inlet gas from the air preheater. Ando (6) reports a limestone FGD system that is achieving 149°F of reheat by this method.

The relative magnitude of the four categories of electric power demand will vary with the type of scrubber and configuration of the FGD system. Typically, more than 80 percent of the process energy will be consumed by the fans and recycle pumps (categories 1 and 2). Most of this process energy is expended specifically for SO₂ absorption; i.e., to overcome the pressure drop of the absorption tower and to recirculate the absorbing slurry. Improvements in scrubber design which reduce the power requirements of the absorber can thus have a significant impact on the total energy demand. For those systems using no reheat or heat exchange, the electric power required for SO₂ absorption will comprise most of the total energy input and large reductions are possible.

A sensitivity analysis of operating variables which affect the energy requirements of limestone scrubbers (7) identified pH as the most important factor related to the absorber. As a practical matter, however, the operating pH is fixed by constraints imposed by reliability and waste production so that it does not offer an effective means of reducing energy demand. It is known, for example, that the limestone stoichiometric ratio--which largely determines pH--must be maintained below 1.17, corresponding to a pH of 5.6, to avoid mist eliminator fouling (8). A pH of about 5.8 is the maximum that can be used in practice for closed loop operation with high sulfur coals. Since this pH corresponds to a stoichiometric ratio of 1.4 to 1.5, a special washing protocol for the mist eliminators must be strictly adhered to for reliable scrubber operation. The tradeoff of absorption efficiency (and energy consumption) for reliability is also encouraged by the high cost of disposal of the excess sludge produced when operating at high stoichiometric ratios. An alternative to varying pH is to employ scrubber additives which enhance mass transfer, such as MgO or adipic acid. These additives have been shown to have a large effect on the liquid-to-gas ratio required to achieve a given SO₂ removal efficiency and, in the case of adipic acid, to also reduce the amount of limestone needed.

The objective of this analysis is to establish, by examination of available data on pressure drop and pumping rates, the energy required for SO₂ absorption (category 1) as a function of removal efficiency. The available data will be compared for scrubbers of different types at a given removal efficiency and pH when operating with a closed water loop and flue gas from combustion of high sulfur coal. Low sulfur coals will require less energy or a given removal efficiency, since mass transfer is enhanced by lower inlet SO₂ concentration. Finally, the effect on energy demand of additives which affect SO₂ mass transfer will be determined.

Procedure

The power required to move flue gas through the scrubber, from the absorber inlet to the mist eliminator outlet, was calculated from pressure drop and gas flow-rate data reported in the literature for a range of superficial velocities, liquid/gas ratios, and internal scrubber packings. A fan of the wet induced-draft type was assumed for each case, operating on saturated flue gas at 125°F. The gas-side power input was added to the power delivered through the slurry recirculation pumps which was calculated from the volumetric flow rates and the minimum discharge pressures required for the given scrubbers. The total power input for SO₂ absorption was thus determined as:

$$P = Q(\Delta P) + L(H) \quad (1)$$

where: P is the total net mechanical power delivered to the scrubber, ft-lb/min;
 Q is the volumetric flow rate of flue gas out of the scrubber (saturated at 125°F), cu ft/min;
 ΔP is the gas pressure drop across the absorber (including the mist eliminator), lb/sq ft;
 L is the slurry recirculation rate through the absorber, cu ft/min;
 and H is the slurry discharge head of the pumps, determined as:

$$H = (H - H_t) \rho + P_n + P_L \quad (2)$$

where: h is the height of the absorber inlet nozzles, ft;
 h_t is the height of the slurry surface in the effluent hold tank, ft;
 ρ is the density of the slurry (64.8 lb/cu ft at 8 percent solids);
 P_n is the spray nozzle pressure drop, lb/sq ft; and
 P_L is the pressure drop in the slurry piping due to friction and acceleration, lb/sq ft.

To make comparisons on a consistent basis, P was divided by the flue gas throughput to obtain the work required per cubic foot of gas cleaned. This net specific-work input, in ft-lb/cu ft, was used to compare the relative efficiencies of different scrubber types for achieving a given SO₂ removal. The gross electric energy demand, in W/cfm of flue gas scrubbed, was obtained by dividing the net work input by the efficiencies of the fan and pump for converting electrical energy to mechanical energy:

$$\text{Gross electric demand} = \frac{0.0226}{\eta_e} \left[\frac{\Delta P}{\eta_f} + \frac{L(H)}{Q \eta_p} \right] \quad (3)$$

where: η_e is the electrical efficiency of the motors;
 η_f is the mechanical efficiency of the fan; and
 η_p is the mechanical efficiency of the pumps.

Table I summarizes the principal features of the scrubber systems. Most of the data are from the prototype test facility operated for EPA by Bechtel National, Inc. from 1972 through 1980 at the TVA Shawnee Power Plant. The pumping heads shown for the TCA (turbulent contacting absorber) and spray tower in Table I represent operation with a 6-ft clearance between the bottom scrubber flange and the surface of the slurry in the effluent hold tank (EHT). Due to an oversized EHT used in the prototypes, most tests were actually conducted with the EHT only one-third full and the pumping heads were 11 ft higher than those indicated. This free space is assumed to be designed out of both scrubbers when the work input is calculated here. An equal and constant value of $p_L = 1000$ lb/sq ft was assumed in all cases in accordance with the recommended practice of maintaining 8 to 10 ft/sec slurry velocity in the recycle lines. An important feature of the three scrubbers, and a necessary condition for meaningful comparisons between them, is that the same limestone type and grind was used in all tests. It contained 95 percent CaCO₃ and less than 3 percent MgCO₃; the grind was 90 percent passing 325 mesh. The scrubber inlet SO₂ concentrations were 2300 to 2800 ppm. The scrubbers operated closed-loop with chloride levels averaging 3000 ppm in the scrubbing liquor.

TABLE I. FEATURES OF PROTOTYPE SCRUBBERS

	TCA	Spray Tower	Cocurrent Scrubber
Scrubber cross section, sq ft	32	50	12.5
EHT slurry level to:			
Upper spray header, ft	33	33	15, 41
Lower spray header, ft	N/A	24	31
Venturi, ft	N/A	20	N/A
Pressure drop across nozzles, psi	5	10	10

Results and Discussion

TCA Scrubber. Head (9) reported SO₂ removal efficiencies of a limestone TCA operated at a feed slurry pH of 5.8 and three levels each of gas velocity and slurry recirculation rate. Those data are plotted in Figure 1 as a function of the net work input, calculated according to Equations (1) and (2). The partially closed symbols denote tests with three beds of nitrile foam spheres, each bed

having 5 in. static depth. The open symbols denote tests without spheres, in which case the absorber internals consisted only of the four bar grids which normally support the TCA spheres.

It is evident from Figure 1 that a net work input of 70 ft-lb/cu ft is required to remove 90 percent of the scrubber inlet SO_2 . For 70 percent removal, 41 ft-lb/cu ft is required. The net work required to remove a given amount of SO_2 was independent of scrubber gas velocity within the range tested, 8.3 to 12.5 ft/sec.

Figure 1 also shows that removal efficiency increases in a continuous manner with work input for operation with and without spheres. Thus, the spheres do not perceptibly increase the work requirement, but greatly improve the SO_2 absorption for a given slurry recirculation rate. The additional pressure drop caused by the spheres was thus fully energy-effective at bed depths up to 5 in. Tests with the bed depth increased to 7.5 in. (by adding more spheres) were not energy effective; the SO_2 removal obtained for a given work input was about 10 percent lower than the curve of Figure 1.

Spray Tower. Figure 2 shows the SO_2 removals reported by Head (9) and by Burbank and Wang(10) for a limestone spray tower, plotted as a function of the net work input. The feed liquor pH was again 5.8 (stoichiometric ratio = 1.4 to 1.5). Gas velocities and slurry recirculation rates were systematically varied from 5.4 to 9.4 ft/sec, and 15 to 30 gpm/sq ft, respectively. The data include scrubber configurations with and without a venturi preceding the spray tower. All data are for single-loop mode of operation; i.e., the venturi and spray tower were fed from a single EHT.

The pumping energy was calculated for the spray tower assuming that two pumps are used for slurry recirculation: one for the two upper spray headers and one for the two lower headers. Equal flows to the upper two headers were assumed for liquid rates up to half the maximum total flow; beyond half maximum flow, the bottom two headers were assumed to receive the remaining flow. The venturi, when used, was assumed to be provided with a third pump. The pressure drop across the spray nozzles was assumed constant at 10 psi.

The spray tower data correlate with work input in a manner similar to the TCA; the only data not following that correlation were the venturi tests at the highest gas velocity, 9.4 ft/sec, indicating an additional 15 ft-lb/cu ft was needed to attain a given SO_2 removal. One can conclude that the venturi is not energy efficient at velocities above 7.4 ft/sec. Comparison of Figures 1 and 2 shows that the total net work required for 90 percent SO_2 removal in the spray tower, 82 ft-lb/cu ft, is about 17 percent higher than the 70 ft-lb/cu ft required by the TCA.

Work is delivered to the spray tower primarily through the slurry pumps. The TCA scrubber delivers most of the work through the fans due to its lower liquid/gas ratio and higher pressure drop. If the mechanical efficiencies of the pumps and fans were

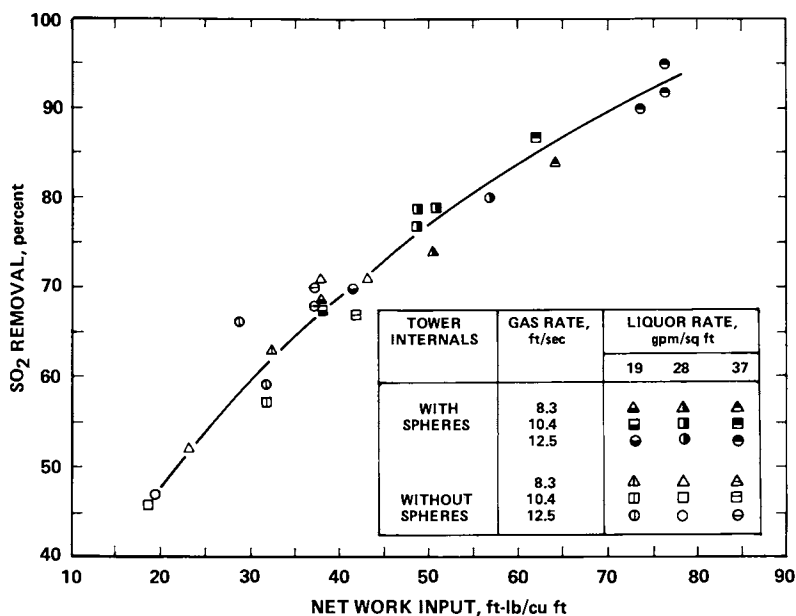


Figure 1. SO₂ removal efficiency of TCA scrubber as a function of net work input, pH 5.8.

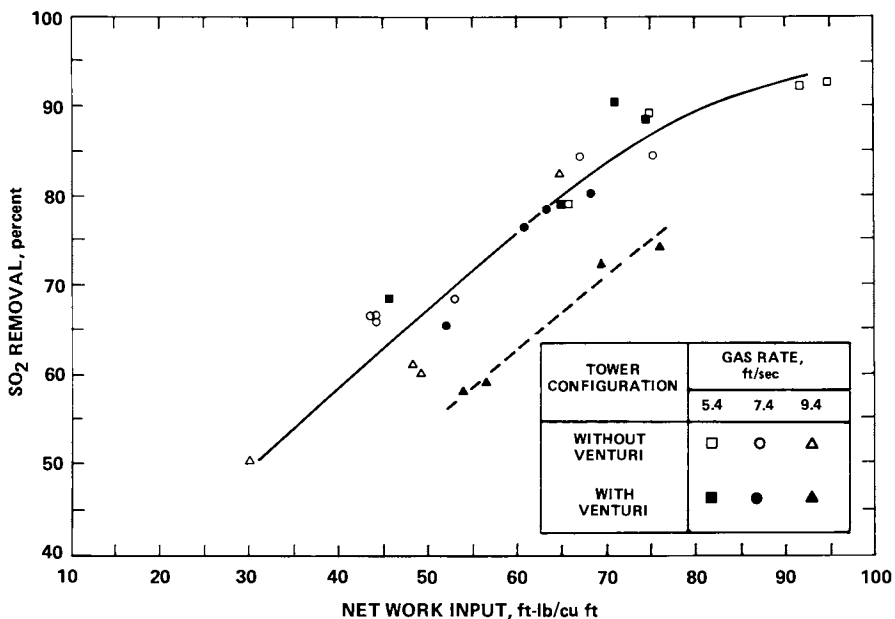


Figure 2. SO₂ removal efficiency of spray tower as a function of net work input, pH 5.8.

equal, then the gross electrical energy demand of the two scrubber types would follow the same relative responses as Figures 1 and 2. Although the efficiency of slurry pumps is generally agreed to be about 60 percent, fan efficiencies are higher--sometimes approaching 80 percent. As a result, the gross electric demand will be lower for scrubbers that deliver most of the work through the fans. Table 2 compares the same data as Figures 1 and 2 on the basis of gross electric demand calculated by Equation (3) for various assumed fan efficiencies. Whereas the spray tower is little affected by fan efficiency, the electric demand of the TCA can be reduced significantly by the use of more efficient fans.

Cocurrent Flow. Henson (11) reported tests with a 45-ft high limestone scrubber in which both the flue gas and the scrubbing slurry entered the top of the tower and moved downward in cocurrent flow. This configuration is capable of higher gas velocities than the countercurrent scrubbers discussed above. The principal advantage expected of this design is a reduction of capital cost due to the smaller scrubber diameter for a given throughput. The scrubber height was varied in those tests as well as gas velocity, L/G, and tower internals. The limestone stoichiometric ratio was again 1.4 mol/mol of SO₂ absorbed. When operated as a 45-ft open spray tower and 18 ft/sec gas velocity, a slurry recirculation rate of 192 gpm/sq ft was required for 88 percent SO₂ removal. Henson reported an increase in pressure across the tower under these conditions due to the energy transferred to the gas by the downward flowing slurry. Using Equations (1) and (2) to calculate the net work input from these data, crediting the work recovered due to the 0.6-in. H₂O pressure gain, yields a value of 119 ft-lb/cu ft. Comparison of this value with Figure 2 shows that the open cocurrent spray tower is less energy efficient than the countercurrent type.

Henson added six 1-1/4 in. thick grids to the cocurrent tower and obtained 90 percent SO₂ removal with a shorter (35-ft) tower and higher (27 ft/sec) gas velocity. A positive 3.0-in. H₂O pressure drop was observed in this case with the slurry recirculation rate again at 192 gpm/sq ft. The net work input was reduced to 91 ft-lb/cu ft due to the lower pumping head. Another test with six 3-3/4 in. grids in the 35-ft tower yielded 6.5-in. H₂O pressure drop at 27 ft/sec gas velocity, but only 112 gpm/sq ft was needed to achieve 90 percent SO₂ removal. The net work input calculated for these conditions is 78 ft-lb/cu ft. Addition of grids to the cocurrent tower thus reduced the work needed for 90 percent SO₂ removal to a level comparable to the countercurrent scrubbers. Since a large part of the work delivered to the grid-packed cocurrent scrubber is through the fan, it will be capable of operating with lower electric power demand than the countercurrent spray tower, as shown by the comparison in Table II. One can conclude from these comparisons that the reductions in capital costs expected from cocurrent high-velocity scrubbers can be realized without penalty in energy demand.

TABLE II. GROSS ELECTRIC ENERGY INPUT FOR
90 PERCENT SO₂ REMOVAL

Mechanical Efficiency of Fan, percent	Gross Energy Input, W/cfm ^a		
	TCA	Spray Tower	Cocurrent Grid Tower
60	3.0	3.45	3.27
70	2.75	3.41	3.07
80	2.51	3.33	2.92

^aPump efficiency = 60 percent; 90 percent motor efficiency.

The gross electric energy demands of the three types of limestone scrubbers are compared in Table III as percentages of the total plant power production. The comparison is based on 2420 cfm per MW (saturated flue gas at 125°F, 1 atm) and 70 percent fan efficiency. In no case does the electric demand for 90 percent SO₂ removal exceed 0.83 percent of production. It is interesting to note that the differential between the highest demand (spray tower) and the lowest demand (TCA) amounts to only 0.16 percent of the total plant power production. From this viewpoint, the simplicity and increased reliability of the spray tower are not expensive attributes in terms of additional energy drain.

TABLE III. ENERGY CONSUMED FOR 90 PERCENT
SO₂ REMOVAL IN LIMESTONE SCRUBBERS^a

Scrubber Type	Percentage of Total Plant Power Production ^b
Spray tower	0.825
Cocurrent grid tower	0.743
Turbulent contacting absorber (TCA)	0.666

^aWet fan, 70 percent efficient;
60 percent pump efficiency.

^bCoal heating value = 11,000 Btu/lb.

Adipic Acid. Any additive which enhances SO_2 mass transfer, especially at low scrubber pH, will increase limestone utilization. The use of adipic acid as an additive to limestone scrubbers has been shown to improve both the SO_2 removal efficiency and limestone utilization at any given set of scrubber operating conditions. As a result, both SO_2 removal efficiency and limestone utilization are increased. A lower work input is also required to achieve a given removal efficiency. Figure 3 shows the effect of 1400 ppm adipic acid in the scrubbing liquor of a TCA system (12); comparison with Figure 1 shows a 30 percent reduction of the work input required for 90 percent SO_2 removal, from 70 to 48 ft-lb/cu ft. Similar plots at other adipic acid concentrations yielded the relationship shown in Figure 4. All of the tests are reported to have been made at a limestone stoichiometric ratio of 1.2, which corresponds to a utilization of 83 percent.

Two options are available. The additive may be used to reduce the energy demand or it can be used to increase limestone utilization. Table IV compares these options, using the 30 percent reduction in gross electric demand as a basis for the evaluation. Since 90 percent removal requires only 0.67 percent of the plant power production (237 kW-hr/ton of SO_2 absorbed) without adipic acid, a 30 percent reduction does not yield sufficient savings in electric power to cover the cost of the additive. If, on the other hand, 2.4 percent or more of the power production were required by the absorber, the value of the power saved would exceed the cost of the adipic acid used, regardless of credits for any other cost reductions. Table IV shows that the alternative approach is most effective--maintaining a higher work input and operating with as little limestone feed (and therefore as little sludge production) as possible. By using the adipic acid to reduce the stoichiometric ratio from 1.4 to 1.1, the value of the limestone saved and the reduced cost of sludge disposal defray the total cost of the adipic acid plus one third of the electric power demand of the absorber. The basis for estimating the effect of adipic acid on utilization is seven runs made in the Shawnee TCA at 1600 ppm concentration and net work input of 72 ft-lb/cu ft. These runs, Nos. 903-2A&B, 907-2L, 928-2A, 932-2A, and 934-2C&D, averaged 95 percent SO_2 removal and 90 percent limestone utilization. The slope of the curve of Figure 1 was used to estimate the energy demand at 90 percent removal.

Table IV also shows that the adipic acid makeup rate must be held below 15.4 lb/ton of SO_2 absorbed in order to recover the cost of the additive when operating at 90 percent limestone utilization. This limit is increased only slightly, to 16.5 lb/ton of SO_2 , at a 97 percent level of limestone utilization. The makeup rate used in Table IV was obtained from two independent Shawnee measurements. One measurement is the average of eight runs (934-2A to -2H) made without fly ash and with 78 percent solids in the discharged sludge; these runs required an average makeup rate of 9.95 lb/ton SO_2 . The second measurement was obtained from

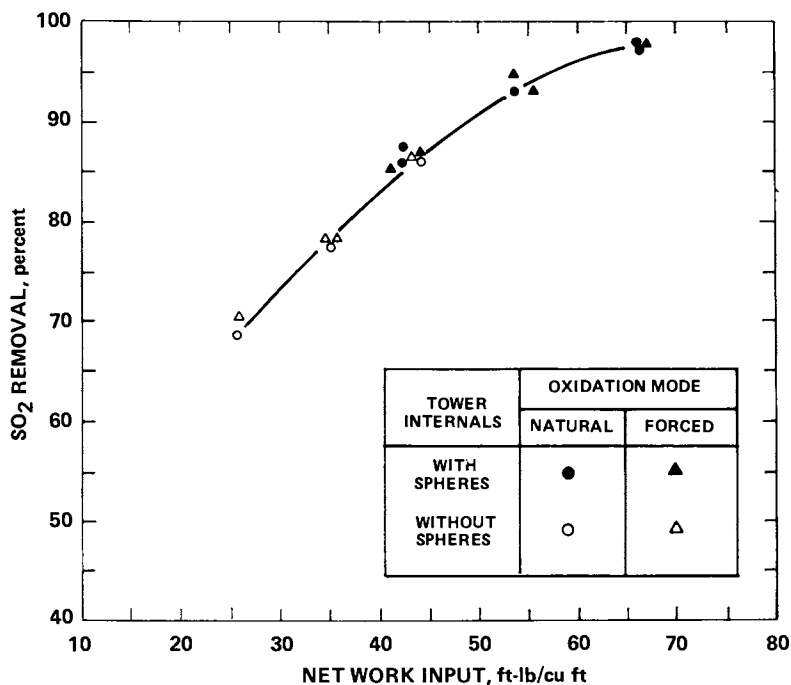


Figure 3. *SO₂ removal efficiency of TCA scrubber vs. net work input with 1400 ppm adipic acid in scrubbing liquor.*

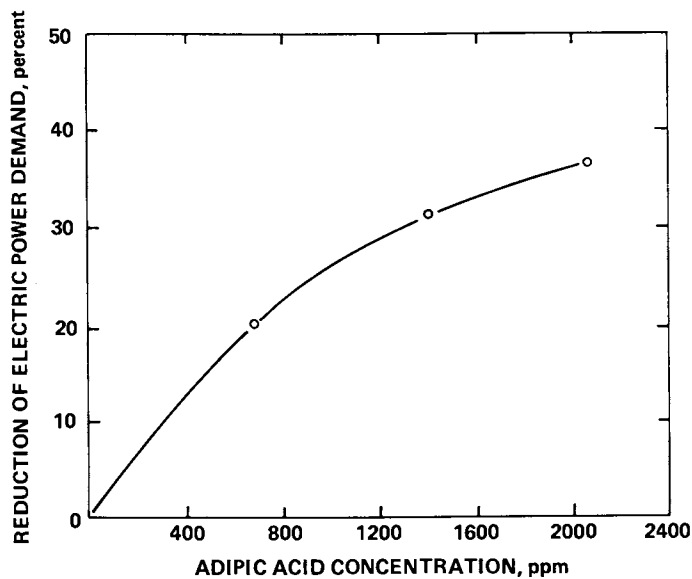


Figure 4. *Effect of adipic acid concentration on gross electric power demand for 90% SO₂ removal in TCA scrubber.*

TABLE IV. COMPARISON OF OPERATING ALTERNATIVES FOR ADIPIC ACID ADDITION

Basis: One ton of SO₂ absorbed in TCA scrubber
 90 percent SO₂ removal efficiency
 Fly-ash-free sludge, 70 percent solids
 Natural oxidation
 Wet fan, 70 percent efficient

	Without Adipic Acid	With Adipic Acid	
Limestone stoichiometric ratio	1.4	1.2	1.1
Dry limestone feed, tons	2.18	1.87	1.71
Sludge produced; tons, dry basis	2.65	2.34	2.18
Power input, kW-hr	237 ^a	166	207
Adipic acid conc., ppm	0	1400	1500
Adipic acid makeup, lb	0	11.9	10.7
Value of limestone saved (@ \$7/ton)		\$2.66	\$3.29
Cost reduction for sludge disposal (@ \$9.4/ton)		\$2.91	\$4.42
Value of power saved		\$2.06	\$0.87
Total saving in operating costs		\$7.63	\$8.58
Cost of adipic acid added (@ \$0.55/lb)		\$6.5	\$5.9
Total saving - cost of additive		\$1.1	\$2.7

^aTotal cost of power for 90 percent SO₂ absorption =
 237 kW-hr x \$0.029/kW-hr = \$6.87

Reliability Run 932-2A, which was made with fly ash, discharged a sludge containing 61 percent solids, and required a makeup of 17.5 lb/ton SO₂. When these data are normalized to a fly-ash-free basis, at equal limestone utilization, and equal sludge moisture, they yield the same makeup rate of 10.7 lb/ton SO₂ for a concentration of 1500 ppm adipic acid in the scrubbing liquor.

The limitation on adipic acid makeup rate likewise implies a minimum acceptable filtration efficiency for break-even operation: on a fly-ash-free basis, the sludge must contain more than 46 percent solids when operating at 90 percent limestone utilization and 1500 ppm adipic acid. For both economic and environmental reasons, filter washing should be employed whenever additives are used in limestone scrubbers.

Figure 3 also shows that 86 percent SO₂ removal can be attained without spheres in the TCA scrubber when using 1400 ppm adipic acid. By increasing the work input by only 5 ft-lb/cu ft, 90 percent SO₂ removal can be expected while eliminating the maintenance and reliability problems associated with the spheres. The necessary work can be delivered by raising the pumping rate or by installing additional grids in the tower. In view of the above discussion, the gross electric demand would be minimized by the latter course.

Fan Location. The fan can be located downstream from the scrubber, in which case it operates on saturated flue gas at 125°F (normally), or the fan can be located upstream, where it operates on hot (ca. 300°F) gas containing about 8 percent moisture. The hot booster fan handles a greater gas volume and therefore requires more energy than the wet fan. A fan located after a reheater will likewise consume more energy than the wet fan because of the higher temperature (ca. 175°F) and the slight additional pressure drop caused by the reheater. Figure 5 is a replot of the data in Figures 1 and 2 to show the gross electric demand of scrubbers using hot booster fans. The spray tower is unaffected: most of the energy is delivered through the pumps and the energy required for 90 percent SO₂ removal remains at 0.83 percent of plant power production. The advantage of the higher-P TCA scrubber virtually disappears, however, increasing from 0.67 percent with a wet fan to 0.73 percent with the hot booster fan. Scrubbers which are preceded by electrostatic precipitators for dry removal of fly ash can use airfoil-type booster fans that provide maximum efficiency. Assuming that a hot fan of this type--and having 80 percent mechanical efficiency--is used with the TCA, the gross energy demand for 90 percent SO₂ removal is 2.80 W/cfm.

Category-2 Demands. The energy consumed by the fan to overcome the pressure drop in that part of the ductwork which is directly associated with the scrubber is chargeable to the FGD system. This includes the modularization ducts and dampers and the reheater, if used. It also includes the energy required to move through the

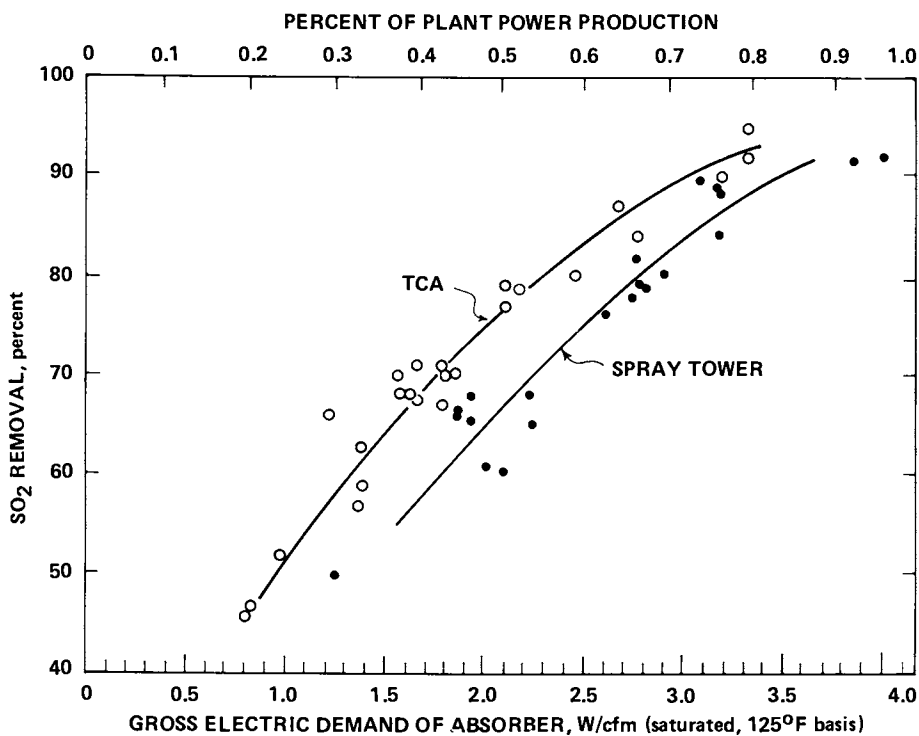


Figure 5. Gross electric power demand of limestone scrubbers using hot (300°F) booster fans.

scrubber any air leaked in via the preheater. With a 2-in. pressure drop in the modularization ducts and 10 percent air leakage, the total process energy required by a spray-tower FGD system operating without reheat is shown in Table V. The energy demand for ancillary motors and raw materials handling was obtained from the total horsepower ratings of equipment listed (13) for a 500-MW power plant.

TABLE V. PROCESS ENERGY REQUIREMENTS
FOR LIMESTONE FGD

Component	Energy Demand, Percent of Plant Power Production
Scrubber (spray tower)	0.83
Ancillary motors and raw materials handling	0.28
Modularization ducts and dampers	0.10
Leakage	0.08
Total	1.29

Sulfur. The energy produced by the combustion of the sulfur in coal is not an insignificant contribution to the total power generated, especially for high sulfur coal. Depending on the ash and water content, 1 lb of 4-percent sulfur coal will yield 1.1 to 1.5 percent more energy than would be obtained if the sulfur were removed prior to combustion. It is significant to note that the total process energy required by FGD systems of current design is within the same range.

Potential for Improvement. Further reductions can be expected in the energy required by the newer generation of limestone FGD systems. The Chiyoda 121 process, which is already offered commercially, eliminates scrubber recycle entirely and reduces energy demands and maintenance problems associated with slurry pumps. The gas-side pressure drop reported (14) for the Chiyoda jet-bubbler absorber is 11.8 in. H₂O at 90 percent SO₂ removal. Disregarding the energy used for air compression (forced oxidation is an integral part of that process) the corresponding net work input is 61 ft-lb/cu ft. By incorporating sludge stacking with the forced oxidation, it affords the prospect of eliminating the clarification and filtration steps which would also affect capital

costs favorably. Another example is the dual alkali system developed by Arthur D. Little, Inc., which uses a clear sodium sulfite solution for SO₂ absorption and limestone regeneration of the spent liquor. Pilot plant tests of this system by EPA (15) have verified that 90 percent SO₂ removal can be achieved with a liquid/gas ratio of only 2.2 gal./Mcf and 7 in. water pressure drop in a sieve-tray absorber. In addition, over 95 percent limestone utilization is obtained. The gross electric demand of the absorber calculated for these conditions by Equation (3), based on the same pump pressure as was used for the TCA calculations, is 1.4 W/cfm. This energy demand amounts to 0.33 percent of the plant power production for the scrubber and 0.79 percent for the entire FGD system, using the same data for other demands as are indicated in Table V. Since it uses a clear solution for SO₂ absorption, this limestone process variation should be particularly well suited for use with the high-velocity cocurrent packed tower developed by TVA. Most important, however, is the potential for operation with minimum sludge production and with a power demand that is less than the energy generated by the combustion of the sulfur in most high sulfur coals.

Conclusions. The analysis leads to the following conclusions regarding limestone FGD scrubbers:

- The net work input required for 90 percent SO₂ removal is 76±6 ft-lb/cu ft (125°F, saturated) of flue gas scrubbed.
- Except for scrubbers using a venturi prescrubber, the specific work input required for 90 percent SO₂ removal is independent of gas velocity to 27 ft/sec.
- The gross electric energy demand of a spray tower is greater than that of a TCA, mainly due to the higher efficiency of fans relative to slurry pumps. The difference between the two scrubber types, however, amounts to only about 0.16 percent of the generated power.
- A 27 ft/sec cocurrent packed tower can achieve 90 percent SO₂ removal with less energy input than a countercurrent spray tower.
- The TCA scrubber is more energy-efficient than either type of spray tower.
- In high-sulfur coal applications, 90 percent SO₂ removal can be attained with a total process energy of 1.3 percent of the plant power production.
- Adipic acid can reduce the electric demand for 90 percent SO₂ removal in a TCA scrubber by 30 percent at a concentration of 1400 ppm. It sets a ceiling on the power demand at 2.4 percent of plant power production; at a higher demand, the value of the power saved exceeds the cost of the additive.
- Adipic acid will be most effective as a means of improving limestone utilization; potential reductions in sludge disposal and limestone makeup costs are greater than the value of electric power savings.

Systems now under development can be expected to reduce the total process energy demands for limestone FGD below the energy generated from the combustion of the sulfur in most high sulfur coals.

Literature Cited

1. Farber, P.S., Livengood, C.D., "Energy and Economic Impacts of Pollution Control Equipment for Coal-Fired Power Plants: An Assessment Model," 1979, presented at 72nd Annual Meeting of the Air Pollution Control Association, Cincinnati, Ohio.
2. Ferrell, J.D., Stenby, E.W., "Interface Design Problems Between Coal Fired Boilers and SO₂ Scrubbing Systems," 1977, Proceedings of the Second Pacific Chemical Engineering Conference; AIChE, Vol. I, 295-302.
3. McGlamery, G.G., Tarkington, T.W., Tomlinson, S.V., "Economic and Energy Requirements of Sulfur Oxides Control Processes," 1979, Proceedings: Symposium on Flue Gas Desulfurization--Las Vegas, Nevada, March 1979, Vol. I, EPA-600/7-79-167a (NTIS PB 80133168), 137-214.
4. Richman, M., "Limestone FGD Operation at Martin Lake Steam Electric Station," *Ibid.*, 613-28.
5. Muela, C.A., Menzies, W.R., Brna, T.G., "Stack Gas Reheat--Energy and Environmental Aspects," 1979, Proceedings: Symposium on Flue Gas Desulfurization--Las Vegas, Nevada, March 1979, Vol. II, EPA-600/7-79-167b (NTIS PB 80133176), 1161-78.
6. Ando, J., "SO₂ and NO_x Abatement for Coal-Fired Boilers in Japan," 1981, Proceedings: Symposium on Flue Gas Desulfurization - Houston, Texas, October 1980, Vol. I, EPA-600/9-81-019a, 85-109.
7. Ruben, E.S., Nguyen, D.G., J. Air Pollut. Contr. Ass. 1978, 28, 12, 1207-12.
8. Epstein, M., Head, H.N., Wang, S.C., Burbank, D.A., "Results of Mist Elimination and Alkali Utilization Testing at the EPA Alkali Scrubbing Test Facility," 1976, Proceedings: Symposium on Flue Gas Desulfurization, New Orleans, March 1976, Vol. I, EPA-600/2-76-136a (NTIS PB 255317), 145-204.
9. Head, H.N., "EPA Alkali Scrubbing Test Facility: Advanced Program, Third Progress Report," 1977, EPA-600/7-77-105 (NTIS PB 274544), 6-5.
10. Burbank, D.A., Wang, S.C., Progress report for EPA Contract 68-02-3114, Bechtel National, Inc., September 1980, 1-8.
11. Henson, L.J., "TVA/EPRI Shawnee Cocurrent Scrubber Test Results," 1980, Proceedings: Fifth Industry Briefing on IERL-RTP Lime/Limestone Wet Scrubbing Test Programs, December 1979, EPA-600/9-80-032 (NTIS PB 80199813), 116-165.
12. Burbank, D.A., Wang, S.C., Progress report for EPA Contract 68-02-3114, Bechtel National, Inc., August 1979, 1-9.

13. Stephenson, C.D., Torstrick, R.L., "Current Status of Development of the Shawnee Lime-Limestone Computer Program," 1979, Proceedings: Industry Briefing on EPA Lime/Limestone Wet Scrubbing Test Programs (August 1978), EPA-600/7-79-092 (NTIS PB 296517), 94-139.
14. Idemura, H., Kanai, T., Yanagioka, H., "Jet Bubbling Flue Gas Desulfurization Process," 1977, Proceedings of the Second Pacific Chemical Engineering Conference; AIChE, Vol. I, 365-70.
15. Borgwardt, R.H., Dempsey, J.H., Chang, S.C., "Dual Alkali Scrubbing of SO₂ at IERL-RTP Pilot Plant," 1980, Progress Report No. 2, U.S. Environmental Protection Agency, Research Triangle Park, NC.

RECEIVED November 20, 1981.

The Limestone Dual Alkali Process for Flue Gas Desulfurization

JAIME A. VALENCIA

Arthur D. Little, Inc., Cambridge, MA 02140

The limestone dual alkali process developed by Thyssen-CEA Environmental Systems, Inc., and Arthur D. Little, Inc., has been tested at laboratory, pilot plant, and more recently at a 20 MW prototype facility. The intent of this last project was to evaluate the technical feasibility of the process at a prototype scale and to develop sufficient technical information leading to the implementation of the process at a full, commercial scale. Throughout two months of testing, excellent SO₂ removal efficiencies in excess of 95% were achieved. Limestone utilizations were also high, over 97%. Further refinement, however, is needed in controlling the properties of the waste solids generated. The status of the technology based on the testing and operating experience gathered to date is the subject of this paper.

Thyssen-CEA Environmental Systems, Inc. (initially Combustion Equipment Associates, Inc.) and Arthur D. Little, Inc., have developed, over the past few years, a dual alkali process for removing SO₂ from flue gas generated in coal-fired utility boilers. This process is based on the absorption of SO₂ in an alkaline sodium solution, followed by regeneration of the absorbing solution by reaction with a second alkali, calcium. These reactions generate insoluble calcium-sulfur salts which are discharged from the system as a moist cake.

The dual alkali process presents three significant advantages over conventional direct lime or limestone scrubbing technology. First, it uses a clear liquor, rather than a slurry, for scrubbing the flue gas. Second, the regeneration of the scrubbing solution and precipitation of waste solids takes place outside the absorber. Thus, the potential for scaling and plugging in the absorber is minimized; and the formation of solids with good dewatering properties is more easily controlled. Third, high SO₂ removal efficiencies (>90%) are easily achieved with alkaline sodium scrubbing solutions by simply adjusting the scrubber operating pH.

0097-6156/82/0188-0325\$06.75/0

© 1982 American Chemical Society

The dual alkali process has been tested extensively at laboratory, pilot plant, and prototype levels using lime (calcium hydroxide) as the source of calcium for the regeneration reactions (1). The performance of the process in these test programs prompted the federal Environmental Protection Agency (EPA) to select it for a full-scale demonstration plant. This lime-based dual alkali system has been installed on a 300 MW boiler at Louisville Gas and Electric's Cane Run Station. The system is currently undergoing a one-year test program.

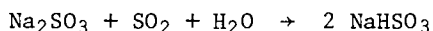
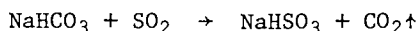
Although the lime-based system is technically and economically viable, a source of calcium cheaper than lime would increase the economic attractiveness of the process. Limestone (calcium carbonate) was recognized early on as a potential source of cheaper calcium for the dual alkali process. Extensive testing of the use of limestone was undertaken at laboratory and pilot plant levels (1, 2). Successful pilot operations using limestone were achieved in 1977 and led to a prototype scale (20 MW) testing of the system, just completed in early 1981 (3). The status of the technology based on the testing and operating experience gathered to date is the subject of this paper.

Description of the Technology

The limestone dual alkali technology consists of four distinct operations: SO₂ absorption, absorbent regeneration, waste solids dewatering, and raw materials storage and feed preparation. A typical process flow diagram is shown in Figure 1.

In the absorption section of the system, SO₂ is removed from the flue gas by contacting the gas with a solution of sodium salts. This is usually accomplished in a tray tower equipped with quench sprays for cooling and humidifying the gas. The scrubbed gas is then reheated to prevent condensation and corrosion in the ducts and stack and to improve atmospheric dispersion after being exhausted from the stack.

The alkaline solution used to remove SO₂ from the flue gas contains sodium sulfite (Na₂SO₃), bisulfite (NaHSO₃), sulfate (Na₂SO₄), chloride (NaCl), and very small amounts of bicarbonate (NaHCO₃). During the process of removing SO₂, the bicarbonate and some sulfite are consumed producing additional bisulfite. The SO₂ removal process can be represented by the following overall reactions:



Although the actual reactions within the absorber are more complex, involving various intermediate ionic dissociations, the above set of simplified, overall reactions is an accurate representation of the overall consumption and generation of the various components.

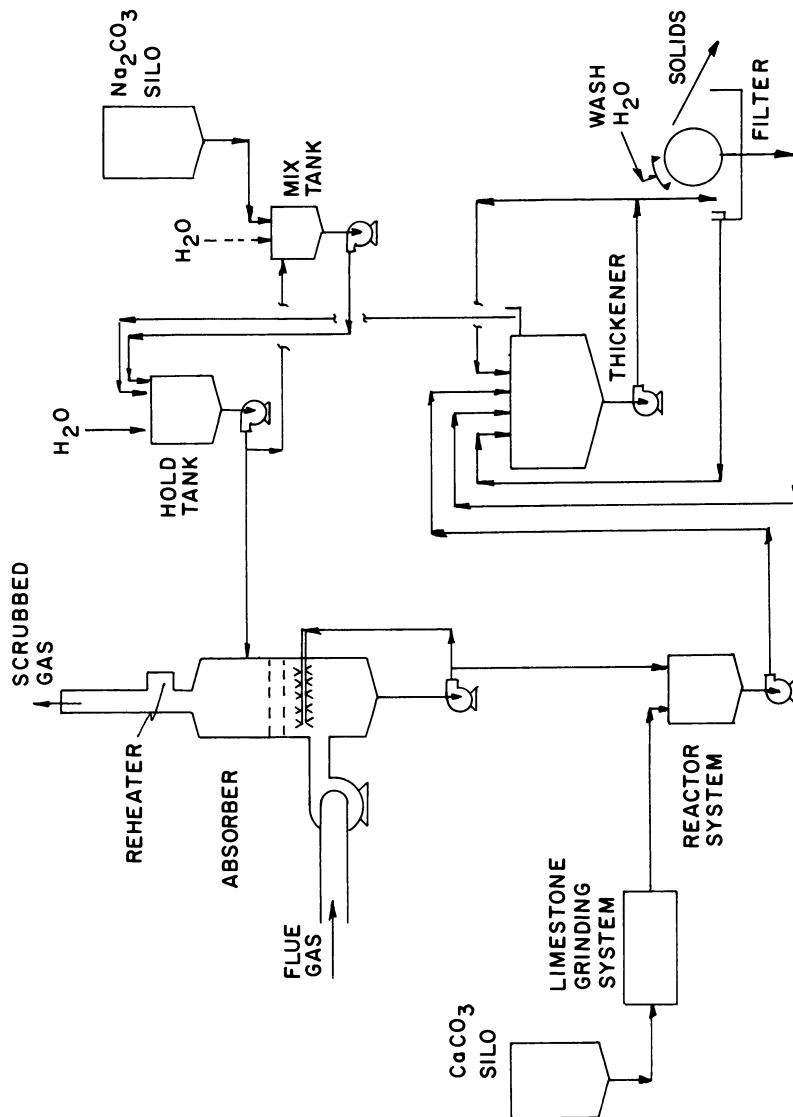


Figure 1. Dual alkali process flow diagram.

Sodium sulfate and sodium chloride do not participate in the SO₂ removal process. In this sense, they are considered "inactive" components. The other alkaline components represent "active" species. Sodium sulfite plays the most important role in the absorption of SO₂ since it is usually present in the greatest concentration. The bicarbonate is present in the absorber feed only in very small amounts. The concentration of these "active" alkaline components is a measure of the SO₂ removal potential of the process liquor, which is conveniently expressed in terms of the "active sodium" concentration where [active sodium] =

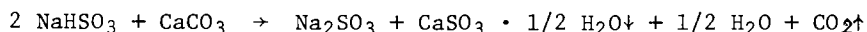
$$2 \times [\text{Na}_2\text{SO}_3] + [\text{NaHCO}_3] + [\text{NaHSO}_3].$$

It must be pointed out that the use of the term "active sodium" is simply one of convenience since it is only an indirect indication of the absorptive potential of the liquor. SO₂ is actually absorbed by or reacts with the sulfite or bicarbonate ions rather than the sodium ion. Also, even though the bisulfite cannot absorb any SO₂, it can be regenerated to sulfite (as will be discussed later) and, therefore, it is a potentially active species. The limestone dual alkali system operates at "active sodium" concentrations of 1.1 to 1.7 M.

The presence of sodium sulfate and sodium chloride is principally the result of secondary absorption reactions. Sodium sulfate is formed by the oxidation of sodium sulfite via reaction with oxygen absorbed from the flue gas. Oxidation also occurs in other parts of the system where process solutions are exposed to air; however, the amount of oxidation is small relative to the oxidation which occurs in the absorber. At steady state, the sulfate must leave the system either as calcium sulfate or as a purge of sodium sulfate at the rate at which it is being formed in the system. Although a practical limit for the level of oxidation that can be tolerated by the limestone dual alkali system has not yet been established, it appears that oxidation rates equivalent to 15 to 20% of the SO₂ removed might be accommodated without intentional purges of sodium sulfate.

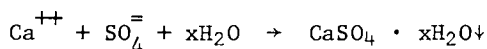
Similarly, sodium chloride is formed in the absorber by the reaction of chloride, present in the flue gas as HCl vapor, with the alkaline sodium solutions. The level of sodium chloride in the system builds up to a steady state concentration, such that the rate at which sodium chloride leaves the system with the washed filter cake is equivalent to the rate at which it is absorbed by the process liquor in the absorber.

The spent scrubbing solution is regenerated by reaction with limestone. This reaction precipitates mixed calcium sulfite and sulfate solids, resulting in a slurry containing up to 5 wt. % insoluble solids. The regeneration process involves basically the following overall reaction:



However, not all of the bisulfite is reacted since the limestone is only moderately basic and the regeneration reaction can only be carried to a pH of 6.0 to 6.5. At these pH's, the bisulfite and sulfite ions exist in significant quantities in the solution in equilibrium with one another.

Simultaneously with the above reaction, a limited amount of calcium sulfate will also be precipitated:



The sulfate co-precipitates with the calcium sulfite, resulting in a mixed crystal (or solid solution) of calcium-sulfur salts. Gypsum is not formed. The relatively high sulfite concentrations in the solution prevent soluble calcium concentrations from reaching the levels required to exceed the gypsum solubility product, and the system operates unsaturated with respect to calcium sulfate.

The regeneration of the absorptive capacity of the spent scrubbing solution is accomplished in a multi-stage reactor system--three to five reactors in series. Both the limestone and the spent solution are fed to the first reactor and pass successively through the other reactors. The effluent from the reactor system is directed to the solids separation section.

The separation of solids is a purely mechanical process involving thickening of the reactor effluent slurry from 2-5 wt. % to 20-30 wt. % solids, followed by filtration to produce a waste filter cake. While the cake is being formed, it is washed with fresh water to recover sodium salts that would otherwise be lost in the process liquor that is entrained in the moist cake. The filter cake represents the only waste discharged from the process. There are no other purges from the system. The clarified and regenerated thickener overflow liquor is fed forward to the absorber thus completing the liquor loop.

Despite washing the cake, a small portion of the sodium salts remains occluded within the calcium-sulfur salts or trapped in interstices of agglomerates which cannot be practically washed from the waste cake. The amount of sodium lost will depend primarily upon the total sodium concentration in the process liquor (which is a function of the amount of oxidation and the chloride content of the coal) and the extent of cake washing. The sodium losses in the filter cake are made up by the addition of sodium carbonate to the system. Typically, the sodium carbonate makeup should amount to less than 5 mole % of the SO_2 removed.

Limestone is the primary raw material used by the process. The amount of limestone needed to regenerate the spent scrubbing solution is reduced slightly due to the soda ash makeup. Under normal conditions, the limestone feed stoichiometry will be slightly less than one mole of available CaCO_3 per mole of SO_2 removed. In order to insure reasonable reactivity, limestone utilization, and good settling properties in the waste solids, the limestone must be ground to the 325 to 400 mesh range and have a high calcium content (>90%) and low magnesium content (<3%).

Development of the Technology

The development of the limestone (as well as the lime-based) dual alkali technology began in the early seventies with laboratory batch regeneration tests (1). These tests confirmed the potential of limestone to regenerate sodium-based scrubbing solutions.

Subsequent laboratory continuous stirred tank reactor (CSTR) tests showed that in generating the waste solids CaSO_4 was being precipitated along with the CaSO_3 even though the solution was not saturated with respect to CaSO_4 . Thus suggesting the possibility that the precipitation of CaSO_4 involved the formation of some sort of solid solution in the $\text{CaSO}_3 \cdot 1/2 \text{H}_2\text{O}$ lattice.

Further laboratory and early pilot plant tests revealed the sensitivity of the limestone utilization (percent of available alkali in the limestone which is reacted) and of the settling behavior of the solids to various process parameters. Reactor temperatures lower than 50°C adversely affected the limestone utilization and the settling of waste solids. High concentrations of soluble magnesium (>2000 ppm), iron (>20 ppm) or sulfate (>1.2 M) had a similar adverse effect. It was also found that the use of a multi-stage reactor system greatly improved the behavior of the solids compared to the single CSTR. Furthermore, it was found that in order to achieve high reaction rates, high limestone utilizations and good settling solids, the active sodium concentration had to be a high one, between 1.2 and 1.8 M.

Based on these findings, two pilot plant (0.5 MW) tests were performed in 1977. Each test lasted a week. These tests were intended to investigate the effect of different types of limestone, soluble magnesium levels, reactor temperature, as well as verify the applicability of the multi-staged reactor system design and high active sodium concentrations. The regeneration of spent scrubbing solution was performed in a four stage reactor system with a total residence time of about two hours. Active sodium concentrations were maintained in the 1.5 to 2.0 M range. Inlet SO_2 concentrations ranged between 3000 and 3500 ppm (dry) and oxygen concentrations between 4.5 and 5.0 vol. % (dry).

The type of limestone used had a major impact on the performance of the system. An excellent overall system performance was achieved while using Fredonia limestone (finely ground, 93 wt. % through 325 mesh and with high calcium content of 96.7 wt. % as CaCO_3). High SO_2 removal efficiencies of up to 95% were easily obtained by adjusting the scrubber bleed pH liquor--between 5.7 and 6.1--by simply changing the feed forward rate of regenerated solution to the absorption tower. Limestone utilizations approached 100%. The solids produced exhibited good settling properties and resulted in a filter cake containing 55 to 65 wt. % insoluble solids.

The performance of the system with Saginaw limestone was not as good. The major difference between these two limestones was the coarser size of the Saginaw limestone particles--only 66 wt. %

through 325 mesh. The SO₂ removal capability of the system with the Saginaw limestone was the same as that with Fredonia limestone. The Saginaw limestone utilization dropped to about 90%; but it was the poor settling of the solids generated with the Saginaw limestone that clearly set the performance of the two limestones apart.

The oxidation experienced by the system amounted to an equivalent of 10% of the SO₂ removed. Approximately 7% of the oxidized sulfur left the system in the form of CaSO₄ and the remaining 3% in the form of Na₂SO₄ with the entrained liquor in the cake. Another important observation was the need to increase the degree of washing of the cake in order to maintain a reasonably low level of sodium losses given the high sodium concentration in the process liquor. The soda ash feed, to make up for sodium losses in the cake, amounted to an equivalent of 5% of the SO₂ removed.

Subsequent laboratory tests with the original Fredonia limestone, with the Saginaw limestone ground to less than 400 mesh and with the fraction of the original Saginaw limestone which passed through a 400 mesh screen, reduced substantially the difference between the performance of these two types of limestone; thus confirming a need for a finely ground limestone as regenerating material.

The Prototype System at Scholz

The successful performance in the pilot plant tests prompted the testing of the technology at a prototype scale (20 MW). The project was sponsored by EPA, who provided most of the funds; by Thyssen-CEA Environmental Systems, Inc. (initially Combustion Equipment Associates, Inc.) who also contributed to the funding of the project; by Gulf Power Company; and by Southern Company Services, Inc.

The existing 20 MW lime-based dual alkali system at Gulf Power Company's Scholz steam plant was recommissioned and modified for operation in a limestone regeneration mode. The generalized diagram presented in Figure 1 is a good representation of the limestone dual alkali system at Scholz, with two exceptions. First, flue gas passed through a venturi scrubber prior to entering the absorption tower. Since the flue gas was being taken from high efficiency electrostatic precipitators, there was, in fact, no need for the venturi scrubber. Rather than removing it from the existing system, the scrubber was used primarily for quenching and saturating the flue gas, operations which also contribute to the SO₂ removal. The regenerated scrubbing solution was fed to the absorber and then passed to the scrubber. A bleed from the scrubber recirculation loop was directed to the reactors for regeneration. Second, the system at Scholz did not include a limestone grinding system as the limestone was received and stored as a finely ground material (>96% through 325 mesh).

A five-stage reactor system, with a total holdup time of approximately 100 minutes, was used. The first reactor was roughly one-fifth the size of the other four equal-sized reactors. An SO₂ injection system was provided to occasionally increase the SO₂ concentration in the inlet gas by 200 ppm or more. The SO₂ was injected upstream of the booster fan.

The prototype system was to undergo a six month testing period to evaluate its performance with regard to SO₂ removal capabilities; raw materials and energy requirements; quality of the waste solids generated; and reliability and ease of operation. Due to economic considerations, however, the test program was reduced from six to two months--February and March 1981. Some limited data was also collected during the startup and break-in testing during the months of December 1980 and January 1981, in which the system operated for 888 hours (37 days) or 60% of the time.

During the testing period, the system operated for 925 hours (38.5 days) or 71.4% of the time, recording an uninterrupted period of operation of 431 hours (18 days). Significant outages were due to bad weather, filter repairs, and solids carryover in the thickener overflow.

The general operating conditions during the break-in period and the system testing period are summarized in Table I. The boiler was fired with coal containing 2.6 to 4.2% sulfur resulting in SO₂ concentrations in the flue gas which typically ranged from 1400 to 2200 ppm. Injection of SO₂ prior to the gas entering the scrubber expanded this range to concentrations as high as 3240 ppm, although SO₂ concentrations usually did not exceed 2500 ppm. The gas load to the system varied between 13,300 and 48,800 dry scfm (equivalent to 6 to 23 MW). Oxygen levels in the flue gas varied between 5 and 11.2 vol. % depending on boiler load.

The liquor in the system had an active sodium concentration normally ranging between 1.4 and 1.7 M, occasionally reaching extremes of 1.1 and 1.8 M. The sulfate concentration reached a steady level of about 1 M. Similarly, the chloride concentration leveled out at 0.05 to 0.07 M.

The overall performance of the system in terms of SO₂ removal, chemical requirements, and properties of the waste cake is summarized in Table II. The performance data is based on overall material balances derived from flue gas analyses, waste cake properties and discharge rates, and raw materials feedrates and inventories.

SO₂ Removal. The SO₂ removal performance of the system was excellent. Inlet SO₂ concentrations during the testing period ranged from 1460 to 3240 ppm (dry volume basis). Outlet SO₂ concentrations, corrected for reheater air dilution, ranged from 29 to 239 ppm. The corresponding SO₂ removal efficiencies averaged to 95.4% for the month of February and 96.7% for the month of March.

TABLE I
 SUMMARY OF SYSTEM OPERATING CONDITIONS
 (December 1980 - March 1981)

<u>Inlet Gas</u>	<u>Range</u>	<u>Average</u>
Gas Load (dry scfm)	13,300-48,800	38,100
SO ₂ Level (ppm, dry basis) ^a	1,460-3,240	2,071
O ₂ Level (% dry volume) ^a	5.0-11.2	7.1

<u>Regenerated Liquor Composition</u>	<u>Range</u>	<u>Typical</u>
pH	5.70-6.40	6.10
Na ⁺ _{act} (M)	1.1-1.8	1.6
SO ₄ ⁼ (M)	0.76-1.07	0.95
Cl ⁻ (M)	0.030-0.087	0.070
Mg ⁺⁺ (ppm)	600-900	750
Ca ⁺⁺ (ppm)	14.5-37.5	22.0

^aBased on data from February and March only, since SO₂ and O₂ meters were not available until mid-January.

TABLE II
SUMMARY OF OVERALL SYSTEM PERFORMANCE
(December 1980 - March 1981)

Month	SO ₂ Removal Efficiency	Limestone Feed		Soda Ash Feed		Limestone Utilization (% of CaCO ₃ Reacted)	Waste Cake %	
		Stoichiometry (mols CaCO ₃ / mol ΔSO ₂)	mol ΔSO ₂	Stoichiometry (mols Na ₂ CO ₃ / mol ΔSO ₂)	mol ΔSO ₂		Range	Average
Break-in Period								
December	--- ^a	---	---	---	---	--	33.6-47.7	37.0
January	93.5% ^a	0.83 ^a	0.83 ^a	0.20 ^a	0.20 ^a	--	36.3-52.0	42.0
System Testing								
February	95.4%	0.82	0.82	0.26	0.26	97	33.3-46.6	38.0
March	96.7%	0.67	0.67	0.33	0.33	98	32.2-42.7	38.0

^aSO₂ analyzer not available until mid-January.

The single most important variable affecting the SO₂ removal was the liquor pH. This strong dependency is clearly shown in Figure 2. SO₂ removal efficiencies greater than 90% could easily be achieved by maintaining a scrubber bleed pH of at least 5.5. Although the SO₂ removal capability improves as the scrubber bleed liquor pH is raised, it begins to level off at a pH of 6. Furthermore, regeneration reactions are carried out at pH's of 6.0 to 6.4. Thus, a limitation is needed on the scrubber bleed pH in order to maintain an adequate control on these reactions and to ensure sufficient reactivity of the liquor. Operating the scrubber/absorber at a bleed pH of 5.7 to 6.0 appears to be a reasonable compromise that provides for high SO₂ removal efficiencies and adequate regeneration of the liquor in the reactors.

The impact of other variables such as inlet SO₂, sodium concentration on the SO₂ removal performance is much smaller than the bleed pH. Their effect falls within the scatter of the data and as such appear to be secondary in nature.

The SO₂ removal performance at Scholz reconfirms the high SO₂ control capability of this technology observed in the previous pilot plant tests where SO₂ removals of 95% were easily achieved by similar manipulation of the scrubber bleed pH.

Limestone Utilization. Two types of limestone were used for regenerating the spent scrubber liquor: Fredonia limestone from Kentucky, ground to 96.4 wt. % through 325 mesh, with a Ca content of 93.6 wt. % as CaCO₃, and Mg content of 4.2 wt. % as MgCO₃; and Sylacauga limestone from Alabama, ground to 97.7 wt. % through 325 mesh, with a Ca content of 95.7 wt. %, and Mg of 1.3 wt. %. The Fredonia limestone was used during the startup and break-in period until the end of December 1980. Thereafter, Sylacauga limestone was used for the remainder of the startup and break-in period and for the entire testing period. The Fredonia limestone was selected for use in the initial period of operation of the system since the successful results in the previous laboratory and pilot plant test programs were obtained with this limestone. Following the stable operation in the month of December, a new limestone was used to test the capability of the system with regard to the use of different limestones. The information below presents the results obtained during the testing period in which Sylacauga limestone was used.

In general, the limestone utilization by the dual alkali system was very good. During the testing period, utilizations in the reactor train effluent ranged from 85 to 95% of the available CaCO₃ in the raw limestone. As the reaction with limestone continued in the dewatering system, the final system utilizations, determined from chemical analyses of the filter cake, ranged from 93 to 100%, averaging at 97.5%. The average limestone feed stoichiometry for the testing period amounted to 0.77 moles of CaCO₃ per mole of SO₂ (the average is based on the hours of operation in each month). The reduction in the limestone feed stoichiometry, from the

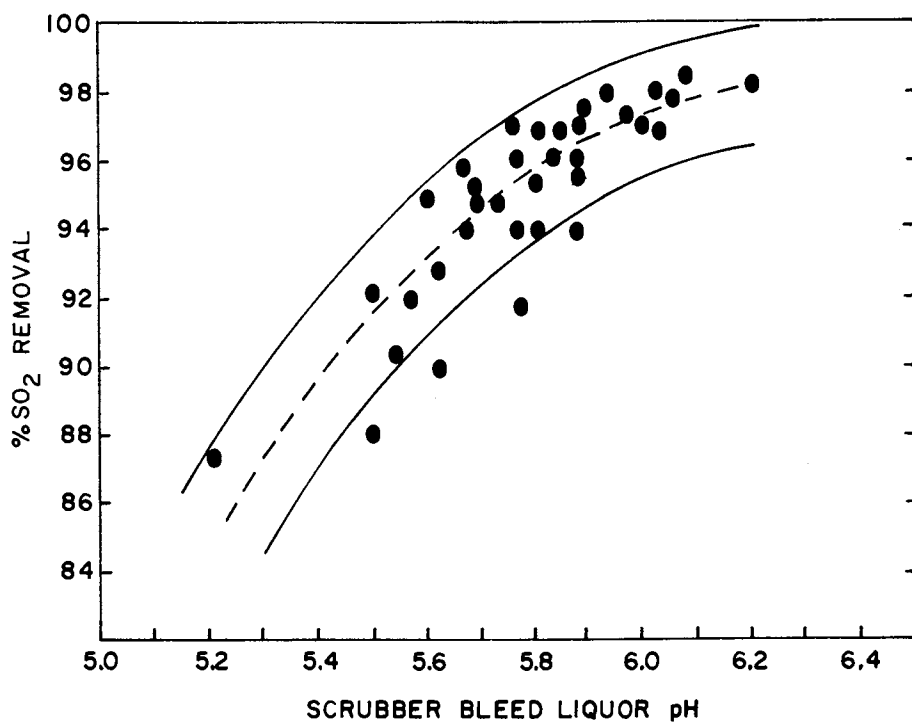


Figure 2. SO_2 removal as a function of scrubber bleed pH. Inlet SO_2 , 1460–3240 ppm; and Na^+_{active} , 1.25–1.75 M.

anticipated of approximately one mole of CaCO_3 per mole of SO_2 , was due to the high soda ash makeup rate. The soda ash makeup requirements are described in a later section.

Analyses were made to determine the progress of the regeneration reactions, and thus limestone utilization, through the reactor train. The results of these analyses are shown in Figure 3. The effect that the solids carried over in the thickener overflow liquor (and thus fed to the reactor train after passing through the absorber and scrubber) had on the limestone utilization in the first reactor is of particular interest. The utilization in this reactor ranged from 23% at solids carryover of 104 ppm to 63% at 1910 ppm. Since the solids carried over in the thickener overflow were essentially fully reacted, they undoubtedly contributed to an "apparent" high limestone utilization in the first reactor. In addition, it is also possible that solids entering the first reactor facilitated the precipitation of calcium sulfur salts. This, in turn, would have promoted an increase in the rate at which calcium from the limestone dissolved in the liquor and reacted with the sodium bisulfite. The high utilizations that accompany the solids carryover have been observed before (1); however, further studies would be needed to verify the exact mechanism involved. As reacting slurry passed through the reactors, the holdup time in the first reactor becomes small (~ 5 minutes) in relation to the overall holdup time in the reactor train (~ 100 minutes), and the spread reduced to limestone utilizations of 82 to 99% in the last reactor. Additional reaction in the thickener further reduced the differences in limestone utilizations.

Thus, it seems that regardless of the extent of reaction achieved in the first reactor, the limestone will be efficiently consumed in the remainder of the reactor train and dewatering system. The solids carryover in the thickener overflow, therefore, do not appear to have a substantial effect on the overall limestone utilization by the system; they do, however, impact on the settling properties of the solids generated as will be discussed later when addressing the properties of the waste solids.

Although very limited information was collected while using Fredonia limestone during the startup and break-in period, all indications were that this limestone exhibited performance characteristics comparable to the Sylacauga limestone used during the testing period.

Oxidation and Sulfate Precipitation. As anticipated, most of the oxidation took place in the absorber/scrubber unit. The levels of oxidation in this unit ranged from an equivalent of 5 mole % of the SO_2 removed, at O_2 concentrations of 5.5 vol. % in the inlet flue gas, to 25 mole % at O_2 concentrations of 8%. Oxidation throughout the remainder of the system amounted to an additional 1 to 5% of the SO_2 removed.

During the stable operation of the system, the sulfate formed in the scrubber/absorber unit, as well as the rest of the system,

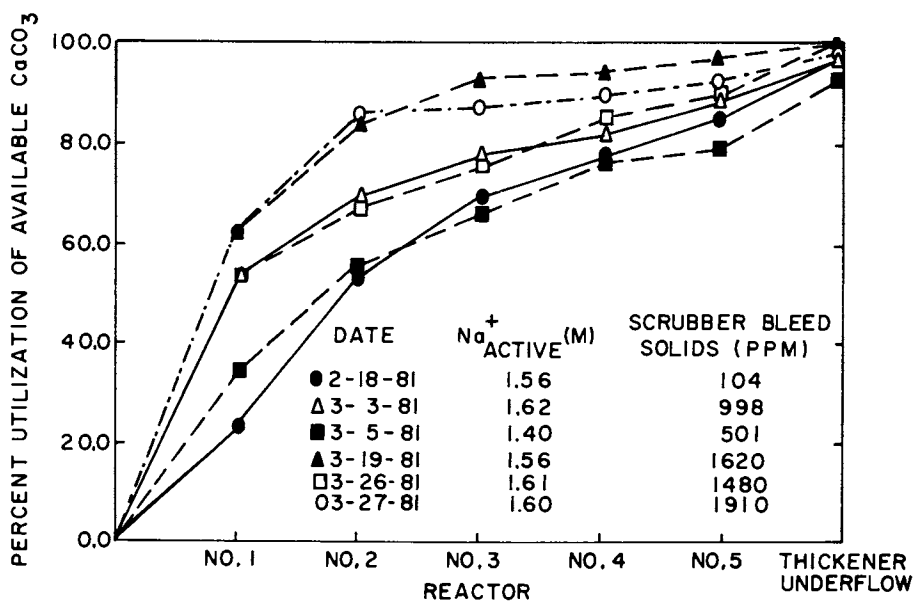


Figure 3. Limestone utilization for reactor studies.

must be removed at the same rate at which it is generated. This removal is effected by the precipitation of calcium sulfate and its discharge as part of the cake solids and by the losses of sodium sulfate in the entrained liquor in the cake. The amount of sulfate co-precipitated with the calcium sulfite is a function of the concentrations of sulfate and sulfite in the reactor liquor. As the concentration of sulfate increases relative to sulfite, the amount of sulfate precipitation increases. Thus, as the rate of oxidation increases, the ratio of sulfate to sulfite in solution will increase until the rate of calcium sulfate precipitation is sufficient to keep up with the rate of sulfate formation by oxidation. This self-adjustment by the system may, however, be limited by the need to maintain a high active sodium concentration which will limit sulfate concentrations (and consequently the sulfate/sulfite ratio) simply by solution saturation considerations. Furthermore, the sulfate/sulfite ratio may also be limited by the need to ensure high limestone utilizations and good solids properties.

Frequent liquor losses from the system, acting for all practical purposes as a frequently used purge stream, did not allow the examination of the full co-precipitation potential of the process. These liquor losses were the result of numerous piping and pump leaks and insufficient surge capacity. The poor condition of the equipment following three years of inactivity and a limited recommissioning were responsible for leaks and numerous other mechanical problems. Excessive inputs of seal water (needed to maintain worn out pumps in operation) combined with heavy rains and very limited surge capacity caused severe system volume balance problems. Rather than allowing tanks to overflow, process liquor had to be purged occasionally.

Thus, a practical limit for the level of oxidation that can be tolerated could not be determined, but it appears that oxidation rates of 15 to 20% might be accommodated by the process. Strict, closed loop operations are needed to verify this assumption.

Settling Characteristics of Waste Solids. The generation of solids with good settling characteristics was the most significant process limitation encountered at Scholz. It essentially accounted for all of the process related outages. Throughout the months of December and February, solids with excellent settling characteristics were generated. The solids settled out to 10% of the initial slurry volume in 6 to 8 minutes. In contrast, the poor solids generated throughout January took hours rather than minutes to settle. Variations in the settling characteristics of the solids in the reactor train effluent are shown in Figure 4. A definite correlation exists between the settling behavior of the reactor train effluent solids and the amount of solids in the scrubber bleed fed to the reactor train. The carryover of fine solids in the thickener overflow, which were fed to the reactors after passing through the absorber/scrubber, promoted the formation of more fine and difficult to settle solids in the reactor train. A similar

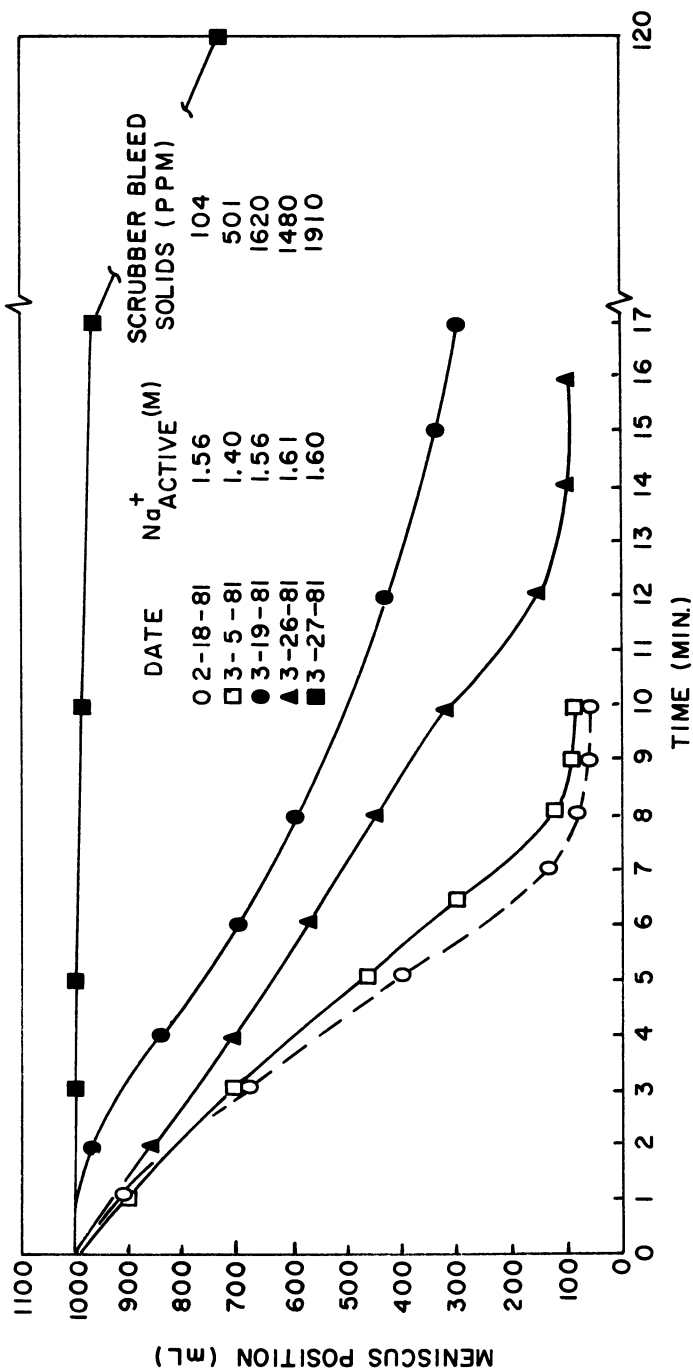


Figure 4. Variations in settling rates of reactor T-5 effluent solids.

behavior was observed in prior laboratory and pilot plant tests. Further verification in the laboratory resulted from running parallel regeneration tests with a scrubber bleed sample containing fine carryover solids and a similar sample from which the solids had been removed in a centrifuge. The settling rate of the solids formed by regenerating the first sample was noticeably slower than the one for the second sample. Analysis of electron micrographs of solid samples taken from the reactor train effluent revealed that the poor settling behavior was associated with the presence of a large percentage of fine, needle-shaped solids. On the other hand, large agglomerated particles, having a much lower surface area to mass ratio, exhibited a much higher settling rate.

In general, a solids carryover in the thickener overflow of 1000 ppm could easily be handled by the system without detrimental effects to the settling properties of the reactor solids. Solids carryover in excess of 5000 ppm, however, resulted in the quick deterioration of the quality of solids generated in the reactors.

The exact mechanism for the initial deterioration of the settling properties is not clearly understood. Unusually cold ambient temperatures during January--as low as 10°F--severely reduced the temperatures in a system not designed to operate in cold weather. As has been discussed before, lowering temperature slows the rate of reaction and contributes to the generation of poor solids. Dissolved magnesium concentrations remained under 1000 ppm and did not appear to have strongly influenced the quality of solids. Sulfate concentrations were typically 1 M and excellent settling solids were produced at sulfate concentrations as high as 1.2 M. Thus, neither the Mg^{++} nor SO_4^- concentrations appeared to be, by themselves, responsible for the poor solids. Dissolved iron concentrations were also investigated as occasionally levels in excess of 50 ppm were detected in the reactors, particularly after a shutdown when exposed carbon steel in pipes or tanks (due to lining failure) might have contributed to the accumulation of dissolved iron. Pilot plant tests run by EPA at its Research Triangle Park facilities confirmed that dissolved iron concentrations in excess of 20 ppm can interfere with the regeneration reactions and result in the production of poor solids. A high level of dissolved iron, however, could not be sustained neither at Research Triangle Park nor at Scholz. Upon restarting the system and maintaining the reactor pH above 6, the dissolved iron concentration dropped very quickly to less than 10 ppm. Therefore, dissolved iron was not thought to be responsible for poor solids either. It is possible that the reactor effluent pH, the limestone feedrate used to control this pH, and the residence time in the reactors might have contributed to the initial formation of poor solids. No meaningful correlation, however, could be established.

Another characteristic of the waste solids was the deterioration of their settling properties with time. This effect was observed on various occasions, most notably during a filter repair downtime. Solids with excellent settling properties had been

generated prior to the shutdown and had accumulated in the thickener precisely because of the inability of the filter to effectively remove the solids. During the eight days of downtime, the solids in the thickener began resuspending as the underflow was continuously recycled to the thickener centerwell to prevent plugging of the line or the thickener discharge cone. It is possible that these agglomerated and quick settling solids began redissolving and recrystallizing, this time into needle-like, poor settling solids.

Although the generation of poor settling solids does not appear to affect the SO₂ removal efficiency or the limestone utilization, it does however impact on the quality of the final waste product. These solids are more difficult to dewater and can result in a waste cake that is too moist, with attendant sodium losses. Furthermore, the advantages of using a clear liquor rather than a slurry in the absorber loop would be lost. Thus, there is still a need to refine the process in order to better control and understand the settling behavior of the waste solids.

Filter Cake Characteristics. Ease of handling and disposing of the waste as well as economic considerations dictate the need for a reasonably dry waste material from which most of the sodium value has been recovered. In general, both of these goals were not achieved at Scholz.

The anticipated insoluble solids content in the cake was 55 wt. % or higher. Yet, throughout the test program, it typically ranged between 35 and 45%. On a few occasions, it reached as high a solids content as 52%, and as low as 32%. The poor mechanical performance of the filter contributed significantly to this problem. Leaks in the internal piping of the filter drum and in the automatic control valve caused substantial losses of vacuum. The properties of the cake itself, which tended to crack during the dewatering cycle also contributed to the loss of the vacuum. The end result was a vacuum level which typically ranged from 5 to 10 inches Hg instead of the 15 to 20 inches Hg that had been anticipated.

Another factor was the inability of the thickener underflow pumps (inappropriately sized for the service) to handle slurries containing much more than 15% solids. This required the dilution of the thickener underflow before being pumped to the filter. A much higher demand was then placed on the already limited capabilities of the filter. The slurry had to be dewatered from 15% solids to 55% instead of from 25 to 55%; thus, more than doubling the amount of filtrate to be removed from the same amount of insoluble solids.

In all likelihood, a properly working and adequately sized filter and associated pumps and piping would have produced a waste cake of the desired concentration, or even exceed it as was the case in the previous pilot plant tests in 1977 when the filter cake typically contained 55 to 65% solids. Limestone dual alkali pilot

plant tests performed by EPA have also produced waste cakes with solids contents in excess of 60%.

The sodium losses in the cake were rather high throughout the Scholz test program. The loss of soluble sodium salts in the cake is reduced by maximizing the solids content in the cake and by using wash water to displace the remaining mother liquor in the cake. At Scholz, two spray banks were used to wash the cake. The use of up to 40 gpm of wash water was anticipated (equivalent to displacing four times the final volume of liquid in cake containing 55% solids). The corresponding sodium losses were anticipated to amount to about 4 wt. % of the insoluble solids content of the cake (equivalent to a Na/Ca ratio of 0.08 in the final cake).

The average number of displacement washes in February was only 1.5 resulting in a high Na/Ca ratio of 0.2 in the discharged cake. In March, the average number of displacement washes was even lower, 0.8, and the Na/Ca ratio was correspondingly higher, 0.4. There were times, however, when up to three displacement washes could be accommodated; the sodium losses were then reduced to 0.03 to 0.04 moles Na per mole Ca, even below the targeted 0.08 moles Na per mole Ca. In general, the use of more than two displacement washes was not possible because of capacity limitations in the piping for handling of filtrate and limitations in the wash water supply.

Soda Ash Consumption. The design of the Scholz system anticipated a makeup rate of 0.04 mole of Na_2CO_3 per mole of SO_2 removed. The actual sodium losses were much higher and were due to not only excessive losses in the cake but also severe liquor losses due to leaks, spills, and liquor purges needed to maintain volume balances. During the testing period, the overall soda ash feed stoichiometry amounted to 0.29 mole of Na_2CO_3 per mole of SO_2 removed. As much as 50% of this amount was needed to make up for cake losses; the remainder was associated with liquor losses.

Both of these problems, their causes, and impacts have already been discussed. The losses in the cake were addressed in the discussion of cake properties and liquor losses were addressed in the discussion of oxidation and sulfate precipitation. It is reasonable to assume that had the mechanical problems and corresponding impacts on the process operation not been present, the makeup rate could have been limited to the design condition. This was clearly demonstrated during the earlier pilot plant tests where soda ash makeup rates amounted to an equivalent of 5 mole % of the SO_2 removed.

Power Consumption. The power consumption by the dual alkali system ranged from 2.5% (0.53 MW) at flue gas rates equivalent to a boiler load of 21 MW, to 5.3% (0.42 MW) at an equivalent load of 8 MW.

The power consumption at Scholz was primarily related to the operation of the F.D. fan. As the pressure drop across the scrubber was typically 2 to 3 times the pressure drop across the

absorber, most of the power consumed by the fan was, in turn, associated with the operation of the venturi scrubber. Thus, in a typical limestone dual alkali application where flue gas is taken from an electrostatic precipitator or a baghouse and the venturi is not required, one would expect the power consumption to be much lower--more in the range of 1 to 1.5% of the power generated at full boiler load.

Process Operability. Process operability, unlike equipment or mechanical operability, refers to the ease with which the system can be operated and controlled, to the ability of the system to adequately respond to varying conditions, and to the ability to tolerate upsets in process chemistry due to mechanical problems or operator oversight.

In general, the process operability of the limestone dual alkali system was good after the first 2 or 3 days of stable operation. It was during these initial days, following any restart of the system, that the major problems with process operability were encountered. The first 24 to 28 hours of operation with limestone feed were critical. Typically, during the first few hours of solids generation, the reactor effluent solids would settle very fast--down to 10% of the initial slurry volume in less than 5 minutes. Thereafter, as the liquor in the system was being turned over, the settling rate would steadily decline to the point where it would take 7 to 10 minutes to effect the same settling. At this point following each startup, the solids settling rate would either level off and a stable operation would be achieved or it would continue deteriorating resulting in significant solids carry-over in the thickener overflow; which as discussed earlier is only conducive to the further deterioration of the quality of the solids.

It is possible that these restart problems were caused by the redissolution of the solids left in the thickener at the time of the outage and subsequent recrystallization into fine crystals. This appeared to be the case in the month of March when, during the eight days of downtime for filter repairs, the solids in the thickener resuspended. This resuspension was further aggravated by the liquor circulation upon restarting the system. Thus, an increasing amount of fines were being carried over to the reactors even before generation of new solids had started.

The symptoms, however, were not necessarily present in each occurrence of the restart problems; and therefore, it appears that other causes also contributed to the problem. Further testing would be needed to identify and correct these causes.

Once the system reached stable operation, the process operability was very good. The system was able to easily accommodate variations in inlet SO₂ concentrations of as much as 500 ppm by simply adjusting the feed forward rate of regenerated solution to the absorber/scrubber in order to maintain a constant scrubber bleed pH. Variations in boiler load and thus in the amount of gas processed by the system were also accommodated in the same fashion.

Upsets to the chemistry of the system were also handled well by the system. These upsets included the carryover of fly ash in the flue gas due to malfunction in the precipitators, the gross overfeeding of limestone due to operator oversight, and the occasional limestone and soda ash feed outages lasting from 1 to 5 hours.

Given the fact that the system was primarily controlled by the pH of the liquor, it is important to make some observations on the effect of pH variations on the process. Controlling the scrubber at a bleed pH above 6.0 provides for SO₂ removals better than 97% but reduces the limestone utilization in the reactors; lowering the scrubber bleed pH to 5.5 to 6.0 results in good limestone utilization. It should be noted however that at scrubber bleed pH's below 5.7, the SO₂ removal efficiency drops below 92%. Operations at scrubber bleed pH of 5.7 to 6.0 should accommodate both good SO₂ removals as well as good limestone utilization.

The reactor train effluent pH ranged from 5.8 to 6.4. Operating the reactor train at an effluent pH below 6.0 for too long (~24 hours) causes the deterioration in the settling properties of the solids. This effect is due to two factors. First, the low pH of the regenerated liquor forces a considerable increase in the feed forward rate to the absorber/scrubber in order to maintain reasonable SO₂ removals, thus shortening the time allowed for solids to settle in the thickener. Second, the limestone utilization in the first reactor becomes very high at such low pH's. Performing such extensive regeneration in a single reactor tank favors the formation of the corresponding solids in a fine, needle-like structure, rather than in the agglomerates that exhibit good settling properties.

The highest pH observed in the reactor train effluent was 6.4, even during periods of gross limestone overfeeding. This may indicate that the process liquor becomes highly buffered at this pH. If future tests prove this to be the case, then the actual control of the regeneration step of this process by pH alone would be questionable.

A common area of concern in the SO₂ scrubbing field is the formation of scale in the system. This was not a major problem at Scholz, although some scale formation took place in the reactors and in the scrubber.

There was a slow buildup of a layer of scale on the walls of the first reactor. Insufficient agitation may have contributed to the deposition of this scale which was primarily made up of calcium sulfite/sulfate solids. The formation of this scale was also evident in the overflow pipe connecting the first and second reactors. This pipe had to be replaced in early March as the 6-inch line had been reduced to a 3-1/2 inch line due to scale buildup. This overflow line was rather long--6 feet--and had an angle of incline of only 3° because of limitations in the existing plant layout. A greater angle of incline may have reduced this scale buildup.

Another type of solids deposition in the form of round/oval beads was also observed in the first reactor. These beads--1/8 to 3/8 inch in size--were also made up of calcium sulfite/sulfate which built up in layers around a seed particle much like the growth of pearls. Scale buildup in the other reactors was minimal. Based on the time of operation at Scholz, it appears that a semi-annual cleaning operation as part of a regular maintenance program might be adequate to control reactor scaling.

A buildup of sodium salts took place at the top of the scrubber, near the wet/dry interface where the flue gas enters the scrubber. It is at this location that the process liquor first contacted the flue gas. A substantial evaporation of water from the scrubbing liquor took place leaving the sodium salts behind. These sodium salts are rather soluble in water and can, therefore, be easily cleaned by a periodic spray wash.

Economic Considerations

Estimates for the cost of installing and operating a limestone dual alkali system on a new 500 MW boiler are presented in this section. Such estimates are based on the current knowledge and understanding of the technology. Modifications in equipment and operation may result from further testing needed prior to commercialization of this process. However, only minor changes are expected; and, therefore, these generalized estimates should be representative of the costs of commercial application of this technology.

The total capital investment for a generalized 500 MW limestone dual alkali system is estimated at \$51.7 million (1980 \$), which is equivalent to \$103.4/kW (3). This generalized system is assumed to be designed for a 95% SO₂ removal efficiency when burning coal containing 3.5% sulfur. The estimated annual operating costs (raw materials, utilities, labor and maintenance, overhead and waste disposal) are estimated at \$10.7 million (1980 \$) or 3.1 mills/kWh.

By comparison a similar 500 MW lime-based dual alkali system would represent a total capital investment of \$46.3 million or \$92.6/kW. This lower cost reflects primarily a simpler reactor system and lower circulation flowrates. The annual operating costs however are much higher, \$13.0 million or 3.7 mills/kWh, which reflects primarily the higher cost of lime. The price differential between limestone and lime more than offsets the higher capital charges, the higher soda ash consumption (5 mole % ΔSO₂ for limestone vs. 2.5% for lime) and the higher consumption, on a weight basis, of limestone (limestone has a higher molecular weight than lime). Thus, the limestone dual alkali system becomes an economically attractive process for flue gas desulfurization.

Conclusions

Both the pilot plant and the prototype tests have demonstrated the excellent SO₂ control capability of the technology. SO₂ removal efficiencies in excess of 95% have been consistently achieved. The use of finely ground limestone is necessary, but at the same time the limestone utilization is quite good--well in excess of 95%. Reasonable soda ash makeup rates were established in the pilot plant tests but could not be verified at Scholz due primarily to the poor mechanical condition of the equipment. Unlike pilot tests where the waste cake contained 55 to 65% solids, similar mechanical and related problems resulted in a very moist waste cake at Scholz. The capability of the system to generate solids with excellent settling properties for sustained periods of operation was initially demonstrated in pilot plant tests and clearly reconfirmed at Scholz. However, poor solids were also generated on various occasions. The mechanism for their formation needs to be better understood so that their generation can be prevented at all times. The practical limits for the tolerance of the system to oxidation are yet to be determined; it appears, though, that the system can tolerate oxidations equivalent to 15 to 20% of the SO₂ removed. The power consumption by the full-scale system should be in the range of 1 to 1.5% of the full boiler output.

The estimated total capital investment for a generalized 500 MW limestone dual alkali system is \$51.7 million, equivalent to \$103.4/kW. The annual operating costs are equivalent to 3.1 mills/kWh.

Thus, the limestone dual alkali technology appears to be technically and economically feasible. However, further testing is needed to reinforce such conclusions and to develop sufficient process information needed for full-scale commercialization purposes.

Literature Cited

1. LaMantia, C. R.; Lunt, R. R.; Oberholtzer, J. E.; Field, E. L.; Valentine, J. R. "Final Report: Dual Alkali Test and Evaluation Program," EPA-600/7-77-050a,b,c, 1977.
2. Oberholtzer, J. E.; Davidson, L. N.; Lunt, R. R.; Spellenberg, S. P. "Laboratory Study of Limestone Regeneration in Dual Alkali System," EPA-600/7-77-074, 1977.
3. Valencia, J. A.; Peirson, Jr., J. F. "Evaluation of the Limestone Dual Alkali System at the Scholz Steam Plant - Final Report," EPA-600/7-81-141b, 1981.

RECEIVED November 20, 1981.

**American Chemical
Society Library
1155 16th St., N.W.**

Control of SO₂ Emissions by Dry Sorbent Injection

JAMES T. YEH, RICHARD J. DEMSKI, and JAMES I. JOUBERT

U.S. Department of Energy, Pittsburgh Energy Technology Center,
Pittsburgh, PA 15236

The use of dry alkali sorbents (sodium bicarbonate, trona, and nahcolite) to control SO₂ emissions from coal-fired boilers was studied while burning coals containing 1 to 3 percent sulfur.

The tests were carried out in an experimental furnace designed to burn 500 lb/hr of pulverized coal. The sorbents were injected into the furnace flue gas as a dry powder, upstream of a baghouse filter. Operating variables considered included baghouse temperature and cleaning cycle time, sorbent particle size, sorbent/sulfur ratio, location of sorbent injection point, and sorbent injection schedule (continuous or intermittent). With the exception of baghouse cleaning cycle rate, each parameter had a significant effect on SO₂ removal efficiency. Up to 95 percent SO₂ removal could be obtained with each sorbent, with the proper selection of operating conditions.

A considerable amount of interest has developed in utilizing dry-sorbent injection as a means of controlling SO₂ emissions from coal-fired industrial and utility boilers.(1-7) A dry sorbent FGD system is one in which an alkaline material is injected into the boiler flue gas as a dry powder or aqueous slurry; the sorbent reacts with SO₂ to form a dry product containing sulfates and sulfites. The mixture of spent material and fly ash is removed from the gas stream by means of an electrostatic precipitator or baghouse filter. The spent sorbent is usually disposed of, but in some cases it may be regenerable or have commercial end uses.(2)

Dry FGD systems offer several advantages over conventional wet scrubbing systems: there is no need for sludge handling equipment; scaling and plugging problems often occurring in wet scrubbers are avoided; lower quality steel can be used for construction of vessels; energy and water consumption is

This chapter not subject to U.S. copyright.
Published 1982 American Chemical Society.

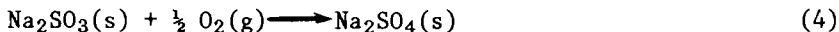
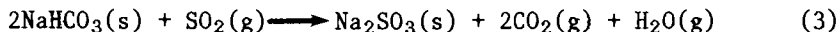
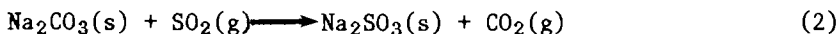
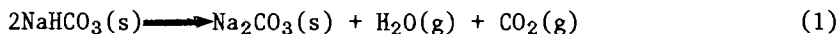
significantly less, even with spray dryer injection; and, finally, recent studies (2, 4, 7) indicate potential economic advantages of dry FGD systems over conventional lime- or limestone-based, wet scrubbing systems. One potential disadvantage of dry FGD systems using sodium-based sorbents is the solubility of the spent material; special approaches may have to be developed to dispose of the waste in an environmentally acceptable manner. (2)

Data reported in the literature indicate that sodium compounds are considerably more reactive than calcium compounds when injected into flue gas as dry powders, although reactivities of the calcium compounds (particularly lime) are increased when they are injected via a spray dryer system. The study described in this paper was confined to dry-powder injection tests with sodium bicarbonate, nahcolite (a sodium bicarbonate mineral), and trona (a sodium carbonate/bicarbonate mineral).

Nahcolite is not currently mined. However, approximately 30 billion tons (27 billion metric tons) of nahcolite are known to be associated with western oil-shale deposits. A study conducted by TRW, Inc., (2) indicates that commercial production of nahcolite for FGD applications would be merited provided a utility market of a least 5000 MW existed. This is equivalent to 1.28 million tons per year (1.16 million metric tons per year) of nahcolite, assuming the use of 1% sulfur coal with 70% SO₂ removal.

Reserves of trona are even larger than those of nahcolite. The bulk of the trona mined currently is converted to sodium carbonate. However, commercial sodium carbonate is not effective for FGD when injected as a dry powder; in earlier tests at PETC, only 30 percent SO₂ removal could be achieved.

The reactions of sodium carbonate and sodium bicarbonate with SO₂ in a flue gas stream can be described by the following equations:



Reaction (1) can occur at temperatures as low as 180°F. The evolution of CO₂ and H₂O vapor occurring in Reaction (1) apparently produces a porous form of Na₂CO₃ at temperatures below 600°F, with a surface area significantly higher than commercially produced Na₂CO₃. Data reported by Ness and Selle (8) indicate that at temperatures above 600°F sintering of the sorbent particles takes place, which results in a decrease in surface area and a corresponding decrease in SO₂ sorptive capacity.

The objective of the tests conducted at PETC was to evaluate the relative effectiveness of the three NaHCO₃ sorbents

mentioned in removing SO_2 from flue gas streams. The tests were carried out in an experimental furnace designed to burn 500 lb/hr of pulverized coal. Parametric studies were conducted to determine the effect of operating parameters on SO_2 removal efficiency and sorbent utilization (gram atoms Na reacted to Na_2SO_4 /gram atoms Na injected). Parameters varied were sorbent/sulfur ratio, sorbent particle size, baghouse temperature and cleaning cycle time, location of sorbent injection point, and sorbent injection schedule (continuous or intermittent). Three types of coal were burned ranging in sulfur content from 1 to 3.1 percent. All tests were conducted at an excess air level of 20 percent.

Experimental

Combustion Test Facility. The 500-lb/hr combustion test facility is shown schematically in Figure 1. The furnace was designed to simulate the performance of an industrial steam generator. The unit is 7 feet wide, 5 feet deep, and 12 feet high, and has a volumetric heat liberation rate of about 16,000 Btu/hr ft³ at a thermal input of 6.5 million Btu/hr. The furnace walls are refractory-lined and water-cooled.

Coal is charged to the hopper, pulverized to a size consist of 70% minus 200 mesh, and then conveyed by the primary air into a recycle coal loop where intimate mixing of coal and air occurs. Four adjustable exit tubes are connected to the recycle loop; these convey the primary air-coal mixture to each of the four burners. Secondary air at 600°F is fed through adjustable swirl vanes surrounding each burner. The flue gas exits the furnace at about 2000°F, passes through a convective heat transfer section, and is then used to preheat the secondary air to the desired inlet temperature. By controlling the air flow through the recuperative air preheater, the flue gas exit temperature can be maintained in the range of 300-475°F.

The dry-sorbent injection system is shown schematically in Figure 2. This rather simple system provides reliable and accurate feeding of solid sorbent. The entire feed mechanism, including sorbent storage, was placed on a weigh scale with digital readout. The sorbent feed rate was constantly monitored from the slope of weight loss vs time.

In most of the tests, dry sorbent was injected into the 12-inch diameter flue-gas duct at the exit of the preheater, 26 feet upstream of the baghouse. The nominal flue gas velocity in the duct is about 50 feet/second, which results in a gas/solid contact time of about 0.5 second prior to entering the baghouse. A few tests were conducted while injecting sorbent at the inlet of the baghouse.

The baghouse is a Mikro-Pulsaire model manufactured by the Pulverizing Machinery Division of the Slick Corporation, and is 6 feet, 6 inches in diameter and 9 feet, 10 inches high. It contains 57 Nomex bags, 8 feet long x 4.5 inches OD. The unit is normally operated at air/cloth ratios of 4-4.5 feet/minute.

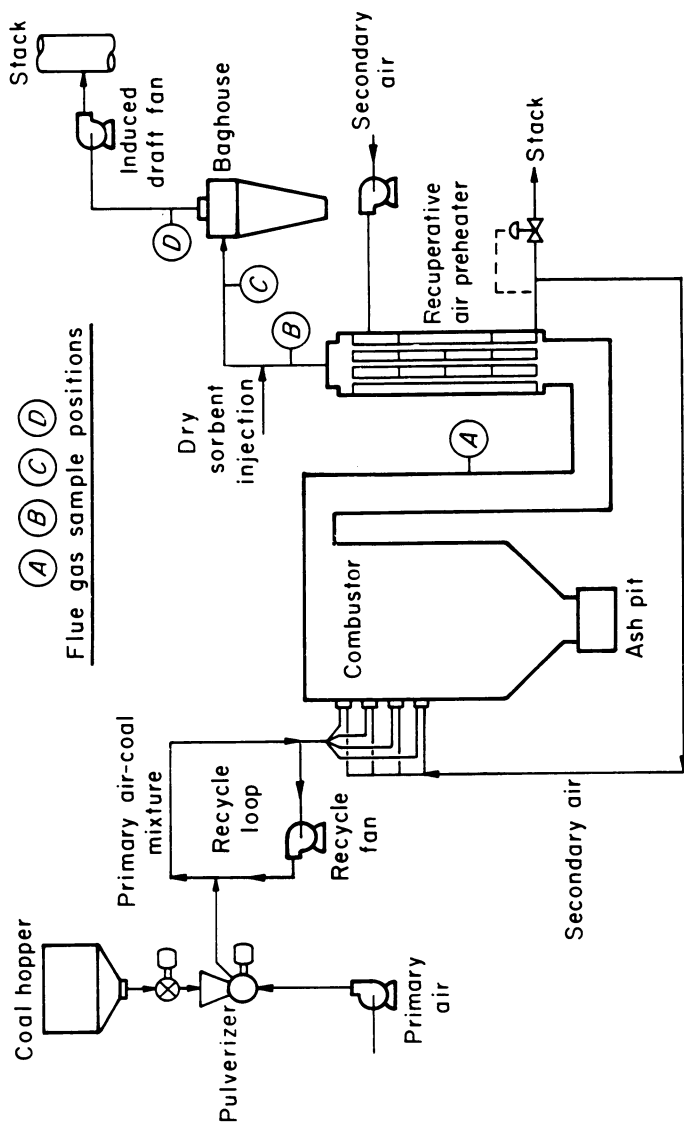


Figure 1. Simplified flowsheet of 500 lb/hr pulverized-coal-fired furnace.

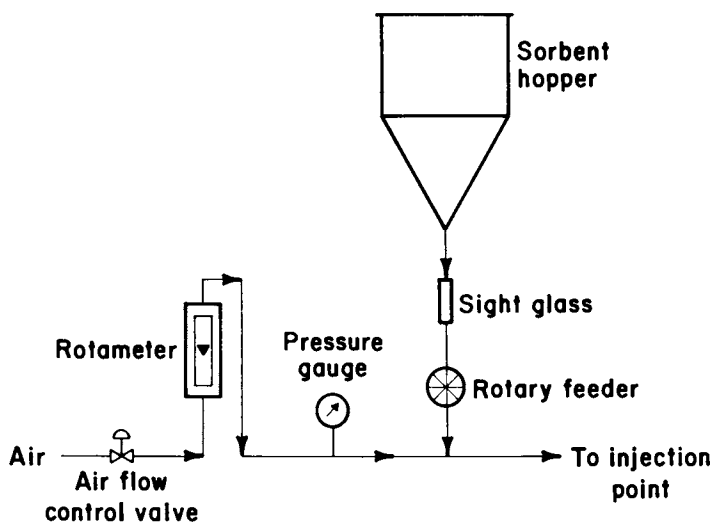


Figure 2. Dry sorbent injection system.

Gas analyses, as well as temperatures, pressures, and flows, are recorded with a computerized data collection system. The flue gas is sampled and analyzed at four locations (see Figure 1): the furnace outlet; the air preheater outlet (prior to sorbent injection); the baghouse inlet; and the baghouse outlet.

A schematic of the gas sampling system is given in Figure 3. Flue gas is drawn through a 15 μm stainless-steel sintered filter located inside the hot flue gas lines. This clean, wet gas passes through heated lines to a refrigeration system where moisture is removed by condensation. The relatively dry gas is then pumped under a positive pressure through a Perma Pure Dryer for additional drying (by osmosis) prior to entering the appropriate instruments. Sampling point D provides continuous measurement and recording of SO_2 , CO , CO_2 , NO_x , O_2 , and total hydrocarbons at the baghouse exit. The process mass spectrometer automatically switches to all four streams and samples each stream for one minute, but can be manually controlled to obtain data at any of the four possible positions. Sample streams A, B, and C are connected through a selector valve to a different set of instruments. Sufficient time was allowed for each instrument to attain a steady state reading before changing sampling location.

Sorbents and Coals Tested

Typical analyses of the nahcolite and trona used in the dry sorbent tests are given in Table I. The nahcolite was supplied by Superior Oil Company from a mine near Rifle, Colorado. The trona was obtained from a Stauffer Chemical Company mine in Rock Springs, Wyoming. The sodium bicarbonate used was USP grade and was ≈ 100 percent NaHCO_3 . Much of the parametric testing was conducted with this material because it is well characterized chemically and is available in carefully graded size consists with the following industrial designations: No. 3 (32 μm mean particle diameter); No. 1 (69 μm); No. 2 (110 μm); No. 4 (115 μm); and No. 5 (180 μm).

TABLE I. TYPICAL ANALYSES OF NAHCOLITE AND TRONA

	Nahcolite	Trona
	(Weight Percent)	
CO_3^-	Not Detected	24.3
HCO_3^-	62.7	25.3
Na	22.1	24.9
K	0.1	0.2
Ca	0.65	1.3
Mg	0.5	0.6
	86.05	76.6

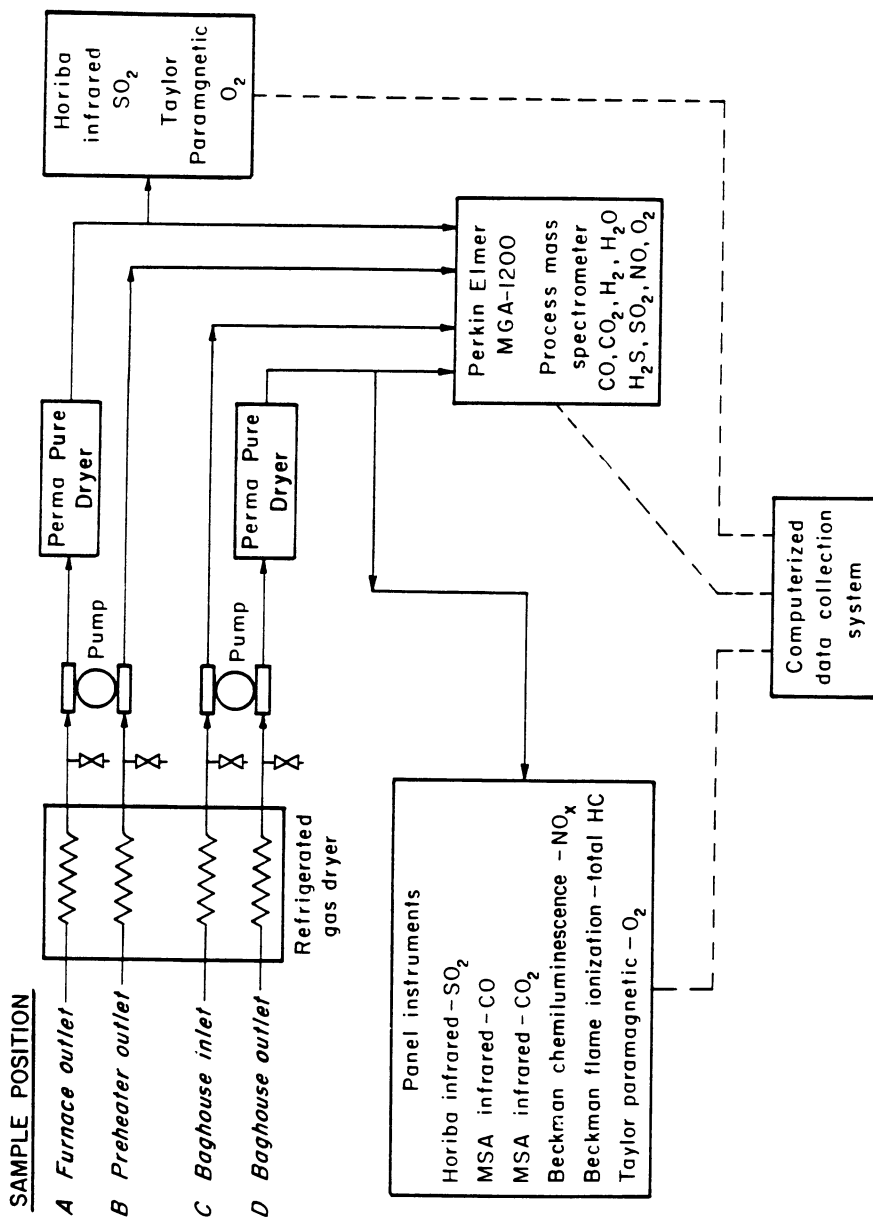


Figure 3. Gas analysis system.

Analyses of the coals tested are given in Table II. Most of the tests were conducted with the 1.6-percent-sulfur Pittsburgh seam coal. Twelve tests were carried out with the 3.1-percent-sulfur West Virginia coal. [This also is a Pittsburgh seam coal, but is referred to as "West Virginia coal" (from Marion County, West Virginia) to facilitate discussion.] Two tests were conducted with the 1.0-percent-sulfur Kentucky coal.

Results and Discussion

Sodium Bicarbonate Tests.

Effect of Na_2/S Ratio. Figure 4 shows the effect of varying the Na_2/S ratio over a range of approximately 0.5 to 2.0 while injecting No. 3 (32 μm) sodium bicarbonate. The baghouse temperature was 400°F, and the baghouse pulse cycle was 15 minutes. There was about a 25°F temperature drop between the sorbent injection point and the baghouse. With this size-consist of NaHCO_3 (the finest grind tested), 90 percent SO_2 removal is achievable at a Na_2/S ratio of 1.3, which corresponds to a sorbent utilization of about 70 percent.

Effect of Temperature. Figure 5 depicts the effect of baghouse temperature on SO_2 removal with No. 1 (69 μm) sodium bicarbonate over the temperature range 350°-450°F. The removal of SO_2 tends to level off at about 80 percent at temperatures in excess of 400°F. In the case of other sorbents, a temperature of 400°F also appears near optimal in terms of SO_2 removal, and this temperature level does not represent a severe operating condition for the baghouse. Thus, most of the testing was carried out at approximately 400°F.

Effect of Sorbent Particle Size. Figure 6 shows the effect of sorbent particle size on SO_2 removal with sodium bicarbonate at a Na_2/S ratio of 2 and a baghouse temperature of 400°F. It will be noted that the SO_2 removal varies approximately linearly with the mean particle diameter of the sorbent, increasing with decreasing particle size. The data indicate that SO_2 removals of 90 percent are achievable at mean sorbent diameters of 65 μm or less, for the conditions stated.

Effect of Location of Sorbent Injection Point. The effect of injecting sorbent at the baghouse inlet versus injecting into the flue gas duct 26 feet upstream at the air heater outlet was examined. The baghouse temperature was maintained at 400°F and cycle time was 30 minutes. Three size consists of NaHCO_3 were used: 32, 69, and 180 μm . All tests were carried out at a Na_2/S ratio of 1.5.

The results indicate no apparent effect with the 32 μm material; SO_2 removal was about 90 percent in each test. However, the effect was significant with the coarser materials.

TABLE II. TYPICAL ANALYSES OF COALS USED

	<u>Pittsburgh</u>	<u>W. Virginia</u>	<u>Kentucky</u>
PROXIMATE ANALYSIS - WT.% (Dry Basis):			
Volatile Matter	37.5	39.1	35.3
Fixed Carbon	53.8	50.2	55.3
Ash	8.7	10.7	9.4
ULTIMATE ANALYSIS:			
Hydrogen	5.0	5.0	5.0
Carbon	75.8	74.2	75.4
Nitrogen	1.5	1.2	1.4
Sulfur	1.6	3.1	1.0
Oxygen	7.4	5.8	7.8
Ash	8.7	10.7	9.4
HEATING VALUE (Btu/lb):			
	13698	13378	13393
MOISTURE IN COAL (As Fired):			
	1.0	1.0	1.0
ASH ANALYSIS:			
Al ₂ O ₃	26.31	20.36	27.99
CaO	2.96	7.30	3.46
Fe ₂ O ₃	13.58	21.88	17.09
K ₂ O	1.58	1.78	0.21
Na ₂ O	0.57	1.37	0.42
SiO ₂	53.96	45.80	48.63
MgO	1.04	1.51	2.2

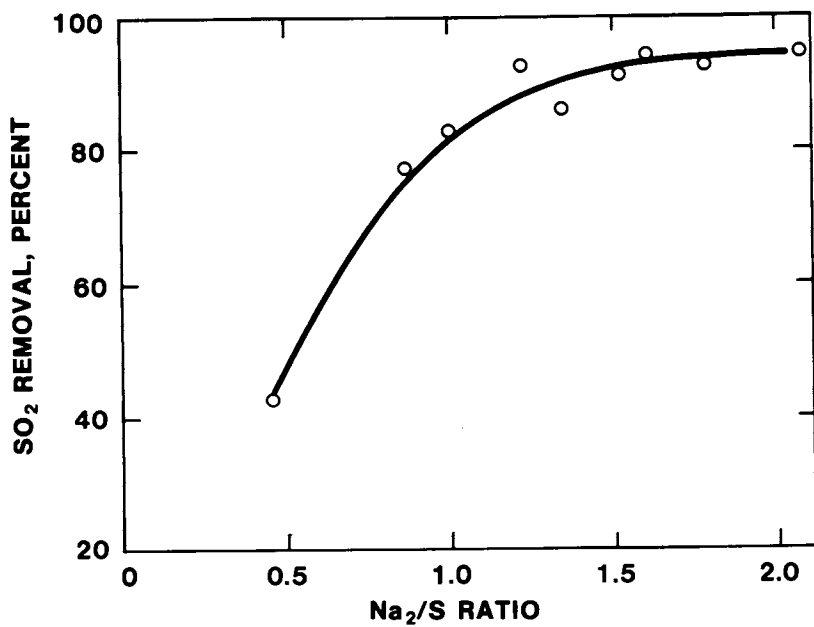


Figure 4. SO₂ removal with NaHCO₃: effect of Na₂/S ratio. Sorbent, No. 3 NaHCO₃ (32 μM); baghouse T, 400°F; and Pittsburgh seam coal (1.6% S).

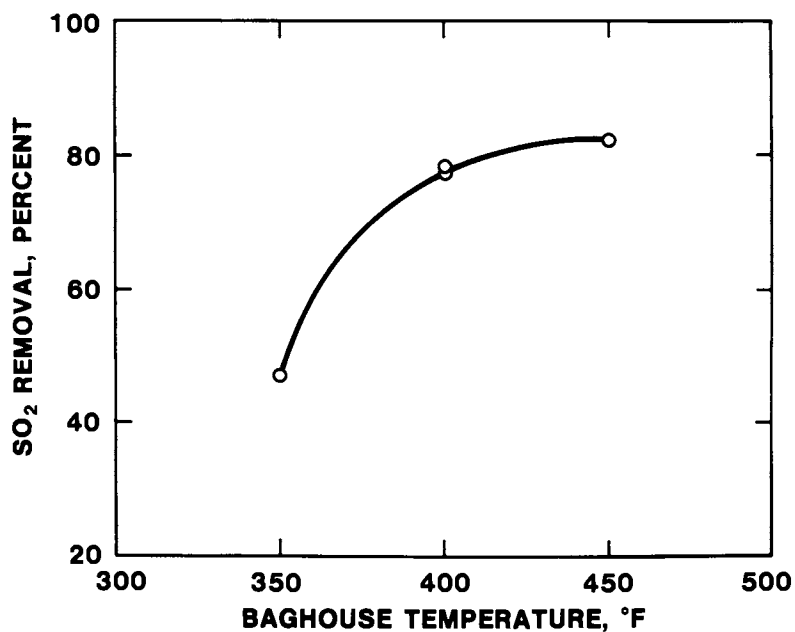


Figure 5. SO₂ removal with NaHCO₃; effect of baghouse temperature. Sorbent, No. 1 NaHCO₃ (69 μm); Na₂/S ratio, 1.30; Pittsburgh seam coal (1.6% S).

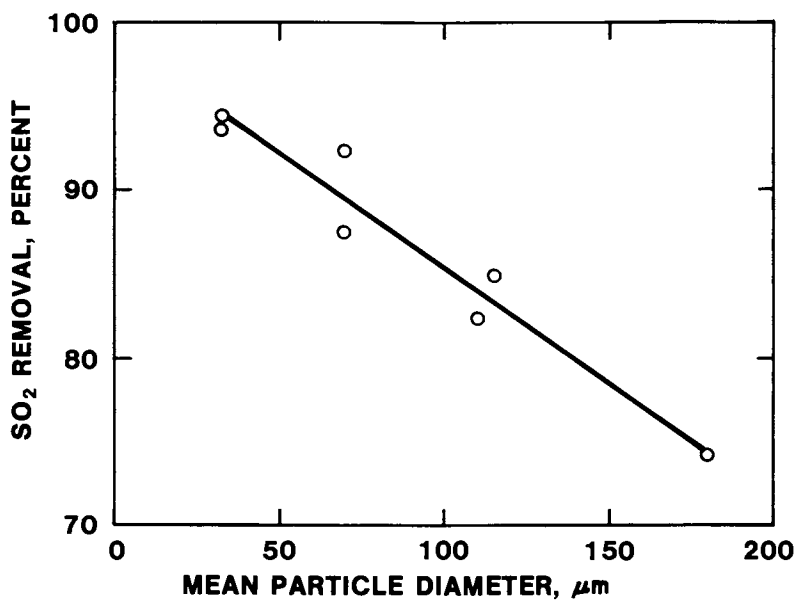


Figure 6. SO_2 removal with $NaHCO_3$: effect of sorbent particle size. Sorbent, $NaHCO_3$; Na_2S ratio, 2; baghouse T, $400^\circ F$; and Pittsburgh seam coal (1.6% S).

With the 69 μm material, SO_2 removal decreased from 87 percent when injecting upstream, to 64 percent when injecting at the baghouse inlet. Corresponding values with the 180 μm material were 64 percent and 43 percent, respectively.

Inasmuch as the gas/solid contact time in the duct is only 0.5 second, it had been anticipated that the effect of injecting upstream would be negligible since the baghouse pulse cycle was 30 minutes. A possible explanation of the effect noted with the coarser materials is that the larger particles may tend to separate from the gas stream upon entering the baghouse and fall to the baghouse bottom. Thus a fraction of the coarser materials would be in intimate contact with the gas considerably less than 30 minutes.

Continuous Versus Intermittent Feeding of Sorbent. Two tests were conducted to determine whether the time-averaged SO_2 removal efficiency and sorbent utilization could be increased by intermittent sorbent injection as compared to continuous feeding. Number 1 NaHCO_3 (69 μm) was used in both tests. The baghouse temperature was 400°F and cycle time was 20 minutes. The results are given in Table III.

TABLE III. EFFECT OF INTERMITTENT SORBENT FEEDING ON SO_2 REMOVAL EFFICIENCY AND SORBENT UTILIZATION

Sorbent Injection Schedule	Na_2/S Ratio	SO_2 Removal (Percent)	Sorbent Utilization (Percent)
Continuous 1 min on, 1 min off	1.30	77.6	59.7
		58.6	45.1
Continuous 3 min on, 1 min off	0.95	65.1	68.5
	0.98	48.0	49.0

Sorbent: No. 1 Sodium Bicarbonate (69 μm)
 Baghouse Temperature: 400°F
 Baghouse Cycle: 20 minutes
 Pittsburgh Seam Coal (1.6% S)

In the first test, the Na_2/S ratio was maintained at an average value of 1.30, and the sorbent feed schedule was 1 minute on (at $\text{Na}_2/\text{S}=2.6$) and 1 minute off. The SO_2 removal efficiency obtained was only 58.6 percent, significantly less than the 77.6 percent value obtained with continuous feeding; sorbent utilization was 45.1 percent versus 59.7 percent with continuous feeding.

The second test was conducted with an average Na_2/S ratio slightly less than 1, and the sorbent feed schedule was 3 minutes on, 1 minute off. Again the SO_2 removal efficiency was

lower with intermittent feeding (48.0 percent) than with continuous feeding (65.1 percent). Sorbent utilization was 49.0 percent as compared to 68.5 percent with continuous feeding.

Tests with Nahcolite

Pittsburgh Seam Coal (1.6 Percent Sulfur). A series of tests was conducted with Pittsburgh seam coal while injecting nahcolite with a mean particle diameter of 37 μm . Figure 7 shows the effect of Na_2/S ratio on SO_2 removal at 400° and 420°F. As expected from the earlier sodium bicarbonate tests (see Figure 5), the slight difference in temperature appears to have no major effect on the removal achieved.

It should be noted that varying the baghouse cycle rate over the range 6 to 30 minutes also had no apparent effect on SO_2 removal. This was found to be true in all other tests performed, regardless of the sorbent employed. It is believed that this is an indication that reactions are confined to only a thin outer layer of sorbent deposited on the filter bags.

For the conditions stated in Figure 7, 90 percent SO_2 removal is achieved at a Na_2/S ratio of 1.1. This corresponds to 82 percent sorbent utilization.

Kentucky Coal (1.0 Percent Sulfur) and West Virginia Coal (3.1 Percent Sulfur). Two tests were conducted with a Kentucky coal containing 1.0 percent sulfur, and six tests were conducted with a West Virginia coal containing 3.1 percent sulfur. Baghouse temperature was maintained at 400-420°F, and the cycle times were either 15 or 30 minutes.

The results for these two coals are shown in Figure 8, along with the smooth curve representing the results for Pittsburgh seam coal discussed above. The results for the Kentucky coal are consistent with the results obtained with the Pittsburgh seam coal. However, the SO_2 removal efficiencies achieved when burning the 3.1%-S West Virginia coal were somewhat lower than those obtained with the Pittsburgh seam coal. The reason for this is not apparent. Intuitively, one would anticipate greater reactivity with the West Virginia coal, as initial SO_2 concentrations should be higher than when burning Pittsburgh seam coal. Also, inspection of the ash analyses given in Table II would suggest, if anything, that the more alkaline ash of the West Virginia coal would result in greater SO_2 removal than with Pittsburgh seam coal, if in fact ash- SO_2 reactions occur. The same phenomenon has been noted by others.(9)

Tests with Trona

A series of ten tests was conducted with trona with a mean particle diameter of 59 μm while burning 1.6%-S Pittsburgh seam coal. Another series of seven tests was carried out with a second batch of trona (32 μm) while burning 3.1%-S West Virginia

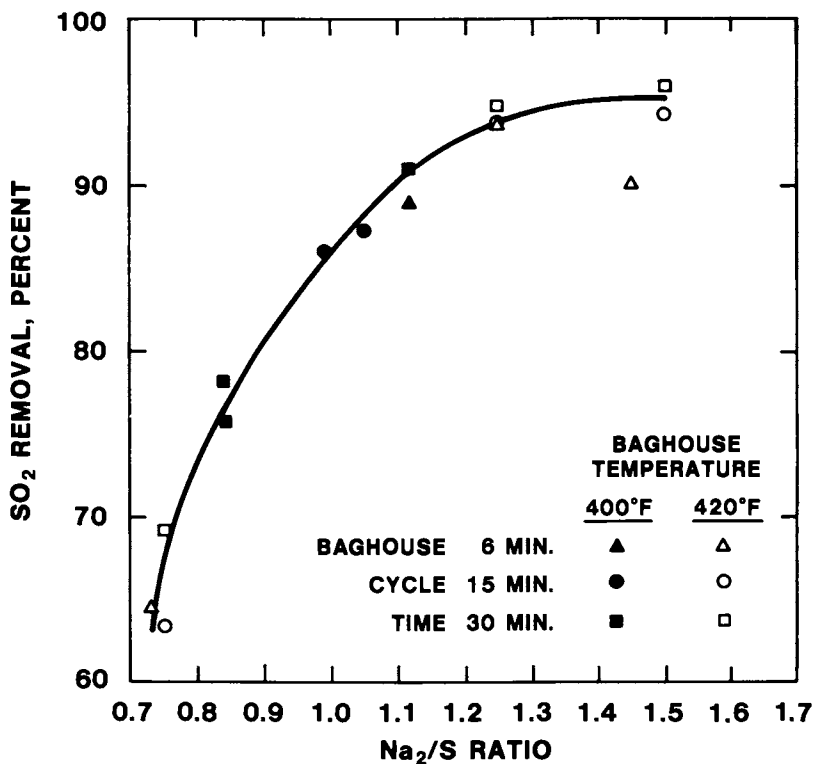


Figure 7. SO₂ removal with nahcolite while burning Pittsburgh seam coal. Sorbent, nahcolite (37 μm); Pittsburgh seam coal (1.6% S).

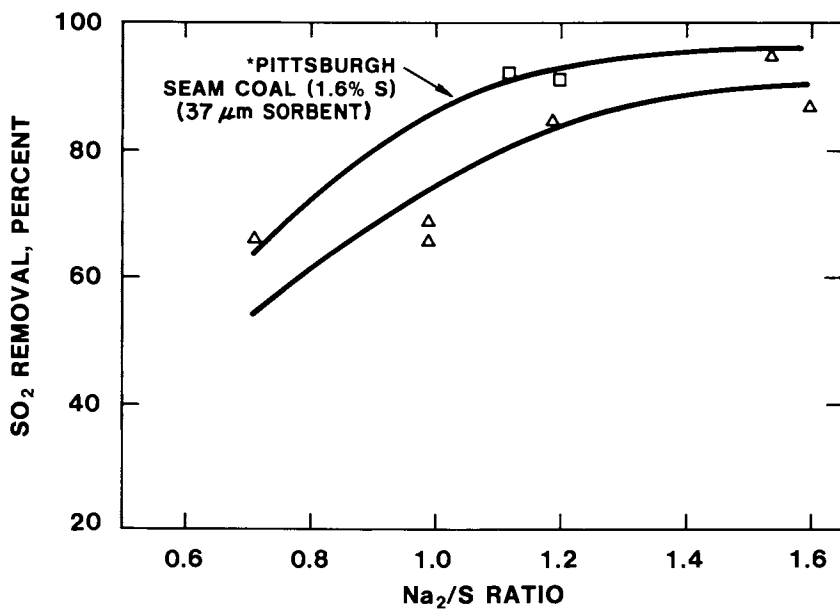


Figure 8. SO_2 removal with nahcolite while burning three types of coal. Sorbent, nahcolite; baghouse T , 400–420°F. Key: \square , Kentucky coal (1.0% S) (37 μm sorbent); \triangle , West Virginia coal (3.1% S) (33 μm sorbent); *, from Figure 7.

coal. The results are plotted in Figure 9. As in the case with nahcolite, higher SO₂ removal efficiencies were achieved while burning Pittsburgh seam coal than with West Virginia coal, although here the difference is more pronounced. In fact, if one were to adjust the West Virginia coal curve to account for particle size effects, the difference would be even greater (a decrease in SO₂ removal efficiency by approximately 3 percentage points at each Na₂/S ratio, assuming the correlation given in Figure 6 is valid).

Conclusions

This study has confirmed that high levels of SO₂ removal can be achieved via dry powder injection of NaHCO₃-bearing sorbents into the flue gas of coal-fired boilers. The mineral nahcolite is particularly effective. Commercially produced sodium bicarbonate is slightly less reactive than nahcolite. The mineral trona was found to be less effective, probably due to the lower bicarbonate content of this material. With all three sorbents, SO₂ removal efficiencies in excess of 90 percent could be achieved, although in some cases at fairly low sorbent utilization efficiencies.

Baghouse temperature had a significant effect on SO₂ removal efficiency, although baghouse cleaning cycle rate had no effect. It appears that a temperature of 400°F provides adequate sorbent reactivity, and this is well below the recommended maximum use temperature of the bags (\approx 450°F).

Sorbent particle size is also important. Removal efficiencies increased with decreasing mean particle size. The finest material tested had a mean particle diameter of 32 μ m. Whether finer grinding is warranted in industrial applications would depend on an economic analysis taking into consideration both increased sorbent utilization and increased grinding costs with finer grinding.

The location of the sorbent injection point appears to be important if coarser materials are used. However, with 32- μ m sodium bicarbonate, there was no difference between injecting sorbent immediately before the baghouse and injecting 26 feet upstream in the flue gas duct. It was also found that continuous injection of sorbent produces better results than intermittent feeding.

Higher levels of SO₂ removal efficiency were achieved with nahcolite and trona while burning the low-sulfur coals (1.0 and 1.6 percent sulfur) than when burning the 3.1 percent-sulfur coal. This cannot be explained, but the same effect has been noted in other studies.

Future investigations at PETC will focus on improving sorbent utilization while burning high-sulfur coals. A spray dryer system has been added to the test facility, and a sorbent recycle system will be installed. The planned work will include an evaluation of the effectiveness of lime and limestone slurry injection.

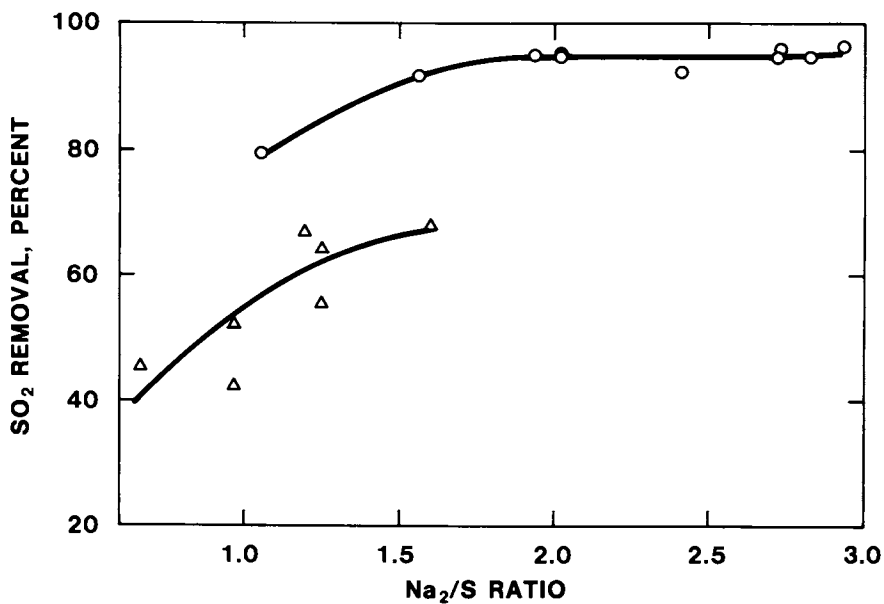


Figure 9. SO_2 removal with trona while burning Pittsburgh seam and West Virginia coal. Sorbent, trona; baghouse temperature, $400^\circ F$. Key: \circ , Pittsburgh seam coal (1.6% S) ($59 \mu m$ sorbent); and \triangle , West Virginia coal (3.1% S) ($32 \mu m$ sorbent).

Conversion Factors

<u>To Convert</u>	<u>Multiply By</u>	<u>To Obtain</u>
Btu	1055.06	Joules
Btu/hr·ft ³	10.3539	Joules/sec·m ³ , watt/m ³
Cubic feet	0.02832	Cubic meter
Fahrenheit (degrees)	(°F-32)/1.8	Centigrade (degrees)
Feet	0.3048	Meters
Pounds	0.4536	Kilograms
Tons	0.9072	Metric Tons

Reference in this report to any specific commercial product, process, or service is to facilitate understanding and does not necessarily imply its endorsement or favoring by the United States Department of Energy.

Literature Cited

1. Midkiff, L. A., "Spray-Dryer System Scrubs SO₂", *Power*, 123, No. 1, 29 (1979).
2. Lutz, S. J., R. C. Christman, B. C. McCoy, S. W. Mulligan, and K. M. Slimak, "Evaluation of Dry Sorbents and Fabric Filtration for FGD", prepared by TRW, Inc. for U. S. EPA, EPA-600/7-79-005, January 1979.
3. Miller, I., "Dry Scrubbing Looms Large in SO₂ Cleanup Plans", *Chemical Engineering*, p. 52, August 27, 1979.
4. Eriksen, P. E., "The Development of Dry Flue Gas Desulfurization at Basin Electric Power Cooperative", Second Conference on Air Quality Management in the Electric Power Industry, Austin, Texas, January 22-25, 1980.
5. Blythe, G. M., J. C. Dickerman, and M. E. Kelly, "Survey of Dry SO₂ Control Systems", prepared by Radian Corp. for U. S. EPA, EPA-600/7-80-030, February 1980.
6. Kelly, M. E. and J. C. Dickerman, "Current Status of Dry Flue Gas Desulfurization Systems", *Symposium on Flue Gas Desulfurization*, Houston, Texas, October 28-31, 1980, pp. 761-776, EPA-600/9-81-0196.
7. Burnett, T. A., K. D. Anderson, and R. L. Torstrick, "Spray Dryer FGD: Technical and Economic Assessment", *Symposium on Flue Gas Desulfurization*, Houston, Texas, October 28-31, 1980, pp. 713-729, EPA-600/9-81-0196.

8. Ness, H. M. and S. J. Selle, "Control of Western Power Plant Sulfur Dioxide Emissions: Development of the Ash-Alkali FGD Process and Dry Adsorption Techniques at the Grand Forks Energy Technology Center", DOE Symposium on Environmental Control Activities, Washington, DC, November 28-30, 1978.
9. Parsons, E. L., L. F. Hemenway, O. T. Kragh, T. G. Brna, and R. L. Ostop, "SO₂ Removal by Dry FGD", Symposium on Flue Gas Desulfurization, Houston, Texas, October 28-31, 1980, pp. 801-852, EPA 600/9-81-0196.
10. Bechtel Corporation, "Evaluation of Dry Alkalis for Removing Sulfur Dioxide from Boiler Flue Gases", EPRI FP207 (Research Project 491-1). Final Report, October 1976.
11. Rajaram, V., I. P. Nielsen, and H. D. Raymond, Mining Engineering, pp. 1699-1703, 1980.
12. Muzio, L. J., J. K. Arand, and N. D. Shah, "Bench Scale Study of Dry SO₂ Removal with Nahcolite and Trona", Second Conference on Air Quality Management in the Electric Power Industry, Austin, Texas, January 1980.
13. Shah, N. D., D. P. Teixeira, and R. C. Carr, "Application of Dry Sorbent Injection for SO₂ and Particulate Removal", Symposium on FGD, Hollywood, Florida, November 1976.
14. Davis, W. T. and T. C. Keener, "Phase I Chemical Kinetic Studies on Dry Sorbents Literature Review", University of Tennessee Report to Department of Energy Grand Forks Center, August 1980.

RECEIVED November 20, 1981.

Characterization of Volatile Organic Components of Nahcolite and Trona

BRUCE W. FARNUM, RONALD C. TIMPE¹, and SYLVIA A. FARNUM

U.S. Department of Energy, Grand Forks Energy Technology Center,
Grand Forks, ND 58202

Nahcolite and Trona were heated at 250-650°, yielding 1.3 and 0.2% volatile organic compounds. Proton and carbon-13 NMR and capillary gas chromatography indicated homologous series of n-alkanes and 1-alkenes from C₉ to C₂₉. The samples resembled shale oil.

Nahcolite, a naturally occurring form of sodium bicarbonate is found as nodules surrounded by oil shale or occasionally in discrete beds (1, 2). The nahcolite may be recovered during shale oil processing (3, 4) and since the mid-1970's has been in some demand as a scrubbing agent for sulfur oxides removal from stack gas. Several studies involving stack gas absorption show that the porous sodium carbonate produced by thermal decomposition of the nahcolite at stack gas temperatures is a very efficient SO₂ absorber (5-9). Grand Forks Energy Technology Center (GFETC) has been investigating the properties of nahcolite as a dry sorbent (10, 11, 12). These studies have included the use of trona, sodium sesquicarbonate (Na₂CO₃·NaHCO₃·2H₂O). Both nahcolite and trona were efficient absorbers of SO₂ with nahcolite being more efficient than trona during dry injection. Absorption of NO_x appeared to be dependant on the conditions and the amount of SO₂ present. Both materials gave an optimum injection temperature around 345° C where the maximum surface area was attained (10). Other reports supporting the use of trona as a viable dry sorbent have also appeared (13).

The present study was initiated to determine the possible emergence of organic materials from the nahcolite or trona into the flue gas and to identify the types of organic compounds involved.

¹ Current address: Mayville State College, Department of Chemistry, Mayville, ND 58257.

Experimental

Nahcolite and trona were obtained from batches of the dry sorbents used in the GFETC study (12). The nahcolite was mined in the Green River Formation of Colorado and obtained from the Superior Oil Co., Denver, CO, via the Utah Power and Light Company. The trona was mined in Wyoming by Stauffer Chemical Co. of Wyoming, Green River, WY. Pyrolysis of the minerals resulted in copious CO_2 evolution, clogging the liquid nitrogen trap. The carbonate, bicarbonate, and water soluble components of the minerals were dissolved in dilute HCl to obtain an insoluble residue for the pyrolysis studies. These materials were pretreated by mixing about 300 g of -100 mesh mineral into 1500 ml of deionized water. The resulting slurry was stirred magnetically for 2-3 hours and the pH was adjusted to 1-2 with concentrated HCl (Ultrex)*. The mixture was allowed to stand for at least 12 hours before it was filtered and air-dried for 3-8 days.

The volatile oils were collected by heating the air-dried, acid washed nahcolite or trona residues in a Vycor or quartz tube in a tube furnace under N_2 to 150° C, 250° C, 400° C and 650° C. Heat up time was 10-20 minutes. The liquid product was collected in a series of traps, consisting of an air cooled condenser, an ice-water trap, and a liquid nitrogen trap, Figure 1.

Mineral characterization studies were carried out by X-ray diffraction (Geology Department, University of North Dakota) and scanning electron microscopy (SEM).

The studies of the volatile oils utilized elemental analyses, dilute solution IR spectroscopy, 200 MHz ^1H NMR, 50 MHz ^{13}C NMR and capillary gas chromatography. The 200 MHz ^1H NMR spectra were run on a Varian XL-200 at a 45° flip angle (5 μsec pulse) with a delay of 5 sec between pulses. The number of pulses varied from 25 to 100. The volume of oil used was 25 μL with CDCl_3 . TMS was added as an internal standard. ^{13}C NMR spectra were run on the same instrument with 100 mg of oil diluted to 1500-2000 μL , pulse angle of 60°, 12 μsec pulse, and a delay of 5 sec. The number of pulses varied from 5000 to 10,000. TMS was the internal standard.

IR spectra were obtained in dilute solution in CCl_4 . A 10 mm near IR silica cell was used. Computerized subtraction of the cell and solvent background was applied. The instrument used was the Perkin-Elmer model 283 with data station.

Capillary gas chromatography was carried out on an Hewlett-Packard* methyl silicone fluid coated, Carbowax 20M deactivated fused silica capillary column, 50m x 0.2mm ID programmed from 100°C to 280°C at 4°/min. A Varian 3700 GC was used with flame ionization detection.

Thermal gravimetric analyses (TGA) were carried out on a DuPont model 951 analyzer.

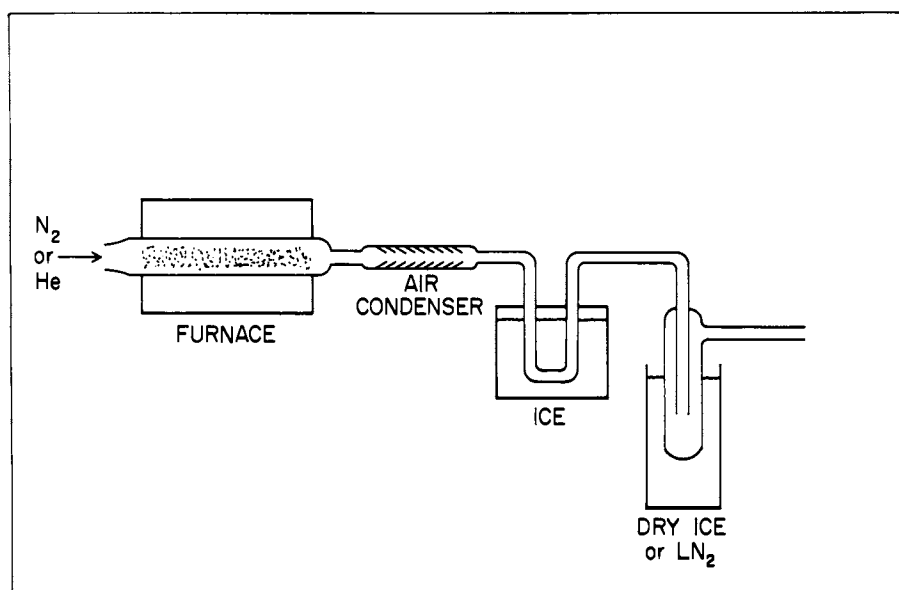


Figure 1. Apparatus for trapping volatile oils from nahcolite and trona.

Results and Discussion

The raw nahcolite and trona are minerals containing sodium carbonate and sodium bicarbonate. Figure 2b shows the x-ray diffraction powder pattern for untreated nahcolite. Patterns for NaHCO_3 and for quartz appear as prominent features. Figure 2a shows the same material after acid-washing, plainly indicating the loss of the NaHCO_3 . SEM microprobe analysis confirmed loss of sodium. The acid insoluble fractions which produced only a minimum of residual CO_2 on heating was much more suitable for use in the determination of volatile organic oils.

Thermal gravimetric analysis showed volatilization of 5.7% of the acid-insolubles of nahcolite and 1.8% of the acid insolubles of trona. After correction to weight of original mineral, the oil represented 1.2% of the nahcolite and 0.3% of the trona. A typical thermogram is shown in Figure 3. The major amounts of oil volatilized between 400°C and 550°C. Table 1 summarizes the data obtained.

Table I
Comparison of Trona and Nahcolite Behavior
with TGA, Acid Slurry Treatment and Volatile Oil Determination

	Trona (%)	Nahcolite (%)
TGA Heating loss, 250-650°C		
acid washed	1.8	5.7
acid washed, corrected to wt. of original mineral	0.3	1.2
Weight loss on acid treatment	94-95	88-89
Oil Yield to 650°C	0.2	1.3

Nahcolite oil, 1.3% of the raw nahcolite, was collected from the three traps after heating at 650°C and was subjected to elemental analysis, Table 2. Additional collections of samples were made with heating terminated at 400°C and 250°C. Elemental analysis data from a run terminated at 400°C also appears in Table 2. The oil that was collected at 400°C was 65% of the total oil yield.

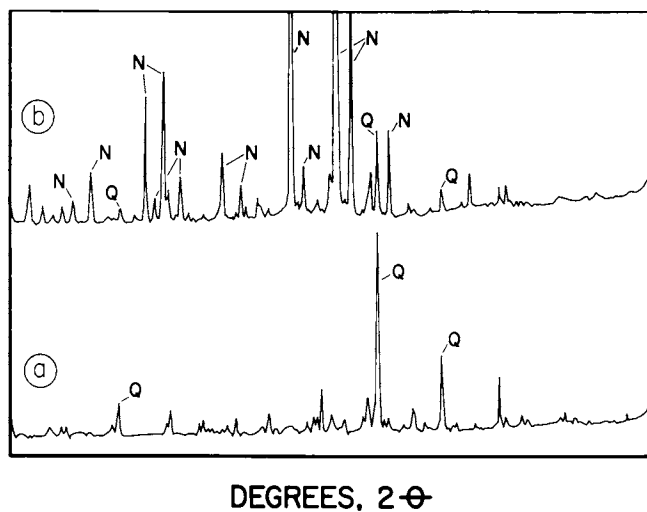


Figure 2. X-ray diffraction patterns for a, acid insolubles of nahcolite and b, nahcolite. Key: N, NaHCO₃; and Q, quartz.

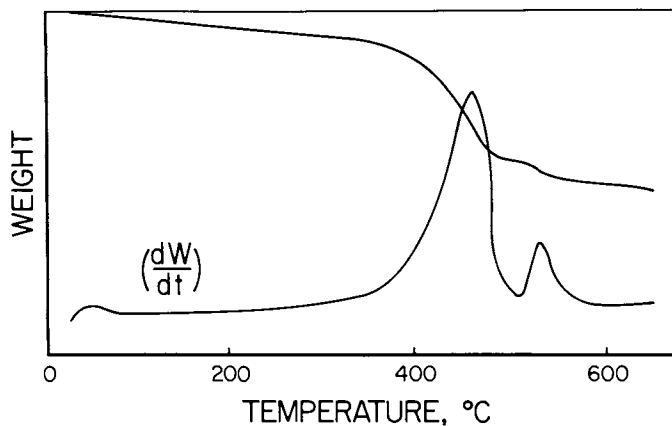


Figure 3. TGA analysis of acid insoluble fraction of nahcolite.

Table II
Elemental Analyses of Nahcolite Oil
Collected on Heating to 650°C

	C (%)	H (%)	N (%)
air condenser	81.2	11.1	1.7
ice trap	82.6	11.9	1.3
LN ₂ trap	81.6	11.6	1.2
Heating to 400°C			
air condenser	84.6	11.4	1.9
LN ₂ trap	81.1	11.3	1.6

The various trap contents were examined by NMR, IR and capillary GC. The 200 MHz ¹H NMR spectrum of the nahcolite oil that was collected up to 400°C is shown in Figure 4a. The CH₃ and CH₂ proton resonances were very prominent indicating alkanes. Terminal olefins were positively identified by the characteristic pattern between 4 ppm and 6 ppm. Figure 4b shows this pattern for one of the standards, 1-octene. The 50 MHz ¹³C NMR spectrum of the same fraction, Figure 5, confirmed the presence of n-paraffins and 1-enes. The capillary gas chromatographic technique used separated the same oil into a recognizable homologous series of alkanes and the corresponding terminal olefins. In this fraction the C-10 through C-28 members of both homologous series were seen. Pristane was present. These are identified in Figure 6a and Table 3. The ¹H NMR spectrum of material collected between 400° and 650° showed long chain n-alkanes with very little unsaturated material present.

Examination of trona oil, 0.2% of the whole trona, collected up to 650°C revealed that the oil was similar in composition to the nahcolite oil. The elemental analyses are shown in Table 4.

Similar patterns of n-alkanes and terminal olefin series peaks were seen for trona oil, Figure 6b. Pristane was recognized.

The IR spectra obtained in dilute CCl₄ solutions were similar for nahcolite and trona oils. Several weak bands were noted (Figure 7). Water, 3700 cm⁻¹ and a phenolic OH stretching frequency at 3605 cm⁻¹ were most obvious.

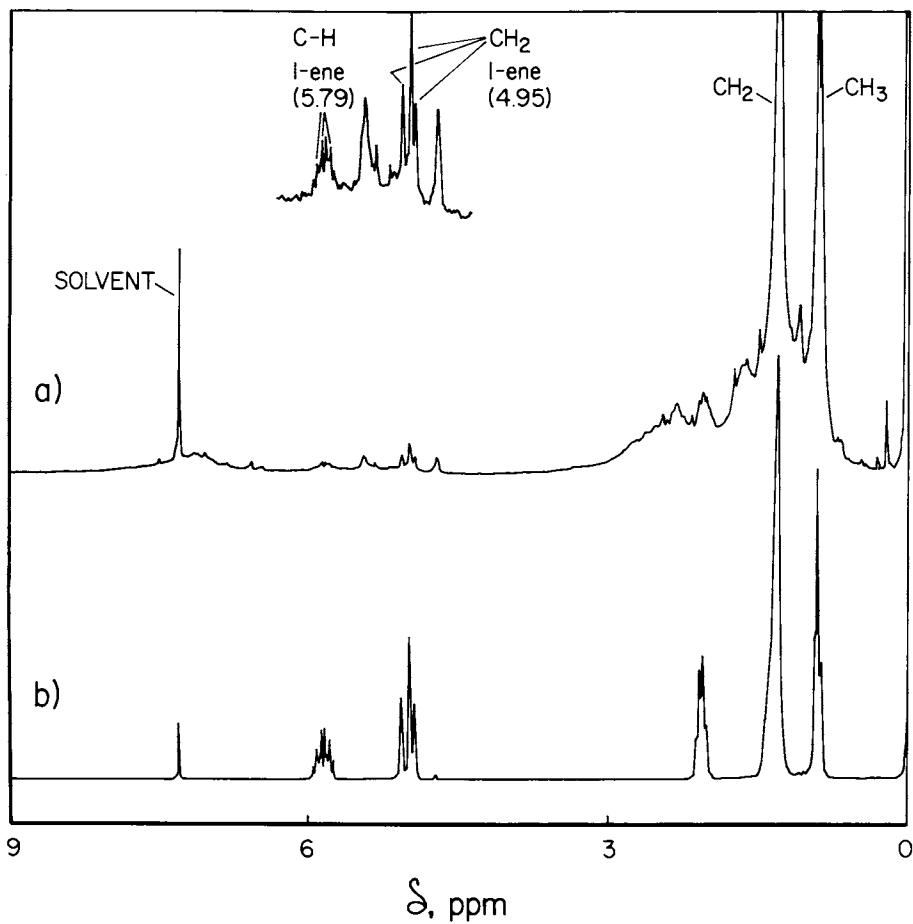


Figure 4. a, ^1H NMR spectrum (200 MHz) of nahcolite oil collected from 250–400°C; and b, standard 200 MHz ^1H NMR spectrum of 1-octene.

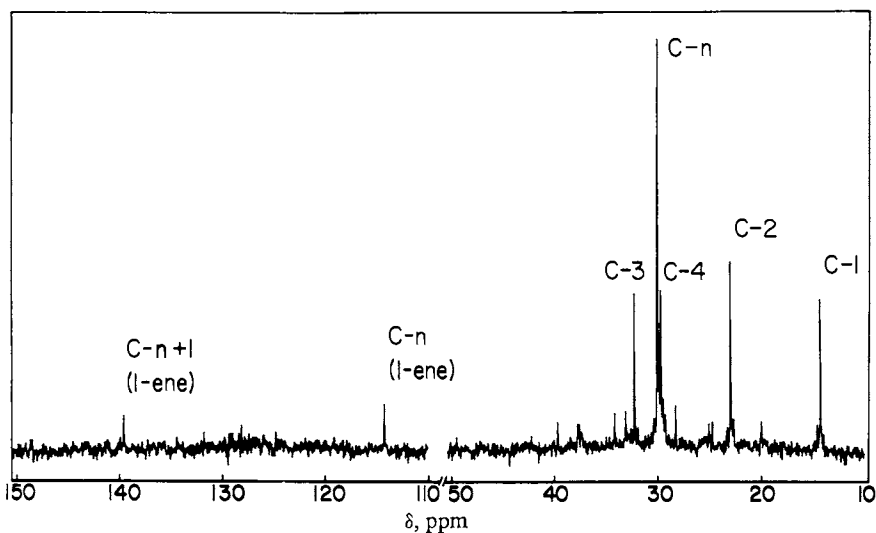


Figure 5. ^{13}C NMR spectrum (50 MHz) of nahcolite oil collected between 250–400°C.

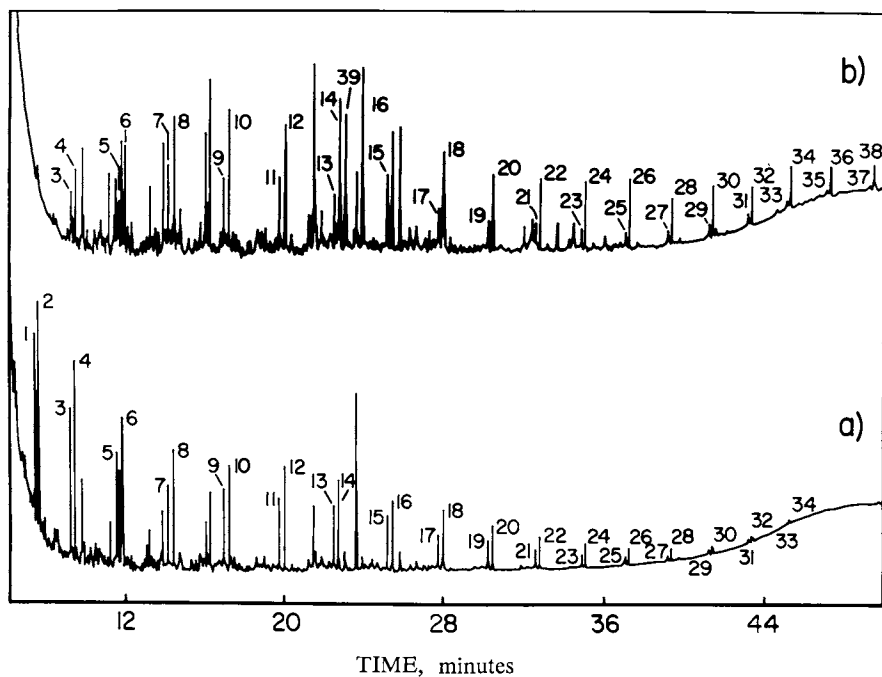


Figure 6. Capillary gas chromatography of a, nahcolite oil collected up to 400°C (liquid N_2 trap); and b, trona oil collected from 250–400°C (liquid N_2 trap), on a HP methyl silicone fluid 0.2 mm \times 50 m fused silica column. Key: see Table III.

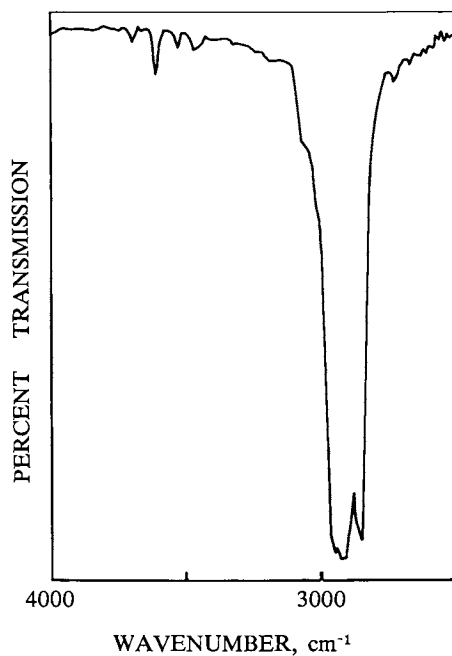


Figure 7. IR spectrum of nahcolite oil collected from 260–400°C, dilute solution in CCl₄.

Table III
Compounds Identified by Gas Chromatography
of Nahcolite and Trona Oils, Figure 6.

1. 1-undecene	14. heptadecane	27. 1-tetracosene
2. undecane	15. 1-octadecene	28. tetracosane
3. 1-dodecene	16. octadecane	29. 1-pentacosane
4. dodecane	17. 1-nonadecene	30. pentacosane
5. 1-tridecene	18. nonadecane	31. 1-hexacosene
6. tridecane	19. 1-eicosene	32. hexacosane
7. 1-tetradecene	20. eicosane	33. 1-heptacosene
8. tetradecane	21. 1-heneicosene	34. heptacosane
9. 1-pentadecene	22. heneicosane	35. 1-octacosene
10. pentadecane	23. 1-docosene	36. octacosane
11. 1-hexadecene	24. docosane	37. 1-nonocosene
12. hexadecane	25. 1-tricosene	38. nonacosane
13. 1-heptadecene	26. tricosane	39. pristane

Table IV
Elemental Analyses of Trona Oil
collected on heating to 650°C

	C (%)	% H	% N
air condenser	81.7	9.9	2.4
ice trap	83.9	11.6	0.7
LN ₂ trap	71.4	9.8	3.4

In summary, the yield of volatile oil was larger for nahcolite than for trona. Thermal gravimetric analysis of the acid insoluble fractions of the mineral yielded good results comparable with the determination of volatile oils by direct heating and weighing.

A significant finding of this study was the fact that the two volatile oils investigated from nahcolite and trona were very similar and that they closely resemble shale oil, both from our observations and from the literature (14, 15). Since the minerals are found in nature near oil shale or in some cases intimately mixed with the shale this is an expected observation. Environmental hazards as well as other oil properties can probably be inferred from studies carried out by numerous investigators with shale oils.

Reference to specific brand names and models is done to facilitate understanding and neither constitutes nor implies endorsement by the Department of Energy.

Acknowledgments

The authors wish to thank Harvey Ness, Frank R. Karner, George Montgomery, Steven A. Benson and Edward F. Bitzan for contributions to the research.

Literature Cited

1. Beard, T.N.; Smith, J.W. In Am. Institute of Chemical Engineers, AIChE Symposium Series (No. 155), 1976, p 32.
2. Desborough, G.A.; Pitman, J.K.; Huffman, C. Jr. Chemical Geology 1976, 17, 13.
3. Weichman, B.E. U.S. Patent 3 821 353, 1974.
4. Chem. Eng. News Jan 10, 1977, 27.
5. Howatson, J., Smith, J.W.; Outka, D.A.; Dewald, H.D. Proc. Fifth Nat. Conf. on Energy and the Environment Nov. 1-3, 1977, Cincinnati, Ohio.
6. Genco, J.M.; Rosenberg, H.S. APCA Journal 1976, 26, 989.
7. Knight, J.H. U.S. Patent 4 062 926, 1977.
8. Doyle, D.J., Electrical World 1977, 32.
9. Howatson, J.; Dewald, H.D.; Outka, D.A.; Diller, D.V.; Cain, M.B.; Smith, J.W. APCA Journal 1980, 30, 1229.
10. Ness, H.M.; Selle, S.J., "Control of Western Power Plant Sulfur Dioxide Emissions: Development of the Ash-Alkali FGD Process and Dry Absorption Techniques at the Grand Forks Energy Technology Center"; presented at the DOE Symposium on Environmental Control Activities, Nov. 28-30, 1978, Washington, D.C.
11. Ness, H.M.; Selle, S.J.; Manz, O.E. "Power Plant Flue Gas Desulfurization For Low-Rank Western Coals"; 1979 Lignite Symposium, May 1979, Grand Forks, N.D., GFETC/IC-79/1, p 117.
12. Stern, F.R. "Laboratory Kinetic Studies on Dry Adsorption of Sulfur Dioxide Using Nahcolite and Trona"; MS Thesis, University of North Dakota, Grand Forks, N.D., 1978.
13. Parsons, E.L., Jr.; Hemenway, L.F.; Kragh, O.T.; Brna, T.G.; Ostop, R.L. "SO₂ Removal by Dry FGD"; presented at EPA Symposium on Flue Gas Desulfurization, Oct. 28-31, 1980, Houston, Texas.
14. DiSanzo, F.P.; Uden, P.C.; Siggia, S. Anal. Chem. 1980, 52, 906.
15. Crowley, R.J.; Siggia, S.; Uden, P.C. Anal. Chem. 1980, 52, 1224.

RECEIVED February 16, 1982.

Conceptual Design and Economics of an Improved Magnesium Oxide Flue Gas Desulfurization Process

T. A. BURNETT and W. L. WELLS

Tennessee Valley Authority, Office of Power, Division of Energy Demonstrations and Technology, Chattanooga, TN 37401

An improved magnesium oxide (MgO) flue gas desulfurization process and its comparative economics are described. Innovations made include the use of a spray dryer, a cyclic hotwater reheater, and a coal-fired fluidized-bed reactor for regeneration of the MgO absorbent. Several technical concerns with the proposed design are addressed, including fly ash and chloride buildup. The economic evaluation shows the process to have a capital investment of about seven percent less than that of a conventional MgO scrubbing process and a 40 percent smaller annual revenue requirement. Finally, a sensitivity analysis is shown relating annual revenue requirements to the byproduct sulfuric acid price credit.

This chapter not subject to U.S. copyright.
Published 1982 American Chemical Society.

INTRODUCTION

TVA's involvement with magnesium oxide (MgO) flue gas desulfurization (FGD) systems extends over a period of years and has been documented in a recent Environmental Protection Agency symposium paper (1). The process described therein utilizes conventional MgO FGD technology and is similar in design to one being installed commercially by Philadelphia Electric Company.

Since the conventional MgO process has not gained widespread acceptance, efforts are underway to make the process more energy efficient, less dependent on fuel oil and, most importantly, more competitive economically with a limestone scrubbing system. This paper is the result of TVA's initial investigation into an improved MgO process. The purpose is to describe the new MgO process, to detail some of the technical uncertainties requiring further development work, and to present preliminary conceptual design economics for this improved MgO FGD system.

INNOVATIVE DESIGN CHANGES

Figures 1 and 2, respectively, show the old and new processes. The major innovations are use of (1) a spray dryer absorber in place of the wet venturi, absorber, centrifuge, rotary dryer combination; (2) a cyclic hot-water reheat system interconnecting thermally the calciner product solids and the effluent gas from the spray dryer absorber; and (3) a coal-fired, fluidized-bed reactor for conversion of magnesium sulfite ($MgSO_3$) and sulfate ($MgSO_4$) to MgO and SO_2 gas. Otherwise, the two systems are very similar, utilizing a regenerable absorbent to recover the sulfur material as a usable commercial grade of concentrated sulfuric acid.

Spray dryer absorbers have recently been adapted for use in FGD systems by numerous vendors and the resulting lime-based FGD processes have been sold for various utility and industrial applications (2). These spray dryer absorbers appear to offer the potential for significant advantages over conventional wet scrubbing technology including (1) elimination of stack gas reheat for most applications, (2) elimination of mist eliminators, (3) production of a dry waste directly, and (4) elimination of the large recirculating pumps and piping. From a theoretical standpoint, there does not appear to be any reason why a spray dryer absorber could not be adapted to the MgO FGD process and offer these same advantages. In fact the production of a dry waste directly in the spray dryer may prove to be the most significant potential advantage since it will

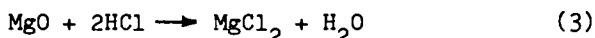
eliminate those processing sections in the conventional MgO FGD process which consume significant amounts of energy (i.e., the scrubber recirculation pumps and the solids separation and drying equipment).

The cyclic hot-water reheater system recovers heat from the product solids cooler in the calcination area and uses this heat to displace steam in the stack gas reheater. The fluidized-bed calciner is fired with station coal rather than expensive No. 2 fuel oil which was used in the previous conventional MgO evaluation. Both of these latter design changes reflect new technology which may require some additional development work before they are accepted as proven for commercial usage.

SPRAY DRYER MgO PROCESS DESCRIPTION

As shown in Figure 2, flue gas from the boiler at about 300°F passes through a 95% efficient ESP to remove most of the fly ash before the flue gas enters the FGD system. The collected fly ash is removed from the ESP hopper, transferred to intermediate storage silos, and trucked to an onsite ash landfill situated one mile from the power unit. The flue gas from the ESP passes through the boiler ID fan, a common plenum feeding the multiple trains of spray dryers, and the ductwork feeding the spray dryer.

The flue gas enters the spray dryer and passes downward through a concentric ring of turning vanes which surround the rotary atomizers. The makeup MgO slurry is pumped to the spray dryer and passes through the internals of the rotary atomizer and is sprayed perpendicularly to the flue gas flow. The resulting intimate mixing of the flue gas and the fine MgO slurry particles results in the following primary reactions:



In addition the following secondary reaction is expected to occur:

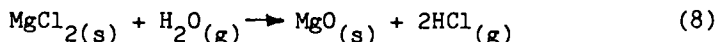
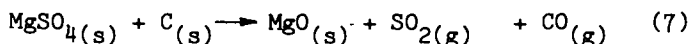
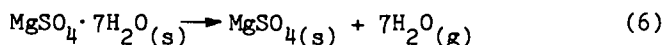
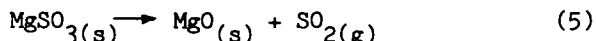


The amount of water in the makeup MgO slurry that is pumped to the spray dryer is controlled such that the flue gas leaves the spray dryer unsaturated. Since no liquid water remains in the flue gas, mist eliminators are not required and the magnesium salts leave the spray dryer as dry particles entrained in the flue gas.

The flue gas leaves the spray dryer at about 150°F and is partially reheated in a cyclic hot-water reheater before entering the baghouse. The water is heated in the product solids cooler in the calcination area and then passed through tubes in the ductwork between the spray dryer and the baghouse, heating the flue gas. The flue gas is reheated approximately 20 F° to prevent condensation in cold spots in the baghouse.

The baghouse is designed to receive flue gas from all trains of the spray dryers and to remove the particulate matter such that the 1979 NSPS for particulate matter (0.03 lb/MBtu) is achieved. The clean flue gas from the baghouse passes through an ID fan and exits through the stack.

The bags in the baghouse are periodically cleaned by reverse air and the mixed magnesium salts and fly ash fall into hoppers at the bottom of the baghouse. These collected solids are pneumatically conveyed to intermediate storage silos. From these silos the solids are pneumatically conveyed to a coal-fired, fluidized-bed calciner. Station coal is removed from the plant stockpile, ground in a grinding mill, and blown into the fluidized-bed calciner. The coal burns in the fluidized bed of MgO pellets to produce heat to maintain the reaction temperatures. Inside the calciner at a temperature of 1600°F the magnesium salts are reconverted to MgO and SO₂ by the following reactions:



The fly ash is assumed to pass through the calciner unreacted. Although MgSO_3 is easily calcined at 1600°F , MgSO_4 (formed in either the absorber or the ash purge section) requires higher temperatures or the presence of carbon for the decomposition reaction to occur. Since carbon in the form of coal is present in the calciner, the MgSO_4 is assumed to be calcined as shown in reaction 7.

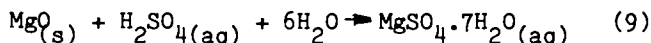
The SO_2 -laden off-gas from the calciner containing the regenerated HCl and the entrained MgO and fly ash passes overhead and into the MgO product cyclone. Approximately 80% of the solids are removed from the off-gas. Since the particle sizes of the MgO and fly ash are conservatively assumed to be very similar, 80% of each are removed. These hot (1600°F) solids pass through a product solids cooler where they are cooled to about 400°F before being pneumatically conveyed to the recycle MgO/ash storage silo for reuse. The heat exchange medium in the product solids cooler is high-pressure water. This hot water passes through the cyclic reheater in the flue gas duct between the spray dryer and the baghouse.

The SO_2 -laden off-gas leaves the MgO product cyclone at 1600°F and preheats the incoming air to the calciner in a fluidizing air heater. The off-gas from the air heater at 880°F is further cooled to 440°F in a spray quench tower and then enters a pulse-jet baghouse where the remaining solids are removed. (A pulse-jet baghouse is used because of the small gas stream to be cleaned.) The clean off-gas passes through a final cleanup section where the 440°F off-gas is cooled by recirculating water sprays to condense some of the water vapor and also to scrub the HCl from the off-gas. This HCl-contaminated water passes to a stripper where compressed air, passing through the water, removes any remaining SO_2 from the water before the water is neutralized and pumped to the clay-lined boiler ash pond.

The SO_2 -laden off-gas from the cooler and the air from the stripper are compressed and sent to a single-contact, single-absorption sulfuric acid plant. Ninety-six percent of the SO_2 is converted to 98% sulfuric acid. Ten percent of this byproduct acid is recycled and used in the MgO FGD process but most is stored onsite and eventually sold as a byproduct. The tail gas from the acid plant containing the unconverted SO_2 is recycled to the flue gas ducts ahead of the FGD system.

The solids from the pulse-jet baghouse at 440°F are pneumatically conveyed to an intermediate storage silo. About two-thirds of the MgO/ash mixture is returned to the recycle MgO/ash storage silo in the feed preparation area while the remaining one-third enters the ash purge section. In this section the MgO/ash mixture is first reslurried with water and then mixed with 98% sulfuric acid from the acid plant. The

sulfuric acid reacts with insoluble MgO to form soluble $\text{MgSO}_4 \cdot 7\text{H}_2\text{O}$, i.e.,



which can then be separated from the ash by filtration. The rotary drum filter separates the ash from the $\text{MgSO}_4 \cdot 7\text{H}_2\text{O}$ solution. The filter cake is washed twice to recover as much of the dissolved $\text{MgSO}_4 \cdot 7\text{H}_2\text{O}$ as practical before the cake is trucked to the onsite ash landfill for disposal.

The filtrate and the wash water containing the $\text{MgSO}_4 \cdot 7\text{H}_2\text{O}$ are pumped to the slurry feed tank in the feed preparation area. Vibrating screw feeders transfer makeup MgO and recycle MgO/ash from 8-hour capacity, in-process feed bins to the prelake mixer where fresh water is added to wet the MgO thus allowing better mixing in the slurry feed tank. Residence time in the mixer is only about two minutes to prevent solidification of the concentrated mix. Makeup water as necessary is added and slaking is completed in the slurry feed tank. The resulting slurry is pumped to the spray dryer as required.

TECHNICAL UNCERTAINTIES

This conceptual design and economic evaluation is based on theoretical considerations only and many of the assumptions used in this design need to be verified in an actual pilot-plant operation. These various design assumptions include: (1) MgO/ash separation, (2) HCl removal and purge, and (3) spray dryer design.

MgO/Ash Separation

The initial and perhaps most critical design assumption is that both the MgO and the fly ash, which are carried out of the calciner and into the MgO product cyclone, have the same particle size distribution and density. This design (i.e., no possibility of physical separation of MgO and fly ash) is a conservative design assumption and adds complexity to the FGD process. It results in the need to recirculate large quantities of the MgO/fly ash mixture through the spray dryer and the calciner. In order to keep the MgO/ash recycle streams to a reasonable size, the mechanical collectors in the main flue gas ducts upstream from the SO_2 absorber, which were used in the initial design because they are relatively inexpensive but yet remove only 80% of the fly ash, had to be replaced with the 95% efficient ESP mentioned earlier.

The FGD waste particles entering the calciner would tend to be larger than the fly ash particles because the larger fly ash particles are removed in the 95% efficient ESP leaving only the smaller (~ 10 micron) particles. The FGD waste particles, although initially small, tend to coalesce in the spray dryer as the atomized slurry dries. Based on information from the lime-based spray dryer FGD systems, it is estimated that the FGD waste particles will be on the order of 50 microns. If this particle size difference between the ash and the MgO particles is still present in the particles leaving the calciner, the MgO particles being the larger of the two would tend to be removed in the MgO product cyclone. The solids passing through the cyclone (and out with off-gas) would thus be enriched in the ash particles. This enrichment would permit smaller recycle streams to be used.

If the MgO and ash particles actually have a significant difference in density/particle size, the ash purge section could be redesigned to include a separation device such as a thickener that could be used to split the solids into an enriched fly ash stream and one enriched in MgO. Since the recycle MgO must be reslurried before entering the spray dryer, wetting this stream would not present any significant problems to the process. The fly ash-enriched stream could then be sent to a smaller ash purge section.

Both of these alternative separation techniques could be evaluated in a spray dryer MgO pilot plant. If either or both of these tests yield satisfactory solutions to the MgO/ash separation problem, it might be possible to reduce the investment and revenue requirements significantly by eliminating the 95% efficient ESP and replacing it with a mechanical collector. Therefore it may also be necessary to perform some test work in a pilot plant to determine the relative densities and particle sizes of the MgO and the ash in the calciner off-gas.

HCl Removal and Purge

The spray dryer MgO FGD system is based on the design assumption that HCl in the flue gas reacts with MgO in the spray dryer to form $MgCl_2$. The $MgCl_2$, along with the fly ash and magnesium-sulfur salts, would then be collected in the baghouse and conveyed to the calciner. Based on a previous theoretical study (3) it is further assumed that in the oxidizing atmosphere of the calciner, the $MgCl_2$ is converted back to MgO and HCl. The MgO is recycled and the HCl remains in the SO_2 -laden off-gas until it reaches the gas cooler where it is removed by the recirculating water sprays. The resulting chloride purge water is neutralized with agricultural limestone and pumped to the boiler ash pond for disposal.

If the HCl is not regenerated in the calciner as is currently expected, one of two design changes must be made and both involve purging a $MgCl_2$ solution from the FGD system. The first alternative is to remove a purge stream from the mixing tank in the ash purge section after the MgO /fly ash mixture has been reslurried (but just before the sulfuric acid is added). At this point in the process $MgCl_2$ would be the only soluble magnesium compound present. Ultimate disposal of this $MgCl_2$ solution, other than in the boiler ash pond, is uncertain and would require further study. The second alternative is to install a guard box in the flue gas ducts between the ESP's and the spray dryers. The guard box would contain a solid absorbent which would preferentially remove HCl from the flue gas. When fully saturated the absorbent would be removed and replaced with a fresh charge. Although this would effectively remove HCl from the flue gas, the $MgCl_2$ purge system would still be required (although on a smaller scale) since HCl would still enter the FGD system from the station coal used as fuel for the fluidized-bed calciner.

Thus it would probably be necessary to determine if the absorbed HCl is in fact regenerated in the calciner. If it is not, a significant change will have to be made in the process design presented here.

Spray Dryer Design

The design for the MgO spray dryer-absorber is based on the data currently available from the lime-based spray dryer systems since data on an MgO -based spray dryer-absorber are currently not available. This assumption is considered to be reasonable since both lime and MgO produce an absorbent slurry and both are Group II element oxides, but primarily because no other data are available.

The MgO system is based on a conservatively designed lime system (i.e., a MgO stoichiometry of 1.8 moles MgO /mole SO_2 absorbed, a 20 F° approach to the flue gas saturation temperature in the spray dryer, etc.). All of the spray dryer design considerations will therefore have to be evaluated in a spray dryer MgO pilot plant.

PRELIMINARY CONCEPTUAL DESIGN ECONOMICS

This section presents comparative economic results for three processes, viz., conventional limestone, spray dryer MgO , and conventional MgO . The results of any conceptual design and economic evaluation depend on the premises chosen initially. The major design and economic premises used for this study are shown in Table I.

TABLE I. MAJOR DESIGN AND ECONOMIC PREMISES

Item	Premise
Power plant	500-MW, new coal-fired boiler
Fuel	11,700 Btu/lb, 15.1% ash, 4% moisture 3.5% sulfur (dry basis)
Heat rate	9,500 Btu/kWh
Operating schedule	165,000 hr, 30-year life; 5,500-hr first-year operation
Particulate removal efficiency	Revised 1979 NSPS
SO ₂ removal efficiency	Revised 1979 NSPS
SO ₂ absorber redundancy	One spare train
Base year	
Capital investment	Mid-1982
Revenue requirements	Mid-1984

Design Premises

The economic evaluation is based on a flue gas cleaning (FGD and fly ash) system to meet the revised 1979 NSPS for both particulate matter and SO₂ for a new, 500-MW coal-fired boiler. The boiler burns a 3.5% sulfur eastern bituminous coal containing 15.1% ash and having a heating value of 11,700 Btu/lb. The boiler has a heat rate of 9,500 Btu/kWh. The FGD system is designed with one spare scrubber train, 50% emergency flue gas bypass around the FGD system, and an onsite landfill located one mile from the boiler. The operating schedule specifies a 165,000-hour, 30-year life for the boiler and 5,500 hours of first-year operation.

Economic Premises

The economic evaluation consists of a study-grade (-20%, +40%) determination of capital investment, first-year annual revenue requirements, and levelized annual revenue requirements. The capital investments are based on major equipment costs (developed from the flow diagram and the material balance) and factored costs for installation, ancillary equipment, and indirect investments. The capital investments are based on mid-1982 costs.

First-year annual revenue requirements consist of raw material, operating, and overhead costs and levelized capital

charges. The levelized annual revenue requirements consist of levelized raw material, operating, and overhead costs as well as levelized capital charges. The levelized raw material, conversion, and overhead costs are calculated by using a levelizing factor of 1.886. This factor is explained in more detail elsewhere (4) and is based on a 10%/yr discount rate, a 6%/yr inflation rate, and a 30-year life of the power unit. Revenue requirements (both first year and levelized) are based on mid-1984 costs.

Economic Evaluation

Since the MgO spray dryer FGD process collects particulate matter as an inherent part of the FGD system, it can be evaluated either as a combined particulate-SO₂ removal system or, with the inclusion of an ESP credit, as an FGD-only process. In this study the spray dryer MgO process evaluation is based on the combined particulate-SO₂ removal system. The primary reasons are that the combined system is easier to explain and that similar evaluations for the limestone scrubbing/ESP and conventional MgO/ESP systems are available from previous studies (2, 5). The conventional MgO/ESP process cost information from the previous study was updated using area scale factors, relative product and gas rates, etc., to put the results on a consistent basis with the current evaluation of the spray dryer MgO process.

All three processes are designed as proven technology, though it is recognized that there are major differences in status of development among these. The spray dryer MgO process is a new design, as yet unproven even on a small pilot-plant scale. The conventional MgO process is based on 100-MW testing at Philadelphia Electric's Eddystone station. The limestone scrubbing process is well-defined and generally considered proven technology with widespread adoption in the electric utility industry. In order to account for design uncertainty, both MgO processes have a contingency factor of 20 percent as part of the capital investment, while the limestone process has a contingency factor of only 10 percent. This contingency factor difference accounts for approximately half of the total capital investment difference.

Capital Investment

Results

The capital investment for the spray dryer MgO FGD process is \$139.5M (\$279/kW) in mid-1982 dollars while that for a comparable limestone scrubbing/ESP process is \$122.0M (\$244/kW) in mid-1982 dollars. The capital investment for the conventional MgO FGD process (including particulate control) is \$149.7M (\$299/kW) in mid-1982 dollars. These costs are summarized in Table II. For full details see Tables A-I, A-II, and A-III in the Appendix.

TABLE II. CAPITAL INVESTMENT SUMMARY

	Capital Investment	
	k\$	\$/kW
Conventional limestone process	121,953	243.91
Spray dryer MgO process	139,497	278.99
Conventional MgO process	149,683	299.37

Comparison

The capital investment for the spray dryer MgO process is approximately 14% higher than that for the comparable limestone scrubbing process. This is not an unexpected result since the MgO process is a regenerable system while the limestone scrubbing process is a throwaway system.

Of the components which make up the capital investment, the direct area investment for raw material handling, feed preparation, gas handling, SO₂ absorption, and waste disposal all are more expensive for the limestone scrubbing process. Because the limestone scrubbing process is a throwaway system, it is not unexpected that the raw material handling, feed preparation, and waste disposal areas are more expensive. The gas handling and SO₂ absorption areas are more expensive due to the wet scrubbing design basis for the limestone process. More expensive materials of construction and more equipment are needed in the wet limestone scrubbing process.

The spray dryer MgO process contains a regeneration section which includes the areas of calcination, off-gas cleanup, sulfuric acid plant, and acid storage and shipping.

There are no comparable areas in the limestone scrubbing process. The \$22 million investment for these areas in the MgO process offsets the lower investment for the other processing areas.

Likewise, the capital investment for the spray dryer MgO process is approximately 7 percent lower than that for the conventional MgO scrubbing process (\$279/kW vs. \$299/kW). The conventional MgO scrubbing process has more equipment, and hence larger investment costs, particularly in the areas of chloride purge, slurry drying, and slurry processing equipment which are not needed in the spray dryer-based system.

Both the spray dryer MgO process and the conventional MgO process contain a regeneration section which includes the areas of calcination, sulfuric acid plant, and acid storage and shipping. The regeneration section in the conventional MgO process also contains the drying area but lacks the off-gas cleaning area. This off-gas cleaning area is not necessary in the conventional process because chlorides are removed upstream and very little fly ash enters the system because of the high-efficiency ESP and the relatively clean nature of No. 2 fuel oil. The chlorides are removed in the off-gas treatment area in the spray dryer MgO process utilizing smaller equipment at a lower cost. The conventional MgO process contains a chloride purge area upstream of the FGD system, which treats the entire flue gas stream resulting in a larger investment cost.

The net effect of these differing area investments for the two processes is that the total direct investment for the spray dryer MgO process is about 6% lower (\$72.0M vs. \$76.2M) than that for the conventional MgO process. This cost advantage for the spray dryer MgO process is further increased as a result of the premise-derived indirect investments (construction expense, contingency, etc.,) and other capital investments (allowance for startup and modification and interest during construction) even though the cost factors (i.e., percentages) for both processes are identical.

The higher direct investment for the conventional MgO process results in the higher indirect investments and other capital investments and hence the total capital investment when these factors are applied.

The calciner area, although considered proven technology in other industrial applications, is as yet incompletely tested in an FGD facility. Further compounding the questions concerning the calciner is the fact that in the spray dryer MgO process it is a coal-fired, fluidized-bed unit whose feasibility and reliability need to be demonstrated. In addition the conversion of $MgSO_3$ to MgO and the reusable nature of the regenerated MgO in a full-scale utility application are unknown. A form of cyclic reheat is also employed here utilizing the waste heat generated in the MgO

product cooler to provide two-thirds of the reheat required by the flue gas (the remainder is provided by steam). The other areas in the spray dryer MgO process are all relatively proven technology and can be adapted to the application envisioned here.

Annual Revenue Requirements

Results

The first-year annual revenue requirements for the spray dryer MgO FGD process are \$28.8M (10.47 mills/kWh) in mid-1984 dollars. The levelized annual revenue requirements for the spray dryer MgO process are \$36.1M (13.13 mills/kWh). The first-year annual revenue requirements for the comparable limestone scrubbing process are \$32.4M (11.78 mills/kWh) in mid-1984 dollars. The levelized annual revenue requirements for the limestone scrubbing process are \$45.2M (16.43 mills/kWh). The first-year annual revenue requirements for the conventional MgO FGD process (including particulate control) are \$40.4M (14.69 mills/kWh) in mid-1984 dollars. Levelized annual revenue requirements are \$56.7M (20.61 mills/kWh). These costs are summarized in Table III. The complete details are presented in Tables A-IV, A-V, and A-VI in the Appendix.

TABLE III. ANNUAL REVENUE REQUIREMENTS SUMMARY

	First-year		Levelized	
	annual revenue		annual revenue	
	requirements		requirements	
	<u>k\$</u>	<u>mills/kWh</u>	<u>k\$</u>	<u>mills/kWh</u>
Conventional limestone process	32,400	11.78*	45,190	16.43*
Spray dryer MgO process	28,800	10.47**	36,113	13.13**
Conventional MgO process	40,400	14.69**	56,683	20.61**

*Onsite solids disposal
 **Byproduct H₂SO₄ credit \$65.00/ton

Comparison

The first-year annual revenue requirements for the spray dryer MgO process are about 11% lower than those for the comparable limestone scrubbing process. This economic advantage for the spray dryer MgO process increases to nearly

20% when the levelized annual revenue requirements are compared. The primary reason for this increased advantage in the levelized annual revenue requirements for the spray dryer MgO process is the low first-year operating and maintenance cost. This low first-year operating and maintenance cost is due to the regenerable nature of the process. It has a low raw materials cost and a high byproduct sales credit.

The first-year and the levelized annual revenue requirements are lower for the spray dryer MgO process because of significant differences in the byproduct credit, energy, and raw material costs. These annual cost savings more than offset the higher capital charges for the spray dryer MgO process.

The byproduct credit for sulfuric acid is the major reason for the lower spray dryer MgO annual revenue requirements. The credit of \$6.0M lowers the first-year annual revenue requirements by 40%. The gypsum produced in the limestone scrubbing process is assumed to be a waste material to be landfilled and thus the limestone scrubbing process does not receive a comparable byproduct credit.

Energy costs are also lower for the spray dryer MgO process. The higher exit temperature of the flue gas from the spray dryer coupled with the cyclic reheat results in a substantially lower steam requirement. The electrical consumption is 25% lower because of the smaller pumps needed for the SO₂ absorption area. The diesel fuel cost is lower because of the smaller volume of material disposed of in the landfill. Raw material costs are lower because of the regenerable nature of the spray dryer MgO process.

There are only two revenue costs which favor the limestone scrubbing process, although they are not large enough to offset the cost advantages enjoyed by the spray dryer MgO process in other areas. These advantages are the labor cost and the levelized capital charges and of these two, only the levelized capital charge difference is of any significance. The limestone scrubbing process has a \$2.7M savings in levelized capital charges but this is offset by the \$6.1M advantage in first-year operating and maintenance costs for the spray dryer MgO process.

In the comparison of the annual revenue requirements for the spray dryer MgO process with those for the conventional MgO process, it is apparent that both the first year and the levelized annual revenue requirements are 40% lower for the spray dryer MgO process (\$28.8M vs. \$40.4M for first year). The most significant difference between the processes is the energy cost, in particular, the fuel oil charges. The spray dryer MgO process uses expensive fuel oil only to operate the waste disposal equipment while the conventional MgO process uses fuel oil, not only for the waste disposal equipment (which is a relatively minor amount) but also to fire the calciner and

thus also to provide heat for the rotary dryers. The slurry drying and calcining areas in the conventional MgO process require fuel oil at a cost of nearly \$8.6M. In contrast the spray dryer MgO process uses station coal at a cost of \$0.7M to fire the calciner. There is also a difference of \$1M in reheat energy costs between the processes in favor of the spray dryer process because of the higher scrubber outlet flue gas temperature and the cyclic reheat used.

Electrical consumption, the other primary energy requirement, is about 10% higher in the spray dryer process but the resulting cost difference of \$0.25M is relatively insignificant compared with the other energy costs.

The other major annual cost difference is the levelized capital charges. These levelized capital charges are calculated as 14.7% of the capital investment and because the spray dryer MgO process has a lower capital investment, its levelized capital charge is approximately \$1.4M less than that for the conventional MgO process. The basis for this levelized capital charge is explained elsewhere (6).

The byproduct credit is not significantly different between the MgO processes because the quantity of sulfuric acid produced is nearly the same for both processes. All other annual costs are approximately the same and do not have a significant effect on the results.

Sensitivity Analysis

Since the annual revenue requirements for the spray dryer and conventional MgO processes appear to be sensitive to the byproduct credit for sulfuric acid, and since sulfuric acid prices have risen dramatically in the last few years, the sensitivity of the first-year annual revenue requirements to the price of byproduct sulfuric acid was projected. The results are shown in Figure 3.

As is apparent from this figure the first-year annual revenue requirements can vary somewhat, depending on the price received from the byproduct sulfuric acid. The base-case credit of \$65/ton of 100% H₂SO₄ results in a first-year annual revenue requirement of 10.47 mills/kWh for the spray dryer MgO process and 14.69 mills/kWh for the conventional MgO process. At a byproduct credit of \$35/ton which is approximately equivalent to the price of sulfuric acid in the past (or which could be the 1984 price netted after transportation costs are subtracted for a utility situated far from the ultimate consumer), the first-year annual revenue requirements for the spray dryer MgO process rise nearly 10 percent to 11.53 mills/kWh. This cost, although slightly lower than that for the limestone scrubbing process, is essentially equivalent given the accuracy associated with this study. For

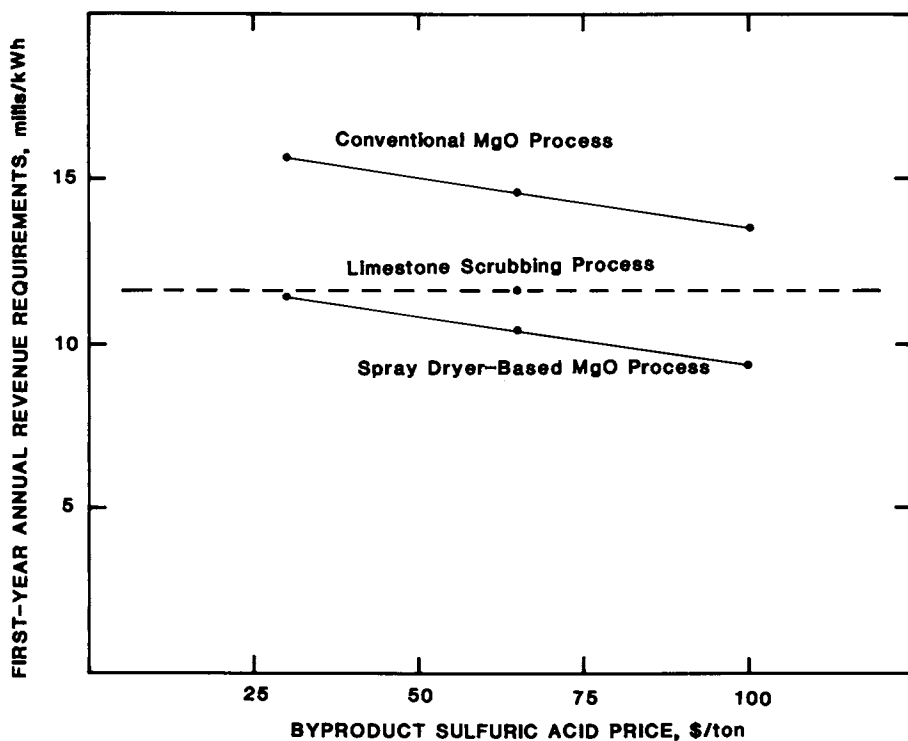


Figure 3. Sensitivity of annual revenue requirements to byproduct sulfuric acid price.

the optimistic \$100/ton byproduct credit case, the first-year annual revenue requirements decrease 13 percent to 9.33 mills/kWh or about 21 percent less than the first-year annual revenue requirements for the base-case limestone scrubbing process. For the conventional MgO process the resulting first-year annual revenue requirements are 13.63 mills/kWh or about 18 percent higher than those for the limestone process.

CONCLUSIONS AND SUMMARY

Conclusions

The primary conclusions of this conceptual design and study-grade economic evaluation are listed below:

1. The spray dryer MgO process appears to have a slight advantage (about 10%) over a comparable limestone scrubbing process in terms of both first-year and levelized annual revenue requirements. This new MgO process, however, has a higher capital investment than the limestone scrubbing process.
2. The spray dryer MgO process has an economic advantage over the conventional MgO process in terms of capital investment (8%), first-year annual revenue requirements (40%), and levelized annual revenue requirements (40%). The primary difference for this large cost advantage for the spray dryer MgO process is due to the lower energy consumption and the use of inexpensive coal to fire the calciner rather than No. 2 fuel oil.

Summary

Based on the results of this initial study, the spray dryer MgO process appears to be a promising new technology. However the design is based on numerous technical assumptions which may or may not be accurate. Therefore a small (~1-MW equivalent) pilot plant will be necessary to test this new FGD process. TVA is planning to pursue funding for a study to determine the cost of such a pilot plant which can confirm these assumptions and assist in creating an economical and technically viable process for converting pollutant material into a useful byproduct.

APPENDIX

Detailed capital and annual revenue requirement costs for the three processes studied here are presented in the following Tables A-I through A-VI.

TABLE A-I. CONVENTIONAL LIMESTONE PROCESS
SUMMARY OF CAPITAL INVESTMENT

(500-MW new coal-fired power unit, 3.5% sulfur in coal;
89.6% SO₂ removal; onsite solids disposal)

<u>Direct Investment</u>	<u>Investment, k\$</u>
Material handling	2,518
Feed preparation	4,618
Particulate removal	9,998
Gas handling	13,653
SO ₂ absorption	20,342
Stack gas reheat	3,325
Solids separation	<u>3,350</u>
Total process capital	59,087
Services, Utilities, and Miscellaneous	<u>3,545</u>
Total direct investment excluding landfill	62,632
Solids disposal equipment	1,007
Landfill construction	<u>3,441</u>
Total direct investment	67,080
<u>Indirect Investment</u>	
Engineering design and supervision	4,384
Architect and engineering contractor	1,253
Construction expense	10,021
Contractor fees	3,132
Contingency	8,142
Landfill indirects	<u>1,348</u>
Total fixed investment	95,360
<u>Other Capital Investment</u>	
Allowance for startup and modifications	7,165
Interest during construction	14,719
Royalties	-
Land	1,070
Working capital	<u>3,639</u>
Total capital investment	121,953
Dollars of total capital per kW of generation capacity	243.91
<u>Basis: TVA design and economic premises.</u>	

TABLE A-II. SPRAY DRYER MgO PROCESS

SUMMARY OF CAPITAL INVESTMENT

(500-MW new coal-fired power unit, 3.5% sulfur in coal;
89.6% SO₂ removal; onsite solids disposal)

	<u>Investment, k\$</u>
<u>Direct Investment</u>	
Material handling	1,124
Feed preparation	755
Gas handling	10,992
Fly ash removal	8,555
SO ₂ absorption	19,894
Calcination	6,906
Offgas cleanup	1,145
Acid plant	11,985
Acid storage and shipping	1,879
Ash purge	<u>966</u>
Total process capital	64,201
Services, Utilities, and Miscellaneous	<u>3,852</u>
Total direct investment excluding waste disposal	68,053
Solids disposal equipment	467
Landfill construction	1,595
Pond construction	<u>1,452</u>
Total direct investment	71,567

Continued on next page.

TABLE A-II. (continued). SPRAY DRYER MgO PROCESS
SUMMARY OF CAPITAL INVESTMENT

Indirect Investment

Engineering design and supervision	4,636
Architect and engineering contractor	1,234
Construction expense	10,635
Contractor fees	2,767
Contingency	15,928
Waste Disposal Indirect Investment	<u>999</u>
Total fixed investment	107,766

Other Capital Investment

Allowance for startup and modifications	10,325
Interest during construction	16,739
Royalties	-
Land	737
Working capital	<u>3,930</u>
Total capital investment	139,497
Dollars of total capital per kW of generation capacity	278.99

Basis: TVA design and economic premises.

TABLE A-III. CONVENTIONAL MgO PROCESS

SUMMARY OF CAPITAL INVESTMENT

(500-MW new coal-fired power unit, 3.5% sulfur in coal;
89.6% SO₂ removal; onsite solids disposal)

	<u>Investment, k\$</u>
<u>Direct Investment</u>	
Material handling	1,278
Feed preparation	405
Gas handling	10,983
Fly ash removal	9,998
SO ₂ absorption	8,664
Stack gas reheat	3,877
Chloride purge	8,206
Slurry processing	1,578
Drying	7,525
Calcination	3,167
Acid plant	10,051
Acid storage and shipping	<u>1,358</u>
Total process capital	67,090
Services, Utilities, and Miscellaneous	<u>4,025</u>
Total direct investment excluding waste disposal	71,115
Solids disposal equipment	461
Landfill construction	1,575
Pond construction	<u>3,028</u>
Total direct investment	76,179

Continued on next page.

TABLE A-III. (continued). CONVENTIONAL MgO PROCESS
SUMMARY OF CAPITAL INVESTMENT

Indirect Investment

Engineering design and supervision	4,871
Architect and engineering contractor	1,316
Construction expense	11,166
Contractor fees	3,023
Contingency	16,785
Waste Disposal Indirects	<u>1,426</u>
Total fixed investment	114,766

Other Capital Investment

Allowance for startup and modifications	10,828
Interest during construction	17,832
Royalties	-
Land	953
Working capital	<u>5,304</u>
Total capital investment	149,683
Dollars of total capital per kW of generation capacity	299.37

Basis: TVA design and economic premises.

TABLE A-IV. CONVENTIONAL LIMESTONE PROCESS

ANNUAL REVENUE REQUIREMENTS

(500-MW new coal-fired power unit, 3.5% sulfur in coal;
89.6% SO₂ removal; onsite solids disposal)

	Annual quantity	Unit cost, \$	Total annual cost, k\$
<u>Direct Costs - First Year</u>			
Raw materials			
Limestone	132,600 tons	8.50/ton	<u>1,127</u>
Total raw materials cost			
Conversion costs			
Operating labor and supervision			
FGD	43,860 man-hr	15.00/man-hr	658
Solids disposal	32,546 man-hr	21.00/man-hr	683
Utilities			
Steam	403,000 MBtu	3.30/MBtu	1,330
Fuel oil No. 2	254,600 gal	1.60/gal	407
Process water	188,200 kgal	0.14/kgal	26
Electricity	65,613,000 kWh	0.037/kWh	2,428
Maintenance			
Labor and material			
Analysis	4,990 man-hr	21.00/man-hr	<u>4,404</u>
Total conversion costs			10,041
Total direct costs			<u>11,168</u>

Continued on next page.

TABLE A-IV. (continued). CONVENTIONAL LIMESTONE PROCESS
ANNUAL REVENUE REQUIREMENTS

<u>Indirect Costs - First Year</u>		
Overheads		<u>3,289</u>
Plant and administrative		14,457
Total first-year operating and maintenance costs		<u>17,927</u>
Levelized capital charges		32,384
Total first-year annual revenue requirements		27,266
Levelized first-year operating and maintenance costs		<u>17,927</u>
Levelized capital charges		45,193
Levelized annual revenue requirements		
	<u>-\$</u>	<u>Mills/kWh</u>
First-year annual revenue requirements	32.38	11.78
Levelized annual revenue requirements	45.19	16.43

Basis: TVA design and economic premises.

TABLE A-V. SPRAY DRYER MgO PROCESS

ANNUAL REVENUE REQUIREMENTS

(500-MW new coal-fired power unit, 3.5% sulfur in coal;
89.6% SO₂ removal; onsite solids disposal)

	Annual quantity	Unit cost, \$	Total annual cost, k\$
Direct Costs - First Year			
Raw materials			
Magnesium oxide	322 tons	460.00/ton	148
Agricultural limestone	1,670 tons	18.75/ton	31
Vanadium catalyst	2,000 liters	3.00/liter	6
Total raw materials cost			
Conversion costs			
Operating labor and supervision			
FGD	59,720 man-hr	15.00/man-hr	896
Solids disposal	21,850 man-hr	21.00/man-hr	459
Utilities			
Steam	66,660 MBtu	3.30/MBtu	220
Bituminous coal	16,748 tons	43.30/ton	725
Process water	165,000 kgal	0.14/kgal	23
Electricity	54,091,000 kWh	0.037/kWh	2,003
Diesel fuel	73,800 gal	1.60/gal	150
Maintenance			
Labor and material	9,900 man-hr	21.00/man-hr	4,869
Analysis			208
Total conversion costs			
			9,553
Total direct costs			
			9,738

Continued on next page.

TABLE A-V. (continued). SPRAY DRYER MgO PROCESS
ANNUAL REVENUE REQUIREMENTS

<u>Indirect Costs - First Year</u>			
Overheads			
Plant and administrative (60% of conversion costs less utilities)			3,978
Marketing (10% of byproduct sales)			605
Byproduct credit	93,010 tonsa	65.00/ton	<u>(6,046)</u>
Total first-year operating and maintenance costs			8,275
Levelized capital charges (14.7% of total capital investment)			<u>20,506</u>
Total first-year annual revenue requirements			28,781
Levelized first-year operating and maintenance costs (1.886 times first-year O&M)			15,607
Levelized capital charges (14.7% of total capital investment)			<u>20,506</u>
Levelized annual revenue requirements			36,113
		<u>MS</u>	<u>Mills/kWh</u>
First-year annual revenue requirements		28.78	10.47
Levelized annual revenue requirements		36.11	13.13

Basis: TVA design and economic premises.
a. 100% H₂SO₄.

TABLE A-VI. CONVENTIONAL MgO PROCESS
ANNUAL REVENUE REQUIREMENTS

(500-MW new coal-fired power unit, 3.5% sulfur in coal;
89.6% SO₂ removal; onsite solids disposal)

	Annual quantity	Unit cost, \$	Total annual cost, k\$
<u>Direct Costs - First Year</u>			
Raw materials			
Magnesium oxide	1,260 tons	460.00/ton	580
Agricultural limestone	2,600 tons	18.75/ton	49
Vanadium catalyst	1,800 liters	3.00/liter	5
Total raw materials cost 634			
Conversion costs			
Operating labor and supervision			
FGD	59,720 man-hr	15.00/man-hr	896
Solids disposal	21,650 man-hr	21.00/man-hr	455
Utilities			
Steam	355,000 MBtu	3.30/MBtu	1,172
Process water	2,085,000 kgal	0.14/kgal	292
Electricity	47,722,000 kWh	0.037/kWh	1,766
Diesel fuel	92,300 gal	1.60/gal	148
Fuel oil (No. 2)	5,374,000 gal	1.60/gal	8,598
Maintenance			
Labor and material	9,900 man-hr	21.00/man-hr	5,130
Analysis			208
Total conversion costs 18,665			
Total direct costs 19,299			

Continued on next page.

TABLE A-VI. (continued). CONVENTIONAL MgO PROCESS
ANNUAL REVENUE REQUIREMENTS

<u>Indirect Costs - First Year</u>			
Overheads			
Plant and administrative (60% of conversion costs less utilities)			4,490
Marketing (10% of byproduct sales)			600
Byproduct credit	92,330 tonsa	65.00/ton	<u>(6,001)</u>
Total first-year operating and maintenance costs			18,388
Levelized capital charges (14.7% of total capital investment)			<u>22,003</u>
Total first-year annual revenue requirements			40,391
Levelized first-year operating and maintenance costs (1.886 times first-year O&M)			34,680
Levelized capital charges (14.7% of total capital investment)			<u>22,003</u>
Levelized annual revenue requirements			56,683
		<u>-\$</u>	<u>Mills/kWh</u>
First-year annual revenue requirements		40.39	14.69
Levelized annual revenue requirements		56.68	20.61

Basis: TVA design and economic premises.
a. 100% H₂S₀₄.

LEGAL NOTICE

Neither the authors, TVA, nor any person acting on their behalf: a. makes any warranty or representation, express or implied, with respect to the use of any information contained in this paper, or that the use of any information, apparatus, method, or process disclosed in this paper may not infringe privately owned rights; or b. assumes any liabilities with respect to the use of, or for damages resulting from the use of, any information, apparatus, method, or process disclosed in this paper.

The contents of this paper do not necessarily reflect the views and policies of the Tennessee Valley Authority. This is a government publication and not subject to copyright.

Literature Cited

1. Marcus, E. G.; Wright, T. L.; Wells, W. L.; Magnesium FGD at TVA: Pilot and Full-Scale Designs, EPA Symposium, Houston, Texas, October 28-31, 1980.
2. Burnett, T. A.; Anderson, K. D.; Technical Review of Dry FGD Systems and Economic Evaluation of Spray Dryer FGD Systems, EPA-600/7-91-014, February 1981.
3. Lowell, P. S.; "Thermodynamic Analysis of the TVA MgSO₃ Colbert Pilot Calciner," Unpublished report prepared for TVA, May 12, 1980.
4. Technical Assessment Guide, EPRI PS-866-SR, June 1978.
5. Anderson, K. D.; Barrier, J. W.; O'Brien, W. E.; Tomlinson, S. V.; Definitive SO Control Process Evaluations: Limestone, Lime, and Magnesia FGD Processes, EPA-600/7-80-001, January 1980.
6. "Premises for Comparative Economic Evaluations of Emission Control Processes," Unpublished report prepared by TVA, April 1981.

RECEIVED November 20, 1981.

INDEX

- A**
- Absorber, spray dryer 382
- Absorption
 gas, film model 195
 gaseous O₂ into bisulfite solution,
 gas volume data 155, 157f, 158
 -reduction processes 140, 145-150
- Acetate, effect, on dissolution rate 91, 93f
- Acetic acid (*see* Acid, acetic)
- Acid(s)
 acetic, effect on limestone
 dissolution 88, 89f
- acrylic
 effect on dissolution
 rate 88, 90f, 91
 hydration 247t
 rate constant 246
- adipic 316-319
 addition, comparison of operat-
 ing alternatives 316, 318t
 concentration
 and scrubber inlet pH on
 sulfur dioxide removal
 in TCA 293, 296f
 and slurry flow rate on sulfur
 dioxide removal in the
 TCA 293-295
 and solids oxidation levels,
 test results 238t
 and spray tower inlet pH with-
 out forced oxidation, sul-
 fur dioxide removal as a
 function 293, 297-299
 on sulfur dioxide removal
 with forced oxidation,
 effects of scrubber inlet
 pH 293, 297-299
 on gross electric power de-
 mand for 90% sulfur
 dioxide removal in
 TCA scrubber 316, 317f
 vs. % sulfate in solids 236, 237f
- content of bench-scale solids
 related % oxidation 234, 235f
- degradation 256, 257f
 correlation coefficient 225, 228f
 determination of Arrhenius
 Activation Energy 232, 233f
 effect of Mn and pH 229, 231f
 in FGD scrubbers 221-242
- Acid (*continued*)
 adipic (*continued*)
 degradation (*continued*)
 results, summary of bench-
 scale system 226t, 227t
 rate 225
 constant for Mn, Mn + Fe,
 and limestone + fly
 ash, effect of pH 229, 231f
 effect of hold tank tem-
 perature 232t
 pH effect 229
- effect
 calcite dissolution 88, 90f
 on limestone dissolution 88, 89f
- enhanced lime tests from
 Shawnee TCA without
 forced oxidation 283f, 285, 286f
- enhanced lime/limestone 267-306
 system operating pH 270, 271
- enhanced limestone
 factorial test results 291-299
 operating costs 304t, 305
- scrubbing
 in spray tower system with
 forced oxidation and
 two tanks 287, 288f
 test programs 272-274
 test results 274-300
- venturi/spray tower system,
 bleed stream oxida-
 tion 291, 292t
- enhanced scrubbing in the TCA
 system without forced
 oxidation 281, 283f
- enhanced scrubbing in the
 Venturi/spray tower
 system 272, 278f
- estimated, losses vs. %
 oxidation 239-241
- mass transfer enhancement 253, 254f
- overall enhancement of sulfur
 dioxide absorption 253, 254f
- oxidative degradation 258t
- physical properties 215t
- as scrubber additive 269-271
- in scrubber solids, coprecipi-
 tation 234-238
- sulfur dioxide removal efficiency
 of TCA scrubber vs net
 work input with 316, 317f

- Acid (*continued*)
- adipic (*continued*)
 - test schedule, Shawnee 272, 273*f*
 - testing as a scrubber
 - additive 276–277
 - use as buffer in commercial scrubbers 187
 - carboxylic
 - conjugated oxidation 255
 - degradation products 268
 - oxidative degradation 258*t*
 - volatility 262
 - fumaric
 - oxidative degradation 258*t*
 - physical properties 251*t*
 - rate constant 246
 - insoluble fraction of nahcolite, thermal gravimetric analysis (TGA) 372, 373*f*
 - nitrous
 - with bisulfite ion, formation hydroxylamine disulfonate by reaction 130, 131
 - reaction of sulfamic acid with 136, 137
 - and sulfite reaction 129, 130
 - organic, effect on limestone dissolution 88–91
 - polyacrylic
 - effect on dissolution rate ... 88, 99*f*, 91
 - impurities 261
 - surface adsorption 91
 - rain 153
 - succinic
 - concentration, dependence of oxidation rate of CaSO_3 180*f*, 182, 186*f*
 - effect on oxidation of CaSO_3 182, 184–188, 184*t*, 185*t*
 - oxidative degradation 258*t*
 - physical properties 251*t*
 - sulfamic
 - energy and entropy formation 135
 - formation 133, 134
 - with nitrous acid, reaction 136, 137
 - sulfopropionic
 - diffusivity 250
 - effect on dissolution rate ... 88, 90*f*, 91
 - oxidative degradation 258*t*
 - physical properties 251*t*
 - unsaturated, sulfonation rates 247*t*
 - Activation, Arrhenius, energy for adipic acid degradation, determination 232, 233*f*
 - Activation energy of calcite dissolution 76
 - Activation energy for Fe-catalyzed sodium sulfite oxidation 179
 - Activity of CaSO_4 when MgSO_4 is added 66*f*
 - Activity coefficient(s)
 - CaSO_4 48*t*
 - mean-ion 59, 65
 - in FGD solution 64*t*
 - MgSO_4 49*t*
 - Na_2SO_4 52*t*, 53*t*
 - Pitzer equations 54, 55
 - Radian mean-ion
 - of CaSO_3 when MgSO_4 is added 69, 70*f*
 - of CaSO_3 when NaCl is added .. 69, 71*f*
 - of CaSO_4 when MgSO_4 is added .. 67*f*
 - of CaSO_4 when NaCl is added 68*f*
 - sensitivity to changes in Pitzer-equation parameters 63, 64
 - single-ion 59
 - SO_2 51*t*
 - strong-electrolyte, in aqueous FGD processes 57–73
 - sulfurous acid 50, 50*t*
 - Additive(s)
 - buffer, for lime/limestone slurry scrubbing 243–265
 - and products of denitrification simultaneous processes 128*t*
 - and products of desulfurization simultaneous processes 128*t*
 - scrubber, advantages of adipic acid 269–271
 - Adipic acid (*see* Acid, adipic)
 - Algorithm, Rung–Kutta–Gill 210
 - Alkali, dual, limestone process for FGD 325–247
 - n*-Alkanes, ^1H NMR spectrum 374, 376*f*
 - Aluminum chloride effect on sulfur dioxide absorption 253
 - Amine disulfonate (ADS) 132
 - hydrolysis 134, 135
 - Amine trisulfonate (ATS) 132
 - hydrolysis 134
 - Ammonia solutions 115, 117
 - saturated with SO_2 , Raman spectrum of solid from auto-redox products 117, 119*f*
 - Ammonia–sulfur dioxide solution, decomposition 117, 118*f*
 - Ammonium bisulfate formation 133, 134
 - Ammonium bisulfite solutions, Raman spectra 115, 117, 118*f*
 - Annual revenue requirements
 - conventional limestone process 405–406*t*
 - conventional MgO process 410–411*t*
 - spray dryer MgO FGD process 395, 407–409
 - to byproduct sulfuric acid price, sensitivity 397–399

- Aqueous solution properties47-55
 Aqueous species, thermodynamic properties13-20*t*
 Arrhenius activation energy for adipic acid degradation, determination232, 233*f*
 Atomic absorption analysis of CaSO₃ 177*t*
 Auto-redox decomposition of sulfur .. 114
- B**
- Baghouse 351
 cleaning cycle rate 365
 temperature effect on SO₂ removal with Na₂HCO₃356, 359*f*
 Barium compounds network approach42, 43*f*
 Barium sulfate, Raman data 115
 Base case operating conditions 104*t*
 Batch reactor, concentration profile of species as function of reaction time137-144
 Bechtel-modified Radian equilibrium computer code 58
 Bechtel modified Radian equilibrium program65, 66*f*
 Debye-Hückel model comparison with64-71
 Bench-scale runs with manganese, iron, limestone, and fly ash, results 230*t*
 scrubber test results224-234
 system adipic acid degradation results, summary226*t*, 227*t*
 system, design 222
 Bicarbonate, sodium, tests356, 358-361
 Binary ion pairs, methods to estimate Pitzer-equation parameters 62, 63
 Bisulfate dissociation, equation 202
 Bisulfite ammonium, solution, Raman spectra 115
 dissociation, equation 202
 and hydrogen ion for oxidation, rate dependence on concentrations162, 163*f*
 ion, formation of hydroxylamine disulfonate by reaction of nitrous acid130, 131
 ion by oxygen, kinetics of oxidation153-171
 oxidation
 in buffered solution, ethanol concentration effect on rate158, 160*f*, 161
 in buffered solution, manganous ion effect on rate158, 159*f*
 kinetics168-170
 in nonbuffered solutions, effect of ethanol161-162, 165*f*
- Bisulfite (*continued*)
 oxidation (*continued*)
 photooxidation data 164
 rate law 158
 rate in nonbuffered solution, manganous ion effect159*f*, 162-164
 and O₂, rate of reaction between158, 159*f*
 and O₂ single-phase experiments, reaction between158-170
 potassium, solutions117, 120
 sodium, solutions117, 120
 solution(s)
 gas volume data for absorption of gaseous O₂155, 157*f*, 158
 Raman spectra of ammonium117, 118*f*
 single-phase experiments rate of O₂ uptake 155
 thermal decomposition113-125
 two-phase experiments, rate of O₂ uptake154, 155
 Bleed stream oxidation, limestone tests with291, 292*t*
 Boiler demonstration, Rickenbacker industrial 300
 Boiler outages 281
 Boundary layer configuration198, 200*f*
 Brassfield 106*t*
 composition 105*t*
 Buffer(s)
 additives for lime/limestone slurry scrubbing243-265
 alternatives on liquid-film enhancement factor, calculated effect253, 254*f*
 with CaSO₃, coprecipitation 261
 comparison of liquid-film enhancement factors with250, 251*f*
 physical properties 251*t*
 p*K*_a effect on SO₂ absorption 261
 reaction mechanism 264
 synthesis245-249
 Buffered solution(s)
 Mn ion effect on rate in HSO₃ oxidation158, 159*f*
 with MnSO₄ and ethanol158-161
 rate law 158
- C**
- ¹³C NMR spectrum of nahcolite oil374, 376*f*
 Calcite
 with CO₂ sparging in CaCl₂, dissolution rate86, 87*f*
 dissolution
 acetic acid effect88, 89*f*

- Calcite (*continued*)
 dissolution (*continued*)
 activation energy 76
 adipic acid effect 88, 90f
 curves 83, 84f
 rate constants 86
 rate, pH effect 107, 108f
 temperature effect 88
 theory 76-82
 molar density 81
 with N₂ sparging in CaCl₂, dissolution rate 86, 87f
 particle size distribution 83, 95t
 surface, calculated solution composition 91, 93f, 94
- Calcium, flux from limestone surface, equation 80
- Calcium carbonate, chemical reactions 100, 101
- Calcium carbonate dissolution 106t
 rate, pH effect 107, 108f
- Calcium sulfate
 activity with added Mg₂SO₄ 65, 66f
 activity coefficients 48t, 69, 70f
 effect of NaCl addition 65, 68f
 conversion to CaSO₃ 173
 forced oxidation of CaSO₃ 268
 formation 329
 molal enthalpy 48t
 Radian mean-ion activity coefficients when MgSO₄ is added 65, 67f
 solid disposal 192
 solubility data with added MgSO₄ 65, 66f
- Calcium sulfite
 activity coefficients when MgSO₄ is added 69, 70f
 blinding of limestone 289
 conversion to CaSO₄ 173-189
 conversion to gypsum 173
 coprecipitation of buffer 261
 dependence of oxidation rate on succinic acid concentration 182, 186f
 dissolution without chemical reaction 202-205
 effect of succinic acid on oxidation 184t, 185t
 forced oxidation to CaSO₄ 268
 mass transfer coefficient 210, 211f
 model slurries, experimental system 195-197
 oxidation
 buffered-solution advantage 193
 clear solution, kinetics 193-194
 experiments in slurries 194-195
 Mn-catalyzed 187, 188t
 results, oxidation 182, 184-188
- Calcium sulfite (*continued*)
 slurries
 model of oxidation 191-220
 physical system model 197-202
 rate equation for batch oxidation 256
 solid 123
 analysis 177t
- Calculator program for thermodynamic calculations 31, 32
- Capillary gas chromatography of nahcolite and trona oils 374, 376f
- Capital investment
 conventional limestone process summary 403-404t
 conventional MgO process summary 401-402t
 limestone scrubbing process 393
- Carbon dioxide
 effect on dissolution rate of CaCO₃ 86-88
 effect on limestone dissolution 86-88
 partial pressure 76
 reaction, rate 79
- Catalyst(s)
 concentration, variable, slurry oxidation model 212, 213f
 influence on thermal decomposition of sulfur 120, 123
 Na₂SO₃ oxidation mixed manganese and iron 182
- Catalyzed slurry oxidation experiments 210-212
- Chain reaction, rate 166
- Charges in Pitzer-equation parameters, sensitivity of activity coefficients 63, 64
- Chelates, ferrous, kinetic and thermodynamic data for reversible NO coordination 147t
- Chelates, metal, kinetics of reactions of NO and sulfur dioxide in aqueous solutions containing 146, 150
- Chemical
 kinetics modeling 137-144
 reaction, model dissolution 205-210
 species important in flue gas desulfurization 44t
- Chloride effect in adipic acid-enhanced limestone scrubbing 271
- Chromatography
 capillary gas, of nahcolite oil 374, 376f
 capillary gas, of trona oil 374, 376f
 gas, of nahcolite and trona oils, compounds identified 378t
- Coal(s)
 analyses 357t
 -burning power plants, SO₂ removal 153-171

- Coal(s) (*continued*)
 -fired furnace 351, 352*f*
 -fired power plants, pollution
 control 308
 Pittsburgh seam 362, 363*f*
 tested 354, 356
 Cocurrent flow 314-315
 Cocurrent grid tower, energy consumed for SO₂ removal 315*t*
 Coefficient of Ca₂SO₃, determination of mass transfer 210, 211*f*
 Coefficients, virial 59-61
 Combustion test facility 351-354
 Compositions
 of limestone samples 105*t*
 reactor feed 104*t*
 scrubber feed 102*t*
 Computer code, Bechtel-modified Radian equilibrium 58
 Computer model, SO₂ wet scrubber 100
 Concentration profile of species as a function of reaction time in
 batch reactor 137-144
 Configuration, boundary layer 198, 200*f*
 Configurations, scrubber 291
 Consumption at Scholz, power 343-344
 Consumption, soda ash 343
 Continuous stirred tank reactor (CSTR) tests 330
 Coprecipitation of adipic acid in scrubber solids 234-238
 Coprecipitation of buffer with CaSO₃ 261
 Correlation coefficient for adipic acid degradation 225, 228*f*
 Cost differential between limestone and lime 99
 Costs relative of organic acids 255*t*
 Coulter method 198
- D**
- Data base for flue gas desulfurization processes 41-56
 Data centers, NBS, future evaluations 55
 Debye-Hückel coefficients 58
 model comparison with Bechtel-modified Radian equilibrium program 64-71
 osmotic-coefficient constant 60
 Decomposition
 ammonia-sulfur dioxide solution 117, 118*f*
 sulfur, auto-redox 114
 thermal, of sulfite, bisulfite, and disulfite solutions 113-125
 thermal, of sulfur, Raman spectroscopy, use 114-115
 thiosulfate as a function of pH 120, 121*f*
- Degradation
 adipic acid 256, 257*f*
 carboxylic acids, oxidative 258*t*
 effect of Mn and pH on adipic acid 229, 231*f*
 in FGD scrubbers, adipic acid 221-242
 oxidative 255-261
 rate, effect of hold tank temperature on adipic acid 232*t*
 results, summary of bench-scale system adipic acid 226*t*, 227*t*
 Degrees of freedom in bulk liquid 205
 Denitrification simultaneous processes, additives and products 128*t*
 Denitrification system, kinetics of reaction in wet flue gas 127-152
 Density, molar, of calcite 81
 Density variations, slurry 212, 214*f*
 Design changes in MgO process 382-385
 Desulfurization processes
 data base for flue gas 41-56
 thermodynamic values 1-39
 simultaneous processes, additives and products 128*t*
 system, kinetics of reaction in wet flue gas 127-152
 Dewatering, solids 271
 Differential size distribution 82
 Diffusion flux balance 204
 Diffusivities 85*t*
 equation 82
 of sulfopropionic acid 250
 Disposal, CaSO₄ solid 192
 Dissociation, equation
 bisulfate 202
 bisulfite 202
 water 202
 Dissolution
 calcite, acetic acid effect 88, 89*f*
 calcite, adipic acid effect 88, 90*f*
 CaCO₃ 106*t*
 with chemical reaction, model 205-210
 curves for calcite 83, 84*f*
 limestone effects of pH, CO₂, and buffers modeled by mass transfer 75-101
 equation, rate 105
 factors affecting magnesium limestone 99-111
 limestone, effect on organic acids 88-91
 Mg₂CO₃ 106*t*
 particle, with no reaction, surface and bulk conditions 206*t*
 rate
 calcite, with CO₂ sparging in CaCl₂ 86, 87*f*
 calcite, with N₂ sparging in CaCl₂ 86, 87*f*
 CaCO₃, calculation 77, 78

- Dissolution (*continued*)
 rate (*continued*)
 difference between limestones 107
 effect of acetate 91, 93f
 effect of organic acids 88, 90f
 Fredonia base case 105
 Fredonia limestone, temperature
 effect 107, 109f
 pH effect on CaCO₃ 107, 108f
 single particle, equation 81
 vs. stirring rate, Fredonia
 limestone 107, 110f
 reactor 83, 84f
 surface conditions 202-205
 theory, calcite 76-82
- Disulfite solution, thermal
 decomposition 113-125
- Dry sorbent injection, control of
 SO₂ emissions 349-368
- Dry sorbent injection system 351, 353f
- Dual alkali process, limestone, for
 FGD 325-347
- Dual alkali system, limestone,
 power consumption 343
- E**
- Economic(s)
 adipic acid-enhanced limestone
 scrubbing 271
 comparison, limestone FGD
 system 390-399
 conceptual design, MgO FGD
 system 390-399
 considerations, limestone dual
 alkali process 346
 evaluations, limestone case 302, 304t
 limestone scrubbing 300-305
- Effluent hold tank (EHT) 311
- Efficiency of NO_x removal 137-144
- Electric
 demand to operate SO₂ scrubbers .. 308
 demand for SO₂ removal 310
 energy, gross, input for 90%
 SO₂ removal 315t
 power demand, gross, of limestone
 scrubbers using hot booster
 fans 319, 320f
 power demand, gross, for 90%
 SO₂ removal in TCA scrub-
 ber, effect of adipic acid
 concentration 316, 317f
- Electric Power Research Institute
 (EPRI) 99
- Electrical consumption, MgO FGD
 process 397
- Electrolyte solutions, statistical
 mechanics 58
- Electron micrographs, analysis of
 solid samples 341
- Elemental analyses of nahcolite oil 374t
 Elemental sulfur conversion 120
- Emission
 control, flue gas 127-152
 control, SO₂ 192
 SO₂ 281
 standards 268
- Energy
 consumed for 90% SO₂ removal
 in limestone scrubbers 315t
 demands for FGD system 319, 321
 formation, Gibbs, calculations 45t
 formation, sulfamic acid 135
 Gibbs, calculation 46t
 requirement for limestone
 FGD 321, 322
 requirements for SO₂ absorption
 in limestone scrubbers 307-324
- Enhancement factor, calculated effect
 of buffer liquid film,
 alternatives 253, 254f
- Enhancement factors, liquid film,
 comparison with buffers 250, 251f
- EPA alkali scrubbing test facility .. 267-306
- Enthalpy
 calculation(s) 45t, 46t
 coordination of NO to metal
 chelates 145, 147t
- molal
 CaSO₄ 47
 MgSO₄ 48t
 Na₂SO₄ 49t
 Na₂SO₃ 53t
 SO₂ 52t
 SO₂ 51t
- standard
 aqueous species 13-20t
 calculation 21-30t
 common gases 3-7t
 solids and liquids 8-12t
- Entropy
 calculation(s) 45t, 46t
 coordination of NO to metal
 chelates 145, 147t
 formation, sulfamic acid 135
 aqueous species 13-20t
 common gases 3-7t
 solids and liquids 8-12t
- EPRI (Electric Power Research
 Institute) 99
- Equations for $-(G^\circ - H^\circ_{298})/RT$.. 21-30t
- Equilibrium constant
 calculation 31, 44, 46t
 coordination of NO to metal
 chelates 145, 147t
 mass-transfer model for CaCO₃
 dissolution 77, 78
- Ethanol, effect on bisulfite oxidation
 in nonbuffered solutions 162, 165f
- Ethanol, rate expression for photo-
 oxidation with 164, 165f

- F**
- Factorial test results, adipic acid-enhanced limestone 291-299
- Fan(s)
- efficiencies 314
 - gross electric power demand of limestone scrubbers using hot booster 319, 320*f*
 - location 319, 320*f*
- Feeding of sorbent 361-362
- Ferrous chelates, kinetic and thermodynamic data for reversible NO coordination 147*t*
- FGD (Flue gas desulfurization)
- chemical species (important) limestone 44*t*
 - dual alkali process 325-347
 - energy requirements 321-322
 - scrubbers, conclusions 322-323
 - process(es), aqueous, Pitzer equations use to estimate strong-electrolyte activity coefficients 53-73
 - capital investment, conventional MgO 393
 - conceptual design and economics, MgO 381-412
 - data base 41-56
 - electrical consumption, MgO 397
 - sensitivity analysis, MgO 397-399
 - scrubber, bench-scale test results 224-234
 - scrubbers, adipic acid degradation 221-242
 - solution, mean-ion activity coefficients 64*t*
 - spray dryer MgO, process, annual revenue 395
 - spray dryer MgO process, capital investment 393
 - system(s)
 - dry, advantages and disadvantages 349-350
 - energy demands 319, 321
 - forced oxidation 173
 - process, conventional MgO 382, 383*f*
 - spray dryer MgO 384*f*
 - technology 191
- Film model for gas absorption 195
- Film theory employed in slurry model 216
- Filter
- cake characteristics 342, 343
 - cake, liquid entrained 239-241
 - capabilities 342
- Flow rate, flue gas 277
- Flue gas
- cleaning system, major design and economic premises 391*t*, 392
 - contents, power plant 127
 - desulfurization (*see* FGD)
- Flue gas (*continued*)
- emission control 127-152
 - flow rate 277
 - monitoring procedures 280
 - washing process, related reactions .. 44
 - wet, simultaneous desulfurization and denitrification system, reaction kinetics 127-152
- Flux balance, diffusion 204
- Flux, molar, balance 204
- Flyash
- analysis 174, 175*t*
 - separation 388, 389
 - removal 385
- Forced oxidation 271
- in FGD 173
- limestone long-term test with one scrubber loop 287-289
 - limestone long-term tests with two scrubber loops 277-281
 - system 274
 - tank, pilot-scale scrubbing system .. 194
- Fredonia
- base case dissolution rates 105
 - composition 105*t*
 - limestone 330, 335
 - dissolution rate vs. stirring rate 107, 110*f*
 - temperature effect on dissolution rate 107, 109*f*
- Free energy, Gibbs calculation 21-30*t*
- Free radical generation by sulfite oxidation 255
- Fumaric acid (*see* Acid, fumaric)
- Furnace, coal-fired 351, 352*f*
- Future evaluations, NBS data centers 55
- G**
- Gas(es)
- absorption, film model 195
 - analysis system 354, 355*f*
 - chromatography, capillary, of nahcolite and trona 374, 376*f*
 - chromatography of nahcolite and trona oils, compounds identified 378*t*
 - common, thermodynamic properties 3-7*t*
 - liquid mass transfer enhancement 249-255
 - volume data for absorption of gaseous O₂ into HSO₃ solution 155, 157*f*, 158
- Gibbs energy calculation 46*t*
- Gibbs energy of formation calculations 45*t*
- Gibbs free energy, standard, calculation 21-30*t*

- Grand Forks Energy Technology Center (GFETC) 369
- Gross electric demand for sulfur dioxide removal 310
- Gulf Power Company's Scholz steam plant 331
- Gypsum, CaSO_3 conversion 173
- Gypsum solubility 329
- H**
- ^1H NMR spectrum of nahcolite oil 374, 375f
- ^1H NMR spectrum of 1-octene 374, 375f
- HA (*see* Hydroxylamine)
- HADS (*see* Hydroxylamine disulfonate)
- HAMS (*see* Hydroxylamine monosulfonate)
- Heat capacity calculation(s) 45t, 46t
- Heat capacity, standard
- aqueous species 13-20t
- common gases 3-7t
- solids and liquids 8-12t
- Heat exchangers, Ljungstrom-type 309
- Hold tank temperature effect on adipic acid degradation rate 232t
- Hydration of acrylic acid 247t
- Hydrochloric acid removal and purge 389, 390
- Hydrogen ion and bisulfite concentration effect on reaction rate for oxidation 162, 163f
- Hydrolysis
- amine disulfonates (ADS) 134, 135
- amine trisulfonate (ATS) 134
- hydroxylamine disulfonate (HADS), rate and mechanism 131, 132
- hydroxylamine monosulfonate (HAMS) 132
- sulfamate (SAM), rate and mechanism 135, 136
- Hydroxyacetic acid, inhibition of sulfite oxidation 260-261
- Hydroxyacetic acid, oxidative degradation 258t
- Hydroxylamine (HA), sulfonation 133-134
- Hydroxylamine disulfonate
- formation, by reaction of nitrous acid with bisulfite ion 130, 131
- rate and mechanism, hydrolysis 131, 132
- sulfonation 132
- Hydroxylamine monosulfonate
- hydrolysis 132
- Hydroxylamine monosulfonate sulfonation 133
- Hydroxylamine trisulfonate, hydrolysis 132
- Hydroxypropionic acid (HP) 248, 249
- effect on dissolution rate 88, 90f, 91
- inhibition of sulfite oxidation 260-161
- physical properties 251t
- β -Hydroxypropionic acid, oxidative degradation 258t
- I**
- IERL-RTP pilot plant test results 276-277
- Injection point, sorbent, effect of location 356, 361
- Injection system, dry sorbent 351, 353f
- Interfacial area per unit volume
- equation 208
- Ion-pair(s) 59
- binary, methods to estimate Pitzer-equation parameters 62, 63
- parameters, estimated 63t
- Ionic diffusivities 82
- IR spectra for nahcolite and trona oils 374, 377f
- Iron
- catalyzed Na_2SO_3 oxidation 179-181
- regression analyses 181t
- S(IV) vs. time 180f
- dissolved, interference with regeneration reactions 341
- and Mn mixed catalysts, Na_2SO_3 , oxidation 182
- J**
- Japanese processes 129
- K**
- Kentucky coal 357t, 362, 364f
- Kinetic(s)
- bisulfite oxidation 168-170
- CaSO_3 oxidation in clear solution 193-194
- data for reversible NO coordination to ferrous chelates 147t
- of formation, hydroxylamine disulfonate 130, 131
- modeling, chemical 137-144
- of oxidation of bisulfite ion by oxygen 153-171
- rate constants for Mn-catalyzed simulated slurry oxidation 212
- reactions of NO and SO_2 in aqueous solutions containing metal chelates 146, 150
- reactions in a wet flue gas simultaneous desulfurization and denitrification system 127-152
- sulfonation reaction 246

L

- Lime test with one scrubber loop and forced oxidation285-287
- Lime tests with one scrubber loop without forced oxidation283*f*, 285, 286*f*
- Lime/limestone
 adipic acid-enhanced267-306
 processes, oxidation of bisulfite ion
 by oxygen153
 scrubber slurry192
 slurry scrubbing, buffer additives243-265
- Limestone
 analysis174, 175*t*
 CaSO₃ blinding289
 case, economic evaluations302, 304*t*
 case with MgO additive302, 303*t*
 dissolution
 effect on organic acids88-91
 effects of pH, CO₂, and buffers
 modeled by mass transfer 75-101
 effects of sulfite91-94
 effect of temperature87*f*, 88
 experimental apparatus and procedure82-86
 factors affecting magnesium99-111
 mass transfer model77-82
- dual alkali
 process326, 327*f*
 advantages325
 economic considerations346
 effect of pH variations345
 for flue gas desulfurization325-347
 operability344-346
 power consumption343
 Scholz prototype system331-346
 SO₂ removal332, 335, 336*f*
 soda ash consumption343
 technology326
 development330
- factorial test results, adipic acid-enhanced291-299
- FGD321-323
- Fredonia330, 335
 dissolution rate vs. stirring
 rate107, 110*f*
 temperature effect on dissolution
 rate107, 109*f*
- and lime, cost differential between .. 99
- long-term test
 with one scrubber loop and forced oxidation287-289
 with one scrubber loop without forced oxidation281-285
 with two scrubber loops and forced oxidation277-281
- process annual revenue requirements, conventional405-406*t*
- Limestone (*continued*)
 process summary of capital investment, conventional403-404*t*
- reactivity
 apparatus102, 103*f*
 experimental approach101-103
 experimental results104-107
 pH and temperature effect104*t*
 stir rate104*t*
 regeneration, overall reaction328
- Saginaw330
- samples, compositions105*t*
- scrubber(s)
 cocurrent flow314, 315
 energy consumed for 90% SO₂ removal315*t*
 energy requirements for SO₂ absorption307-324
 fan location319
 using hot (300°F) booster fans, gross electric power demand319, 320*f*
- scrubbing
 adipic acid-enhanced
 economics271
 in spray tower system with forced oxidation and two tanks287, 288*f*
 test programs272-274
 test results274-300
 economics300-305
 process, capital investment393
- spray tower312-314
- Springfield229
- Sylacauga335
- tests with bleed stream
 oxidation291, 292*t*
 testing with forced oxidation272
 utilization334*t*, 335, 337, 338*f*
 in adipic acid-enhanced system .. 270
 for reactor studies337, 338*f*
 sensitivity330
- Liquid entrained in filter cake239-241
- Liquid film enhancement factor, calculated effect of buffer alternatives253, 254*f*
- Liquid film enhancement factors with buffers, comparison250, 251*f*
- Liquids, thermodynamic properties .. 8-12*t*
- Ljungstrom-type heat exchangers309
- Loop analysis42

M

- Magnesium limestone dissolution, factors affecting99-111
- Magnesium, spray dryer, FGD process, capital investment393
- Magnesium carbonate dissolution106*t*

- Magnesium oxide
 additive, limestone case with302, 303*t*
 FGD process
 annual revenue requirements,
 conventional410-411*t*
 annual revenue requirements for
 spray dryer395, 407-409*t*
 capital investment,
 conventional393, 401-402*t*
 capital investment summary,
 spray dryer400*t*
 conceptual design and
 economics381-412
 description, spray dryer385-388
 design changes382-385
 electrical consumption397
 regeneration section400
 sensitivity analysis397-399
 FGD system
 conceptual design economics390-399
 HCl removal and purge389, 390
 process, conventional382, 383*f*
 spray dryer384*f*
 -fly ash separation388, 389
- Magnesium sulfate
 activity coefficient49*t*
 addition to CaSO₄, activity65, 66*f*
 addition, CaSO₄, Radian mean-ion
 activity coefficients65, 67*f*
 addition to CaSO₄, solubility data65, 66*f*
 molal enthalpy49*t*
- Maleic acid rate constant246
- Manganese
 catalytic effect on sulfite oxidation260
 -catalyzed
 CaSO₃ oxidation187, 188*t*
 Na₂SO₃ oxidation176, 178-179, 181*t*
 regression analyses181*t*
 S(IV) vs. time176, 178*f*
 simulated slurry oxidation,
 kinetic rate constants212
 concentration effect on slurry
 model oxidation212, 213*f*
- iron, limestone, and fly ash, results
 of bench-scale runs with230*t*
 and iron mixed catalysts, Na₂SO₃
 oxidation182
 and pH effect on adipic acid
 degradation229, 231*f*
- Manganous
 concentration effect on photooxi-
 dation rate of bisulfite166, 167*f*
 ion effect on bisulfite oxidation rate
 in buffered solution158, 159*f*
 ion effect on bisulfite oxidation
 rate in nonbuffered
 solution159*f*, 162-164
- Mass transfer
 coefficient of CaSO₃,
 determination210, 211*f*
- Mass transfer (*continued*)
 enhancement by adipic acid253, 254*f*
 enhancement, gas/liquid249-255
 model75-101
 model for CaCO₃ dissolution77-82
 S(IV) ions from solid to liquid
 equation207
- Mathematical model for scrubber
 slurry191
- Mean-ion activity coefficients59, 64*t*, 65
 in FGD solution64*t*
- Metal chelates144
 formation and dissociation rate
 constants of nitrosyl145-149
 kinetics of reactions of NO and
 SO₂ in aqueous solutions
 containing146, 150
- Metal ion effect on thermal decom-
 position of sulfur120, 123
- Mineral characterization studies379
- Mixing parameters61, 62
- Model
 -dissociation with chemical
 reaction205-210
 oxidation in CaSO₃ slurries191-220
 solutions210-215
- Modeling
 chemical kinetics137-144
 reactions considered and rate
 constants148*t*, 149*t*
 slurry oxidation195
- Molal enthalpy47
 CaSO₄48*t*
 H₂SO₃50*t*
 MgSO₄49*t*
 Na₂SO₄53*t*
 Na₂SO₃52*t*
 SO₂51*t*
- Molar density of calcite81
- Molar flux balance204
- N
- Nahcolite350
 acid-insoluble, x-ray diffraction
 pattern372, 373*f*
 analyses354*t*
 characterization of volatile organic
 components369-379
 oil(s)
 ¹³C NMR spectrum374, 376*f*
 capillary gas chroma-
 tography374, 376*f*
 compounds identified by gas
 chromatography378*t*
 elemental analyses374*t*
 ¹H NMR spectrum374, 375*f*
 IR spectrum374, 375*f*
 tests362-365

- Nahcolite (*continued*)
 thermal gravimetric analysis of
 acid-insoluble fraction 372, 373*f*
 and trona, apparatus for trapping
 volatile oils 370, 371*f*
 and trona behavior with TGA 372*t*
 x-ray diffraction powder
 pattern 372, 373*f*
 National Bureau of Standards tables 21–30*t*
 National Bureau of Standards, data
 centers, future evaluations 55
 Network approach for barium
 compounds 42, 43*f*
 Nitric acid oxidation to NO₂ 137, 139*f*
 Nitric oxide
 coordination to ferrous chelates,
 kinetic and thermodynamic
 data for reversible 147*t*
 coordination to metal
 chelates 144, 145, 147*t*
 kinetics of reaction with metal
 chelates 146, 150
 oxidation to NO₂ 127, 129
 Nitrite ions, reaction
 pH effect 140*f*, 144
 with sulfite 137–144
 SO₂ concentration effect 141*f*, 144
 temperature effect 142*f*, 145
 Nitrite and sulfite ions interaction
 reaction scheme 129, 130
 Nitrogen oxides 127, 129
 Nitrogen–sulfur complexes 129
 Nitrosulfonic acid formation 129, 130
 Nitrosyl metal chelates, formation and
 dissociation rate constants 145–149
 Nitrous acid (*see* Acid, nitrous)
 NO_x removal efficiency 137–144
 Number of particles in experimental
 run 198
- O
- Occlusion in solids 239–241
 1-Octene, ¹H NMR spectrum 374, 375*f*
 Oils, volatile, studies 370, 371*f*
 Olefins, ¹H NMR spectrum 374, 375*f*
 Operating alternatives for adipic acid
 addition, comparison 316, 318*t*
 Organic acid(s)
 effect, on dissolution rate 88, 90*f*
 effect of limestone dissolution 88–91
 relative costs 255*t*
 solutions, sulfite oxidation 173–189
 Organic volatile components of
 nahcolite and trona,
 characterization 369–379
 Osmotic coefficient constant, Debye–
 Hückel 60
 Osmotic coefficient, Pitzer equation .. 54
- Oxidation
 –absorption–reduction
 processes 128*t*, 129
 beginning at three pH values 212, 215*f*
 bisulfite ion by oxygen, kinetics 153–171
 in buffered solution, ethanol con-
 centration, effect on rate in
 bisulfite 158, 160*f*, 161
 in buffered solution, manganous ion
 effect on rate in bisulfite 158, 159*f*
 of CaSO₃, effect of succinic
 acid 184*t*, 185*t*
 in CaSO₃ slurries, model 191–220
 Fe-catalyzed Na₂SO₃ 179–181
 forced 271, 274
 in FGD 173
 kinetics of bisulfite 168–170
 levels, solids, test results for adipic
 acid concentration 238*t*
 Mn-catalyzed CaSO₃ 187, 188*t*
 Mn-catalyzed Na₂SO₃ 176, 178,
 179, 181*t*
 model, slurry, variable catalyst
 concentration 212, 213*f*
 modeling of the slurry 195
 Na₂SO₃ 176
 pH effect on S(IV) species 176, 178*f*
 nonbuffered solutions, bisulfite 161–162
 in nonbuffered solutions, ethanol
 effect on bisulfite 162, 165*f*
 sulfite, in organic acid solutions 173–189
 percent vs. total adipic acid
 losses 234, 235*f*
 photooxidation data for bisulfite 164
 rate dependence on concentrations
 of bisulfite and hydrogen
 ion 162, 163*f*
 rate in nonbuffered solution,
 manganous ion effect on
 bisulfite 159*f*, 162–164
 regression analyses of Mn and
 Fe-catalyzed Na₂SO₃ 181*t*
 regression analyses of Na₂SO₃ 183*t*
 slurry model, pH measurements 216, 217*f*
 states, sulfur 115–117
 and sulfate precipitation 337, 339
 sulfite 256, 257*f*
 to sulfate 113–125
 in variable concentration
 slurries 212, 214*f*
 Oxidative degradation 255–261
 carboxylic acids 258*t*
 Oxidizing system in scrubber, of pH
 effect on solubility 202, 203*f*
 Oxyacids ions of sulfur 116*t*
 Oxygen
 kinetics of HSO₃⁻ oxidation 153–171
 gaseous, gas volume data for
 absorption into bisulfite
 solution 155, 157*f*, 158

- Oxygen (*continued*)
 rate of reaction between HSO_3^- 158, 159f
 single-phase experiments, reaction
 between HSO_3^- 158–170
 uptake by bisulfite solution, single-
 phase rate experiments 155
 uptake by bisulfite solutions, two-
 phase rate experiments 154, 155
 Ozone as oxidant 137
- P**
- Partial pressure, CO_2 76
 Particle(s)
 dissolution with no reaction, surface
 and bulk conditions 206t
 number in experimental run 198
 size
 distribution 198, 201f
 of CaCO_3 83, 85t
 sorbent effect on SO_2 removal
 with NaHCO_3 356, 360f
 surface conditions 204
 Pitzer composition 105t, 106t
 pH
 effect on adipic acid degradation
 rate constant 229, 231f
 behavior of slurry model 212, 215f
 decomposition of thiosulfate 120, 121f
 effect
 adipic acid degradation rate 229
 on CaCO_3 dissolution rate 86, 87f,
 107, 108f
 on limestone dissolution 86
 on limestone reactivity 104t
 on nitrite ions reaction 140f, 144
 on S(IV) species, oxidation
 of Na_2SO_3 176, 178f
 on solubility, oxidizing system
 in scrubber 202, 203f
 on sulfite ions reaction 140f, 144
 measurements for slurry model
 oxidations 216, 217f
 operating, adipic acid-enhanced
 lime/limestone system 270–271
 scrubber bleed, SO_2 removal as
 a function 335, 336f
 spray tower inlet, effect on SO_2
 removal 293, 297–299
 variations, effect on limestone dual
 alkali 345
 Photooxidation
 data for bisulfite oxidation 164
 with ethanol, rate expression 164, 165f
 manganous concentration effect on
 bisulfite rate 166, 167f
 Physical properties of buffers 251t
 Pilot-scale scrubbing system with
 forced oxidation tank 194
 Pittsburgh coal 357t
 Pittsburgh seam coal 362, 363f
 Pitzer equation(s)
 activity coefficient 54, 55
 calculations 65, 66f
 curves for CaSO_3 69, 70f
 osmotic coefficient 54
 parameters for binary ion pairs 62, 63
 parameters, sensitivity of activity
 coefficients 63, 64
 summary 59–61
 use to estimate strong-electrolyte
 activity coefficients in aqueous
 FGD processes 53–73
 pKa of buffer, effect of SO_2 absorption 261
 Pollution control for coal-fired
 power plants 308
 Polyacrylic acid (*see* Acid, poly-
 acrylic)
 Polydisperse size distribution 83, 85t
 Polythionates formation 120
 Potassium bisulfite solutions 117, 120
 Potassium sulfite solutions 117, 120
 Power
 consumption at Scholz 343–344
 demand, gross electric, of limestone
 scrubbers using hot booster
 fans 319, 320f
 input for SO_2 absorption 310
 plant flue gas contents 127
 plants, SO_2 removal, coal-
 burning 153–171
 Precipitation, solids, test results for
 adipic acid addition 236t
 Precipitation, sulfate, and
 oxidation 337, 339
 Process(es)
 absorption–reduction 140, 145–150
 description, spray dryer MgO 385–388
 energy requirements for limestone
 FGD 321t
 FGD, limestone dual alkali 325–347
 Japanese 129
 lime/limestone oxidation of bisul-
 fite ion by oxygen 153
 limestone dual alkali, advantages 325
 operability of limestone dual alkali
 system 344–346
 oxidation–absorption–
 reduction 128t, 129
 in SO_2 scrubbing, chemical
 reactions 192
 Program, Bechtel-modified Radian
 equilibrium 65, 66f
 Program, calculator for thermo-
 dynamic calculations 31, 32
 Prototype system at Scholz 331–346
 Pumps, thickener underflow 342

R

- Radian
 effective curve for $\text{CaSO}_3\text{-NaCl}$ 69, 71*f*
 equilibrium computer code,
 Bechtel-modified 58
 equilibrium program, Bechtel-
 modified 65, 66*f*
 compared with extended Debye-
 Hückel model 64-71
 mean-ion activity coefficients
 CaSO_3 when MgSO_4 is added 69, 70*f*
 CaSO_3 when NaCl is added 69, 71*f*
 CaSO_4 when MgSO_4 is added 67*f*
 CaSO_4 when NaCl is added 68*f*
- Raman spectra data
 ammonium bisulfite
 solution 115, 117, 118*f*
 barium sulfate 115
 mixture of trithionate and
 tetrathionate 120, 122*f*
 solid from auto-redox products
 of ammonia solution saturated
 with SO_2 117, 119*f*
- Raman spectroscopy use in thermal
 decomposition of sulfur 114-115
- Rate
 adipic acid degradation 225
 chain reaction 166
 constants for calcite dissolution 86
 equation 82
 formation and dissociation of
 nitrosyl metal chelates 145-149
 kinetic, for Mn-catalyzed simu-
 lated slurry oxidation 212
 for sulfonation 246
 used for modeling, reactions
 considered 148*t*, 149*t*
- dependence on concentrations of
 bisulfite and hydrogen ion for
 oxidation 162, 163*f*
- equation
 for batch oxidation of CaSO_3
 slurry 256
 equation for dissolution 105
 for Fe and Mn-catalyzed
 Na_2SO_3 oxidation 179
 for reaction of sulfamic with
 nitrous acid 136
- equation for sulfite transfer from
 solid particles to liquid phase 208
- expression for photooxidation with
 ethanol 164, 165*f*
- law for buffered solutions 158
- laws for bisulfite oxidation 158, 169*t*
- of oxidation of CaSO_3 , dependence
 on succinic acid con-
 centration 182, 186*f*
- Rate (*continued*)
 of O_2 uptake by bisulfite solution,
 single-phase experiments 155
 of O_2 uptake by bisulfite solutions,
 two-phase experiments 154, 155
 reaction between HSO_3^-
 and O_2 158, 159*f*
 of sulfite oxidation 255
- Reaction(s)
 between HSO_3^- and O_2 single-phase
 experiments 158-170
 considered and rate constants used
 for modeling 148*t*, 149*t*
 kinetics in wet flue gas simultaneous
 desulfurization and denitrifica-
 tion system 127-152
 of sulfamic acid with nitrous
 acid 136, 137
 vessel used for single-phase experi-
 ments on O_2 uptake by bisul-
 fite solution 155, 156*f*
- Reactivity
 apparatus, limestone 102, 103*f*
 limestone experimental
 approach 101-103
 limestone, experimental results 104-107
- Reactor
 batch, concentration profile of
 species as function of reaction
 time 137-144
 dissolution 83, 84*f*
 feed composition 104*t*
 slurry 195-197
 studies, limestone utilization 337, 338*f*
- Regeneration
 limestone, overall reaction 328
 reactions, dissolved Fe interference
 with 341
 section, MgO process 400
- Regression analyses of Na_2SO_3
 oxidation 183
 Fe-catalyzed 181*t*
 Mn-catalyzed 181*t*
- Removal efficiency of NO_x 137-144
- Removal efficiencies of SO_2 311, 313*f*
- spray tower as a function of net
 work input 312, 313*f*
- TCA scrubber as function of net
 work input 311, 313*f*
- Rickenbacker industrial boiler
 demonstration 300
- Runge-Kutta-Gill algorithm 210
- s**
- S(IV) ions from solid to liquid,
 mass transfer equation 207
- S(IV) ions production 207

- S(IV) species, pH effect on Na_2SO_3 oxidation176, 178f
- S(IV) vs. time for Fe-catalyzed Na_2SO_3 oxidation 180f
- S(IV) vs. time for Mn catalyzed Na_2SO_3 oxidation176, 178f
- Saginaw limestone 330
- Scale formation 345
- Scholz power consumption343-344
- Scholz prototype system331-346
- Scholz system
 general operating conditions332, 333t
 overall performance332, 334t
 SO_2 removal performance 332, 335, 336f
 additive, adipic acid advantages 269-271
- Scrubber(s)
 additive, adipic acid testing276-277
 adipic acid degradation221-242
 bench-scale, test results224-234
 bleed pH, SO_2 removal as
 function335, 336f
 bleed stream 291
 commercial, adipic acid use
 as buffer 187
 computer model, SA_2 wet 100
 configurations 291
 feed composition102t
 inlet pH and adipic acid concentration effect on SO_2 removal
 in TCA293, 296f
- limestone
 energy consumed for 90% SO_2 removal 315t
 energy requirements for SO_2 absorption307-324
 fan location 319
 FGD, conclusions322-323
 using hot booster fans, gross electric power demand319, 320f
 effect of pH on solubility, oxidizing system202, 203f
 prototype features 311t
 slurry(ies)
 model, sulfite oxidation rate 193
 mathematical model 191
 physical system model197-202
 solids, coprecipitation of
 adipic acid234-238
 SO_2 , diagram of closed loop222, 223f
 TCA311, 312
 units, liquid phase 47
- Scrubbing
 adipic acid-enhanced limestone, in spray tower system
 with forced oxidation and two tanks287, 288f
 in TCA system without forced oxidation281, 283f
- Scrubbing (*continued*)
 adipic acid-enhanced (*continued*)
 in venture/spray tower system272, 278f
- agent(s)
 analyses354, 356
 for sulfur oxides removal from stack gas369-379
 tests362-366
 economics of limestone300-305
 process, limestone, capital investment 393
 process, slurry 76
 slurry, buffer additives for lime/limestone243-265
 system with forced oxidation tank, pilot-scale 194
 test facility, EPA alkali267-306
- Selective catalytic reduction 150
- Sensitivity of activity coefficients to changes in Pitzer-equation parameters63, 64
- Sensitivity analysis, MgO FGD process397-399
- Settling characteristics of waste solids339-342
- Settling rates of waste solids339, 340f
- Shawnee
 adipic acid test schedule272, 273f
 TCA without forced oxidation, adipic acid-enhanced lime tests from283f, 285, 286f
- test
 blocks274, 275t
 facility 274
 results 274
- Single-ion activity coefficients 59
- Single particle agglomerate, sulfite/sulfate198, 199f
- Single particle dissolution rate equation 81
- Size distribution, particle198, 201f
 CaCO_3 83, 85t
- Slurry(ies)
 CaSO_3 oxidation model191-220
 conditions during dissolution202-205
 density variations212, 214f
 equation for total sulfite concentration in 209
 flow rate effect on SO_2 removal in TCA293-295
 liquid phase sulfite concentration .. 207
 model
 film theory 216
 oxidations, pH measurements 216, 217f
 pH behavior212, 215f
 scrubber physical system197-202
 oxidation
 experiments, catalyzed210-212

- Slurry(ies) (*continued*)
 oxidation (*continued*)
 model, variable catalyst concentration 212, 213*f*
 modeling 195
 particle representation 198, 200*f*
 particles, sulfite/sulfate 198, 199*f*
 reactor 195-197
 scrubbing, buffer additives for
 lime/limestone 243-265
 scrubbing process 76
 Soda ash consumption 343
 Sodium bicarbonate
 baghouse temperature effect on
 SO₂ removal with 356, 359*f*
 reaction with SO₂ 350
 sorbent particle size effect on
 SO₂ removal with 356, 360*f*
 tests 356, 358-361
 Sodium bisulfite solutions 117, 120
 Sodium carbonate reaction with SO₂ .. 350
 Sodium chloride
 addition, effect on activity coefficient of CaSO₃ 65, 68*f*
 addition, effect on activity coefficient of CaSO₄ 65, 68*f*
 formation 328
 Sodium sesquicarbonate (*see* Trona)
 Sodium sulfate
 activity coefficients 53*t*
 formation 328
 molal enthalpy 53*t*
 Sodium sulfite 328
 activity coefficients 52*t*
 molal enthalpy 52*t*
 oxidation 176
 Fe-catalyzed 179-181
 rate equation 179
 regression analyses 181*t*
 S(IV) vs. time 180*f*
 Mn-catalyzed 176, 178*f*
 regression analyses 181*t*
 rate equation 179
 S(IV) vs. time 176, 178*f*
 pH effect on S(IV) species 176, 178*f*
 regression analyses 183*t*
 solutions 117, 120
 Solid(s)
 dewatering 271
 occlusion 239-241
 oxidation levels, test results for
 adipic acid concentration 238*t*
 precipitation, test results for adipic acid addition 236*t*
 samples, electron micrographs
 analyses 341
 thermodynamic properties 8-12*t*
 waste, settling characteristics 339-342
 waste, settling rates 339, 340*f*
- Solubility
 calculations 69
 data, experimental, for CaSO₄
 when MgSO₄ is added 66*f*
 gypsum 329
 oxidizing system in scrubber,
 pH effect 202, 203*f*
 sulfate 198
 sulfite 198
 Solution, aqueous, properties 47-55
 Solutions of model 210-215
 Sorbent(s)
 feeding 361-362
 injection point, location effect 356, 361
 injection system, dry 351, 353*f*
 particle size, effect on SO₂ removal
 with NaHCO₃ 356, 360*f*
 tested 354, 356
 Spray dryer
 absorbers advantages over wet
 scrubbing 382
 MgO FGD process
 annual revenue requirements 395
 capital investment 393
 description 385-388
 process, summary of capital
 investment 400*t*
 process annual revenue
 requirements 407-409*t*
 Spray tower 312-314
 energy consumed for SO₂ removal 315*t*
 as a function of net work input,
 SO₂ removal efficiency 312, 313*f*
 system with forced oxidation and
 two tanks 287, 288*f*
 Springfield full-scale demonstration .. 300
 Springfield limestone 229
 Stack gas absorption studies 369
 Stir rate effect on limestone
 reactivity 104*t*
 Stirring rate, vs. Fredonia limestone
 dissolution rate 107, 110*f*
 Stokes-Einstein relationship 82
 Succinic acid (*see* Acid, succinic)
 Sulfamate (SAM), hydrolysis rate
 and mechanism 135, 136
 Sulfamic acid (*see* Acid, sulfamic)
 Sulfate
 barium, Raman data 115
 calcium
 activity coefficients 48*t*
 CaSO₃ forced oxidation 268
 CaSO₃ conversion to 173
 formation 329
 molal enthalpy 48*t*
 calcium, oxidation results 182, 184-188
 solid disposal 192
 magnesium, activity coefficient 49*t*
 magnesium, molal enthalpy 49*t*

- Sulfate (*continued*)
- percentage vs. adipic acid concentration in solids 236, 237*f*
 - precipitation 337, 339
 - slurry particles 198, 199*f*
 - sodium, formation 328
 - solubility 198
 - sulfite oxidation 113-125
 - /sulfite, single particle agglomerate 198, 199*f*
- Sulfite
- effects on limestone dissolution 91-94
 - ions reaction
 - pH effect 140*f*, 144
 - SO₂ concentration effect 141*f*, 144
 - temperature effect 142*f*, 145
 - and nitrite ions reaction in aqueous solutions 137-144
 - and nitrite ions interaction, reaction scheme 129, 130
 - and nitrous acid reaction 129, 130
 - oxidation 256, 257*f*
 - cost-effective alternative 262
 - factors that influence 260-262
 - free radical generation 255
 - hydroxyacetic acid inhibition 260-261
 - hydroxypropionic acid inhibition 260-261
 - Mn catalytic effect 260
 - in organic acid solutions 173-189
 - rate 255
 - in scrubber slurries model 193
 - of sodium 176
 - to sulfate 113-125
 - thiosulfate inhibition 260
 - particle geometry 216
 - potassium solutions 117, 120
 - slurry
 - equation for total concentration 209
 - liquid phase concentration 207
 - oxidation model 191-220
 - particles 198, 199*f*
 - sodium 328
 - solutions 117, 120
 - solubility 198
 - solution, thermal decomposition 113-125
 - transfer from solid particles to liquid phase, rate equation 208
- Sulfocarboxylic acid 246-248
- Sulfosuccinic acid effect on dissolution rate 88, 90*f*, 91
- Sulfonation
- hydroxylamine 133, 134
 - hydroxylamine disulfonate 132
 - hydroxylamine monosulfonate 133
 - rate constants 246
 - rates of unsaturated acids 247*t*
 - reaction kinetics 246
- Sulfopropionic acid (*see* Acid, sulfopropionic)
- Sulfur 321
- auto-redox decomposition 114
 - catalysts influence on thermal decomposition 120, 123
 - elemental, conversion 120
 - nitrogen complexes 129
 - oxidation states 115-117
 - oxyacids ions 116*t*
- Sulfur dioxide
- activity coefficients 51*t*
 - absorption
 - adipic acid effect on 253, 254*f*
 - aluminum chloride effect 253
 - buffer p*K*_a effect 261
 - in limestone scrubbers, energy requirements 307-324
 - power input 310
 - ammonia solution, Raman spectra of solid from auto-redox products 117, 119*f*
 - ammonia solution thermal decomposition 117, 118*f*
 - concentration effect, sulfite and nitrite ions reaction 141*f*, 144
 - conversion to sulfuric acid 153, 387
 - emissions 281
 - control 192
 - by dry sorbent injection 349-368
 - standards 268
 - kinetics of reaction with metal chelates 146, 150
 - molal enthalpy 51*t*
 - NO_x as oxidizing agent 127
 - reaction with Na₂CO₃ and NaHCO₃ 350
 - removal
 - efficiencies 311, 313*f*
 - and sorbent utilization, effect of intermittent sorbent feeding 361*t*
 - of spray tower as function of net work input 312, 313*f*
 - of TCA scrubber as function of net work input 311, 313*f*
 - of TCA scrubber vs. net work input with adipic acid 316, 317*f*
 - with forced oxidation, effects of scrubber inlet pH and adipic acid concentration 293, 297-299
 - as a function of adipic acid concentration and spray tower inlet pH without forced oxidation 293, 297-299
 - as a function of scrubber bleed pH 335, 336*f*
 - gross electric demand 310

- Sulfur dioxide (*continued*)
 removal (*continued*)
 with NaHCO_2 356, 358*f*
 baghouse temperature
 effect 356, 359*f*
 sorbent particle size effect 356, 360*f*
 with nahcolite 362, 364*f*
 while burning Pittsburgh
 seam coal 362, 363*f*
 ninety percent, energy
 consumed 315*t*, 316, 317*f*
 performance of Scholz
 system 332, 335, 336*f*
 process 192
 overall reactions 326
 from stack gases 153
 in TCA
 effect of adipic acid concentration and slurry flow
 rate 293–295
 effects of scrubber inlet pH and adipic acid concentration 293, 296*f*
 with trona while burning
 Pittsburgh seam and West Virginia coal 362, 365, 366*f*
 scrubber, diagram of closed
 loop 222, 223*f*
 scrubbers, electric demand to
 operate 308
 scrubbing, processes chemical
 reaction 192
 solubility in water 250
 wet scrubber computer model 100
 Sulfuric acid, byproduct, price,
 sensitivity of annual revenue
 requirements 397–399
 Sulfuric acid, SO_2 conversion 387
 Sulfurous acid activity coefficients 50
 Sulfurous acid, molal enthalpy 50*t*
 Surface conditions during dissolution 202–205
 Sylacauga limestone 335
 Synthesis, buffer 245–249
- T**
- TCA (*see* Turbulent contacting absorber)
 Temperature effect
 baghouse, on SO_2 removal with
 NaHCO_3 356, 359*f*
 dissolution rate, Fredonia
 limestone 107, 109*f*
 limestone dissolution 87*f*, 88
 limestone reactivity 104*t*
 nitrite ions reaction 142*f*, 145
 settling properties of waste solids .. 341
 Temperature effect (*continued*)
 sulfite ions reaction 142*f*, 145
 hold tank, on the adipic acid
 degradation rate 232*t*
 Tetrathionate and trithionate mixture, Raman spectra 120, 122*f*
 Thermal decomposition
 SO_2 -ammonia solution 117, 118*f*
 sulfite, bisulfite, and disulfite
 solutions 113–125
 sulfur
 influence of catalysts 120, 123
 Raman spectroscopy 114–115
 thiosulfate intermediates 117, 120
 Thermal gravimetric analysis of
 acid-insoluble fraction of
 nahcolite 372, 373*f*
 Thermodynamic
 calculations, calculator program ... 31, 32
 data for reversible NO coordination
 to ferrous chelates 147*t*
 properties
 aqueous species 13–20*t*
 common gases 3–7*t*
 data base 42
 liquids 8–12*t*
 solids 8–12*t*
 values for desulfurization
 processes 1–39
 Thickener underflow pumps 342
 Thiosulfate
 decomposition as function
 of pH 120, 121*f*
 inhibition of sulfite oxidation 260
 intermediates in thermal decomposition of sulfur 117, 120
 solutions 120
 Time, reaction, in a batch reactor,
 concentration profile of species
 as function of 137–144
 Trithionate and tetrathionate mixture,
 Raman spectra 120, 122*f*
 Trona 350
 analyses 354*t*
 apparatus for trapping volatile
 oils 370, 371*f*
 characterization of volatile organic
 components 369–379
 and nahcolite behavior with TGA .. 372*t*
 oil, capillary gas chromatography
 374, 376*f*
 oils, compounds identified by gas
 chromatography 378*t*
 tests 362, 365, 366*f*
 Turbulent contacting absorber (TCA)
 comparison of trona and nahcolite
 behavior with 372*t*
 effect of adipic acid concentration
 and scrubber inlet pH on
 SO_2 removal 293, 296*f*

Turbulent contacting absorber

(continued)

- effect of adipic acid concentration and slurry flow rate on SO₂ removal293-295
- energy consumed for SO₂ removal 315*t*
- scrubber311, 312
 - effect of adipic acid concentration on gross electric power demand for 90% SO₂ removal316, 317*f*
 - as a function of net work input, SO₂ removal efficiency 311, 313*f*
 - vs. net work input with adipic acid, SO₂ removal efficiency316, 317*f*
- system without forced oxidation, adipic acid-enhanced scrubbing281, 283*f*

U

- UV light effect on bisulfite photooxidation163-165

V

- Valeric acid formation 255
- Venturi/spray tower system, adipic acid-enhanced scrubbing272, 278*f*
- Venturi/spray tower system, bleed stream oxidation, adipic acid-enhanced limestone291, 292*t*
- Virial coefficients59-61
- Volatility of carboxylic acid 262
- Volatile oils studies370, 371*f*

W

- Water dissociation equation 202
- Waste solids
 - deterioration of settling properties
 - with time 341-342
 - settling characteristics 339-342
 - temperature effect on settling properties 341
- West Virginia coal357*t*, 362, 364*f*

X

- X-ray diffraction powder pattern for nahcolite372, 373*f*